

(NASA-CR-192962) PROCEEDINGS OF  
THE SEVENTH ANNUAL SUMMER  
CONFERENCE. NASA/USRA: UNIVERSITY  
ADVANCED DESIGN PROGRAM (USRA)  
325 p

N93-29712  
--THRU--  
N93-29761  
Unclas

G3/01 0160576

**Proceedings of the  
7th Annual Summer Conference**

**NASA/USRA**

**University Advanced Design Program**

**Hosted by  
Kennedy Space Center  
June 17-21, 1991**

**NATIONAL AERONAUTICS & SPACE ADMINISTRATION  
UNIVERSITIES SPACE RESEARCH ASSOCIATION**



**NASA/USRA  
UNIVERSITY ADVANCED DESIGN PROGRAM**

**PROCEEDINGS OF THE  
7th ANNUAL SUMMER CONFERENCE**

**June 17-21, 1991**

**NASA/USRA UNIVERSITY ADVANCED DESIGN PROGRAM  
7th ANNUAL SUMMER CONFERENCE**

The NASA/University Advanced Design Program is operated by the Universities Space Research Association (USRA) under a contract with NASA Headquarters (NASW-4435). Inquiries regarding the program may be directed to:

USRA Advanced Design Program Office  
3600 Bay Area Boulevard  
Houston, Texas 77058  
(713)480-5939  
FAX: (713)480-8862

## IN MEMORIAM

*This Proceedings volume is respectfully dedicated to the memory of Mr. Melvin J. Hartmann who died on August 17, 1991. Mr. Hartmann retired from NASA Lewis Research Center in 1990 after 47 years of outstanding service to NACA and NASA. He last served as Director of University Programs where he coordinated research at NASA and universities. Prior to that he was Director of Aeronautics, supervised projects for space vehicles, and was Director of Science and Technology. His many awards included the Presidential Citation and the Exceptional Scientific Achievement Medal. Mr. Hartmann was a staunch supporter of the Advanced Design Program. He will be missed by his many friends and colleagues associated with the program.*

## FOREWORD

### **The Program**

*The Advanced Design Program (ADP) is a unique program that brings together students and faculty from United States engineering schools with engineers from the NASA centers through integration of current and future NASA space and aeronautics projects into the university engineering design curriculum. The ADP was conceived in 1984 as a pilot project to foster engineering design education in the universities and to supplement NASA's in-house efforts in advanced planning for space design. Nine universities and five NASA centers participated in the first year of the pilot project. Two years later a similar program was added, focusing on advanced aeronautics design. Close cooperation between the NASA centers and the universities, the careful selection of design topics, and the enthusiasm of all participants have resulted in a very successful program that now includes forty-one universities, eight NASA centers, and one industry participant.*

*The Advanced Space Design Program study topics cover a broad range of projects that could be undertaken during a 20-30 year period beginning with the deployment of the Space Station Freedom scheduled for the late 1990's and embracing both manned and unmanned endeavors.*

*The Advanced Aeronautics Design Program study topics typically focus on nearer-term projects of interest to NASA, covering the spectrum from small, slow-speed vehicles through large, supersonic passenger transports, and on through hypersonic research vehicles. The systems approach to the design problem is emphasized in both the space and aeronautics projects. The student teams pursue the chosen problem during their senior year in a one- or two-semester capstone design course and submit a comprehensive written report at the conclusion of the project. Finally,*

*student representatives from each of the universities summarize their work in oral presentations at the Annual Summer Conference, sponsored by one of the NASA centers and attended by the university faculty, NASA and USRA personnel, and aerospace industry representatives.*

### ***The Proceedings Volume***

*As the Advanced Design Program has grown in size, it has also matured in terms of the quality of the student projects. The comprehensive final reports are distributed through the National Technical Information Service. However, the results of the studies reach only a small audience, principally those who attend the Summer Conference. In order to broaden the distribution, a Proceedings volume, which summarizes the project results and roughly parallels the Conference presentations, is published. The present volume represents the student work accomplished during the 1990-91 academic year reported at the Seventh Annual Summer Conference hosted by Kennedy Space Center, June 17-21, 1991.*

### **ACKNOWLEDGMENTS**

*This publication was made possible through the efforts of a great many people. First of all, we are grateful to the students, the university faculty, and their teaching assistants for the excellent technical work. Second, we are indebted to those individuals from NASA Headquarters and from the NASA centers who conceived the program in the beginning, have provided valuable guidance to both USRA and the universities throughout, and through their keen interest in the student projects, are in large part responsible for the boundless enthusiasm of the students. Finally, we thank the staff of the Publications Services Office of the Lunar and Planetary Institute for the excellent work in the preparation of the final Proceedings volume.*

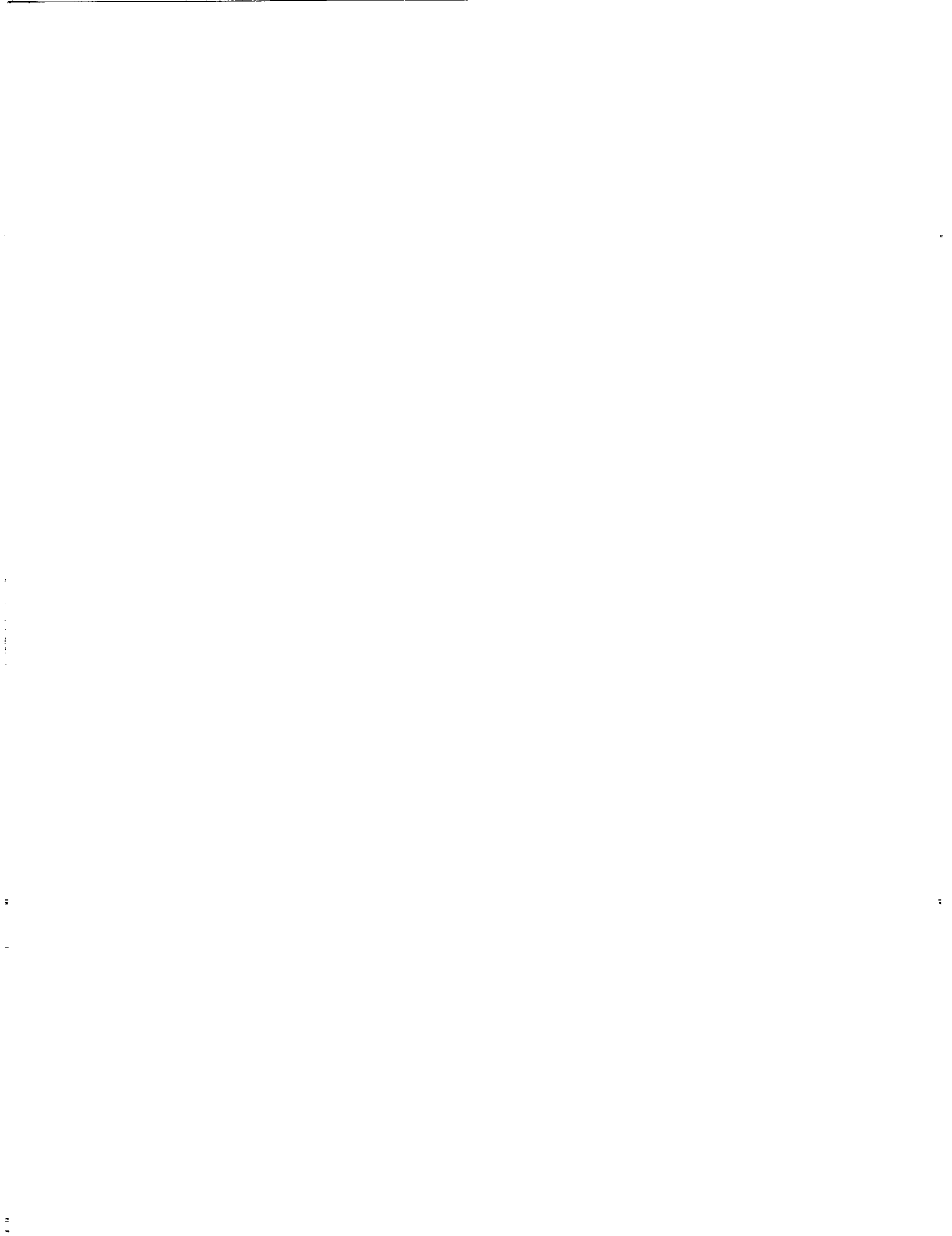
— USRA Advanced Design Program Office

# TABLE OF CONTENTS

|   |          |
|---|----------|
| <b>Foreword</b>   | iii      |
| <b>AERONAUTICS PROJECTS</b>   |          |
| AUBURN UNIVERSITY<br>Summary of 1990-91 Aeronautics Design Projects <i>-omit</i>  | 3-0      |
| CALIFORNIA STATE POLYTECHNIC UNIVERSITY, POMONA<br>High-Altitude Reconnaissance Aircraft                                      | 11-1     |
| CALIFORNIA STATE POLYTECHNIC UNIVERSITY, SAN LUIS OBISPO<br>Project Summary   | 19-2 ✓   |
| CALIFORNIA STATE UNIVERSITY NORTHRIDGE<br>Project ARES II: High-Altitude Battery-Powered Aircraft                             | 29-3     |
| CASE WESTERN RESERVE UNIVERSITY<br>Conceptual Design of a Two-Stage-to-Orbit Vehicle  | 35-4     |
| THE UNIVERSITY OF KANSAS<br>Preliminary Design of an Advanced General Aviation Aircraft                                       | 45-5 ✓   |
| UNIVERSITY OF NOTRE DAME<br>Design Study to Simulate the Development of a Commercial Transportation System                    | 57-6     |
| THE OHIO STATE UNIVERSITY<br>The Design of Two-Stage-to-Orbit Vehicles  | 65-7     |
| ECOLE POLYTECHNIQUE FEMININE<br>ASUR  | 77-8     |
| PURDUE UNIVERSITY<br>Design of a Turbofan Powered Regional Transport Aircraft   | 83-9     |
| WORCESTER POLYTECHNIC INSTITUTE<br>Solar Powered Multipurpose Remotely Powered Aircraft                                       | 89-10    |
| <b>SPACE PROJECTS</b>   |          |
| THE UNIVERSITY OF ALABAMA IN HUNTSVILLE<br>A High-Temperature Furnace for Applications in Microgravity                        | 97-11    |
| UNIVERSITY OF ARIZONA<br>Advanced Design for Orbital Debris Removal in Support of Solar System Exploration                    | 105-12 ✓ |
| UNIVERSITY OF CALIFORNIA, LOS ANGELES<br>1990/91 Project Summaries  | 113-13 ✓ |
| UNIVERSITY OF CENTRAL FLORIDA<br>Design, Building, and Testing of the Postlanding Systems for the Assured Crew Return Vehicle | 117-14 ✓ |
| UNIVERSITY OF COLORADO<br>Earth to Lunar CELSS Evolution  | 123-15 ✓ |
| UNIVERSITY OF FLORIDA<br>Design of Biomass Management Systems and Components for Closed Loop Life Support Systems             | 133-16   |

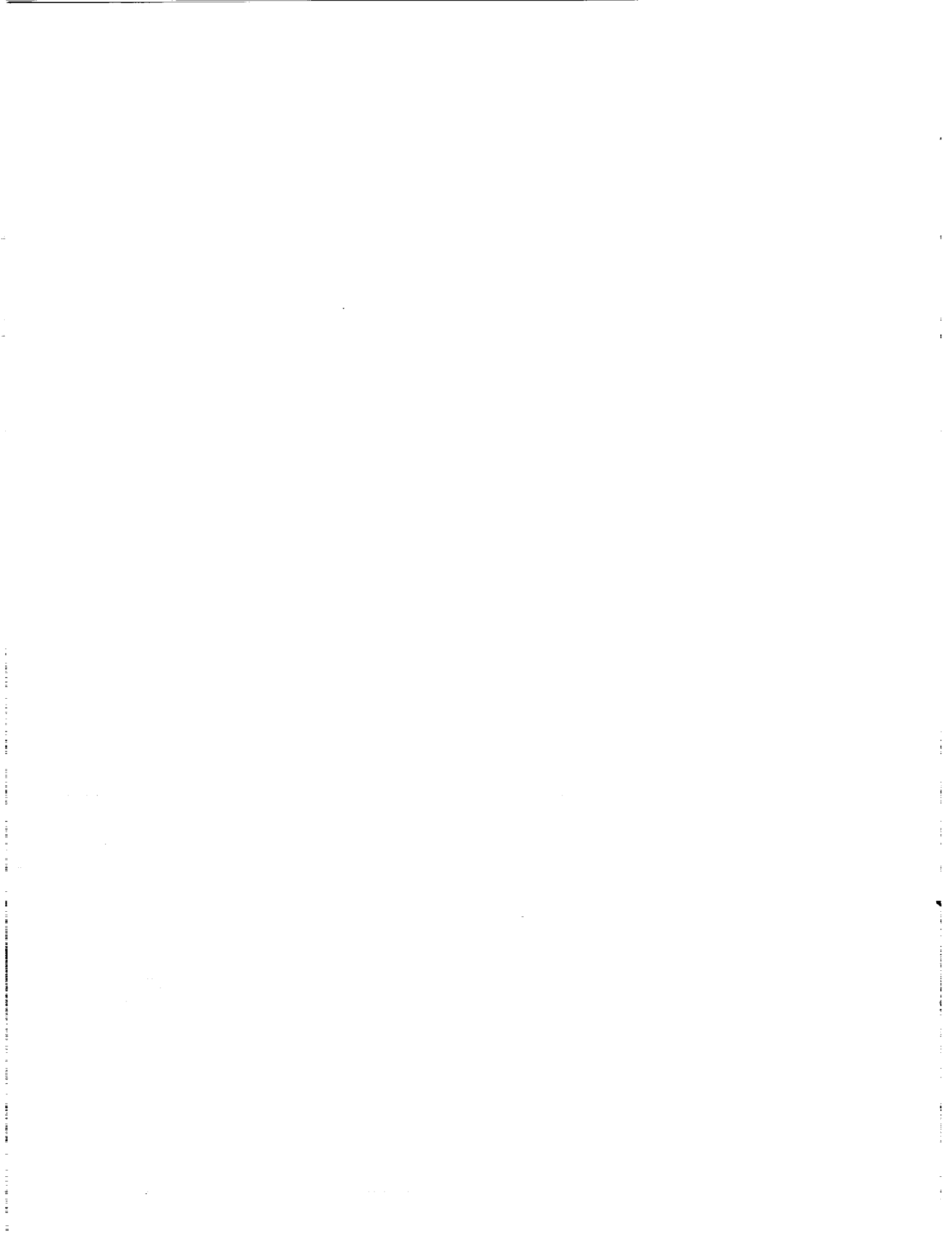
|   |        |
|---|--------|
| FLORIDA A&M UNIVERSITY/FLORIDA STATE UNIVERSITY<br>Lunar Lander Ground Support System                           | 139-17 |
| GEORGIA INSTITUTE OF TECHNOLOGY<br>1990-91 Project Summaries  | 143-18 |
| GEORGIA INSTITUTE OF TECHNOLOGY<br>1990-91 Project Summaries  | 145-19 |
| UNIVERSITY OF HOUSTON<br>Solar Energy Emplacement Developer   | 149-20 |
| UNIVERSITY OF IDAHO<br>Exercise/Recreation Facility for a Lunar or Mars Analog                                  | 155-21 |
| KANSAS STATE UNIVERSITY<br>Automation of Closed Environments in Space for Human Comfort and Safety              | 159-22 |
| UNIVERSITY OF MARYLAND<br>Delta Advanced Reusable Transport (DART) An Alternative Manned Spacecraft             | 165-23 |
| UNIVERSITY OF MARYLAND<br>Taurus Lightweight Manned Spacecraft Earth Orbiting Vehicle                           | 177-24 |
| UNIVERSITY OF MARYLAND<br>Walking Robot: A Design Project for Undergraduate Students                            | 187-25 |
| MASSACHUSETTS INSTITUTE OF TECHNOLOGY<br>Project Copernicus: An Earth Observing System                          | 191-26 |
| UNIVERSITY OF MICHIGAN<br>Project MEDSAT  | 197-27 |
| UNIVERSITY OF MICHIGAN<br>Project UM-Haul: A Self-Unloading Reusable Lunar Lander                               | 205-28 |
| UNIVERSITY OF MINNESOTA<br>Mars Integrated Transportation System Multistage Mars Mission                        | 213-29 |
| UNIVERSITY OF MINNESOTA<br>Single-Stage Mars Mission  | 219-30 |
| NAVAL POSTGRADUATE SCHOOL<br>Multipurpose Satellite Bus (MPS)   | 227-31 |
| THE OHIO STATE UNIVERSITY<br>Project WISH: The Emerald City   | 237-32 |
| OLD DOMINION UNIVERSITY<br>From Orbital Debris Capture Systems Through Internal Combustion Engines on Mars      | 241-33 |
| PENNSYLVANIA STATE UNIVERSITY<br>Mars Sample Return Mission Two Alternate Scenarios                             | 249-34 |
| PRAIRIE VIEW A&M UNIVERSITY<br>Mars Habitat   | 253-35 |
| UNIVERSITY OF PUERTO RICO<br>Selenia: A Habitability Study for the Development of a Third Generation Lunar Base | 265-36 |
| RENSSELAER POLYTECHNIC INSTITUTE<br>The Lightcraft Project  | 275-37 |

|   |          |
|---|----------|
| THE UNIVERSITY OF TEXAS, AUSTIN<br>ASPEC—Solar Power Satellite  | 281 - 38 |
| THE UNIVERSITY OF TEXAS, AUSTIN<br>B&T—Lunar Landers  | 287 - 39 |
| THE UNIVERSITY OF TEXAS, AUSTIN<br>Spacey's Rockets—Personnel Launch System/Family of Heavy Lift Launch Vehicles    | 291 - 40 |
| THE UNIVERSITY OF TEXAS, AUSTIN<br>RS Landers—Lunar Lander  | 295 - 41 |
| THE UNIVERSITY OF TEXAS, AUSTIN<br>SPECS—Orbital Debris Removal   | 299 - 42 |
| THE UNIVERSITY OF TEXAS, AUSTIN<br>1990-91 Project Summaries  | 301 - 43 |
| U.S. NAVAL ACADEMY<br>Mars Aquarius Mission and Titan Explorer  | 305 - 44 |
| UTAH STATE UNIVERSITY<br>Thermion: Verification of a Thermionic Heat Pipe in Microgravity                           | 309 - 45 |
| VIRGINIA POLYTECHNIC INSTITUTE AND STATE UNIVERSITY<br>Solar Electric Propulsion Cargo Spacecraft for Mars Missions | 313 - 46 |
| UNIVERSITY OF WASHINGTON<br>Antares: A Low Cost Modular Launch Vehicle for the Future                               | 317 - 47 |
| UNIVERSITY OF WISCONSIN-MILWAUKEE<br>Genesis II: Advanced Lunar Outpost   | 329 - 48 |
| WORCESTER POLYTECHNIC INSTITUTE<br>Rotational Fluid Flow Experiment   | 335      |



---

***Aeronautics Projects***



# SUMMARY OF 1990-91 AERONAUTICS DESIGN PROJECTS

## AUBURN UNIVERSITY

MIT  
FD 3  
P 11

Auburn University's design groups have completed preliminary study of two design approaches for a new regional aircraft. These projects were sponsored by the NASA/USRA Advanced Design Program and were proposed by S. J. Morris, center mentor at Langley Research Center. The topics proposed are (1) design of a turboprop commuter aircraft, and (2) design of a jet commuter aircraft.

### THE LANGLEY TURBOPROP COMMUTER DESIGN

#### Introduction

This design was undertaken in response to a request for proposal by the NASA Langley Research Center for the design of a regional transport aircraft to meet the apparent demands of a future market. One purpose of this design project is to surpass current regional/commuter aircraft capabilities by using advanced technologies. Another purpose is to make spoke-to-spoke and spoke-to-hub flight more desirable and more feasible. The design requirements as outlined by Langley are (1) short-to-medium range capabilities for regional transport, (2) improved passenger comforts and seamless service; (3) a speed suitable for a commuter service aircraft; (4) low levels of cabin noise; (5) high lift capabilities; (6) materials that meet FAA strength requirements at lower weights; (7) fuel efficiency and low seat-per-mile costs; (8) a seating capacity of 35 to 50 passengers.

There is no current American design for this type of transportation. Furthermore, market forecasts show that in the next 10 years the commercial aviation industry will increase dramatically. Airports will become more congested, and the number of airports will increase. An obvious demand for more regional transports to provide service between the smaller airports and hubs will be generated. Forecasters also predict that the trend will favor commuters seating over 40 passengers.

Overall, the commuters of the 1990s need to produce a safe, comfortable, and economic means of regional transportation. These commuters must be adaptable to the major hubs, but possess short take-off (high lift) capabilities for smaller airports.

The report contains an analysis of the proposed design. Major areas of interest include aerodynamics, stability, performance, propulsion, structures, and materials. In addition, areas such as cabin layout, avionics, and production cost were considered. Figure 1 is a 3-view drawing of the proposed commuter aircraft.

#### Aerodynamics

As a starting point for analyzing the aerodynamics of the proposed aircraft, some initial sizing schemes for the wing, horizontal tail, and vertical tail surfaces had to be determined. From the derived areas of these control surfaces, the appropriate shape for the surfaces were carefully determined in order to meet structural constraints as well as maximize the possible aerodynamic gains.

Wing sizing was the first consideration, and the wing area needed was determined using an equation from *Airplane Design: Part 1 Preliminary Sizing of Airplanes*<sup>(1)</sup>. The wing area was calculated to be 867 sq ft with a wing span of 100 ft.

After the wing area was determined, the next task was to develop a wing shape that would best meet the need of the aircraft. High aspect ratio wings are beneficial in that they have low induced drag characteristics, good for single-engine climb-outs and gliding flight. However, a structural penalty must be paid for high aspect ratio wings since they are usually very long and slender. An aspect ratio of 11.53 was chosen to take advantage of the drag benefits without structural complexity. The leading edge of the wing was swept 16.11° to assist in achieving cruise Mach numbers greater than 0.6.

A natural laminar flow airfoil, model NLF(1)-0215F, was chosen for its excellent performance characteristics at the desired cruise speed of 360 knots. Laminar flow airfoils delay the transition of the flow over the wing, thus preventing the high parasite drag of turbulent flow. A good laminar flow airfoil combined with smooth fabrication methods can produce a wing with laminar flow over about 50-70% of the wing. High lift devices are necessary to achieve short take-off and landing performance. Through the use of double slotted Fowler flaps and leading edge slats, a takeoff  $C_L$  of 1.9 and a landing  $C_L$  of 2.5 can be achieved. The Fowler flaps increase the effective camber and wing area creating greater lift capability at low airspeeds. The slats, aside from extending the stall point of the wing, also create a larger wing area and camber. The double slotted Fowler Flaps are 11 ft in length and will be used in pairs on each side of the wing. When deployed, they will increase the wing area by two-thirds of the clean flap area. The slats designed for this aircraft are in two sections per wing. Each is 16.0 ft long and covers 70% of the leading edge.

The ailerons typically extend from about 50% to 90% of the wing span. For this high aspect ratio aircraft, such large ailerons are not needed, so the ailerons are 12.5 ft long and extend from 65% to 90% of the wing span.

With this wing information the horizontal and vertical tail areas can be determined by using the Tail Volume Coefficient Method<sup>(2)</sup>. Using this method the horizontal tail area was calculated to be 200 sq ft and the vertical tail area is 125 sq ft. After the tail areas have been calculated, the geometry for a T-tail can be determined, along with the rudder and stabilator size.

The geometry is a traditional T-tail geometry with the vertical tail standing 11.5 ft high and a taper ratio of 0.4. The leading edge sweep of the vertical tail is 35°. The rudder is 9.0 ft long

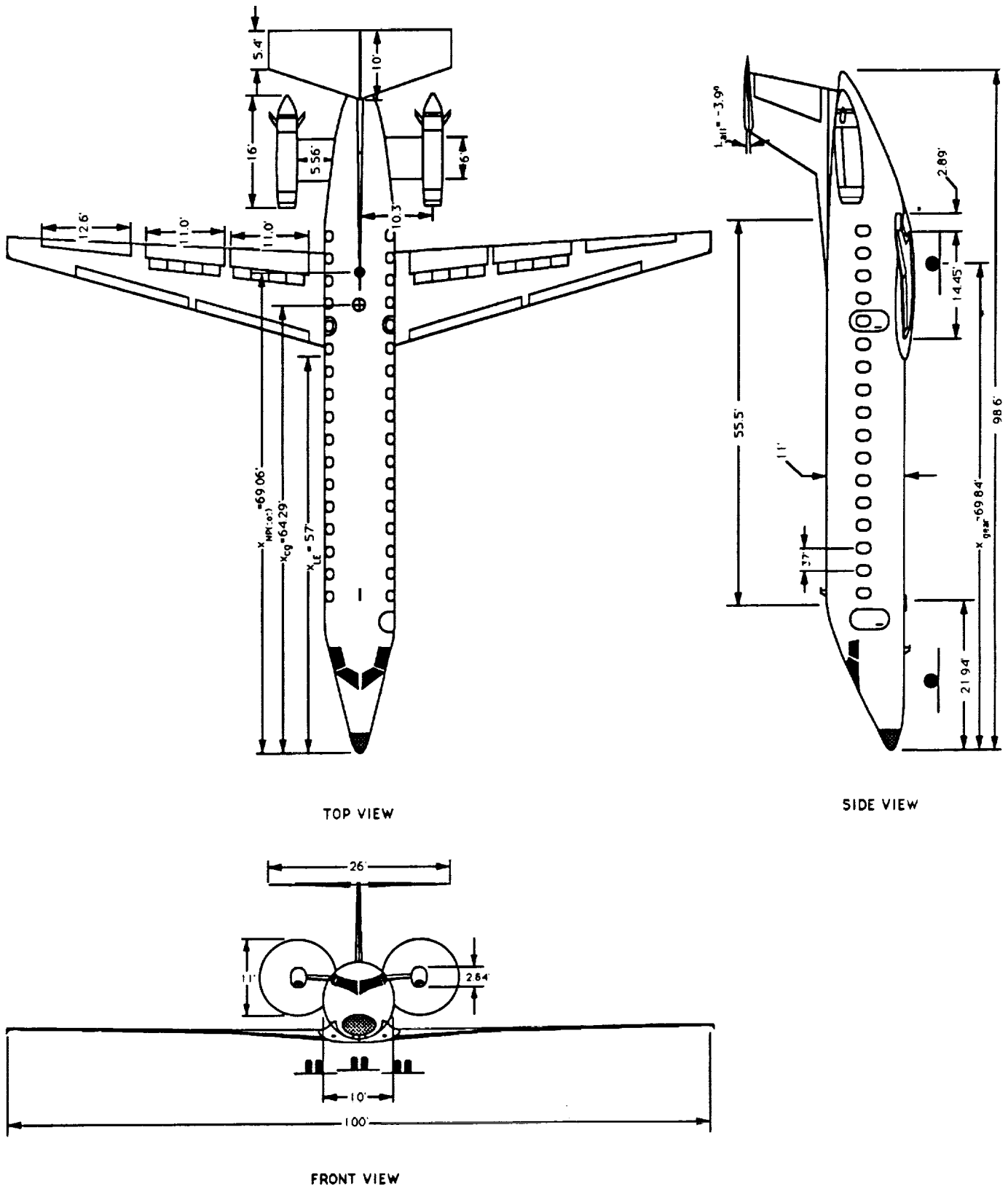


Fig. 1. 3-View drawing of Langley turboprop.

and 40% of the chord in width. The stabilator or horizontal tail has a leading edge sweep of  $22^\circ$ . This tends to make the tail stall after the wing which is an important control feature. The stabilator has a total span of 21.85 ft and a taper ratio of 0.54.

### Stability

The stability of an aircraft is essential to its operation in flight. The extent of the stability analysis done on this aircraft was limited to the static longitudinal stability, combined with some general theory considerations for the static lateral stability problem.

In order to evaluate the static longitudinal stability, it is first necessary to determine the location of both the center of gravity (c.g.) and the wing-body-tail neutral point. In finding the c.g., the location and the weight of each part of the airplane must be accounted. For the purposes of this project, approximations were made using available data in order to complete this calculation. Table 1 shows the weights and distances (measured from the tip of the nose cone) for the different aircraft parts.

From the analysis in Table 1, it can be noted that both permanent and variable-weight components are included. While the structural components will not change with various loading conditions, passenger, baggage, and fuel weights and moments will change. It is necessary to evaluate aircraft stability at many loading conditions to ensure that the plane is capable of flight regardless of the loading variables. Table 2 shows some different loading situations along with the corresponding c.g. locations, static margins, and  $C_{M\alpha}$ s. Though there are many other possible conditions, Table 2 includes the extreme conditions (i.e., worst-case loading arrangements). With the stability requirements met for these extremes, no other loading conditions will present a stability problem. For each of these conditions, the value of  $C_{M_0}$  is positive, which, combined with the negative value for  $C_{M\alpha}$ , yields a trimmable, stable aircraft.

TABLE 1. Component weights, positions, and moments for c.g. of the aircraft.

| Component                      | Weight (lb) | Position (ft) | Moments (ft <sup>3</sup> lb) |
|--------------------------------|-------------|---------------|------------------------------|
| Nose Gear                      | 217         | 11.25         | 2,441                        |
| Fuselage                       | 9,731       | 57.19         | 556,496                      |
| Engines                        | 2,678       | 87.35         | 233,923                      |
| Vertical Tail                  | 1,054       | 90.60         | 95,492                       |
| Horizontal Tail                | 1,679       | 97.43         | 163,585                      |
| "Dry" Wing                     | 4,050       | 67.60         | 273,780                      |
| Main Gear                      | 1,225       | 69.84         | 85,554                       |
| Empty Weight                   | 20,634      |               |                              |
| 51 Passengers<br>(180 lb each) | 9,180       | 49.69         | 456,154                      |
| Fuel<br>(max. loading)         | 8,800       | 67.60         | 594,880                      |
| Front Baggage                  | 1,300       | 49.20         | 63,960                       |
| Aft Baggage                    | 1,300       | 79.50         | 103,350                      |
| Misc. Weight                   | 20,580      |               |                              |
| TOGW                           | 41,214      |               |                              |

TABLE 2. Stability characteristics at various loading configurations.

| Loading Condition                                | c.g. Location | Static Margin | $C_{M\alpha}$ |
|--|---------------|---------------|---------------|
| Fully loaded (51 passengers and bags, full fuel) | 64.29         | 0.4790        | -0.0533       |
| No passenger and bags, full fuel                 | 68.16         | 0.0905        | -0.0156       |
| No passengers and bags half full                 | 68.24         | 0.0827        | -0.0148       |
| No passengers and bags, 20% fuel                 | 68.29         | 0.0769        | -0.0143       |
| Empty (no passengers and bags, no fuel)          | 68.34         | 0.0724        | -0.0138       |

With regard to the lateral stability, calculations were not performed to determine actual stability values. This is due to a lack of data required to do these calculations. However, general lateral stability theory was applied in the design of the aircraft. First, the wings were designed with approximately  $5^\circ$  of dihedral in order to establish roll stability. Many low-wing aircraft use such dihedral because of the tendency it gives the aircraft to level its wings when placed at some bank angle. This concept of roll stability applies in level flight because if a gust suddenly lifts a wing, the plane will automatically return to level flight. Next, the vertical tail and rudder were chosen to have large enough surface areas to produce any needed yawing moments necessary for side-slip or unbalanced engine thrust. The dorsal fin leading into the vertical tail not only separates the incoming flow to the tail (thus lowering the pressure drag on the tail), but more importantly also stabilizes the aircraft in a spin condition. In all, our lateral stability elements have been estimated, based on historical data, to yield our desired stability characteristics.

### Propulsion

In order to meet the goals for this design, the propulsion system must meet, and in some cases exceed, current standards in propulsion technology. These standards include such subjects as fuel efficiency, cruise speed, and interior and exterior noise levels. The propulsion system chosen for this design is the GM/Allison GMA 2100 advanced technology turboprop engine in a pusher configuration. This advanced turboprop design offers a high propulsive efficiency at a relatively high Mach number compared to both the turbofan and the conventional turboprop. The engines will be mounted on either side of the far aft portion of the fuselage below the high T-tail. This configuration will allow clean flow over the natural laminar flow wing and reduce interior noise levels.

Some of the advanced features of the GMA 2100 that make it appealing for this design are the full authority digital engine control system (FADEC), composite propellers, and a powerful and efficient engine core. The FADEC system coordinates the engine power and blade pitch and manages propeller synchronizing and synchrophasing functions through the use of a single power lever.

The Dowty Rotol blades chosen for this design are made of a polyurethane foam core sandwiched between two carbon fiber spars that run from the blade tip to the root. This assembly

is then covered with a glass fiber or a carbon/fiber/glass-fiber shell, and spray coated with a protective polyurethane. This process produces very low weight blades, which enables considerable simplification of the control system.

### Performance

To predict the performance parameters of the aircraft, we had to first estimate the drag polar using Roskam's *Methods of Estimating Drag Polars of Subsonic Aircraft*<sup>(3)</sup>. Calculations yielded the following relation.

$$C_D = 0.0183 + 0.032C_L^2$$

The next consideration was takeoff performance.  $C_{Lmax}$  at takeoff was calculated to be 1.49. This value yielded a stall speed of 96.4 knots at a density altitude of 12,000 ft. The takeoff velocity was calculated to be 99.3 knots with a total takeoff distance, of 3526.3 ft. The maximum rate of climb from this density altitude at takeoff speed was determined to be 1762.5 ft/min, and climb velocity was calculated to equal 107.9 knots.

Several quantities were necessary for calculating cruise performance. The lift coefficient of the aircraft, cruising at a velocity of 360 knots and an altitude of 25,000 ft, was determined to be 0.23, with a corresponding drag coefficient of 0.02 and a value of  $C_L/C_D$  of 11.5. These values were then used to calculate a range of 2046 n.m. The specific range was computed to be 0.233 n.m./lb of fuel.

Landing performance was evaluated according to Federal Aviation Regulations (FAR) part 25 guidelines. The velocity required to clear a 50-ft obstacle was determined to equal 107.7 knots, and the aircraft's velocity when it makes contact with the ground is 95.3 knots. The velocity of the aircraft at braking was calculated to be 80.95 knots. These velocity values were then used to determine the various forces and distances associated with landing. The total landing distance was calculated to be 3711.3 ft.

### Structures

The structural layout of the wing is one of the most crucial design considerations. A wing structure must be able to withstand loads from lift, drag, and thrust components of the aircraft, while also serving dual purposes such as a fuel and landing gear storage.

The wing design for this commuter will use spars made of high-strength composites because the wing is long, thin, and wet. A conventional front-rear spar arrangement was selected to allow the central part of the wing to transfer all loads to the fuselage. A shear-web style spar is desirable because webs will carry loads even when they are severely damaged. Cost will also be lower for a web design because it requires only a simple cutting operation. The ailerons are laid out with the leading edge parallel to the rear spar. Flaps will run the entire distance of the wing inboard of the ailerons, with the same chord-length ratio as the aileron. For rib placement, the conventional spanwise rib arrangement will be used. This arrangement is light, easily manufactured, and low in cost. The wing skin will consist of integrally stiffened panels with the

z-shape because they have been proven effective as light-weight, high-strength constructions. The fuel tanks will be a leak-proof integral design expending the fuel from inboard outward.

The point where the wings join the fuselage is a critical area as far as structures are concerned. Since the wings produce large bending moments, the structure must be designed so that these moments will pass between the wings through the fuselage. A constant-depth box will be used because of its simple geometry and the resulting low manufacturing cost. In addition, it provides a total continuity in the upper cover, and minimizes spar and rib sizes, thus lowering the weight.

Another important structural area considered is the landing gear. A tricycle arrangement with two wheels on the nose gear, and two wheels on each main gear will be used. The main gears will be stored in a joint wing/fuselage junction.

### Materials

Materials selection involves various considerations, and is often a compromise between mechanical properties and cost and manufacturing. Historically, the most important decisions are based on mechanical properties, such as strength, toughness, and corrosion resistance. Other important decisions are based upon producibility, cost, and fabrication characteristics. Aside from cost penalties, a reduction in empty weight is an excellent means of reducing lift-induced drag, and therefore fuel consumption.

Since weight is an important consideration, we plan to use as many composite and advanced metal alloys as possible. Among the advanced materials considered are carbon-fiber composites and aluminum lithium (Al-Li).

Carbon-fiber composites, such as graphite-epoxy, are the most commonly used composites because they are easily molded and have excellent strength-to-weight ratios. Carbon-fiber composites are suitable for the areas critical to the structural integrity, such as the wing carrythrough box, fuselage bulkheads, and pressure bulkheads. Also, since graphite epoxy has high corrosion resistance and durability, it may replace members that were previously made of conventional materials, such as fairings, doors, and some leading edges. Other applications for fiber composites would include glass fiber coatings on the nose cone and the fuselage rear cone.

Aluminum lithium is less dense than conventional alloys with comparable strengths, and it also has a higher stiffness, leading to further weight savings. Al-Li will be used on some leading edges, fuselage skin, skin for doors and access panels, and fuselage stringers.

### Cost Analysis

The cost of an aircraft in the design phase is extremely difficult to analyze. Cost projection to any degree of accuracy is virtually impossible due to the unpredictability of the economy from year to year. To evaluate the cost of a single airplane is relatively meaningless because total unit cost decreases with respect to production quantity; therefore, a full-scale component cost estimation based on variable production quantities was

conducted. The total production cost should range from \$6.4 million to \$5.3 million for an annual production quantity ranging from 30 to 100 units.

## THE FM-007, AN ADVANCED COMMUTER FOR HUB-TO-SPOKE TRANSPORTATION

### Introduction

The specifications for an advanced jet commuter aircraft design includes the need for a 500-n.m. range, a cruise speed of Mach 0.7, natural laminar flow wings, and 50 to 70 passenger capacity.

The need for more advanced commuter aircraft is now emerging due to the aging of current aircraft such as the DC-9 and the Boeing-737. Also the need for hub-to-spoke service is increasing because of the rapid growth of airports that are already congested. Studies show that by the year 1992, 58 major airports in the world will be in a serious state of overcongestion. To alleviate this problem, advanced technology must be applied to new commuter aircraft to shorten runway lengths, increase payload, and decrease fuel consumption.

### External Geometry

The FM-007 incorporates three external features different from conventional commuter aircraft. These are an oval fuselage, three lifting surfaces, and an upper surface blown flap. Figure 2 shows a 3-view of the proposed commuter design.

The oval fuselage was used to decrease the amount of unused space and increase passenger comfort. This shape also generates more lift than a standard circular fuselage, thus contributing to the STOL capabilities of the aircraft.

The three-lifting-surface configuration includes canards, wings, and a horizontal tail. The canards are mounted on the lower surface of the fuselage and are placed 16.9 ft from the nose of the aircraft. To decrease cabin noise from the engine exhaust, the wings are placed slightly aft of the center of gravity. A T-tail is used to decrease downwash effects created by the blown flap. These three surfaces act together to counteract nose-down pitching moments. They also help reduce drag by decreasing the total lifting surface area needed.

The airfoils selected for the lifting surfaces are chosen for their cruise lift and drag characteristics. To decrease drag, a laminar flow airfoil is used for the wing. The airfoil chosen is the HSNLF (1)-0213F, which provides a high coefficient of lift, 0.26 at 2° incidence, and drag is small at Mach 0.7. The tail sections are NACA 0012 airfoils, which were chosen because of their symmetry and because they provide a  $C_L$  of 0.2 at an incidence angle of 0.2°. The airfoil for the canard had to have a high coefficient of lift so the NACA 2412 airfoil was chosen because it provides a  $C_L$  of 0.622 at an angle of incidence equal to 3°.

To achieve STOL performance, the FM-007 incorporates an upper surface blown flap. The flap generates lift by circulating the exhaust from the two engines over the wing and deflecting it downward. The lift created is separated into three components: (1) the basic wing lift; (2) the vector component of the engine exhaust in the lift direction; and (3) the wing lift due to

supercirculation. The total lift generated can be as high as three to four times that of a conventional airfoil. This extra lift is used to decrease the takeoff and landing distances. In case of a critical engine failure the turbines of the two engines are cross-coupled to the fan of the opposite engine. This is done in order to reduce the asymmetric lift that would be generated if an engine failed, and thus allow continued safe flight at low speeds. This allows STOL performance even with an engine out. This type of powered lift was chosen for its ease of incorporation into a commuter design and for its superior decreased noise characteristics.

### Structures

Material selection was an important part of the design of FM-007. Instead of using standard aluminum alloys, aluminum alloys containing lithium have been chosen for most of the airplane. The fuselage will be composed primarily of Al 2090, an aluminum-copper-lithium-magnesium alloy. This alloy is comparable to the standard Al2024 aluminum-copper alloys used in airplanes today but has a lower density.

Also, when considering compound structures, the wings have been given special attention, since aircraft wings are usually constructed of more than one material. On the lower wing surface, the Al2090 alloy will be used because of the cyclic tension loading. One important point about these aluminum lithium alloys is that they are experimental at this time, and the life span of these materials is unknown.

The internal structure of the wings will also be made of aluminum lithium alloys. Al2090 will be the main alloy used in the spars. Al2090 is currently used in extruded leading-edge stiffeners in the wings of the Airbus A330 and A304, which are currently in production. The successful use of Al2090 in these planes proves that this material can be used in the main spar and stiffener structure of the aircraft.

The c.g. was determined by using the tip of the nose as a datum point and locating distances from the datum to the c.g. of different components of the airplane. For each component (wings, canards, tails, etc.) of the airplane, the component's c.g. was estimated by either numerical calculation or geometrical approximation. The weight of each component was also similarly determined by numerical calculation or geometrical approximation. Then a spreadsheet was employed to maximize c.g. calculations since the spreadsheet allows for alteration of airplane components and quick recalculations for determination of center of gravity.

### Avionics

The avionics of the FM-007 incorporates the latest in glass cockpit technology and some of the top-of-the-line digital avionics. The basic "T" information such as attitude, altitude, heading, airspeed, and vertical speed along with complete flight direction commands will be contained in the 8 × 8-in primary flight display (PFD). The PFD replaced each of these single instruments with one cathode ray tube (CRT), which reduces weight and also reduces the pilot's workload since several instruments do not have to be scanned at one time. These avionics are needed because of the steep takeoff and landing

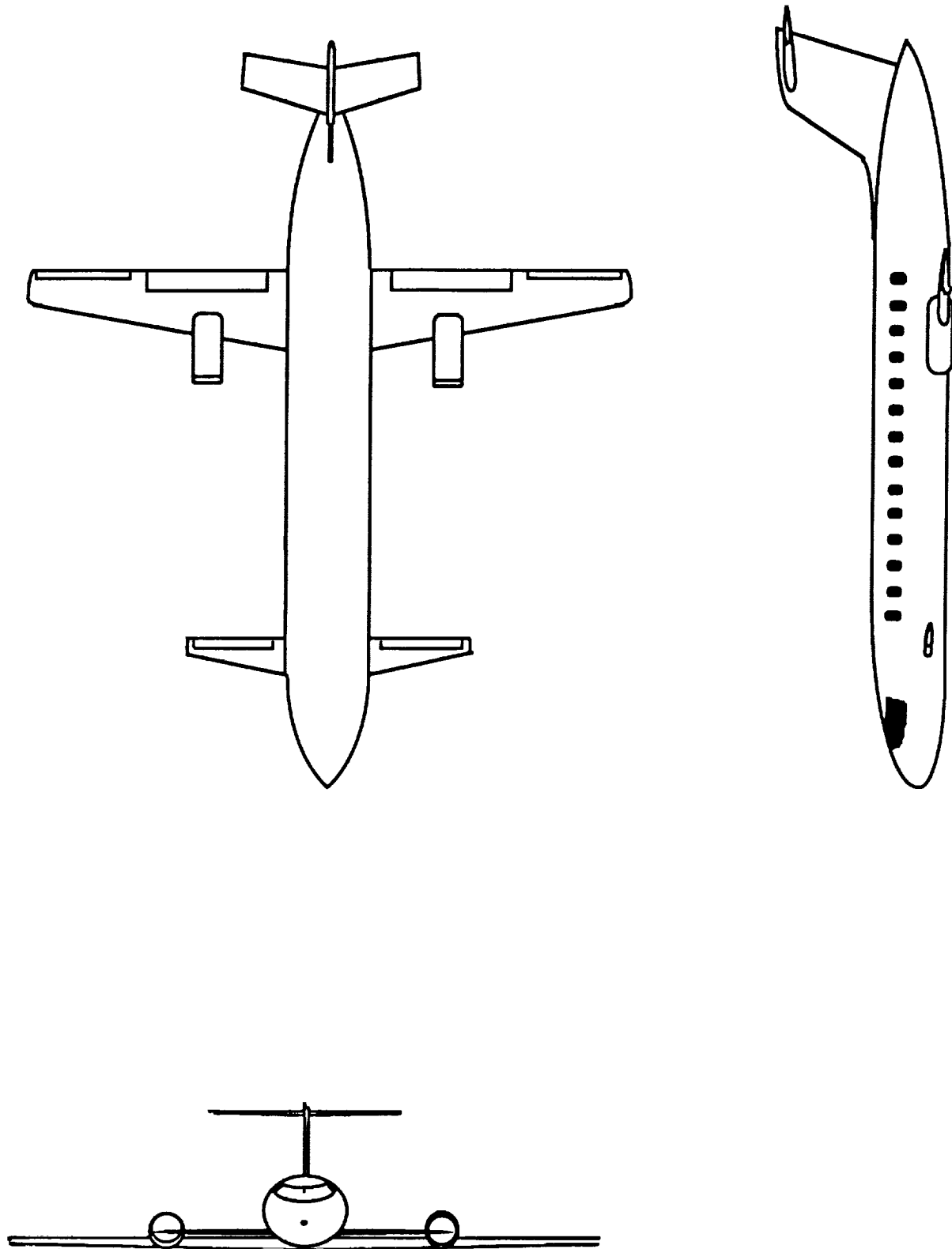


Fig. 2. 3-View drawing of FM-007.

flight path angles used by a STOL aircraft. These flight paths require increased pilot attention and any decrease in pilot workload is desirable.

### Conclusions

The FM-007 is an advanced design STOL commuter aircraft that uses the best flight technology available. Drag is reduced by using natural laminar flow airfoils, the three lifting surfaces, and the fuselage design. Thrust is used to create lift to provide the aircraft with short takeoff and landing capabilities. The TAY 620 engines are among the most fuel-efficient engines on the market, which helps to decrease the amount of fuel weight needed and thus decreases total weight. Also, the FM-007 is composed of primarily 2090-T83, a relatively low-density aluminum alloy. The landing gear is a dual-wheel tricycle design that ensures safety in the event of a flat tire, and plane stability during takeoff and landing. The avionics of the FM-007 consists of the latest in glass technology and digital instrumentation.

The aircraft's specifications and theoretically calculated data have been tabulated in Tables 3 through 6.

### REFERENCES

1. Roskam J. (1985) *Airplane Design: Part I: Preliminary Sizing of Airplanes*. Roskam Aviation and Engineering Corporation, Ottawa, KS.
2. Raymer D. P. (1989) *Aircraft Design: A Conceptual Approach*. AIAA Education Series, American Institute of Aeronautics and Astronautics, Inc., Washington, D.C.
3. Roskam J. (1971) *Methods for Estimating Drag Polars for Subsonic Aircraft*. J. Roskam, Lawrence, KS.

TABLE 3. External geometry.

|                      |            |                 |
|----------------------|------------|-----------------|
| Planform Area        | 533.3      | ft <sup>2</sup> |
| Wing Span            | 73.2       | ft              |
| Root Chord           | 10.0       | ft              |
| Tip Chord            | 4.6        | ft              |
| Sweep                | 10.0       | deg             |
| M.A.C.               | 7.28       | ft              |
| Thickness Ratio      | 0.134      | —               |
| Vertical Tail Area   | 299.4      | ft <sup>2</sup> |
| Horizontal Tail Area | 264.9      | ft <sup>2</sup> |
| Canard Area          | 84.39      | ft <sup>2</sup> |
| Fuselage Length      | 92.0       | ft              |
| Cross Sectional Area | 74.2       | ft              |
| Fuselage Dimensions  | 10.5 × 9.0 | ft              |
| Flap Area            | 191.4      | ft <sup>2</sup> |

TABLE 4. Cabin geometry.

|  |       |                 |
|--|-------|-----------------|
| Number of Seats                            | 70    | —               |
| Seat Width                                 | 17    | in              |
| Seat Height                                | 42    | in              |
| Seat Pitch                                 | 36    | in              |
| Arm Rest Right Side                        | 3     | in              |
| Arm Rest Left Side                         | 2     | in              |
| Seats Abreast                              | 5     | —               |
| Aisle Width                                | 19    | in              |
| Aisle Height                               | 82    | in              |
| Carry on Baggage Allotment (per passenger) | 3.1   | ft <sup>3</sup> |
| Wardrobe (total floor area)                | 9.56  | ft <sup>2</sup> |
| Restroom                                   | 14.5  | ft <sup>2</sup> |
| Galley                                     | 14.44 | ft <sup>2</sup> |
| Flight Attendant Seat Width                | 15    | in              |
| Door                                       | 3 × 6 | ft              |
| Cockpit Length                             | 12    | ft              |
| Luggage Volume                             | 196   | ft <sup>3</sup> |
| Compartment Hold                           | 400   | ft <sup>3</sup> |

TABLE 5. Weights and center of gravity.

|                    |        |    |
|--------------------|--------|----|
| Empty Weight       | 20572  | lb |
| Fuel Weight        | 2000   | lb |
| Max Takeoff Weight | 40000  | lb |
| Max Landing Weight | 40000  | lb |
| Forward cg         | 52     | ft |
| Aft c.g.           | 54     | ft |
| Static Margin      | 0.9417 | ft |

TABLE 6. Performance.

|                      |         |                    |
|----------------------|---------|--------------------|
| FAR Takeoff Distance | 1486    | ft                 |
| FAR Land. Distance   | 884     | ft                 |
| Cruise Velocity      | Mach .7 | —                  |
| Stall Speed          | 120     | ft/s               |
| Takeoff Thrust       | 22000   | lb                 |
| Wing Loading         | 75      | lb/ft <sup>2</sup> |
| Range                | 545     | nmi                |



this reason, the airfoils tended to experience laminar separation bubbles and compressibility effects, which must be avoided. Each group analyzed several different airfoils and modified them to best suit their needs. A computer code authored by Mark Drela called XFoil was used to modify and analyze the airfoils<sup>(5)</sup>. The code was able to tailor the pressure distribution to reduce shocks and flow separation. XFoil is prone to errors in integration. This manifests itself in excessive peaks in the pressure distribution at the leading edge and a slightly higher Mach number distribution as compared to test data for similar airfoils. However, despite these potential problems the performance characteristics of the final modification compare well with published data for similar airfoils designed for low Reynolds number flight<sup>(6)</sup>.

The airfoils were modifications of the LA203A, the Eppler 1230, and the Lissaman 7769, which were chosen by the Gryphon, the SHARP, and the HAMMER groups, respectively. Drag polars are displayed in Figs. 10 and 11. One disadvantage of the LA203A modification was an excessive pitching moment of  $-0.17/\text{radian}$ . The Gryphon group decided to compensate for the resulting trim drag by delaying the onset of separation with submerged vortex generators.

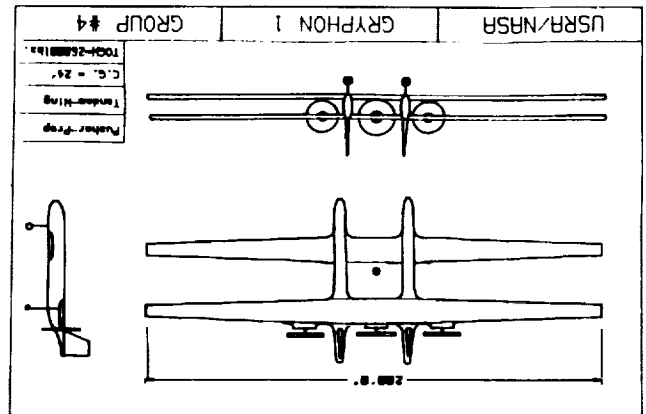


Fig. 7. Gryphon.

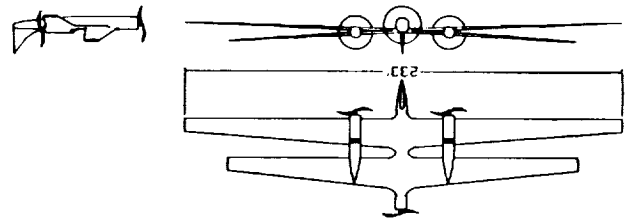


Fig. 8. HAMMER.

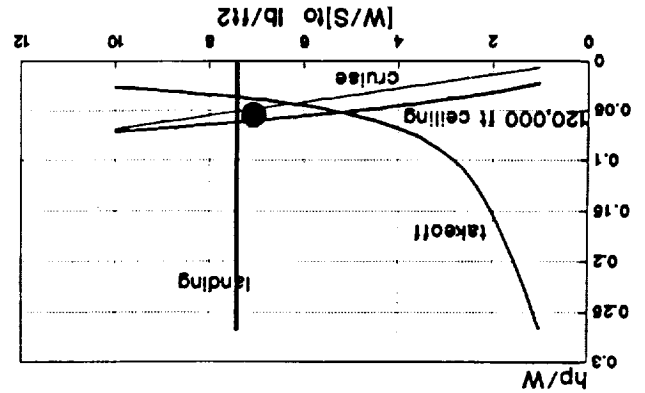


Fig. 9. Constraint diagram.

effects of Mach buffet and low-speed, low-Reynolds-number flight, a cruise Reynolds number of between 500,000 and 600,000, and a cruise Mach number of between 0.6 and 0.65 were selected by each group. The cruise Reynolds number was the design driver in the airfoil design.

### Airfoil Design

The airfoil design criteria are high lift and low drag at cruise conditions. In addition, the rarefied flow at the cruise altitude introduces low Reynolds number aerodynamic phenomena. For

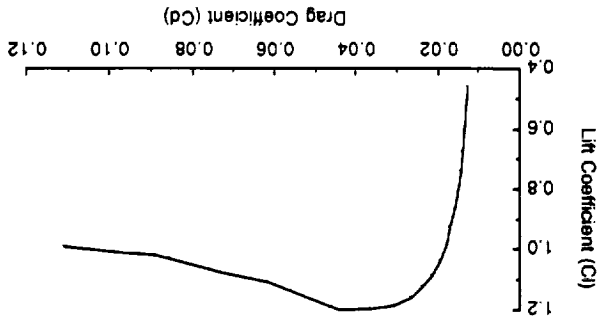


Fig. 11. Eppler 1230 drag polar.

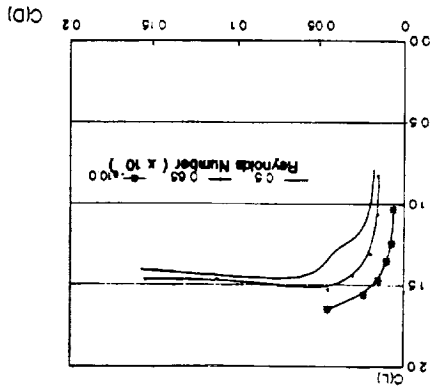


Fig. 10. LA203A drag polar.

The tandem wing, like the joined-wing and the biplane configurations, minimizes the span by using two wings instead of one. At the same time, the wing bending and structural weight are better than the monoplane configuration as shown with the Rutan *Voyager* aircraft. The resulting structural weight for the *Voyager* was 9.7% of the total weight compared to 25% for most conventional monoplane configurations. The tandem-wing configuration also provides a lower induced drag. If interference effects between the two wings are not considered, the induced drag is half that of a monoplane. Interference effects can be reduced significantly by employing a negative stagger, which places the rear wing away from the downwash of the front wing. It should be noted that the drag reduction is not always realized, as indicated from the *Voyager* data, which suggested an increase in aerodynamic drag over conventional

in the future to verify the analysis procedure. Wind tunnel testing should be done as a biplane. However, it some have referred to it as a joined-wing hybrid. However, it engines. Classifying this aircraft as a biplane is controversial; There are also reinforcing struts located under the tips are to prevent the tips from touching when the wing is further. Figure 6 shows a three-view. The struts that join the the advantages of the design, this aircraft is being considered that the strut interference may not be sufficient to undermine is interference from the wing struts. Allowing for the possibility and has good propeller clearance. Its most apparent disadvantage required may render it cost ineffective.

A twin-boom biplane is structurally sound, minimizes the span, wing aircraft is not a proven design. Therefore, the extra testing dynamic penalties by using swept wings. In addition, the joined- acrobatic efficiency and high structural strength. Unfortunately, like the flying wing, the joined wing incurs some aero- The joined-wing aircraft at first seems ideal with its high figure can be found.

A canard configuration has advantages and disadvantages similar to a flying wing. No justification for using a canard con- twin-boom fuselage, so this design was eliminated. while maintaining case of analysis. However, the structural loads hand, a twin-boom fuselage would relieve the structural loads be difficult for a single fuselage to counteract. On the other

From the sizing chart shown in Fig. 9, it is evident that in order to meet the constraints, the wing loading was limited to a range of 6 to 7 psf. In order to achieve wing loadings of this magnitude at altitude, the aerodynamic parameter  $M^2 C_L$  had to be maximized<sup>(1)</sup>. To avoid Mach buffet, the upper limit on Mach number was approximately 0.7. With the upper limit for the cruise speed known, the maximum tolerable Reynolds number per unit chord was determined. The lower limit for the Reynolds number was set at approximately 300,000, where the drag rise with increasing Reynolds number increases sharply. Even before a Reynolds number of 300,000 is reached, it is clear from Fig. 10 that a decrease in Reynolds number results in an increase in drag. In order to balance the contradicting

## AERODYNAMICS

In summary, the three designs chosen for further investigation were a biplane configuration and two tandem-wing configurations. The three projects are called SHARP, Gryphon, and HAMMER, respectively.

In summary, the three designs chosen for further investigation were a biplane configuration and two tandem-wing configurations. The three projects are called SHARP, Gryphon, and HAMMER, respectively.

Two of the non-airplane considerations for this project were balloons and sounding rockets. Balloons are currently being used with some effectiveness, but their range varies from 100 to 1000 ft. and they are not controllable. Sounding rockets have also proven effective in the past, but they too have range restrictions compounded by an endurance of only minutes. Conventional runway, balloon ascent, and towed takeoff were the three alternatives considered most feasible for an aircraft with spans in excess of 200 ft. The conventional runway proved to be the simplest alternative, requiring the least amount of ground support personnel and equipment. A balloon ascent and towed takeoff added performance to the aircraft by decreasing the amount of fuel needed at takeoff. The added performance did not outweigh the complexity as calculations progressed, so a conventional runway was used.

Several launch methods were considered. Conventional runway, balloon ascent, and towed takeoff were the three alternatives considered most feasible for an aircraft with spans in excess of 200 ft. The conventional runway proved to be the simplest alternative, requiring the least amount of ground support personnel and equipment. A balloon ascent and towed takeoff added performance to the aircraft by decreasing the amount of fuel needed at takeoff. The added performance did not outweigh the complexity as calculations progressed, so a conventional runway was used.

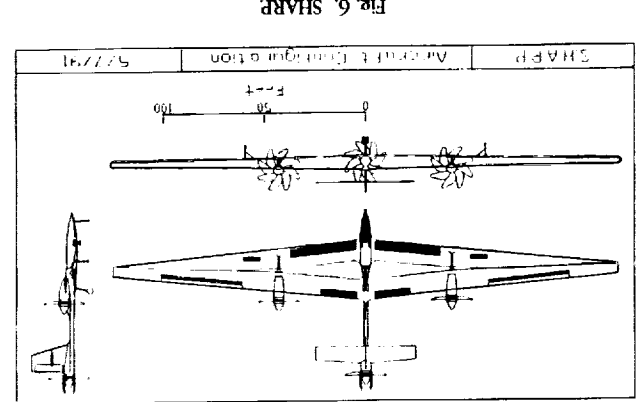


Fig. 6. SHARP

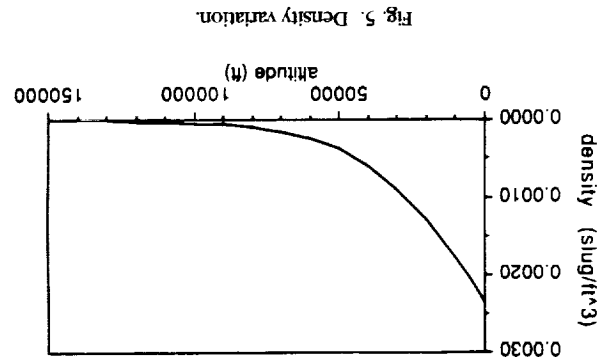


Fig. 5. Density variation.

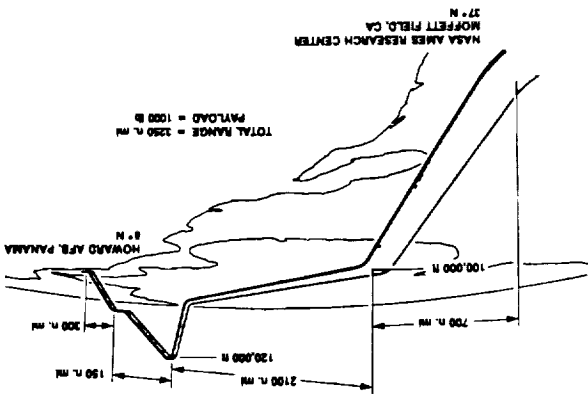


Fig. 4. NASA Ames to Panama, 3250 n.m. at 30 km (100,000 ft) with excursion to 37 km (120,000 ft).

and high-wing planform areas. Figure 5 illustrates the variation of air density with altitude. All these adverse effects become more significant with decreasing Mach number. The Mach number chosen must balance the contradictory effects of compressibility and air density. The air sampling equipment also dictates the cruise time and range. Stratospheric scientists are unable to obtain an accurate mapping of the ozone layer without extensive measurements over a large area.

The aircraft must be operational by the year 2000 in order for maximum utility from this vehicle. In mid-1993, the Cryogenic Limb Array Etalon Spectrometer (CLAES), an instrument designed to monitor the ozone layer on the Upper Atmosphere Research Satellite scheduled for launch in 1991, will cease operation. The first Earth Observing System (EOS) sensors are scheduled to become operational in 1996 at the earliest. After EOS comes online, the aircraft will be used to cross-calibrate measurements from EOS and ground-based sensing instruments<sup>(1)</sup>.

CONFIGURATIONS

Configurations for the three high-altitude research aircraft were selected according to the following criteria: (1) large wing area—minimum span, maximum aspect ratio, (2) maximum aerodynamic efficiency, (3) low wing-tip bending or twisting, (4) minimal structural weight, (5) ample ground clearance, and (6) minimum cost.

The configurations considered for these aircraft are (1) flying wing, (2) monoplane, (3) canard, (4) joined wing, (5) biplane, and (6) tandem wing.

The flying wing has a high aerodynamic efficiency because it has no horizontal tail. However, it has the disadvantage of stability problems coupled with poor takeoff rotation attributed to the lack of propeller ground clearance. The controllability of a flying wing can be increased by sweeping the wing, but this yields a decrease in laminar flow and reduced aerodynamic efficiency. These factors rendered this design undesirable. The monoplane has the advantage of being a simple, proven configuration. The disadvantage is that the large wing span required would produce excessive bending moments that would

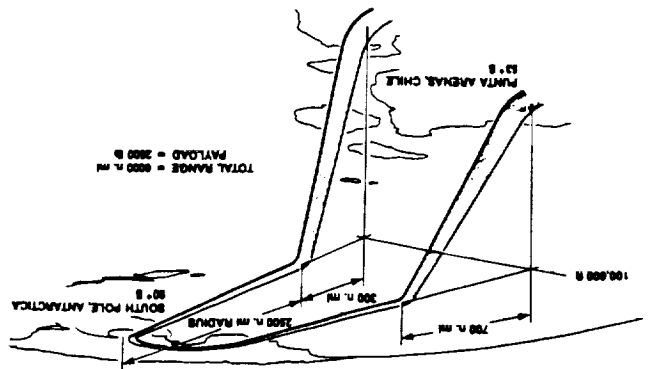


Fig. 1. Chile to South Pole to Chile, 5000 n.m. at 30 km (100,000 ft).

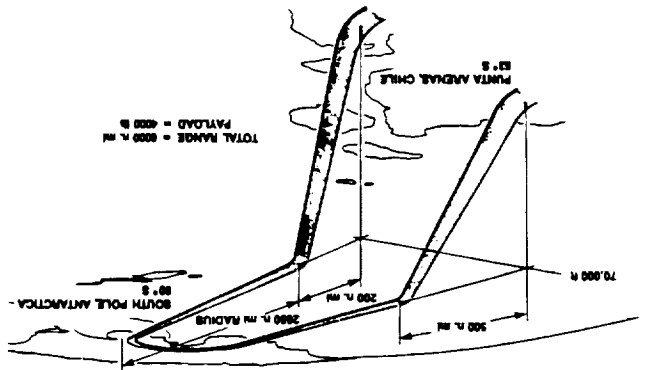


Fig. 2. Chile to South Pole to Chile, 5000 n.m. at 21 km (70,000 ft).

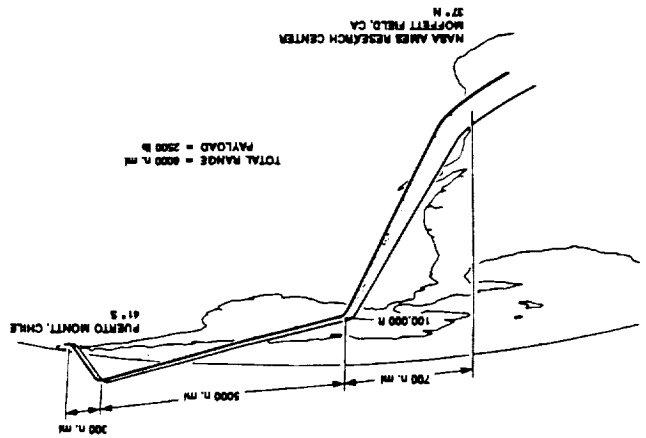


Fig. 3. NASA Ames to Chile, 5000 n.m. at 30 km (100,000 ft).

HIGH-ALTITUDE RECONNAISSANCE AIRCRAFT

CALIFORNIA STATE POLYTECHNIC UNIVERSITY, POMONA

51-05  
160577  
P-8

At the equator the ozone layer ranges from 65,000 to 130,000+ ft, which is beyond the capabilities of the ER-2. NASA's current high-altitude reconnaissance aircraft. This project is geared to designing an aircraft that can study the ozone layer. The aircraft must be able to satisfy four mission profiles. The first is a polar mission that ranges from Chile to the South Pole and back to Chile, a total range of 6000 n.m. at 100,000 ft with a 2500-lb payload. The second mission is also a polar mission with a decreased altitude and an increased payload. For the third mission, the aircraft will take off at NASA Ames, cruise at 100,000 ft, and land in Chile. The final mission requires the aircraft to make an excursion to 120,000 ft. All four missions require that a subsonic Mach number be maintained because of constraints imposed by the air sampling equipment. Three aircraft configurations have been determined to be the most suitable for meeting the requirements. The performance of each is analyzed to investigate the feasibility of the mission requirements.

INTRODUCTION

The recent discovery of the ozone hole above the North Pole has prompted the scientific community to accelerate investigations of humans' impact on the environment. The existence of the ozone hole has raised concern that the predictions of stratospheric scientists may come true. In 1974 two chemists from the University of California, F. Sherwood and M. Molina, theorized that the ozone layer was being destroyed by chlorofluorocarbons. Unless ozone depletion in the Earth's atmosphere is controlled, radiation levels at the surface may increase to harmful levels. To effectively investigate the ozone layer, NASA needs to develop a high-altitude aircraft that will reach altitudes of 130,000+ ft. To hasten development of the technology and methodology required to design an aircraft that can reach these altitudes, the NASA/USRA program has been working closely with industry and universities. With the data retrieved from this aircraft, scientists and politicians perhaps will be able to formulate an emissions control plan that will diminish the rate of degeneration of the ozone layer.

DESIGN SPECIFICATIONS

The objective is to develop three possible designs for an aircraft that can cruise at 100,000 ft and sample the ozone layer at this altitude. Ideally, the scientific community would like the aircraft to meet the four mission profiles depicted in Figs. 1-4<sup>(1)</sup>. The requirements and constraints are listed as follows:

1. The aircraft must fly subsonically at all stages of the mission. If the aircraft is manned, it must have redundant life-support systems and be pilot friendly. If an unmanned mission is chosen, proof that it is a better alternative must be provided.
3. The crosswind capability must be a minimum of 15 knots with moderate to severe turbulence.
4. Spoilers or alternative lift dump devices are to be provided for low wing loading landing.
5. For safety and flexibility, two engines are a minimum.
6. The hangar is 110 x 70 ft.
7. The aircraft enters production before the year 2000.

These specifications meet most of the demands of the stratospheric scientists. The results of previous studies have shown that flight at 100,000 ft with a range of 3250 n.m. is possible<sup>(2)</sup>. Unfortunately, the current ER-2 missions at altitudes of 60,000 to 70,000 ft do not give an accurate estimate of the chemical activity within the ozone layer at the equator. The ozone layer at the tropics is within the range of 65,000 to 130,000+ ft, as opposed to 50,000 to 100,000 ft at the mid-latitudes and 35,000 to 95,000 ft at the poles. This fact, coupled with an airplane's ability to follow an experimenter-chosen path, makes an airplane meeting the above specifications an ideal ozone testing platform<sup>(1)</sup>.

Some of the constraints are imposed by the sampling equipment, which is a modification of that in current use on the ER-2<sup>(3)</sup>. Increase in air temperature and the dissociation of flow cause problems with air sampling as compressibility effects become significant; therefore, the Mach number must be below the transonic regime. At the same time, low air density (0.00003211 slugs/ft<sup>3</sup>) at altitude implies low wing loadings available through the USRA program.

DESIGN PROCESS

The 1990-1991 school year was the third in a three-year ongoing project on a high-altitude reconnaissance aircraft. The assignment project on the beginning of each year is to perform a preliminary design analysis to determine the aircraft that best fits the requirements. If such an aircraft is not deemed feasible, the aircraft must still be designed, with those requirements that are not approachable indicated in the concluding comments. Suggestions for making the Request for Proposal feasible are also requested. During the fall quarter, three groups were formed. Each group investigated design drivers for the aircraft and did preliminary research for configuration, propulsion system, and airfoil selection. The groups reconvened during the winter quarter to commence their design. The final design iteration was completed, and the final report was compiled in the spring quarter. These were assembled into three volumes and made available through the USRA program.

**Propeller Design**

There were two main criteria for designing the propellers. The first and foremost was that the tip velocities cannot exceed the drag divergence Mach number. Since the air density is so low, the propellers lose their ability to transfer power at higher altitudes. This results in an increased diameter and RPM. For a conventional propeller configuration the necessary diameters are on the order of 25 to 35 ft. If a propfan propeller configuration is used, employing a blade sweep of 38°, the propeller diameters range from 16 to 20 ft with an increase in cruise efficiency of 3%.

All three groups opted for a pusher configuration to minimize flow disturbance over the wing. The disadvantage to a pusher configuration is that each time a blade passes through the wake of the wing it experiences a different loading than the freestream condition, which results in blade fatigue. This problem was eliminated by constructing the blades from composite materials. The SHARP group chose to fold the rearmost propeller on takeoff to increase ground clearance. The propeller will open during flight as a result of the centrifugal force produced by the engine rotation.

**Performance**

With low wing loadings, takeoff is not a problem. The takeoff distances were on the order of 1300 ft, and high lift devices in the form of flaps and slats were generally considered unnecessary. During landing, spoilers and other lift dump devices were employed. The landing distance for the SHARP project was 3537 ft. It should be noted that the SHARP's rearmost engine will be shut down for takeoff and landing. Because of this, the Gryphon and H.A.M.M.E.R. configurations take off and land in less than 75% of the SHARP value.

Using energy-state approximation methods, a minimum fuel-to-climb trajectory was found to minimize the weight of the aircraft without significantly increasing the time to climb. An ideal fuel-to-climb curve results in the aircraft climbing at stall speed, so the climb profile was designed to have a 10% margin over stall speed. The fuel consumed to reach 100,000 ft was 1200 lb. The climb velocity profile is shown in Fig. 12.

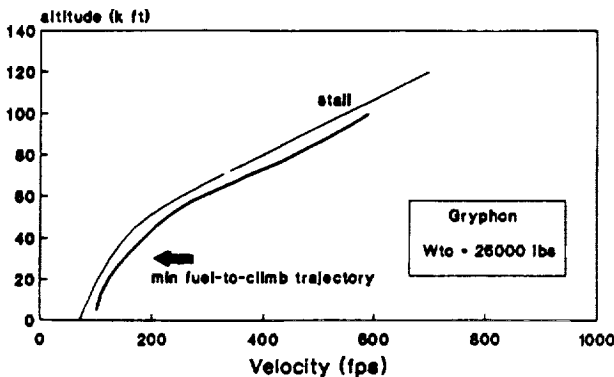


Fig. 12. Climb velocity profile.

The flight envelope for all three aircraft is similar. The aircraft are constrained by the stall velocity at lower speeds and by maximum power at higher speeds. Typically, high-altitude aircraft have a very narrow flight envelope. These three designs are no exception, as shown in Fig. 13.

Figure 14 shows the variation of the power required as fuel is consumed for the cruise condition. It is clear that the aircraft is flying within its power requirements at all times.

**PROPULSION SYSTEM**

The powerplant for this aircraft must be able to operate with a low specific air consumption. The 6000-mile range requirement necessitates that the powerplant have a low specific fuel consumption. Since the aircraft operates at subsonic velocities and very high altitudes, the aircraft's wings are large and heavy. This requires an engine that is capable of producing large amounts of power at altitude. The final requirements are to keep the engine and its systems as light as possible and to develop this system with current technology.

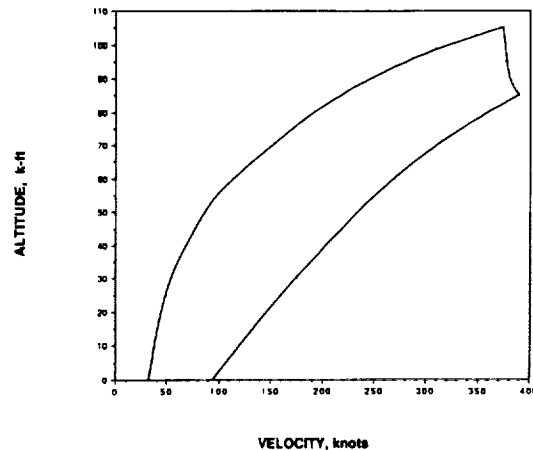


Fig. 13. Flight envelope.

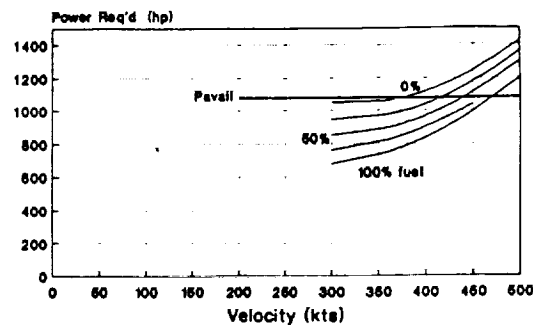


Fig. 14. Variation of power required.

**Powerplant Selection**

The driving constraint for engine selection is air consumption at altitude. The air consumption must be low for the engine to produce power at altitude. Figure 15 shows typical specific air consumption values for the engines examined. The second constraint is propulsion system weight, which must be kept as low as possible. Figures 16 and 17 show typical specific fuel consumption and specific weight values for the engines examined.

The subsonic cruise velocity combined with the high specific air consumption of turbojet and turbofan engines make it impossible for them to produce any meaningful thrust at altitude. Turboprops follow the same trend as the turbojet, producing little power at altitude. The hydrazine engine is also an unlikely candidate since it has an extremely high specific fuel consumption and is extremely toxic.

Internal combustion engines have a relatively low specific air and fuel consumption. Nonetheless, they are unable to produce enough power at altitude without some type of turbocharging. The Lockheed HAARP Project designed a turbocharg-

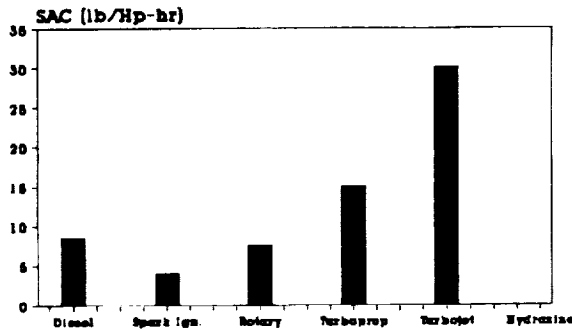


Fig. 15. Specific air consumption.

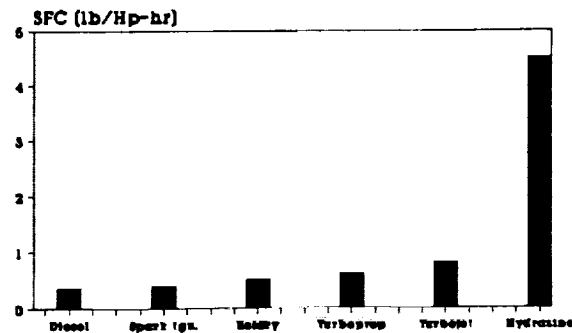


Fig. 16. Specific fuel consumption.

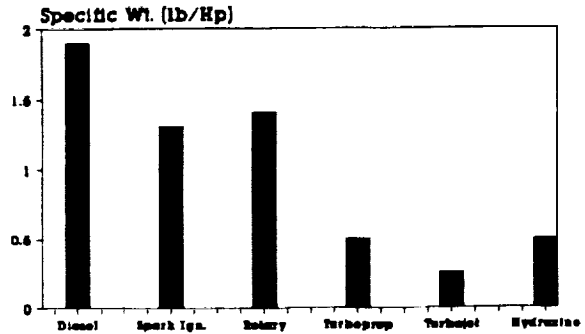


Fig. 17. Specific weight.

ing system to operate with an internal combustion engine at an altitude of 100,000 ft. Of the three internal combustion engines examined, diesel, rotary, and spark ignition, the spark ignition engine had the best mix of specific air consumption, specific fuel consumption, and specific weight.

Other engine technologies such as microwave propulsion, laser propulsion, nuclear propulsion, and electrical propulsion were examined. Practical versions of these engines are not feasible with present-day technology; therefore, there is no merit in further investigation. Thus, the spark ignition engine was selected as the best choice for the high-altitude propulsion system.

**Engine Configuration**

The Teledyne Continental GTSIOL 550 engine with three stages of turbocharging now in the preliminary design stages was chosen for this project. At altitude, the engine produces 400 hp with a specific fuel consumption of 0.45 lb/hp/hr. The overall dimensions are 33.5 inches high by 42.5 inches wide by 42.64 inches long. The total weight with the turbocharged system is 1900 lb<sup>(7)</sup>.

**Engine Cooling**

Cooling the engine at altitudes above 80,000 ft is a design challenge because of the low air density. The cooling techniques investigated are (1) using the fuel as a coolant with the wings acting as radiators; (2) liquid cooling with conventional radiators; (3) using oil coolant radiators; (4) use the fuel tanks as heat sinks; and (5) recycling heat in a steam turbine. In reality, none of these techniques were able to reject enough heat and still maintain a reasonable volume. A combination of two or more of the techniques is necessary.

**WEIGHTS AND STRUCTURES**

A typical weight breakdown is shown in Fig. 18. The takeoff gross weight varied from 25,000 lb to 30,000 lb depending on the mission and configuration. The aircraft structural analysis was constrained by the gust loading as shown in Fig. 19. Typical wing deflections are shown in Fig. 20.

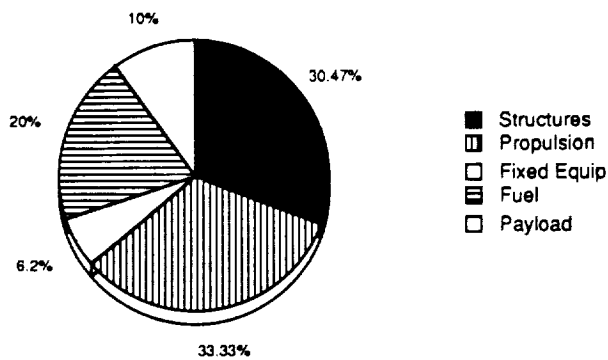


Fig. 18. Weight breakdown at takeoff = 30,000 lb.

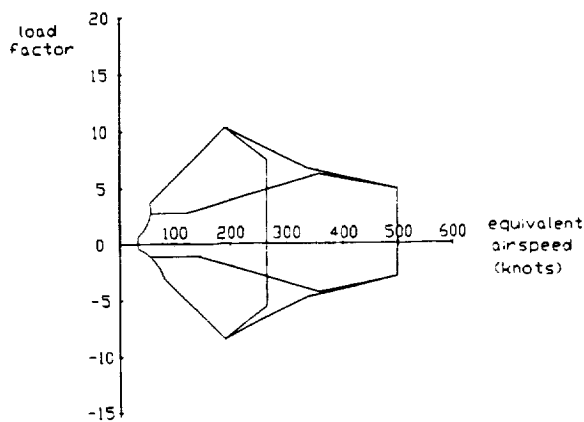


Fig. 19. Combined V-n diagram.

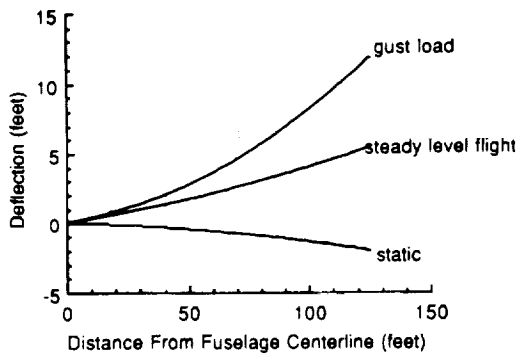


Fig. 20. Wing deflections.

**Material Selection**

To meet the wing loading requirements dictated earlier and still maintain the necessary strength, the wings were designed with composite materials and averaged a wing weight per unit

area of 1.2 lb/ft<sup>2</sup>. This is an attainable goal since both the *Daedulus* and the *Voyager* aircraft had lower wing weight per unit area. The material selection criteria are (1) high strength, (2) corrosion resistance, and (3) low density. Some of the materials considered and their properties are listed in Table 1.

TABLE 1. Material Properties Comparison.

| Material | Young's Modulus (psi) | Tensile Strength (psi) | Density (lb/in <sup>3</sup> ) |
|----------|-----------------------|------------------------|-------------------------------|
| Steel    | 30(10) <sup>6</sup>   | 110(10) <sup>3</sup>   | 0.278                         |
| Aluminum | 10(10) <sup>6</sup>   | 61(10) <sup>3</sup>    | 0.101                         |
| Titanium | 16(10) <sup>6</sup>   | 141(10) <sup>3</sup>   | 0.160                         |
| Gr/PAI   | 10(10) <sup>6</sup>   | .                      | 0.056                         |
| Gr/epoxy | 8.0(10) <sup>6</sup>  | 70(10) <sup>3</sup>    | 0.053                         |
| B/epoxy  | 9.6(10) <sup>6</sup>  | 85(10) <sup>3</sup>    | 0.068                         |
| Kevlar   | 18(10) <sup>6</sup>   | 525(10) <sup>3</sup>   | 0.052                         |
| Spectra  | 25(10) <sup>6</sup>   | 435(10) <sup>3</sup>   | 0.035                         |

\* Compressive strength = 95(10)<sup>3</sup>

Kevlar has the highest strength, but Spectra has the highest strength-to-weight ratio. Graphite Polyamide-imide acts best in compression. On the other hand, Graphite/Epoxy costs less than all three. H.A.M.M.E.R. was primarily designed with Graphite/Epoxy. Gryphon chose a combination of Graphite/Epoxy and Graphite Polyamide-imide, and SHARP chose Kevlar and Spectra 1000. Manufacturing with Spectra 1000 will prove to be expensive since it has not been used extensively.

**MANNED VS. UNMANNED**

Manned flight would be preferred by the stratospheric scientists since the pilot could monitor the aircraft rather than relying on data links for every desired action. Also, many countries may not allow an unmanned aircraft of this magnitude within their airspace. To put a man in the cockpit greatly increases the cost, complexity, and weight of the aircraft. The longer missions are on the order of 18 hours. It may not be reasonable to expect a pilot to remain in a space suit under cramped conditions for such a long period of time. For these reasons, all three projects chose to design an unmanned aircraft with an optional manned module that could be used for shorter flights and flights over populated areas.

**COST**

The total life cycle cost for these aircraft is \$181 million. This number includes RDT&E, acquisition, operations, and disposal. Figure 21 shows the percent breakdown of life cycle cost. If two aircraft are built, each aircraft will cost \$89.4 million over the course of its life. From the figure, it is apparent that the highest percentage of cost is attributed to RDT&E. The only way this number can be reduced is to postpone building this aircraft.

These figures were checked using a program produced by David Hall Consulting, under contract with NASA<sup>(8)</sup>. The results indicated a RDT&E cost of \$191 million and an acquisition cost of \$51 million.

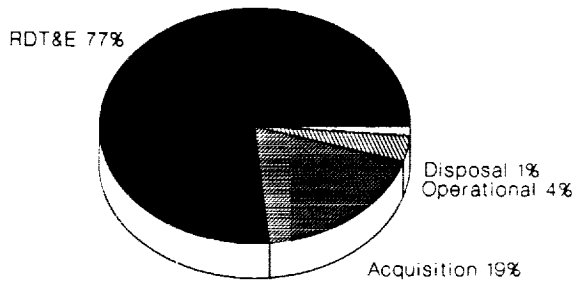


Fig. 21. Life cycle costs.

### SUMMARY OF RESULTS

Table 2 contains a selective summary of the results obtained for each of the three configurations.

TABLE 2. Summary of Results

|                                  | Gryphon | SHARP | H.A.M.M.E.R. |
|----------------------------------|---------|-------|--------------|
| Span - fore                      | 202     | 250   | 186          |
| (ft) - aft                       | 202     | 250   | 233          |
| MAC - fore                       | 8.4     | 8.4   | 12.4         |
| (ft) - aft                       | 8.4     | 8.4   | 11.6         |
| Aspect Ratio - fore              | 14      | 31.25 | 15.1         |
| - aft                            | (eff)   | 31.25 | 20.1         |
| Wing Area (ft <sup>2</sup> )     | 3400    | 4000  | 5000         |
| Empty Weight (lb)                | 17200   | 21000 | 16800        |
| C.g. at take-off (ft)            | 25.7    | 28.3  | 34.2         |
| Gross Take-off Weight (lb)       | 26000   | 30000 | 26000        |
| Time to Climb (hrs) <sup>†</sup> | 1.7     | 4.1   | 2.5          |

\* measured from nose

<sup>†</sup> mission one

1. All the design requirements were met except for the excursion to 120,000 ft in the fourth mission. Since the absolute ceilings of these aircraft were between 110,000 and 115,000 ft, it was determined that it would be unreasonable to expect a first-generation aircraft to zoom to altitudes of 120,000 ft. Perhaps after sufficient flight testing, a rocket-assisted zoom could be achieved.

2. The hangar requirements could be met by folding or removing the wings. A study should be done to determine if it would be cheaper over the life of the aircraft to build new hangars for housing.

3. Wind tunnel testing must be done on all three configurations. Interference effects caused by joining the wings at the tips for the SHARP configuration are still uncertain. The H.A.M.M.E.R. and Gryphon configurations positioned their wings for minimum drag. With wind tunnel testing, it can be determined if the drag is less than that for a conventional monoplane.

4. The exact combination of cooling methods to achieve the desired heat rejection deserves further research.

5. With RDT&E costs on the order of 140 to 190 million dollars it is difficult to determine who could finance this aircraft.

6. A high-altitude, ozone sampling platform configured with one or more three-stage turbocharged internal combustion engines is feasible.

### ACKNOWLEDGMENTS

The author, Renee Anna Yazdi, thanks Anne Nunes, Jose Rivera, Craig Burton, Susan Lee, Cara Zylla, and Darren Hayashi, the group leaders. She would also like to acknowledge the hard work of the individual team members. Our NASA sponsor Mark Moore did much to keep us on track. Many others at NASA gave their time and energy to assist us. The USRA staff gave us the opportunity to participate in the program and then taught us how to make the most of the opportunity. The Lockheed Corporation, Teledyne-Continental Motors, and Hughes Aircraft provided us with insight into the problem from industry's standpoint. Finally, the author would like to credit Professor P. A. Lord, the instructor in charge of aircraft design at California State Polytechnic University, Pomona.

### REFERENCES

1. "Global Stratospheric Change," NASA Conference Publication 10041, July 15-16, 1989.
2. "High Altitude Atmospheric Research Platform, Information Package," The Lockheed Corporation, Burbank, California, February 1990.
3. Memorandum dated July 13, 1988- To: Distribution, From: SSG/Chief, Atmospheric Experiments Branch, Subject: Very-High-Altitude Platform Aircraft Exploratory Studies, Reply to Attn of: SSG:245-5/136.
4. Cambers, Alan and Reed, Dale, "A Very High Altitude Aircraft For Global Climate Research," Unmanned Systems, Summer 1990, pgs. 14-19.
5. Drela, Mark, XFOIL software, MIT.
6. Miley, S. J., "A Catalog of Low Reynolds Number Airfoil Data for Wind Turbine Applications," Rockwell International Corporation, Subcontractor No. PFY12781-W, February 1982.
7. Benway, Ralph, Teledyne Continental Motors Corporation Information Package, October 1990.
8. David Hall Consulting contracting to CODE FAS, NASA/Ames Research Center, N.A.S. Moffett Field, CA 94035.

## PROJECT SUMMARY

## CALIFORNIA POLYTECHNIC STATE UNIVERSITY, SAN LUIS OBISPO

S2-05  
160578  
P. 10

California Polytechnic State University's design project for the 1990/91 school year was the design of a close air support aircraft. There were eight design groups that participated and were given requests for proposals. These proposals contained mission specifications, particular performance and payload requirements, as well as the main design drivers.

The mission specifications called for a single pilot weighing 225 lb with equipment. The design mission profile consisted of the following:

1. Warm-up, taxi, take off and accelerate to cruise speed.
2. Dash at sea level at 500 knots to a point 250 nmi from take off.
3. Combat phase, requiring two combat passes at 450 knots that each consist of a 360° turn and an energy increase of 4000 ft. At each pass, half of air-to-surface ordnance is released.
4. Dash at sea level at 500 knots 250 nmi back to base.
5. Land with 20 min of reserve fuel.

The request for proposal also specified the following performance requirements with 50% internal fuel and standard stores:

1. The aircraft must be able to accelerate from Mach .3 to .5 at sea level in less than 20 sec.
2. Required turn rates are 4.5 sustained g at 450 knots at sea level. A 6.0 instantaneous turn rate was also required at the same conditions.
3. The aircraft must have a reattack time of 25 sec or less. React time was defined as the time between the first and second weapon drops.
4. The aircraft is allowed a maximum take off and landing ground roll of 2000 ft.

The payload requirements were 20 Mk 82 general-purpose free-fall bombs and racks; 1 GAU-8A 30-mm cannon with 1350 rounds; and 2 AIM-9L Sidewinder missiles and racks.

The main design drivers expressed in the request for proposal were that the aircraft should be survivable and maintainable. It must be able to operate in remote areas with little or no maintenance. Simplicity was considered the most important factor in achieving the former goal. In addition, the aircraft must be low cost both in acquisition and operation.

The following are the summary of the aircraft configurations developed by the eight groups.

## THE SNODOG

With the design mission profiles and objectives discussed above in mind, we would like to present the future of close air support: the SnoDog. Configuration results are summarized in Fig. 1. This highly maneuverable aircraft has a low-aspect-

ratio, 20° aft swept wing incorporating a supercritical airfoil for low weight and larger fuel volume. The SnoDog has twin low-bypass turbofan engines, twin booms, two canted vertical stabilizers, a high cross-mounted horizontal stabilizer, and minimal avionics. The cost per aircraft is \$14.8 million.

For the SnoDog, a low, conventional wing with a supercritical airfoil was chosen. The placement of the wing was made to facilitate ordnance accessibility, to enhance maintainability, and to reduce the length of the landing gear struts. Structurally, a low wing allowed for spar carry-through to occur with minimal internal interference. In addition, the wing spars are used to help support the engines. Although visibility is not as good as with a high wing position, the SnoDog's wing is placed as far aft as possible to maximize visibility. An aspect ratio of 6 was selected as a compromise between the better aerodynamic performance of a high-aspect-ratio wing and the low cost, simplicity, and desirable ride qualities of a low-aspect-ratio wing. The wing is swept aft 20° to increase the critical Mach number. This also allowed the wing to be thicker, thus reducing the wing weight and creating ample space to store most of the SnoDog's fuel.

The cockpit and engines for the SnoDog are contained in a conventional fuselage. The empennage, however, is supported by twin booms. This configuration was selected for several reasons. A conventional fuselage was needed to provide the internal area necessary for the pilot, internal systems, and cannon. Twin booms, however, are lighter structurally than a conventional fuselage (although a slight drag penalty is paid). Having twin booms allowed complete separation of the redundant control systems, a survivability feature. Finally, engine accessibility is greatly enhanced. The engines can be pulled straight out of the back without any empennage interference.

For the SnoDog, two vertical stabilizers were used, canted inward 12°, coupled with a high cross-mounted horizontal stabilizer. The location of the horizontal tail was selected to keep it out of the hot jet exhaust, to keep it in the freestream flow at high angles of attack, and to facilitate engine removal. The twin vertical tails are a survivability feature: the SnoDog can fly with one stabilizer severely damaged.

The SnoDog's twin low-bypass turbofan engines are located above the wing and to the rear of the fuselage. Each engine has its own inlet located above the wing and surrounding the fuselage. This inlet placement minimizes foreign object damage (FOD) and reduces the amount of cannon exhaust gases ingested. Two engines were selected to increase survivability (the SnoDog is capable of flying with one engine out) and to achieve the thrust needed with minimum engine size. The engines are placed close together to minimize the differential

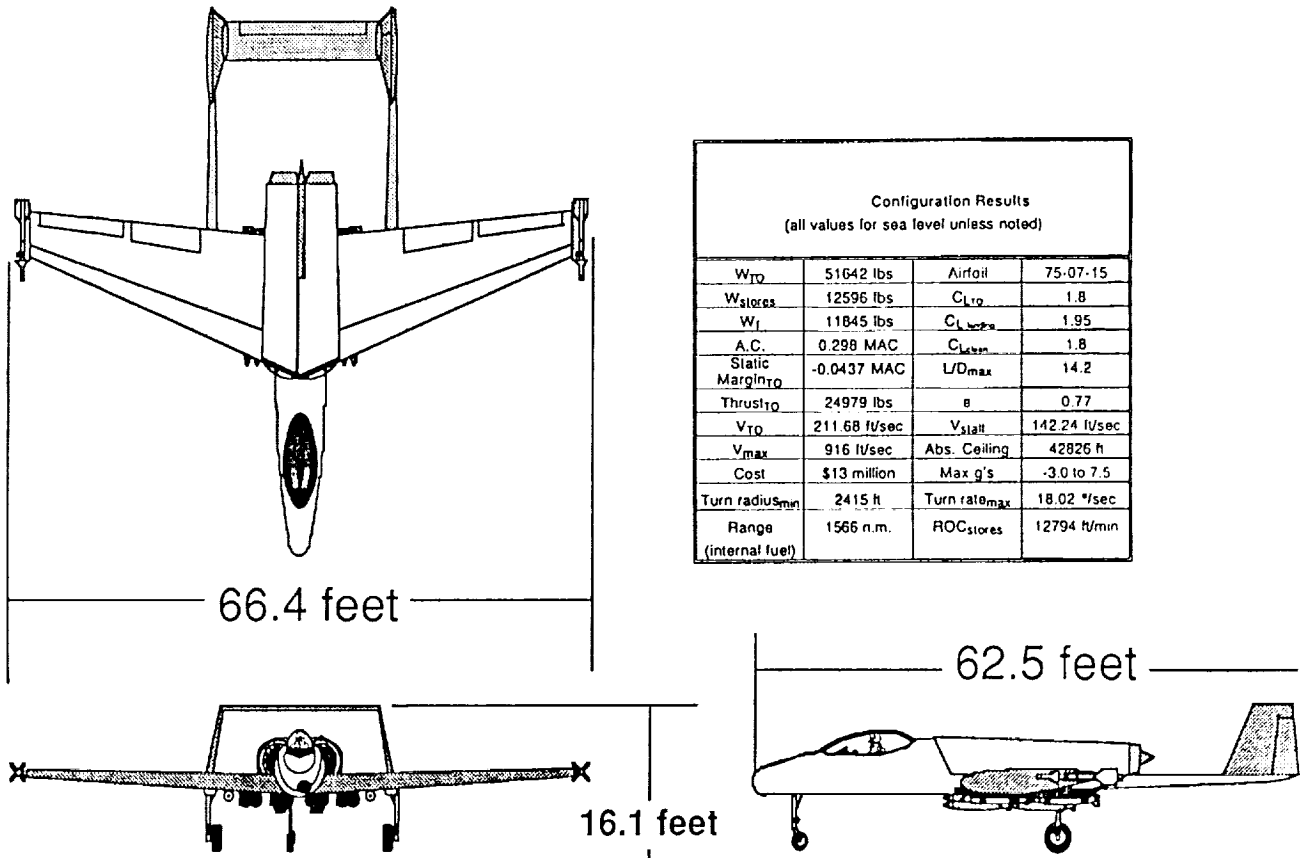


Fig. 1. SnoDog.

thrust in an engine-out situation, and are separated by a Kevlar shield to help contain a catastrophic engine failure.

Design analysis indicates that the SnoDog meets or exceeds all mission requirements. The primary design driver for the SnoDog, simplicity, has resulted in a highly maneuverable, highly survivable, low-cost aircraft. Two advanced design concepts were used. First, the inherent instability of the aircraft necessitates a fly-by-wire system. Secondly, the SnoDog employs a supercritical airfoil. The SnoDog uses proven combat avionics, balancing mission needs and low cost. Finally, the SnoDog uses conventional structural technology, and uses practically no composites to increase maintainability.

#### THE GUARDIAN

The close air support role is a highly specialized role for an aircraft to perform. The plane must be more maneuverable, more survivable, and more easily maintainable than other fighter aircraft. The Guardian was designed with the intention of meeting all these CAS requirements using innovative methods.

The first aspect one would notice in observing the aircraft is its unique configuration, Fig. 2. The configuration layout was designed with survivability and maintainability in mind. The rear

wing/forward canard placement gives the pilot better visibility of the ground, as well as increased maneuverability over conventional designs. The canard-wing configuration makes the Guardian more maneuverable and hence more survivable. The canard serves a multipurpose role of providing horizontal attitude control, gun exhaust control, and wing stall prevention. Stall prevention is critical in close air support operations where the plane is operating close to the ground. The other advantage of a canard as opposed to an elevator is that it is a lifting surface, much like the wing. The canard was placed low in order to keep canard downwash from interfering with the engine inlets as much as possible.

The engines are rear mounted above the wing. The wings themselves provide the engines with protection from ground fire. Engines were placed far enough forward on the top of the wing so as to mask most of the exhaust infrared signature from enemy heat-seeking weapons below. The engine nacelles were not completely buried in the fuselage in order to provide easier access to the engine compartment for maintenance in front-line operations. The twin vertical tails are designed for redundancy as well as additional protection for the engines against weapons fire, and as a heat signature mask.

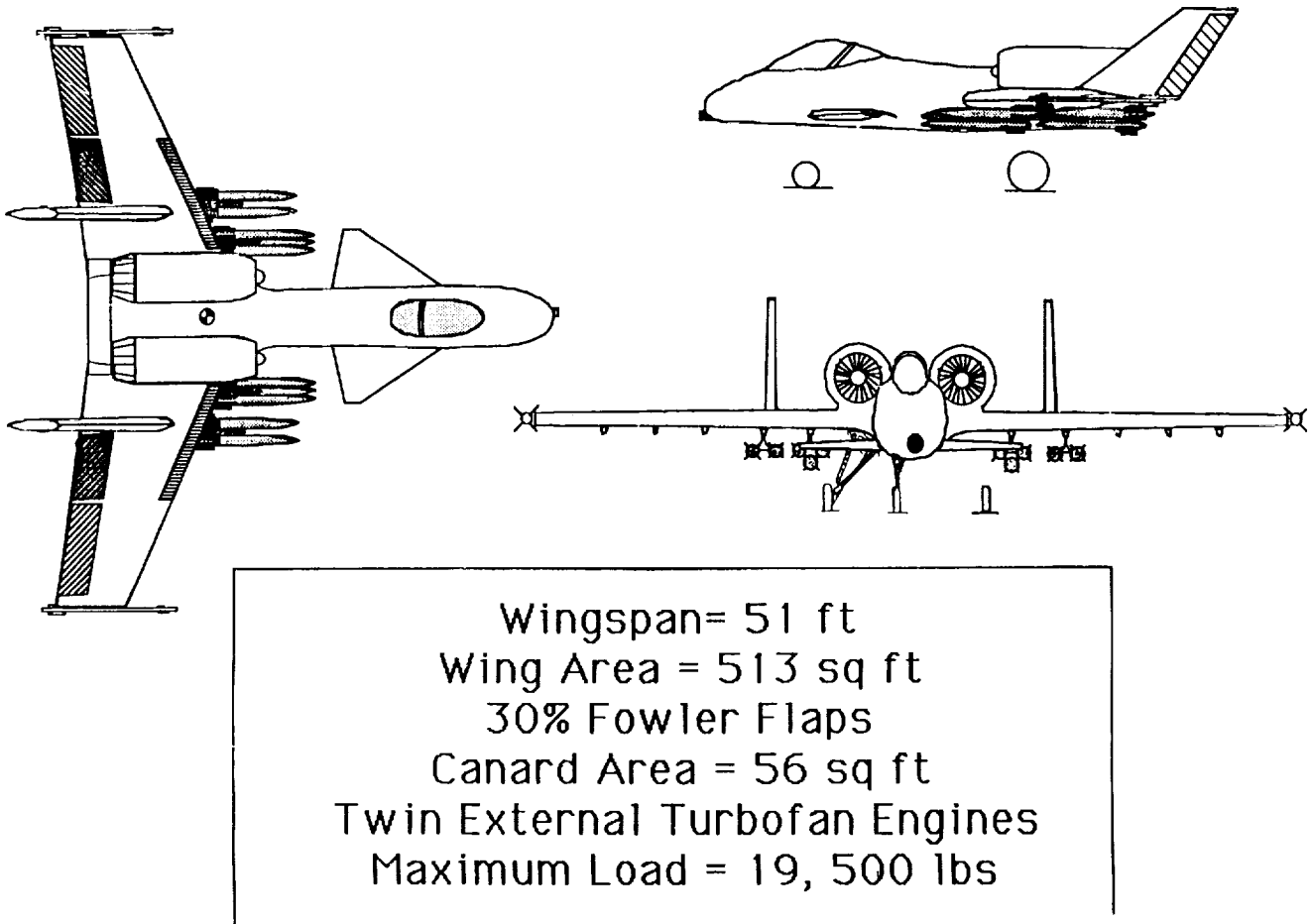


Fig. 2. Guardian CAS.

The propulsion system was designed with simplicity and cost efficiency in mind. The Guardian is one of the two California Polytechnic designs not to use afterburning engines. It was decided not to employ augmented engines in the final design. Although augmented engines provide the advantage of smaller size and weight for the same thrust-to-weight ratio, the fuel consumption was considered unreasonable. The design requirements specified the aircraft to have a 500-n.m. attack radius at an attack speed of 500 knots, about Mach 0.76. An engine that must dash at augmented power settings would require far more fuel to meet the range requirements. Thus, a low-bypass-ratio turbofan engine was selected.

The Guardian's onboard systems were designed to help reduce the pilot's workload as much as possible, as well as keep it up to date in the high-tech environment of the future. The systems include a fly-by-wire flight control system with electrically controlled hydrostatic actuators, using HOTAS flight control, LANTIRN targeting and navigation system, onboard electronic counter measures, a passive radar warning receiver, and a full complement of communications.

Ground support requirements were kept to a minimum. By implementing a fly-by-wire flight control system, a hydraulic charging system is not needed on the ground. Since the aircraft

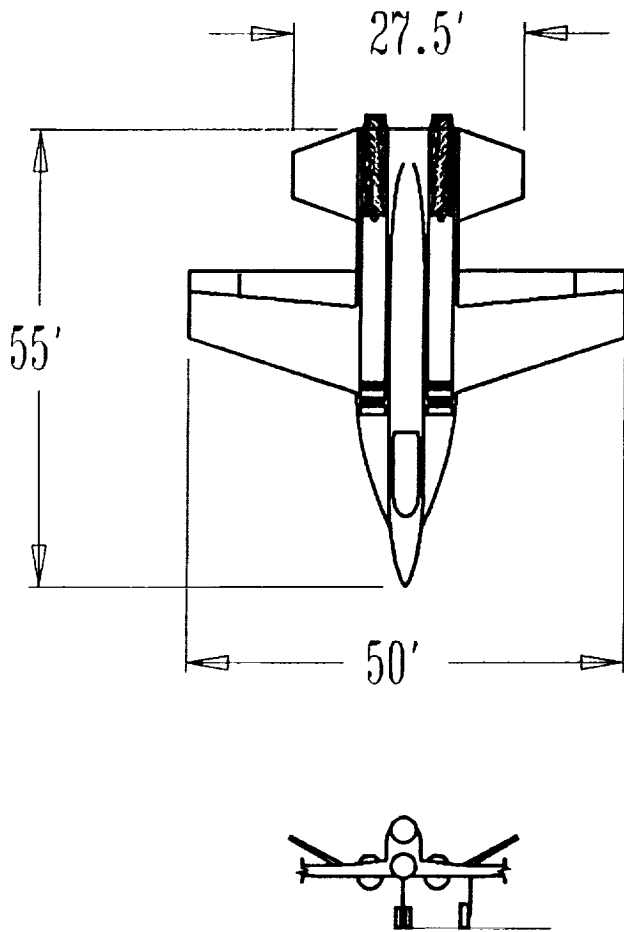
carries an onboard auxiliary power unit, ground-based electrical sources are not needed. The only necessary ground support needed is a fuel source, a GAU-8 cannon reload cart, a liquid oxygen cart, and a powered hoist to mount ordnance to the underside of the wing. Reloading points are placed so as to allow all ground operations to occur at once without any single operation interfering with another.

Every attempt was made to make manufacturing as simple and cost effective as possible. Linear tapered wing spars and the external placement allows for simpler and more cost effective manufacturing. Composite materials were not used extensively because of difficulty in maintenance in the field and cost of manufacturing.

Close air support is primarily the protection of ground forces. With an aircraft designed as survivable, maintainable, rugged, and reliable as this, ground troops can feel at ease knowing that the Guardian will be watching over them, day and night.

#### THE A-2000

The A-2000 is a futuristic attack aircraft capable of delivering massive firepower in the highly lethal arena of modern combat, Fig. 3.



| Differential Stabilizer |                 |                 |
|-------------------------|-----------------|-----------------|
|                         | Wing            | (one tail only) |
| Area (ft <sup>2</sup> ) | 600.0           | 75.3            |
| Span (ft)               | 50.0            | 9.12            |
| MGC (ft)                | 12.44           | 8.56            |
| Aspect Ratio            | 4.17            | 1.11            |
| LE Sweep (deg)          | 17.8            | 16.8            |
| Taper Ratio             | 0.5             | 0.5             |
| Root Chord (ft)         | 16.0            | 11              |
| Thickness Ratio         | 0.10            | 0.06            |
| Dihedral (deg)          | 0               | 30              |
| Incidence (deg)         | 0               | variable        |
| Airfoil                 | NACA 65-410     | NACA 0006       |
|                         | <b>Aileron</b>  | <b>Flap</b>     |
| Chord Ratio             | 0.3c            | 0.3c            |
| Span Ratio              | 0.76 - 1.0      | 0.24 - 0.76     |
|                         | <b>Fuselage</b> | <b>Cockpit</b>  |
| Length (ft)             | 55.0            | 7.0             |
| Max Height (ft)         | 7.0             | 5.2             |
| Max Width (ft)          | 9.0             | 3.6             |

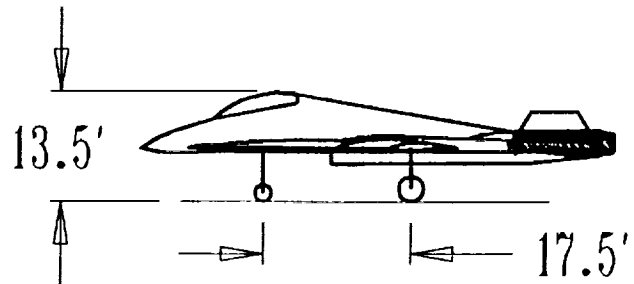


Fig. 3. A-2000.

Short take off and landing distances (1500 ft) are achieved by a combination of minimizing weight, the use of a single slotted flap covering over 50% of the wing span, and a leading edge extension (LEX) to increase lift. The LEX creates a strong vortex flow over the inward portion of the wing creating an additional nonlinear lift distribution. It also serves to strengthen the boundary layer, thus delaying flow separation and aiding high angle-of-attack flight performance. The vortex flow created by the LEX will also help to reduce the problem of gun gas ingestion into the engine by drawing the gas up over the top of the wing and away from the inlets. Auxiliary inlets above the wing open up for take-off while the primary inlets, which are below the wing, simultaneously close off. This considerably reduces the chances of foreign object damage to a turbine blade while operating on a rough, unprepared runway.

The A-2000 is highly maneuverable in the low-altitude, high-speed environment of close air support. Maneuverability is enhanced by moderate load factors (7.5 g), high afterburner thrust levels (27,500 lb static), and high lift coefficients. The use of strictly internal fuel tanks for all but the ferry mission helps keep parasite drag to a minimum.

The A-2000 is capable of providing support in a variety of roles. These include antiarmor, precision attack, battlefield interdiction, and maritime patrol. A variety of hardpoints are supplied for both weapons and external fuel tanks. The GAU-12 cannon in conjunction with armor-piercing rounds allows the A-2000 to defend against enemy tanks, armored vehicles, and a variety of ground targets, while offering a considerable weight savings over the GAU-8 specified in the request for proposal.

Keeping the level of complexity to a minimum has reduced the need for extensive ground support. An auxiliary power unit (APU) allows the A-2000 to self start, requiring smaller ground crews, while the use of proven technologies and readily accessible components minimizes the maintenance requirements.

#### THE MANX

The Manx fighter aircraft is offered as a viable replacement for existing close air support (CAS) aircraft, Fig. 4. The Manx is designed to outperform existing CAS aircraft by integrating

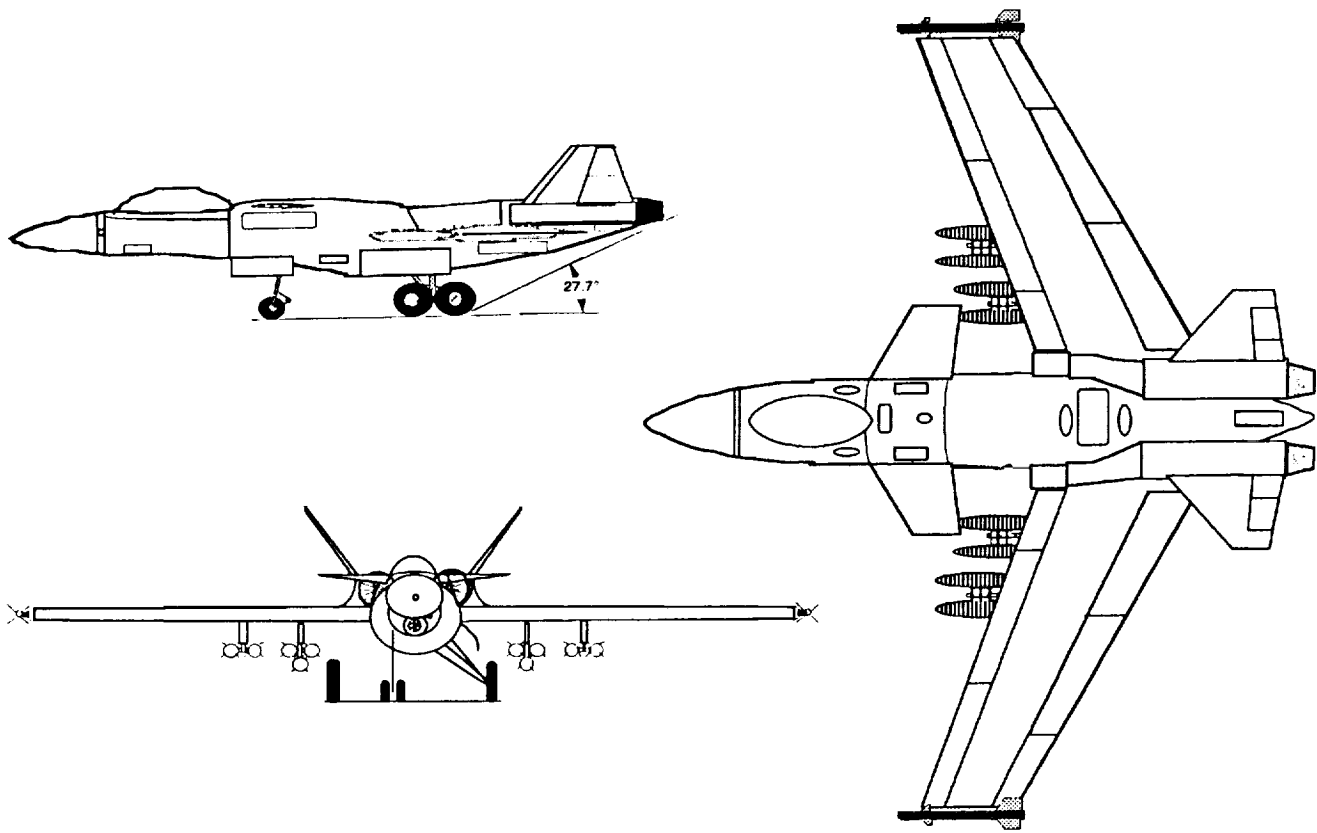


Fig. 4. Manx Fighter.

new technologies in aircraft configuration, avionics, weapons deployment, survivability, and maintainability.

The Manx's forward-swept wing, canard configuration will allow for a smaller, lighter-weight aircraft that is more efficient than existing aircraft. This configuration contributes to improved maneuverability, better stall characteristics, and offers a stable platform from which weapons can be aimed accurately.

The Manx incorporates an aeroelastically tailored, cantilever midwing that is swept forward  $25^\circ$  at the quarter chord. The wing airfoil section is a NACA 65-210. Additional lift for take off, landing, and maneuvering is achieved by integrating both Fowler flaps and leading edge slats.

The Manx fuselage has been designed with a fineness ratio of 8 to reduce drag. The fuselage is semimonocoque with aluminum-lithium frames, aluminum alloy longerons and composite skins.

The Manx is equipped with a canard that is a fully movable surface. This canard is primarily used for pitch control, but also enhances roll capability when used differentially in conjunction with the ailerons. The canards are also employed as a speed brake during landing.

Twin vertical tails provide the stability required for one-engine inoperative flight, well as giving the Manx the redundancy needed to survive in a high-threat environment. The swept cantilever tails are canted  $35^\circ$  to place them out of the wake of the fuselage at high angle of attack.

A tricycle landing gear is provided to allow the Manx added stability and ruggedness. The gear retracts forward. This design allows the gear to be deployed by gravity and locked into position by dynamic pressure in the case of power failure or damage. The nose gear is a dual arrangement while the main gear is a tandem design. The tires are low pressure to allow for operations from soft grass or packed sand fields.

The Manx is equipped with twin low-bypass turbojet power plants, each producing 16,000 lb of thrust at sea level. The engines produce power required to meet the required performance of the design and also provide redundancy in case of engine failure or damage. Engine inlets have been placed above the wing to reduce the possibility of foreign object damage to the engine.

The single pilot is situated in a forward-mounted air-conditioned and pressurized cockpit that has been designed

to increase pilot visibility. The cockpit is enclosed by single-piece polycarbonate canopy that opens upward. The pilot and all vital avionics are surrounded by a Kevlar shield which provides protection from small and medium ground fire.

The Manx employs a triple-redundant irreversible fly-by-wire control system to signal the electrohydrostatically driven control surfaces. The Manx also uses a stability augmentation system (SAS) to help the pilot control the 17.8% longitudinally unstable aircraft. Additional avionics used in the Manx include terrain following/avoidance radar/IR, global positioning satellite navigation and targeting, forward looking infrared (FLIR), and LANTIRN navigation/targeting pods.

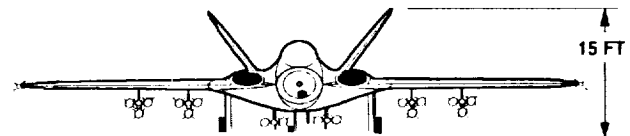
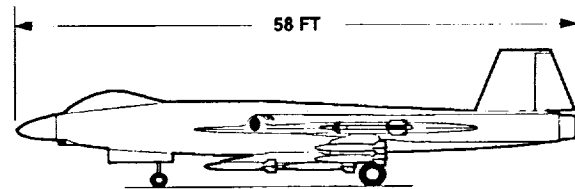
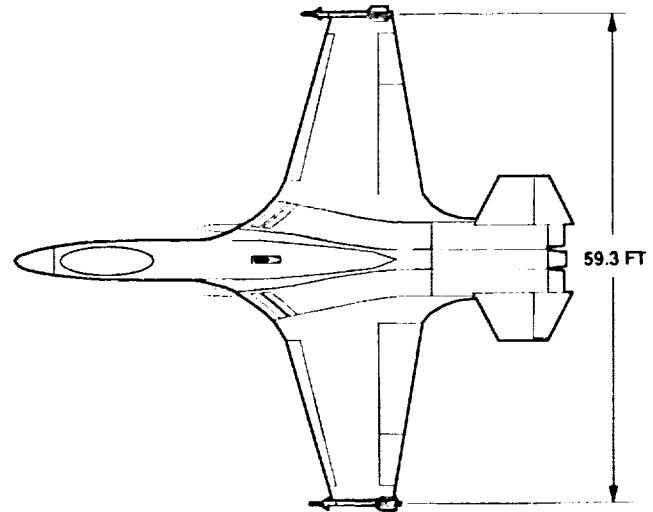
There are 10 hard points available for weapons carrying capability. AIM-9L Sidewinders are carried on each wing tip and 20 Mk-82 bombs are carried on 4 wing hard points for the design low-level mission. Other weapons can be integrated using the additional hard points as the missions require.

### THE CYCLONE

The future battlefield will require an effective close air support aircraft able to protect friendly troops and wreak destruction on the enemy. The Cyclone design group has produced an aircraft capable of these tasks.

The conventional configuration of the Cyclone reduces the costs that are incurred during the research and development phases of a new aircraft design, and the proven ability of this configuration in existing aircraft makes it a wise choice for the Cyclone, Fig. 5. The blended wing-fuselage reduces the interference drag and results in a greater fuselage volume allowing for all the required fuel to be carried in the fuselage. On top of this, the refueling port gives the Cyclone midair refueling capabilities, greatly extending its operational range and endurance. The engine inlets are set off the fuselage to minimize ingestion of gun gas produced by the GAU-8 30-mm cannon, and they allow for undisturbed flow into the engine intake. Furthermore, the small leading edge extensions inboard of the engine inlets create vortices that entrain the gun gas over the fuselage and further prevent gun gas ingestion into the engines. Use of the v-tail and an augmented flight control system reduces the structural weight and skin friction drag of the Cyclone. The bubble canopy used on the Cyclone provides excellent visibility for the pilot in all directions, allowing him to see possible threats or targets. The titanium tub surrounding the cockpit also increases the pilot's safety by protecting him from small arms fire.

The aerodynamics of the Cyclone include a supercritical airfoil to reduce the compressibility drag at higher Mach numbers. In conjunction with the leading edge flaps and trailing edge single-slotted flaps, this airfoil provides enough lift for the aircraft to allow it to land and take off in short distances. The wing configuration and large internal fuel volume of the Cyclone allow it to carry its large payload into battle even if the battlefield is far away. Furthermore, the design instability of the Cyclone makes it maneuverable, and as the fuel is consumed on the way to the battle the aircraft becomes even more maneuverable. The Cyclone's propulsion system includes two low-bypass, augmented turbofan engines buried inside the fuselage where they are protected. They provide an excellent dash speed at



#### MAIN WING PLANFORM GEOMETRY:

|                 | SPECIFICATION  |
|-----------------|----------------|
| AIRFOIL         | SUPER CRITICAL |
| ASPECT RATIO    | 5              |
| C/4 SWEEP ANGLE | 8 DEGREES      |
| THICKNESS RATIO | 0.12           |
| TAPER RATIO     | 0.35           |
| WING SPAN       | 59.3 FT        |
| SURFACE AREA    | 703.5 SQ FT    |

Fig. 5. Cyclone: A close air support aircraft for tomorrow.

sea-level for this type of aircraft and, with afterburner, the Cyclone has more than enough power for combat maneuvering.

In conclusion, the Cyclone is the choice for the future in close air support.

### THE RAPTOR

The Raptor was designed around a cranked-arrow, canard, twin vertical tail configuration, Fig. 6. The cranked-arrow configuration was selected as the optimal blend of high-speed drag reduction and low-speed maneuverability. The wing employs single-slotted flaps and flaperons for additional lift capabilities and roll control. The canards are mounted on the upper surface of the inlets for minimal disruption of incoming airflow into the inlet. In addition, the canards can be independently controlled for supplementary roll control. The twin vertical tails give adequate engine-out control, even with one vertical tail inoperable. The Raptor sets down, after completing its mission, on a conventional tricycle landing gear configuration.

The wing structure is composed of six tapered spars, to decrease weight and increase survivability. The majority of the airframe is composed of aluminum for its high strength-to-weight ratio and ease of manufacturing. Composites are used sparingly in only the canard and vertical tails for their fatigue resistance in combatting buffeting at high angles of attack.

The Raptor performance is unequalled by any other competitor. With design weapons load, the Raptor launches off the runway in a mere 1605 ft. The Raptor will execute a normal landing in only 1124 ft, and land after an aborted takeoff in only 1800 ft. The Raptor can be ferried up to 3020 nmi on internal fuel alone. A sea-level combat radius with design weapons load of 475 nmi can be achieved. Acceleration from Mach 0.3 to Mach 0.5 is achieved in a neck-breaking time of 7.7 seconds. A 45,000 ft per min maximum rate of climb is attained by the Raptor at sea level. These two outstanding performance parameters combine to allow a combat pass (consisting of a 360° turn and 4000-ft energy increase) to be performed in 23.8 s, giving the Raptor one of the fastest reattack times possible. This top-of-the-line aircraft will cost the taxpayer a mere 12.6 million dollars.

| Raptor Specifications       |                     |
|-----------------------------|---------------------|
| Wing Area                   | 500 ft <sup>2</sup> |
| Wingspan                    | 45 ft               |
| $\Delta\alpha_4$ (inboard)  | 53°                 |
| $\Delta\alpha_4$ (outboard) | 26°                 |
| Overall Length              | 61.5 ft             |
| Overall Height              | 17 ft               |
| Canard Area                 | 94 ft <sup>2</sup>  |
| Vertical Tail Area          | 160 ft <sup>2</sup> |
| Empty Weight                | 22700 lbs           |
| Design Weight               | 46500 lbs           |
| Max Thrust                  | 36500 lbs           |

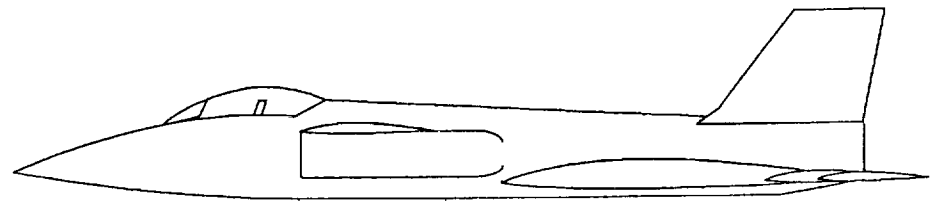
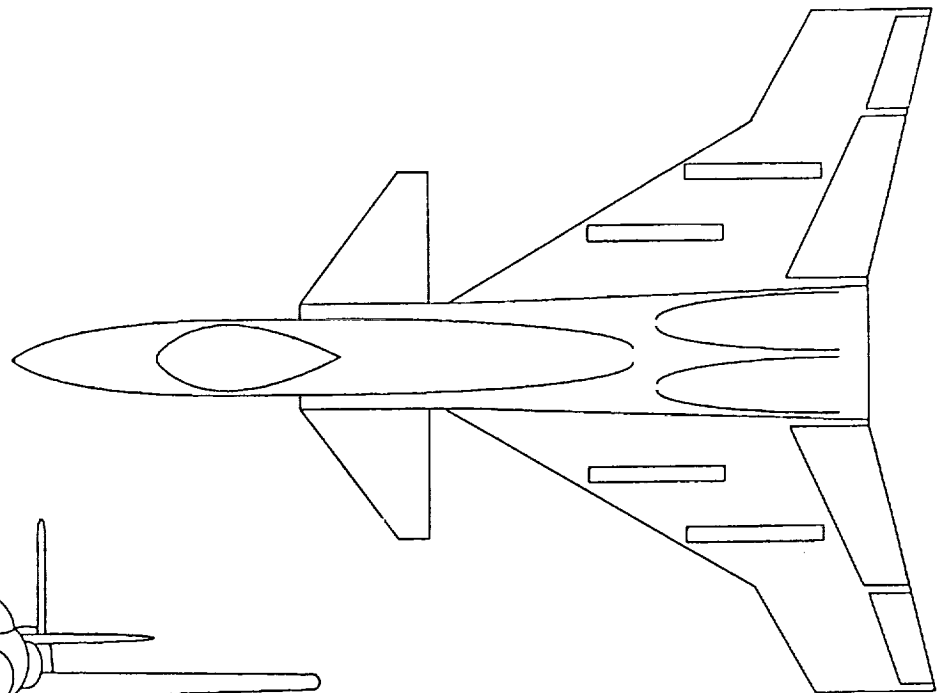
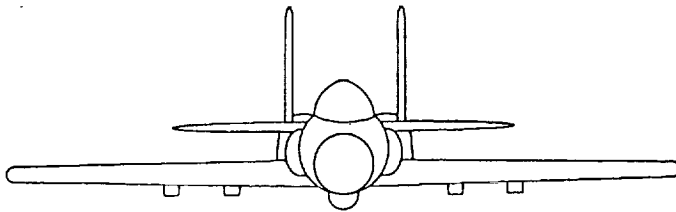


Fig. 6. The Raptor.

The cockpit was designed for maximum ease of use by the pilot by employing large reconfigurable multifunction displays. Also, the next generation of ejection systems is used in the form of the Boeing CREST ejection seat. Pilot visibility is excellent, with  $16^\circ$  over the nose and  $41^\circ$  over the side.

To enable day and night, as well as bad weather operations, the Raptor is equipped with an internally mounted LANTIRN targeting and navigation system. In addition, a Pave Penny sensor was included to allow for target handoff from friendly ground or air units. For protective measures, a flare and chaff system was placed in the rear of the aircraft between the two engines.

Battlefield maintenance and ground support is kept to a minimum by the inclusion of an auxiliary power unit and an airframe-mounted accessory drive. The canards and vertical tails are interchangeable by design for ease of replacement.

The awesome sight of a fully laden Raptor, carrying 36 Mk 82 bombs on its seven high-capacity hardpoints, is sure to strike fear into the hearts of even the most battle-hardened enemy commanders.

### THE SCORPION

Technology has caused battlefield warfare to become increasingly complex. The concept of the close air support aircraft has not changed, but the close air support aircraft and its role has had to continually evolve to maintain pace with the battleground. The primary goal of the Scorpion design team was to design an aircraft that met today's needs as well as fulfill tomorrow's. The design process resulted in an aircraft that is rugged, reliable, and capable of flying in adverse operating conditions. The Scorpion exceeds all mission requirements and is capable of fulfilling additional roles. The Scorpion excels in range, payload capabilities, and rate of climb.

The Scorpion has a conventional configuration, with twin tails, twin engines, and tricycle landing gear sized for rough field operation, Fig. 7. The wing is a conventional planform with a  $20^\circ$  leading edge sweep. The lift augmentation system includes leading edge slats, Fowler flaps, and flaperons. The horizontal tail is a fully controllable stabilator arrangement, also with a  $20^\circ$  leading edge sweep. The engines are separated to provide better survivability, and the inlets were placed high, on top of the wings, extending to the leading edge to provide uniform freestream flow and to help prevent foreign object ingestion during take-off and landing ground time. The Scorpion also features a bubble canopy for better pilot visibility— $20^\circ$  down the nose and  $45^\circ$  laterally. The location of the vertical tails, forward of the horizontal stabilators, allow for maximum simultaneous deflection of the rudders and stabilators as well as simplifying the internal structural layout of the empennage. The twin-canted vertical tails also allow for better survivability and increased controllability in high-angle-of-attack flight conditions.

The object of the Scorpion design concept was to produce a neutral or marginally stable close air support aircraft. The static margin of the Scorpion is 2% stable, which allows for excellent maneuverability with survivability. The aircraft is maneuverable, but controllable in the event of system failure. Through the use of a double-redundant fly-by-wire system, the survivability of the aircraft is further enhanced. Marginally stable

aircraft also offer the advantage of having minimal trim drag, as well as eliminating the need for complex avionics, thus minimizing costs. Other electronic systems used in the Scorpion include a passive infrared all-weather navigation and target acquisition system that also decreases the effectiveness of radar-seeking anti-aircraft weapons.

The aforementioned characteristics enhance the performance of the Scorpion. The performance parameters determined include specific excess power, range-payload capabilities, and the flight envelope. The Scorpion's maximum rate of climb at Mach 0.5 at sea-level is 12,500 fpm. The maximum range with payload is 2006 nmi and the maximum ferry range is 4300 nmi at a best cruise altitude of 38,000 ft. For a 4.5-g sustained turn, the maximum turn rate is  $17^\circ$  per sec at a turn radius of 1700 ft. This allows for a reattack time of 21 sec. The Scorpion is capable of taking off from a 1600 ft. hard, dry strip and can land within 1589 ft.

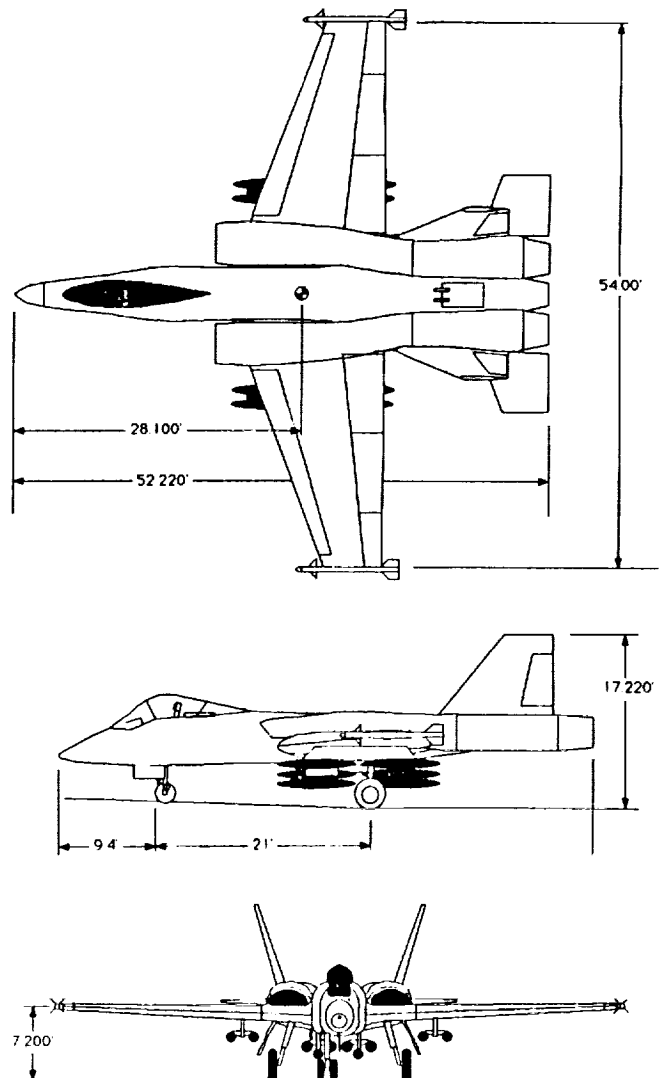


Fig. 7. Three-view of Scorpion.

The Scorpion was designed to meet the battlefield requirements of the future, while emphasizing low-cost (\$17.5 million 20-year life cycle cost), low-maintenance, high survivability, multirole capabilities, and low pilot workload to enhance combat performance.

### THE ELIMINATOR

The Eliminator is the answer to the need for an affordable, maintainable, survivable, high-performance close air support aircraft, Fig. 8. As important as close air support is, the U.S. is facing a desperate need for a new aircraft to fill this role. The challenge for the future will be to produce a close air support aircraft that will be able to stand up to a high-tech, fast moving, and incredibly deadly battlefield. In addition, the future aircraft must be versatile enough to adapt to any possible mission it might be called upon to perform during war or peacetime, with a minimum need for maintenance or service. Most importantly, the aircraft of the future must be affordable.

It is vital that it employ a combination of new and proven technologies to achieve a blend that gives high performance and survivability.

The Eliminator is a fixed-wing aircraft, with two GE F404-400 turbofan engines, and a high-canard, low-wing, twin-tail configuration aircraft. The total length of the aircraft is 55 ft, with a wingspan of 53 ft, and a total planform area of 517 ft<sup>2</sup>. Since the take-off weight is 55,000 lb, the maximum wing loading is 110 psf. The maximum thrust from the two engines with afterburners is 30,000 lb, making the maximum power loading at take-off 0.55. Without the afterburners, the maximum thrust is 22,000 lb. The afterburners provide the Eliminator with an excess power up to 300 ft/s. Without afterburners the Eliminator has up to 185 ft/s in excess power. This power was required to meet the 2000-ft ground roll requirement, and also provides maneuvering power in combat situations.

The main wing and the canard use a NACA 63-412 airfoil. The canard has been designed with a trailing edge extension, or TEX, in order to assure smooth flow into the engine inlets.

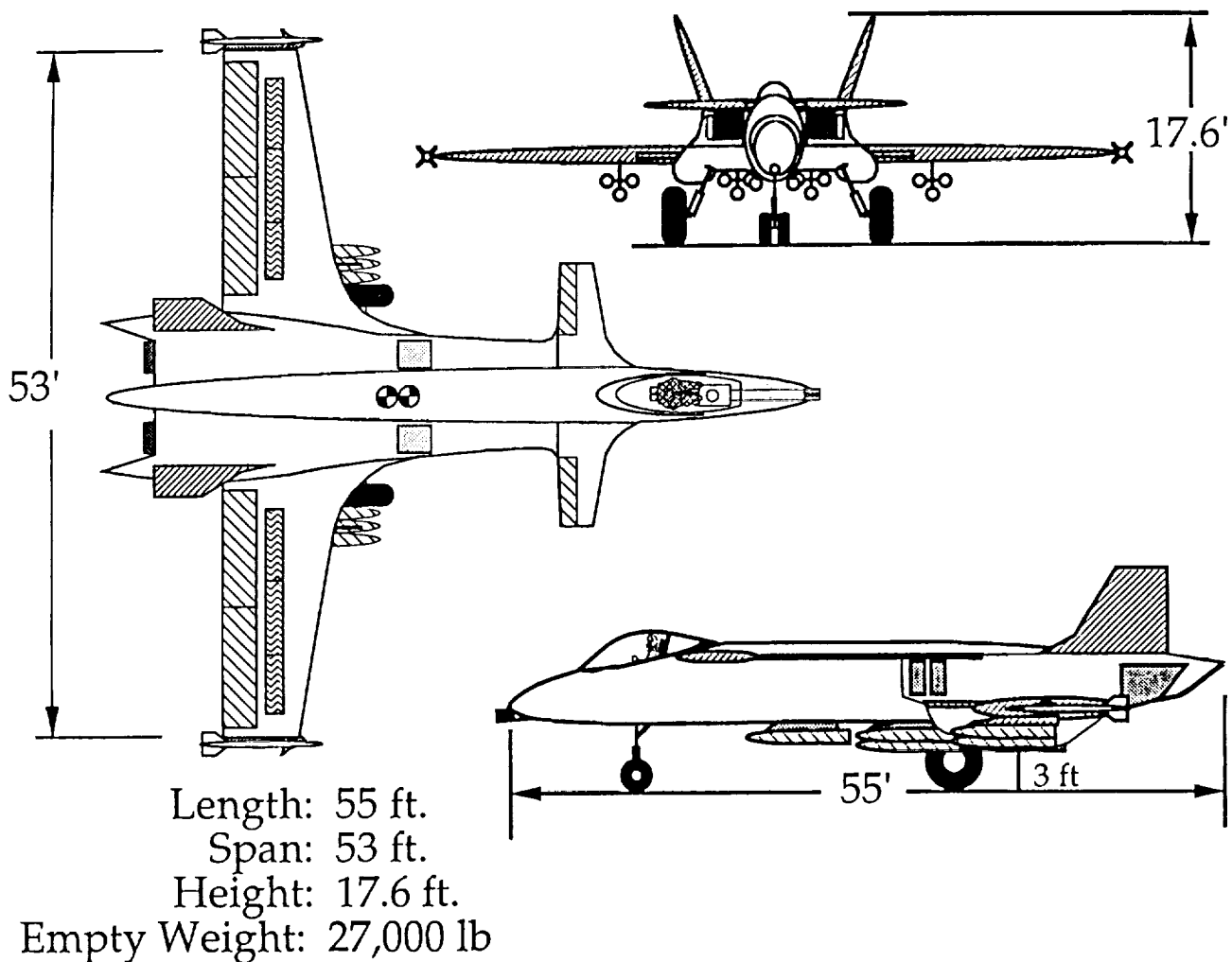


Fig. 8. Eliminator.

Pressure relief doors were added to the TEX, just behind the inlets, to release the air trapped at high angles of attack, and thus reduce the pressure buildup in front of the inlet. The doors should also act as vortex generators, producing vortices over the fuselage, thus increasing the lift of the fuselage slightly.

The main wing uses Fowler flaps to provide a high boost to the lift coefficient at take-off, enabling the Eliminator to exceed the runway length requirement of 2000 ft with a mere 1760 ft ground roll for take-off and 1810 ft for landing. Should it be necessary to land in a shorter distance, the pilot may employ the airbrakes, which are mounted directly on the side of the aircraft, extending from the trailing edge of the main wing to the rear of the fuselage. The tires of the Eliminator have been oversized, and inflated to approximately 65 psi, to allow operation from hard dirt runways. Operation from soft grass fields is possible with a temporary metal runway implemented.

The Eliminator has been designed to have a maximum instability of 23%, resulting in an extremely maneuverable aircraft. A dual fly-by-wire control system will therefore be employed to aid the pilot in maneuvering. The primary control system is powered by the generators. The secondary control system has been located as spatially distant from the primary wires as possible in order to avoid the destruction of both systems in the case of a hit. Should it be necessary, the pilot may use the secondary system, which is run either by the generators, the APU (both located between the engines), or the battery, located in the nose of the aircraft.

The avionics used by the Eliminator have been chosen for their usefulness and cost effectiveness. A radar system is not employed, primarily because it is not necessary for this type

of aircraft. In addition, extensive radar systems are typically very costly and it has been attempted to keep the cost of the Eliminator as low as possible. Therefore, for the purpose of target identification, a passive system has been chosen—the Pave Penny system, located under the center of the fuselage. For defensive purposes, a radar warning system (antennae located in the tail and nose) will be used to inform the pilot when to employ the chaff and flares for electronic countermeasures.

The Eliminator's primary mission is close air support, but it can easily be converted for antiarmor use. In addition, the Eliminator can do maritime patrols, antiradiation missions, and interdiction missions, among others. These different roles make the Eliminator a flexible and capable aircraft for all services.

One design objective was to keep the cost of the aircraft as low as possible. The Eliminator achieves this goal, with a flyaway cost of \$14.6 million. Included in this cost were the conventional aluminum alloys and composites of which the Eliminator is built, its relatively simple avionics systems, and the Eliminator's weight and maximum speed, among many other factors.

Although this is only a preliminary design, and much work and analysis would need to be done before the Eliminator could be considered a finished concept, there is a great deal of cause for enthusiasm. The Eliminator meets or surpasses all the requirements that drove its design and has emerged as a capable aircraft that can be used to fulfill many missions. Although designed for close air support, it has become evident that the Eliminator could fill many roles, and could be acquired as a single plane air force. This alone makes it a remarkable aircraft. The Eliminator: It's not a threat; it's a promise.

**PROJECT ARES II: HIGH-ALTITUDE BATTERY-POWERED AIRCRAFT**

**CALIFORNIA STATE UNIVERSITY NORTHRIDGE**

53-05  
160579  
P. 5

A high-altitude, battery-powered, propeller-driven aircraft has been designed and is being built by undergraduate students at California State University, Northridge. The aircraft will fly at an altitude of 104,000 ft at Mach 0.2 (190 ft/sec) and will be instrumented to record flight performance data, including low Reynolds number propeller and airfoil information.

This project will demonstrate the feasibility of electric-powered flight in a low-density, low-temperature Earth environment that models the atmosphere of Mars. Data collected will be used to design a Mars aircraft to investigate the surface of Mars prior to manned missions.

The instrumented payload and the mission profile for the high-altitude Earth flight were determined. Detailed aerodynamic and structural analyses were performed. Control, tracking, and data recording subsystems were developed. Materials were obtained and fabrication begun.

The aircraft has a 32-ft wing span, a wing area of 105 sq ft, is 17.5 ft long, has a 12-in payload bay, and weighs 42 lb. It is composed primarily of lightweight materials, including Mylar, and composite materials, including graphite/epoxy and aramid core honeycomb sandwich.

Low-altitude flight testing to check guidance and control systems and to calibrate data-gathering instruments will take place this summer, followed shortly by the 104,000-ft flight.

**INTRODUCTION**

The Universities Space Research Association (USRA), in association with NASA, has sponsored a three-year undergraduate design project in the Mechanical Engineering Department at California State University, Northridge (CSUN). The overall project objective is to design a heavier-than-air craft to fly in the lower martian atmosphere, investigating geological and atmospheric features as a prelude to a manned Mars mission.

The first year's design team (ARES I) investigated the martian mission and made recommendations for mission profile, payload, aircraft configuration, and delivery of the craft to Mars. Now, in the second year of the project, a new student team (ARES II) has designed an aircraft to be built and flown on Earth. This prototype, currently being fabricated at CSUN, will demonstrate the feasibility of the Marscraft by flying on Earth.

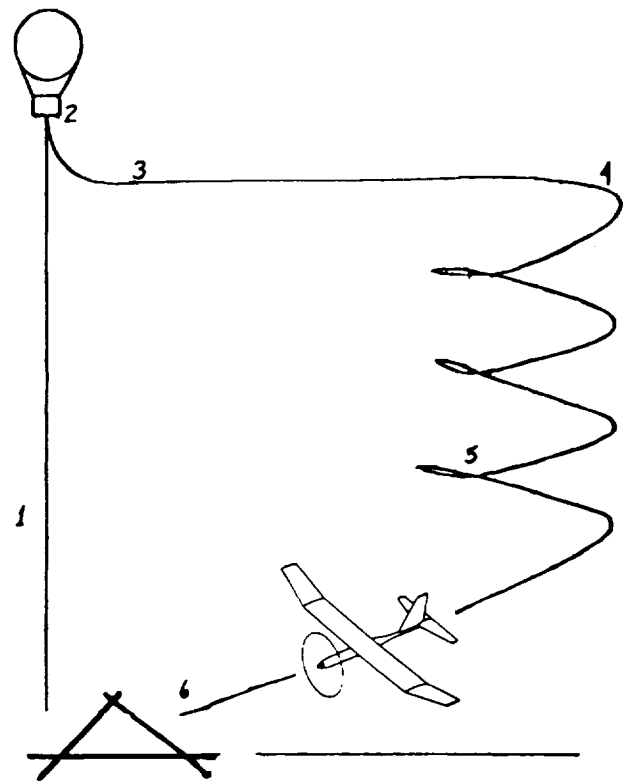
The aircraft will fly at 104,000 ft at Mach 0.2, a flight regime closely resembling the martian mission in the following important parameters: atmospheric density and temperature, Reynolds numbers, and lift coefficient. A successful Earth flight will demonstrate the feasibility of the Mars mission and craft.

For a meaningful demonstration, the Earth prototype will carry an instrument payload to measure and record aircraft performance data. This data will be useful in verifying the design concepts and analytical model developed by the student team and providing a baseline for design of the actual Marscraft, as well as providing valuable low-Reynolds-number propeller and airfoil information.

The high-altitude flight is planned for this summer (1991) at Edwards Air Force Base.

**MISSION PROFILE**

To achieve the stated objectives, the mission profile detailed in Fig. 1 was developed. A balloon will take the aircraft to 110,000 ft and release it. After 3 min of programmed level flight and maneuvers within a 25 by 8 mile test area at Edwards AFB, the aircraft will descend and land under manual control.



| Phase | Description  |
|-------|--|
| 1-2   | Balloon launch and ascent. Release aircraft nosedown at 110,000 ft.        |
| 2-3   | Pullout to level flight at 104,000 ft. Maximum 3-g load occurs at point 3. |
| 3-4   | Preprogrammed level flight and maneuvers for 3 minutes.                    |
| 4-5   | Descend. Wind gusts below 50,000 ft can be dangerous.                      |
| 5-6   | Land under manual control.   |

Fig. 1. Mission profile.

Prior to the high-altitude flight, low-altitude test flights will be made to test guidance and control systems and to calibrate data gathering instruments.

**AERODYNAMIC DESIGN**

The basic requirement was to design an aircraft for electrically powered flight at 104,000 ft (a low-Reynolds-number regime). The selected airfoil, the RG15-PT, is suitable for low Reynolds numbers. It has a low design coefficient, small variations in L/D as a function of Reynolds number, and is fabricable due to its simple shape. The expected Reynolds number at altitude is 60,000. See Fig. 2 for additional airfoil details.

Since the Mars craft will very likely be solar powered, the Earth prototype was planned as a solar vehicle too; but due to cost, availability, and low energy density, solar cells were waived in favor of nickel-cadmium batteries for this design. Nevertheless, several key aerodynamic design decisions were made based on the presence of solar cells, as will be discussed.

A trade study was performed based on small payloads, available motor horsepower, wing loading vs. velocity, and, finally, wing loading vs. aspect ratio. An optimum aspect ratio of 10 was determined. A carpet plot incorporating these variables resulted in the simultaneous optimization of wingspan (32 ft), velocity (190 ft/s), and weight (42 lb). Subtracting the known weights of the propulsion and avionics systems from this weight resulted in the target structural weight fraction, to be discussed later.



- LOW DESIGN COEFFICIENT  $C(L) = 0.63$
- SMALL L/D VARIANCE FOR DIFFERENT REYNOLDS NUMBERS
- 8.9% THICKNESS
- SIMPLE SHAPE FOR EASE OF FABRICATION

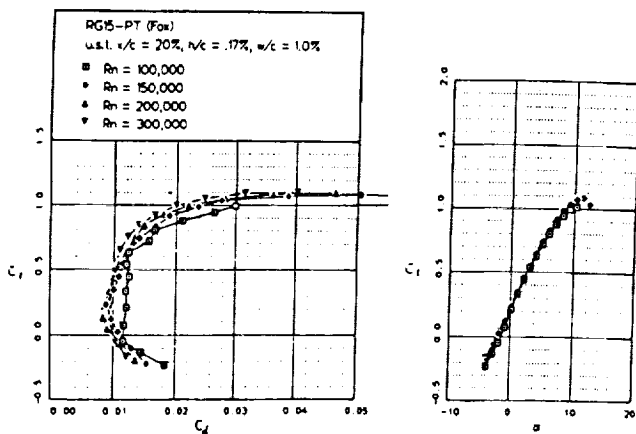


Fig. 2. Airfoil data.

The wing area was as large as possible to allow for the greatest number of solar cells. Ailerons were eliminated for the same reason. To simplify fabrication, the wing has a 20-ft-span constant chord center section with 6-ft tapered outboard sections. To improve stability, the outboard sections have a taper ratio of 7.5, all in the leading edge, to give a sweep effect, and a 13° dihedral, giving the equivalent of a 5° total wing dihedral.

The tail was designed in conventional configuration, although an inverted V-tail could still be built. The conventional tail is preferred for landing, since the aircraft will not have landing gear. Symmetric airfoil sections were selected for both vertical and horizontal tail sections. Ailerons were not used; instead, a large rudder and elevator were designed to control pitch, roll, and yaw.

The fuselage was designed in a one-piece "guppy" shape, tapering from a payload bay to a tail boom. This configuration simplified structural analysis, eliminated stress concentrations associated with a separate boom attachment, and simplified fabrication. The wetted area was reduced by rounding the square cross-section, and drag was reduced by giving the payload bay a slightly sculptured profile.

The propulsion system includes an 7-ft propeller, driven by a 1.6-hp electric motor through a belt-driven gear reducer, powered by nickel-cadmium batteries (see Fig. 3.) With a smaller payload, or reduced structural weight, the same system can be powered by K7 solar cells. All the cells can be placed in the wing beneath the clear Mylar skin.

A summary of final aircraft specifications is provided in Fig. 4.

**STRUCTURAL DESIGN**

Large structural elements were divided into finite segments, allowing the analysis of a tapered geometry with nonlinear distribution of loads, moments, and properties. All loads were multiplied by a load factor and safety margin, and the resulting moments used to determine stresses, deflection, and rotation

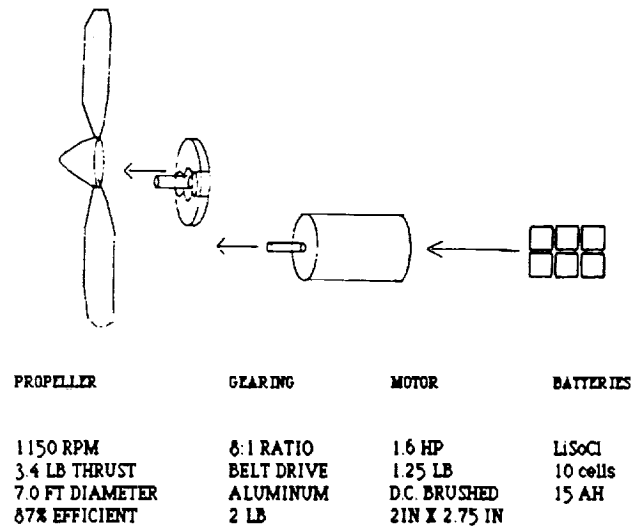
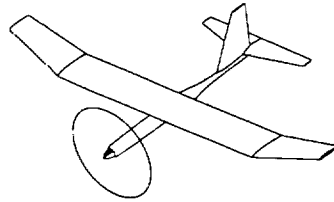


Fig. 3. Propulsion schematic.

| PERFORMANCE       |            | WING         |                     |
|-------------------|------------|--------------|---------------------|
| Altitude          | 104,000 ft | No sweep     |                     |
| Vel (cruise) Mach | 0.02       | Wing Area    | 105 ft <sup>2</sup> |
| Vel (cruise)      | 190 ft/sec | Aspect Ratio | 10                  |
| Vel (climb)       | 180 ft/sec | Taper Ratio  | 0.5                 |
| Vel (stall)       | 172 ft/sec | b            | 32.3 ft             |
| Load Factor       | 3 G        | C (root)     | 3.5 ft              |
| Safety Factor     | 1.2        | C (tip)      | 2.2 ft              |
|                   |            | C Bar        | 3.34 ft             |
|                   |            | Y Bar        | 7.18 ft             |

| DESIGN PARAMETERS |                        |
|-------------------|------------------------|
| Wing Loading      | 0.4 lb/ft <sup>2</sup> |
| Weight            | 42.0 lb                |
| Hp/wt             | 0.038                  |
| Wt/Hp             | 26.18                  |



| VERTICAL TAIL |                       | HORIZONTAL TAIL |                    |
|---------------|-----------------------|-----------------|--------------------|
| A             | 1.6                   | A               | 6                  |
| Taper ratio   | 0.4                   | Taper ratio     | 0.4                |
| S             | 11.89 ft <sup>2</sup> | S               | 18 ft <sup>2</sup> |
| b             | 4.36 ft               | b               | 10.39 ft           |
| C (root)      | 3.89 ft               | C (root)        | 2.47 ft            |
| C (tip)       | 1.56 ft               | C (tip)         | 0.99 ft            |

Fig. 4. Aircraft specifications.

of structural assemblies. The geometry, material, or configuration of each assembly was modified until the computed stresses, deflections, and rotations met acceptable limits, and were then refined to reduce weight.

Table 1 indicates the target weight summary. Note that the structure comprises 42% of the total aircraft weight, and the wing alone weighs 0.1 lb/sq ft. Recent advanced aircraft data (e.g., the Gossamer *Penguin*) suggest that these targets are achievable.

A maximum load factor of 3 g was determined from an aerodynamic analysis of the launch. Four-g loads due to gusts may be encountered at 50,000 ft (during descent), determined from velocity-load diagrams. Nevertheless, it was decided to use a design load factor of 3 g to help reduce weight, and fly on a low-gust day. Similarly, a safety factor of 1.2 was selected, even though 1.5 is typical in aircraft applications.

TABLE 1. Weight Summary

| Item         | Weight (lb) |
|--------------|-------------|
| Structure    |             |
| Wing         | 10.5        |
| Fuselage     | 12.0        |
| Tail         | 3.0         |
| Propulsion   |             |
| Propeller    | 4.4         |
| Motor        | 1.6         |
| Gear reducer | 2.0         |
| Batteries    | 2.5         |
| Payload      | 6.0         |
| Total        | 42.0        |

TABLE 2. Final Material Selection

| Item                       | Material  |
|----------------------------|---|
| Ribs                       | Composite sandwich: 1/4" aramid honeycomb core with 7 mil, 1-ply graphite/epoxy (g/e) facings |
| Torsion box                | g/e sandwich, all four sides  |
| Leading and trailing edges | 7 mil, 1-ply g/e  |
| Skin                       | 0.5 mil Mylar, adhered and heat shrunk  |
| Fuselage                   | 7 mil, 1-ply g/e, with local stiffening   |

For simplification of the wing analysis, it was assumed that the torsion box alone would carry all loads. Normal spanwise stresses at every box segment were determined using advanced beam theory. The maximum stress in a given segment was then compared to the local buckling stress, determined from thin-plate buckling theory. Predicted failure stress was kept at least 20% higher than the maximum stress, wing tip deflection was kept less than 1 in, and tip rotation was less than 2°.

The fuselage was designed similarly to the wing torsion box. A mostly square cross section was adopted to simplify (1) wing and tail attachment, (2) analysis and design, and (3) tooling and fabrication. The tail section was patterned on the wing.

A number of tests were conducted to provide insight into the behavior and characteristics of certain structural component materials and fabrication methods. A rib test fixture was built to determine the lowest-weight rib configuration that could sustain the applied load. A thin-film skin test was performed to evaluate skin deflection under load and to observe the behavior of film and adhesive at low temperatures (-70°F). Lastly, some informal allowable testing was performed to confirm assumptions regarding adhesive and composite strength in tension at low temperatures. The tests were useful in confirming or modifying the selection of materials.

A wide range of materials was considered for all structural elements. Primary selection criteria were availability, cost, density, and ease of tooling and fabrication. Table 2 indicates the final materials selection. Figure 5 shows the final configuration.

### AVIONICS

Systems for flight control and tracking, testing, and data recording were designed, tested, and assembled. Flight control will be provided via modified radio-controlled model aircraft hardware. The transmitter station will include an amplifier and directional antenna to boost the control signal to the required range. The aircraft will carry a miniature radio transponder to aid in radar tracking. The control system incorporates a fail-safe feature whereby the aircraft assumes a preprogrammed descent profile in the event of a loss of control signal.

The aircraft will carry sensors to measure and record airspeed, altitude, ambient temperature, motor power consumption, and propeller thrust and speed. This information will be stored for later retrieval by the flight data recorder (FDR). The FDR uses the latest in LSI and surface-mount chip technology to pack what is, in essence, a complete microcomputer onto a few square inches. The FDR will also provide sensor signal conditioning and supply regulated reference voltages.

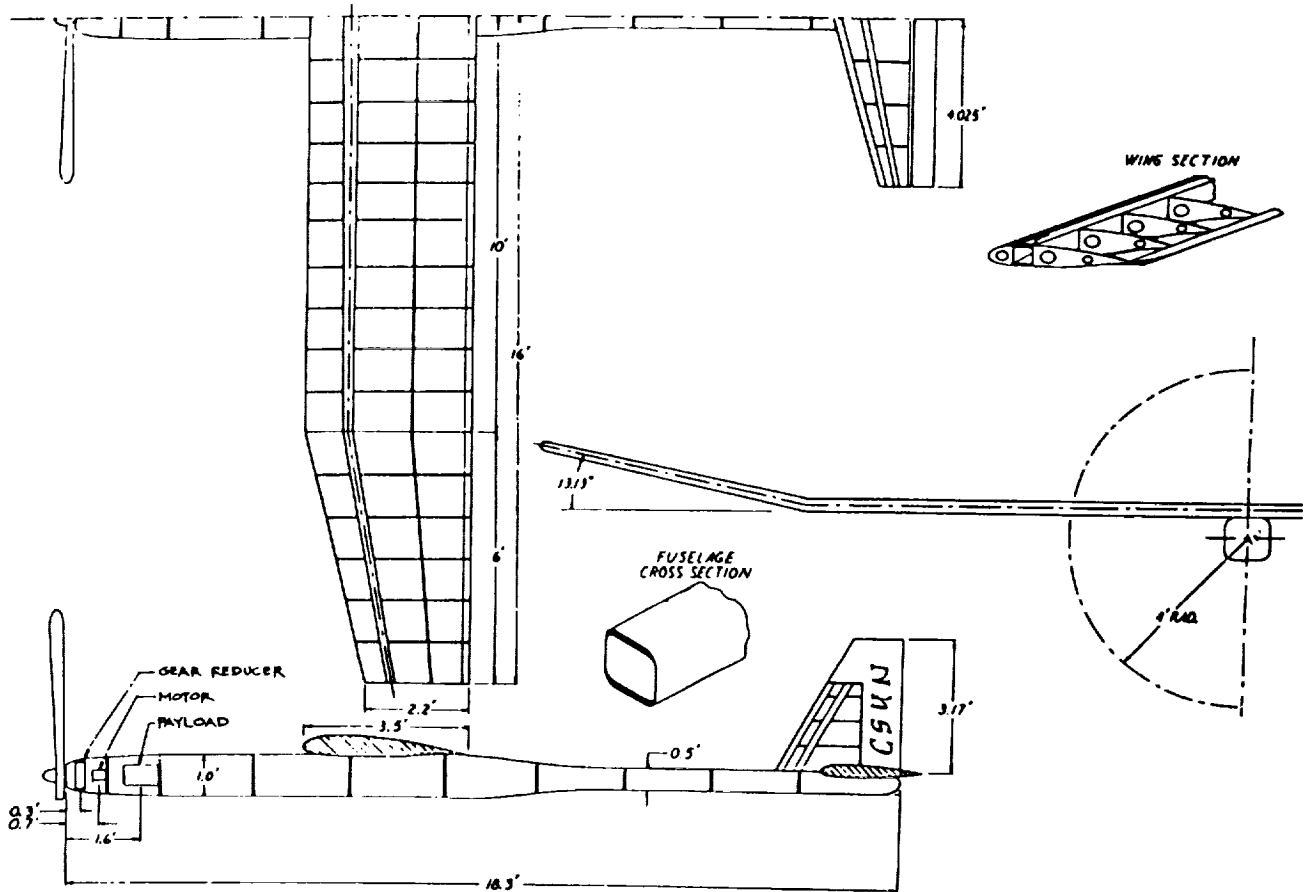


Fig. 5. Configuration drawing.

Additionally, the aircraft will carry a wing pressure port scanner system to record air pressure differentials at 32 different chord-wise wing locations. This data will validate the computational fluid dynamics model.

Because of low ambient temperatures at altitude ( $-70^{\circ}\text{F}$ ), the instrumentation package will be insulated. The FDR will be able to monitor and regulate the payload bay temperature with the aid of a small film resistance heater. Power for the onboard avionics will be provided by a dedicated carbonmono-fluoride lithium battery. The FDR will be furnished independently with a battery backup. Figure 6 illustrates the control, data collection, and flight data recorder schematics.

### BUDGET

In a project of this scope, the required instrumentation and materiel support is substantial. Thanks to the generous donations of interested industrial associates, the fabrication phase has proceeded on schedule with a continuing promise of success. Table 3 is a budget of this year's work.

### FABRICATION

The aircraft is being constructed entirely by the student team. Individual elements and major subassemblies are being built and tested, and redesigned if necessary, before final construction.

TABLE 3. Budget

| Item            | Cost, \$ |
|-----------------|----------|
| Avionics        | 8,600    |
| Propulsion      | 3,800    |
| Structure       | 19,000   |
| Mission Support | 5,300    |
| Travel          | 5,800    |
| Total           | 42,500   |

Most of the structural components were made from fiber/epoxy sheets or composite sandwich (an aramid honeycomb core with graphite/epoxy facings). Molds, made of wood or sheet metal, were built, surfaced with putty and enamel paint, then prepared with release agents to accept the wetted cloth. Curing was done in vacuum. A brief discussion of fabrication methods used for the major components follows.

The wing is being built in three sections (a 20-ft center section and two dihedral sections), due to fabrication space limitations and transportation difficulties. The wing torsion box for each section was laid up full length in two L-shaped pieces and assembled with epoxy. Mylar tape was used to attach the ribs to the box, and to face the edges of the ribs for skin attachment. The leading and trailing edge caps were made in 4-ft sections and adhered to the ribs. The Mylar skin, in 50-in wide strips,

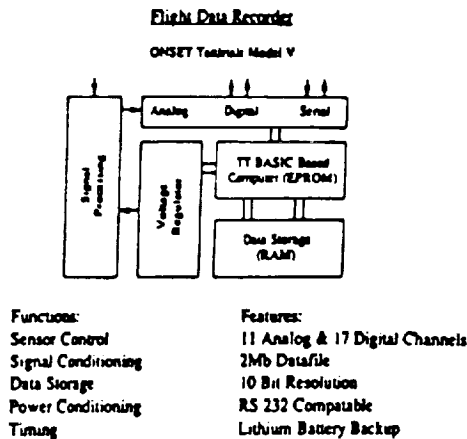
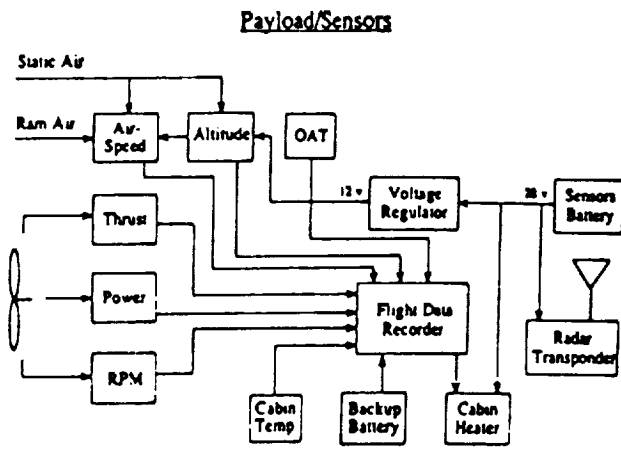
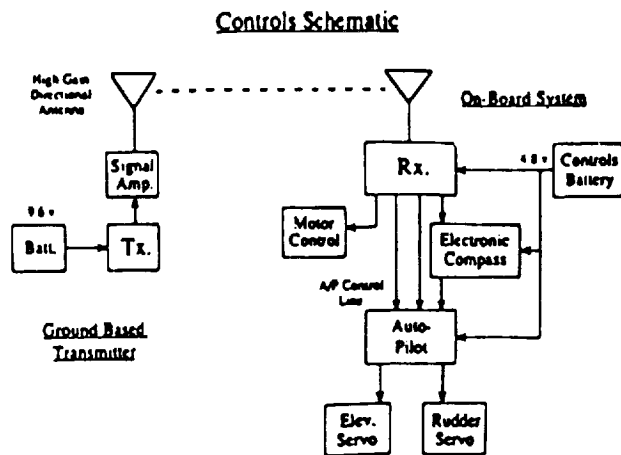


Fig. 6. Avionics schematics.

tail, motor, and payload mounting. The two halves were attached with adhesive tape and epoxy at the seam and around the bulkheads.

Tail assemblies were built similarly to the wing. Aluminum brackets were made to secure the wing and tails to the fuselage and permit disassembly for transport.

### CONCLUSION

Through the successful flight of a high-altitude Earth prototype aircraft, CSUN Mechanical Engineering students hope to verify the feasibility of a heavier-than-air craft for the martian atmosphere. Though the prototype is battery-powered, it is reasonable to expect the Marscraft to be solar-powered.

Some of the major design challenges included (1) using low Reynolds number airfoils, (2) electric motor selection and power system development, (3) low Reynolds number propeller design, (4) structural analysis of composite aircraft components, and (5) high-altitude, low-density atmospheric flight performance.

The data collected from various onboard sensors will be used to build a database that can be used to improve the aircraft design for subsequent flights. Next year's Project Ares III will benefit from our experience in aircraft structural design and fabrication, in high-efficiency aerodynamic design (verified by CFD), and in aircraft guidance and control with onboard data acquisition. With this knowledge, future design objectives can include detailed aircraft subsystems such as flaps, slots, landing gear, video cameras, autonomous control systems, and refined aerodynamic and structural designs.

The Ares II design team has responded to a difficult challenge: the design and fabrication of an all-composite, high-altitude, electrically powered aircraft. In the summer of 1991, we will fly this aircraft at an altitude of 104,000 ft. This accomplishment will generate world-wide interest and set CSUN and its students apart for having flown at an altitude never yet achieved by propeller-driven aircraft.

### ACKNOWLEDGMENTS

The project Ares II consists of Ed Avetesian, Tony Banh, Doug Boobar, Chris Charan, Jerry Gaudreau, Scott Gordon, Elise Gravance, David Hooper, Elizabeth Kralian, Bogdan Macri, Denise Mah, Doug Meyer, Margie Monsen, Craig Morton, Fred Mugford, Mel Navarro, Ermin Nazareno, George Renteria, Richard Shafiroff, Ralph Valencia, and Tammy Yeast.

was adhered chordwise to the wing skeleton and heat shrunk. Connectors were made to join the 6-ft dihedral sections to the center wing section.

The fuselage has a symmetrical cross-section, so the top and bottom halves were made full-length from the same mold. Bulkheads were installed for shape control and for the wing,



# CONCEPTUAL DESIGN OF A TWO-STAGE-TO-ORBIT VEHICLE

CASE WESTERN RESERVE UNIVERSITY

54-05  
160580  
P-9

A conceptual design study of a two-stage-to-orbit vehicle is presented. Three configurations were initially investigated with one configuration selected for further development. The major objective was to place a 20,000-lb payload into a low Earth orbit using a two-stage vehicle. The first stage used air-breathing engines and employed a horizontal takeoff, while the second stage used rocket engines to achieve a 250-n.m. orbit. A two-stage-to-orbit vehicle seems a viable option for the next-generation space shuttle.

## INTRODUCTION

The space shuttle system currently in use by NASA uses a conventional method of rocket boost to place a payload in orbit. The space shuttle is essentially a cargo bay assisting in no way on the ascent trajectory. Its advantage comes at the end of its flight as it uses aerodynamic forces to return for a landing and be refurbished and put back into orbit. Another method exists to place a payload in orbit: this method involves using aerodynamic forces to assist in the ascent trajectory. The vehicle can either be flown to orbit directly from a runway using aerodynamic lifting forces as much as practical, or it can be boosted by one or more stages. This vehicle would resemble the X-15 experimental research airplane in overall configuration.

It was decided to use horizontal takeoff for the boost stage of a Two-Stage-to-Orbit vehicle. The horizontal takeoff would use less fuel than a vertical-type liftoff system because the engine would not have to produce enough thrust to support the weight. It could make maximum use of aerodynamic forces for lifting instead of just contributing to the drag of a typical vertical launch system. Two stages were chosen for this vehicle. The first stage was to take advantage of the high specific impulse of air-breathing engines and aerodynamic lift as much as practical. The booster stage would then separate from the orbiter and return to land and be reused. The orbiter would then ascend using the lower specific impulse rocket propulsion, but without the weight of the now-inactive airbreathing engines, associated fuel system, and the inefficient aerodynamic lifting devices.

Three configurations of the Two-Stage-to-Orbit vehicle were proposed for research. The first proposal was to put the orbiter on the bottom or even inside the booster. The second was to take a more radical approach to the problem of orbiter location and place the orbiter on the front of the booster vehicle. The third and final proposal was to take a more conventional approach and place it on the top of the booster. These proposals had their advantages and disadvantages and were given equal consideration.

The bottom mounting would simplify separation problems with the orbiter being basically dropped from the booster. However, a larger vehicle would result and the landing gear system would be complicated. The propulsion system would also be split up, reducing the inlet efficiencies. This proposal was rejected. The orbiter position on the front of the booster would enable its wing to provide some lifting force in the ascent.

This would result in a reduced weight for the booster due to the smaller wing area required because the booster would not have to support the entire weight of the vehicle. With the orbiter positioned on the top, minimal contribution could be made to the total vehicle lift. However, the front-mounted orbiter would have a forward-moving center of gravity and would become excessively stable as the flight progressed. This would result in large trim drags. Also, the front-mounted orbiter would complicate landing gear design and also would complicate the separation procedures. The vehicle stability at separation would change dramatically, with a large rearward shift in the center of gravity. This could result in an instantaneous instability at separation and would require very large pitching control surfaces and fast, powerful actuators.

The front-mounted orbiter was rejected in favor of the more conventional "piggy-back" design. This design was then developed in more detail for the final conceptual design proposal.

## BOOSTER DESIGN

### Aerodynamics

**Configuration.** An overall booster-orbiter gross takeoff weight was determined through a series of size iterations to be 1,112,000 lb. The booster was to make up 820,000 lb of the total weight, with the orbiter taking up the remaining 300,000 lb. A wing loading of 84 lb per sq ft at takeoff was selected to give adequate takeoff performance without the need for auxiliary propulsion takeoff devices. An overall tailless delta configuration was chosen in order to reduce drag at high Mach numbers. The wing was configured as a double-delta planform, with the leading edge swept at 79°-60°. The initial 79° sweep was essentially a leading edge extension (LEX) designed to produce a pitch-up moment to help compensate for the rearward shift of the aerodynamic center as the vehicle passes from subsonic to supersonic flight. The LEX would also reduce the requirement for wing elevons to produce a downward force to maintain static stability.

All-moving tailplanes are located on the wing-tips. The purpose of the tailplanes is to minimize the decrease in lift associated with aft-mounted elevon controls on tailless delta configurations. They also increase the effectiveness of longitudinal control at low speeds and especially at takeoff, where the aircraft must be pitched to an angle of attack for a high lift coefficient. The

all-moving tailplanes were hinged at the trailing edge to increase their lift coefficients. At high speeds, when the required lift coefficient is small and where aileron reversal becomes a problem, the tailplanes are locked out and longitudinal control is taken over by the elevons. This would give the main wing a cranked-arrow type configuration resulting in better efficiency.

To minimize the effect of the elevon with the wing flow field, the directional control surfaces were placed between the wing and the tailplanes. This location gave an endplate-type effect and increased the effective aspect ratio (Fig. 1).

The fuselage was designed with an overall fineness ratio of 7.5. The fuselage was "coke-bottled" to decrease wave drag. The overall length of the booster vehicle was 303 ft with a wingspan of 218 ft (Fig. 2).

**Airfoil design.** The airfoil section of the booster was specially designed for this project for low wave drag, low heating load, and adequate longitudinal control at high speeds. Two proposals for airfoil sections were designed with the main difference in the leading edge radius. The first had a sharp leading edge to decrease wave drag. The second had a radius/chord ratio of 0.0083 (Fig. 3).

This blunt leading edge reduced the lift-to-drag ratios by approximately 50%. However, no active cooling would be used, and it did have adequate aerodynamic characteristics (Figs. 4 and 5). All supersonic aerodynamic calculations were done using a linearized flow technique.

**Computational fluid dynamics method.** A linearized flow technique was used to calculate the wing aerodynamic characteristics. Due to the formation of shock waves, the linearized flow technique could not be used at Mach numbers close to 1. The linearized flow model was used in a computer program that required the geometry to be entered in (Fig. 6). The program calculates total lift and drag on the wing by summing up the section lifts and drags by using similar airfoil sections. It calculates the lift and drag on an airfoil section of unit depth starting at the exposed root chord. It then uses a linear model to determine the new airfoil parameters. The planform of the wing must be entered into the program. A linear wing twist model is also incorporated.

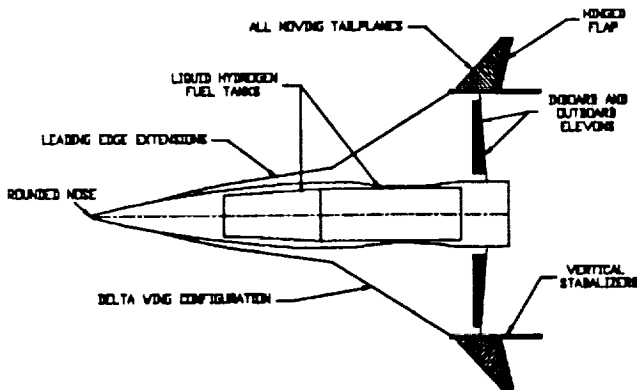
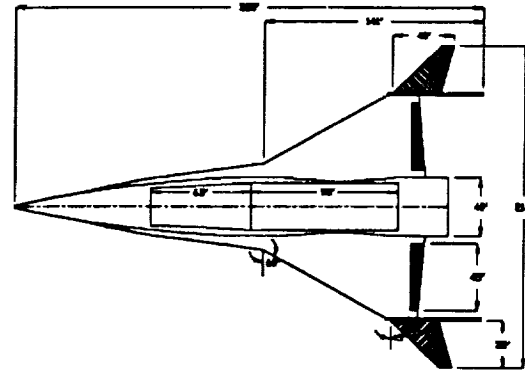


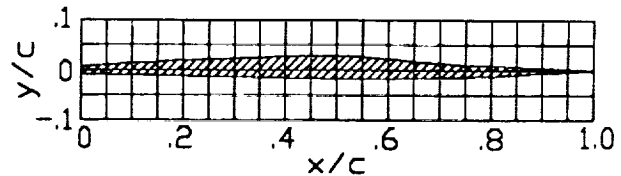
Fig. 1. Key design features.



Aircraft Specifications

|                    |                |
|--------------------|----------------|
| Aspect Ratio       | 1.8            |
| S ref              | 13,320 sq ft   |
| S exp              | 750 sq ft      |
| S lex              | 830 sq ft      |
| S tailplane        | 630 sq ft each |
| Sweep le           | 60°            |
| Sweep te           | -5°            |
| Taper Ratio        | 13%            |
| Sweep Tailplane le | 45°            |
| Sweep Tailplane te | 14°            |
| Taper Ratio Tail   | 25%            |

Fig. 2. Booster planform view.



Specifications

- Maximum thickness/chord ratio - 0.04 @ x/c = 0.5
- Leading edge radius/chord ratio - 0.0083
- Positive camber

Fig. 3. Airfoil section proposal number 2.

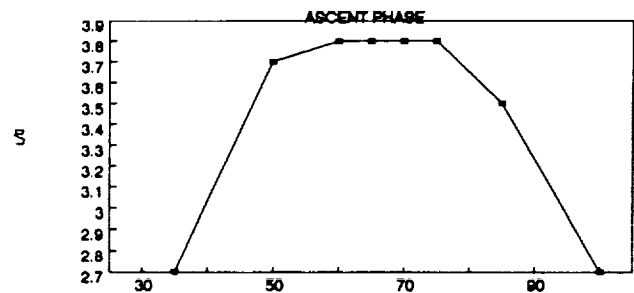


Fig. 4. Lit-to-drag ratio vs. altitude in thousands.

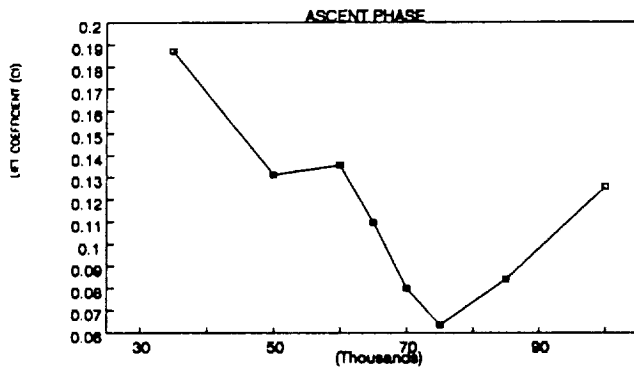


Fig. 5. Lift coefficient vs. altitude in thousands.

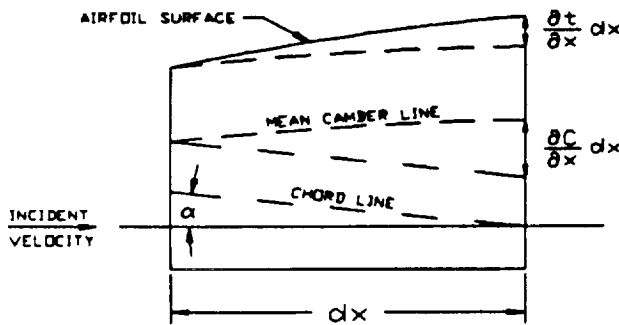


Fig. 6. Surface model used in linearized flow program.

## Propulsion

**Trajectory analysis.** The first consideration in the design of the propulsion system was to compute the trajectory of the booster. This was done by using the energy method. The energy method consisted of generating various curves and then analyzing them to obtain the most efficient flight path. These curves consisted of specific energy heights, specific fuel consumption contours, and a structural limit curve. A minimum fuel-to-climb analysis was then performed. This was accomplished by connecting the points of tangency of the energy heights and the fuel consumption curves, while remaining below the structural limit. For low Mach numbers, this strategy does not apply due to the fact that the curves are essentially perpendicular. Therefore, the aircraft will fly at relatively low altitudes until it reaches approximately Mach 0.8. At this point, the vehicle will climb to approximately 35,000 ft while remaining subsonic. At this point, the vehicle will perform what is sometimes referred to as a "transonic fall." The aircraft literally begins to fall or dive. This is advantageous in two ways. First the fall accelerates the vehicle through the transonic region and second, it requires no additional fuel to perform the maneuver.

After surpassing the transonic region, the minimum fuel-to-climb approach was performed. Near Mach 2.0 and beyond, the points of tangency of the two curves lie approximately along

the structural limit. Therefore, what was done was to follow a path that moved along the structural limit, but with a safety margin of 5000 ft at any point. The vehicle will follow this path and continue to accelerate up to Mach 6.5 at an altitude of 68,000 ft. At this point the vehicle would simply trade a portion of its kinetic energy for potential energy and quickly climb to the required 100,000 ft with no additional power required from the engines.

**Boundary layer considerations.** The beginning of the inlet is located 162 ft from the nose of the vehicle. At low Mach numbers the boundary layer that is built up from the forebody can be quite substantial. In light of this fact, boundary-layer thickness was calculated and subsequently graphed as a function of Mach number. The results revealed that the boundary-layer thickness ranged from 1.75 ft at subsonic speeds to 1.25 ft at supersonic speeds. A channel-type boundary-layer diverter was selected as a remedy to this problem. This method entails shifting, or in this case, lowering the propulsion system a certain calculated height. The diverter consists of two components. First, a diverter ramp, essentially a wedge, channels the flow around the inlet. In addition to the ramp, a splitter plate extends beyond the start of the diverter ramp to ensure that none of the boundary layer's outer edge is spilled into the inlet.

With this method of boundary-layer removal, the design is assured of strictly high-energy flow entering the turbojet for its full operation time. As for the ramjet, any excess boundary layer that might form can be funnelled through the turbojet. However, at higher Mach numbers, the boundary-layer thickness becomes smaller, so the channel-type diverter should suffice.

**Engine selection.** An over/under turboramjet with liquid hydrogen fuel was the engine of choice for the propulsion system. This engine was the most attractive choice due to its high performance characteristics. The turbojet produces 160,000 lb of static thrust. This was based on an existing turbojet engine scaled to meet the specifications of the mission. Five turbojets were selected based on the minimum thrust required, maximum weight, and size constraints. The engine measures 26 ft long with a maximum diameter of 4.5 ft. The ramjet's cross sectional area is approximately one-third of the turbojet's, measuring 1.5 ft.

**Inlet design.** The inlet used was a two-dimensional, dual-ramp, variable geometry, mixed compression inlet. Mixed compression was necessary to decelerate the flow and turn the flow back toward the engine compartments. For subsonic flight, the inlet is flat with a normal shock at the throat. As the vehicle accelerates, the inlet will continually change to induce the required oblique shocks. The inlet design Mach number is 6. This is a 7-shock inlet with two main shocks touching the cowl lip and then a series of reflected shocks and finally a normal shock at the throat. The first ramp measures 28 ft long while the second measures 40 ft. Maximum deflection is 2.5° and 3.5° respectively.

**Nozzle integration.** Once a cycle analysis was done on both the turbojet and the ramjet, and exit Mach numbers were obtained, a calculation of the exit area of the throat was performed. For the turbojet, a converging-diverging, variable geometry, axisymmetric nozzle was chosen. For the ramjet, a nonaxisymmetric, "half" converging-diverging nozzle was selected. Both of these nozzles satisfy the operating conditions of the system throughout the booster's ascent.

**Structure**

**Materials.** The booster is designed to achieve a speed of Mach 6 at an altitude of 100,000 ft. This hypersonic speed induces high skin friction on the vehicle. In turn, high temperatures on the order of 1000-2000° are encountered. The highest temperatures on the vehicle will occur at stagnation points. Areas of concern were the leading edges of the wings and the nose. The materials investigated included titanium aluminide, titanium-based metal matrix composites, carbon-carbon composites, ceramic-matrix composites, copper-matrix composites, and beryllium alloys. The final material selection consisted of titanium aluminide for the skin, a carbon-carbon composite for the nose, and titanium for the understructure.

**Weight breakdown.** The final weight breakdown of the booster is shown below in Table 1 and Fig. 7. This data includes the gross weight of the orbiter, which will be given in detail in the orbiter section of the report.

TABLE 1. Final weight breakdown of booster

|                  |              |
|------------------|--------------|
| Fuselage         | 209,361 lb   |
| Wings            | 230,729      |
| Vertical Tails   | 22,512       |
| Landing Gear     | 68,230       |
| Thrust Structure | 4,569        |
| Total Structure  | 535,401 lb   |
| Engines          | 80,400 lb    |
| Fuel Tank        | 16,000       |
| Subsystems       | 40,506       |
| Fuel             | 160,000      |
| Payload          | 301,300      |
| GLOW             | 1,133,000 lb |

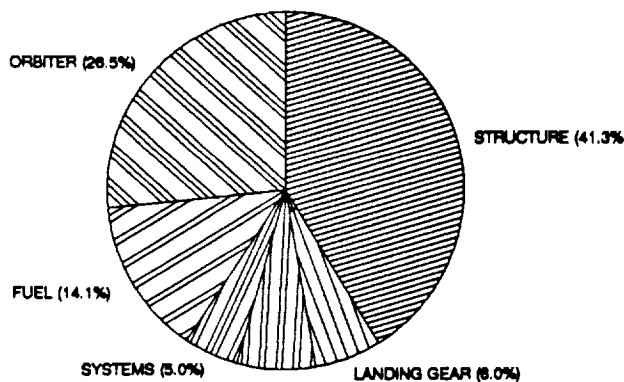


Fig. 7. Booster weight breakdown (takeoff configuration).

ignite its engines to create the first velocity impulse (20,245 ft/s). This impulse will place the orbiter into an elliptical orbit, which will have the 100,000-ft altitude as its perigee.

For the most efficient orbit transfer, the second major velocity impulse will occur at the apogee of the elliptical transfer orbit, which is located at 250 n.m. The velocity impulse (4125 ft/s) will place the orbiter into a circular orbit at this altitude. The

timing of the mission must be such that the orbiter and space station rendezvous at approximately this transfer point. In order to allow for a more flexible launch time, the orbiter may be placed in a circular holding orbit, although doing so will increase the necessary amount of fuel.

A third velocity impulse will be required to place the orbiter into the same elliptical transfer orbit so that it can deorbit.

**ORBITER DESIGN**

**Orbiter Trajectory**

During the entire trajectory, three major velocity impulses will be necessary. The first major velocity impulse will occur soon after separation from the booster. At the release point, the orbiter will be at 100,000 ft and traveling at Mach 6. At the maximum altitude of the booster's trajectory, the orbiter will be released, and the booster will perform a zero-g pushover. Once the booster has reached a safe distance, the orbiter will This final impulse is 4121 ft/s, bringing the total velocity impulse required for the mission to 28,490 ft/s. A diagram showing the various orbits is shown in Fig. 8.

**Aerodynamics**

**Wing design.** The initial size estimate for the orbiter wing was based on conditions at landing. Given a lift coefficient of 1.0, a density at sea level of 2.3675E-03 slugs/cu ft, and a landing speed of 300 ft/s, a wing loading of 106.5 lb per sq ft was calculated. Given an initial weight estimate of approximately 90,000 lb, a wing area of 880 sq ft was found. However, if this wing area was implemented, the majority of its surface would lie within the fuselage, leaving very little exposed area for control. Therefore the wing area was increased by approximately 50% to 1200 sq ft. A diagram of the wing, showing all relevant data, is presented in Fig. 9.

The airfoil used for both the wing and tails was designed to withstand the high temperatures encountered during reentry. It was determined that a 6-in leading edge radius would safely withstand the heating values. Therefore, a symmetric airfoil with a 6-in leading edge radius and a maximum thickness-to-chord ratio of 12% was designed.

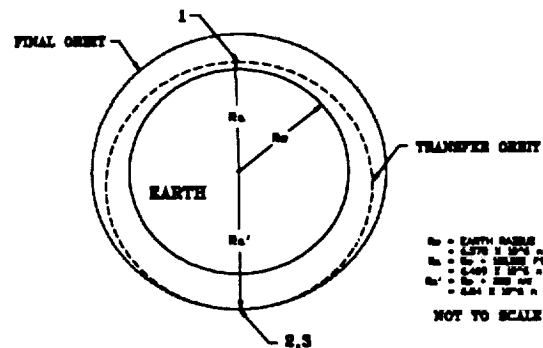


Fig. 8. Orbiter trajectories.

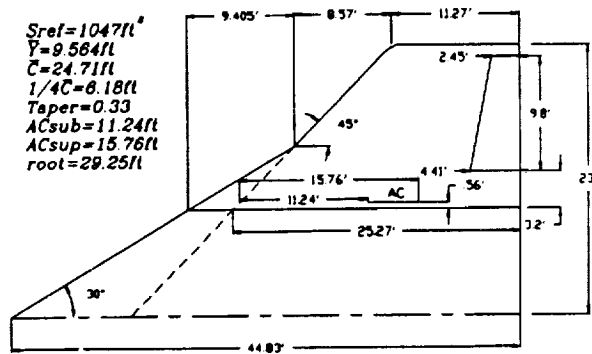


Fig. 9. Wing dimensions.

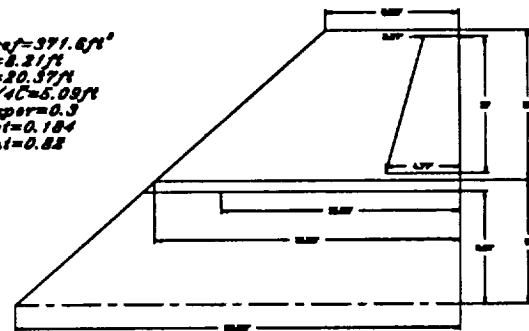


Fig. 10. V-tail dimensions.

**Tail design.** In an effort to minimize weight, the vertical and horizontal tails were replaced by a V-tail. The V-tail was intended to reduce the wetted area of the tails. With a V-tail, the horizontal and vertical tail forces are the result of horizontal and vertical projections of the force exerted upon the "V" surfaces. In addition, V-tails offer reduced interference drag.

A trapezoid was selected as the basic shape of the V-tail in an attempt to avoid complexity. An 11 ft span from the outer edge of the fuselage was arbitrarily selected and used in the initial calculations. Figure 10 shows a side-view of the V-tail and includes all relevant data pertaining to the V-tail.

**Stability and control.** Both conditions for static longitudinal stability were met by the orbiter for all four flight regimes: supersonic flight with payload, supersonic flight without payload, subsonic flight with payload, and subsonic flight without payload. The moment coefficient at an absolute angle of attack of  $0^\circ$  is positive provided the angle of attack of the orbiter is positive. Also, the slope of the moment coefficient about the center of gravity is negative for all flight conditions.

The static margins for the various flight regimes differ considerably. The wings were placed on the orbiter so as to provide a minimum static margin of 10%. This occurs when the orbiter is flying subsonically without a payload. However, due to the dramatic shift in the location of the center of gravity when a payload is present, the static margin increases to 50% when the orbiter is flying supersonically and 40% when it is subsonic. These large static margins would produce excessive trim drags which would make it difficult to pilot the orbiter.

**Re-entry trajectory.** The reentry trajectory from 250 n.m. was calculated in two parts. The first section of the reentry was from orbital altitude to 300,000 ft. At these high altitudes, the atmosphere is so thin that aerodynamic effects are negligible. In the second section, below 300,000 ft, aerodynamic forces are no longer negligible.

Above 300,000 ft, the reentry trajectory was calculated using the equations of motion for a two-body problem. These equations were then integrated to determine the vehicle's position, velocity, and angle of descent as a function of time. A plot of the orbiter's altitude as a function of time is shown in Fig. 11.

Below 300,000 ft, the reentry was determined by aerodynamic forces. The equations of motion were again integrated to determine the altitude, velocity, and angle of descent of the

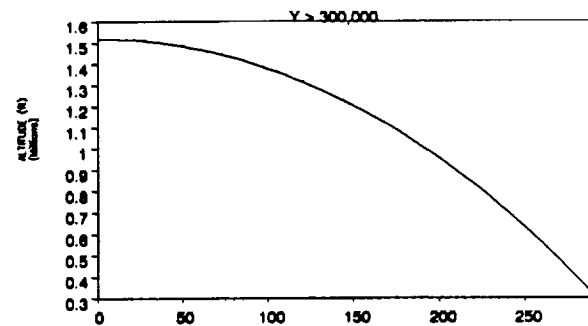


Fig. 11. Orbiter reentry (&gt;300,000 ft vs. time).

orbiter as a function of time. A check was included to ensure that the deceleration would not exceed 3 g. A plot of the orbiter's altitude vs. time for this section is shown in Fig. 12.

Overall, the orbiter's reentry path is similar to that of the shuttle's. However, there are a large number of oscillations present in the data. These oscillations could be dampened with a controller that was too complex to develop in the allotted time period.

**Aerodynamic heating.** The aerodynamic heating incurred upon atmospheric reentry affects many aspects of the orbiter's design, most importantly, structure weight. The temperatures that occur during a typical reentry require that the windward surfaces of the orbiter be covered with a temperature-resistant material. The available materials can result in a large weight penalty; therefore, the aerothermodynamic environment of the orbiter was carefully considered.

Both temperature and heat transfer rate, along with heat load, were calculated at the orbiter nose and the wing leading edge, two areas of severe heating effects. These quantities are functions of velocity, altitude, material emissivity, and airframe geometry.

The results of the heating calculations can be seen in Figs. 13 and 14. The maximum heat load that the material can withstand is 70,480 Btu/sq ft. The heat loads for the orbiter's nose and leading edges are both well below this value. While the maximum values of  $T_w$  at the nose and leading edges appear excessively high, this is due to the oscillatory nature of the reentry trajectory. If the reentry could be managed more effectively and the oscillations in velocity and altitude could be reduced, the maximum values of  $T_w$  would be more

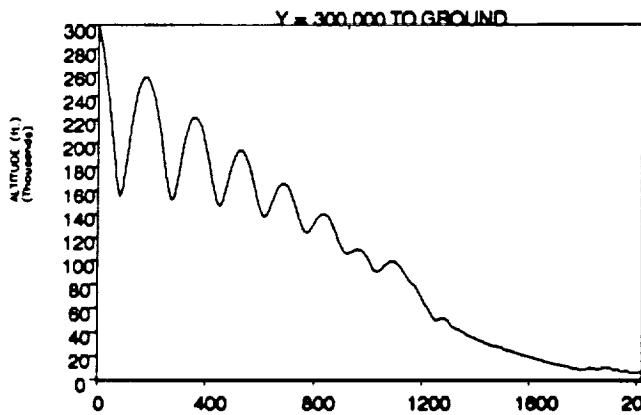


Fig. 12. Orbiter reentry (300,000 ft to ground vs. time).

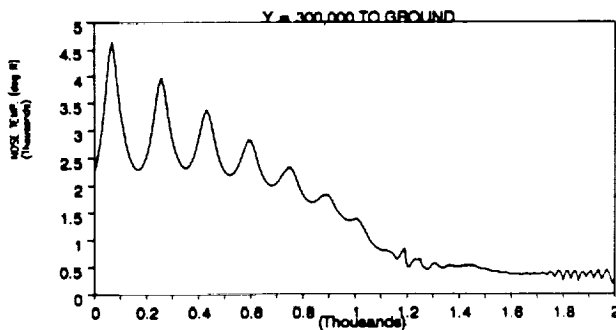


Fig. 13. Orbiter reentry (Nose temperature vs. altitude).

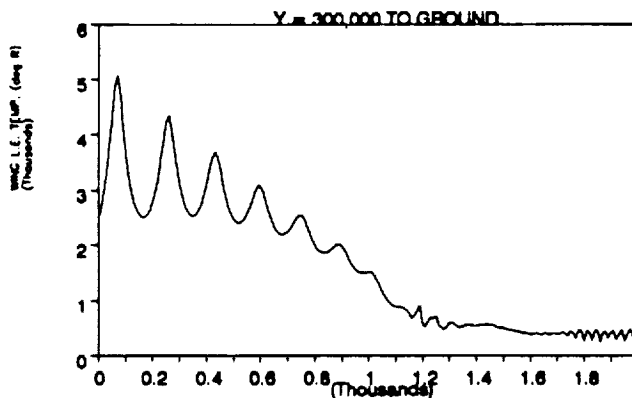


Fig. 14. Orbiter reentry (Leading edge temperature vs. altitude).

reasonable. Wall temperatures around 3000°F would be possible. This temperature is within the range that materials available in the near future will withstand without severe weight penalty.

**Landing performance.** The final aerodynamic calculation was to investigate the distance traveled by the orbiter once it touched down. Two landing conditions were considered:

landing with a payload and landing without a payload. The first of these yielded a total ground roll of approximately 8600 ft, and the second resulted in a total ground roll of just over 6700 ft. Both of these conditions assume that the orbiter's fuel tanks are empty.

### Propulsion

In designing the propulsion system for the orbiter, several performance requirements had to be met. It was of primary importance that the system be sufficient to provide the necessary thrust to obtain orbital velocity and to facilitate orbital transfers. A second requirement was that the vehicle be equipped with control thrusters to allow for translation and rotation in all axes. Encompassing all other requirements was the stipulation that the overall system weight, including propellants, be as low as possible.

The first step taken in the design of the system was to research the available propellants and to choose that primary fuel/oxidizer combination that would best meet the stated requirements. After examining several possible combinations, it was decided to use liquid hydrogen as the fuel and liquid oxygen as the oxidizer. Having selected the propellants, it was then possible to proceed with the design of the system components.

**Main engine.** The function of the main engine in this vehicle is to provide the necessary thrust to reach orbital velocity from an initial release velocity of 6000 ft/s. It was decided that the main engine would not be used for orbital transfers and thus could be designed specifically for high-thrust, long-duration firing, eliminating major concerns for transient operation and wide throttling requirements. These functional requirements can be met by the "next-generation SSME," which was specified as the main engine. Estimates were then made on the engine's performance based upon recent data and expected advances in materials technology in future years.

**Orbital maneuvering engines.** The OMEs serve to provide the required thrust for orbital transfers and major maneuvering. Thus the engines must be designed to be restartable and to have controllable thrust vectors for precise maneuvering. Based on the preliminary configuration of the orbiter fuselage, it was decided that a pair of engines, mounted on each side of the main engine would be the most effective configuration. An advantage of this type of mounting is that the maneuvering engines need only be gimballed to obtain pitching moments, since yaw moments can be obtained by simply decreasing the thrust from one of the OMEs. As for fuel, since the hydrogen and oxygen tanks are a permanent part of the vehicle, it was decided that it would be advantageous to design the engines to operate with this fuel/oxidizer combination.

The actual engine design was based primarily on information presented in a paper entitled *Advanced LO<sub>2</sub>/LH<sub>2</sub> Space Engine Characteristics*, published by Rocketdyne. The final design has both engines gimballed for thrust vector control, and the exit plane of the OMEs coinciding with the exit plane of the main engine, to avoid external nozzle damage. A single propellant feed system was chosen with separate flow control valves for each engine to facilitate thrust modulation. A schematic of the mounting scheme can be seen in Fig. 15.

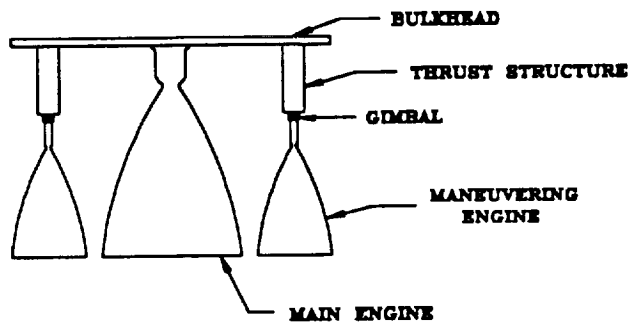


Fig. 15. Orbital engine mounting.

**Attitude control rockets.** The attitude control rockets have the primary function of controlling the orientation of the vehicle while in space. Thus a main requirement of these rockets is that enough thrust is produced so that maneuvers may be performed within a reasonable time allotment. A second requirement is that each rocket can be restarted thousands of times, and that each burn time be controllable to within a few hundredths of a second, providing precise maneuvering capabilities.

A detailed analysis was performed and it was determined that a minimum of 16 thrusters would be needed, and that a redundant thruster for each required should be included, insuring that no one thruster failure could disable the attitude control system. For fuel, it was decided to use monomethyl hydrazine and nitrogen tetroxide with a gas pressure feed system. Major engine specifications are presented in Table 2.

TABLE 2. Engine specifications

|                           |                |
|---------------------------|----------------|
| SSME:                     |                |
| Maximum Thrust            | 493,000 lb     |
| $I_{sp}$                  | 493 s          |
| Weight                    | 5362 lb        |
| OME:                      |                |
| Maximum Thrust            | 7500 lb (each) |
| $I_{sp}$                  | 493 s          |
| Weight                    | 266 lb (each)  |
| Attitude Control Rockets: |                |
| Maximum Thrust            | 900 lb (each)  |
| $I_{sp}$                  | 300 s          |
| Weight                    | 30 lb (each)   |

## Structures

**Wing design.** Once the total area and shape of the wing was determined, it was possible to make estimates of the internal structural layout and the skin thicknesses. A sparswise lift distribution was determined to range from 2081-989 lb at the tip of the wing. These lift calculations were based on area increments from the root to the tip of the wing, using a wing loading of 84 lb/sq ft. The wing weight was estimated to be 4.5 lb/sq ft. The net lift was found by subtracting the incremental wing weight from the lift. From this, the shear force and bending moment distributions were calculated.

The internal structure of the wing consists of three spars. Two spars are load bearing and are located at 0.2 and 0.8 chord lengths from the leading edge. The third spar is smaller and non-load bearing. It is used for lateral support of the ribs. The two load-bearing spars are located on the lower edge of the wing, while the third is on the upper edge. These spars were modeled as I-beams. The leading edge spar is a 12-in I-beam with a flange width of 6 in, a thickness of 0.4375 in, and a web thickness of 0.25 in. The trailing edge spar is tapered from a height of 12 in to 3 in at the tip. It has a flange dimension of 6 in by 0.3125 in and a web thickness of 0.25 in. The center spar has a flange that is 3 in by 0.25 in and a web that is 6 in by 0.25 in. The two load bearing spars are connected by 12-in I-beam carrythroughs. The carrythroughs are fastened to the fuselage frame members as well as the wing fillets.

The ribs are fabricated from a sheet of 1/8-in thick titanium with 70% of the area cut out for weight reduction. Each rib has a 2-in-wide flange around it to facilitate the skin mounting. There are 10 ribs per wing. A schematic of the wing structure is shown in Fig. 16.

**Fuselage design.** The fuselage is composed of circular frame elements that are connected by a network of 12 stringers placed equally around the circumference of the fuselage. The frame element was designed to fit the size requirements of the tanks, payload area, and outer shell. The frame element consists of a fabricated circular I-beam with a 12-in-high web and a 2-in-wide flange on both sides. Both the web and flanges were constructed from 1/8-in-thick titanium. To minimize weight, we included 24 6-in-diameter cutouts, which are located in pairs between the spars. Figure 17 shows this frame element. These frame members are connected by a series of 12 stringers. These I-beam-shaped members have a 12-in-high web and a 2-in-wide flange, each of which are 1/8-in thick. There are 16 frame members spaced equally along the length of the fuselage. In addition, there are three bulkheads: two are fore and aft of the payload bay and a third serves as the thrust structure to which the engines are mounted.

**Thermal protection system.** The selection of the thermal protection system was based upon weight, maximum temperature limit, system simplicity, and available information. The

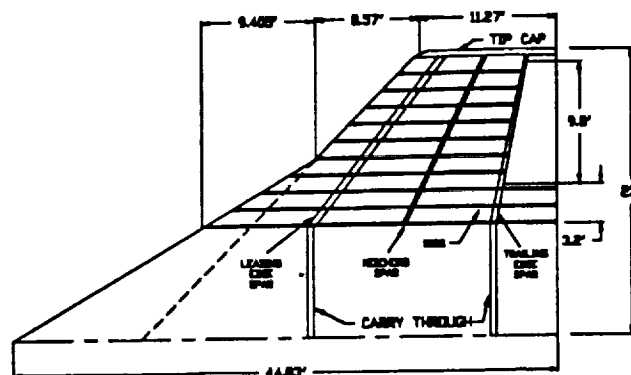


Fig. 16. Wing structure.

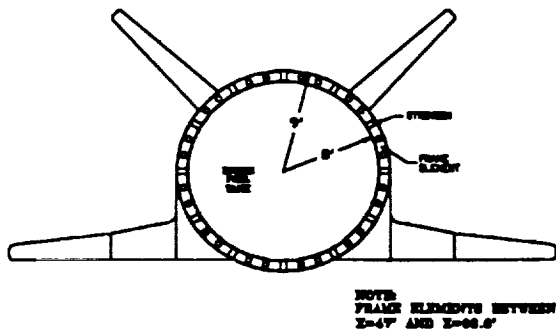


Fig. 17. Structural cross section.

Fiber-Fiber Rigid Composite Insulation (FRCI) system was selected. FRCI is a ceramic composite silica and aluminabosilicate fiber. This serves as the insulation layer.

A coating of RCG is applied to the FRCI insulation to protect it from aerodynamic stresses. Polymide graphite was selected as the structural skin of the orbiter. It has an operational temperature limit of over 500°F and is very lightweight. The insulation tiles are glued to the polymide graphite skin with RTV 560, a high-temperature adhesive. A final weight breakdown of the orbiter can be found in Table 3 and Fig. 18 along with a two-view of the orbiter in Fig. 19.

TABLE 3. Orbiter weight breakdown (lb)

|                                    |                |
|------------------------------------|----------------|
| Wings                              | 4,985          |
| Wing (TPS)                         | 2,740          |
| V-Tail                             | 1,500          |
| V-Tail (TPS)                       | 529            |
| Fuselage                           | 10,063         |
| Fuselage (TPS)                     | 9,203          |
| Nose                               | 3,000          |
| Nose (TPS)                         | 2,510          |
| Nose Gear                          | 1,000          |
| Main Gear                          | 4,000          |
| LOX Tank                           | 1,634          |
| LH <sub>2</sub> Tank               | 3,811          |
| N <sub>2</sub> O <sub>4</sub> Tank | 50             |
| MMH Tank                           | 43             |
| <b>Total Structure</b>             | <b>45,067</b>  |
| <b>Total TPS Weight</b>            | <b>14,982</b>  |
| <b>Propulsion Group</b>            |                |
| Main Engine                        | 5,362          |
| OMEs                               | 532            |
| Total                              | 5,894          |
| <b>Subsystems</b>                  |                |
| Control                            | 10,000         |
| Hydraulic                          | 5,000          |
| Crew Compartment                   | 4,280          |
| Total                              | 19,280         |
| <b>Total Empty Weight</b>          | <b>70,241</b>  |
| <b>Maximum Payload</b>             | <b>20,000</b>  |
| <b>Fuel Weights</b>                |                |
| LOX                                | 179,600        |
| LH <sub>2</sub>                    | 29,930         |
| N <sub>2</sub> O <sub>4</sub>      | 1,010          |
| MMH                                | 490            |
| Total                              | 211,030        |
| <b>Gross Weight</b>                | <b>301,271</b> |

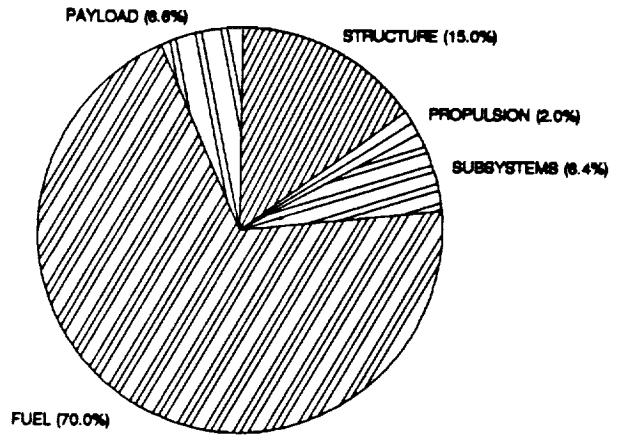


Fig. 18. Weight breakdown at gross takeoff weight.

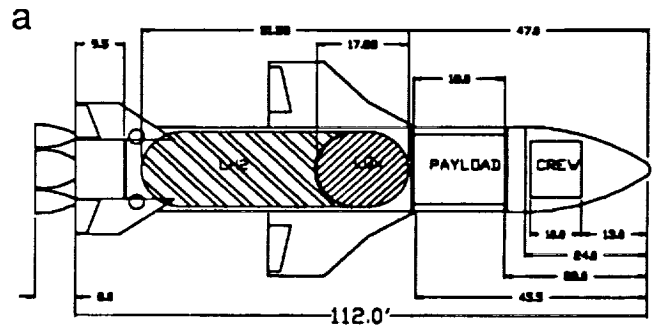
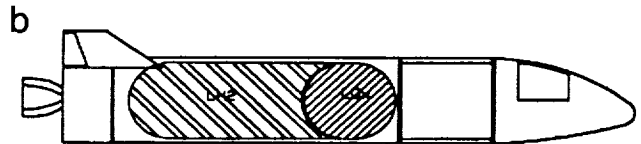


Fig. 19. (a) Orbiter top view.



(b) Orbiter side view.

### CONCLUSION

The final design is presented in Fig. 20. This conceptual design has the following three advantages over the space shuttle. First, the use of high specific impulse air-breathing engines during its initial ascent reduces the mission's fuel requirements and thus the cost of placing the payload into orbit. Second, unlike the space shuttle, this vehicle was designed to be completely reusable, thereby further reducing its cost by eliminating the need for substantial refurbishment after each mission. Third, due to the reduction in turnaround time, NASA's profitability would increase both in absolute and in per unit terms by expanding the capacity to launch more missions per year and reducing the cost of each as well.

Unlike proposed single-stage-to-orbit vehicles, the orbiter of this design does not have the added weight of air-breathing engines to carry into space. This reduces the fuel requirement, thereby further reducing the cost of each mission. This conceptual design of a two-stage-to-orbit vehicle appears to be a viable option for the next-generation space shuttle.

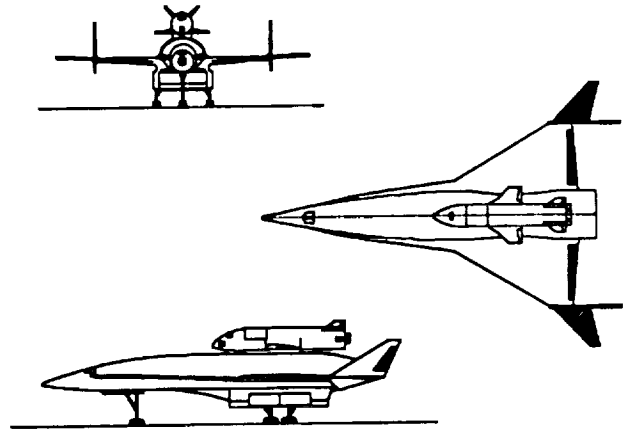


Fig. 20. Final design of two-stage-to-orbit vehicle.



**PRELIMINARY DESIGN STUDIES OF AN ADVANCED  
GENERAL AVIATION AIRCRAFT**

**THE UNIVERSITY OF KANSAS**

55-05  
160581  
p. 12

Preliminary design studies are presented for an advanced general aviation aircraft. Advanced guidance and display concepts, laminar flow, smart structures, fuselage and wing structural design and manufacturing, and preliminary configuration design are topics to be discussed. This project was conducted as a graduate-level design class under the auspices of the KU/NASA/USRA Advanced Design Program in Aeronautics. This paper will present the results obtained during the fall semester of 1990 (Phase I) and the spring semester of 1991 (Phase II).

**NOMENCLATURE**

|       |  |
|-------|--|
| ACQ   | Acquisition                                    |
| AEP   | Airplane estimated price                       |
| APT   | Advanced Personal Transport                    |
| ATC   | Air traffic control                            |
| C/A   | Coarse/acquisition                             |
| CAT   | Category                                       |
| COM   | Communications                                 |
| DEU   | Drive electronics unit                         |
| DISP  | Disposal                                       |
| DMU   | Digital memory units                           |
| EMI   | Electromagnetic interference                   |
| FAA   | Federal Aviation Administration                |
| FBL   | Fly-by-light                                   |
| FBW   | Fly-by-wire                                    |
| GA    | General aviation                               |
| GPS   | Global positioning system                      |
| HERF  | High-energy radio frequencies                  |
| HSNLF | High-speed natural laminar flow                |
| HUD   | Heads-up display                               |
| IFR   | Instrument flight rules                        |
| IGG   | Integrated GPS/Glonass                         |
| ILS   | Instrument landing system                      |
| INS   | Inertial navigation system                     |
| KU    | The University of Kansas                       |
| LCC   | Life cycle cost                                |
| LCD   | Liquid crystal display                         |
| MAC   | Mean aerodynamic chord                         |
| MAN   | Manufacturing                                  |
| NAS   | National Airspace System                       |
| NAV   | Navigation                                     |
| NLF   | Natural laminar flow                           |
| OPS   | Operations                                     |
| RDTE  | Research, development, testing, and evaluation |
| RPM   | Rotations per minute                           |
| SSSA  | Separate surface stability augmentation        |
| T-O   | Take-off                                       |
| USRA  | Universities Space Research Association        |
| VFR   | Visual flight rules                            |

Flight control systems of today's GA airplanes are still the same as those of 50 years ago: cables, pulleys, and bell-cranks: this represents 2-3% of the design takeoff weight of the airplane. In addition, tailoring mechanical control systems to today's handling quality requirements is fraught with problems, most of these caused by friction and cable-tension problems associated with mechanical control systems. By switching to a fly-by-light or fly-by-wire system, much of this weight and all of the handling quality problems can be eliminated.

Cockpit instrumentation has been improved since 1945 only in the sense that the instruments are more capable and marginally more reliable. The typical GA cockpit has anywhere from 150 to 300 clocks, bells, whistles, and switches. In terms of airplane design takeoff weight, this amounts to 3-10%. Revolutionary cockpit design would start from scratch: with an empty panel. Through a functionality analysis that gives priority to user friendly features, a new cockpit design should emerge with only very few displays, bells, whistles, and switches. This should eliminate a lot of weight and complexity. Heads-up displays should be considered as a replacement of all existing displays.

Navigation and communication with the FAA's ATC system in today's GA airplanes is very cumbersome and extremely user unfriendly. Since 1945 the ATC environment has grown more and more hostile toward GA airplanes. Most of these procedures can and should be automated through the use of onboard microprocessors. ATC coupling with GPS/Glonass should be considered. Optical disk storage of en-route and terminal guidance should be considered.

Airplane structural design and manufacturing is still done mostly with conventional riveted aluminum materials. Recent developments with Arall (Aramid-aluminum), Glare, and other types of composite materials opens the way to significantly lighter structures. The recently developed outside-in tooling approach makes it possible to design even aluminum structures with surface tolerances that allow for the attainment of laminar flow. In addition, electrical signal and power paths should be integrated into the structure so that these paths also carry part of the air loads.

The flight controls in GA airplanes are still so-called "rate command control systems." The potential exists to change this to attitude or decoupled response command systems. This is, in fact, the logical way to proceed if FBL and/or FBW are used.

**1. INTRODUCTION**

Since 1945, when Beech Aircraft corporation came up with the Model 35 Bonanza, speed and range performance of GA airplanes have not improved to any significant extent. With few exceptions, GA airplanes of today are still turbulent flow airplanes. Laminar flow airplanes are now feasible.

44 INTENTIONALLY BLANK

This would lead to the complete elimination of many accidents that are fundamentally caused by the rate command nature of today's flight controls.

The purpose of this paper is to present the preliminary design results of an advanced aircraft design project at the University of Kansas. The goal of the project was to take a revolutionary look into the design of a general aviation aircraft including those items mentioned above. This project was conducted as a graduate-level design class under the auspices of the KU/NASA/USRA Advanced Design Program in Aeronautics. The class is open to aerospace and electrical engineering seniors and first-level graduate students. This paper will present the results obtained during the fall semester of 1990 (Phase I) and the spring semester of 1991 (Phase II). References 1 through 17 are reports documenting the work completed in Phase I and references 18 through 25 document the work completed in Phase II.

## 2. PRELIMINARY SIZING

A market survey was conducted to create a database of information that could be used as a reference in preliminary design work. It was also used to identify and compare current and potential designs that would offer competition for the planned design, provide specific aircraft information characteristics to aid in configuration design and development, and identify potential voids in the current market. The market survey included 16 aircraft that were considered to be potential competitors for the planned design in the 4-10 passenger range. The two main competitors in the survey were considered to be the Piaggio P-180 Avanti and the Socata/Mooney TBM-700. Performance data for the 16 aircraft were collected. These data included range, number of passengers, maximum cruise speed, rate of climb, and service ceiling. By plotting the range vs. number of passengers for the 16 aircraft, voids in the general aviation market were located. The Advanced Personal Transport (APT) was selected to be a 6-passenger aircraft capable of a 1200-n.m. range. The average values of selected performance parameters for the 16 aircraft are listed in Table 1.

The mission specifications were selected to make the APT competitive with those aircraft studied in the market survey. The mission specifications are 6 passengers, 175 lb each, with 30 lb of baggage each; range of 1200 n.m. with reserves of 10% mission fuel; 420-kt cruise speed; takeoff field length of 2000 ft at sea level conditions; landing field length of 2500 ft at sea level conditions; maximum rate of climb of 4000 ft/min;

TABLE 1. Average values of performance parameters.

|             |                        |
|-------------|------------------------|
| 7575 lb     | Empty weight           |
| 13244 lb    | Maximum takeoff weight |
| 55.2 psf    | Maximum wing loading   |
| 2.73 lb/lb  | Maximum power loading  |
| 2730 ft     | Takeoff field length   |
| 3797 ft/min | Maximum rate of climb  |
| 389 kt      | High-speed cruise      |
| 1858 n.m.   | Maximum range          |
| 38000 ft    | Service ceiling        |
| \$4 million | Cost                   |

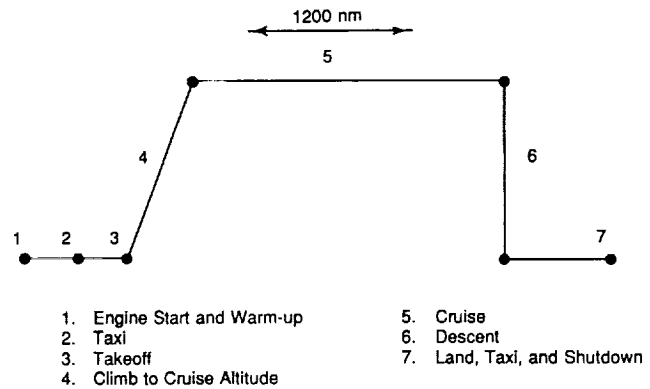


Fig. 1. Mission Profile.

twin turboprop powerplant; 8000-ft cabin at 45,000 ft; FAR 23 certification; and 45,000-ft service ceiling.

The mission profile is shown in Fig. 1.

## 3. CONFIGURATION DESCRIPTION AND CABIN LAYOUT.

Two configurations, a tractor and a pusher, were designed to meet the mission specifications. A twin-boom three-surface configuration was selected for the APT pusher layout. This configuration provides a high degree of structural synergism by allowing the aft pressure bulkhead, wing carry-through mount, and main landing gear mount to form one integral fail-safe unit. Recent research<sup>(26,27)</sup> has shown that, for the same basic geometry, three-surface configurations typically have a higher trimmed lift-to-drag ratio than either conventional or canard configurations. The research has also shown that three-surface layouts can have lower trim drag over a wider center of gravity range than do two-surface layouts. Flap-induced pitching moments can be automatically trimmed by incorporating a flap on the canard that is "geared" to wing flap deflection.

A three-view and table of geometry of the final design is shown in Fig. 2. One of the primary features of this layout is that it was designed to attain a high extent of NLF. All flying surfaces use NLF airfoils, and the fuselage features a pusher propeller and smooth NLF forward fuselage. The wing is swept forward 15° (measured at the leading edge), and features a midwing location to decrease fuselage interference drag. A strake is incorporated at the wing root to stiffen the wing root against the high torsional loads inherent with forward swept wings. The strake also provides local strengthening for tail boom support and increases the available volume for fuel.

The horizontal tail was located at the top of the vertical tails to place it above the propeller slipstream, which reduces structural noise and fatigue and should allow attainment of natural laminar flow on the tail surface. Ventral fins mounted on the underside of the tail booms insure against prop strikes if the airplane is over-rotated. A standard retractable tricycle landing gear arrangement was selected, with the nose gear retracting forward into the nose and the fuselage-mounted main gear retracting aft into the area underneath the wing. Crosswind landing gear is used to allow the APT to land in a crabbed

Table of Geometry of the Pusher APT Configuration

|                           | <u>Wing</u>        | <u>Horiz. Tail</u> | <u>Vert. Tail</u> | <u>Canard</u> |
|---------------------------|--------------------|--------------------|-------------------|---------------|
| Area (ft <sup>2</sup> )   | 130                | 31.7               | 38.6              | 8.0           |
| Span (ft)                 | 36.0               | 11.9               | 6.5               | 7.8           |
| Aspect Ratio              | 9.97               | 4.5                | 1.1               | 3.8           |
| Sweep Angle               | -15°(@L.E.)        | 0°                 | 40°(@L.E.)        | 0°(@0.10c)    |
| M.A.C. (ft)               | 3.28               | 2.6                | 4.2               | 1.00          |
| Taper Ratio               | 0.35               | 1.0                | 0.4               | 0.70          |
| Dihedral Angle            | 3°                 | 0°                 | 90°               | -5°           |
| Incidence Angle           | 1°                 | 0°                 | 0°                | 3°            |
| Twist Angle               | 0°                 | 0°                 | 0°                | 0°            |
| Airfoil                   | Custom NLF Section | "                  | "                 | "             |
| Thickness Ratio           | 0.13               | 0.09               | 0.09              | 0.11          |
| Control Surf. Chord Ratio | 0.25               | 0.30               | 0.32              | N/A           |
| Control Surf. Span Ratio  | 0.72-1.00          | 0-0.98             | 0.20-0.85         | N/A           |
| Flap Chord Ratio          | 0.25               | N/A                | N/A               | 0.35          |
| Flap Span Ratio           | 0.19-0.72          | N/A                | N/A               | 0.21-1.00     |

|                  | <u>Cabin</u> | <u>Fuselage</u> | <u>Overall</u> |
|------------------|--------------|-----------------|----------------|
| Length (ft)      | 11.17        | 29.33           | 34.75          |
| Max. Height (ft) | 4.67         | 5.42            | 9.92           |
| Max. Width (ft)  | 4.58         | 4.92            | 43.40          |

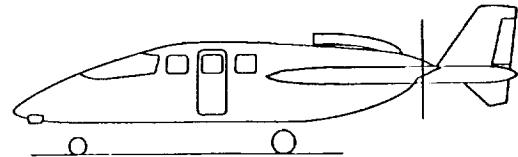
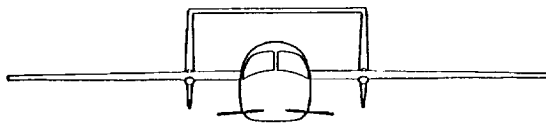
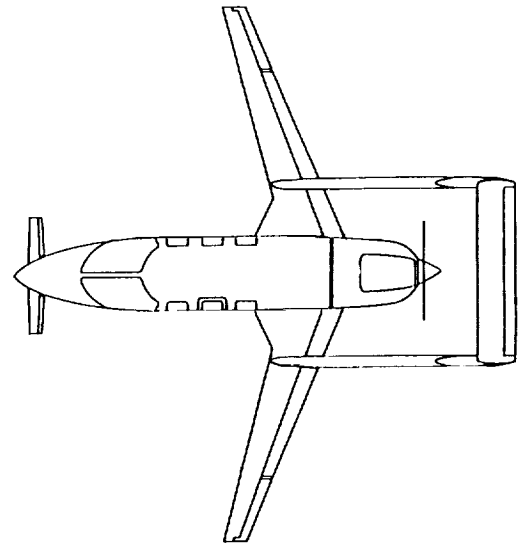


Fig. 2. Three-view of the APT pusher configuration.

configuration. Cabin access is provided by an air-stair door on the left fuselage, which is a convenient feature usually found only on larger turboprops and business jets.

A conventional configuration was selected for the APT tractor layout. This layout provides good balance and flexible wing placement. It should also reduce development costs due to the extensive database of similar airplanes. A three-view and table of geometry of the tractor layout are shown in Fig. 3. As can be seen, the layout is rather conventional and is similar to many popular GA airplanes.

To allow a fair comparison with the pusher configuration, the tractor configuration uses the same cabin layout (Fig. 4) and wing geometry. However, the pusher design was iterated to meet the mission specifications, resulting in a smaller wing than the tractor configuration, the design of which was not iterated. A low wing arrangement was selected to allow the wing carry-through structure to pass under the cabin and to allow simple wing mounted landing gear. A T-tail arrangement was used to remove the horizontal tail from the turbulence of the fuselage and propwash, which can allow a small reduction in tail area and should allow attainment of NLF on the tail surface. A standard retractable tricycle landing gear arrangement was selected, with the nose gear retracting underneath the engine and the main gear retracting into the wing. Crosswind gear

is also used for the tractor configuration. Cabin access is achieved by first stepping up onto the wing and then entering a side-hinged door located on the left side of the fuselage.

Unlike the pusher configuration, there was no practical place in the fuselage of the tractor configuration to mount the weather radar. Consequently, the radar was mounted in a pod on the left wing, similar in arrangement to that of the Cessna P-210 Centurion.

The cabin layout of the APT was sized by comparison with similar current GA airplanes, and the final layout is shown in Fig. 4. The cabin dimensions selected for the APT are relatively large compared to similar airplanes because current small GA airplanes are not known for cabin comfort. To improve marketability, the cabin of the APT was designed to ease this problem as much as practical, without causing undue weight or drag penalties. The fuselage cross section of the APT is shown in Fig. 5, and features a circular upper and a rounded square lower cross section. This arrangement was selected as a compromise between the structural efficiency of a fully circular cross section and the low wetted area and volume penalties of a fully square cross section. An illustration of a proposed APT cockpit layout is shown in Fig. 6. The layout features two sidestick controllers, one on each side of the cabin, and a center console containing the speed control handle. Due to the high degree of automation

Table of Geometry of the Tractor APT Configuration

|                           | Wing               | Horiz. Tail | Vert. Tail |
|---------------------------|--------------------|-------------|------------|
| Area (ft <sup>2</sup> )   | 151.7              | 36.4        | 27.3       |
| Span (ft)                 | 42.7               | 12.8        | 5.6        |
| Aspect Ratio              | 12.0               | 4.5         | 1.2        |
| Sweep Angle               | -15°(@L.E.)        | 9°(@L.E.)   | 40°(@L.E.) |
| M.A.C. (ft)               | 3.89               | 2.87        | 5.7        |
| Taper Ratio               | 0.35               | 0.7         | 0.4        |
| Dihedral Angle            | 3°                 | 0°          | 90°        |
| Incidence Angle           | 1°                 | 0°          | 0°         |
| Twist Angle               | 0°                 | 0°          | 0°         |
| Airfoil                   | Custom NLF Section | "           | "          |
| Thickness Ratio           | 0.13               | 0.09        | 0.09       |
| Control Surf. Chord Ratio | 0.25               | 0.30        | 0.32       |
| Control Surf. Span Ratio  | 0.72-1.00          | 0-0.98      | 0.20-0.85  |
| Flap Chord Ratio          | 0.25               | N/A         | N/A        |
| Flap Span Ratio           | 0.19-0.72          | N/A         | N/A        |
|                           | Cabin              | Fuselage    | Overall    |
| Length (ft)               | 11.17              | 29.33       | 34.75      |
| Max. Height (ft)          | 4.67               | 5.42        | 9.92       |
| Max. Width (ft)           | 4.58               | 4.92        | 43.40      |

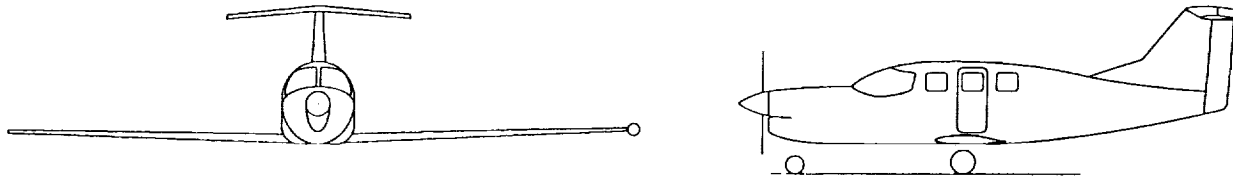


Fig. 3. Three-view of the APT tractor configuration.

in the flight control system, neither rudder pedals, brake pedals, flap handles, or landing gear handles are required<sup>(12)</sup>. The layout features a HUD projected directly onto the windshield and a single LCD touch screen. The LCD will display all required systems information and will also be used for data entry; therefore, no other instruments or separate data entry devices are required in the cockpit. One interesting feature of this cockpit arrangement is that it allows incorporation of a sliding table or tray, which can be slid out from under the control panel to hold aeronautical charts, maps, or even drinks.

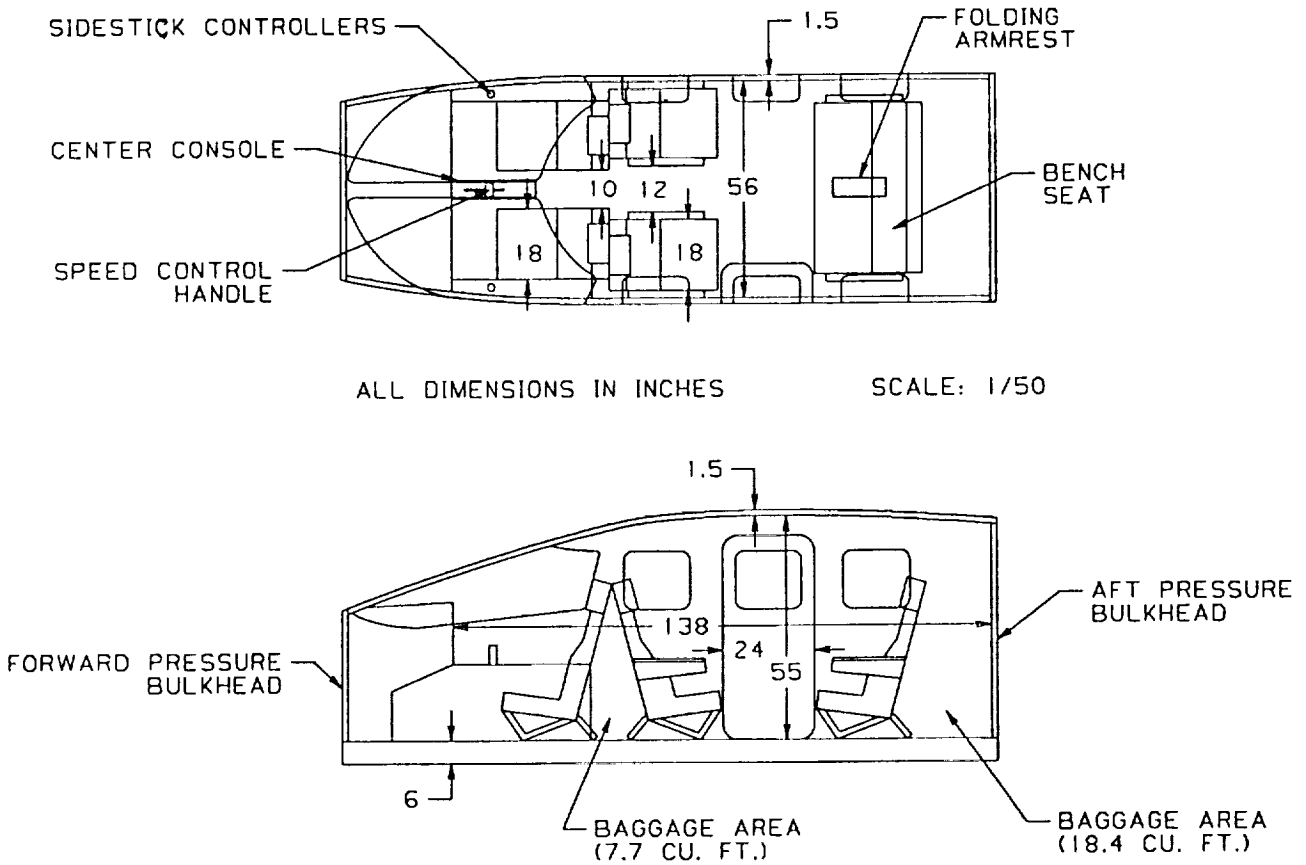
#### 4. ADVANCED GUIDANCE AND DISPLAY

The overall objective of the navigation system was to reduce pilot workload. If possible, the pilot should not have to do anything except fly the airplane. A pilot workload study was conducted<sup>(2)</sup> to determine the workload a pilot must complete to make typical flights under two scenarios: the 1990 ATC system and the proposed IGG system. Each scenario included procedures for both VFR and IFR. From this study, it was estimated that at least a 30% reduction in pilot workload would be experienced due to the time saved from the capability of the IGG to monitor the navigation instruments. Additional workload reduction is possible because the pilot does not have to

fly and communicate at the same time. Reductions are also expected since the pilot is no longer monitoring multiple instruments. Another objective was to be able to navigate vertically as well as horizontally with great accuracy using only onboard computers and positioning satellites. In this way, the onboard computer could build an approach into any airport even if no instrument approaches were established.

The GPS is a method of navigation using a constellation of satellites with known positions to calculate current position. Both the U.S. and the Soviet Union have been working individually on establishing a network of satellites. The NAVSTAR satellite system is the name given to the U.S. effort in global positioning. The system consists of 24 satellites, only 85% of which are presently in orbit. The constellation is expected to be completed by 1993. The satellites are grouped in six orbital planes with four satellites in each plane. Each satellite has a one-day ground track repeat, meaning that it will pass over the same spot once a day.

Each satellite contains almanac information about its orbit and position, and transmits it to the onboard receiver. Time delays measured in the signal are then used to calculate the distance from the satellite to the receiver. By tracking multiple satellites, the position of the airplane is triangulated from the known positions of the satellites. The satellites transmit two



ALL DIMENSIONS IN INCHES SCALE: 1/50

Fig. 4. Cabin layout of the APT.

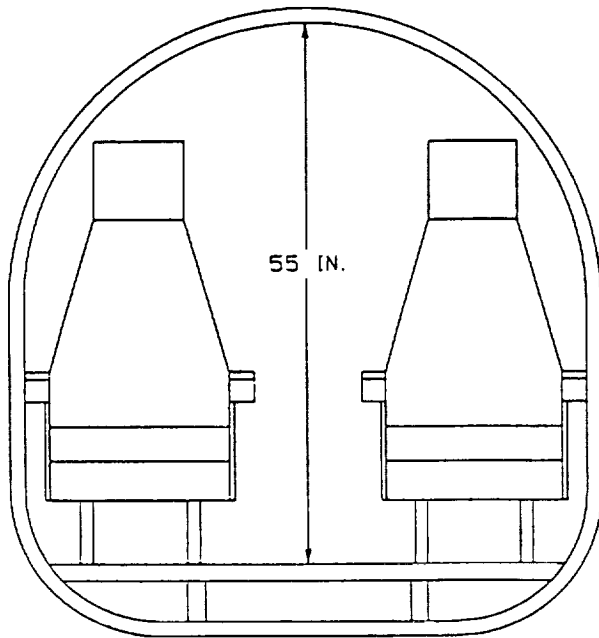


Fig. 5. APT cabin cross section.

codes. The P code has high accuracy and is encrypted and presently restricted to use by the military. A C/A code is available for civilian use, but its accuracy is limited to 50 m. The C/A code is simply a degraded form of the P code. The NAVSTAR system results in the ability to know longitude, latitude, and altitude at any given time.

Glonass represents the Soviet effort in global positioning. The main difference between the U.S. and Soviet systems is that Glonass is in a slightly lower orbit with an eight-day ground track repeat. The satellites are grouped into three orbital planes with eight satellites in each plane. This results in less consistent coverage over a given area. With NAVSTAR, there is a 10-hour period for which these eight satellites are in reception range for a given area. Satellite coverage can be expected over that area at the same time of day, every day, using only eight satellites. Even with 10 satellites, Glonass only repeats every eight days, resulting in inconsistent times of area coverage.

GPS can be used to update an INS to reduce the time-cumulative errors. GPS has the problem that the time delays used to calculate position result in a time lag. This means that the indicated position of the airplane is actually a few seconds behind the actual position. INS, however, can reduce this 12-second lag to instantaneous update rates resulting in higher position accuracy.

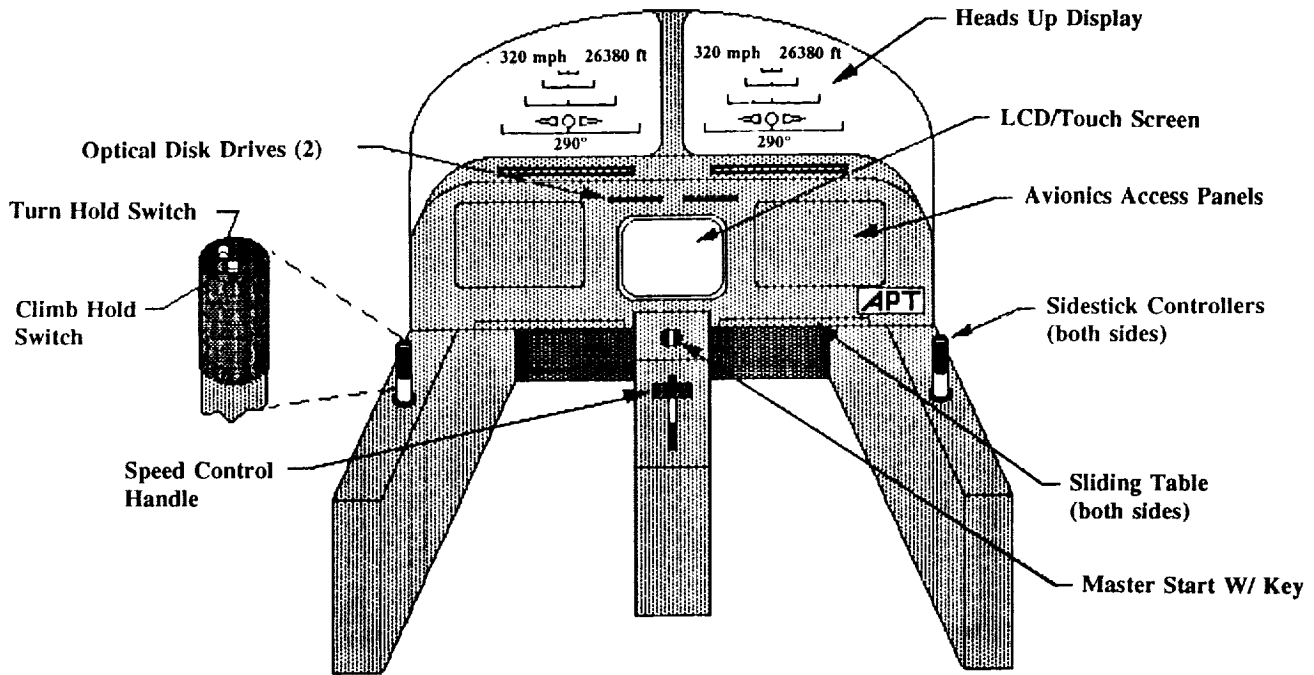


Fig. 6. Proposed cockpit layout of the APT.

The use of differential multichannel GPS receivers will increase the accuracy of the navigation system. By continuously tracking multiple satellites with multiple receivers, the efficiency of the updates is increased, and the noise in the signal and the power required to maintain lock on a satellite are reduced compared to a single receiver cycling through several satellites. The result of this when coupled with INS yields horizontal accuracies that will allow for zero visibility ground navigation and approach accuracies to satisfy CAT II approach criteria.

By the year 2000, advances in the NAS should allow for a GPS-equipped airplane to navigate point to point. It is doubtful, however, that they will allow an airplane without communications to enter controlled airspace. This depends on the advances made in the Data-Link system currently in use. Data-Link allows ATC to talk directly to onboard computers and to issue departure clearances. In the next 10 years, the system should be able to handle all traffic and routing information autonomously.

The only foreseen problem in the NAS is that automatic computer-generated approaches with CAT II criteria will not be allowed. To account for this by the certification date, an ILS system will have to be incorporated. It is believed, however, that GPS-based navigation will reach certification for en-route, DME, ADF, and VOR operations. The only unwanted addition to the APT instrumentation is a dual King KX-155 equivalent NAV/COM. This will not increase panel complexity. It can be worked in as an extra module and therefore does not increase pilot workload, only system complexity.

The complete navigation package will allow complete autonomous flight planning and management, with the exception of some communication requirements for traffic avoidance. It will allow point-to-point navigation with continuous flight information available to the pilot and will also allow CAT II approaches even into undeveloped fields where no approaches are established. The cost of the navigation system is estimated at \$400,000.

The overall objective of the display system was to take a revolutionary look into possible improvements in cockpit instrumentation with an eye toward automation and user friendly operation. Ideally, the instrumentation and the display formats used in this cockpit should enable any pilot to fly this airplane under any weather conditions.

The advanced display system is composed of a map computer, DMUs, the DEU, a HUD, and a multifunction touch-screen display. The map computer is an optical disk-based system that handles all operating system functions, input processing, and the control of both the DEU and the multifunction display. The DEU provides the power, information, and control to the HUD.

The HUD, with the combiner integrated into the windscreen, performs two functions. It incorporates all flight-crucial information into the pilot's heads-up field of view. In this way, the pilot will never have to take his eyes off where he is flying to try and find an important piece of information from a cluttered instrument panel. By providing the pilot with a wide field-of-view display that can use pictorial representations of the outside world, the influences of spatial disorientation can be greatly reduced.

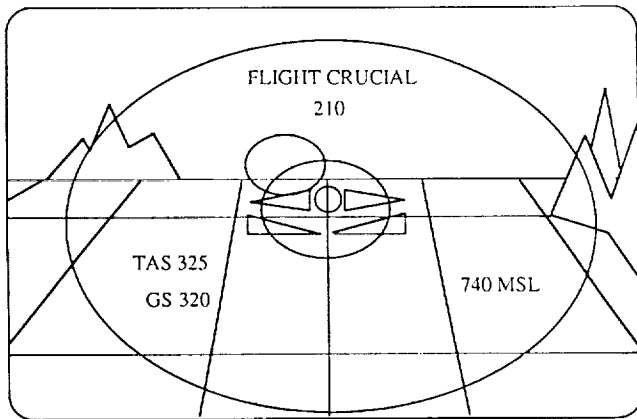


Fig. 7. Head-ups display in flight mode.

The multifunction/touch-screen display is used to display all non-flight-crucial information and for pilot interfacing. The multifunction display would be used for things such as flight planning/changes, monitoring of airplane systems and flight status, display of low priority Data-Link communications, etc. An example of what the HUD would display during flight is shown in Fig. 7. The price of the display system is estimated to be \$600,000.

### 5. PROPULSION SYSTEM INTEGRATION AND PERFORMANCE EVALUATION

For reasons of efficiency throughout the flight envelope, a turboprop powerplant and propeller were selected as the propulsion system of the APT. Two Garrett TPE331-15 engines are connected to a single shaft through a Soloy twin-pac gearbox. These engines power a Hartzell HC-E5N-3L/L8218 propeller.

A survey of several manufacturers was conducted to determine a pool of propeller candidates that may be used on the APT. The five-bladed Hartzell HC-E5N-3L/L8218 was selected from this pool as the propeller for the APT. Due to the large power plant, the Hartzell HC-E5N-3L/L8218 was not able to accept all the power available at its original diameter. To keep the propeller tip Mach number at an acceptable level, the rotational speed had to be decreased from 1885 to 1687 RPM, and the diameter was increased from 85 to 95 in. The designers of the HC-E5N-3L/L8218 specifically designed the blades to operate in a range where tip Mach numbers reached 1.0. The tips of the HC-E5N-3L/L8218 use the most advanced transonic airfoil cross-sections. Three-dimensional effects are taken into account for precise tailoring of blade twist. As a result, the manufacturer claims that the tips are lightly loaded and fly at less than 2° angle of attack at this flight condition. Therefore, the transonic losses are 75% to 90% lower than a traditionally designed blade.

The power plant and propeller installation for the pusher configuration is shown in Figs. 8 and 9. A small shaft extension, which does not appear on the tractor configuration, was added to the gearbox of the pusher configuration to allow better fairing of the aft end of the aircraft. To reduce ducting losses, short

inlet ducts with gradual bends were used. Both engines are supported by one very rigid support truss to minimize gearing mismatch at the engine power takeoff shaft. For maximum accessibility, it was determined that the truss should have hinged members that would swing up and out when a certain engine accessory needs to be replaced or receive maintenance. An oil cooler is incorporated to improve reliability and lower maintenance. Firewalls and a fire suppression system have been included for safety, and chip count sensors were included for prognostics/diagnostics. Torque, RPM, and fuel flow instruments are integrated into the onboard computer for system monitoring.

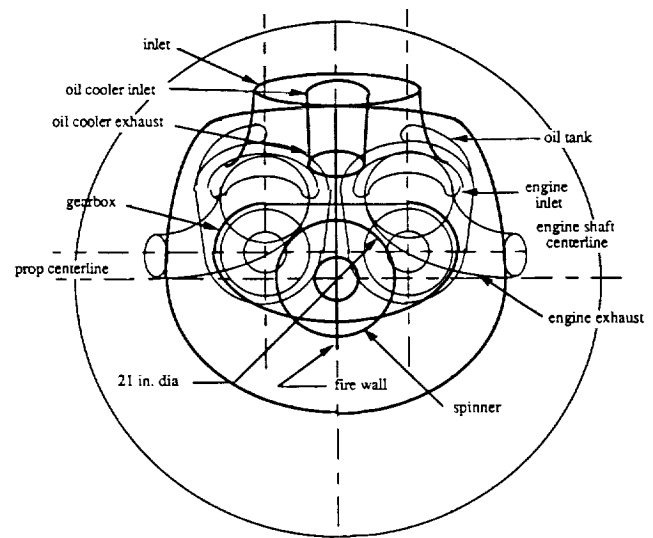


Fig. 8. Front view of the propulsion system integration for the APT pusher.

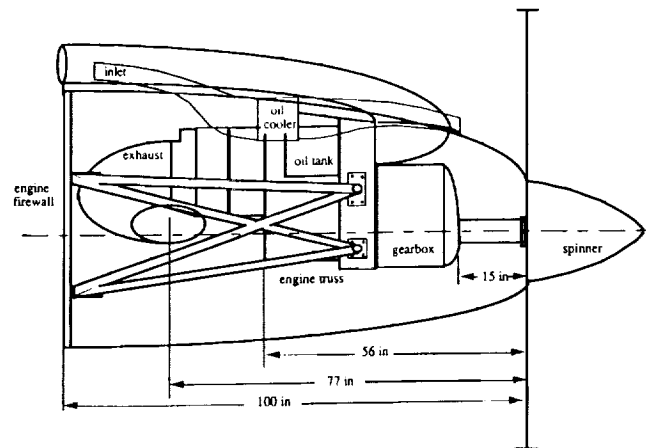


Fig. 9. Side view of the propulsion system integration of the APT pusher.

## 6. AIRFOIL DESIGN

The airfoil, designated as HSNLF-3012, is designed for a cruise Mach number of 0.73 at a Reynolds number of  $5 \times 10^6$ . The HSNLF denotes "High Speed Natural Laminar Flow" and the 3012 denotes a cruise lift coefficient of 0.30 and thickness ratio of 12% chord. At these conditions, approximately 60-70% laminar flow boundary layers are expected on the upper and lower surfaces. In addition, a maximum lift coefficient of 1.4 at a Mach number of 0.1 and Reynolds number of 2 million is a design condition.

The HSNLF(1)-0213 airfoil was used as a basis for the design. Because the HSNLF(1)-0213 airfoil drag-rise Mach number is too low for the APT design cruise speed conditions, some modifications had to be made. The drag rise Mach number was increased by decreasing the thickness ratio of the airfoil and by giving the wing sweep. After scaling down the HSNLF(1)-0213 and reshaping the airfoil afterbody, the desired conditions were met. The airfoil maintains natural laminar flow on 58% and 70% of the upper and lower surfaces respectively.

## 7. WEIGHT AND BALANCE

The component weights and the aircraft balance were determined<sup>(28)</sup>. Table 2 lists the results of the weight estimations. The weights for the pusher configuration are higher because it was resized in Phase II design to meet the mission specifications.

The center of gravity travel is 9 in (20% of the wing MAC) for the tractor configuration and 7 in (15% of the wing MAC) for the pusher configuration. Typical c.g. ranges for similar aircraft are 8-16 inches and 10-21% of the wing MAC<sup>(29)</sup>. This indicates that the results for the APT are reasonable.

## 8. STABILITY AND CONTROL

The stability and control derivatives for both APT configurations were estimated for three flight conditions (power approach, climb, and cruise)<sup>(30)</sup>. Both configurations were determined to be trimmable in all three flight conditions investigated.

It is important to the pilot that certain modes of motion of the airplane are well behaved. The longitudinal and lateral-directional mode shape characteristics of both configurations were calculated<sup>(30)</sup> for the same three flight conditions used in calculating the stability and control derivatives. The tractor configuration satisfies level 1 flight requirements in the phugoid mode in all three flight conditions. The pusher, however, has slightly low damping ratios in both cruise conditions. Both configurations satisfy level 1 short-period flight requirements for all three flight conditions. The spiral mode requirements for level 1 flight are satisfied for both configurations, but the spiral mode is too stable in all three conditions for the tractor and in power approach for the pusher. Decreasing the wing dihedral will alleviate this. Both configurations satisfy the requirements for level 1 dutch roll flying qualities except for the pusher configuration in both cruise conditions. This can also be corrected by changing the wing dihedral or the size of the vertical tail. Both configurations satisfy the roll requirements for level 1 flying qualities in all three flight conditions.

## 9. STRUCTURAL CONSIDERATIONS

The wing and fuselage structural layouts and manufacturing processes were determined for the pusher configuration. The fuselage skin is to be made of Glare 3, the upper wing skin of 7075 aluminum, and the lower wing skin of 2024 aluminum.

TABLE 2. Comparison of the APT with the competition.

|                                 | APT<br>Pusher | APT<br>Tractor | Socata/Mooney<br>TBM-700 | Beech<br>Starship | Piaggio<br>P-180 |
|---------------------------------|---------------|----------------|--------------------------|-------------------|------------------|
| <i>Weights</i>                  | 7,264         | 6,247          | 6,510                    | 14,400            | 10,510           |
| Maximum Takeoff weight (lb)     |               |                |                          |                   |                  |
| Standard empty weight (lb)      | 4,311         | 3,661          | 3,637                    | 10,320            | 6,700            |
| Maximum useful load (lb)        | 2,800         | 2,800          | 2,646                    | 4,280             | 3,810            |
| Maximum wing loading (psf)      | 55.9          | 41.2           | 32.2                     | 51.3              | 61.95            |
| <i>Performance</i>              | 1,961         | 2,050          | 1,936                    | 3,280             | 2,415            |
| T.O. Fieldlength (ft) [sls,isa] |               |                |                          |                   |                  |
| Maximum climb rate (fpm)        | 4,000         | 4,650          | 2,380                    | 3,100             | 3,650            |
| Best climb rate speed (kt)      | 260           | 243            | 123                      | 180               | 160              |
| Clean stall speed (kt)          | 76            | 77             | 75                       | 99                | 105              |
| Landing stall speed (kt)        | 60            | 63             | 61                       | 84                | 82               |
| Service ceiling (ft)            | 45,000        | 44,000         | 30,000                   | 41,000            | 41,000           |
| Normal cruise speed (kt)        | 310           | 300            | 282                      | 270               | 320              |
| at altitude of (ft)             | 40,000        | 44,000         | 30,000                   | 35,000            | 41,000           |
| High speed cruise (kt)          | 415           | 350            | 300                      | 335               | 400              |
| at altitude of (ft)             | 20,000        | 25,000         | 26,000                   | 22,000            | 27,000           |
| Fuel flow for:                  | 323           | 330            | 312                      | ---               | 460              |
| Normal cruise (lb/hr)           |               |                |                          |                   |                  |
| High speed cruise (lb/hr)       | 708           | 700            | 320                      | 984               | 860              |
| Maximum range (nm)              | 1,300         | 930            | 1,000                    | 1,450             | 1,800            |

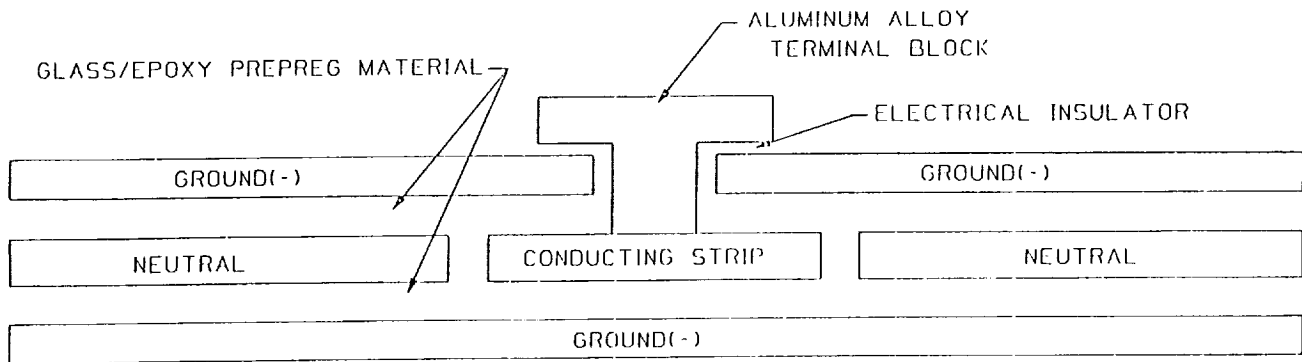


Fig. 10. Smart structure power bus and tap configuration.

The supporting structures of both components will be made of conventional aluminum alloys. Both the wing and the pressurized section of the fuselage were analyzed with a finite structural element program to size the structural members. Outside-in tooling methods will be used to improve surface smoothness of the components to allow for the attainment of natural laminar flow. Skin splices and surface waviness and gaps will be within required levels<sup>(31)</sup> to maintain natural laminar flow.

The APT will incorporate the use of smart structures. The use of embedded sensors in a laminate material can play four key functions: monitoring of the manufacturing process, allowing nondestructive evaluation of each individual structure at any point in the manufacturing or assembly process, vehicle health monitoring, and complementing the flight control system.

Optical fibers will be used for data transmission to take advantage of their immunity from electromagnetic interference and also to take advantage of the savings in weight (about 4%) and volume over conventional copper wire bundles. Optical fiber sensors will be incorporated into the aircraft using the smart-skin approach primarily for vehicle health monitoring. Power transmission by optical fiber will only be considered an option for low power (3 W or less) applications such as simple electronic circuits and active sensors. Optical fibers intended for sensing applications will be standard fiberoptic glass. Optical fibers intended for data transmission will be of the polycarbonate type because of the simpler connection systems and the ease of repair associated with this type of fiber. Optical fibers to be used for data transmission will be too thick to be embedded in the Glare laminate regardless of the type of fiber used, and will therefore be attached to the inner surface of the Glare panels.

Coatings for the fiberoptic cables were selected to ensure protection from the heat generated during the manufacturing of the laminate and the strain from dynamic loadings during flight. It was determined that optical fibers used for data transmission will be coated with acrylate to protect and insulate them from shock and stress, and optical fibers intended for sensing applications will be coated with Polyamide B, a thermoset material.

The possibility of using aluminum alloy strips, integrated into one or more of the aluminum layers of the Glare laminate, as power busses was also investigated. This would allow the electrical bus to be used as a structural member and could lead to a substantial weight savings. A schematic of this concept is shown in Fig. 10. The feasibility of this concept is yet to be verified and warrants further research. A major concern is the reparability and redundancy requirements of such a system. The imbedded strips would make it difficult to repair. The solution accepted at this time is to have triply redundant busses. If an area is damaged, it would be repaired only structurally. The damaged power bus would be "turned off" and the system would simply tap into one of the backup strips.

## 10. SYSTEMS

The layout of the major systems of the APT was designed for both configurations. These systems include the pressurization, pneumatic, air conditioning, oxygen, fuel, de-ice, escape, avionics, electrical, and primary flight control systems. A specialized electro-impulse de-icing system was designed to accommodate maintenance concerns without depreciating the amount of obtainable laminar flow. Detailed analyses were also conducted on the electrical and primary flight control systems. All system conflicts that have been identified have been corrected.

Trade studies were conducted on rate command, attitude command, and decoupled response command flight control systems. A decoupled response control system was selected for the APT because it offers advantages over the rate and attitude command systems. A decoupled response control system significantly reduces pilot workload and improves the handling qualities over conventional rate command systems, especially during low-visibility IFR flight conditions. It has the potential to make flying an airplane as easy and safe as driving a car. The system is particularly well suited for operation by novice and infrequent pilots, though it is also easily adapted to by experienced pilots. Each primary response variable of the airplane is a function of only one cockpit control position, which provides intuitive and easy-to-learn operation. The system automatically compensates for speed and trim changes due to flap

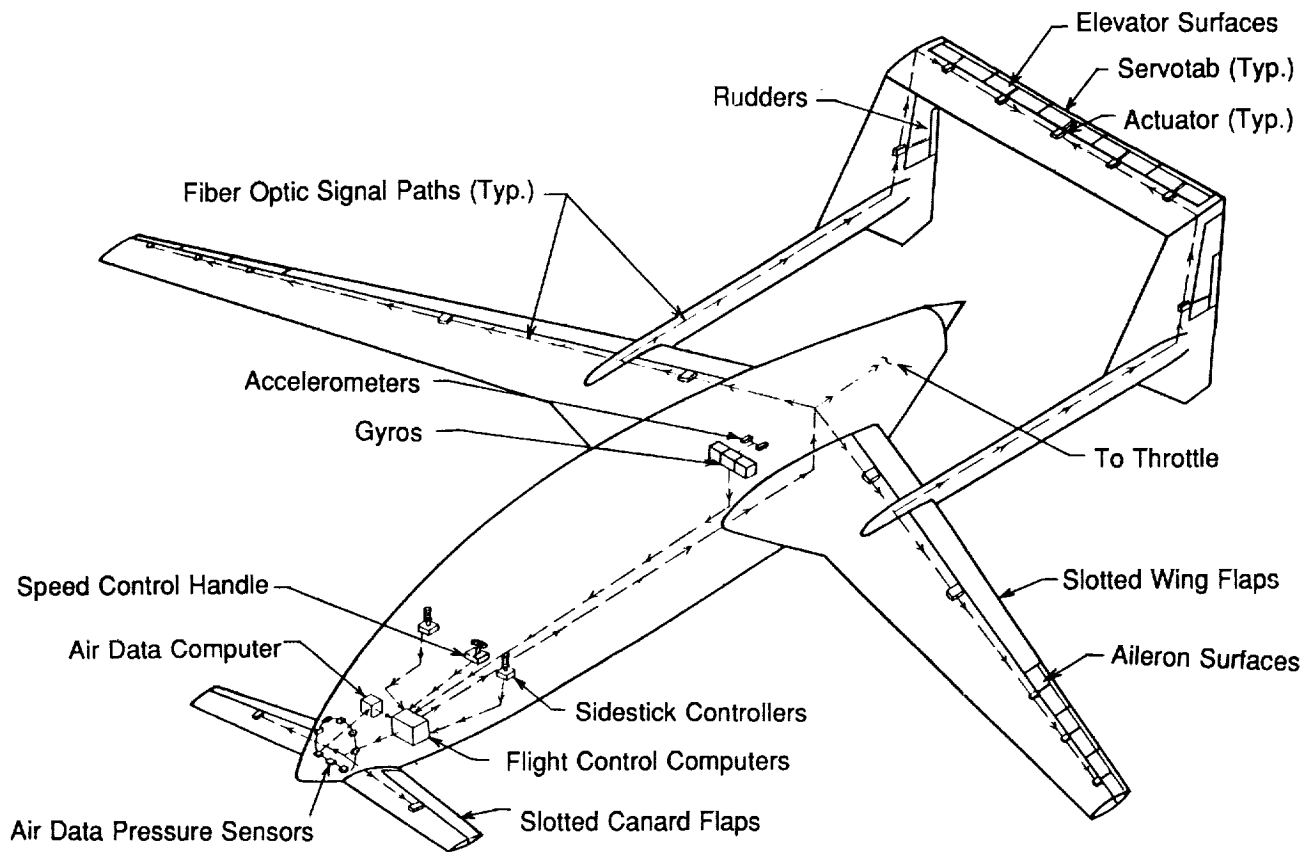


Fig. 11. Preliminary flight control system layout.

deflection, landing gear extension, and steep turns. This considerably decreases pilot workload, especially during approach and balked landing flight conditions. The system makes the type and sign of the steady-state airplane responses the same as those of the initial response, again providing intuitive operation. The system automatically damps out the annoying phugoid oscillation.

Trade studies were also conducted for several flight control system arrangements: reversible mechanical, reversible mechanical with SSSA, and irreversible fly-by-wire/fly-by-light (FBW/FBL). Due to the importance of providing enhanced flying qualities to the APT project, the mechanical reversible system was immediately eliminated from consideration since it did not allow practical stability augmentation. In general, the results showed that the SSSA system should be less expensive to develop, build, and certify, more reliable due to the mechanical primary controls, and easier to certify due to the extensive database of similar airplanes and the relative simplicity of the system. The irreversible FBL system was, in general, the higher performance system since it gives much better handling qualities, allows the safety of flight envelope protection, potentially weighs less, and reduces pilot workload and training requirements. It was apparent that if the cost, reliability, and certification problems of FBL could be overcome, it was the best choice

for the flight control system of the APT. Considering recent technological advances in areas such as microprocessors, fiberoptics, and electromechanical actuators, it seems likely that by the time of certification of the APT in 1999 these problems can be practically overcome<sup>(32)</sup>. As a result, an irreversible FBL control system was selected for the APT (Fig. 11).

Several control surface/actuator arrangements were investigated for the APT flight control system. A multiple-segment control surface arrangement was selected to provide redundancy in the case of actuator failure, using the following segment numbers: seven aileron segments (per aileron), five elevator segments, and two rudder segments (one on each vertical tail). One of the primary advantages of this multiple surface arrangement is that it was designed to provide a constant actuation force for all control surfaces. Hence, one common actuator can be used for all control surfaces, which should provide significant cost and maintenance advantages. Servotab actuation of the control surfaces was selected to allow use of a smaller actuator (for the same control power), which provides the advantage that the actuators should be lighter, less expensive, and have smaller power requirements.

An iron bird has been built and tested. The iron bird involved a simulation of an aileron-tab configuration for lateral control, an investigation to see if a servotab can be used to control

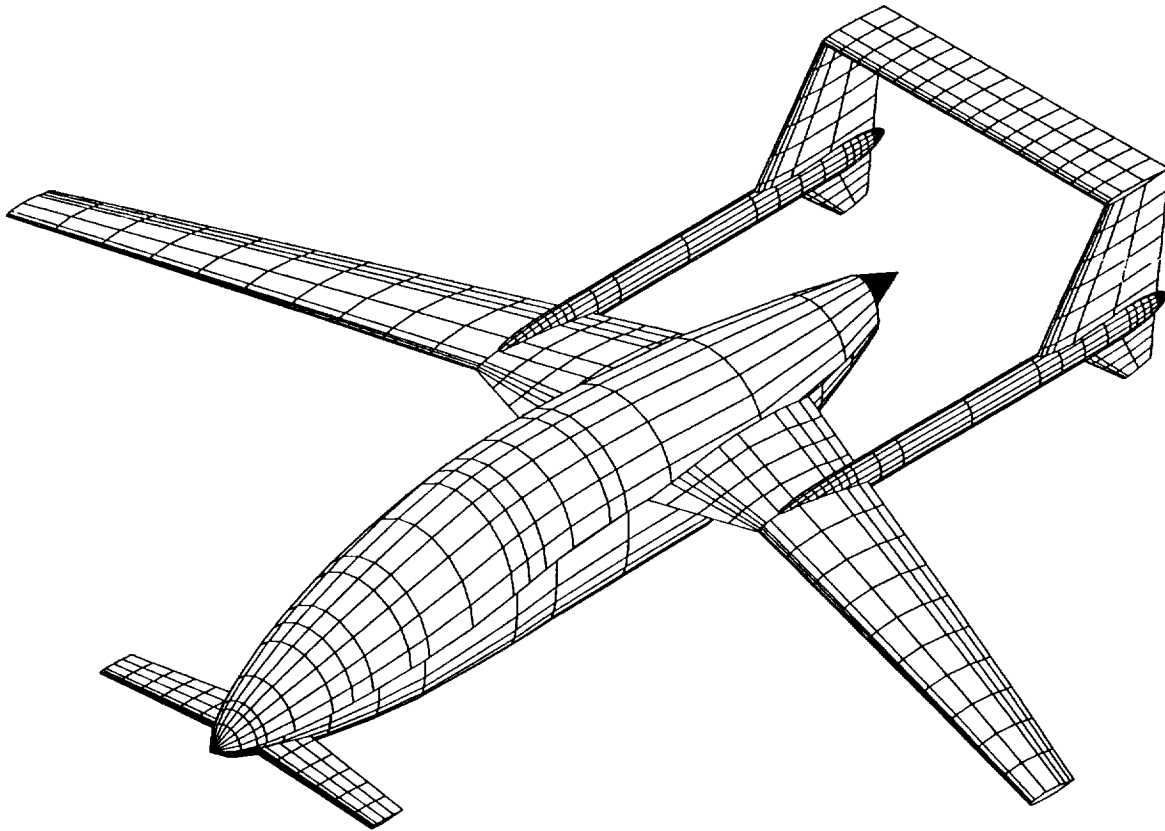


Fig. 12. 3D ACAD model of the APT Pusher configuration.

the aileron surface. The advantage of this configuration is the elimination of the heavy and costly actuators needed to control the ailerons.

Trade studies were conducted between electrical signal paths (FBW) and fiberoptic signal paths (FBL). A FBL arrangement was selected primarily because fiberoptic signals are inherently immune to environmental effects such as EMI, HEMP, and lightning strikes. Fiberoptic cables are also lighter than equivalent electrical cables<sup>(18)</sup>.

To enhance the safety of the APT, a flight envelope protection system will be incorporated. This system will feature protection of the following variables: airspeed, angle of attack, load factor, pitch attitude angle, and bank angle. Such a system can greatly enhance safety by preventing beginning and infrequent pilots from placing the airplane into an unsafe attitude, and by giving the pilot quick and positive access to the entire flight envelope of the airplane.

Due to the FBL control system, the need for large, bulky center-mounted control columns has been eliminated. Experience with civil aircraft such as the Airbus A320, the Rutan Long-Eze, and the new Lancair IV has shown that sidestick controllers provide an unobstructed view of the cockpit panel and allow much easier access to the cockpit. The sidestick controller allows a more comfortable cockpit layout for the

pilots and provides more flexibility in flight deck arrangement. Perhaps the most important advantage of sidesticks is that pilots simply tend to like flying with them. The APT cockpit layout will thus feature sidestick controllers, with one provided on each side of the cabin. Two switches located on the top of each sidestick will be provided to command climb hold and turn hold functions. A single-speed control handle is mounted on the center console of the cockpit, where it is accessible to both pilots. The speed control will be used to command speed both on the ground and in flight, and functions in a manner similar to the cruise control of an automobile. Due to the extensive flight envelope protection used in the APT flight control system, artificial feel units on the sidestick controllers should not be required. Experience with the Airbus A320 has shown that simple linear springs in the controller work well, and also provide the pilot with a more comfortable interface than if an artificial feel unit were employed.

## 11. PERFORMANCE AND COST

The performance capabilities of both configurations of the APT are shown in Table 2. Table 2 also compares the APT configurations with the primary competitors: the Piaggio P-180, the TBM-700, and the Beech Starship. The pusher configuration

TABLE 3. Project cost estimates for the APT aircraft (pusher configuration)

| Year 2000 dollars, 200 aircraft with 20-year service life |               |
|---|---------------|
| RDTE Cost   | 62.7 million  |
| ACQ Cost  | 641 million   |
| OPS Cost  | 6.87 billion  |
| DISP Cost   | 76.5 million  |
| LCC   | 7.65 billion  |
| AEP   | 3.516 million |

meets all the requirements defined in the mission specification. This required the resizing of the entire aircraft. The APT configurations compare favorably with the competitors in Table 2.

Table 3 contains the breakdown of the estimated total APT project costs. These cost estimates are based on year 2000 dollars, with a production run of 200 aircraft, with a service life of 20 years, and were determined by the methods of reference 33.

## 12. CONCLUSIONS

Phases I and II of the preliminary design of an advanced GA aircraft have been completed. It was determined that an IGG-equipped airplane can lead to a 70% reduction in pilot workload. Also, using differential GPS/INS interface, CAT II approaches and zero-visibility ground operations are possible. Through the use of a heads-up display unit and a multifunction touchscreen display, all other flight instrumentation can be excluded.

Glare is planned for the skins of the APT fuselage and conventional aluminum will be used for the wing skins. Outside-in tooling methods will be used in the manufacturing processes of the APT to achieve the smooth surfaces required to maintain natural laminar flow. Electrical power is to be distributed by a triple-redundant, embedded power bus system. Further research needs to be done regarding the design and special manufacturing requirements of an embedded power bus system.

The APT will have a FBW, decoupled response flight control system that will provide control system operations that should greatly improve flying qualities. The pusher design was iterated in Phase II to meet all the performance requirements (Fig. 12).

## REFERENCES

- Burgstahler, Huffman, Ryan, *Market Survey Report for the Advanced Personal Transport*, The University of Kansas, 11 September 1990.
- Axmann, Knipp, Roper, Wenninger, *Pilot Work Load Study*, The University of Kansas, 20 September 1990.
- Hoffmann, Rodkey, Roper, *Advanced Guidance and Display Study*, The University of Kansas, 30 November 1990.
- Axmann, Knipp, *Equipment List for Typical Aircraft and Proposed APT*, The University of Kansas, 4 October 1990.
- Burgstahler, Huffman, *Mission Specification for the Advanced Personal Transport*, The University of Kansas, 20 September 1990.
- Barrett et al., *Preliminary Design of Two Configurations*, The University of Kansas, 15 December 1990.
- Anderson, Jackson, *Loads Analysis of the Advanced Personal Transport*, The University of Kansas, 4 December 1990.
- Chronister, Jackson, *Fuselage Design and Manufacturing Study*, The University of Kansas, 4 December 1990.
- Bauguess, Weiss, *Wing Layout, Design and Manufacturing Tolerances of the Advanced Personal Transport*, The University of Kansas, 12 December 1990.
- Hoffmann, Wu, *Electrical System Design Considerations for the Advanced Personal Transport*, The University of Kansas, 20 November 1990.
- Dreiling, Weiss, *Results of Investigation into the Use of Smart Structures for the Advanced Personal Transport*, The University of Kansas, 4 December 1990.
- Shumate, Woolpert, *Primary Flight Control System Study*, The University of Kansas, December 1990.
- Axmann, Knipp, *System Layouts for the Advanced Personal Transport*, The University of Kansas, 30 November 1990.
- Bauguess, Lawson, Woolpert, *Maintenance and Repairability Study*, The University of Kansas, 13 November 1990.
- Dirkzwager, Schlatter, *Natural Laminar Flow Airfoil Design for the Advanced Personal Transport*, The University of Kansas, 9 November 1990.
- Barrett, Chronister, *Design, Construction, and Test of the Iron Bird*, The University of Kansas, 11 December 1990.
- Gomer, Roskam, *Design Developments for Advanced General Aviation Aircraft*, SAE Technical Paper 911022.
- Evans, DeMoss, *Electrical System Report for the Advanced Personal Transport*, The University of Kansas, April 1991.
- Knipp, Dirkzwager, *Manufacturing Plan and Cost Analysis for the Advanced Personal Transport Pusher Configuration*, The University of Kansas, May 1991.
- Dirkzwager, *Structural Design of the Advanced Personal Transport Pusher Configuration*, The University of Kansas, May 1991.
- Knipp, Keiter, Demoss, *Advanced Guidance and Display Study for the Advanced Personal Transport*, The University of Kansas, April 1991.
- Barrett et al., *Design, Construction, Test and Evaluation of an Aileron-Servotab Iron Bird*, The University of Kansas, May 1991.
- Barrett et al., *Preliminary Airframe Design for the Advanced Personal Transport Pusher Configuration*, The University of Kansas, May 1991.
- Barrett et al., *Primary Flight Control System Design Considerations for the Advanced Personal Transport*, The University of Kansas, May 1991.
- Evans, Smith, Wenninger, *Maintenance and Repairability Study for the Advanced Personal Transport*, The University of Kansas, May 1991.
- Kendall, *The Minimum Induced Drag, Longitudinal Trim and Static Longitudinal Stability of Two-Surface and Three-Surface Airplanes*, AIAA Report 84-2164.
- Selberg, *Analytical Study of Three-Surface Lifting Systems*, NASA TN 850866.
- Roskam, *Airplane Design Part V: Component Weight Estimation*, Roskam Aviation and Engineering Corporation, Ottawa, KS, 1989.
- Roskam, *Airplane Design Part II: Preliminary Configuration Design and Integration of the Propulsion System*, Roskam Aviation and Engineering Corporation, Ottawa, KS, 1989.
- Roskam et al., *Advanced Airplane Analysis Program (AAA)*, The University of Kansas.
- Holmes, *Manufacturing Tolerances for Natural Laminar Flow Airframe Surfaces*, AIAA Paper 85063.
- Tucker, "Advances in Flying Control System", from the conference *Civil Avionics - The Future International Scene*, Royal Aeronautical Society, London.
- Roskam, *Airplane Design Part VIII: Airplane Cost Estimation: Design, Development, Manufacturing, and Operating*, Roskam Aviation and Engineering Corporation, Ottawa, KS, 1989.

# DESIGN STUDY TO SIMULATE THE DEVELOPMENT OF A COMMERCIAL TRANSPORTATION SYSTEM

56-05

160582

P-8

## UNIVERSITY OF NOTRE DAME

Seven teams of senior-level Aerospace Engineering undergraduates were given a Request for Proposals (RFP) for a design concept of a remotely piloted vehicle (RPV). The RPV designs were intended to simulate commercial transport aircraft within the model of "Aeroworld." The Aeroworld model was developed so that the RPV designs would be subject to many of the engineering problems and trade-offs that dominate real-world commercial air transport designs, such as profitability, fuel efficiency, range vs. payload capabilities, and ease of production and maintenance. As part of the proposal, each team was required to construct a prototype and validate its design with a flight demonstration.

### INTRODUCTION

The purpose of this design project is to provide a simulation of the design process for development of a commercial transportation system. The project has been formulated to expose the design students to numerous issues related to the systems design process. Due to the limitations on experience, time, and resources in a single undergraduate engineering course, one appears to have two options in the formulation of the design project: either to select a complex project in which only certain aspects of the design process can be considered, or to select a simpler project in which the design process can be addressed in more depth.

The second of the two options has been selected for this project. Since one of the final products required is a flying aircraft, the nature of the project is limited to those types of systems that can be readily manufactured by the student design teams. Since the area of interest was a commercial transportation system, the problem was modeled in a rather simple fashion. The development of an aircraft system capable of transporting groups of "passengers" to and from a variety of destinations is a complex task involving geographic, demographic, economic, and technical issues. A problem that attempted to integrate a number of these issues was formulated. It should be stressed that the emphasis was placed on the design process, not the final product. The course goals are listed below and the project, as defined in the Request for Proposals (RFP), was intended to help achieve these course goals.

- Introduce the student to system design methodology and, in particular, aircraft design.
- Illustrate the interactive interface between each of the technologies that influence the performance of a system.
- Provide an opportunity to integrate each of the independent technical disciplines at a level where the students understand the technology and can effectively use the appropriate tools.
- Develop an understanding of the planning, coordination, and communication necessary in a team project.
- Expose the students to numerous phases of the system development process, from problem definition to system operation.

- Provide the opportunity to experience the process of translating ideas into an actual product.

Each of these goals is addressed in the context of a team-oriented, mission-directed, aircraft design project. The following section describes the project in some detail and the results of the individual student team designs.

### RFP: COMMERCIAL AIR TRANSPORTATION SYSTEM DESIGN

The mission and semester project details were defined in the following RFP. This request placed some additional requirements and constraints on the basic mission specifications. The design teams were notified that certain aspects of the mission were open for modification, given sufficient justification for these changes.

Commercial transports operate on a wide variety of missions ranging from short 20-minute commuter hops to extended, 14-hour flights that travel across oceans and continents. To satisfy this wide range of mission requirements, "families" of aircraft have been developed. Each basic airplane in the family was initially designed for a specific application, but from that basic aircraft numerous derivative aircraft are often developed. The design of the basic aircraft must allow the derivative aircraft to be developed.

Though they may differ in size and performance, all commercial designs must also have one common denominator: They must be able to generate a profit. This requires compromises between technology and economics. The objective of this project will be to gain insight into problems and trade-offs in the design of a commercial transport system. This project simulates numerous aspects of the overall systems design process so that you will be exposed to many of the conflicting requirements encountered in a systems design. Because of the limited time allowed for this single course a "hypothetical world" has been developed and you will be provided with information on geography, demographics, and economic factors. You will be asked to design a basic aircraft configuration and derivative aircraft that will have the greatest impact on a particular market. The project will not only allow you to perform a systems design

study, but will provide an opportunity to identify those factors that have the most significant influence on the system design and design process. Formulating the project in this manner will also allow you the opportunity to fabricate the prototype for your aircraft and develop the experience of translating ideas into hardware, and then validate the hardware with prototype flight testing.

### Problem Statement

The project goal will be to design a commercial transport that will provide the greatest potential return on investment in a new airplane market. Maximizing the profit that your airplane design will make for your customer, the airline, will be the primary goal. You may choose to design the plane for any market in this fictitious world from which you believe the airline will be able to realize the most profit. This will be done by careful consideration and balancing of the variables such as the number of passengers carried, range/payload, fuel efficiency, production costs, and maintenance and operation costs. Appropriate data for each is included later in the project description.

The "world" market in which the airline will operate is shown in Fig. 1. Additional information is provided to indicate the passenger load between each possible pair of cities each day. This ranged from 20-500 passengers per day. Other useful information about each city including details on location, runway length, and number of gates available to your airline and their size will be provided. The airline may operate in any number of markets provided that they use only one airplane design and its derivatives (your company does not have the engineering manpower to develop two different designs for them). Consider derivative aircraft as a possible cost-effective way of expanding its market.

### Requirements

1. Develop a proposal for an aircraft and any appropriate derivative aircraft that will maximize the return on investment gained by the airline through careful consideration and balance of the number of passengers carried, the distance traveled, the fuel burned, and the production cost of each plane. The greatest measure of merit will be associated with obtaining the highest

possible return on investment for the airline. You will be expected to determine the ticket costs for all markets in which you intend to compete. The proposal should not only detail the design of the aircraft but must identify the most critical technical and economic factors associated with the design.

2. Develop a flying prototype for the system defined above. The prototype must be capable of demonstrating the flight worthiness of the basic vehicle and flight-control system and be capable of verifying the feasibility and profitability of the proposed airplane. The prototype will be required to fly a closed figure-eight course within a highly constrained envelope. A basic test program for the prototype must be developed and demonstrated with flight tests.

### Basic Information for Aeroworld

The following information is to be used to define special technical and economic factors for this project. Some are specific information; others are ranges that are projected to exist during the development of this airplane. (Note real time is referred to as RWT, Aeroworld time as AWT.)

1. Passengers = standard ping-pong balls. Remember these are "passengers" not cargo, therefore items like access, comfort, safety, etc., are important.
2. Range = distance traveled in feet.
3. Fuel = battery charge in milli-amp hours (mah) (RWT).
4. Production cost = \$400 per dollar spent on the prototype + \$100 per prototype construction man-hour (RWT).
5. Maintenance (timed battery exchange) = \$500 per man-minute (RWT).
6. Fuel costs = \$60-\$120 per milli-amp hour RWT.
7. Regulations will not allow your plane to produce excessive noise from sonic booms; consider the speed of sound in this world to be 35 ft/s.
8. The typical runway length at the city airports is 75 ft. This length is scaled by a runway factor in certain cities.
9. Timescale is 1 minute AWT = 30 RWT minutes.
10. The world has uniform air density to an altitude of 25 ft and then is a vacuum.
11. Propulsion systems: The design, and derivatives, should use one or a number of electric propulsion systems from a family of motors provided by the instructor.
12. Handling qualities: The aircraft must be able to perform a sustained, level 60-ft-radius turn.
13. Loiter capabilities: The aircraft must be able to fly to the closest alternate airport and loiter for one minute RWT.
14. There are two existing modes of transportation in Aeroworld that offer competition to your market: An average train fare costs \$6.25 per 50 ft + \$50 flat rate; an average ship fare costs \$8.00 per 50 ft + \$65 flat rate.

To satisfy the mission objectives, Design Requirements and Objectives (DR&O) were established by each design team. Development of DR&O for each team was based on the priorities set by each team. The primary items identified in the DR&O were passenger and range requirements, aircraft gate requirements, and certain manufacturing requirements. With these goals established, each group member developed a basic aircraft concept and from the individual concepts, a team concept was

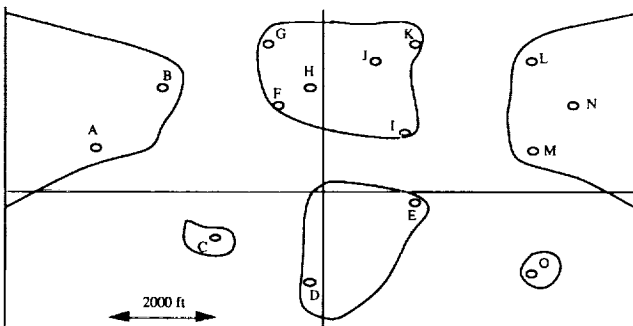


Fig. 1. Geography of "Aeroworld."

selected. The team concept was then used as the baseline configuration and preliminary design studies were performed to develop each concept.

### CONCEPT DESCRIPTIONS

The following summaries provide an overview of each of the seven concepts and address specific technical merits and limitations. Included are selected three-view representations of the aircraft. These summaries are meant to give a brief description of each design, and further technical detail on each proposal is available upon request. These are edited versions of the final proposal executive summaries.

#### Alpha Group: The *Behemoth Apteryx*

Alpha Design Group formulated a design for an aircraft called the *Behemoth Apteryx*. The design is a compilation of efforts both to fulfill requirements imposed by the project definition and to optimize efficiency in both performance and construction. The basic aircraft configuration is a conventional, high-wing monoplane with aft-mounted tail.

We decided to limit the wingspan to 5 ft to be able to utilize all gates in Aeroworld while having a solid, unhinged wing. A SPICA airfoil section with a wingspan of 60 in and a chord of 14 in was selected. This required flying relatively close to  $C_{L_{max}}$ , the maximum allowable cruise velocity, and  $\alpha_{stall}$ . These risks were recognized and it was decided that they could be overcome. With such a short wingspan and thus small area and aspect ratio, the next critical constraint was minimal weight. The small area meant a large wing loading, thus every effort was made to minimize weight.

Considering the two major limiting factors, the design can be summarized as follows: Propulsion is to be provided by an Astro-15 electric motor and a 650-mah battery pack. The fuselage is 44 in long with a maximum width of 7 in and will hold 50 passengers plus 2 crew members. The structure consists of a balsa wood and spruce truss structure for the fuselage and balsa wood spars and ribs for the wing. The entire aircraft will be covered with plastic coating. Control will be accomplished by means of an elevator, a rudder, and ailerons. Given the target commercial market, fleet size, and ticket price, the purchasing airline could make \$840 million per year and Alpha Design would make \$4,316,800 on the sale of that fleet.

Potential problems with the *Behemoth Apteryx* result mostly from the 5-ft wingspan restriction. To achieve a realistic cruise  $L/D$ , the aircraft must cruise at 32 ft/sec or  $M = 0.91$ . The takeoff speed is 29 ft/sec, which is also relatively high. However, the design is very versatile in that it can access any airport gate and any runway without additional ground crew handling associated with a hinged wing. It also is extremely easy and inexpensive to build, which keeps the purchase price down, thus making it a very marketable aircraft. This aircraft can beat all existing modes of travel in cost, speed, and convenience. This would make air transportation the ultimate in travel in Aeroworld. We feel that the benefits we receive from our self-imposed restrictions well justify the risks in design.

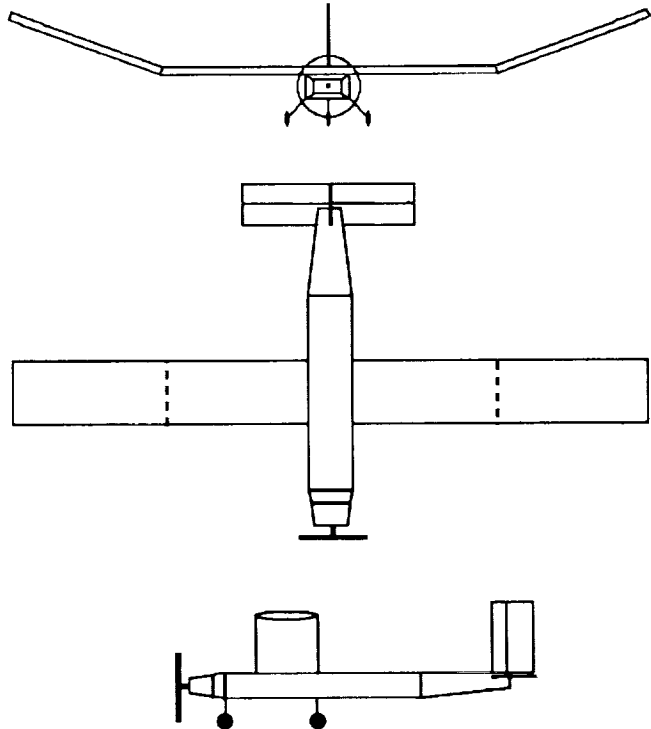


Fig. 2. Beta Group Concept.

#### Beta Systems: *El Toro*

*El Toro* has been designed to operate as a commercial transport that can profitably meet the needs of the Aeroworld market for both the manufacturer and the airline. From mission studies conducted of the Aeroworld market, it was determined that an aircraft range of 6000 ft plus loiter time would be able to serve about 90% of the market. It was also determined from these studies that an aircraft capacity of 50 passengers would best meet the needs of the market. *El Toro* meets both of these market requirements with a range of 25,000 ft and a capacity of 51 passengers. The present design for *El Toro* will profitably meet the requirements for operation in Aeroworld with a ticket price comparable to the ticket prices of current transportation. The extended range of *El Toro* allows for numerous flights before the battery pack must be changed. This drastically reduces the operating costs to the airlines, allowing them to charge less for a ticket or to realize a higher profit margin. The unit production cost for the airplane is estimated to be \$162,000, including all material, systems, and labor.

The aircraft was a conventional, high-wing design shown in Fig. 2. The airfoil selected for *El Toro* is the SPICA, chosen for its high lift coefficient at low Reynold's number and its ease of construction. The wing is sized for minimum power required at cruise while meeting structural requirements. The wing has a span of 8.33 ft and an aspect ratio of 10. The wing is hinged at 2 ft on either side of the fuselage to allow folding of the wing on the ground to enter any airport gate.

The propulsion system for *El Toro* was sized for takeoff in 60 ft with enough extra power to overcome changes in runway conditions, aircraft weight, and aircraft aerodynamics. The propulsion system consists of a propeller-electric motor combination with the prop mounted at the front of the fuselage.

Maximum passenger comfort and safety established a majority of the stability and control design requirements. Longitudinal stability and control will be achieved with the horizontal tail with elevator. Directional stability and control will be achieved with an aft vertical tail with a rudder. Lateral stability will be achieved with a high wing with dihedral. Ailerons are not used because of the hinged wings.

One of the most critical areas in this airplane's structural configuration is the hinge design of the wing. The feasibility of this technology must be demonstrated in order to justify the airplane design, for without folding wings, *El Toro* would not meet the gate requirements of Aeroworld. One of the primary purposes of the technology demonstrator will be to show that a working folding wing can be constructed.

Beta Systems is confident that *El Toro* will be a successful and profitable airplane in Aeroworld for both the manufacturer and the airlines. This success will continue into the future with a family of derivative aircraft. Possible derivatives will have extended or shortened fuselages, larger or smaller engines, or capabilities to be converted for cargo or military applications.

#### Delta Group: The *Nood Rider* 821

The *Nood Rider* aircraft provides a fast, efficient, and relatively inexpensive alternate mode of transportation to the people of Aeroworld. In addition, the *Nood Rider* is able to expand with the growing needs of the market. The *Nood Rider* offers safety far superior to that of its competitors. A number of the routes the aircraft will be used on will be over large bodies of water. With its twin engine configuration, the aircraft can remain safely airborne while diverting to the nearest airport. Although the aircraft cannot take off with one engine out, it can be brought to a stop safely with adequate control.

The *Nood Rider* cruises at a velocity greater than or equal to that of our competitors. At a cruise velocity of 34 ft/sec, the *Nood Rider* will be able to move passengers to their destinations with a large time savings. Since the passenger is paying a premium for air transportation, we felt it important to maximize this time savings. With the absence of a drag penalty for flying at Mach numbers close to one, there is no disadvantage with flying at this velocity.

The passenger payload of 50 and the foldable wingspan of the *Nood Rider* gives a greater flexibility in our departure schedule (Fig. 3). The on-ground wingspan of 5 ft allows the *Nood Rider* to use all the gates available in Aeroworld. The relatively small passenger payload allows multiple daily departures from every city in Aeroworld. Flexibility in planning an itinerary is paramount in every traveler's needs, and the *Nood Rider* is able to satisfy them.

Maintaining the aircraft was always an important consideration. The engines, mounted on pylons extending from the fuselage, are easily accessible. This allows easy routine maintenance or replacement of the engine if necessary. The structure of the entire aircraft is of the simplest design. The

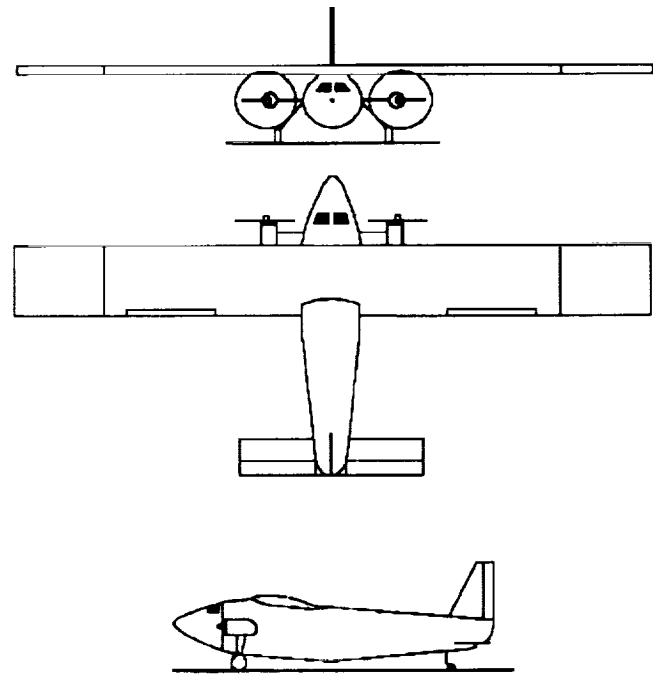


Fig. 3. Delta Group Concept.

wing is a three-spar structure with ribs and stringers. The empennage is a two-spar configuration of similar construction. The fuselage consists of circular bulkheads with longerons running between. All this allows easy maintenance and repair.

With a cruise range of 4200 ft, the *Nood Rider* is able to remain competitive with the other modes of transportation in Aeroworld. The selling price is \$368,000. The per-flight operating cost of the aircraft is \$70,843. Charging the passenger a ticket price of \$12 per 50 ft (15.24 m) plus a flat fee of \$100, allows the operator to recoup all the operating costs, which include depreciation for yearly replacement of the aircraft, even when flying at a passenger load factor of 0.70. This makes the *Nood Rider* a viable alternative to trains or boats.

#### Gamma Group: The *Pale Horse*

The *Pale Horse* is a conventional RPV that will operate in Aeroworld as a 30-passenger aircraft. The major design concerns were cost, range, and passenger comfort. Economic analysis concludes that approximately 150 aircraft flying 8 missions of an average distance of 2150 ft per mission will comfortably accommodate the needs of Aeroworld. A rate of \$12 per 50 ft plus a \$50 flat rate will be profitable to the airlines and will be competitive with the other modes of transportation in Aeroworld.

The *Pale Horse* uses the SD7062 airfoil. The rectangular wing, with an 8-ft span and 10.5-in chord, will be mounted high on the fuselage with 10° of dihedral for increased roll stability. The wing will be hinged 1.5 ft from each wing tip to utilize the 5-ft as well as 7-ft gates at Aeroworld airports. The hinge enables the wing tips to be folded upward during loading and unloading in the airport gates.

Passengers will be seated in two rows of 15, with a center aisle for safety and comfort. Aft of the passenger cabin will be space for a restroom as well as a galley. Beneath the passenger area will be a luggage storage hold that will also house the control system and linkage.

An Astro-15 electric motor will be used to power the *Pale Horse*. Connected to the motor will be a Tornado 10-6 propeller, and driving the motor will be thirteen 1.2 V/1.2 ah batteries connected in series. This propulsion system enables the aircraft to be maneuverable with a desirable rate of climb and a takeoff distance less than 38 ft. The flight range for one battery pack is over 20,000 ft; therefore, a fully charged *Pale Horse* can fly its 8 daily flights including taxi and delay times on a single charge. This reduces Aeroworld gate times, thus allowing quicker turnovers between flights. In addition, this reduces maintenance costs, which allows the airlines to pass the savings on to passengers.

Concerns in the design include the hinge design and structural failure resulting from the inexperience of the manufacturers. Prototype studies give encouraging results for the effectiveness of the hinge. Throughout the design, large factors of safety have been included to reduce the apprehension for the latter concern.

#### Kappa Group: The *Initial Guess*

This aircraft is designed to generate profit in the market that is currently dominated by the train and boat transportation. The main priority of the design team was to develop an extremely efficient aircraft that could be sold at a reasonable price. The *Initial Guess* offers a quick and safe alternative to the existing means of transportation at a competitive price. The cruise velocity of 28 ft/sec allows all flights to be between 20 and 45 min, which is a remarkable savings in time compared to travel by boat or train.

The *Initial Guess* is propelled by a single Astro-05 engine with a Zinger 10-6 propeller. The Astro-05 is not an extremely powerful engine, but it provides enough thrust to meet the design and safety requirements. The major advantage of the Astro-05 is that it is the most efficient engine available. The fuel efficiency of the Astro-05 is what puts the Kappa Aerospace aircraft ahead of the competition. The money saved on an efficient engine can be passed on as lower ticket prices or increased revenue.

The *Initial Guess* has a payload of 56 passengers and a wingspan of 7 ft. The 7-ft wingspan allows the aircraft to fit into the gates of all of the cities that are targeted. Future endeavors of Kappa Aerospace will include fitting a stretch version of The *Initial Guess* with a larger propulsion system. This derivative aircraft will be able to carry more passengers and will be placed on the routes in greatest demand.

The fuselage and empennage are made of a wooden truss configuration, while the wing is made of a rib/spar configuration. The stress-carrying elements are made of spruce, the non-stress-carrying elements are made of balsa. The wing is removable for easy access to the fuselage. The easy access to the batteries will keep maintenance costs down.

The *Initial Guess* will cost \$246,000 to produce. The ticket price will be \$75 flat fee and \$12/50 ft. This ticket price will generate profit at the most expensive fuel price and, assuming

that the plane flies at capacity, the production cost will be made back in 49 flights. The *Initial Guess* provides an extremely rapid return on investment and will be competitive with the already existing modes of transportation.

#### Theta Group: The *Hotbox*

The *Hotbox* is a 40-passenger commercial aircraft designed to have a minimum range of 5500 ft and cruise at a velocity of 30 ft/sec. The aircraft is designed to serve the longer-range, overseas market in Aeroworld. The driving force behind the design was to generate the greatest possible return on investment and profit for an Aeroworld airline. This goal, at least in an underlying sense, influenced all aspects of the design. Because of the seven-week engineering timeframe, ease of construction and simplicity of design also had a primary influence on the design. In addition, space restrictions (disassembled aircraft must fit in a 2' x 3' x 5' box) imposed significant limitations on aircraft design.

From these primary design goals, a set of secondary drivers evolved. First, in order to serve all the airports in the overseas market, the *Hotbox* was required to be able to use a 5-ft gate. A weight requirement was set at 4.5 lb in order to maximize aircraft efficiency. Finally, a single-engine system was chosen because it minimized system weight, complexity, and cost. From these primary and secondary design goals, the *Hotbox* was born.

The *Hotbox* is estimated to cost \$152,000 Aeroworld dollars (AD) and will sell for \$200,000 AD. A ticket price of \$38 flat rate plus \$9.70 per 50 ft is recommended. This ticket price is, on an average flight, 15% higher than the ticket cost of a ship. Because of the time savings involved with air travel, this excess cost is considered acceptable. A market consisting of 27 routes and 316 flights per day is estimated to generate a \$42.3 million AD net income and a 53.8% annual return on investment.

The propulsion system for the *Hotbox* consists of a nose-mounted Astro 15 electric-powered motor and a Top Flight 12-6 propeller. Early in the design process, studies indicated that the Astro 15 motor would provide sufficient power for all phases of the mission and better cruise performance than other motors considered. After ordering this motor, however, weight considerations became an increasing concern in the design of the *Hotbox*. The Top Flight 12-6 was used because it allowed minimum battery weight and was the only propeller considered that met the 60-ft takeoff requirement.

A SPICA airfoil was selected for the *Hotbox* based on the ease of construction of its flat bottom and its positive lift and drag characteristics. In order to provide acceptable wing loading, the *Hotbox* has a wing area of 7.33 ft<sup>2</sup>. Aircraft aspect ratio is 8.72. To simplify construction, no sweep, taper or twist was incorporated into the wing design. The wing consists of a spar and rib construction with a plastic sheet skin. In order to fit into the 5-ft gates of Aeroworld, the *Hotbox's* 8-ft wing must be hinged. The primary hinge mechanism will be enclosed in the wing and located at the quarter chord and 26.75 in from the fuselage centerline.

A fuselage of rectangular cross section will contain the propulsion system, control system, and a passenger bay with 2 x 20 seating. The center of gravity (c.g.) is located at 30% chord

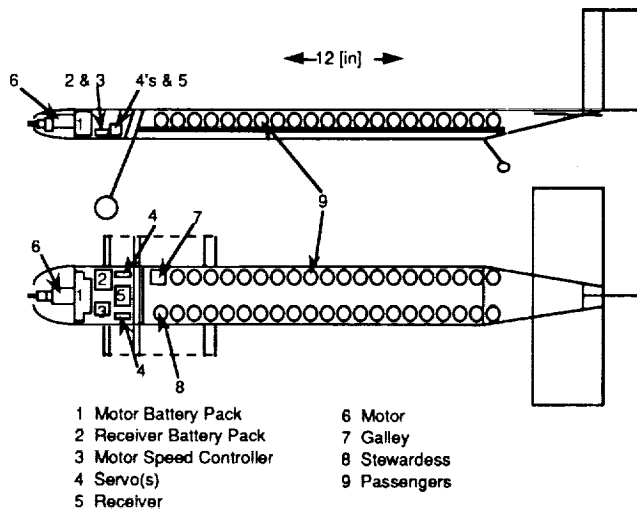


Fig. 4. Theta Group Concept - Internal Layout.

with the aircraft fully loaded and at 21.5% chord without passengers. Figure 4 is a schematic illustration of the internal arrangement.

The final design of the *Hotbox* provides for takeoff distance of 26.5 ft and normal cruise range of 17,000 ft. Maximum range and maximum endurance for the aircraft are 20,600 ft and 14.3 min respectively.

#### Zeta Group: The *Valkyrie*

The *Valkyrie* is a flying wing concept designed to serve as a high-volume commuter transport in Aeroworld (Fig. 5). The technology demonstrator seeks to validate the flying wing design as a superior alternative to the conventionally configured aircraft used in the modern airline industry. The 5.02-lb *Valkyrie* has a wingspan of 84 in (7 ft), which results in an aspect ratio of 4.9. The root and tip chords measure 23 and 11 in, respectively, forming a taper ratio of 0.48.

The *Valkyrie* employs the NACA 2R<sub>2</sub>12 airfoil section. A 2° reflex in the trailing edge of this airfoil provides a zero moment coefficient about the aerodynamic center over the applicable range of angles of attack. Furthermore, the rear 20% of the chord across the entire span comprises the elevator and ailerons. This configuration, along with a judicious positioning of the c.g. location, allows the *Valkyrie* to trim during cruise at an angle of attack of 8°. Although reflexing the trailing flap to trim does increase the drag generated by the wing by raising the  $C_{D0}$  to 0.0314, the overall drag produced by this configuration remains small compared to similarly sized conventional designs with drag-inducing fuselages.

A leading edge wing sweep of 13.2° and a 2° dihedral have been incorporated to provide lateral stability. Ailerons have been designed to provide adequate roll control power. Yaw stability is provided by triple vertical stabilizers. Yaw control is achieved through the use of a rudder on the center vertical stabilizer. With this configuration, it is possible to land in a crosswind of 10 ft/s.

The *Valkyrie* is a semimonocoque structure manufactured from spruce and balsa wood covered in plastic mylar skin. The internal ribs are spaced 3.5-in apart to provide comfortable seating for the maximum carrying capacity of 100 passengers. The NACA 2R<sub>2</sub>12 airfoil, with its 12% maximum thickness ( $t/c$ ) provides sufficient volume to comfortably carry the maximum passenger load. In addition to adequate passenger space, the *Valkyrie* must have sufficient usable volume to house the fuel and control system. Two large, solid balsa wood ribs form the central corridor of the aircraft, housing the motor, batteries, and avionics.

The AstroFlight Cobolt 25 electric engine will power the *Valkyrie*. It is designed to take off in less than 20 ft. To eliminate the difficulties associated with rotating the aircraft at takeoff, the wing is mounted on its landing gear at the takeoff angle of attack of 8°. A velocity of 26.7 ft/s is required to generate sufficient takeoff lift. Once airborne, the *Valkyrie* climbs to the cruise altitude of 20 ft, then flies at 32 ft/s on a closed, figure-eight loop. In turns, the *Valkyrie* can either increase its speed or deflect its control surfaces to maintain the cruise altitude. On landing, the aircraft must touch down at a speed of approximately 26 ft/s to maintain trimmed conditions.

Finally, the *Valkyrie* provides a greater payload-to-weight ratio than a conventionally configured aircraft of comparable weight. Considering the requirements, the *Valkyrie* is the most efficient design for the specified mission.

#### DESIGN ISSUES

The following brief sections address issues in the major areas of weights, structures, propulsion, aerodynamics, stability/control, economics, and production, and describes the concept technology demonstrators and their flight validation.

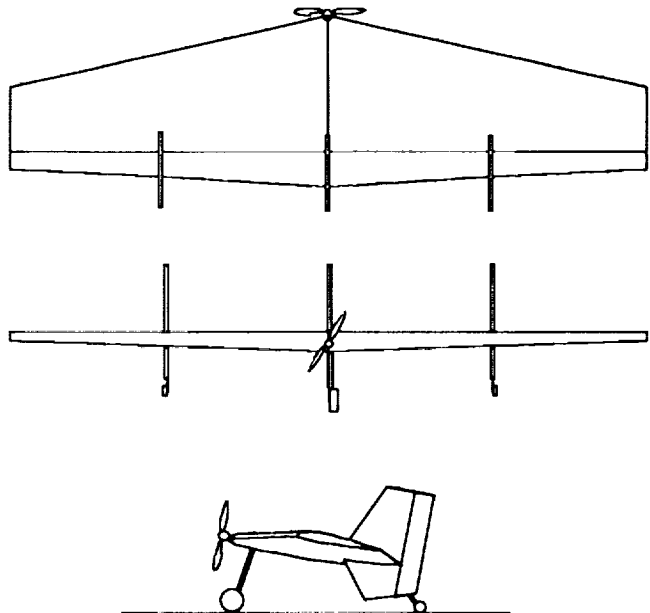


Fig. 5. Group Zeta Concept - the *Valkyrie*.

## Weights

Each team was concerned about keeping overall weight to a minimum. Previous design studies have provided a reasonable database for component weights, but accurate initial estimates are difficult because they significantly depend on manufacturing techniques. Payload weight was not a significant issue, though payload volume was. C.g. control was usually achieved by positioning of the relatively heavy motor batteries.

## Structures

Manufacturing considerations imposed the greatest constraints on the structural design. Certain unique features such as a circular fuselage, multiple-engine configurations, and, in particular, folding wings provided challenges in structural design. Because of limited manufacturing expertise, the design teams were often cautious in adopting nontraditional structural concepts. Since total time required for the fabrication phase was a significant cost factor, manufacturing constraints were present in the structural designs.

## Propulsion

For safety and other reasons related to development of the technology demonstrators, electric propulsion systems were required. Integration of the battery storage, electric motor performance, and propeller selection proved to be critical in determining the success of the concepts. Takeoff power requirements exceeded the low-speed, steady-cruise requirements. Various computer-based methods were developed to provide performance predictions since analytic models of the electric motor performance are available. Performance predictions for the propellers operating in this low Reynolds number regime are difficult and the flight validation indicated that a number of the propeller selections were inappropriate. The size of the propulsion systems ranged from the O35 to the 25 and unfortunately weight and cost were not directly proportional to power available. The twin-engine concept developed by Delta Group presented a technical risk. The engines were readily accessible and simultaneous control appeared to be effective. During flight test, asymmetric thrust developed either because of differences in the motors or the propellers. Resolution of this problem would have required additional testing.

## Aerodynamics

Wing design was driven by the conflicting requirements of gate dimensions and the desire for high aspect ratio to achieve optimum cruise performance. Only one group attempted to develop the minimum span wing (5 ft). Others selected either rigid wings that met the larger gate requirement or folding wing tips. Certain aerodynamic considerations such as taper, twist, or complex airfoil geometries were often eliminated from consideration by anticipated problems with fabrication. The Mach number limit did not carry with it a penalty for approaching the limit and was therefore only invoked for safety considerations associated with the indoor flight tests. Most groups attempted

to achieve cruise near  $L/D_{max}$  but the preliminary drag predictions are difficult in this low Reynolds number regime.

The primary payload, citizens of Aeroworld, was relatively lightweight, but occupied significant volume. Space/comfort requirements for the passengers as well as baggage and required services were not well defined, leading to different interpretations by individual groups. Fuselage size was influenced by the design passenger load. The influence of fuselage design on the drag did not appear to be a critical design issue since cruise drag was not a design driver.

## Stability and Control

Concerns were primarily those of maintaining adequate static pitch stability and the roll control necessary to perform the closed course maneuvers. This was usually accomplished with two channels of control, elevator and rudder, in order to eliminate the weight and complexity of the additional control for ailerons. A number of the groups did effectively integrate aileron control, but pilot response did not imply that these designs handled any better than the two-channel systems. Previous designs developed to fly in the same constrained airspace had demonstrated the feasibility of the control concepts and, other than issues related to control surface sizing and actuator installation, few significant problems were encountered.

The *Valkyrie* flying wing design was a unique development that presented a certain technical risk. C.g. control in this design was particularly difficult and a number of post PDR changes had to be made to the design prior to flight validation. This aircraft may have performed more like a fighter than a transport.

## Economics

In light of the overall design goal of generating a profit, a direct comparison of each concept would be desirable. Because of the limited time allowed and rather liberal interpretation of some of the initial guidelines, this direct comparison is not possible. Most of the design groups interpreted fuel cost, production time, and production costs as primary cost drivers. Since each used similar total battery capacities and the total fabrication times were comparable (each group fabricated the technology demonstrator in about two weeks), system cost predictions yielded similar values. This implies that the aircraft carrying the greatest number of passengers might be the most profitable, if flights were full.

Complete system economic studies were beyond the scope of this project, but it did make the groups aware of certain economic drivers in the design process.

## Production

Since each group has limited manufacturing experience and a very short time to construct the technology demonstrator, many early decisions are based upon perceived problems in production. Airfoil complexity, wing taper, fuselage cross section, type and placement of the control systems, and internal structural arrangement are all influenced by the manufacturing

requirement. Available tooling and materials also affect the design process. The time constraints make it more difficult to incorporate new technologies or materials.

The requirement to produce a product in a finite time, with a limited budget, is probably the most important design driver. Every decision appears to be influenced by this factor.

### Technology Demonstrators

Each design team constructed its prototype during the last three weeks of the project. They were issued Futaba Attack 4 radio systems, as well as their respective engines. All construction took place in the Notre Dame Aerospace Design Lab, where simple construction equipment was provided. After a construction period of approximately two weeks, a series of taxi tests were performed to test the systems and to check the aircraft for basic flight worthiness and controllability. All seven aircraft experienced problems, especially in the areas of c.g. placement, tuning of the control surfaces, landing gear stiffness and alignment, propeller selection, and propulsion system battery performance.

On May 3, 1991, the flight demonstrations were held. All seven aircraft successfully performed takeoff and sustained, controlled flight. All the aircraft handled very well under the control of an experienced pilot with the exception of the Delta Group plane, which experienced significant thrust asymmetry as mentioned above. The Theta Group aircraft appeared to handle exceptionally well even at very low cruise speeds. The Zeta Group flying wing design provided the most dramatic flight, though its performance may not have been particularly characteristic of a commercial air transport. Considering the lack of experience of the builders and the time constraints placed on the teams, this flight demonstration was considered a great success and showed the students the difference between a conceptual success and success in the real world.

### CONCLUSIONS

The purpose of this course is multifaceted. Students entered the course with the knowledge required to complete the mission. The learning process involved the ability to incorporate that information into a design. They were shown the design process from start (the RFP) to finish (the prototype). They were immersed into many real-world problems faced by engineers. These included working in a team and integrating seven engineers' ideas and work into one design. They were given the opportunity to experience the construction process, and how to bridge the gap between a concept on paper and a flightworthy aircraft.

The attempt to simulate numerous issues related in commercial transportation system design through the use of an RPV system appeared to be successful. The limited time available to address so many complex issues precluded attention to great detail in any area.

### ACKNOWLEDGMENTS

This project was supported by NASA/USRA Advanced Aeronautics Design Program. Technical assistance and guidance was provided by the Boeing Company under the coordination of Mr. Cal Watson. Other contributions from the Boeing Company include the comments and recommendations of Mr. Robert Kelley-Wickemeyer and Mr. Steve Ford during the development of the RFP and the participation of Mr. George E. Bean and Dr. Gerald C. Paynter in the preliminary design review. The course was presented by Drs. Stephen M. Batill and Robert C. Nelson, and graduate teaching assistants David Carey and Kevin Costello. Finally, thanks go to Mr. Joseph Mergen, Mr. Tony DeRoza, Mr. Joel Preston, and Mr. Mike Swadener for their technical assistance and advice throughout the semester.

# THE DESIGN OF TWO-STAGE-TO-ORBIT VEHICLES

THE OHIO STATE UNIVERSITY

57-05  
160583  
P. 11

Two separate student design groups developed conceptual designs for a two-stage-to-orbit vehicle, with each design group consisting of a carrier team and an orbiter team. A two-stage-to-orbit system is considered in the event that single-stage-to-orbit is deemed not feasible in the foreseeable future; the two-stage system would also be used as a complement to an already existing heavy lift vehicle. The design specifications given for this project are to lift a 10,000-lb payload, 27 ft long by 10 ft diameter, to low Earth orbit (300 n.m.) using an air breathing carrier configuration that will take off horizontally within 15,000 ft. The staging Mach number and altitude were to be determined by the design groups. One group designed a delta wing/body carrier with the orbiter nested within the fuselage of the carrier, and the other group produced a blended cranked-delta wing/body carrier with the orbiter in the more conventional piggy-back configuration. Each carrier used liquid hydrogen-fueled turbofanramjet engines, with data provided by General Electric Aircraft Engine Group. While one orbiter used a full-scale Space Shuttle Main Engine (SSME), the other orbiter employed a half-scale SSME coupled with scramjet engines, with data again provided by General Electric. This paper presents the two groups' conceptual designs, along with the technical trade-offs, difficulties, and details that surfaced during the design process.

## INTRODUCTION

In previous years, The Ohio State University (OSU) Advanced Aeronautical Design Program (AADP) has focused on hypersonic design concepts ranging from 250-passenger commercial jets to 10-passenger executive jets to a Mach 10 scramjet test bed. Continuing with the hypersonic design trend at OSU, this year's project was the conceptual design of a two-stage-to-orbit vehicle. Until last year, most of the hypersonic design efforts were cruise concepts that lent themselves to optimization during the cruise regime. A two-stage-to-orbit vehicle is an accelerator, and thus no steady-state optimization is really possible.

The last space shuttle (Endeavour) has already been built, and although the space shuttle program is not near cancellation or termination, the Challenger accident showed that the U.S. space program is strongly dependent upon the space shuttle. A complementary (not replacement) orbital lift system would be a logical step, making the U.S. space program more versatile when the new system has access to space. Another consideration is that the space shuttle program incurs large operating costs by employing a veritable standing army of support personnel. These costs can be alleviated by having a system that operates as an aircraft, not a rocket, yielding an additional benefit of a quick turnaround time. This points toward a single-stage-to-orbit vehicle (i.e., NASP) or a two-stage-to-orbit vehicle (i.e., Sanger/Horus), with the latter mode less of a technology risk, as well as being nearer-term technology. Therefore, a two-stage-to-orbit vehicle is seen as a compromise between the operational costs associated with an expendable heavy lift rocket and the technical difficulties of a single-stage-to-orbit vehicle.

## DESIGN SPECIFICATIONS

The design specifications for the conceptual two-stage-to-orbit vehicles were laid out to conform with vehicles of similar concept, yet allow sufficient latitude for each group to design a vehicle as they saw fit. As far as a specific mission for this type

of vehicle, a quick relief flight to Space Station *Freedom*, supplying men, materials, and equipment was considered to be one of the primary missions.

It was specified that the carrier take off within 15,000 ft using only air breathing propulsion (no rocket assist), accelerate to the staging point, where the orbiter will separate and carry a 10,000-lb payload to 300 n.m. or low Earth orbit (LEO), at an orbital speed of 25,400 ft/s. The payload chosen is roughly one-fifth-scale in volume and weight of the space shuttle cargo bay. This size is estimated to encompass 90% of all current and future orbital payloads. Note that the staging Mach number and altitude are not specified and are to be determined by each group. The design specifications can be summarized as follows:

- Air breathing carrier propulsion
- Payload: 27 ft long  $\times$  10 ft diameter  
10 passengers plus  
10,000 lb (total weight)
- Low Earth orbit (300 n.m., 25,400 ft/s)
- Take off distance  $\leq$  15,000 ft

## DESIGN SERIES OUTLINE

A conceptual design project of this magnitude is indeed challenging, and thus the OSU hypersonic design series is expanded from the usual four-credit-hour design class to a program spanning the entire academic year. The series consists of a one-credit-hour seminar during the Autumn Quarter, a four-credit-hour Aerospace Vehicle Design Course during Winter Quarter, and a three-credit-hour Advanced Vehicle Design Course during Spring Quarter.

During Autumn Quarter a series of seminars are scheduled where professionals from industry and academia are invited to OSU to discuss not only aircraft design problems in general, but also problems specifically associated with hypersonic aircraft.

Winter Quarter is when most of the vehicle design is accomplished. The students were divided into two design groups, each having a carrier and an orbiter team. The teams were set up to duplicate industry design teams, each having a team leader and field specialists in areas such as propulsion and aerodynamics. The groups began with a calculation of weights and dimensions from an estimated ascent trajectory that included current aerodynamic and propulsion models. The staging Mach number and altitude was altered for a minimum system weight (both carrier and orbiter). Once a staging point was chosen, the task was to design two vehicles that must work together as one system. Each design team then worked to optimize their respective vehicles, mostly in the form of improving ascent trajectories. At the end of Winter Quarter, neither group had a fixed configuration due to the time involved in choosing an acceptable staging point.

Because Spring Quarter was an elective, there was a 25% reduction in students and a subsequent reorganization within the design teams, which took time and put the design groups on a tight schedule. Refinement of the ascent trajectories was continued, and the areas of stability and control, heat transfer, inlet design, and material selection were investigated. Further refining of the vehicle systems indicated that the ascent trajectory and orbiter weight were the critical elements in weight optimization.

The continuation of the design series to include a second quarter was critical due to the fact that some of the problems that occurred during Winter Quarter were not solved until the Spring Quarter, as well as allowing the students to refine their designs, and allowing more insight into the design process.

#### VEHICLE DESIGNS

The design groups operated independently and were in friendly competition throughout the design classes. They were encouraged to design different two-stage-to-orbit vehicles while still collaborating between groups to a small extent to aid each other in weak areas.

Although a manned or unmanned vehicle was not specified, both groups automatically used manned orbiters because passengers were assumed. At first, an unmanned carrier was considered, but after considerable debate and inquiries at Wright Patterson Air Force Base and NASA Lewis Research Center it was determined that the workload on the orbiter crew would be too great with preflight checks to allow them to fly the vehicle to the staging point.

##### Scarlet Group

|                          |            |
|--------------------------|------------|
| Length                   | 210 ft     |
| Takeoff Distance         | 9860 ft    |
| Takeoff Weight           | 808,210 lb |
| Staging Altitude         | 80,000 ft  |
| Staging Mach Number      | 5.5        |
| Carrier Mission Time     | 35 min     |
| Carrier Mission Distance | 788 mi     |
| Time to Orbit            | 44 min     |

The Scarlet Group configuration (Fig. 1) has a takeoff weight of 808,210 lb and stages at Mach 5.5 at 80,000 ft. The primary

design concept for the Scarlet Group was to gain orbital altitude and velocity quickly, while keeping the design simple. This led to a typical wing/body carrier, but with the orbiter situated within the rear portion of the carrier fuselage. This location eases the loading process, eliminates the additional drag due to an exposed orbiter, and makes staging safer during separation. Due to the minimum time (and distance) conditions set by the group, the vehicle is overpowered during the ascent trajectory to gain as much acceleration as possible, within engine and human restrictions. Extensive optimization of the ascent trajectory through energy-state methods was conducted to compensate for the overpowered propulsion system. Upon staging, the orbiter executes a full SSME thrust acceleration out of the atmosphere to achieve orbit in a total time of 44 min.

##### Scarlet Carrier

|               |                      |
|---------------|----------------------|
| Length        | 210 ft               |
| Wing Span     | 150 ft               |
| Height        | 69 ft                |
| Panform Area  | 8000 sq ft           |
| Aspect Ratio  | 2.81                 |
| Fueled Weight | 423,250 lb           |
| Propulsion    | 8 GE Turbofanramjets |

The Scarlet carrier (Fig. 2) is a 210-ft-long high delta wing/cylindrical body configuration to allow for simplified analysis and easy manufacturing. The eight liquid hydrogen-fueled, full-scale GE turbofanramjets are located under the wings next to the body in a square "quad-pod" formation. The canards are used during takeoff and landing, as well as during staging to enhance stability and controllability.

##### Scarlet Orbiter

|                |             |
|----------------|-------------|
| Length         | 138 ft      |
| Wing Span      | 65 ft       |
| Height         | 13 ft       |
| Planform Area  | 1311 sq ft  |
| Aspect Ratio   | 1.5         |
| Staging Weight | 385,000 lb  |
| $\Delta V$     | 19,835 ft/s |
| Propulsion     | 1 SSME      |

The Scarlet orbiter (Fig. 3) is a 138-ft-long low delta wing/body configuration similar to the space shuttle with the exception of retractable canards to be used exclusively for landing. Near the orbital altitude the SSME is throttled back to 65%, eventually cutting thrust altogether for LEO acquisition.

##### Gray Group

|                          |            |
|--------------------------|------------|
| Length                   | 207 ft     |
| Takeoff Distance         | 13,843 ft  |
| Takeoff Weight           | 710,000 lb |
| Staging Altitude         | 90,000 ft  |
| Staging Mach Number      | 6.0        |
| Carrier Mission Time     | 137 min    |
| Carrier Mission Distance | 2300 mi    |
| Time to Orbit            | 71 min     |

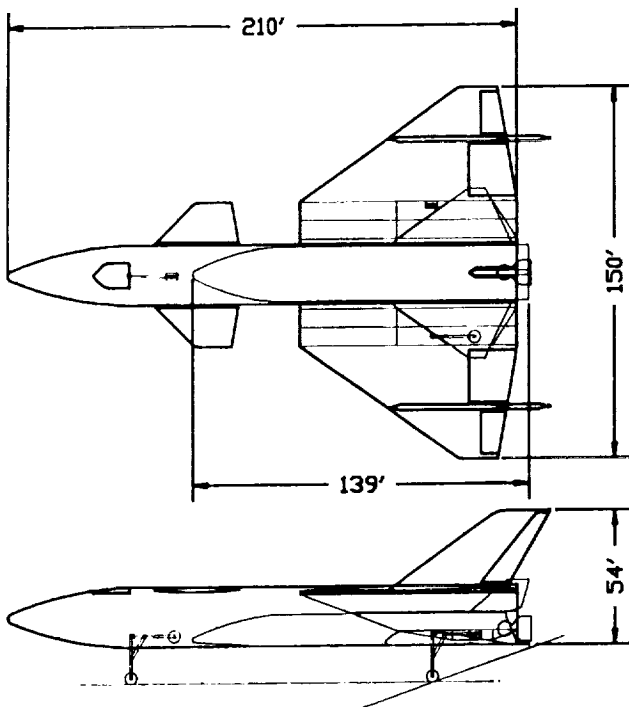


Fig. 1. Scarlet configuration.

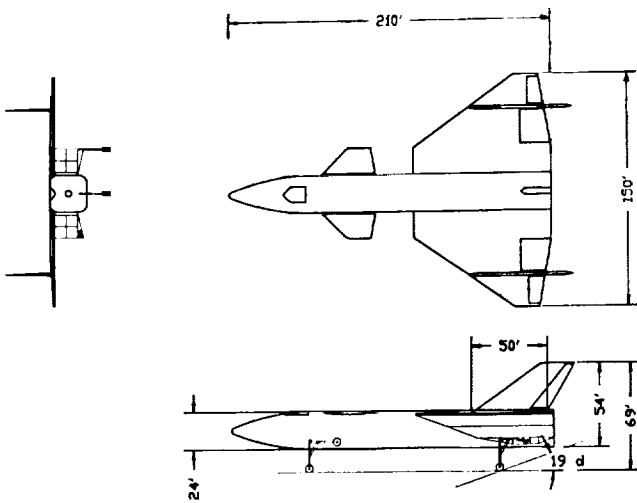


Fig. 2. Scarlet carrier.

The Gray Group configuration (Fig. 4) has a takeoff weight of 710,000 lb and stages at 90,000 ft at Mach 6.0. The Gray Group elected to design a vehicle that achieves orbit with the use of air-breathing engines. This drove the configuration to more of a blended wing/body carrier with the orbiter located in a piggy-back position. This allows the turbofanramjets to be placed together close to the centerline, allowing for a single propulsion module (inlets, engines, and nozzles). Due to the orbiter location, it will be necessary to dive during staging to

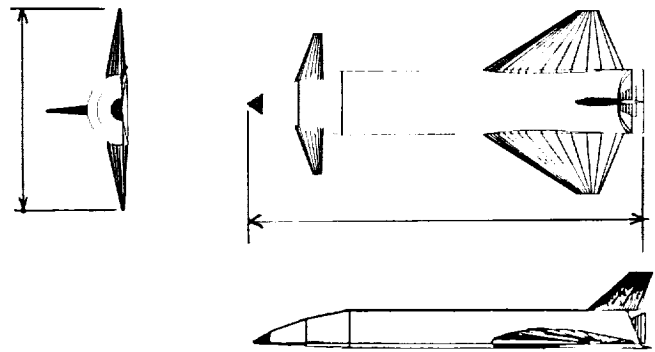


Fig. 3. Scarlet orbiter.

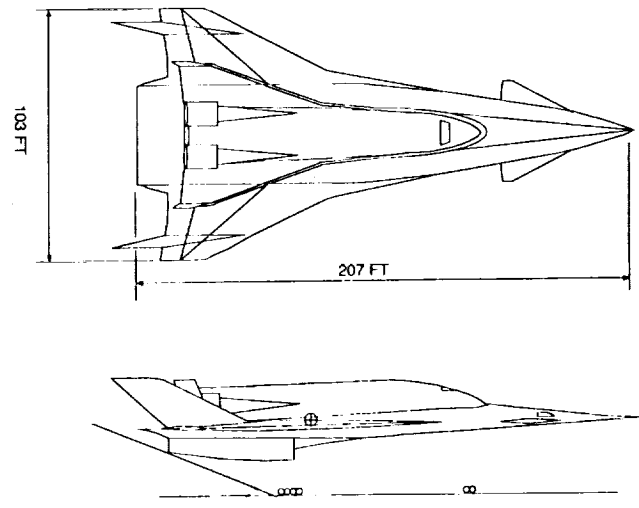


Fig. 4. Gray configuration.

make a clean and safe separation. In order to accelerate efficiently, the Gray Orbiter utilizes scramjets until Mach 12, decreasing the  $\Delta V$  requirements for the rocket; thus only a one-half-scale SSME was needed. This decreased the staging weight by 63,000 lb (17%), further reducing the weight of the entire system. While efficient acceleration reduces takeoff weight, it also produces a time to orbit of 71 min.

**Gray Carrier**

|               |                      |
|---------------|----------------------|
| Length        | 207 ft               |
| Wing Span     | 103 ft               |
| Height        | 46 ft                |
| Planform Area | 6500 sq ft           |
| Aspect Ratio  | 1.46                 |
| Fueled Weight | 390,000 lb           |
| Propulsion    | 6 GE Turbofanramjets |

The Gray carrier (Fig. 5) is a 210-ft-long blended cranked delta wing/body configuration giving a cleaner design. The six liquid hydrogen-fueled, 150%-scaled GE turbofanramjets are

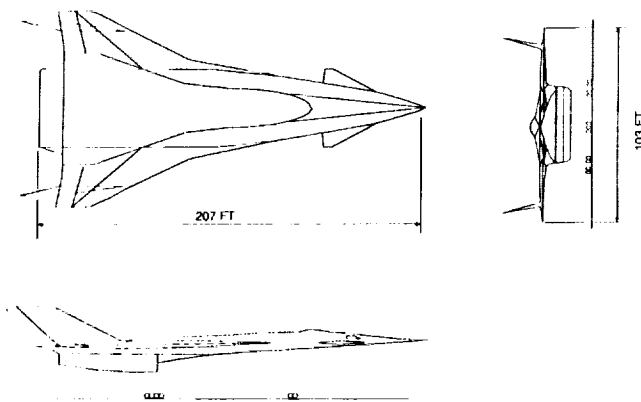


Fig. 5. Gray carrier.

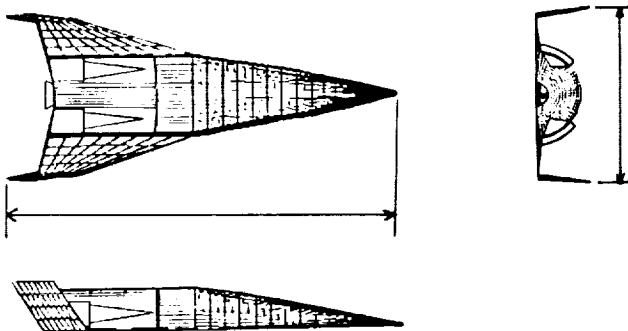


Fig. 6. Gray orbiter.

located in a row at the rear of the aircraft allowing for better engine-out characteristics.

#### Gray Orbiter

|                |                          |
|----------------|--------------------------|
| Length         | 130 ft                   |
| Wing Span      | 61 ft                    |
| Height         | 15 ft                    |
| Planform Area  | 1212 sq ft               |
| Aspect Ration  | 0.8                      |
| Staging Weight | 317,000 lb               |
| $\Delta V$     | 19,288 ft/s              |
| Propulsion     | 8 GE Scramjets, 1/2 SSME |

The Gray orbiter (Fig. 6) is a 130-ft-long low delta wing/half cylinder body configuration with the vertical stabilizers on the wing tips so they are not washed out at high angles of attack. The Gray orbiter employs eight GE scramjets and one-half SSME, which yields a lighter propulsion system because the scramjet oxidizer is not carried on the vehicle. This lowers the required internal volume, which further decreases the structural weight. While a scramjet and one-half SSME propulsion package is more efficient for flight through the atmosphere, lower accelerations are produced, and a longer flight time results.

## DESIGN APPROACH

A two-stage-to-orbit vehicle is essentially an accelerator, making optimization for a point along the mission profile (i.e., a cruise phase) unreasonable. Therefore, optimization of the trajectory itself was considered, with the ascent being the crucial phase. Due to the accelerating nature of the mission profile, the constantly changing propulsion and aerodynamic conditions needed to be continually incorporated into the ascent profile. The following sections outline different technical aspects covered during the design process.

### Propulsion

To produce an acceptable propulsion system, an engine and fuel must be matched over the required flight regime. Figure 7 shows a mass and volumetric energy density comparison for various fuels for air-breathing engines. Methylcyclohexane (MCH) is advanced endothermic fuel that breaks down into toluene and hydrogen just prior to combustion. While liquid hydrogen has a high mass energy density, a penalty is incurred due to its low volumetric density. Due to the short ranges and flight times of the vehicles there were no real volume constraints, and since weight minimization was necessary, both groups chose liquid hydrogen as a fuel for both the carrier and orbiter.

With the fuel chosen, an engine unit capable of operating over the desired mission must be employed. Figure 8 shows the performance for several candidate engines, and it is seen that the propulsion characteristics for a vehicle that operates over a large range of Mach numbers is discontinuous in nature. Because of this, the propulsion system was the final driver in the determination of the staging point.

**Carrier.** Since high staging Mach numbers were desired, a combination of an efficient turbofan for the subsonic and low supersonic flight regimes and a ramjet for the high supersonic and hypersonic flight regimes was chosen. Higher staging Mach numbers would be desirable to minimize orbiter weight, but the addition of another separate scramjet module was not worth the weight, drag, or complexity penalties.

The three typical turbofanramjet configurations are shown in Fig. 9: wrap-around, over/under, and tandem. Since both carriers are inherently long and thin for supersonic flight, a tandem turbofanramjet configuration was chosen by both teams due to its higher slenderness ratio (length/diameter).

General Electric provided a performance database for a turbofanramjet scheduled for entry in 2005 (Fig. 10). The performance data were given for a full-scale engine with scaling limits of 65% to 150%. The Scarlet carrier uses eight full-scale engines and the Gray carrier uses six 150%-scale engines.

Figure 11 gives the net thrust (ram drag is included) as it varies with Mach number and altitude for the full-scale turbofanramjet. The engine data assume a mil-spec inlet and nozzle. While complete inlet and nozzle designs were not completed due to time constraints, it was determined that the mil-spec requirements could be met.

**Orbiter.** The staging point had a significant effect on the orbiter weight. While staging altitude was a factor, the staging Mach number had the greatest impact on the orbiter weight due to the  $\Delta V$  required to get to the orbital velocity of 25,400

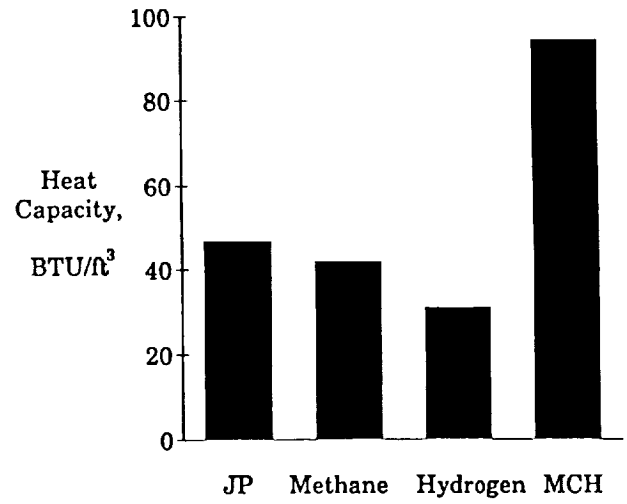
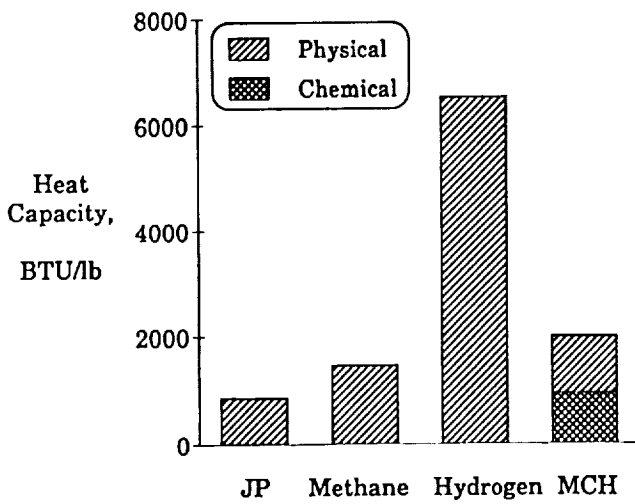


Fig. 7. Fuel comparison.

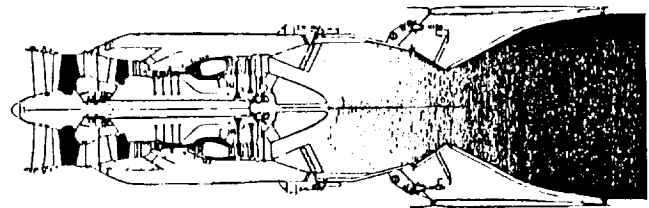
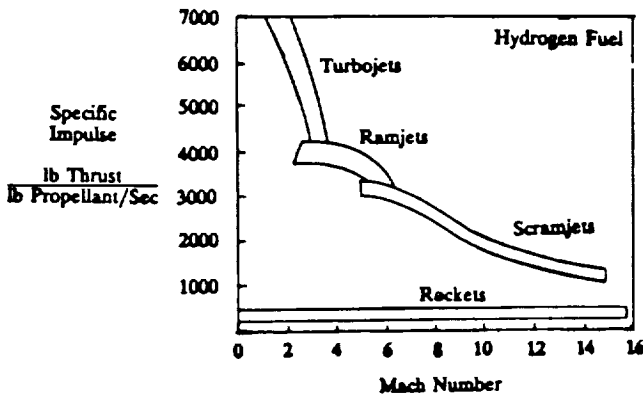


Fig. 10. G.E. turbofanramjet.

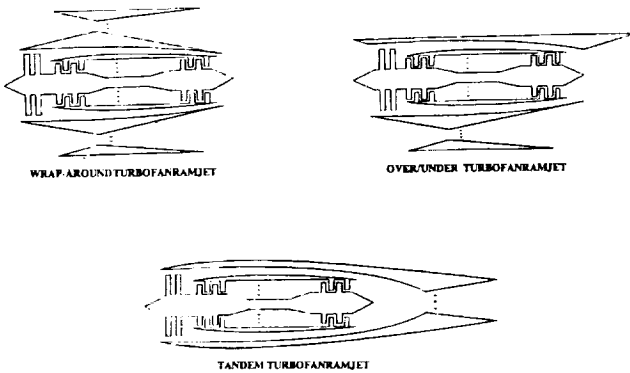


Fig. 9. Turbofanramjet concepts.

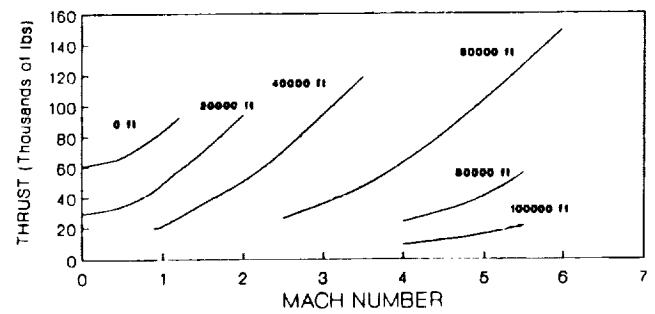


Fig. 11. Thrust vs. Mach number.

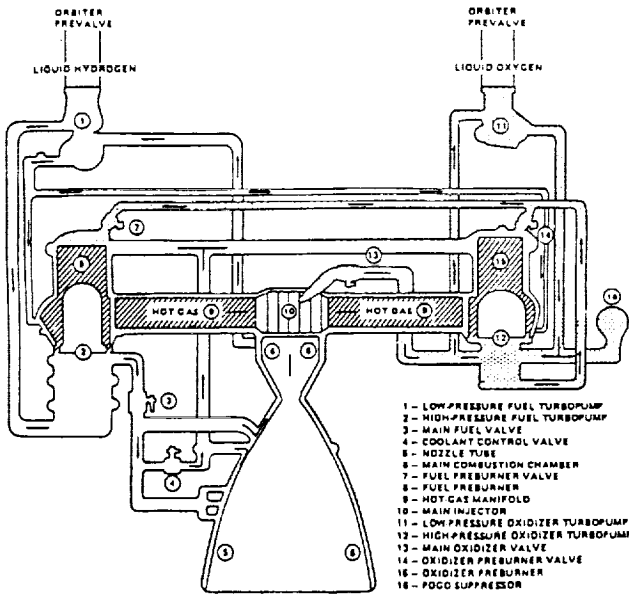


Fig. 12. SSME schematic.

ft/s.  $\Delta V$  is the main driver in the fuel weight, which accounts for about 80% of the orbiter staging weight.

Since LEO was the final destination, a rocket propulsion unit is required to accelerate through space. Due to the availability of performance and weight data, as well operational verification, both orbiter teams originally chose the liquid hydrogen/liquid oxygen-fueled SSME, schematically shown in Fig. 12. A full-scale SSME produces 470,000 lb of thrust in a vacuum. The SSME is throttled at 109% sea level thrust from ignition to near LEO, where it is throttled back to 65%. Prior to achieving orbit, the SSME is shut down and the orbiter acquires LEO with minimum thruster control.

The Gray orbiter team decided to use scramjets (Fig. 13) in order to minimize the fuel (specifically the oxidizer) use by the SSME. By accelerating to Mach 12 using scramjets, the  $\Delta V$  for the SSME was reduced from 19,288 ft/s to 13,364 ft/s allowing the SSME to be scaled down by 50% in thrust and weight.

The scramjet performance data was provided by General Electric and is given in Fig. 14. The Gray orbiter team uses eight scramjets to accelerate to Mach 12 then a one-half scale SSME to achieve orbit. This propulsion system did have its penalties in the added weight and complexity of inlets and nozzles for the scramjets, an active thermal protection system, as well as a greater technology risk. Inlets for the scramjets were investigated, and a single, fixed ramp, supersonic inlet (no throat) was chosen over a movable ramp system. This was because the slight improvements in efficiency of the variable ramps did not outweigh the associated weight, length, and complexity penalties. A weight reduction of 63,000 lb (17%) was realized due to using an eight scramjet/one-half scale SSME propulsion system instead of a single full-scale SSME.

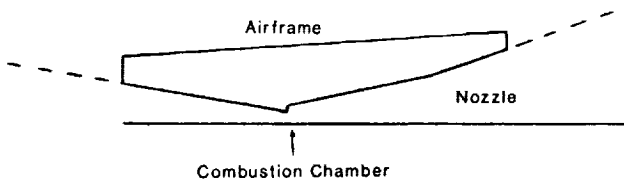


Fig. 13. Scramjet module.

**Aerodynamics**

The aerodynamic analysis of the vehicles was accomplished through a variety of techniques including (but not limited to): component drag build up, comparison with similar experimental results, shock-expansion theory, and subsonic potential theory.

**Carrier.** A typical drag polar for both carriers is shown in Fig. 15. Notice that the highest drag coefficients occur at Mach 1.1. This drove the propulsion system to be scaled for the transonic flight regime. The low drag coefficients occurring at Mach 6 are the result of the generally sleek configuration suited for high supersonic flight.

**Orbiter.** As seen in Fig. 16, the typical lift and drag coefficients do not change drastically for the ascent from staging to orbit. The aerodynamic characteristics of the Gray orbiter influence its shape more than the Scarlet orbiter for two reasons: the Gray orbiter accelerates through the atmosphere using scramjets, and upon ascent from takeoff it is exposed to the freestream riding piggy back on the Gray carrier, whereas the Scarlet orbiter quickly accelerates out of the atmosphere, and is housed within the fuselage of the Scarlet carrier upon ascent.

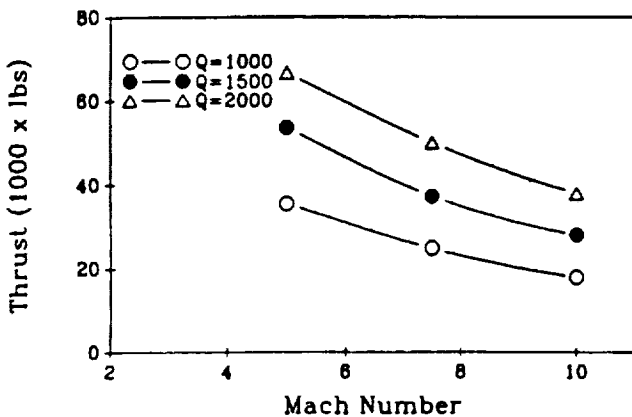


Fig. 14. Scramjet performance.

**Stability and control**

Stability and control was one of the final sections of the vehicle designs considered by the two design groups. Longitudinal static

stability was determined for three critical points in the mission: takeoff, staging, and landing. In addition to the stability and control problems associated with takeoff and landing operations, a two-stage-to-orbit vehicle must execute a staging maneuver. With Stability Augmentation Systems (SAS) available, static stability at staging is not a requirement, but controllability is. Fuel management systems help stability by controlling the center of gravity travel, which in turn reduces the trim drag of the vehicle.

While it is acceptable for a hypersonic aircraft to be unstable at some point along the mission profile, a two-stage-to-orbit vehicle has a special problem as there is a sudden abrupt movement of the center of gravity upon staging. This center of gravity shift is not only in the longitudinal direction, but also in the vertical direction (Fig. 17). This affects longitudinal, lateral, and roll controllability, and therefore it is necessary to know the amount of control necessary during the staging maneuver. While the vehicles are statically stable at all points along the mission profile, including before and after staging, a dynamic stability analysis was not completed for the staging maneuver.

**Trajectory**

Incorporating constantly changing aerodynamic and propulsion models into a specific trajectory that does not lend itself to optimization was indeed difficult. The ascent trajectory was found to be a strong force in the takeoff weight of the system due to the fuel burned during accelerating ascent. The staging point was found to be the main driver in the weight of the orbiter due to the  $\Delta V$  needed required to achieve LEO. Parametric studies were conducted to show the effect of staging altitude and Mach number on the weight of the vehicle. It was found that the staging altitude had only a slight effect on the vehicle weight, whereas the staging Mach number had a significant effect, especially on the orbiter weight. As the staging Mach number increased, the carrier weight increased and the orbiter weight decreased, but the carrier weight increased at a slower rate than the orbiter weight decreased; thus, the system takeoff weight decreased for increasing staging Mach numbers. In the end, the staging Mach number was specified by the maximum speed of the propulsion unit.

**Carrier.** Both carrier teams followed similar flight profiles (Fig. 18) typical of two-stage-to-orbit vehicles: take off, accelerate and climb towards Mach 1, punch through the transonic regime, accelerate until a specified constant dynamic pressure ( $q$ ) is attained, follow this constant  $q$  until the staging point, stage at the specified Mach number and altitude, then descend and possibly cruise at a maximum lift-to-drag ratio until landing. Both groups chose a maximum  $q$  of 1500 psf based on research into similar conceptual hypersonic vehicles. The Gray carrier team simply iterated on the trajectory profile until a minimum fuel-to-stage was obtained.

The Scarlet carrier team chose to optimize the entire trajectory profile up to the constant  $q$  intersection using energy-state methods (Figs. 19 and 20). The set of curves in Fig. 19 represent constant total energy levels (kinetic plus potential energy). The contour plot in Fig. 19 is excess power of the aircraft, which shows exactly where the vehicle can accelerate, climb, or a

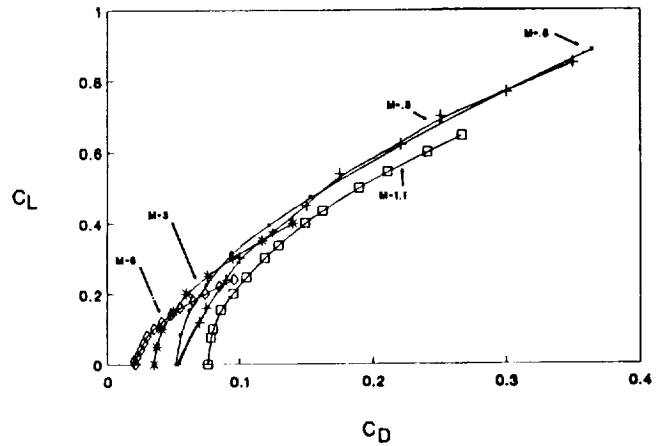


Fig. 15. Carrier  $C_L$  vs.  $C_D$ .

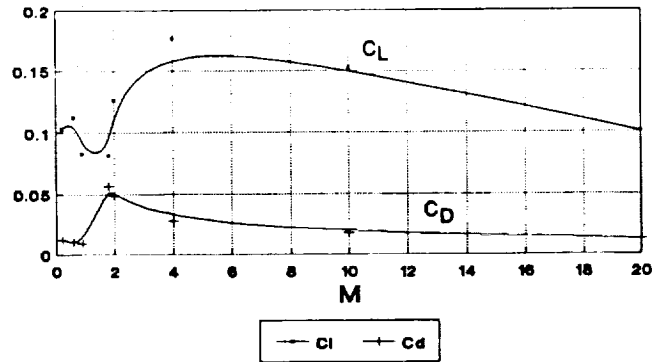


Fig. 16. Orbiter  $C_L$  and  $C_D$  vs.  $M$ .

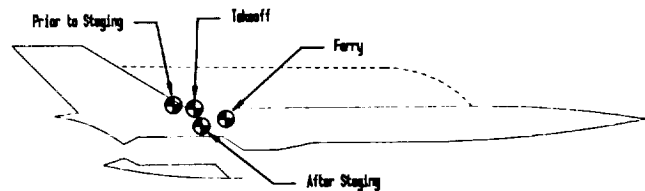


Fig. 17. Center of gravity travel.

combination of both. By flying through the set of points where a constant energy curve is tangent to an excess power contour, a minimum-fuel-to-climb trajectory is obtained.

By further defining specific excess power as excess power divided by thrust and specific fuel consumption, the thrust pinch is seen to occur at Mach 1.6 (Fig. 20). The vehicle is actually flying from the subsonic excess power region to the supersonic excess power region. If the excess thrust (thrust-drag) is decreased, a bottleneck is produced between these two excess

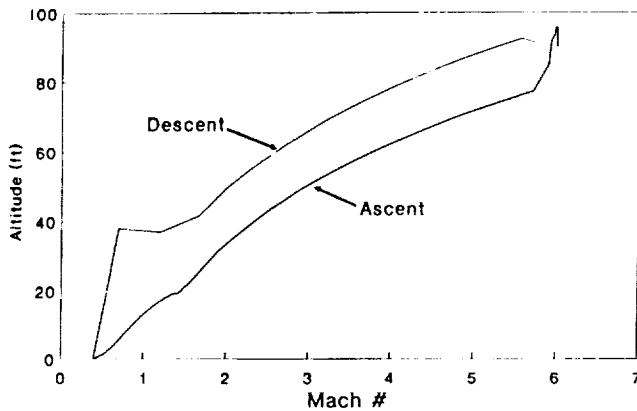


Fig. 18. Mission acceleration.

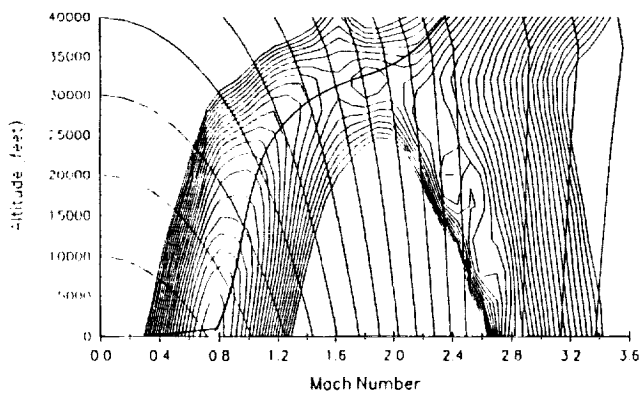


Fig. 19. Minimum fuel to climb.

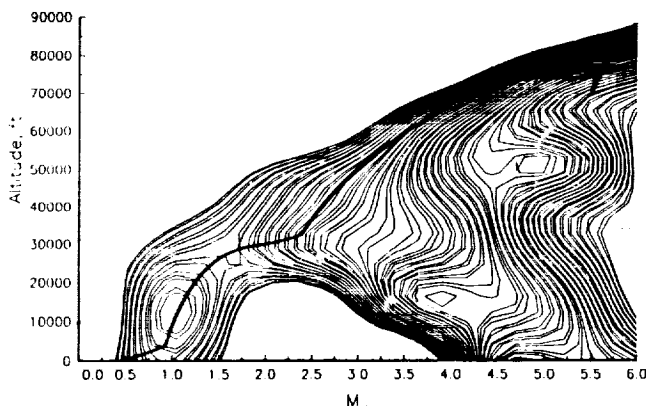


Fig. 20. Specific excess power.

power regions, and a further decrease in excess thrust completely separates the two regions. When this occurs, it becomes impossible to traverse the transonic flight regime.

Once staging occurs (the carrier and the orbiter actually separate), the carrier undergoes an instantaneous weight reduction of roughly 50%, causing the net lift of the carrier to dramatically increase. This, coupled with the stability fluctuations during staging due to the center of gravity shift, causes the staging process to be potentially precarious.

The Gray Group starts staging at Mach 6.0 at 90,000 ft, then dives while staging to avoid a collision with the released orbiter mounted on the carrier upper surface. The Scarlet Group stages at Mach 5.5 and 80,000 ft and avoids the collision problem by releasing the orbiter out from under the carrier, allowing the increase in net lift to pull the carrier up and away from the orbiter.

After staging, both carriers then descend on another constant  $q$  line that will maximize range. The Scarlet carrier will land in Florida, and the Gray carrier returns to the original takeoff location (Fig. 21).

**Orbiter.** Both the Scarlet orbiter and Gray orbiter design teams used ENTRAN (Entry Trajectory Analysis Program) provided by Wright Patterson Air Force Base. The code specifies a final condition on orbital altitude, speed, and weight, and then backs down an ascent trajectory. The propulsion parameters are then changed to intersect the trajectory at the desired point (i.e., the staging point).

The Scarlet orbiter uses a full-scale SSME, and therefore backed down the ascent trajectory from ENTRAN to intersect the staging point. The Scarlet orbiter mission profile consists of a 109% thrust SSME burn, throttle down to 65% thrust, and then cut thrust just before orbit is achieved in order to coast into the orbital altitude with minimum use of control thrusters. The Gray orbiter uses scramjets to accelerate and climb to Mach 12 and 150,000 ft, thus backs down the ENTRAN ascent trajectory to this point. There it initiates a full burn of the one-half-scale SSME, then cuts thrust to coast into LEO. Figure 22 shows a comparison of the two orbiter ascent trajectories.

Both orbiters execute similar reentry maneuvers by skipping off the atmosphere (Fig. 23). These reentry trajectories were also computed by ENTRAN. As the loads on the orbiter exceed a specified level the orbiter "skips" to a higher altitude losing kinetic energy and radiating heat, then descends again with decreased kinetic energy, repeating this procedure until a complete reentry into the atmosphere can be executed.

## Weight

The structural weights of the vehicle were computed by comparison with similar vehicles designed by NASA, industry, and academia. The carrier design teams kept their structural weight percentage in line with similar vehicles at approximately 35% of the fully fueled carrier alone weight (no orbiter). Similarly the orbiter structural weight was approximately 10% of the staging weight. The Scarlet orbiter team went on to verify their structural weight on a component basis. By taking a survey of five similar orbiter vehicles, they were able to obtain an average

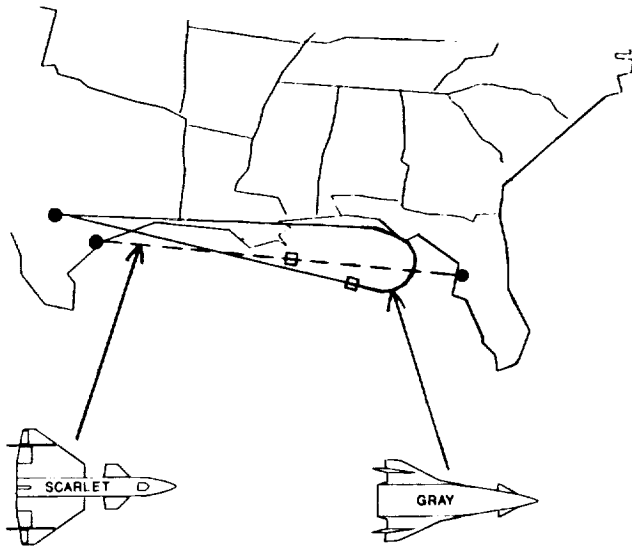


Fig. 21. Mission courses.

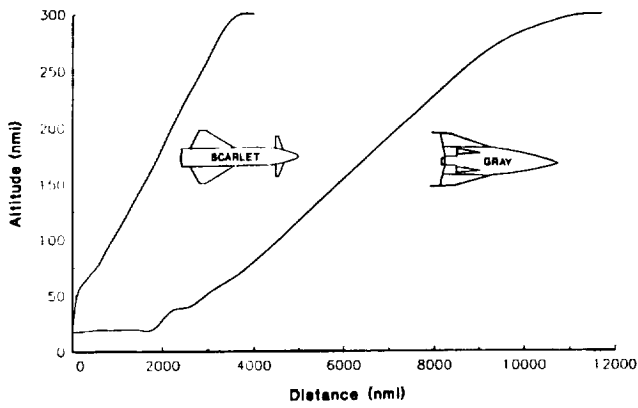


Fig. 22. Orbiter trajectories.

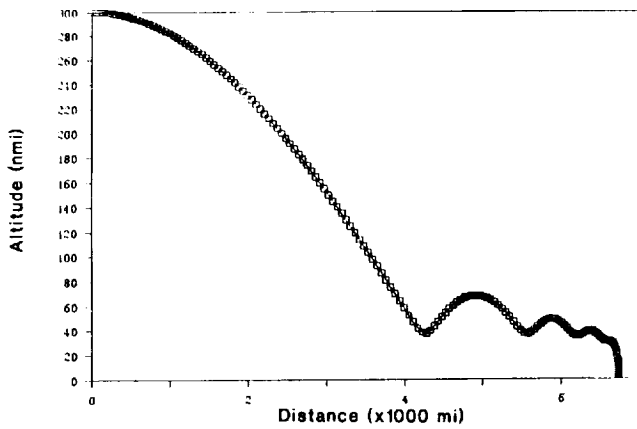


Fig. 23. Reentry trajectory.

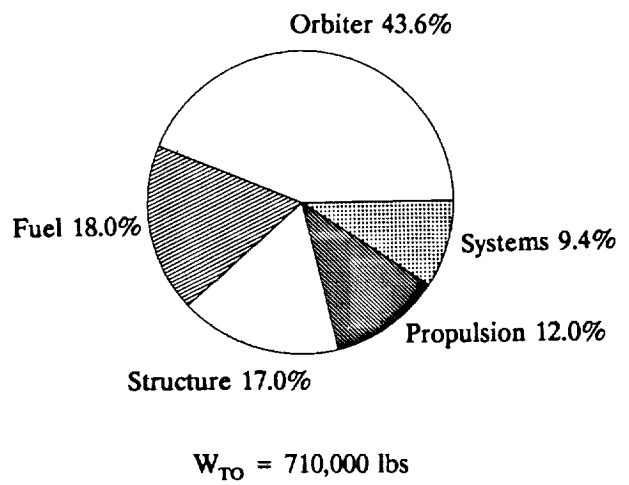
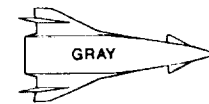
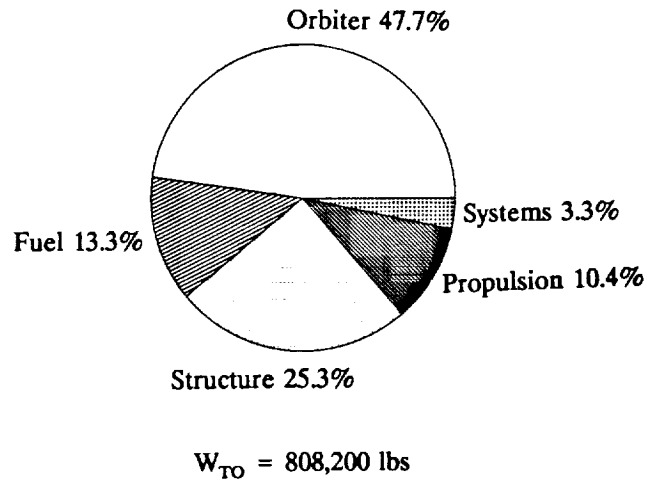
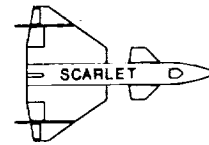
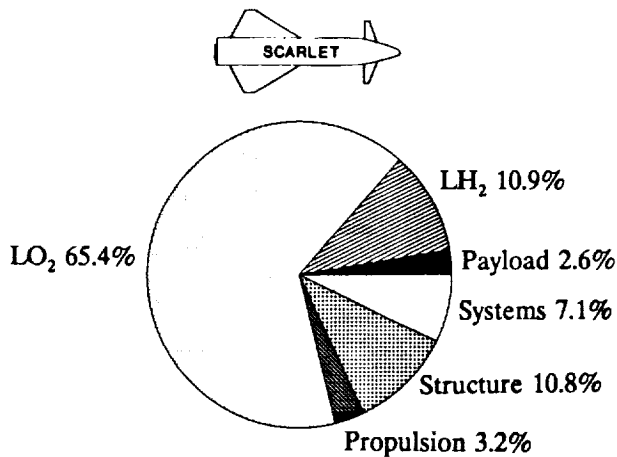
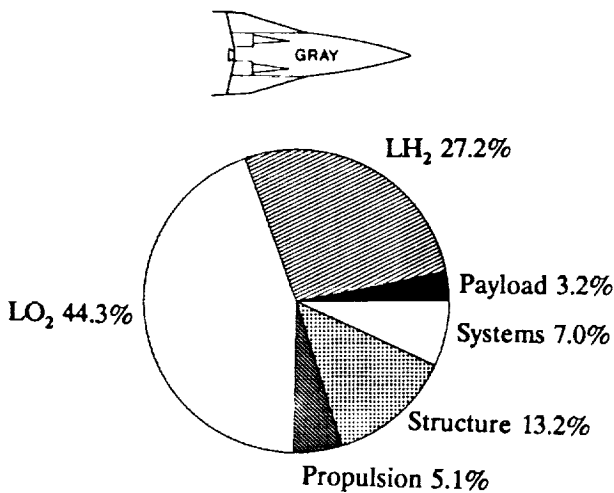


Fig. 24. Carrier weights.



$W_{ST} = 385,200$  lbs



$W_{ST} = 317,000$  lbs

Fig. 25. Orbiter weights.

weight per area for different components (i.e., wings, fuselage, etc.) of their orbiter. They found that the original weight percentage estimation was indeed valid. Figures 24 and 25 show the carrier and orbiter weight comparisons, respectively.

The orbiter staging weight was the most significant single weight of the vehicle. Small changes in the orbiter weight produced larger changes in the system weight because the orbiter is essentially the payload of the carrier. The primary driver in the orbiter weight is the staging-to-burnout mass ratio, a strong function of staging Mach number due to the  $\Delta V$  to a fixed 25,400 ft/s orbital velocity (Fig. 26).

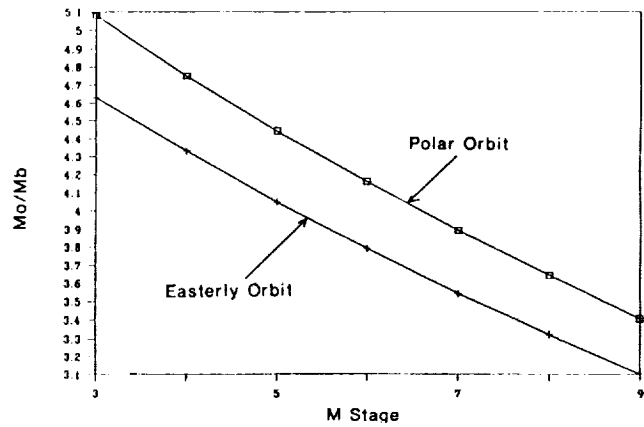


Fig. 26. Mass ratio vs. staging Mach number.

**PRACTICAL EXPERIENCE**

The OSU hypersonic design class is set up to give the participating students a taste of the "real world." Until this design series, the students never worked together on different parts of the same project, only on the same homework assignments as their classmates. Not only does the design team approach demonstrate the technical compromises of aircraft design, but also the personal interactions that are associated with working in a group. This academic year's project had a two-tier organization within each group; the students worked together as design teams, and the carrier and orbiter teams interacted together to form the design group. Because there was no project leader for each design group, the individual design teams compartmentalized their efforts, with the carrier and orbiter teams in each group unaware of what the other was doing. This was alleviated by the Graduate Teaching Assistant (GTA) assuming the position of project leader for both design groups. This allowed the GTA to subtly direct the projects, while still having the students actually design the vehicles (i.e., no heavy-handed intervention).

TABLE 1. Vehicle comparisons

|                      |                     |                         |
|----------------------|---------------------|-------------------------|
| Length               | 210 ft              | 207 ft                  |
| Wing Span            | 150 ft              | 103 ft                  |
| Planform Area        | 8000 sq ft          | 6500 sq ft              |
| Carrier Weight       | 423,200 lb          | 390,000 lb              |
| Orbiter Weight       | 385,000 lb          | 320,000 lb              |
| Takeoff Weight       | 808,200 lb          | 710,000 lb              |
| Carrier Propulsion   | 8 TFRJets<br>(100%) | 6 TFRJets<br>(150%)     |
| Orbiter Propulsion   | 1 SSME              | ½ SSME &<br>8 Scramjets |
| Staging Mach Number  | 5.5                 | 6.0                     |
| Staging Altitude     | 80,000 ft           | 90,000 ft               |
| Orbiter $\Delta V$   | 19,835 ft/s         | 19,288 ft/s             |
| Carrier Mission Time | 35 min              | 137 min                 |
| Time to Orbit        | 44 min              | 71 min                  |

### SUMMARY

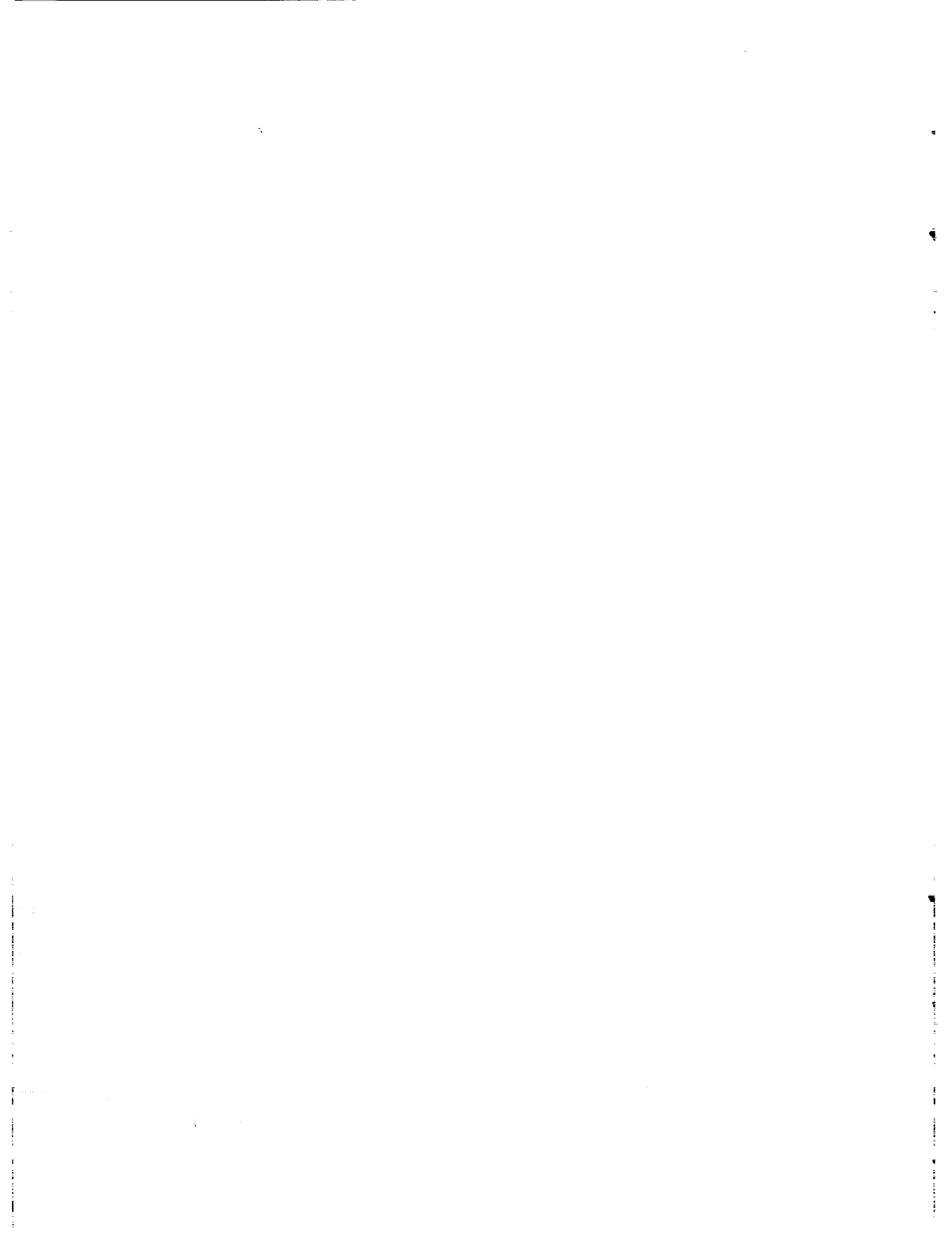
Two complete designs of a conceptual two-stage-to-orbit vehicle have been developed by two independent student design groups. Table 1 provides a direct comparison of the two vehicles.

These vehicles were designed as a complement to the current U.S. space program, which is heavily dependent on the space shuttle. A two-stage-to-orbit vehicle is seen as a compromise between the operating costs of a next-generation heavy lift rocket system and the technical obstacles of a single-stage-to-orbit vehicle.

The most notable contrast between the two vehicles is the almost 100,000-lb difference in takeoff weight. This is primarily due to the larger weight of the Scarlet orbiter, which must

accelerate over a larger  $\Delta V$ , using a less efficient propulsion system (all rocket). This produces a greater staging weight due to the amount of fuel burned, and a larger orbiter staging weight produces a larger "payload" weight for the carrier, thereby increasing the weight (and size) of the Scarlet carrier.

While there are still questions to be addressed pertaining to two-stage-to-orbit vehicles, this design project was well worth the effort of the students, providing them with insight and instruction into the conceptual design process.



ASUR

ECOLE POLYTECHNIQUE FEMININE

S8-05  
160584

P-5

INTRODUCTION

The Ecole Polytechnique Feminine (E.P.F) is a French engineering school for women. The students who presented the project at the Summer Conference are in the fourth year of a five year program. For the second time, the E.P.F worked on a aeronautical project with the Ohio State University. This year, the theme of our study was to design a hypersonic carrier aimed to launch an orbiter at Mach 6, a range of 375 miles and an altitude of 95,000 ft.

We called our plane ASUR. In French ASUR means the blue sky, the same sky that links our countries across the ocean. Moreover, ASUR is an anagram of USRA.

This work benefits from work on reusable hypersonic aircraft in Europe, and especially on two of them: STAR-H and Sanger. STAR-H is a French project. This hypersonic aircraft would replace Ariane 5 in launching a shuttle smaller than Hermes. Sanger is a German project. Its objective is to launch a manned shuttle called HORUS, but Ariane 5 would be kept for heavy cargo launches. These two projects are in competition in Europe to be a launcher of the European Space Agency.

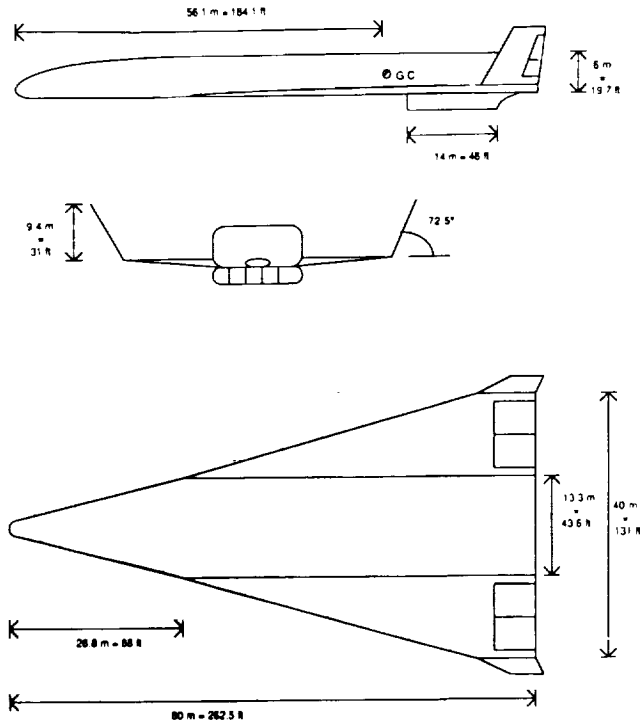


Fig. 1. ASUR 3-view.

GEOMETRY

The carrier's geometry (Fig. 1) has been determined from the fuel volume necessary to accomplish the worst case mission scenario: that separation is impossible and the carrier comes back with the orbiter and lands with almost no fuel.

The parameters known at the beginning of the study were the weight of the orbiter:  $W_{orbiter} = 136$  tons (2,990,823 lb), and the specific impulse of our engine:  $I_{sp} = 2000$  s.

Some other data we needed were given by other work on hypersonic aircraft:  $\Delta V = 400$  m/s; carrier's dry mass  $W_{d,carrier} = 166$  tons (366,030 lb); takeoff velocity  $TOV = 100$  m/s; the lift-off coefficient  $C_{lift-off} = 0.37$ ; the aspect ratio  $\lambda = 1$ ; and body width is equal to 1/3 of the wing span.

These data allowed us to calculate the fuel volume, the plane's geometry, and the tank specifications.

Fuel Volume

The carrier's takeoff gross weight (TOGW) and fuel volume (V) were found to be  $TOGW = 370$  tons (815,850 lb), and  $V = 971.3$  m<sup>3</sup> (256,645 gallons), respectively.

Geometry

The wing area is simply deduced from the equation  $S = 1600$  m<sup>2</sup> (17,222 sq ft). The span of the delta wing is also easily obtained:  $b = 40$  m (131 ft).

We know that the body width is equal to 1/3 of the wing span and that the forward section has to remain constant, so we deduce the dimensions of the backward body as seen in Fig. 2.

Current work on hypersonic design advises us to take a wing sweep of 74°, from the beginning of the backward body. We also obtain the length of the winglets (8 m). Moreover the winglets are designed to provide better aerodynamic efficiency; that's why the extremities of the winglets of the carrier and the orbiter are in the same plane.

For the given backward body dimensions, we have two possibilities to store the required volume of hydrogen, using two or three tanks of the same length. We choose the 2 tanks configuration because it allows us to put an extra small tank between the two large ones.

Weight

To estimate the weight of different parts of the aircraft (Table 1), we use a statistical approach using several of Concorde's derivation methods and also methods applied to high speed military aircraft.

76  
INTERNATIONALLY MEANS

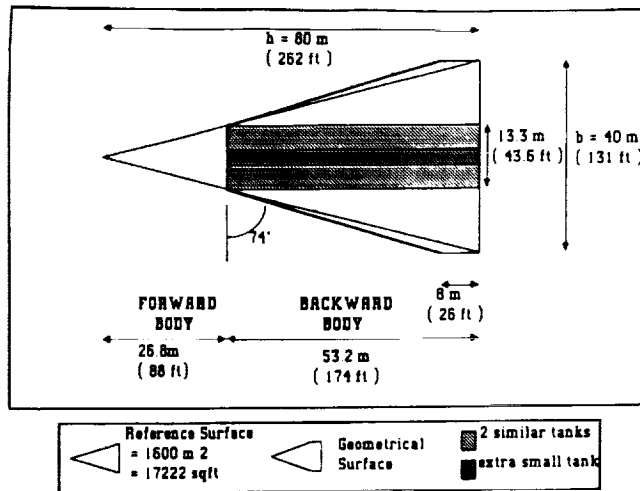


Fig. 2. Geometry.

TABLE 1. Component Weights and c.g.

| Component                  | Weight |        | Center of Gravity Position $x_i$ |       |
|----------------------------|--------|--------|----------------------------------|-------|
|                            | tons   | lbs    | m                                | ft    |
| Wings                      | 42     | 92593  | 59                               | 193.6 |
| Forward body               | 5.35   | 11795  | 17.6                             | 57.74 |
| Backward body              | 36.65  | 80798  | 53.2                             | 174.5 |
| Winglets                   | 6      | 13228  | 78                               | 255.9 |
| Nosegear                   | 1.3    | 2866   | 17.6                             | 57.74 |
| Principal nosegear         | 11.7   | 25794  | 55.9                             | 183.4 |
| Engines                    | 16     | 35273  | 69                               | 226.4 |
| Inlet                      | 10     | 22046  | 61                               | 200.1 |
| Tanks                      | 14     | 30864  | 53.2                             | 174.5 |
| Fuel system                | 4      | 8818   | 53.2                             | 174.5 |
| Flight control system      | 3      | 6614   | 55.9                             | 183.4 |
| Auxiliary control system   | 0.1    | 220.5  | 55.9                             | 183.4 |
| Instruments                | 0.1    | 220.5  | 17.6                             | 57.74 |
| Hydraulic system           | 7      | 15432  | 55.9                             | 183.4 |
| Power supply               | 3.5    | 7716   | 55.9                             | 183.4 |
| Navigation & communication | 1      | 2205   | 17.6                             | 57.74 |
| Installations              | 2      | 4410   | 55.9                             | 183.4 |
| Oxygen                     | 0.04   | 88.2   | 17.6                             | 57.74 |
| Fire extinction            | 0.2    | 441    | 69                               | 226.4 |
| Air conditioning & APU     | 1      | 2205   | 55.9                             | 183.4 |
| Defrosting                 | 0.2    | 441    | 55.9                             | 183.4 |
| Ventilation                | 0.3    | 661.5  | 17.6                             | 57.74 |
| Crew                       | 0.4    | 882    | 17.6                             | 57.74 |
| Fuel unfit for consumption | 4      | 8818   | 53.2                             | 174.5 |
| Oil                        | 0.1    | 220.5  | 55.9                             | 183.4 |
| TOTAL                      | 170    | 374779 |                                  |       |

## STABILITY

To analyze the stability, we calculate the relative position between the center of gravity and the aerodynamic center. We can observe that the aerodynamic center (F) is positioned just before the center of gravity (G) in reference to the aircraft's nose (O); OG = 56.13 m (184.7 ft); OF = 55.9 m (183.4 ft).

Thus our plane can be considered slightly unstable. But at supersonic and hypersonic speeds, the aerodynamic center moves backward by approximately 12 m and makes it stable. Moreover, a computer simulation shows that the little instability of our aircraft can be easily corrected with automatic flight controls.

## MATERIALS

Because ASUR flies at high speed (Mach > 4), its structure will experience high temperature. The materials that will be used for the structure, need to have light weight, good mechanical properties, resistance to corrosion and ablation, reusability, and good protection of the rest of the aircraft from heat.

There are several possibilities. They include titanium materials (but temperatures between 900°F and 1000°F damage the structure); carbon-carbon materials which keep their specifications of resistance at high temperatures; and titanium/plastic alloys joined to a new aluminium/titanium and carbon composite which resist high temperatures and decrease the weight of the plane. We choose this last solution but they are not yet developed.

Whatever material is chosen it will undoubtedly face the same kind of problems. Thermal gradients cause heat fatigue which is very harmful for a plane that has to be reusable. The discontinuity of temperatures lead to internal stresses and deformations that can induce cracks in the structure (the tanks). A dangerous brittleness of the steel landing-gear appears at 200°C, so they must be protected. The equipment necessary for heat protection (fuel, landing-gears) and the recooling of the leading edge of the wings will make the aircraft heavier.

## PROPULSION

The optimization of future space launchers depends mainly on the choice of the combined cycle propulsion concept. We use two solutions: the turbo-rocket-ramjet and the turbo-expander-rocket (Fig. 3). The choice between these two solutions is difficult because both engines have similar performance. But all the mission calculations have been made with the turbo-expander-rocket.

### Turbo-Rocket-Ramjet (TRR)

The TRR flies in a rocket mode to Mach 3 and then in a ramjet mode. The airbreathing operation of a turbo-rocket-ramjet is limited to a flight Mach number of about 6 because of high temperatures. The specific impulse is not very high compared to some other combined cycle propulsion concepts but it has the advantages of a lower weight and less technological complexity.

### Turbo-Expander-Rocket (TER)

Hydrogen is heated before burning in the combustion chamber, which allows the gas to be released through the turbine. Thus we have an expansion effect, not a combustion effect, which is why the engines consume less and the specific impulse increases. But drawbacks are the weight and the technological complexity of the cooling system.

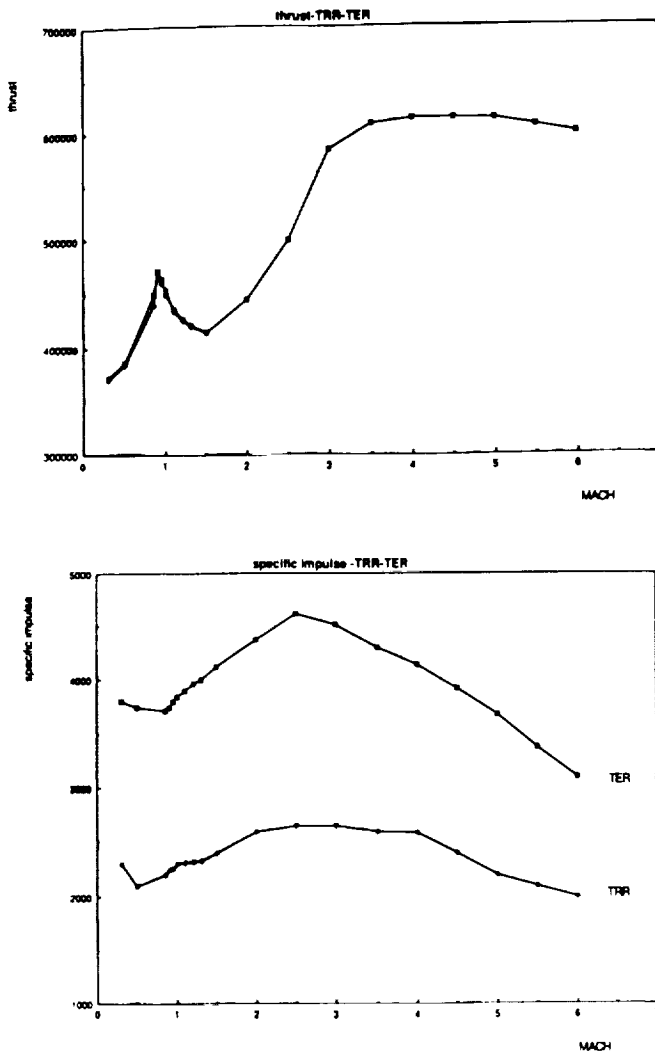


Fig. 3. Thrust and Specific Impulse Calculations.

We have to launch the orbiter at Mach 6 at 30 kilometers, so we need 5 airbreathing engines. They are necessary to overcome the drag rise at Mach 1.3.

### Fuel

For a hypersonic aircraft, fuel determines the structure of the plane because of storage and tank dimensions. We use cryogenic fuel. We have three possibilities:  $LH_2 + LOX$ ;  $LH_2$ ; or Methane. Methane has a very high density and can be used easily but it has a very short functioning time and is less energetic than the others.

$LH_2$  and  $LH_2 + LOX$  are more energetic and have a longer functioning time. Moreover, they can be used to cool the structure, but the supply system is complex and storage is difficult.

$LH_2 + LOX$  and  $LH_2$  are the best solutions for future hypersonic aircraft. We choose  $LH_2$  because  $LH_2 + LOX$  increases the takeoff weight. Instead of  $LOX$ , ASUR uses oxygen from the air because it flies below 35 km and we consider that the atmosphere has enough oxygen density at those altitudes. The orbiter uses  $LH_2$ . If it can't be launched, ASUR has to return with the orbiter and more fuel will be consumed than has been planned. Because the orbiter and ASUR use the same fuel, ASUR could use fuel from the orbiter to return. On the other hand, if the launch can be made, ASUR could top off the orbiter's tank just before the separation.

### Inlet

We choose the Sanger solution of 5 separate inlets, one for each engine.

### DRAG

We calculate first stage drag and composite drag and compare the two to show the influence of the second stage on the first stage (Fig. 4).

For the drag polar equation  $C_d = C_{d_0} + k \cdot C_l^2$ ,  $C_{d_0}$  is the zero lift drag coefficient and  $k$  the induced drag coefficient. We calculate these two coefficients (Fig. 4). On the  $C_{d_0}$  curves, we can see that the orbiter has more influence in the supersonic and hypersonic domain than in the subsonic one because of the wave drag which depends on pressure distribution. The  $C_l/C_d$  ratio decreases until Mach 1.3 and then it increases regularly, but it doesn't reach very big values. This ratio has been calculated during the climb part of the mission. The thrust-drag curve of the composite shows us that we need 5 engines to overcome the drag rise at Mach 1.3.

### MISSION

Some mission specifications are expected to allow the second stage flight. We have to launch the orbiter at Mach 6.0 with an altitude of between 95,000 and 100,000 ft at a range of 375 miles. From this information, we choose the mission profile (Fig. 5).

We decided to define a climb phase along a constant indicated airspeed as it was nearly the minimum fuel climb path to Mach 6.0, 95,000 ft. Then, the orbiter is separated from ASUR. And, ASUR alone, makes a turn and descends along the same constant indicated airspeed.

### Climb Phase

The composite climbs along an constant indicated airspeed of 550 knots to the separation point. In order to verify our assumption, we ran a program that gives us the specifications and amount of fuel consumed at each flight point. Drag study results, engine curves, and the constant indicated airspeed curves were input to the program. With a takeoff weight of 370 tons (815,850 lb), the aircraft uses 40 tons (88,200 lb) during climb. With 64 tons (141,120 lb) of usable fuel remaining, we could achieve the mission, but the reserve fuel quantity wouldn't be acceptable. So, we decided to add a little tank between the

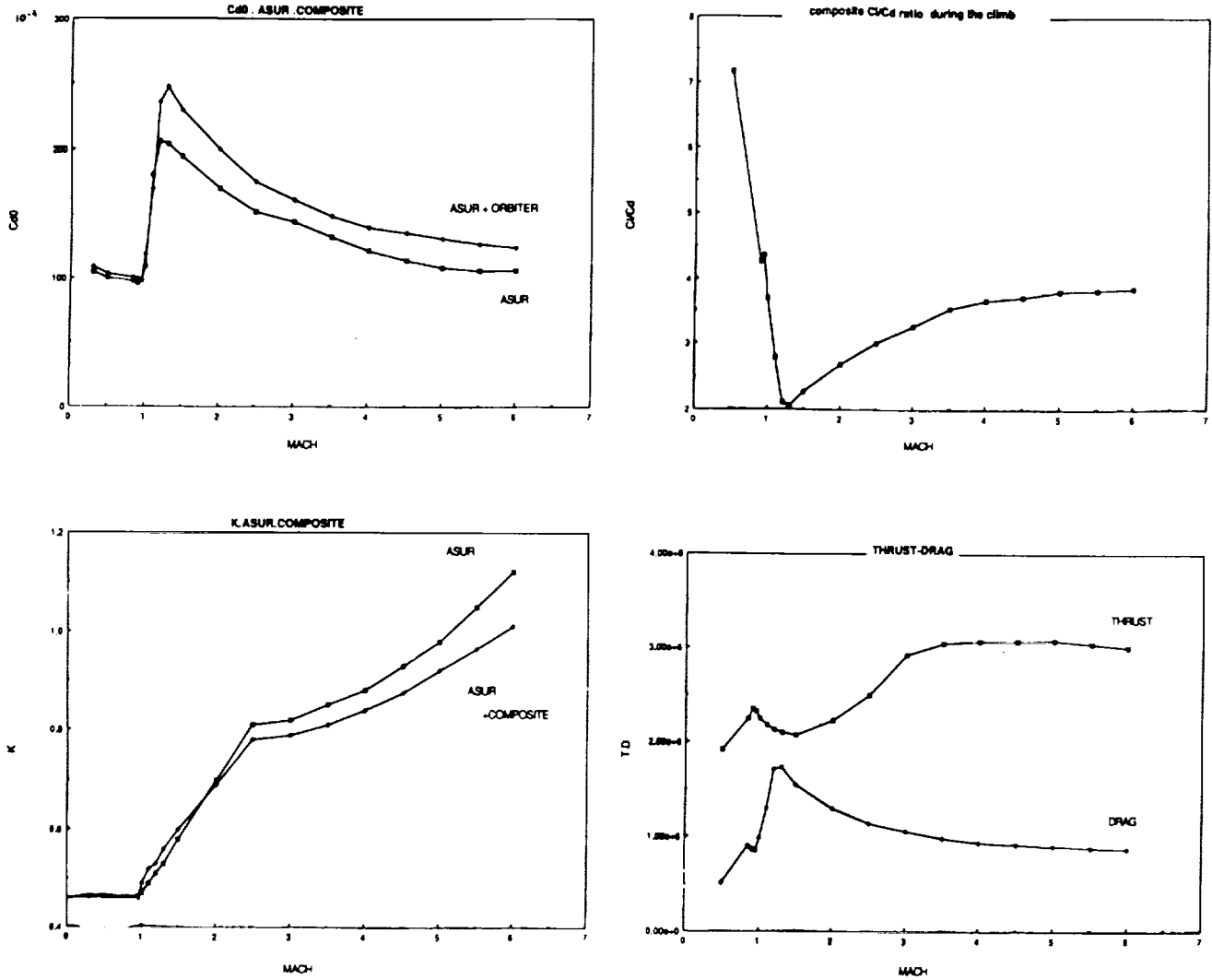


Fig. 4. Drag Calculations.

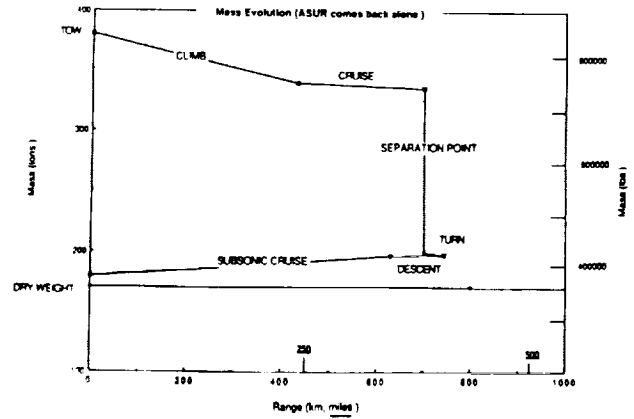
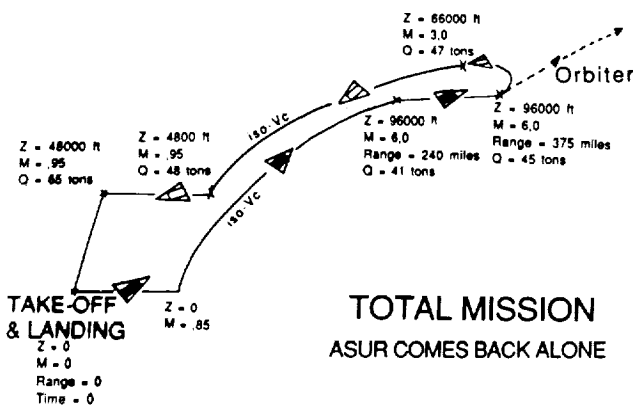


Fig. 5. Mission Profile.

two others containing 10 tons (22,050 lb). Even if we don't use the whole quantity of fuel, the excess would be used to fill up the orbiter's tank. We ran the program again with a takeoff weight of 380 tons (837,900 lb). We obtain a consumption of 41 tons (90,405 lb), with 33 tons (72,765 lb) of fuel left. The other results are equal to the specifications expected for the Mach number and the altitude, but the ranges are lower: 445 km (240 miles). To obtain the 375 miles expected, we decide to add a hypersonic cruise of 135 miles consuming 4 tons (8,820 lb). Notice that we keep the constant indicated airspeed until Mach 6.0 because the combustion chamber doesn't reach its limitation at this speed.

### The Separation Point

At this point, the orbiter needs to be sustained because it is not launched with its engines operating. To achieve this, there must be a way of off-setting it from the carrier craft. We can think about jacks to put the orbiter in incidence. We can also imagine a separation similar to missiles. In this case, ASUR is going down when the orbiter goes straight on. Between these two solutions, the most realistic is the second one: jacks won't withstand very high temperatures.

### Return Phase

We also examined the scenario when the orbiter isn't launched. It is not the worst case because in this configuration ASUR can use the orbiter's fuel. We decide that the takeoff point is also the landing point. This allows the composite to take off from any coastal airport to minimize noise over populated areas. ASUR has to turn and reduce engine thrust. Then it descends at the same constant indicated airspeed and cruises subsonically ( $M = 0.95$ ) at an altitude optimized to minimize fuel consumption.

### Conclusion

Finally, we find the mission is successful. All the specifications are met and the consumed fuel quantity is lower than the usable fuel. Even if the orbiter is not launched, we find that the mission is successful. The time to climb is 750 seconds and the total time is 2,800 seconds for a distance of 1,000 miles when ASUR comes back alone and 3,400 seconds for a distance of 1,050 miles for the composite.

The next step is to loop the calculation and redefine the geometry and the masses.

### TAKEOFF STUDY

To determine the takeoff run, we developed a program using takeoff gross weight :  $TOGW = 380$  tons (837,742.5 lb); wing area =  $1600 \text{ m}^2$  (17,222.3 sq ft); maximum lift = 0.53; drag =  $0.0815 + 0.46 \cdot C_d^2$ ; lift gradient =  $0.027/^\circ$ ; and maximum thrust = 1,900,000 N.

We obtained the following results: ASUR need 35.4 seconds to take off and a runway of 2.4 km (7,887 ft) which is the length of runways in traditional airports.

### CONCLUSION

The aircraft we designed meets the specifications given by the Ohio State University. In France, people from aeronautical firms like Aerospatiale and ONERA were interested in our project and offered us their technical support. However, this project can't be considered as a conclusion in itself but as a first iteration which, we hope, could sustain later studies.

ASUR belongs to a new category of reusable launchers. It opens new horizons for space conquest.



# DESIGN OF A TURBOFAN POWERED REGIONAL TRANSPORT AIRCRAFT

PURDUE UNIVERSITY

59-05  
160585  
P. 6

The majority of the market for small commercial transport aircraft is dominated by high-efficiency, propeller-driven aircraft of non-U.S. manufacture. During the past year senior student design teams at Purdue developed and then responded to a Request For Proposal (RFP) for a regional transport aircraft. The RFP development identified promising world markets and their needs. The students responded by designing aircraft with ranges of up to 1500 n.m. and passenger loads of 50 to 90. During the design project, special emphasis was placed upon keeping acquisition cost and direct operating costs at a low level while providing passengers with quality comfort levels. Twelve student teams worked for one semester developing their designs. This report describes several of the more successful designs and those that placed a high premium on innovation. The report also illustrates the depth of detail and analysis in these student efforts.

## BACKGROUND: THE REGIONAL AIRLINE INDUSTRY

The Federal Aviation Administration defines the regional transport industry as "those air carriers that provide regularly scheduled passenger service and whose fleets are composed predominantly of aircraft having 60 seats or less." The regional transport industry's primary goal is to provide air transport from small secondary airports to large metropolitan and international airports served by commercial air carriers. The market for aircraft to perform this mission is dominated by high-efficiency, propeller-driven aircraft, with the bulk of the aircraft manufactured by companies outside the United States.

Since airline deregulation began in the late 1970s the differences between regional airlines with small aircraft and larger air carriers have become less distinct. In 1978 regional airlines operated at a level of approximately 49,500 passengers per carrier. By 1988 this average had risen to 180,200, an increase of 205%. This growth of the regional industry outpaced the other parts of the commercial airline industry. The Federal Aviation Administration (FAA) predicts that the number of revenue passenger miles on regional carriers will nearly double between 1988 and the year 2000.

Areas of high growth are likely to be in Europe and Asia, and, to a lesser extent, the United States. However, in the U.S. there is a greater acceptance of the regional airline industry by the public and increasing numbers of commercial partnership agreements, called code-sharing, between small carriers and the major carriers. These agreements are essential to the survival of regional airlines because their financial health is tied to the health of the major airline partner. In 1989, 43 of the 50 largest regional companies participated in code-sharing agreements with major carriers.

The European industry today resembles the U.S. industry immediately after deregulation. European traffic has had recent increases near 17% per year. European airlines have not yet begun the U.S. practice of code-sharing, but it is only a matter of time before this occurs.

In general, world growth of regional traffic, including Asia, is expected to remain healthy and growing into the foreseeable future. The number of new units required to fill demand for new aircraft and replacements for older aircraft has been predicted to be as high as 6000 aircraft through 1998.

On the other hand, problems such as airport congestion have occurred as an increasing amount of air traffic has been scheduled to converge at major hub airports in the United States and in Europe. To ease this crowding, new regional routes have been developed to bypass these hub-spoke combinations. As a result, the regional airlines both serve and compete with major air carriers.

The trend toward hub-bypass and point-to-point regional carrier operation has changed the original mission of regional airlines. This change requires new capabilities from the aircraft serving these missions. These new capabilities either are not met by existing aircraft or are not met efficiently. The current average route length or stage length is 150 to 250 n.m. for regional transport. These shorter routes are served primarily by small capacity, propeller-driven aircraft. Some predictions see the stage length increasing to over 300 n.m. with maximum ranges of over 1000 n.m. required on some routes. In this case, the turbofan engine becomes competitive.

In addition to efficiency, airlines must consider passenger convenience, comfort, and cabin noise levels. Regional airlines (and their passengers) will demand faster, quieter aircraft with more passengers on each flight so that they can serve markets efficiently and competitively. Passengers accustomed to the comfort, speed, and in-flight amenities of major air carriers will come to expect the same attributes on the regional routes. This so-called seamless service between larger carriers and smaller carriers will be a major criterion in the design of new regional aircraft.

Finally, regional airlines must continue to be capable of operating from small community airports. Many of the important smaller airports have runway lengths of as little as 5000 ft. In addition, the smaller communities have stringent noise require-

ments. These FAR 36 noise requirements and the desire to keep passenger cabin noise at low levels will impose important constraints on the designer.

### OBJECTIVES

During the past year the mission of 12 Purdue senior student design teams was to develop and respond to a Request For Proposal (RFP) for a regional transport mission. This RFP contained performance requirements chosen by individual teams on the basis of their perception and analysis of the transport market as it will exist in 1995. Special emphasis was placed upon designing to cost, a cost that includes aircraft acquisition cost and operational cost (DOC). Designs incorporating unusual features and creativity were encouraged. The result of this study was not only a perception of what a regional transport should look like, but also an idea of what students thought the most important markets would be.

Although the semester provides a 14-week work schedule, each team had only about 10 weeks to conceive and develop its design concept. The first four weeks of the semester were used to develop market studies and to acquire special design skills such as aircraft weight estimation, design sensitivity techniques, and other traditional techniques.

### TEAM REQUIREMENTS

Each design team was subject to stringent analytical, conceptual and reporting requirements for their design. It was required that extensive information on aerodynamic performance be generated together with stability, control, and flying quality information. The structural loads, member layout, and weights and balance information were also required. Coupled with the weights information were the requirements for guarantees that the landing gear could support the ground loads and would meet minimum tip-over and takeoff clearance requirements.

The ability to perform the required transport mission from takeoff to cruise to landing with required reserves was rigorously checked using analytical procedures that ranged from highly preliminary to extremely sophisticated. These checks used class-developed performance computer codes and, in many cases, the Flight Performance and Optimization (FLOPS) code developed by NASA/Langley and modified at Purdue for use on the personal computer. To obtain performance data it was necessary to have extensive engine data. Such data is usually a closely held secret of engine manufacturers.

To remedy the problem of obtaining accurate engine data, two personal computer codes, ONX and OFFX, were used. These codes can match and generate crucial engine performance data such as fuel flow at various Mach numbers, altitudes and power settings. These codes were used extensively by the USRA Teaching Assistant during the summer of 1990 and a videotape and set of assignments were formulated for class use.

These codes were used to modify the engine cycle and inlet temperatures as required to meet the specific missions of the design team aircraft. In some cases this required extensive redesign of the three engine designs that the students were given at the beginning of the class.

The final result of each team's work was a detailed, 100-page design report, an executive summary of this report, and a 25-page mid-term report that was evaluated by a team of technical writing experts from the Thiokol Corporation. What follows is a summary of some of the data presented in these reports.

### THE VALUE OF TIME AND THE COST OF SPEED

Time is money. Time is of value to a passenger on a regional transport, but it also costs money to acquire the speed necessary to save time. This cost is reflected in all of the empirical relations used to estimate aircraft cost.

Figure 1 shows the amount of time required to complete a trip as a function of airspeed. This so-called timescoping analysis shows a knee in the curve. At Mach numbers or airspeeds above this knee, there is very little change in the trip time as Mach number increases. In general, the knee moves right to larger airspeeds when the range of the aircraft increases. For short-range aircraft, it is not important that the aircraft be extremely fast.

Because of the market factors that governed each group's design, the 12 teams independently arrived at the conclusion that it was unnecessary to have the aircraft travel extremely fast. In addition, because aircraft acquisition cost increases with cruise Mach number, cruise speeds were kept down so that they ranged from Mach 0.70 to 0.82. These cruise Mach numbers can be compared to longer range aircraft that may cruise up to Mach 0.90.

### PASSENGER LOADS, RANGE, AND REQUIREMENTS

Recent trends in the regional transport business have been directed toward development of aircraft with up to 100 seats and ranges up to 1500 n.m. As a result, the RFPs developed by the 12 design teams displayed a wide range of seating and range objectives. Figure 2 shows this data for the 12 design groups and compares it to two other aircraft now in service.

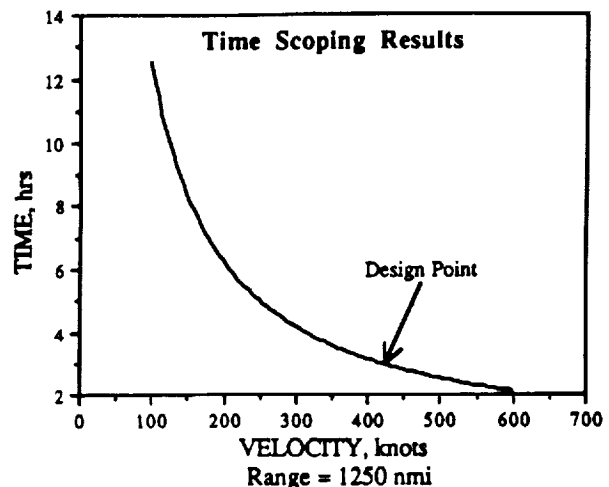


Fig. 1. Trip time vs. airspeed.

The smallest aircraft developed at Purdue has a passenger capacity of only 50 with a range of 800 to 900 n.m. (with reserves). The largest aircraft is designed to hold 90 passengers and had a range of 1650 n.m., comparable to the Fokker 100.

Design groups identified the European and Asian markets as being more promising than the U.S. market. As a result, while they used FAR standards in their work, design teams also used the Association of European Airlines Requirements (AEA) as a standard.

While the AEA standards repeat many of the FAR requirements for safety, they also set minimum standards for passenger comfort in terms of such items as seat pitch. All 12 aircraft meet these AEA standards and use AEA guidelines to calculate DOC. Let us now consider some of the designs generated by the design teams and their features. Note that all of these designs are required to carry a cockpit crew of two.

**THE WAG-78**

The WAG-78 is a 78-passenger aircraft with a range of 1100 n.m. It is designed to cruise at  $M = 0.80$  at 35,000 ft with an operational ceiling of 39,000 ft. The aircraft will take off from a runway longer than 5500 ft on a standard day in Denver. This design is a modification of a design that has appeared during the past ten years and is shown in Fig. 3.

The WAG-78 provides an example of a departure from conventional subsonic aircraft design because it uses the joined wing concept developed several years ago. This joined wing has a rear wing surface that acts both as a horizontal tail and as an external strut to stiffen and strengthen the wing. The takeoff gross weight (TOGW) of this aircraft is 54,900 lb with an empty weight of 30,500 lb. Some weight savings were achieved because of the joined wing structural design.

The WAG-78, like all the other student designs, was powered by a redesigned General Electric TF 34 engine. This engine was resized and slightly redesigned to develop a thrust of 11,900 lb.

Two engines were used for this design to satisfy one engine inoperative (OEI) requirements and so that the engines would be capable of developing thrust levels sufficient to meet the takeoff requirements and OEI criteria. The thrust-to-weight ratio for this aircraft is rather large so that the aircraft can climb rapidly to its cruise altitude.

The designers of the WAG-78 were conservative in their estimates of the number of aircraft that they could market. They predicted that they would be able to sell 175 aircraft over an 11 year development and production cycle. This number did not include the 5 test aircraft that they chose for a development phase that was to last 3 to 5 years. This unusually large number of test aircraft were thought to be necessary because of the new joined-wing design feature that they proposed to use.

The WAG-78 designers estimated a development and testing cost of \$810 million and production costs of \$2.262 billion. A cash bucket analysis shown in Fig. 4 was used to estimate the price of this aircraft to be \$20 million if the cost of capital is 18%. Operating costs for an 1100-n.m. trip were estimated at \$2060 to give a low 3.6 cents per revenue seat mile assuming a 66.7% load factor.

The WAG-78 design team compared their design to the BAe 146-100 and the DeHaviland Dash 8-400 and found that the

**Design Teams' Market Profile**

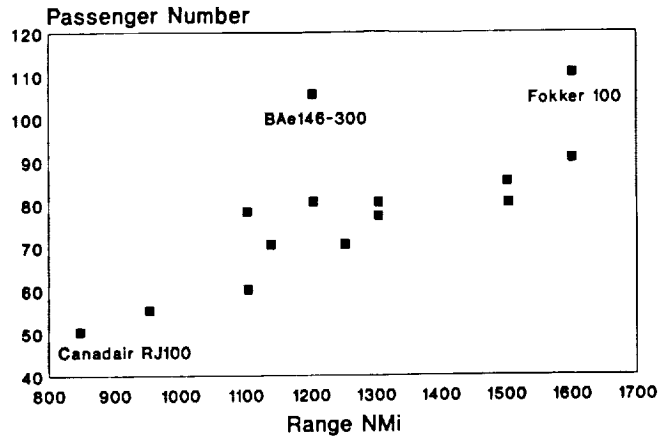


Fig. 2. Design team passenger number vs. range.

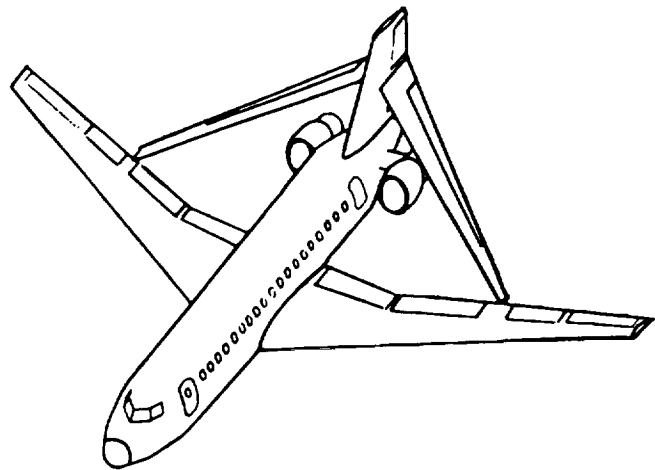


Fig. 3. WAG-78 Joined Wing Design.

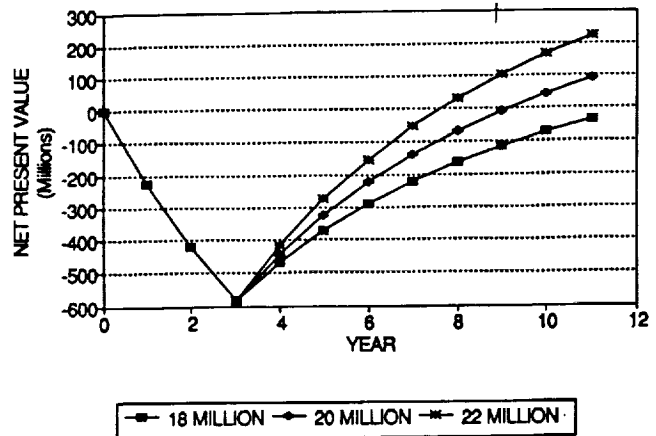


Fig. 4. Cash Bucket Price Analysis.

WAG-78 cost 0.5 to 1 million dollars more than these aircraft. On the other hand, it could be operated at a seat mile cost of about 10% less than the BAe 146-100 and only slightly more than the Dash 8. The Dash 8 is a turboprop aircraft and, in its latest stretched version, its range has been reduced to 800 n.m. at a speed of 350 knots.

### THE ARCA-60

Design reviews with industrial representatives were held during both semesters of design team activity. Design representatives included a marketing authority, a propulsion and maintenance expert, and an airline pilot. The airlines represented included Southwest Airlines, USAir and Northwest Airlines.

In all cases, the teams were encouraged to simplify their designs and to consider flight operations and maintenance. While this advice was valuable, it also tended to discourage configuration innovation. As a result, aircraft external features evolved to become somewhat traditional.

An excellent example of a well-conceived, traditional, DC-9-like design is the ARCA-60, shown in Fig. 5. This aircraft has seating for 60 passengers with an 1100-mile range and enough fuel to fly to an alternate airport 200 n.m. away and hold for 30 minutes. It has a maximum Mach number of 0.80 and cruises at 35,000 feet at  $M = 0.75$ .

Extensive studies were done by the ARCA-60 aerodynamicist to obtain an efficient airfoil shape for low drag. These efforts led to the choice of a NASA supercritical airfoil, the SC(2)-0412. An Euler code analysis of the section estimated the drag divergence Mach number of this section to be 0.75. This code was used to accurately model the nonlinearities that occur in transonic flow.

The ARCA-60 wing was mounted low on the fuselage to allow for aft mounting of the engines and easy storage of the landing gear. Aft mounting of the engines resulted in the requirement

for a T-tail design. Although the c.g. movement during flight is minimal, the ARCA-60 requires a large tail volume to rotate the nose on takeoff from short runways. The extra cruise drag from this configuration was regarded by the design team to be acceptable.

The ARCA-60 has a predicted TOGW of 60,300 lb and a wing loading of 75 psf at takeoff. The wing quarter chord sweep is  $20.4^\circ$  to help reduce torsional loads while maintaining aerodynamic efficiency. After extensive analysis, a taper ratio of 0.2 was chosen so that the lift distribution approached that of a minimum drag, elliptical spanwise lift distribution.

The thrust per engine was 9650 lb and is much lower than the WAG-78. With engine cost estimated at \$2.4 million per aircraft, the ARCA-60 is estimated to cost \$19 million. This number is based on a production run of 300 and a cost of capital of 10%. This latter cost is low compared to the 18% estimate of the WAG-78 team. The ARCA-60 program is estimated to last for 20 years and to produce a profit of \$819 million.

As shown in Fig. 6, the cabin cross-section is designed for comfort. This feature is also present in the other 11 designs.

### THE SRT-80 AIRCRAFT

The SRT-80 design, shown in Fig. 7, is representative of several designs produced during the project (note that this image is produced by a mesh generation program and some distortion in engine placement will occur when the computer screen image is printed). This aircraft resembles the 737/757 class of aircraft with wing-mounted engines. This aircraft can cruise at Mach 0.80 and carries 80 passengers a distance of 1200 n.m. with reserves. It has a wing loading of 55 psf to allow it to take off from 5500-ft runways at 2000 ft above sea level.

The aircraft has a span of 94 ft and a length of 93 ft. The wing itself has a dihedral angle of  $5^\circ$  for stability. At a design

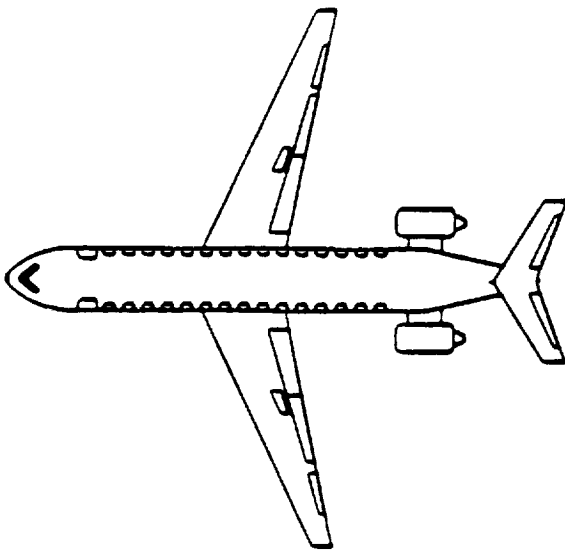


Fig. 5. The ARCA-60 Aircraft.

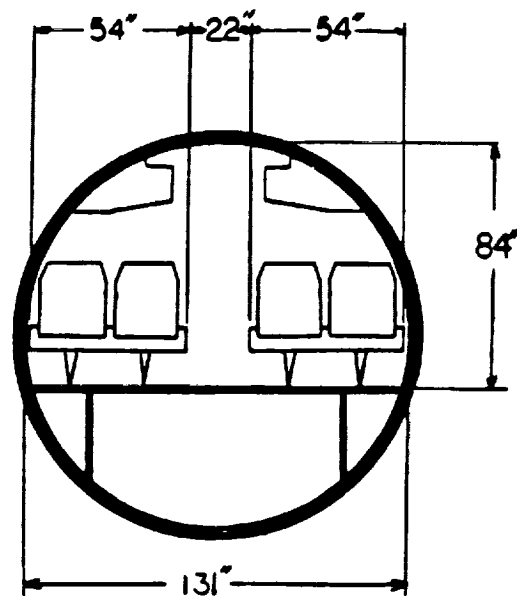


Fig. 6. Cabin Cross-section.

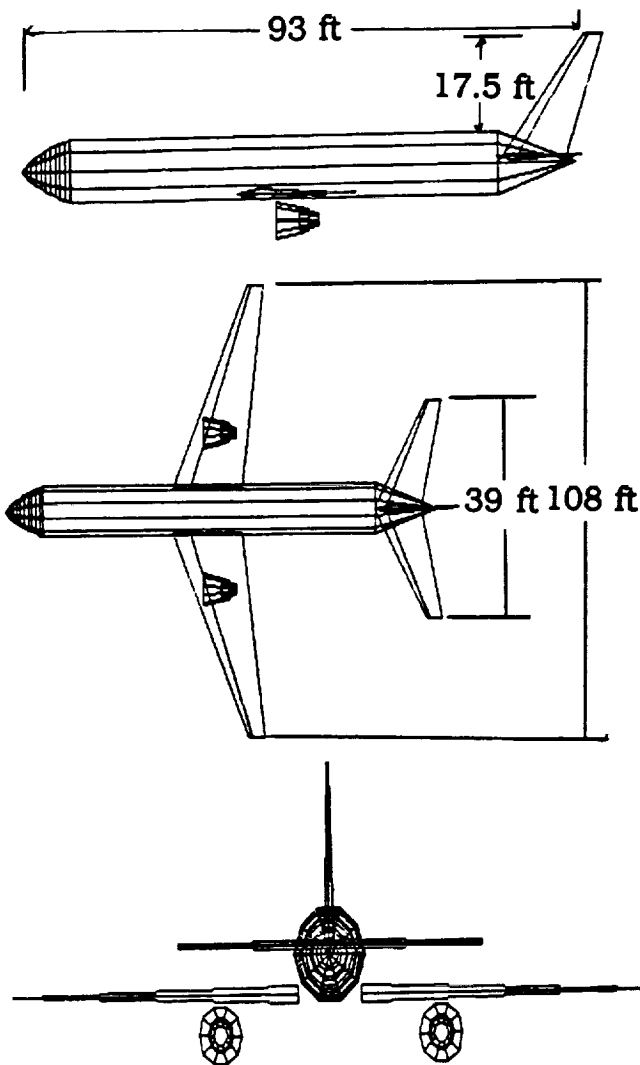


Fig. 7. The SRT-80.

TOGW of 60,900 lb this aircraft will use 9400 lb of fuel to complete its mission. The engines on the SRT-80 are designed so that the integrated airframe and propulsion units will generate 101 seat miles (n.m.) per gallon of fuel.

The engines are modified versions of the GE TF 34 turbofan design. They were scaled up to increase the thrust from each engine. The TF 34 was selected by the SRT-80 team because of its superior fuel efficiency. The propulsion specialist increased the bypass ratio from 6.23 to 7.0 to increase thrust by almost 7% and to decrease fuel consumption by over 4%.

Like most of the designs, the structure of the SRT-80 is composed primarily of aluminum, with small amounts of composites used in non-load-bearing structure. The structure is estimated to be 40.1% of the TOGW. Passengers and baggage are an additional 31.6% while the systems and equipment are 3.3%. The remaining weight is due to passengers and their baggage.

**THE WOMBAT**

The last airplane to be reviewed is a blend of conventional design with a few unconventional features. This design, shown in Fig. 8, began as a design that closely resembled the BAe-146 or the C141. The high wing was judged by the designers to be desirable because of its handling qualities during the landing in ground effect. Wing mounted engines were used for or ease of access. Landing gear is stowed in a blister pod in the fuselage and meets tip-over criteria.

The Wombat has a wing span of 92.2 ft, a length of 105 ft and weighs 66,950 lb to give it a wing loading of 89 psf at takeoff. The Wombat is designed to carry 70 passengers, but will also be available in a stretch version that will carry 100 passengers. The projected cost is \$22 million.

The design team became concerned about cabin noise from the engines and overhead hydraulic lines as well as the potential for blade damage from an engine failure in flight. As a result, they moved the wing back instead of attaching the engines to the fuselage as a number of other design teams had done. This necessitated the addition of a canard to raise the nose at takeoff. It also generated concern for the effects of the canard tip vortices on the engine intakes.

The aerodynamicist and the stability and control specialist cooperated to place the wing and canard properly to reduce trim drag in flight. The result was an optimized three-lifting-surface aircraft shown in Fig. 8.

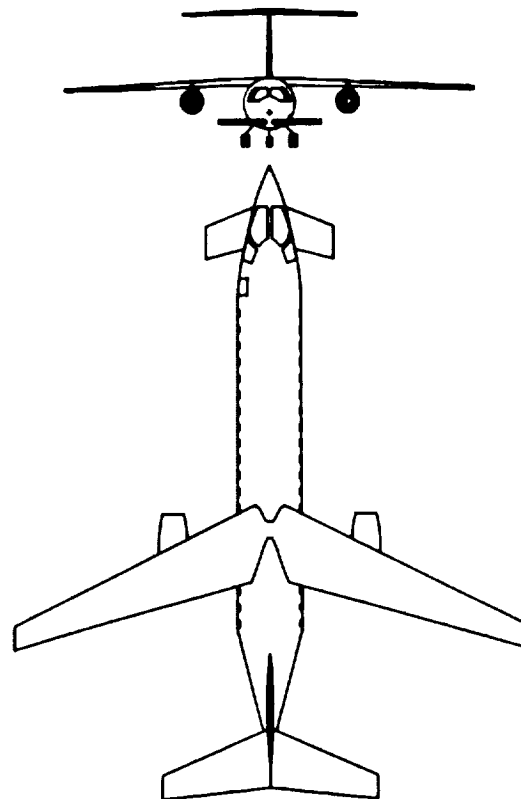


Fig. 8. The Wombat (note difference in scales).

The fuselage of this aircraft is to be constructed of Arall. This composite material has an organic fiber material sandwiched between layers of aluminum. This material should be safer and deaden sound from the engines better than conventional aluminum.

### CONCLUSION

The Purdue design class considered the engineering/economic task of designing a regional transport aircraft with turbofan engines. Market considerations drove this design to passenger capabilities of about 70 passengers. As a result, one of the three available engines, the GE TF 34, was the clear choice of the 12 teams that participated.

One agreement among the design teams was that the regional transport market would grow. As a result, a successful design will have a good chance of returning a profit to its investors. Because of the emphasis placed upon practicality and economy, most aircraft have a conventional appearance. In addition, most aircraft use minimal amounts of composite materials for construction and have conventional controls. On the other hand, all groups embraced supercritical airfoil technology.

The emphasis upon cost and price of the aircraft required a model to predict these numbers. The teams developed such models and the ability to judge the desirability of trading one technology against another. In the long run, it is the clear relationship between market forces and engineering decisions that will prove to be the most valuable aspect of this design experience.

**SOLAR POWERED MULTIPURPOSE REMOTELY POWERED AIRCRAFT**

**WORCESTER POLYTECHNIC INSTITUTE**

510-05  
160586  
P-6

Environmental problems such as the depletion of the ozone layer and air pollution demand a change in traditional means of propulsion that is sensitive to the ecology. Solar-powered propulsion is a favorable alternative that is both ecologically harmless as well as cost effective. Integration of solar energy into designs ranging from futuristic vehicles to heating is, therefore, beneficial to society. The design and construction of a Multipurpose Remotely Piloted Vehicle (MPRPV) seeks to verify the feasibility of using solar propulsion as a primary fuel source. This task has been a year-long effort by a group of eight students, divided into four teams, each dealing with different aspects of the design.

The aircraft has been designed to take off, climb to the design altitude, fly in a sustained figure-eight flight path, and cruise for approximately one hour. This mission requires flight at Reynolds numbers between 150,000 and 200,000 and demands special considerations in the aerodynamic design to achieve flight in this regime. Optimal performance requires a lightweight configuration with both structural integrity and maximum power availability. The structural design and choice of solar cells for the propulsion were governed by weight, efficiency, and cost considerations.

The final design is an MPRPV weighing 35 N that cruises at 7 m/s at the design altitude of 50 m. The configuration includes a wing composed of balsa and foam NACA 6409 airfoil sections and carbon fiber spars, a tail of similar construction, and a truss structure fuselage. The propulsion system consists of 98 12.5%-efficient solar cells donated by Mobil Solar, a NiCad battery for energy storage, and a folding propeller regulated by a lightweight and efficient control system. The airfoils and propeller chosen for the design have been researched and tested during the design process.

aircraft to remain within a reasonable distance from the ground control. Once at altitude, a sustained figure-eight pattern tests the aircraft characteristics over a variety of maneuvers.

**Aircraft Configuration**

The proposed vehicle is shown in Figs. 1 and 2. General data and design parameters are summarized in Table 1.

The configuration consists of a nonconventional, high-wing aircraft with two carbon fiber composite support struts primarily important in maintaining structural integrity. The two composite

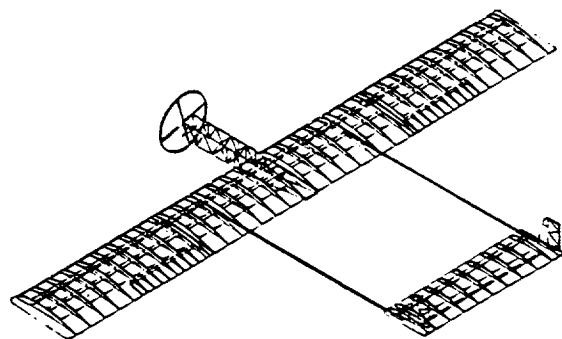


Fig. 1. Final design—Isometric view.

**INTRODUCTION**

**Mission Requirements**

This study investigates the possibilities for a remotely controlled solar-powered aircraft. Ultimately the aircraft will be able to perform a sustained figure-eight flight pattern at an altitude of 50 m using only solar power. The mission will be carried out in several flight stages including launch, climb to altitude, and pattern flight.

The aircraft will be launched away from the Sun employing a catapult system to provide some initial altitude. Maximum power will be received when the aircraft is traveling away from the Sun, resulting from the incidence of the solar array with respect to the Sun. Therefore the best climb rate will be achieved when flying in this direction. A circular climbing pattern will be used, to compensate for slow climb rates and enable the

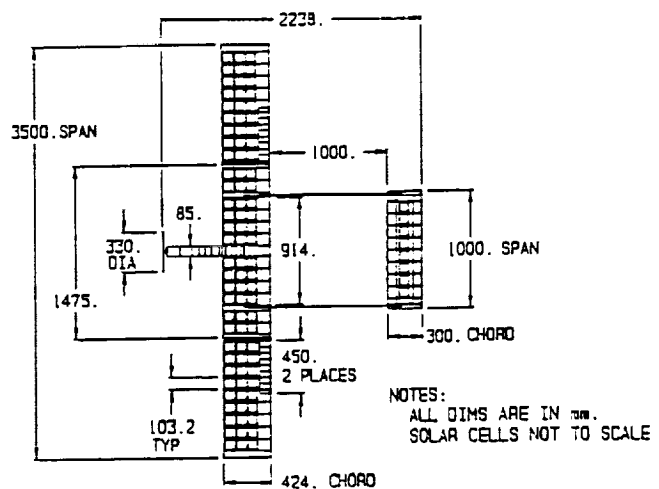


Fig. 2. Final design—Top view.

TABLE 1. General data.

|                     |             |                        |
|---------------------|-------------|------------------------|
| Weight              | $W_{gross}$ | 40 N                   |
| Wing Area           | S           | 1.48 m <sup>2</sup>    |
| Wing Loading        | W           | 27.03 N/m <sup>2</sup> |
| Aspect Ratio        | AR          | 8.25                   |
| Wingspan            | b           | 3.5 m                  |
| Cruise Altitude     | h           | 50 m                   |
| Cruise Velocity     | V           | 7 m/s                  |
| Design Lift Coeff   | $C_L$       | 0.83                   |
| Design Lift-to-Drag | L/D         | 15.75                  |
| Cruise Power Req'd  | P           | 15.9 W                 |
| Design Load Factor  | n           | 7                      |

rods extend from the main spar in the wing to the spar of the horizontal stabilizer. This becomes of primary importance during both takeoff and landing, as large wing tip deflections could result in catastrophic failure.

A solar propulsion system, which includes 98 photovoltaic solar cells supplied by Mobil Solar Corporation, powers the aircraft. The cells directly power an Astro-Flight Cobalt 0.05 motor that drives a folding Aero-Haute 13 × 6.5" pitch plastic propeller. As a safety feature, a switch is included to provide access to a NiCad battery backup system.

The electronics equipment is housed in a small fuselage, connected to the underside of the main wing. The fuselage was built using a balsa truss structure covered with a mylar coating. The truss structure provided the fuselage with the necessary strength to safely house the electronics equipment under all anticipated loads, while minimizing the weight.

The wing and horizontal tail both have a prismatic planform with aerodynamic characteristics of NACA 6409 airfoil sections. The wing has a span of 3.5 m and a chord of 0.424 m, resulting in an aspect ratio of 8.25. The wing is attached to the fuselage at an angle of attack of 4°. At level flight conditions, this angle of attack produces a total wing  $C_L$  of 0.72 and downwash of -2°. The tail has a span of 1 m and chord of 0.3 m, resulting in an aspect ratio of 3.33. The  $C_L$  of the tail is 0.22 and efficiency assumed is 85%. The design at level flight conditions has an airplane lift coefficient of 0.83 and drag coefficient of 0.053 resulting in a configurational lift-to-drag ratio of 15.75.

In addition, the aircraft is equipped with a variety of control devices including two ailerons, two rudders, and an elevator. These are directed with an onboard receiver that uses four electronic servos to control their motion.

## DESIGN AND ANALYSIS

### Aircraft Sizing and Weight Estimation

The required mission mandates the proposed vehicle be powered solely by the Sun; therefore, the design was optimized for maximum power and minimum weight. A model aircraft provided by a kit was constructed and flown. This aircraft was not solar powered, but did provide a reasonable initial weight estimation and power requirement for the proposed solar-powered vehicle. Solar propulsion was integrated into the design and the configuration was iteratively improved until a final and unique vehicle was obtained. Tables 2 through 5 break down

TABLE 2. Wing component masses.

| Wing                | Parts | Mass (g) | % Wing |
|---------------------|-------|----------|--------|
| Ribs                | 30    | 99.2     | 4.8    |
| Leading Edge        | 1     | 84.2     | 4.1    |
| Trailing Edge       | 1     | 104.4    | 5.1    |
| Spar Webs           | 33    | 44.8     | 2.2    |
| Skin (Mylar)        |       | 192.9    | 9.3    |
| Solar Braces (foam) | 270   | 33.7     | 1.6    |
| Wing Tips (foam)    | 2     | 36.1     | 1.7    |
| Carbon Rods         | 2     | 91.0     | 4.4    |
| Solar Cells         | 90    | 856.8    | 41.5   |
| Servos              | 2     | 43.0     | 2.1    |
| Wiring              |       | 55.1     | 2.7    |
| Reinforcing Ribbs   | 10    | 340.0    | 16.5   |
| Fasteners           | 10    | 82.2     | 4.0    |
| Wing Total          |       | 2063     | 100    |

TABLE 3. Fuselage component masses.

| Fuselage            | Mass (g) | % Fuselage |
|---------------------|----------|------------|
| Balsa Frame         | 111.6    | 12.5       |
| Skin (Mylar)        | 12.3     | 2.5        |
| Servo               | 21.5     | 2.4        |
| Wiring              | 37.9     | 4.2        |
| Motor & Gearbox     | 225.7    | 25.3       |
| Propeller           | 32.9     | 3.7        |
| Receiver Battery    | 97.0     | 10.9       |
| Receiver            | 44.0     | 4.9        |
| Speed Control       | 54.8     | 6.1        |
| On/Off Switch       | 10.3     | 1.2        |
| Emergency Batteries | 234.3    | 26.2       |
| Landing Gear        | 23.6     | 2.6        |
| Fuselage Total      | 905.9    | 100        |

TABLE 4. Tubular strut masses.

| Tail Strut       | Mass (g) | % Strut |
|------------------|----------|---------|
| Carbon Tubes (2) | 225.1    | 80.9    |
| Wiring           | 53.2     | 19.1    |
| Strut Total      | 278.3    | 100     |

TABLE 5. Tail component masses.

| Tail                | Parts | Mass (g) | % Tail |
|---------------------|-------|----------|--------|
| Ribs                | 9     | 14.2     | 4.5    |
| Leading Edge        | 1     | 20.0     | 6.422  |
| Spar Webs           | 9     | 6.4      | 2.0    |
| Elevator            | 1     | 34.8     | 10.8   |
| Skin (Mylar)        |       | 42.0     | 13.4   |
| Solar Braces (foam) | 16    | 2.0      | 0.6    |
| Carbon Rods         | 2     | 2.6      | 0.8    |
| Solar Cells         | 8     | 76.2     | 24.3   |
| Vertical Tail       | 2     | 20.2     | 6.4    |
| Servos              | 2     | 43.0     | 13.7   |
| Reinforcing Ribbs   | 2     | 21.6     | 6.9    |
| Fasteners           | 2     | 31.2     | 10.0   |
| Tail Total          |       | 313.4    | 100    |

the actual masses for individual elements of the plane and also show the percent contribution of each to its element section of the plane.

**Aerodynamic Design and Analysis**

The wing has been designed to have a span of 3.5 m and a chord length of 0.424 m from its root to wing tip. A prismatic planform was selected to achieve the maximum amount of power per wing area. The flight regime corresponding to a Reynolds number of approximately 200,000 involves difficulty with viscous effects associated with the boundary layer and prediction of laminar separation bubbles. The computational methods at our disposal have proven inaccurate due to the physics of the flow. Reliable experimental data were obtained from *Soartech 8: Airfoils at Low Speeds*<sup>(1)</sup>. Three airfoil sections were considered and their lift-to-drag ratios vs. angle of attack are shown in Fig. 3. The NACA 6409 was determined to be well suited to thermal sailplane gliding due to its aerodynamic performance at the design point. This airfoil has a maximum of 9% thickness and 6% camber both located at 40% chord and generates a  $C_L$  of 0.72 at level flight with an attack angle of 4°. Using the Eppler code<sup>(2)</sup> the inviscid distribution of pressure for an angle of attack of 4° was determined.

The tail is similarly designed with the aerodynamic shape of the NACA 6409 and a prismatic planform of dimensions 0.3 m (chord length) × 1 m (span). This component has an angle of attack of 0° and generates a  $C_L$  of 0.2206 at level flight. Tail efficiency is assumed to be 85%.

The effects of finite wing length on the two-dimensional lift and drag curves were investigated using a Fourier series representation developed by Glauert (1937). The prismatic wing

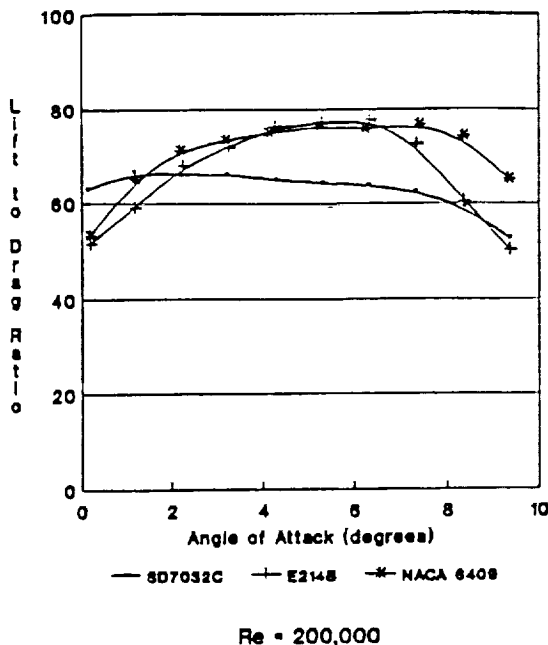


Fig. 3. Comparison of airfoil sections.

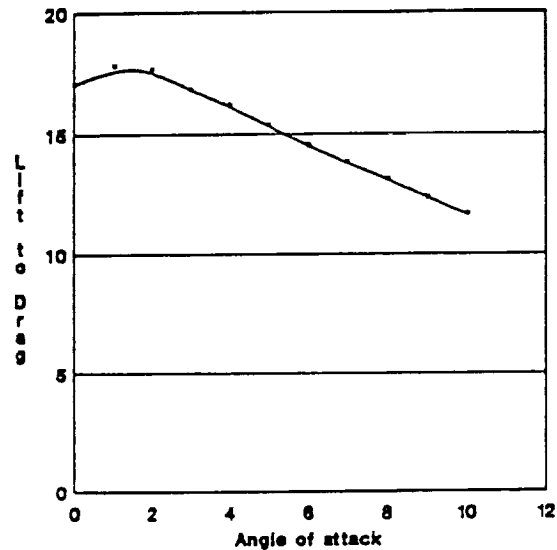


Fig. 4. Configurational lift-to-drag curve.

design of this aircraft deviates from the elliptic wing resulting in a 4% loss in lift and an 8% increase in drag. Twist and taper of the wing could alleviate these problems, yet these options were not implemented due to construction difficulties.

To determine the optimum operational point for the given configuration, a study of the variation of excess power with attack angle was administered. An attack angle of 4° was chosen corresponding to a trimmed tail at -2° (an angle of attack of 0° corresponding to the horizontal). The configurational lift-to-drag curve resulting from this study is shown in Fig. 4.

**Structural Design and Analysis**

This configuration employs a semimonocoque (stressed skin) structure composed of a balsa skeleton with a transparent mylar skin covering, providing a lightweight aerodynamic frame. Carbon fiber rods running the span of the wing and tail are the major strengthening elements in the wing and tail design. This spanwise spar consists of a 3.3-mm-diameter carbon fiber rod joined by balsa spar webs to create an I-beam structure. Structural half-models were created and analyzed using a professional version of ANSYS. Increasing levels of detail were incorporated during the course of the academic year.

Applying the maximum anticipated load (equivalent to a gust-induced aerodynamic lift of seven times the aircraft weight, simulating the design load factor) resulted in compressive and tensile stresses within the structure much less than those allowable for each component given its material properties. The maximum deflection and angle of twist in the wing are 0.24 m and 11.5° respectively, occurring in the wing tips. The tail is restrained at its tips by the connections to the carbon fiber supports and experiences a maximum deflection of only 0.515 mm at its midspan. The results of the ANSYS analysis substantiates the material selection and structural design by verifying the structure will not fail under the greatest anticipated loading.

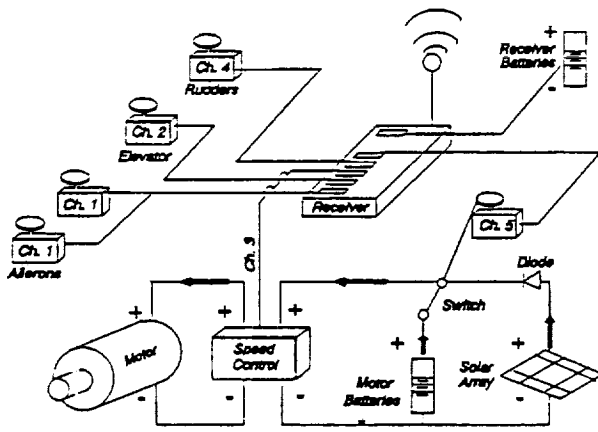


Fig. 5. Controls layout.

**Controls and Interface**

The modified remote control radio system and the necessary hardware for controlling deflecting surfaces and switches via servomotor, shown in Fig. 5, is the essence of the controls and interface scheme.

A propulsion powerplant divided into three subsections is employed. This system includes 98 solar cells, 7 rechargeable nickel-cadmium batteries, 1 DC motor, and 1 propeller, as shown in Fig. 5. This power circuit enables three modes of operation. In one mode the solar array is the sole source of input power. A second scenario occurs when the motor is turned off and the NiCad batteries are in parallel with the solar array: the array will charge the batteries provided the array has a high enough voltage and produces sufficient current. The option of using power from both the NiCad batteries and the solar array is also available.

The Sun is the only source of electrical input energy and the solar cells serve as the primary source of input power by converting the solar energy into electrical energy. The NiCad batteries serve as a safety feature, both as a secondary power source and a means of supplying short bursts of energy to the system when needed (i.e., for takeoff and critical maneuvers). The solar array and NiCad batteries are connected in parallel via a remotely controlled switch in series with the DC motor. The subsections were optimized to work together and the solar propulsion system was integrated into the final configuration.

Characteristics of solar cells were examined and several types of cells were considered. Finally, 12.5%, 3.75 x 3.75" cells were selected for the current design. The cells are of high quality and relatively good efficiency, yet their size and low power/weight ratio presents considerable constraints. The cells are placed within the wing and tail on foam supports. The supports are mounted on the rib sections to provide protection and maintain the aerodynamic quality of the configuration. Shading from the rib sections is inevitable. However, placing the cells as close as possible to the upper surface of the airfoil shape greatly alleviated this problem.

Decrease in transmittance caused by the mylar coating was theoretically and experimentally evaluated. Using the Fresnel

reflection equations<sup>(3)</sup> and data provided by the cell manufacturer, the theoretical transmittance of the mylar coating was determined to be around 80%. Experimental evaluation yielded a transmittance of 90%.

A random sample of solar cells was tested on February 27, 1991, and the resulting current-voltage (I-V) and power curves were determined. A current adjustment was determined and applied to the experimental results. Voltage change as a function of both cell and ambient temperature was estimated<sup>(4)</sup>, taking into account the effect of light intensity. The ambient temperature for the test data was adjusted by +10° to account for the "greenhouse effect" within the wing. Applying the current and voltage adjustments to the experimental data, the I-V and power curves were estimated for a given flight date light intensity and current values (see Figs. 6 and 7). The Astro Cobalt 05 electric, geared motor and a two-bladed, folding propeller with a diameter of 33 cm and pitch of 16.5 cm manufactured by Aero-Haute were chosen for their combined efficiency. A combined contour plot of electrical input power, shaft torque, shaft RPM, and motor efficiency vs. voltage and current is shown in Fig. 8. Three motor-propeller combinations were tested in

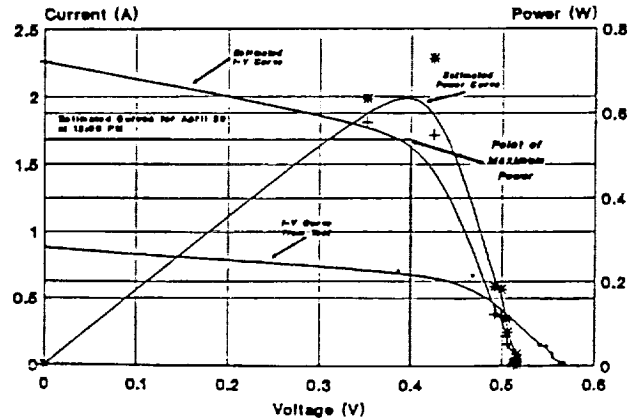


Fig. 6. Solar cell current-voltage curves.

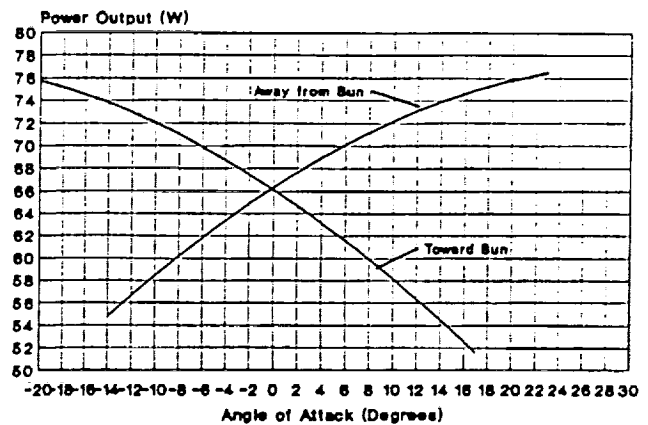


Fig. 7. Estimated power from solar cell curves.

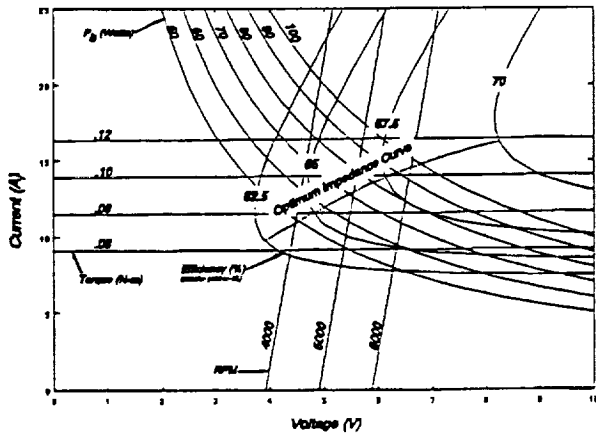


Fig. 8. Combined contour plot for design motor.

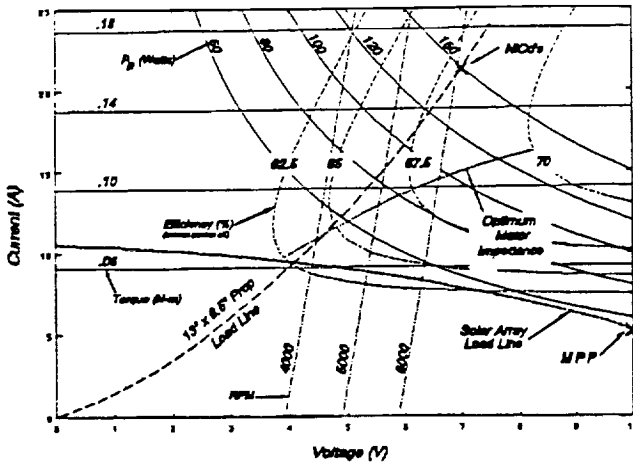


Fig. 9. Combined contour plot for design motor—Propeller setup.

the WPI wind tunnel under conditions similar to those in flight. Figure 9 illustrates the results of the tests performed for the chosen motor-propeller combination.

**Stability**

Longitudinal and lateral stability were evaluated by classical analysis methods<sup>(5)</sup>. The tail and support struts were sized to provide static longitudinal stability<sup>(6)</sup>. The effects of expected gust-induced loads in the longitudinal direction (pitch) results in a rate of change of the pitching moment with the total airplane lift of -0.1415, giving static stability to the configuration. In order to study the longitudinal dynamic stability of the configuration, the long- and short-period oscillatory modes of motions were examined. A second-order differential equation of the plane's motion was derived from Newton's second law and the damping ratio and natural frequency were determined. Results of the longitudinal dynamic stability analysis at the design point are given in Table 6.

TABLE 6. Dynamic longitudinal stability.

| Motion       | Frequency | Period |
|--------------|-----------|--------|
| Long Period  | 0.948     | 2.12 s |
| Short Period | 0.045     | 7.07 s |

The vertical tail and dihedral were sized to provide lateral stability. The vertical tail has a volume coefficient of 0.018, which is very close to the typical value of 0.02 for a sailplane<sup>(7)</sup>, and furnishes directional stability. Dihedral stability is achieved by adding a small positive dihedral angle of 5° at a location of 0.75 m from the wing root, tending to return the aircraft to its equilibrium position once it has been disturbed by a rolling moment<sup>(7)</sup>.

**Performance and Mode of Operation**

Solar propulsion is very appealing because it is harmless to the environment and cost efficient. The performance of a vehicle, however, is very dependent on the weather, time of day, location, season, and efficiency of its solar-power system. The available solar cells for this aircraft configuration were not the most efficient or lightweight, yet did allow for excess power for takeoff and climb. A computer code was developed to predict the performance of the aircraft in level flight (see Fig. 10).

The aircraft is designed to climb in a circular flight path to an altitude of 50 m in 6.7 min, as shown in Fig. 11. This mission requires 7 complete revolutions about a 200-m field. The climb rate is a function of the angle of incidence between the Sun and the solar cell array; the aircraft climbs at a rate of 0.155 m/s away from the Sun and 0.093 toward the Sun.

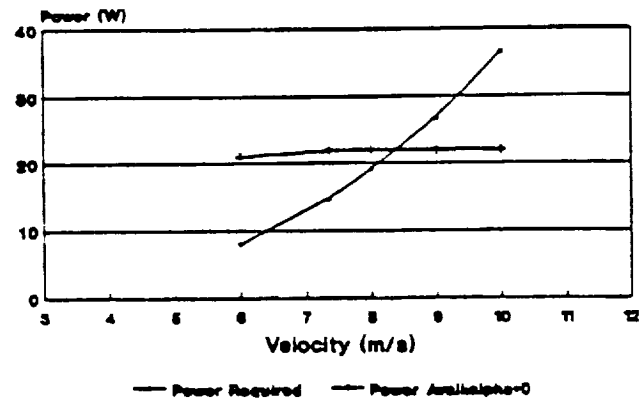


Fig. 10. Design power curve.

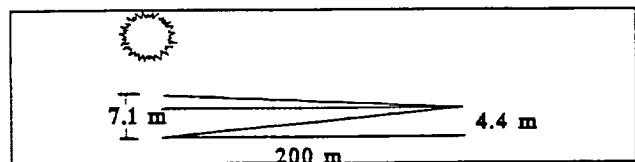


Fig. 11. Circular climb pattern.

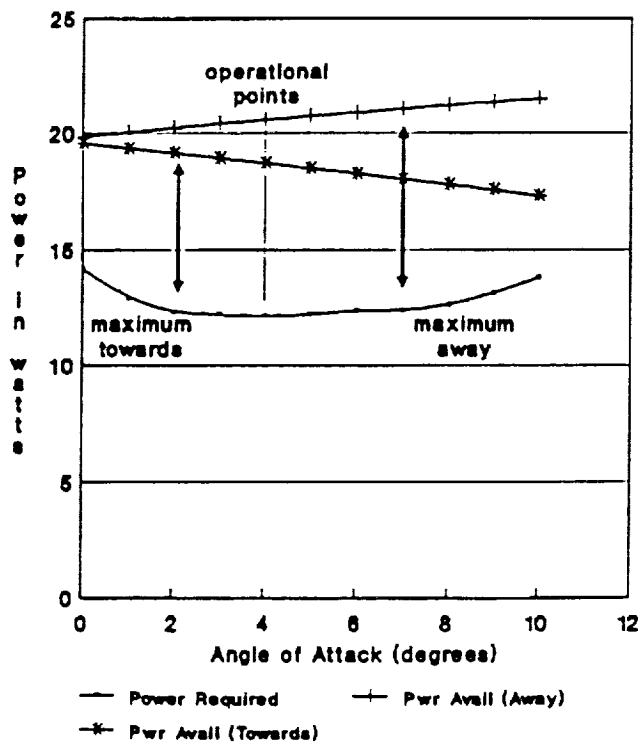


Fig. 12. Optimization of excess power with angle of attack.

At the design altitude, 15.9 W is required from the propulsion system to maintain flight at 7 m/s. A sustained figure-eight flight pattern will be achieved with an angle of attack of 4°, banking angle of 4°, and a turning radius of 79 m. Figure 12 shows the optimization of excess power with respect to the attack angle of the wing.

### Construction Procedure

The final design of the solar-powered vehicle was meticulously constructed with every attempt to maintain the aerodynamic features and weight budget for each component and any additional items not initially allotted for. To facilitate transport, storage, and construction, modular features were incorporated into the final configuration. Consideration was given to the connections in order to maintain the structural integrity of the original design. Currently the aircraft is being prepared for a test flight to establish the effectiveness of the control system and its overall stability.

### Environmental Impact

Society is faced with various self-induced environmental problems. Implementation of solar energy as a replacement to traditional energy resources provides an economical solution. The design and construction of this solar-powered aircraft attempts to contribute to this cause and encourage future research into alternative energy resources.

### CONCLUSIONS

A preliminary study of a solar-powered MPRPV designed to operate at approximately sea level indicates that it is currently feasible to integrate solar propulsion into the design of airborne vehicles. Increased research on the potential of and possibilities for solar energy is encouraged.

### ACKNOWLEDGMENTS

The assistance and technical support of the NASA contacts, WPI faculty, Mobil Solar, and many other interested aircraft modeling enthusiasts are very greatly appreciated. Special thanks to Art Glassman, our NASA/USRA mentor and the advising professors, Prof. William W. Durgin, Prof. Andreas N. Alexandrou, Prof. Ralph F. Cohn, Prof. Vahid Motevalli, Prof. David J. Olinger, Prof. Joseph J. Rencis, Prof. Clark, and Kurt Heinzmann for their faithful guidance. The educational assistance on low Reynolds number flight vital to the required mission provided by Don Harvey and Dan Somers, both affiliated with NASA Langley, has been invaluable. Also thanks to the many helpful students from WPI especially Adam Szymkiewicz, Jason Makofsky, and Kyle Jacobson for sharing their expertise.

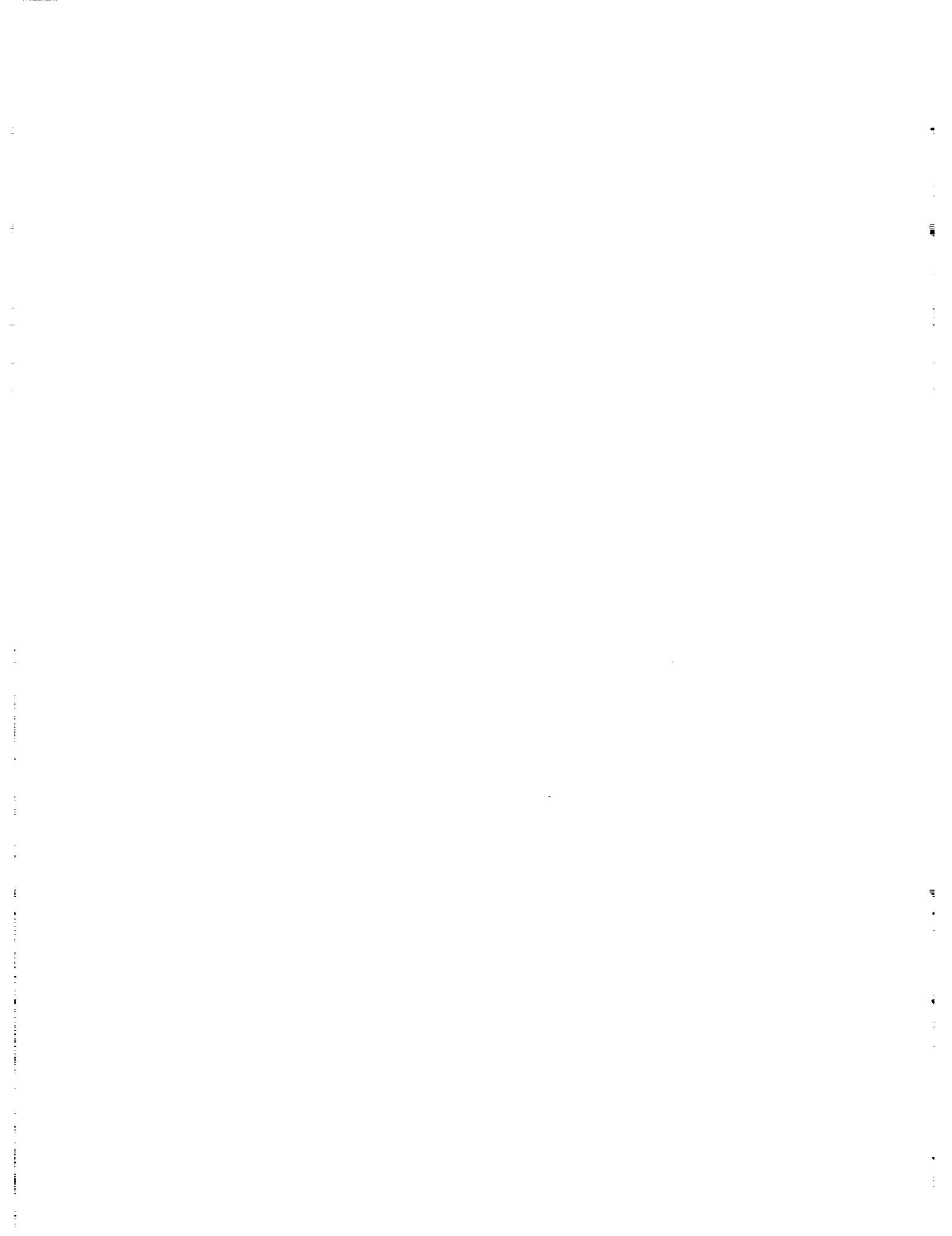
### REFERENCES

1. Selig, M., J. Donovan, and D. Fraser. 1989. *Soartech 8: Airfoils at Low Speeds*.
2. Eppler, R. and D. Somers. 1980. "A Computer Program for the Design and Analysis of Low-Speed Airfoils, Including Transition." NASA TM 80210.
3. Duffie, J. and W. Buckner. 1980. *Solar Engineering of Thermal Processes*. John Wiley and Sons, Inc., New York.
4. Buresch, M. 1983. *Photovoltaic Energy Systems: Design and Installation*. McGraw-Hill Inc., New York.
5. Nelson, R. 1989. *Flight Stability and Automatic Control*. McGraw-Hill, New York.
6. Shevell, R. 1983. *Fundamentals of Flight*. Prentice-Hall, Englewood Cliffs, New Jersey.
7. Raymer, D. 1989. *Aircraft Design: A Conceptual Approach*. American Institute of Aeronautics and Astronautics, Inc., Washington, D.C.

omit

---

***Space Projects***



**A HIGH-TEMPERATURE FURNACE FOR APPLICATIONS  
IN MICROGRAVITY**

**THE UNIVERSITY OF ALABAMA IN HUNTSVILLE**

S11-14  
1605BT  
P-8

Technology in the area of material processing and crystal growth has been greatly furthered by research in microgravity environments. The role of efficient, lightweight furnaces with reliable performance is crucial in these experiments. A need exists for the development of a readily duplicated, high-temperature furnace satisfying stringent weight, volume, and power constraints.

A furnace has been designed and is referred to as the UAH SHIELD. Stringent physical and operating characteristics for the system have been specified, including a maximum weight of 20 kg, a maximum power requirement of 60 W, and a volume of the furnace assembly, excluding the batteries, limited to half a Get-Away-Special canister. The UAH SHIELD furnace uses radiation shield and vacuum technology applied in the form of a series of concentric cylinders enclosed on either end with disks. Thermal testing of a furnace prototype has been performed in addition to some thermal and structural analysis. Results indicate the need for spacing of the shields to accommodate the thermal expansion during furnace operation. In addition, a power dissipation of approximately 100 W and system weight of approximately 30 kg has been found for the current design.

**INTRODUCTION**

The low-gravity environment of space provides researchers with conditions suitable for furthering technology in the areas of materials processing and crystal growth. The effects present during terrestrial materials processing experiments such as sedimentation and buoyancy-driven convection are greatly reduced in microgravity<sup>(1)</sup>. Thus, the ability to produce high-quality crystals such as zinc selenide and high-temperature refractory materials is a viable objective in space. These improved materials have direct implications for advanced research in metallurgy and applications in optical computers, and electro-optical devices, among other areas.

Although ideal in principal, research in microgravity is very limited for most investigators due to limited access and on-orbit restrictions. Considerable energy losses tolerated on Earth can not be accommodated in space. For flight applications, a system must be robust to withstand the vibrational loads induced on launch and re-entry, while being reliable to provide a standard level of performance over many flights<sup>(1)</sup>. In addition, volume, weight, and safety considerations, along with experimental requirements, pose a great challenge to designers of hardware for microgravity research.

Several furnaces such as NASA's Crystal Growth Furnace (CGF) and NASA's Advanced Automated Directional Solidification Furnace (AASDF) are being developed to meet the needs of various researchers. The design of these furnaces is driven by the factors mentioned above, as well as their key experimental requirements which are summarized in Table 1. Both the CGF and the AASDF support a maximum hot zone operating temperature ranging from 1500° to 1600°C and utilize conventional solid insulation in conjunction with liquid cooling. In order to satisfy design objectives, the CGF and AASDF are massive furnaces by weight and volume with sizable energy requirements. In particular, the CGF furnace module and auxiliary components measure 60.9 cm in diameter, with a height of 162.5 cm and

TABLE 1. Key experimental requirements for the AASDF and CGF<sup>(2,3)</sup>

| Furnace | Max. Temp. C° | Sample O.D. cm | Sample Length cm | Translation mm/hr | Other                           |
|---------|---------------|----------------|------------------|-------------------|---------------------------------|
| AASDF   | 1500          | 2.0            | 25               | 0.5 -50.0         | Multizone                       |
| CGF     | 1600          | 2.0            | 20               | 0.24-498          | Multizone<br>Auto Sample Change |

requires 1250 W power<sup>(2)</sup>. The AASDF furnace container is 43 cm in diameter, 130 cm in height, requires 775 W power, and weighs 213 kg<sup>(3)</sup>.

The role of efficient, lightweight furnaces with reliable performance is crucial for materials processing in microgravity environments. While satisfying a broad range of experimental requirements, the high cost and limited accessibility of the AASDF and the CGF restrict their simultaneous use by several investigators. A need exists for the development of a readily duplicated, high-temperature furnace satisfying stringent weight, volume, and power constraints.

**PROBLEM STATEMENT AND DESIGN REQUIREMENTS**

The objective of this research was to design an efficient, high-temperature furnace that would satisfy the requirements of two materials processing experiments for the development of zinc selenide crystals and high-temperature refractory materials. The furnace will be candidate for flight on the shuttle or other orbital carrier in a Get-Away-Special (GAS) canister-sized volume. The experiment will be designated to occupy a nonman-rated volume. Weight and power requirements must be compatible with several carriers such as the GAS, the Hitchhiker, and the Complex Autonomous Payload (CAP) programs accommodated in the shuttle and also on the Orbital Free Flyer, the Commercial Experiment Transporter (COMET).

The furnace designed is referred to as the UAH SHIELD. This furnace has been developed with the intent to provide a maximally efficient facility for materials processing. Stringent physical and operating characteristics were specified in an attempt to satisfy this objective. These requirements include a maximum weight of 20 kg, excluding batteries, and a maximum power of 60 W. The volume of the furnace assembly and auxiliary components, excluding the batteries, is limited to half a GAS canister. In particular, this is a payload volume of 2.5 cu ft defined by a payload with a diameter of 19.75 in and a height of 14.13 in<sup>(4)</sup>.

Experimental conditions to be accommodated by the UAH SHIELD furnace include a maximum centerline temperature of 1660°C obtainable for a 2-cm-diameter specimen. A second thermal performance capability required is a temperature profile restricted to low gradients. This specification consists of obtaining a centerline temperature of 1050°C to be maintained over an entrance length of 5 cm. This constant temperature is to be followed by a thermal gradient of 10°C/cm over the next 5 cm of a silica quartz ampoule with the dimensions of 2 cm in diameter and 22.0 cm in length. The furnace must be able to translate with respect to the specimen at a minimal rate of 2 mm/day for a distance of 2 cm. In addition, the entire assembly must tolerate a vacuum environment.

Other design requirements for the UAH SHIELD furnace include the preservation of structural and thermal performance in the harsh environment to which it is subjected. The furnace assembly must be able to maintain its structural integrity under an applied launch load of 12 g on the launch axis and 6 g on each transverse axis<sup>(4)</sup>. In addition, a 12.9 g overall root-mean-squared random vibration level must be withstood. Thermal environmental parameters applied to GAS can payloads are highly dependent on orbital conditions and the internal heat produced by payload items. Steady state orbital bay temperature range from -160° to 100°C. A worse case approximation of half the container's temperature, based on a power dissipation of 60 W, should be assumed to be 25°C. In addition to the key design parameters previously mentioned, considerations were required with respect to furnace reusability, ease of sample changing, safety, materials availability, and compatibility of materials, among others.

#### DESCRIPTION OF THE UAH SHIELD FURNACE

The stringent power, volume, and weight requirements stipulated have dictated a radical departure in design from the use of solid insulation commonly found in conventional high-temperature furnaces. The UAH SHIELD furnace utilizes radiation shield and vacuum technology to achieve its efficiency. The SHIELD design consists of a series of concentric cylinders, referred to as radial shields, enclosed on either end with disks or end shields as shown in Fig. 1. Two designs currently being considered to maintain the spacing between the shields and minimize losses due to conduction include the use of dimples pressed into the shields and the use of a cone to position the radial and end shields. Variable spacing of the shields is proposed in an attempt to accommodate the thermal expansion.

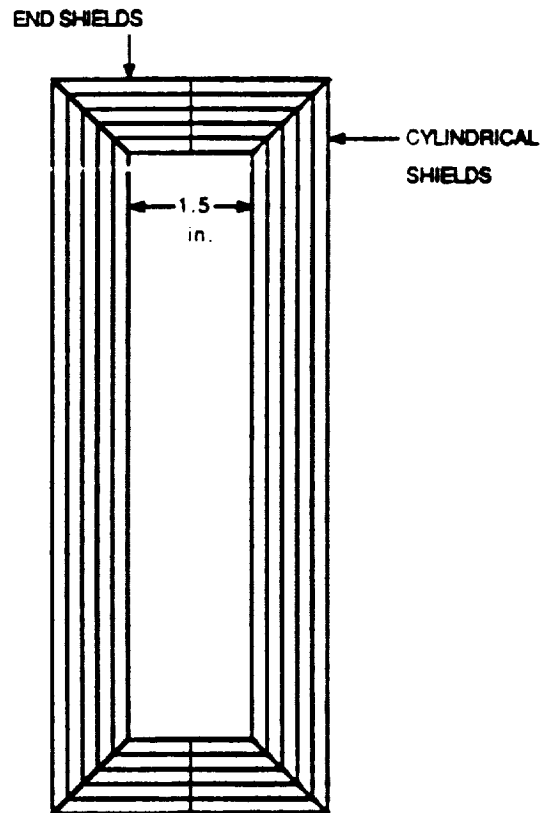


Fig. 1. UAH SHIELD furnace insulation.

The radiation shields are to be constructed from low-emissivity materials to reduce the net radiation transfer between the series of surfaces. In addition, the interior region of the furnace module will be exposed to temperatures of 1660°C and above, requiring materials with high melting and recrystallization temperatures. The shields are proposed to be made of a 0.005-in thick niobium alloy, WC-103, with a melting point of approximately 2400°C<sup>(5)</sup>. For temperatures below 1063°C, which is below the melting point of gold, gold-plated niobium will be utilized. Emissivity as a function of temperature for niobium, gold and with several other materials, is illustrated in Fig. 2<sup>(6)</sup>. Niobium was selected based on its high melting and recrystallization temperature, as well as its relatively low emissivity, density, and thermal conductivity values. As seen from the graph, the use of gold at temperatures below its melting point is advantageous because of its highly desirable emissive properties. The radial and end shields are depicted in Fig. 3, showing a longitudinal, cross-sectional view of the furnace module.

Internal to the shields is the ceramic heating core, which is proposed to be alumina oxide. The core must be supported in a simple but effective manner, allowing easy access to the sample. For the core support, the UAH SHIELD furnace uses caps made from niobium alloy having a cup section that surrounds the core and a thin walled tube section projecting

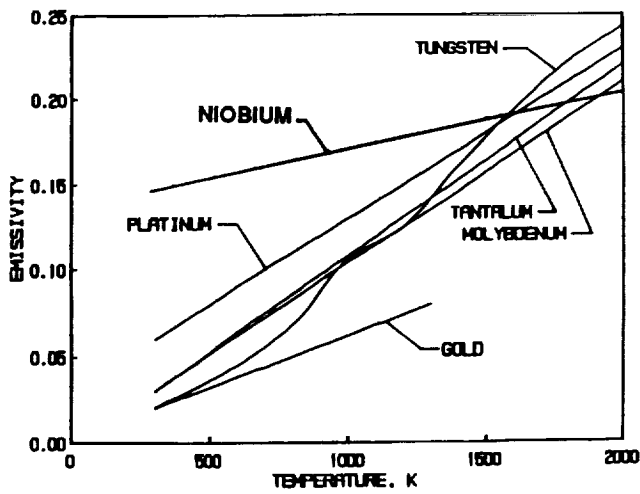


Fig. 2. Emissivity vs. temperature.

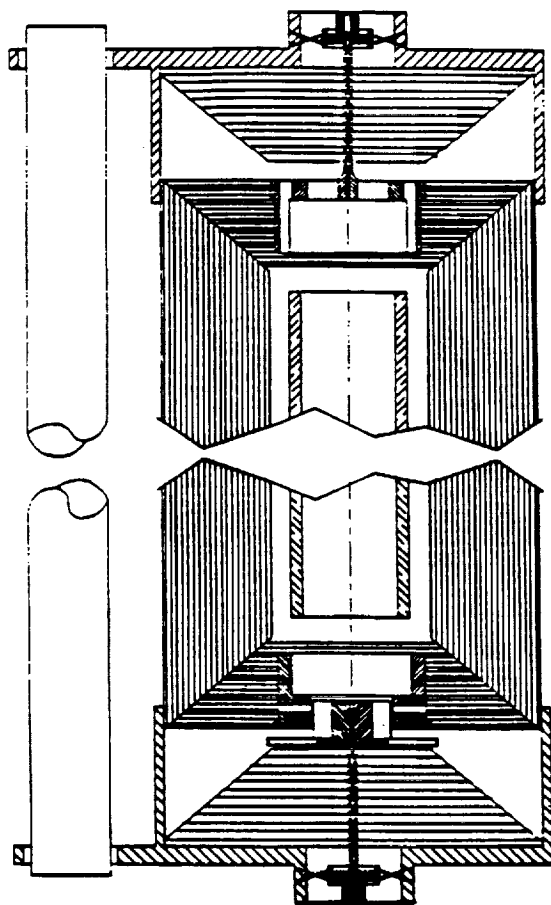


Fig. 3. UAH SHIELD furnace cross-sectional view.

through the end shields as shown in Fig. 3. The core caps are attached to niobium alloy hubs. A system of wires or spokes is proposed to provide interfacing between the hubs and the external structure for support, in addition to minimization of heat loss.

The external structure of the furnace module is supported through endcaps made of 6061-T6 aluminum. The endcaps allow the outer radiation cylinder to be supported, in addition to providing an anchoring base for the spoke system that supports the internal core. A longitudinal view of this part is also shown in Fig. 3. The endcaps are designed to have two tangs on their perimeter to allow the insertion of a translation support rod and a threaded translation rod. The bearing rod and threaded rod are supported by pillow blocks mounted in the GAS can. The furnace module and auxiliary components within the GAS can are shown in Fig. 4. The configuration of the endcaps, threaded rod, and bearing rod with respect to their positioning in the GAS can are clearly depicted in this illustration. Translation of the furnace is accomplished by programming the vacuum-compatible controller to the prescribed rate and duration. With a stepper motor geared for the desired translation, rotation of the threaded rod is performed through a belt-sprocket system.

As specified in the requirements, the specimen is to remain stationary with respect to the furnace translation. In addition, the ampoule/specimen must be supported so that vibration is minimized, alignment in the core is maintained, conduction losses through the furnace are minimized, and sample changing is permitted. The ampoule support system is based on the

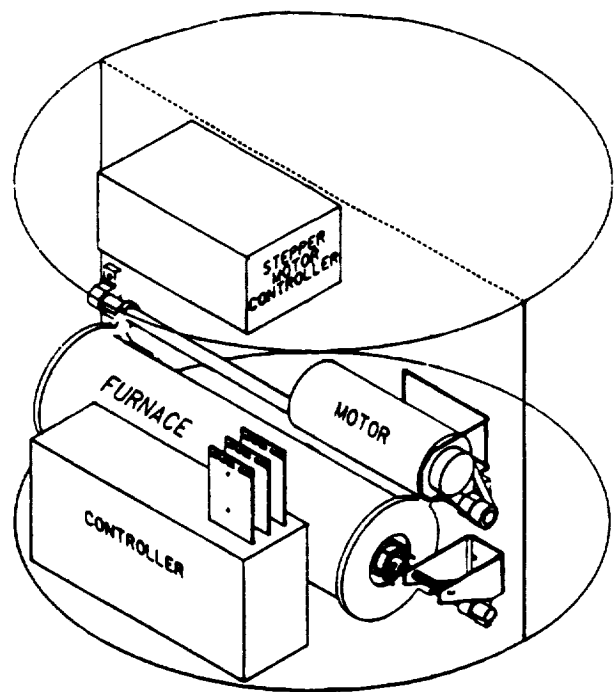


Fig. 4. The UAH SHIELD furnace within 1/2 a GAS Can.

suspension of the ampoule between two rigid supports anchored external to the furnace. The suspension of the specimen is performed using a unique system of support wires and accommodates the elongation of the wires during furnace operation.

The control system for the UAH SHIELD furnace includes a power source, temperature controls, heating elements, and a microprocessor-based controller in order to satisfy the experimental conditions of a 1660°C maximum temperature. The power for this system will be supplied by two zinc-silver oxide batteries. Three thermocouples are to be positioned within the core at different locations along its axial length. This will allow temperature measurements to be obtained and relayed back to an amplifier module and the controller. An additional thermocouple is to be placed within the GAS can to monitor its temperatures. A 60% platinum/40% rhodium alloy wire is proposed for use as the heating elements.

### METHODOLOGY AND RESULTS

Evaluation of the UAH SHIELD furnace has been performed based on experimental, analytical, and numerical techniques. To investigate the feasibility of the proposed design, thermal testing of a prototype has been conducted. Thermal analysis using numerical techniques has been performed in order to evaluate and ultimately optimize the design of the insulation and the supporting structures. Finally, structural evaluation based on hand calculations and finite element analysis has been performed on various components of the supporting structure of the furnace.

#### Thermal Testing

Early research on the UAH SHIELD furnace assumed a radial shield configuration consisting of a helix surrounding the furnace core. An initial experiment was performed to investigate the feasibility of this design concept. The objective of this test was to determine if the thermal expansion would be accommodated using radiation shields fabricated in the form of a helix with dimples separating successive layers.

The prototype developed was made of AISI 300 series stainless steel measuring 19 ft long, 15 in high, and 0.005 in thick. Dimples of approximately 0.02 in high and having a 0.02-in radius were pressed in the stainless steel sheet using a template and applying a rolling procedure. The sheet was then wound into 70 layers containing approximately 1600 dimples. The final prototype is 15 in high, with an inner diameter of 2.75 in and an outer diameter of 7.0 in. Using an alumina core wrapped with nichrome wire, an internal heat source was developed to be inserted within the prototype. Two thermocouples were used for measurements of temperature within the furnace core and on the outer shield. To support the shields, the core, and the internal thermocouple, as well as minimizing axial heat losses, the ends of the shields were insulated using endcaps. The endcaps were fabricated from 310 ceramic foam<sup>(7)</sup>. The table-top configuration of the test set-up is shown in Fig. 5.

The prototype furnace was heated to a temperature of 700°C and temperature readings from both thermocouples were recorded for a total of 102.5 min. The steady-state temperature of the outer shield was found to be 152.7°C. Fluctuations of

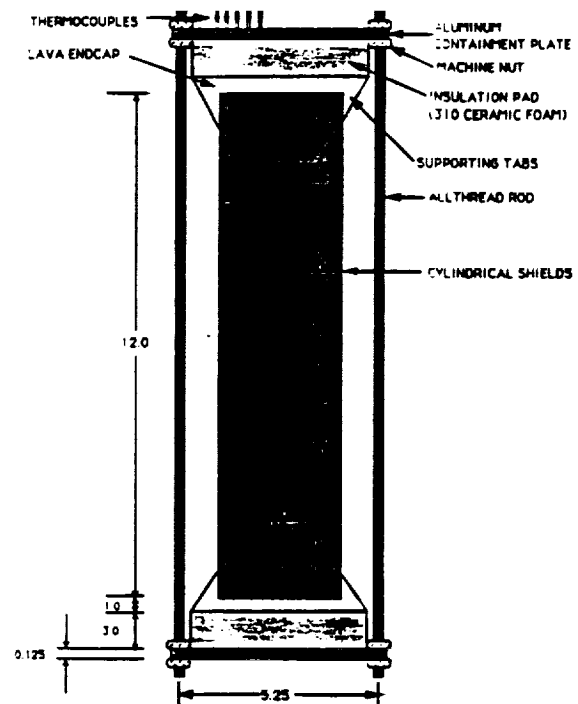


Fig. 5. Experimental set-up for Test 1.

5°C for the outer shield temperature were observed and attributed in part to convection from room air currents. After the test was completed and the furnace thoroughly cooled, the heat shields were unwound and inspected. The innermost shields, those experiencing the greatest temperatures, exhibited severe wrinkling and crimps. This result indicated that the inner shields were being deformed when expansion was restricted by the outer shields, which were expanding a different amount. In addition, a large amount of oxidation was evident on the innermost shields indicating the need for an inert atmosphere during testing. The results from this initial test revealed that the helix configuration of radial shields was inadequate during furnace operation and did not accommodate the thermal expansion.

An iteration in the design of the radial insulation was performed, resulting in the current design of the UAH SHIELD furnace consisting of concentric cylinders with more spacing. This radial insulation was described in an earlier section in this paper. Theoretically, the current radial insulation design addresses many of the problems encountered in the initial design. A second experiment has been proposed and a prototype developed in an attempt to verify the design with respect to thermal expansion qualitatively.

The prototype developed to model the current UAH SHIELD design consists of 9 concentric cylinders with wider spacing. The cylinders were fabricated by spot welding 0.005-in thick sheets of inconel 600. All cylinders were 12 in long while the inner cylinder had an inner diameter of 1 in and the outer cylinder had an inner diameter of 1.555 in. Interior to the

cylindrical shields, a 1.0-in alumina core wrapped with nichrome wire was positioned. Thermocouples of 0.055 in were located between each shield to monitor the temperature distribution throughout the furnace prototype. As in the previous test, endcaps were used to support the shields and the core, and to minimize axial heat losses.

The testing protocol to be followed involves performing the experiment in a bell jar to simulate the actual environment of the furnace. Using a bell jar and a turbopump system, a pressure on the order of  $10^{-5}$  atm will be produced. The core of the prototype will be heated to 700°C and thermocouple readings will be made every 30 sec until the outer shield has reached a steady-state temperature. Following this general approach, it is hoped that qualitative evaluation of the furnace design may be made.

**Thermal Analysis**

Thermal analysis using numerical techniques has been performed in an attempt to evaluate the dissipation of heat and ultimately optimize the design of the insulation and the supporting structures in the UAH SHIELD furnace. In the analysis of the furnace insulation, it was assumed that the heat loss was governed by radiation alone, thus conduction was neglected. A program was developed to determine the number of radial shields required to satisfy the given boundary conditions assuming various heat rates. The radial shields were modeled assuming infinite concentric cylinders as described by the following equation<sup>(8)</sup>.

$$q_{rad} = \frac{SBC \cdot A \cdot (T_i^4 - T_j^4)}{\frac{1}{E_i} + \frac{1 - E_j}{E_j} \cdot \frac{r_i}{r_j}} \quad (1)$$

In this equation,  $q_{rad}$  is the heat loss due to radiation; SBC is the Stefan-Boltzman constant having a value of  $5.67 \times 10^{-8}$  W/(m<sup>2</sup>K<sup>4</sup>); A is the surface area;  $T_i$  is the temperature of shield i;  $T_j$  is the temperature of shield j;  $r_i$  is the radius of shield i;  $r_j$  is the radius of shield j;  $E_i$  is the emissivity of shield i; and  $E_j$  is the emissivity of shield j.

The boundary conditions applied in this analysis assumed the largest possible temperature extremes exist. Thus, the given temperatures of the inner and outer shields were 1700°C and 20°C respectively. The shields were assumed to be 0.005 in thick, separated by a constant vacuum space of 0.01 in, with the innermost shield having an inner radius of 0.775 in. The inner shields were assumed to be composed of the niobium alloy WC-103 until a calculated shield temperature below 1063°C was found. Below 1063°C, the melting point of gold, the shields were assumed to be gold plated. The material properties used in this analysis are given in Table 2 where the emissivities are shown to be a function of temperature (K). In the Fortran program developed, iterations were performed to evaluate the number of shields required to satisfy the given boundary conditions assuming various heat rates. Equation (1) was solved for the temperature of the jth shield allowing the temperature distribution throughout the radial insulation to be

TABLE 2. Selected material properties of the UAH SHIELD insulation.<sup>(5,9)</sup>

| Material | Density kg/m <sup>3</sup> | Emissivity                       | Melting Point °C |
|----------|---------------------------|----------------------------------|------------------|
| WC-103   | 8850                      | $3.75 \times 10^{-5}T + 0.1325$  | 2400             |
| Gold     | 19300                     | $5.29 \times 10^{-5}T + 0.00914$ | 1063             |

TABLE 3. Results of radial shield analysis.

| Shield # | Power W | Weight kg |
|----------|---------|-----------|
| 101      | 55      | 8.24      |
| 118      | 50      | 10.44     |
| 141      | 45      | 13.63     |
| 175      | 40      | 19.45     |

determined. In order to simplify the program a conservative assumption was made that the values of emissivity for adjacent shields were the same.

The resulting number of shields and the corresponding weights for values of heat loss ranging from 40 W to 55 W are shown in Table 3. The values of power dissipation assumed in the analysis were chosen since they fell below the 60 W allowed for the entire furnace. For a 15-W reduction in heat from 55 W to 40 W, it is seen that the number of shields required increases almost 75% and the weight more than doubles. The change in weight and size or diameter of the radial insulation as a function of power is clearly depicted in Fig. 6. From this graph, a sharp increase in weight is seen as the power loss is reduced beyond approximately 45 W. This value of power dissipation, 45 W, was chosen to determine the number of shields used in the UAH SHIELD furnace. For this heat loss, 124 niobium alloy shields and 26 gold-plated shields are required, resulting in a weight of 13.77 kg and an outer diameter of 5.8 in. This value of power dissipation through the radial shields allows flexibility in other areas of the furnace design such that power losses of up to 15 W may be accommodated and still allow satisfaction of the maximum heat loss requirement. The outer

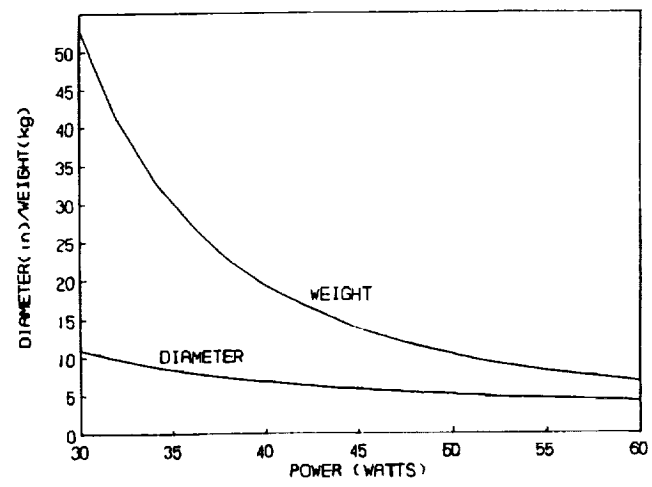


Fig. 6. Power vs. weight and diameter.

diameter of the shielding, 5.8 in, may clearly be accommodated in the volume allotted for the furnace. However, the weight of the shielding is almost 70% of the total weight allowed. The temperature distribution as a function of shield number is given in Fig. 7 for a power loss of 45 W. In this graph, the advantage of using gold plating with its low emissivity at temperatures below 1063°C is seen by the sharp temperature gradient over the outer gold-plated shields. This result translates to savings in the number of total shields over that required if niobium alone had been used.

A simple comparison was made to illustrate the effectiveness of the UAH SHIELD furnace in reducing power dissipation over that permitted with conventional solid insulation. For a heat loss of 45 W through the radial shields, it was found that 141 shields were required, resulting in an inner insulation radius of 0.775 in and an outer radius of 2.9 in. A determination was made of the heat transfer through a solid cylinder with the same dimensions as that of the radial insulation. The radial heat transfer rate for a solid cylinder with a logarithmic temperature distribution is given by the following expression<sup>(8)</sup>.

$$q_{\text{cnd}} = \frac{2 \cdot \pi \cdot L \cdot k \cdot (T_{s,1} - T_{s,2})}{\ln(r_2/r_1)} \quad (2)$$

In this equation,  $q_{\text{cnd}}$  is the heat loss due to conduction;  $\pi$  is a constant having a value of 3.14159;  $L$  is the length of the cylinder;  $T_{s,1}$  is the inner surface temperature;  $T_{s,2}$  is the outer surface temperature;  $r_1$  is the inner radius of the cylinder;  $r_2$  is the outer radius of the cylinder; and  $k$  (W/mK) is the value of thermal conductivity.

The length of the solid cylinder was assumed to be 13 in, an average value of the length of the radiation shields. Zirconia was used in the analysis due to its relatively low thermal conductivity value of approximately 0.23 W/mK at 1650°C<sup>(10)</sup>. In both the analysis of the radial shields and the solid insulation, the boundary conditions applied included an inner temperature of 1700°C and an outer temperature of 20°C. Approximately 600 W of power dissipation was found for the solid cylinder

described. This analysis does not account for the change in conductivity with temperature; however, it is highly significant that 13 times the heat loss is obtained for solid insulation with approximately the same dimensions as that of radiation shielding.

Thermal analysis of the end shields was performed to determine the heat loss based upon a given number of shields and the applied boundary conditions. For a first approximation, the end shields were modeled as large parallel plates governed by the following equation<sup>(8)</sup>

$$q_{\text{rad}} = \frac{\text{SBC} \cdot A \cdot (T_i^4 - T_j^4)}{\frac{1}{E_i} + \frac{1}{E_j} - 1} \quad (3)$$

where the constants shown are the same as those given in equation (1). A-1 in end shield insulation height was assumed per end, resulting in 66 individual shields available. The shields were assumed to be 0.005 in thick and separated by a vacuum space of 0.01 in. An iterative procedure was performed to calculate the heat loss with an inner shield temperature of 1700°C and an outer shield temperature of 20°C. The inner shield diameter was assumed to be 1.55 in while the outer shield diameter was assumed to be 5.8 in. Equation (3) was manipulated to find the end shield temperature distribution, where the emissivity values of adjacent shields were approximated to be equivalent. As before, the innermost shields were assumed to be composed of the niobium alloy WC-103 until a calculated shield temperature below 1063°C was found. Below this temperature, the emissive properties of gold were used in the calculations. The results obtained through this analysis yielded a heat loss of approximately 3 W per end. The 1-in end shield insulation was found to be comprised of 59 niobium shields and 7 gold-plated shields. The weight of the end shields was found to be approximately 1.5 kg total.

The core support was identified as the primary heat sink within the furnace structure. Thus, thermal analysis using the finite element method (FEM) was performed in an attempt to evaluate and optimize the design of this component with respect to heat loss. As described earlier, the core support is composed of a cap having a cup section that surrounds the core, and a thin walled tube section projecting through the end shields to the hubs and ultimately to the endcap rim through a system of wires or spokes. A two dimensional axisymmetric model of the core cap, tube, hub, and spoke section designs were created using ANSYS (Swanson Analysis System, Inc.) finite element software. The core support tube section was defined using quadrilateral elements. Heat loss in this region was assumed to be governed by Fourier's law of conduction. Radiation exchange between the hub and the rim was modeled using one-dimensional, axisymmetric elements. The cross-sectional area for the discrete spokes was found and an equivalent cross-sectional area, axisymmetric, thin disc was used to model the area for conduction transfer in this component. At nodes on the inner surface, a temperature of 1700°C was applied. Those nodes representing the rim were assumed to be at a temperature of 20°C. The axisymmetric model is shown in Fig. 8 and contains 878 elements and 939 degrees of freedom.

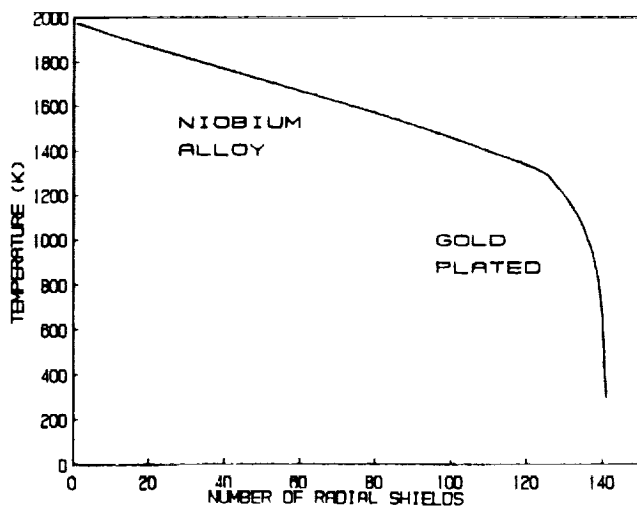


Fig. 7. Radial shield number vs. temperature for  $Q = 45$  W.

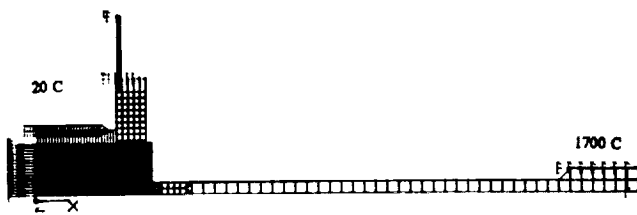


Fig. 8. Axisymmetric model of the core support structure.

In the preliminary design of the UAH SHIELD furnace, the core support components were assumed to be made of tantalum. The current design uses a niobium alloy, however, in this analysis the material properties for tantalum were used. ANSYS's capability to enter up to a fourth degree polynomial for thermal conductivity as a function of temperature was used in this analysis. The polynomial used is of the form<sup>(8)</sup>

$$k = 57.598 + 2.518 \times 10^{-3} T + 1.846 \times 10^{-6} T^2 - 6.537 \times 10^{-10} T^3 \quad (4)$$

where the unit of temperature is degrees C. A value of 0.11, which is fairly constant over the range of 300 K to 1100 K, was used for the emissivity of tantalum<sup>(9)</sup>. The results yielded a 19.3 W heat loss for the core support per end of the furnace<sup>(11)</sup>. With a power dissipation of 45 W through the radial insulation and 6 W through the end shields, this value of heat rate through the core support causes the total heat loss of the furnace to exceed the required 60 W.

In an attempt to assist in the redesign of this component to optimize the heat loss, further analysis was performed. A simplified version of the model described above was used in this second investigation. Only the core support tube section was used resulting in the hub, spoke, and radiation assumptions being neglected. This simplified model consisted of 59 elements and 109 degrees of freedom. The model was analyzed using various values of conductivity given as a function of temperature. The heat flow was determined and divided by the cross-sectional area of the thin-walled tube to obtain the heat flux. The resulting conductivity vs. heat flux is given in Fig. 9. This graph may

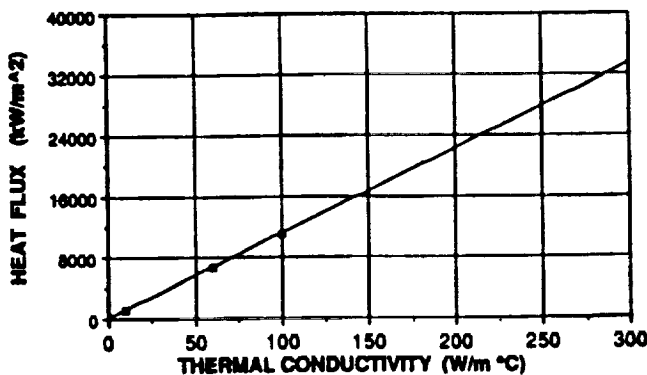


Fig. 9. Thermal conductivity vs. heat flux.

be used to allow a first approximation of the required cross-sectional area for an optimized design of this component given a thermal conductivity value and a desired heat loss.

### Structural Analysis and Safety Considerations

Structural evaluation based on hand calculations and finite element analysis has been performed on various components of the supporting structure of the UAH SHIELD furnace. Some of the key analyses performed are briefly reviewed here. The total weight of the structural and translation components was found to be approximately 7.5 kg. The forces in the 0.025-in tungsten ampoule support wires were calculated to verify their integrity under a launch condition of 12 g on the launch axis. A factor of safety greater than 1.5 was found for the ampoule suspension system.

An iteration in the design of the aluminum endcaps has been performed based on a preliminary finite element analysis of this component. The 6061-T6 aluminum endcaps and tangs were modeled separately using three-dimensional isoparametric elements. The forces due to acceleration were assumed to be transferred through the flanges to the endcap body. ANSYS structural analysis software was used in this investigation. The results indicated that severe stress concentrations were present at the junction of the tangs or flanges and the endcap body. The maximum principal stresses in these locations were found to exceed the yield strength of the material. Subsequently, a redesign of this part was performed where corners were filleted and material redistributed in an attempt to reduce stress concentrations. In order to evaluate the current endcap design, a three-dimensional model of this component has been created for future analysis on a Cray X/MP supercomputer. The model has been refined and consists of 2768 elements having 13,000 degrees of freedom.

The area of safety is a critical aspect in any design project. Applicable safety procedures and requirements have been reviewed at each step in the design of the UAH SHIELD furnace. A preliminary hazard analysis of the payload was performed and a safety data package for Get Away Special payloads was compiled in accordance with NASA's "Get Away Special Payloads Safety Manual" and "NASA's Safety Policy and Requirements Manual."<sup>(12,13)</sup> Materials used within the UAH SHIELD furnace assembly have been selected based upon safety ratings prescribed by Marshall Space Flight Center's "Materials Selection List for Space Hardware Systems."<sup>(14)</sup> In addition, a preliminary materials listing has been developed for the system designed.

### CONCLUSIONS

The objective of this research was to design an efficient, high-temperature furnace that would satisfy the requirements of two materials processing experiments for the development of zinc selenide crystals and high-temperature refractory materials. The UAH SHIELD furnace has been designed in an attempt to address many of the needs specified by these experiments. In addition, the UAH SHIELD furnace was developed to provide researchers with a readily reproducible, high-temperature furnace satisfying stringent weight, volume, and power constraints. The criteria imposed upon the system have dictated a radical departure in

design from the use of solid insulation commonly found in conventional high-temperature furnaces. The UAH SHIELD furnace insulation using radiation shields has been shown to be significantly effective in reducing the power dissipation when compared to solid insulation under similar conditions.

Thermal testing of a furnace prototype has demonstrated the importance in the design of the radial shields coupled with the thermal expansion of the system. The results from the initial test revealed that the helix configuration of radial shields was inadequate during furnace operation and did not accommodate the thermal expansion. This finding motivated a redesign of the radial insulation from a helix configuration to concentric cylinders with wider spacing. A second test using the current radial insulation design, as outlined earlier, should aid in a qualitative evaluation of the furnace design. Future quantitative experimentation needs to ultimately be performed by testing the actual furnace design with its specified materials under true operating conditions.

Through thermal analysis of the insulation and core support structure, a power dissipation of approximately 100 W was found for the UAH SHIELD furnace design. This value exceeds the specified 60 W, but is still well below that required for the CGF furnace or the AADSF. Further analysis and eventual testing is necessary to better approximate the heat loss through the insulation, taking into consideration conduction paths. Redesign and analysis of the core support must be performed in order to optimize this design with respect to the power dissipated. To insure a low gradient thermal profile can be accommodated with this system, further research in this area is essential.

Evaluation of the furnace component dimensions indicate the system may be assembled in half the volume of a Get Away Special canister, excluding the batteries. However, the weight of the furnace has been found to be approximately 30 kg, excluding the batteries. Once again, this value is still below the weight specified for the AADSF. Eventual structural analysis and testing is suggested for all components within the furnace assembly to verify their integrity under simulated launch conditions.

While the UAH SHIELD furnace has many areas requiring further analysis and testing, efforts to date have resulted in the development of a high-temperature furnace that is fundamentally different from most conventional systems. Theoretical results indicate that considerable reductions in power dissipation, volume, and weight are potentially feasible with this unique furnace when compared to solid insulation furnaces. The ultimate goal for future research in the design of the UAH SHIELD furnace is to provide a maximally efficient facility for materials processing in microgravity environments.

#### ACKNOWLEDGMENTS

Support for this research was provided by NASA/Universities Space Research Association Advanced Design Program. This report summarizes a year-long effort conducted through a senior-level mechanical engineering course for the research and

development of a high-temperature furnace. This work has been performed over 3 quarters by approximately 50 students under the direction of Dr. Francis C. Wessling, professor of mechanical engineering, and assisted by Sara B. Fair, graduate teaching assistant. We would like to thank Frank Swalley, Sherry Walker, Susan Spencer, Dr. Lehosky, Curtis Bahr, and Dave Lovell from the NASA Marshall Space Flight Center, for their assistance throughout the course of this research.

The students involved in this project include: B. Adams, C. Ballard, S. Boone, D. Bortnick, H. Burton, B. Campbell, T. Clemmons, G. Cough, D. Dawson, C. Donoghue, A. Dudley, T. Estes, J. Garrison, W. Gooch, G. Griffin, C. Hendren, B. Hunt, T. Keller, K. Kennamer, R. Kinnane, G. Kirkham, R. Langston, S. Lee, E. Litkenhous, D. Little, M. McGuire, P. McCoy, C. Melanowski, D. Miller, S. Miller, T. Mitchell, E. Palmer, D. Reeves, D. Richardson, J. Shultz, J. Smith, P. Stephens, J. Stogner, M. Ward, S. Weir, C. Wheeler, B. Whitsett, Jon Williams, Juan Williams, L. Wilson, M. Wilson, D. Wisener, and K. Worcester.

Questions concerning this document should be referred to Francis C. Wessling Ph.D., (205) 895-6620, Department of Mechanical Engineering, The University of Alabama in Huntsville, Huntsville AL 35899.

#### REFERENCES

1. Rosenthal B. N., Krolikowski C. R. (1990) Programmable Multi-Zone Furnace for Microgravity Research. *J. Amer. Inst. of Aeronaut. and Astronaut.*, 91, 0781, 1-6.
2. NASA Publication, *Crystal Growth Furnace (CGF)*, Marshall Space Flight Center, Experiment Payloads Projects/JA51, January 1989.
3. NASA Publication, *Advanced Automated Directional Solidification Furnace (AADSF)*, Marshall Space Flight Center, Experiment Payloads Projects/JA51, January 1989.
4. NASA Publication, *Get Away Special (GAS) Small Self-Contained Payloads Experiment Handbook*, Goddard Space Flight Center, Special Payloads Division, 1989.
5. Teledyne Wah Chang Albany, (1990) *Niobium*, pp. 15-16.
6. Touloukian Y. S. and Ho R. W. (1970) *Thermophysical Properties of Matter: Thermal Radiative Properties-Metallic Element and Alloys*, Vol. 7, Plenum, Washington
7. Cotronics Corporation, *Ceramics and High Temperature Materials Handbook*, p. 13. Brooklyn, NY.
8. Incropera F. P. and Dewitt D. P. (1990) *Fundamentals of Heat and Mass Transfer*. Wiley, New York.
9. Dewitt D. P. and Touloukian Y. S. (1970) *Thermophysical Properties of Matter VII*, IFI/Plenum, New York, p. 474.
10. Touloukian Y. S. and Ho R. W. (1970) *Thermophysical Properties of Matter: Thermal Radiative Properties-Non Metallic Solids*, Vol. 8, Plenum, Washington.
11. McGuire M., personal communication, May 1991.
12. NASA Publication, *Get Away Special Payloads Safety Manual*, NASA, 1986.
13. NASA Publication, *Safety Policy and Requirements*, NSTS 1700.7B, Lyndon B. Johnson Space Center, 1989.
14. NASA Publication, *Materials Selection List for Space Hardware*, Marshall Space Flight Center, HDBK-527.

# ADVANCED DESIGN FOR ORBITAL DEBRIS REMOVAL IN SUPPORT OF SOLAR SYSTEM EXPLORATION

UNIVERSITY OF ARIZONA

512-18  
160588  
P. 7

The development of an Autonomous Space Processor for Orbital Debris (ASPOD) is the ultimate goal of this project. The craft will process, *in situ*, orbital debris using resources available in low Earth orbit (LEO). The serious problem of orbital debris is briefly described and the nature of the large debris population is outlined. This year, focus was on development of a versatile robotic manipulator to augment an existing robotic arm; incorporation of remote operation of robotic arms; and formulation of optimal (time and energy) trajectory planning algorithms for coordinating robotic arms. The mechanical design of the new arm is described in detail. The versatile work envelope is explained showing the flexibility of the new design. Several telemetry communication systems are described which will enable the remote operation of the robotic arms. The trajectory planning algorithms are fully developed for both the time-optimal and energy-optimal problem. The optimal problem is solved using phase plane techniques while the energy optimal problem is solved using dynamics programming.

## INTRODUCTION

The problems presented by orbital debris have been gaining attention in recent years. Science writers<sup>(1-4)</sup> and the popular news media<sup>(5-9)</sup> have lucidly described these problems. The orbital debris problem merited a report from the General Accounting Office<sup>(10)</sup> describing the threats to future space stations and other space operations. The Advanced Design team at the University of Arizona continues to develop a spacecraft that will economically remove the large debris through local resource utilization. The fundamental idea is to concentrate solar energy into a point-focus and cut the debris into precise shapes that the robotic arms can assemble into a manageable configuration. After having processed several debris pieces three disposal modes exist: (1) retrieval by the shuttle; (2) precise splashdown into the oceans; or (3) planned burn-up during atmospheric reentry.

A study conducted by the University of Arizona in 1989 showed that there were 386 objects in Earth orbit that qualify as large debris (mass 1,500 kg). Each object included in this list has a sufficient orbital lifetime to ensure its existence past the year 2000. This study also identified several specific orbital inclinations where a majority of the large debris exists (Fig. 1).

Mission feasibility studies have shown that one Autonomous Space Processor for Orbital Debris (ASPOD) could process at least five of the large pieces of debris with reasonable propellant requirements<sup>(11)</sup>. This is accomplished by taking advantage of nodal regression differences and through the use of classic Hohmann transfers.

This year's work focused on the development of a versatile robotic manipulator, investigation of remote operation of the existing solar collector and a new robotic arm, and the formation of trajectory planning algorithms for coordinated robotic arms carrying a common object. This report is a summary of the work.

This year, five new students were involved in the ASPOD design. Four were involved with design and fabrication of a robotic manipulator, while the other student refined the solar

tracking device and investigated telemetry systems for future use. In addition, two local high school students were actively involved in the project.

Since the launch of Sputnik in 1957, satellites have orbited the Earth, completed their missions, then burned upon reentry into the atmosphere. Unfortunately, it sometimes takes decades to complete this last step. Three decades into the space age, the amount of junk orbiting the Earth has mushroomed. It includes everything from long-dead satellites, which outnumber working satellites<sup>(1)</sup>, to rocket boosters, clamps, satellite shields, explosive bolts, and even sewage.

Space pollution poses a number of problems. Orbital debris creates a collision hazard for manned and unmanned spacecraft. Defunct satellites falling from orbit, especially those with nuclear power sources, imperil everyone on the ground. Ground-based astronomers already have had observations marred by light reflected from satellites and other orbiting chunks of material passing in front of telescopes<sup>(2)</sup>.

The problem of collision with orbital debris is much more severe than most people imagine. At orbital velocities (typically 7-10 km/s) in LEO, a 1-g mass possesses the same kinetic energy

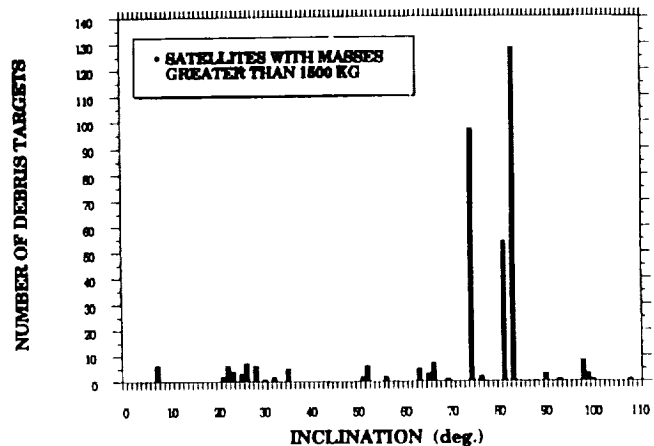


Fig. 1. Inclination where large debris population exists.

as a 50-g bullet travelling at 3300 ft/s (approximately 1000 m/s); a more easily understood analogy is that a 25-g piece of orbital debris in LEO possesses the same energy as a 3000-lb automobile travelling at 60 mph<sup>(3)</sup>. The large pieces of junk (dead satellites, and rocket boosters) are not the immediate problem. They are easily trackable by radar and avoided by manned and unmanned spacecraft. The real problem occurs when these large pieces collide with each other, becoming many thousands of smaller, untrackable, and potentially disastrous projectiles. Excerpts from recent letter written by Dr. Kumar Ramohalli of the University of Arizona, address some of the misconceptions of the orbital debris problem.

Several myths have been propagated regarding orbital debris. (1) The millions of smaller pieces pose a hazard: the eight thousand or so larger ones are not hazardous and can be avoided. [The truth is that these large ones, left alone can create innumerable smaller ones through collisions; we had better remove them while they are still trackable.] (2) Space debris is likely to become a major problem only after 2000 A.D. Why waste our resources trying to build spacecraft to mitigate the future hazards? [The truth is it takes a minimum of ten years to conceptualize, design, fabricate, test and qualify any spacecraft. So the time to start is now.] (3) We know so little about space debris that many more studies are needed for characterization; retrieval can wait. [The truth is that there exists an extensive data bank, continuously updated, on the larger debris. In fact we even have their trajectories, geometry, mass, and sometimes even the remaining propellant in them.]

We could go on, but the point should be clear. These stalling arguments can only be interpreted as a general lack of interest in accepting a problem that is growing at an alarming rate. Don Kessler's own estimates show that space operations could become very hazardous by 2010.

We have approached various authorities, including DoE, DoD who are interested in toxic waste clean-up here on Earth. An autonomous robot that is equipped with solar furnaces and pattern recognition capabilities, image processing, digital filtering, and *in-situ* chemical processing can be sent terrestrially to hazardous waste sites and will detoxify the wastes. Thus, the space-derived technologies may have more immediate applications here on Earth too.

Dr. Ramohalli has proposed using solar energy to process these large pieces of debris, making disposal or reclamation easier. A solar focal-point metal cutter will focus the Sun's energy to a point with an intensity great enough to cut the material. The ASPOD prototype currently consists of a solar powered metal cutter mounted on a wheel table that has been fitted with a telescope equatorial mount to maintain focus of the Sun. One robotic arm has been designed and built to operate satisfactorily with the ASPOD prototype. The space-based unit will need two arms to insure that the final movement imparted to the debris will not cause the severed piece to move toward the fragile lenses and mirrors of the metal cutter.

#### ROBOT MANIPULATOR ARM

Design requirements for the robot manipulator arm call for a rather large working envelope. The arm must be able to retrieve the target debris at a safe distance; it must manipulate the debris at the focal point, position cut pieces near the mirrors, and stow unusable pieces in the storage bin. For the one-fifth scale prototype a stationary robot would need a reach of over ten feet. This year's design team developed a six-degree-of-freedom

robotic arm with the additional feature of a mobile mount that reduced the necessary length of each segment. Upon assembly and testing, the robotic arm satisfied all design specifications.

#### DESIGN OF THE MOBILE MOUNT

The mobile mount is a rotating base for a manipulator. The base is designed to maximize the working envelope of the manipulator arm while minimizing its length and weight requirements.

A top view of the mount is shown in Figs. 2 and 3. The power needed for the mobile mount comes from a parallel shaft TENV gear motor, which is geared down before driving the shaft that goes through the ASPOD platform. The shaft is supported by ball bearings and drives an arm that sits on shoulders machined into the shaft. The other end of the arm rotates with the shaft, thus providing the mobility. The manipulator will "ride" on the far end of the arm near the guide wheel assembly. The guide wheel assembly prevents the arm from moving normal to the ASPOD platform as well as resisting torsional twisting. The arm is guided by a track that is attached to the ASPOD platform.

#### SHAFT ASSEMBLY

The center point of the mobile mount assembly is the central shaft. This shaft supports the torque generated by the weight of the manipulator. The maximum torque, as defined by the static and dynamic model of the manipulator, is approximated at 55 lbf-ft. Carbon steel was the material chosen for the shaft because of its relatively high modulus of rigidity and its availability. The diameter chosen for this design was 1.5 inch. A 13.5 × 14.5-in steel plate supports the shaft. This material was chosen for its high strength and availability. The plate was mounted beneath the ASPOD platform, secured by half-inch bolts to the metal frame of the platform. SKF Industries, Inc. #FY 1 1/2 TM bearings were used to support the shaft. These bearings support both radial and axial loads and are relatively low in cost. The bearings make a sandwich around the steel plate thus supporting the shaft (see Figs. 2 and 3).

#### MOBILE ARM AND WHEEL GUIDE ASSEMBLY

The primary considerations in the design of the mobile arm were: (1) attachment to the central shaft, (2) torsional deflection under the maximum calculated load, and (3) attachment to the wheel guide assembly. A 1.5-in central shaft extends from the top of platform. The maximum torque on the arm was calculated at 650 lb/in. The wheel guide assembly will be mounted to 6061-T6 1.5-in square stock. With these considerations in mind, the arm was designed and fabricated out of 2 × 5 rectangular aluminum (wall thickness = 3/16 in) which was determined to satisfy the design requirements. The machining modifications are shown in Figs. 2 and 3. The wheel guide assembly is responsible for supporting the mobile arm vertically as well as resisting torsional twisting. It was determined that four 6200 series double shield ball bearings will be supported by 10 × 40-mm grade-8 bolts mounted in adjustable supports machined from 6061-T6 aluminum stock. Hardware

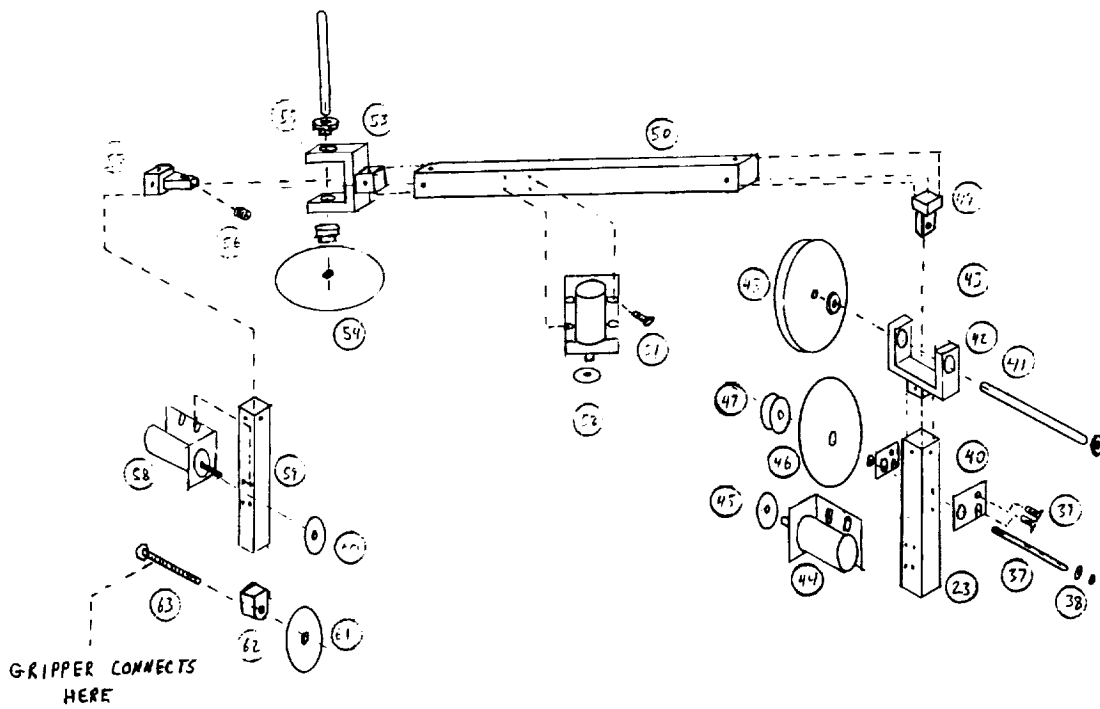


Fig. 2. Manipulator Components.

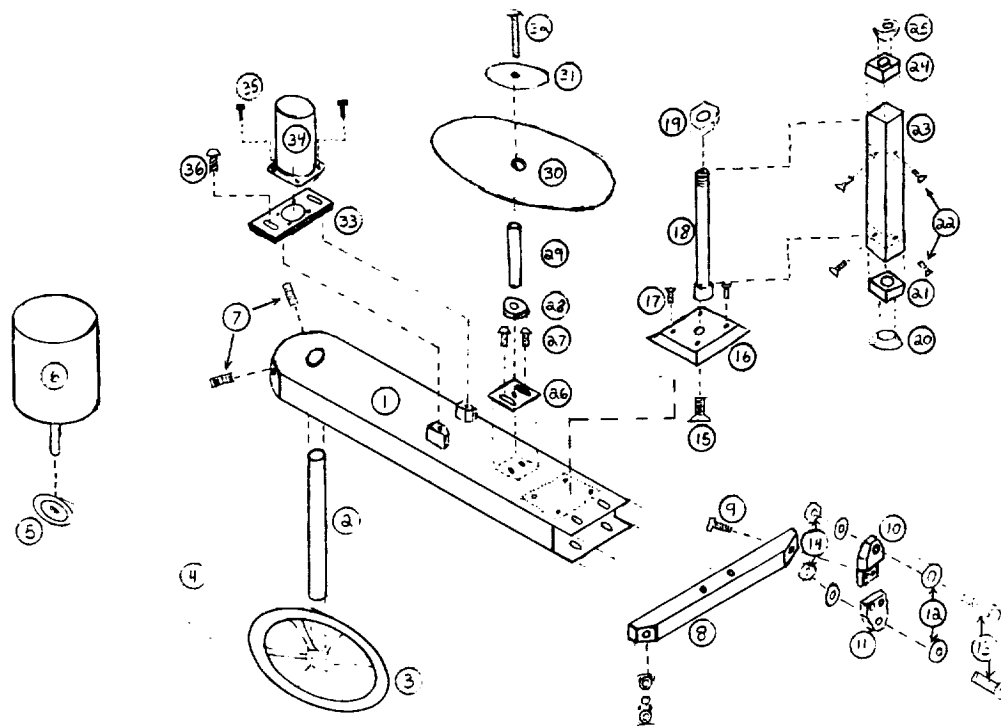


Fig. 3. Rotation Assembly.

is shown in Figs. 2 and 3. After assembly, testing indicated that all components performed as designed. There was no measurable deflection at the wheel/track interface or at the shaft/arm interface.

### TRACK AND TRACK MOUNTS

For the mobile arm, a track was required to allow for movement from one side of the ASPOD platform to the other. The track needed to allow for a guide wheel assembly that would resist motion perpendicular to the mobile mount. After much consideration we decided to use a piece of 3/16-in cold-rolled steel, 2 1/2 in wide. The piece of steel, approximately 12 ft long, was formed into a 5-ft-diameter circle. The track was then mounted to a piece of 3/4-in plywood, which was mounted to the ASPOD platform. In mounting the track to the ASPOD platform, we needed a mount that would allow for complete motion of the mobile arm on the inner diameter of the track. To do this, 3/8-in holes were drilled every 6 inches in the track. A 3/8 × 2-in allen cap screw was used to mount the track to a 4 × 4-in piece of angle that was mounted to the plywood platform. This mounting system for the mobile arm guide wheel assembly allows for the complete motion of the mobile arm in the inner diameter of the track and would also allow no motion perpendicular to the mobile mount.

### MANIPULATOR LINK AND JOINT MATERIAL

After consideration of various materials the decision was made to use aluminum alloy 6061-T6 for the construction of the manipulator links and joints. This alloy, which contains both magnesium and silicon, was chosen because of its good formability, machinability, weldability, and its good corrosion resistance. The temper designation, T6, means this alloy has been solution treated and artificially aged. The major reason for its selection was its relative availability and low cost compared to the other materials considered. Table 1 lists some of the important physical and mechanical properties.

### DEFLECTION AND MOMENT ANALYSIS

The manipulator links will be numbered I, II, and III, beginning at the mobile mount and moving toward the free end of the arm. The shape and dimensions of each link were chosen by using a combination of the availability of a particular material shape and the minimum size needed to attach the necessary actuators to the link's end. Table 2 shows the dimensions of the links. All links are hollow square tubes enabling the routing of wires through their centers.

Using these dimensions, a deflection analysis was performed to make certain that these links would meet the specification of a maximum deflection of 1 cm (0.39 in). This is defined as the difference in deflection between the loaded link and the unloaded link. It will be assumed that the unloaded link will have a 100% repeatability in positioning. Then, if the loaded link can be positioned within 0.39 in. of the unloaded link, the specification will be considered satisfied. A rough schematic of the assembled manipulator can be seen in Fig. 4. The dimensions shown are those dimensions necessary for a deflection and torque analysis. The deflection results are listed in Table 3.

TABLE 1. Al 6061-T6 Properties.

| Properties               | Units               | Value |
|--------------------------|---------------------|-------|
| Yield Strength           | kpsi                | 40    |
| Ultimate Strength        | kpsi                | 45    |
| Modulus of Elasticity    | 10 <sup>6</sup> psi | 10.3  |
| Modulus of Rigidity      | 10 <sup>6</sup> psi | 3.8   |
| Density                  | lbs/in <sup>3</sup> | 0.098 |
| Strength to Weight Ratio | 10 <sup>6</sup> in  | 105.1 |

TABLE 2. Link Dimension.

| Link         | Dimension (in) | Weight (lb) |
|--------------|----------------|-------------|
| I (square)   | 2 × 2 1/8 × 12 | 1.1         |
| II (square)  | 2 × 2 1/8 × 24 | 2.2         |
| III (square) | 2 × 2 1/8 × 12 | 1.1         |

As is evident from the difference values in Table 3, the chosen link dimensions fully meet the deflection design specifications. Using these links, the moments developed at the attached end of each link were calculated. The results from calculations for loaded and unloaded can be seen in Table 4.

These values are important because they can be translated into torque requirements for the actuators between the links if one considers static conditions only. It is obvious that any final torque values must contain dynamic as well as static requirements. The equation for the Lagrangian method (1) for determining torque clearly shows that the torque is

$$\tau = (ml_c^2 + I)\ddot{\theta} + mgl_c \cos(\dot{\theta}) \quad (1)$$

the sum of the potential energy (static) and the kinetic energy (dynamic) terms. The necessary torques can be calculated from (1) ignoring the kinetic energy term if the angular acceleration can be kept several orders of magnitude less than the potential energy acceleration term "g". This will result in a situation where only static conditions will be necessary to calculate torques. By investigating Fig. 5, it is clear that if the time frame can be kept below 30 seconds, torque values can be established by considering static requirements alone, as the angular acceleration term will result in a dynamic value several orders of magnitude less than the static term.

The time in this figure will be the time required to move the link from a vertically down position to a vertically up position. An angular velocity of 1/2 rpm corresponds to a time of 30

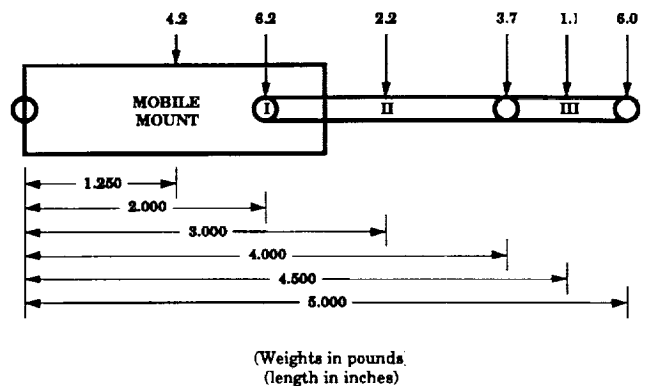


Fig. 4. Deflection and Torque Parameters.

TABLE 3. Link Deflections.

| Link | Unloaded (in) | Loaded (in) | Difference (in) |
|------|---------------|-------------|-----------------|
| I    | 0.0054        | 0.0054      | <0.0001         |
| II   | 0.0134        | 0.0135      | 0.0001          |
| III  | 0.0006        | 0.0007      | 0.0001          |

TABLE 4. Link End Moment Requirement.

| Link         | Unloaded (lb-in) | Loaded (lb-in) | Difference (lb-in) |
|--------------|------------------|----------------|--------------------|
| I            | 285.61           | 287.11         | 1.50               |
| II           | 285.61           | 287.11         | 1.50               |
| III          | 78.60            | 79.35          | 0.75               |
| Mobile Mount | 888.0            | 891.75         | 3.75               |

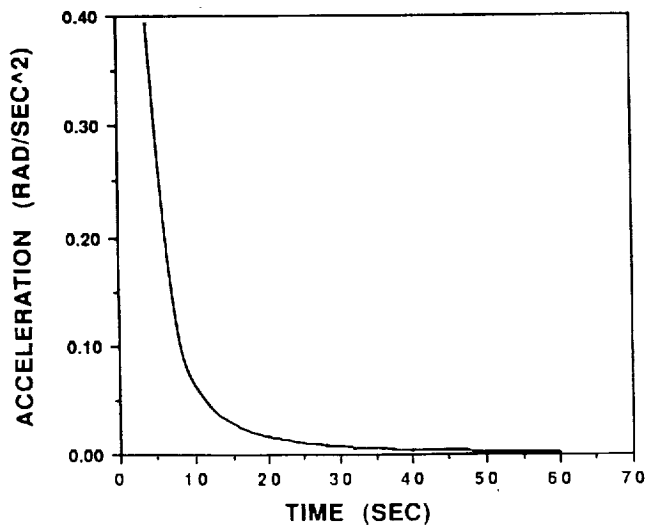


Fig. 5. Acceleration Requirements.

sec, and it is clear that this time-frame is approximately the point where the acceleration begins to rise very rapidly. It is clear that if the angular velocity can be kept at 1/2 rpm or lower, the Lagrangian equation can be solved to a high degree of accuracy while considering only the static or potential energy term alone. The Lagrangian equation shows the difficulty in representing on Earth a manipulator designed for space. On Earth, the dominant acceleration term is gravity. As shown, this is at least four times the magnitude of the angular acceleration term. However, in orbit this gravity term will be zero and angular acceleration will be the controlling parameter regardless of how small it might be.

### JOINTS AND ACTUATORS

To join the manipulator, links together it was necessary to manufacture joints that allow the required degrees of freedom for each link. The joints are fashioned similar to a yoke, as shown in Fig. 2 (#42 and 53) are made of 6061-T6 aluminum. The shaft is connected to the female portion of the yoke by antifriction radial bearings, which also is connected to the male portion of the yoke as shown in Fig. 2. For the rotary motion, a sprocket set is used in conjunction with a DC motor. For the motion

between links I and II a double sprocket pair is used. For the motion between links II and III a single sprocket pair is used. The motors are connected to the links by means of a mount, also shown in Fig. 2.

The torque required for the joint connecting links I and II is 4569.6 oz-in and 1257 oz-in for the joint connecting links II and III. The torques were calculated as for the manipulator links. For links I and II a double sprocket pair with a reduction of 16:1 was used. This resulted in the required torque at the motor to be 285.6 oz-in. A permanent-magnet DC gear head motor with a maximum torque of 400 oz-in was used, giving a safety factor of 1.4 at maximum load. For links II and III a single sprocket pair with a reduction of 6:1 was used. This resulted in the required torque at the motor to be 209.6 oz-in. A permanent-magnet DC gear head motor with a maximum torque of 400 oz-in was also used, resulting in a safety factor of 1.9 at maximum load.

### WRIST AND GRIPPER

The wrist assembly is designed to provide bending and rotational motion for the gripper. Bending motion is provided by the rotation of a 200 oz-in DC gear head motor. As shown in Fig. 2, a shaft connected to the gripper controls its rotational motion. This shaft is supported by two ball bearings positioned in a gripper end-block machined from solid aluminum. The shaft is driven by a 3:1 ratio sprocket pair connected to the motor. A 3.5-in extension piece connects the shaft to the supporting collar. This moves the rotation point closer to the center of gravity so the demands on the motor are reduced. With the extension piece and sprocket pair, there is a safety factor of 4.7 on this motor.

Rotational motion is provided by a DC motor connected directly to the gripper. The output shaft of the motor rotates a 1/4-in shaft that extends through a supporting collar. The supporting collar is a hollow aluminum piece that encases two ball bearings with a 1/4-in inner diameter. This shaft is rigidly attached to the housing for the push/pull motor, which controls the gripper (Fig. 3).

The gripper was adapted from a manipulator that is no longer functional. It is solid aluminum with a series of 1/4-in holes drilled through the solid part of the gripper to reduce weight. The gripper weighs 2.0 lb. A push/pull motor encased in the lower part of the gripper controls the gripper action. Figure 3 shows this assembly.

### TELEMETRY

The telemetry system for the ASPOD is designed to control the robotic arm and to simulate future operation of the system in space. A few telemetry subsystem requirements are:

- A duplex communication link (i.e., a transmitter and a receiver at both remote and local sites)
- A self-contained power source for the system on the remote end
- Real time operation
- Redundancy (for space application)

Taking these factors into account, a Radio Modem and a Photonic telemetry system were chosen for evaluation.

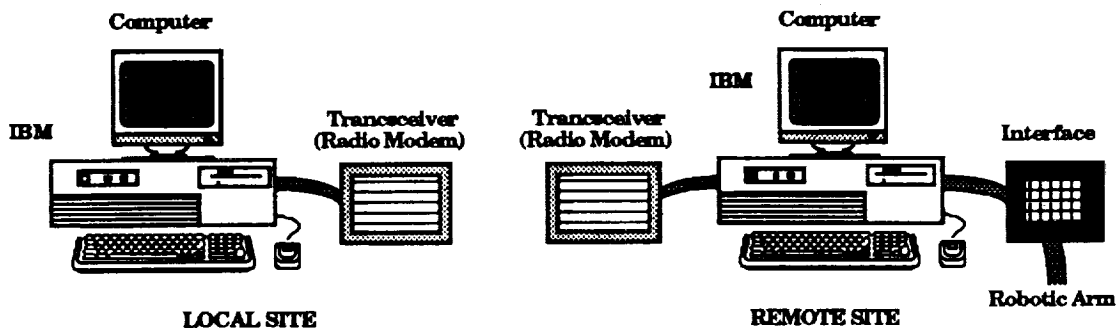


Fig. 6. 1991-1992 Radio Modem Telemetry System.

### Telemetry Systems

The Radio Modem telemetry system (see Fig. 6) is composed of a lap-top IBM PC connected to a transceiver (radio modem) and an interface at the remote site. At the local (user) site an IBM PC is connected to a transceiver. The computers are linked to the modems with an RS-422 serial port.

To simulate the telemetry system to be used in space, a self-contained power source (for the remote site) has been proposed. Wires will connect the computer and modem, the computer and interface, and the power source to the computer and modem. The power source to be used is solar energy.

Likewise, the Photonic telemetry system uses local resources to operate. This system is an optical-pulse-powered sensor system that converts an incoming optical pulse (or a series of pulses) to a voltage by an array of photovoltaic cells. There is no external power source required for the (remote) sensing end. This system improves the performance of the conventional two-wire electronic telemetry system because there are fewer electronic components, and therefore less heat to be dissipated. Additionally, this system isolates the electronic components, which reduces the electromagnetic interference (EMI) between links of the beam.

Both Radio Modem Optical Link telemetry systems have duplex communication links, a self-contained power source (for the remote end), and operate in real time. Redundancy could be applied, but it is only needed for space application. Nevertheless, there are disadvantages to each system. A direct line-of-sight must be maintained for both systems. This requirement is not as strict for the Radio Modem telemetry system as for the Photonic telemetry system. However, once a direct line-of-sight is achieved for the laser, the signals through radio frequency (RF) waves will fade occasionally (throughout the month) due to sunspots.

### ASPOD Telemetry System

The Radio Modem telemetry system will be used for ground application on the ASPOD project. It will still simulate space operation by having a self-contained power source and radio frequency (RF) shield (for each part of the system) to block out radio frequency interference (RFI). However, the Photonic

telemetry system should be incorporated into the future design for space application. The final system will need a radiation shield to minimize RFI.

### Solar Tracker

A solar tracking system was designed to use the Sun's energy to cut orbital debris. For this system to work effectively as well as efficiently, the ASPOD solar cutter must be directly aligned with the Sun (in elevation and azimuth) to obtain a maximum amount of solar energy. This alignment is required to focus energy to a point faster than it can be conducted, convected, reflected, emitted, or radiated away<sup>(1)</sup>. The solar tracking system is composed of two directional systems (one for elevation and the other for azimuth), and a control box. Within each directional system is mounted gear train apparatus, a 90-V DC motor, and a pair of solar photovoltaic cells.

### Solar Photovoltaic Cells

The solar photovoltaic cells are arranged in right-angled configurations. These sensors are mounted on the ASPOD with the bisector of the angle between the cells perpendicular with the focal axis of the solar cutter. Depending on which solar cell is receiving the most solar flux, a voltage difference (positive or negative) will result. However, if the solar flux is of equal intensity on each solar cell, the voltage difference will be zero. This voltage output is sent to the control box which then sends a signal to the servo motor. Note that the two directional systems are independent of each other.

The voltage is related to the direction of the solar tracker in the following manner: If the voltage difference across the solar cells is zero, the solar tracker is in direct alignment with the Sun; if there is a positive or negative voltage difference, then the tracker is leading or lagging the Sun.

### ACKNOWLEDGEMENTS

Summary report prepared by Dr. Kumar Ramohalli and Micky Marine, James Colvin, Richard Crockett, Lee Sword, Jennifer Putz, Sheri Woelfle. The support from USRA and technical

monitoring of Mr. James D. Burke of JPL are gratefully acknowledged. We also would like to thank Mr. Milton Schick who contributed toward the new robotic arm.

#### REFERENCES

1. Beard, Jonathon. *Sweeping Up Space Junk*, Discovery, December 1988, p.22.
2. Lechleitner, Hans. *Raumpfleger Dringend Gesucht*, March 1989, p154. Geo in German
3. Beard, Jonathon. *Verdens Forste Flyvende Skraldemand*, Danish Science, December 1988, p46.
4. Stewart, Doug. *Eyes in Orbit Keep Tabs on the World in Unexpected Ways*, Smithsonian, December 1988, p70.
5. Erickson, Jim. *Engineer Plans to Clean the Heavens*, Arizona Daily Star, February 21, 1987.
6. Stiles, Edward. *Space Junk*, Tucson Citizen, February 27, 1987.
7. Hodge, Carl. *'Sweeper' Would Gather Space Debris*, Arizona Republic, August 14, 1988.
8. Stiles, Edward. *U of A Robot Will Collect Space Junk*, Tucson Citizen, September 23, 1988.
9. Turner, Mark Holman. *Trashed in Space*, American Way, May 15, 1989.
10. *General Accounting Office Report*, April 1989.
11. Ramohalli, Kumar, et al. *Autonomous Space Processor For Orbital Debris*, USRA Summer Conference, June 12, 1989.



1990/91 PROJECT SUMMARIES

UNIVERSITY OF CALIFORNIA, LOS ANGELES

S/3-12  
160589  
P-4

This document summarizes four projects carried out in 1990/91 at the University of California, Los Angeles, under NASA/USRA sponsorship. One of the projects described is a mission design, the three others include the design and construction of space-related hardware and testing.

**MANNED VOYAGE TO MARS WITH PERIODIC REFUELING FROM ELECTRICALLY PROPELLED TANKERS**

Twenty-four UCLA students, in groups of four, participated in a mission design for a manned expedition to Mars based on the concept of midcourse refueling from electrically propelled tankers launched ahead of the manned mission. The study was conducted during the 1991 spring term.

Some of the student groups opted for non-nuclear propulsion of the manned ship, based on LOX and LH<sub>2</sub>; others opted for one based on nuclear-thermal propulsion. The first option is illustrated below.

Electric thrusters, such as the already well-developed ion engines of the electron bombardment type, can have a very large specific impulse, but, for realistic levels of electric power, they have low thrust resulting in very long travel times. In this mission analysis, it is proposed to combine their advantage (high I<sub>sp</sub>) with the advantage of chemical propulsion (high thrust) by midcourse refueling of the chemically propelled, manned ship from electrically propelled, unmanned tankers.

The tankers, which would be orbiting for periods of from three to eight years, would be launched a corresponding number of years before the launch of the manned ship. In addition to their own propellant (e.g., liquid argon), the tankers would carry a much larger quantity of LOX and LH<sub>2</sub> for transfer to the manned ship. In the present proposal, the tankers' electric power would be provided by a 2- to 5-MW<sub>e</sub> nuclear reactor with, for instance, a potassium Rankine-cycle power converter. Boiloff of the cryogenic propellants would be recondensed by sorbent pumps using the reactor's waste heat.

Refueling the manned ship *n* times is equivalent to an (*n* + 1)-fold increase in I<sub>sp</sub>. Because of the very high I<sub>sp</sub> of the tankers, the total mass that must be assembled in LEO is greatly reduced.

A second feature that may or may not be applied to such a mission is to produce all the LOX, even that for the initial fueling, either from lunar soil or, alternatively, from the martian atmosphere. In the latter case, the tankers would start from LEO with only hydrogen, land on Mars, autonomously manufacture the LOX, ascend to a low altitude orbit about Mars by expending a relatively minor amount of LOX and LH<sub>2</sub>, and return to LEO (or to orbital matching for a midcourse rendezvous with the manned ship). The advantage of this scenario is that the difference in total energy (gravitational plus kinetic) per unit mass is  $3.3 \times 10^7 \text{ m}^2/\text{s}^2$  for ascending from the ground to LEO (assumed here and in what follows as the Space Station *Freedom* altitude) vs. only  $6.6 \times 10^6 \text{ m}^2/\text{s}^2$  for the ascent from

the Martian surface to a low Mars orbit (assumed as 200 km altitude). Because of the high I<sub>sp</sub> of the tankers, the transport from Mars vicinity to Earth vicinity is sufficiently efficient in propellant usage to reduce by a major factor the total mass that must be brought up to LEO.

Ordinarily, low thrust, electrically propelled spacecraft are intended to apply thrust parallel to the instantaneous flight path. This results in a spiral path, nearly circular at all times, about the astronomical body. However, such a path will not allow rendezvous with a manned ship that is on an efficient, short-travel-time trajectory. In this case, it is advantageous to put the entire burden for the needed matching of position and velocity on the tankers. This can only be accomplished by applying thrust at an angle to the tankers' flight path (except at the periapsis where the angle is zero). For the trajectories of interest, it can be shown that, as a consequence of thrusting obliquely to the flight path, roughly half of the ΔV is lost.

Figure 1 illustrates a mission that provides for 58 days stay-over on Mars, with a 204-day round-trip time. As indicated in Fig. 1, the manned ship trajectory is at first depressed below the Earth's orbit, thereby gaining enough speed to compensate for the lower mean angular velocity of Mars. The velocities indicated are those pertaining to the heliocentric, nonrotating reference frame.

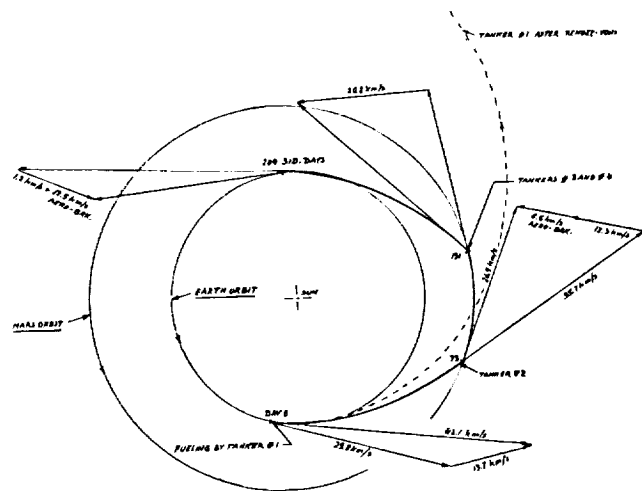


Fig. 1. 200-day mission to Mars, with refueling from electrically propelled tankers

112  
UNIVERSITY OF CALIFORNIA, LOS ANGELES

Five tankers are required (four, if LOX is transported from the ground to LEO). The first load of propellant is sufficient for Earth escape on a hyperbolic trajectory. The next fueling takes place in close proximity to Earth.

A mass of 35,000 kg for the Command/Service Module of the manned ship is assumed (the Mars Lander and equipment left on Mars are assumed to be already in low Mars orbit, transported there by one of the cargo ships). Propulsion of the manned ship is assumed to be by LOX/LH<sub>2</sub> with a vacuum I<sub>sp</sub> of 480 s (based on a mixture ratio of 7.0 and a large extended exit cone). Aerobraking into the Mars atmosphere with ΔV = 8.5 km/s, and into the Earth's atmosphere upon return with ΔV = 12.5 km/s has been assumed. The ΔV requirements for the several flight events and masses for the manned ship ascent to Mars are listed in the Table 1. (Similar values also apply to the return trip.)

For the tankers, an I<sub>sp</sub> of 16,000 s and an electric-to-ion energy efficiency of 0.80 is assumed. These parameters are achievable with current technology. The nuclear reactor power plant, including power conversion, radiator, and the minimal shielding required for an unmanned vehicle, is sized at 4.2 MW<sub>e</sub>. A mass-to-power ratio of 8 kg/kW is assumed. Typical operating times are three to eight years, depending on the rendezvous location and velocity. This results in a combined powerplant and ion thruster propellant mass of 68,000 kg, or about 20% of the total tanker mass (including both LH<sub>2</sub> and LOX). The thrust is 40 N.

In LEO, the mass of each tanker (with LH<sub>2</sub>, but without LOX, which is assumed in this study to be autonomously manufactured on the Moon or on Mars) is given in Table 2. The total mass in LEO per mission is 600 metric tons for five tankers and the Command/Service Module.

Table 1. ΔV Requirements.

| ΔV<br>km/s | LOX/LH <sub>2</sub> Mass,<br>metric tons |       | Total Mass,<br>metric tons |       | Event                                  |
|------------|--|-------|----------------------------|-------|--|
|            | initial                                  | final | initial                    | final |  |
| 3.5        | 247                                      | 99    | 282                        | 134   | Earth escape at parabolic speed        |
| 6.3        | 99                                       | 0     | 134                        | 35    | tanks are emptied                      |
| 0          | 0  | 247   | 35                         | 282   | refueling                              |
| 7.4        | 247                                      | 24    | 28                         | 259   | Earth escape at 13.7 km/s (solar ref.) |
| 2.5        | 24                                       | 0     | 59                         | 35    | tanks are emptied                      |
| 0          | 0  | 247   | 35                         | 282   | refueling                              |
| 9.8        | 247                                      | 0     | 282                        | 35    | retro thrust at Mars                   |

Table 2. Tanker Masss.

| Component               | Mass, metric tons |
|-------------------------|-------------------|
| LH <sub>2</sub>         | 27                |
| Ion thruster propellant | 34                |
| Powerplant              | 34                |
| Structure, etc          | 18                |
|                         | total 113         |

A drawback of midcourse refueling by electrically propelled tankers is the narrow launch window for the manned ship. So as not to miss the rendezvous in case of launch delay, the tankers must be provided with some chemical propulsion capability, comparable to the shuttle OMS engines. Thus, to provide for a launch window of six days, an additional ΔV capability of about 5% would be needed.

Mission safety can be increased by providing for more than the minimum number of tankers, with the goal of making possible a safe abort during any part of the mission, even though one particular refueling may have been missed. For subsequent missions, it may be possible to use tankers that served as backup in earlier ones. For example, the zero-thrust orbit of the tanker intended for the first refueling is shown in Fig. 1 (dashed line). Its orbital period about the Sun is 2.7 years.

A considerably lower LEO mass than the 600 metric tons estimated could be achieved if the stay-over time on Mars is reduced to, say, 15 days.

### GROUND SPEED OF BALLOONS ON MARS

In an international mission to be launched to Mars in 1996, Soviet-built balloons in the planet's atmosphere will carry scientific instruments in a gondola and also in a drag rope (the Snake). During the martian night, when the balloons are cold and descend, the Snake will be in contact with the ground. Instruments, such as a gamma ray spectrometer and an instrument to measure ground speed, have been proposed for incorporation into the snake.

In cooperation with the NASA Jet Propulsion Laboratory and the Planetary Society in Pasadena, California, a student-designed prototype instrument and drag rope have been built. The instrument is intended to measure the approximate speed with which the rope slides over the terrain. When traveling at several meters per second over rough, rocky, and sandy surfaces, the rope will be bouncing and flexing with high accelerations. In addition to withstanding the harsh martian environment, the rope must not snag between rocks or other formations; thus, no instrumentation can be allowed to protrude from the rope's smooth surface.

The device designed and built by students at UCLA is similar in concept to one designed by students at the University of Utah, who are also participants in the USRA Advanced Design Program.

The principle of operation is illustrated in Fig. 2. Inside the guide rope are two pairs of accelerometers, separated by a distance along the guide rope of approximately 2 m. In each pair, the accelerometers are oriented orthogonally to each other and orthogonal to the length of the guide rope. When sliding over and around rocks, there will be a time lag in the voltage outputs from the rear accelerometers with the corresponding outputs from the accelerometers in front. The speed of the guide rope over the ground can then be inferred from forming the convolution integral of the accelerations

$$C(t, \lambda) = \int_{\tau=t-T}^t a_1(\tau a_2(\tau - \lambda)) d\tau$$

where  $a_1$  is the voltage from one of the rear accelerometers,  $a_2$  the voltage from the corresponding front accelerometer,  $\lambda$  the (unknown) lag time, and  $T$  the "window time" (the time interval for which the data are kept in memory by the computer). The best approximation to the true time lag is found by computing the centroid, or weighted mean, of  $C(t, \lambda)$  as a function of the time  $t$ . The speed of the guide rope is found by dividing the known accelerometer distance by the time lag.

To check the theory of operation of the instrument, the students developed computer programs that calculated the best value for the guide rope speed for assumed ground profiles. These included one or two "rocks," represented as Gaussians, with a superimposed ground roughness, represented by a pseudorandom function.

At the time of writing, field tests with the student designed device are in progress on the UCLA campus (Fig. 3).

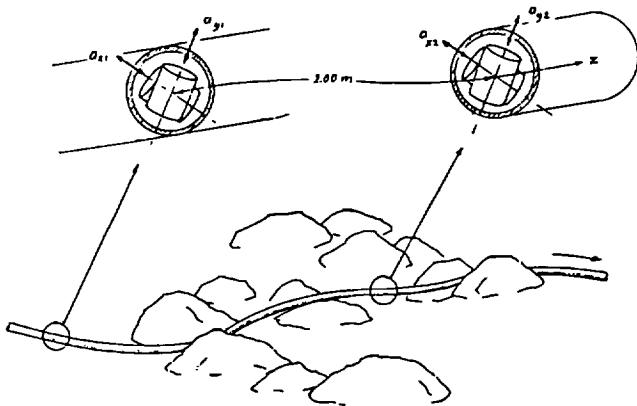


Fig. 2. Drag rope speed measurement by accelerometers



Fig. 3. Field test of "Snake."

### TRIPOD LUNAR LANDING STRUCTURE

In this project, the students were given the task of designing, building, and testing a simple tripod truss of their own design, which was to simulate on a small scale a lunar landing structure.

The specifications were as follows. The tripod had to support a vertical load (the space vehicle) at three strong-points forming a horizontal equilateral triangle with 15-in sides. At its base, there were to be again three strong-points (the landing pads) forming a horizontal equilateral triangle with 36.6-in sides. The height of the tripod was prescribed as 18 in.

The students were encouraged to invent their own truss structure that would connect the top three strong-points to the lower three. They were given the choice of two sizes of low-cost, seamless tubing (1020 carbon steel, 30,000 psi yield strength, 48,000 psi ultimate strength, Young's modulus 29,100,000 psi). One size of tubing had a diameter of 1/2 in, with 0.035-in wall thickness; the other had a 3/4-in diameter with the same wall thickness. The total weight of the structure could not exceed 7.50 lb.

A great variety of structures, one of them shown in Fig. 4, were proposed by the students. They were then asked to make all necessary calculations to predict the maximum load at yield that would be sustained by their design. After completion of the designs and calculations, the students cut and fitted the steel tubing. (Welding was done by a professional welder.) Each structure was tested on a simple testing machine made from an existing hydraulic press and a carefully calibrated load cell.

The entries were judged on two points: (1) the ratio of the maximum sustained load (at yield) to weight; and (2) the percentage of the difference between the maximum load as calculated by the student and the actual one measured on the testing machine.

The structural failures encountered by the students' designs were of several different types: They included Euler buckling, thin wall local buckling, exceedance of the yield strength in a tension member, and overall structural instability (violation of the rules governing the rigidity of a truss). The largest load sustained by any of the structures was 4360 lb.

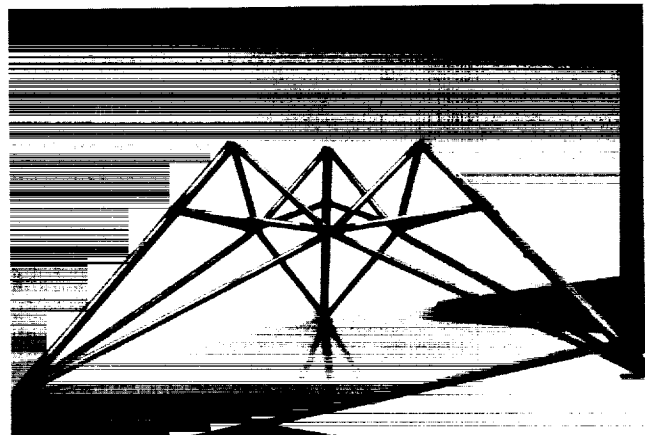


Fig. 4. One of the tripod landing structures designed, built, and tested by the students.

### GRAPPLING/DOCKING DEVICE ACCOMMODATING LARGE LATERAL AND ANGULAR MISALIGNMENTS

In space operations, the mating of two space vehicles is a necessary and ever more frequent maneuver. Docking mechanisms and procedures in use today work well and are usually reliable, but allow for only quite narrow margins of angular and lateral displacements. They require intensive active control, usually by a human operator.

Several methods of joining spacecraft in flight have been developed in the past. The first method employed by the U.S. space program was the relatively simple method typified by the Apollo missions. Although reliable, it required very close control and sometimes necessitated repeated attempts before a successful docking was accomplished. The second method, still in use today in the shuttle orbiter fleet, uses an articulated arm that places the female section of the capture system over the male section. The female section then locks onto the male section, completing the capture and allowing the arm to maneuver the grappled vehicle into the desired position. This method, which has proven to be very successful, is well suited for the capture of an inactive payload module by a manned vehicle that supplies the necessary control signals.

A different approach was used in the (now canceled) Orbital Maneuvering Vehicle (OMV) program, with the OMV to be guided and docked by remote control. This approach was inherently problematic because of the large speed-of-light delay between initiated control action and verification by the controller of the actual event.

In one of the USRA-sponsored design classes at the UCLA, the students developed several ideas for a new docking mechanism that would allow a large lateral misalignment (of the order of one half of the radius of the grappling space vehicle) and an angular misalignment of at least  $20^\circ$ .

The first of these designs involved a deployable capture cone on one of the vehicles, and a long flexible probe on the other, an approach resembling the one used in aircraft refueling.

The second design investigated consisted of a circular capture plate (the end plate of the vehicle) with a hooked lip around its edge and a collapsible tripod on the other vehicle. In the docking maneuver, the legs of the tripod are collapsed together as one or several of them strike the capture plate. The force of the impact forces the legs apart where they lock into place under the lip. The dynamics of this mechanism, however, proved to be very difficult to analyze in any detail and was beyond the scope of this class.

By comparison, the analysis of the dynamics of the cone-probe docking system proved to be relatively simple. The problem was modeled as a bending spring, telescoping outward from the probe-carrying vehicle and telescoping back into it as the docking progresses. From the spring and damping characteristics, the forces on the two vehicles were calculated as functions of the relative angular and lateral displacements and the relative velocities of the two vehicles. To simplify this first analysis, the heavier of the two vehicles was treated as fixed, while the lighter vehicle was free to translate and rotate, depending on its mass and moments of inertia.

The students then designed models of the two spacecraft to demonstrate the cone-probe docking mechanism. Capture in these models is accomplished autonomously by the activation of solenoids that grip the probe and an electric motor that retracts the probe to bring the two vehicles together in the final phase of the docking.

This design is presently being constructed by the School of Engineering machine shop and is expected to be an exhibit at the 1992 USRA Summer Conference.

# DESIGN, BUILDING, AND TESTING OF THE POSTLANDING SYSTEMS FOR THE ASSURED CREW RETURN VEHICLE

UNIVERSITY OF CENTRAL FLORIDA

5/4-16  
160590  
P-5

The design, building, and testing of the postlanding support systems for a water-landing Assured Crew Return Vehicle (ACRV) are presented. One ACRV will be permanently docked to Space Station *Freedom*, fulfilling NASA's commitment to Assured Crew Return Capability in the event of an accident or illness. The configuration of the ACRV is based on an Apollo Command Module (ACM) derivative. The 1990-1991 effort concentrated on the design, building, and testing of a one-fifth scale model of the egress and stabilization systems. The objective was to determine the feasibility of (1) stabilizing the ACM out of the range of motions that cause seasickness and (2) the safe and rapid removal of a sick or injured crewmember from the ACRV. The development of the ACRV postlanding systems model was performed at the University of Central Florida with guidance from the Kennedy Space Center ACRV program managers. Emphasis was placed on four major areas. First was design and construction of a one-fifth scale model of the ACM derivative to accommodate the egress and stabilization systems for testing. Second was the identification of a water test facility suitable for testing the model in all possible configurations. Third was the construction of the rapid egress mechanism designed in the previous academic year for incorporation into the ACRV model. The fourth area was construction and motion response testing of the attitude ring and underwater parachute systems.

## INTRODUCTION

For years, America's journey into space has demonstrated the benefits associated with working in the unique environment of microgravity. Continuing in this tradition, an ambitious and far reaching program to further the advancement of space technology has been launched. With Space Station *Freedom*, the United States enters an era marked by a permanent presence in space. The space station allows continuous rather than intermittent operations to be conducted in orbit. The space station opens doors to many new methods of research and experimentation. Included are better opportunities to observe the Earth and forecast future trends from a vantage point only partially exploited by previous shuttle missions.

Space Station *Freedom* is planned to have a permanent crew of four. The crew will be rotated and resupplied by flights of the Orbiter on an interval currently planned for three months. Because of isolation and potentially hazardous conditions involved in space operations, NASA is committed to the policy of Assured Crew Return Capability for space station crews in the event (1) a medical emergency occurs and an ill, injured, or deconditioned crewmember must be rapidly transported from the space station to a definitive health care facility on Earth; (2) a space station catastrophe forces a rapid evacuation of the crew from the station; and/or (3) the National Space Transportation System becomes unavailable, and an orderly evacuation of the crew from the space station becomes necessary.

These events, or Design Reference Missions (DRMs), can be met by a concept known as the Assured Crew Return Vehicle (ACRV). Currently, NASA is considering three classes of ACRVs: water landers, runway landers, and open land, or nonrunway landers.

The task objectives detailed in this report were developed in conjunction with Kennedy Space Center ACRV project managers and are limited to what is required for a water landing ACRV and postlanding operations. The configuration of the ACRV

is based on an Apollo Command Module (ACM) derivative. The designs presented are associated with the development of one-fifth scale models of the ACRV egress and stabilization systems developed at the University of Central Florida during the 1989-1990 academic year.

## UCF ACRV DESIGNS DEVELOPED PREVIOUSLY (1989-1990)

Returning an ill, injured, or deconditioned crewmember back to Earth aboard a water landing ACRV requires new technologies and operational procedures. The possibility of further injury or illness may compromise the mission. Following are general design considerations and solutions investigated by the senior-level Mechanical and Aerospace Engineering Design classes during the 1989-1990 academic year. The design considerations were from the point immediately after splashdown to rescue by recovery forces.

The first consideration was providing crew egress and rescue personnel support subsystems to ensure the safe and rapid removal of an ill or injured crewmember from the ACRV by recovery forces. A Special Purpose Emergency Egress Couch was designed to medically support a sick or injured crewmember during the ACRV mission. This couch provides a self-contained environment and space for necessary medical equipment. To aid in the movement of the couch from the ACRV floor to the hatch location, a Four Link Injured Personnel Egress Mechanism (FLIPEM) was developed. Support to the rescue personnel is provided by the placement and design of properly located hand-holds, supports, and platforms.

The second consideration was the proper orientation, attitude control, and stabilization systems required for the ACRV in the marine environment. Experience gained from previous Apollo water landings showed that some sea and weather conditions cause severe discomfort to the crew. In the case of an injured crewman this may cause further aggravation of an existing injury,

or even death. Postlanding orientation of the ACRV is achieved through the use of three, 6.2-ft diameter, CO<sub>2</sub>-charged balloons similar to those used during the Apollo program. Attitude control systems were designed that automatically deploy three multichambered ring segments. One segment resides under the hatch and has a 6 × 6 × 3-ft appurtenance to act as a stable platform for the rescue personnel. Multiple underwater parachute assemblies were designed to provide motion reduction through the principles of inertia and viscous drag associated with moving large volumes of water.

The third consideration dealt with providing full medical support to an ill, injured, or deconditioned crewmember aboard the ACRV from the time of separation from the space station to rescue by recovery forces. While living and working on the space station, the astronauts will be involved in extravehicular activities and other demanding jobs. It is likely that an injury may occur that requires emergency medical care available only at a hospital on Earth. Partial medical support, medical support equipment and monitors, and oxygen administration and control systems were addressed. Partial medical support is accomplished by employing the Thomas Transport Pack currently used aboard the shuttle. Extensive research was performed to select suitable medical support equipment and monitors as required by NASA. Each piece of equipment was integrated into unified packages and power requirements were addressed. Oxygen is supplied to a deconditioned crewmember, seated at a regular flight couch, by a nasal cannula and excess oxygen filtered out by an air-dump system. The medical couch is supplied by an independent O<sub>2</sub> system for a period of six hours after egress.

The rescue team may not arrive at the craft for an extended period of time. Consequently, the fourth consideration was to provide for the comfort and safety of the entire crew from splashdown to the time of rescue. Addressed were design solutions for food, water, waste management, atmosphere, contaminant/odor control, and environmental control systems. Food systems chosen rely on space shuttle contingency bars for proven application and low volume and weight. Water supply systems use plastic squeeze bottles. The waste management system is a derivative of the Apollo-style waste bag system. Modifications are necessary to qualify for use by men and women. The standard sea-level atmosphere inside the ACRV is generated by a system using two 3000-psi tanks of O<sub>2</sub> and N<sub>2</sub>. The contaminant and odor control design uses lithium hydroxide and charcoal filter systems used extensively in the space program. An ammonia boiler environmental control system was designed to supplement the existing system after the craft descends through 100,000 ft to the time of rescue.

#### 1990-1991 UCF ACRV DESIGN TASKS

During the 1989-1990 year, the Engineering Design classes examined solutions in support of postlanding operations for the ACRV. The 1989 fall semester class selected designs in the areas of (1) crew egress and rescue personnel support, (2) orientation, attitude control, and stabilization, (3) medical support systems, and (4) crew survival systems. The 1990 spring semester class, with new students, was responsible for providing greater detail to the designs selected in the fall semester. The design requirement was increased in the 1990-1991 academic

year from one semester to two semesters. The students participating in the conceptual design during the fall semester now continue with building and testing in the spring semester. The task objectives for the 1990-1991 Engineering Design class were to determine the feasibility of the previously developed egress and stabilization systems for deployment on the ACRV. Working models of these systems were designed, built, and tested. The scale selected for the development of these systems was one-fifth. Four design teams were formed and tasked as follows:

#### Design Team #1—ACRV Model Construction

The responsibility of the ACRV Model Construction team was to design, build, and test a one-fifth scale model based on the Apollo Command Module (ACM) such that the egress and stabilization systems can be incorporated and tested. The model was required to accurately simulate the geometric and dynamic characteristics of the ACM derivative for testing purposes.

#### Design Team #2—Water Test Facility Identification

The Water Test Facility team was responsible for identifying a test facility where stabilization tests on the ACRV model can be performed. This included researching existing facilities as well as establishing designs for a permanent facility at the University of Central Florida. As a result of the investigation an existing facility was selected for testing and the building and testing phases of a permanent facility were not pursued.

#### Design Team #3—Rapid Egress Systems

The objective of the Rapid Egress System team was to design, build, and test the Four Link Injured Personnel Egress Mechanism (FLIPEM) optimized during the previous year. The FLIPEM consists of three parts: the lift mechanism, the extension support mechanism, and the restraint mechanism. The lift mechanism must translate the couch platform from the ACRV floor to the hatch location. The extension support mechanism provides the means to move the couch platform a specified horizontal distance out of the hatch for recovery. The restraint mechanisms are required to ensure the FLIPEM remains in the stowed position prior to deployment, and to prevent movement of the couch on the platform during FLIPEM operation.

#### Design Team #4—Stabilization Control Systems

The objective of the Stabilization Control Systems team was to determine, through modeling, the feasibility of reducing heave, surge, and pitch motions of the ACRV model on water using an underwater parachute system. The underwater parachute system should stabilize the ACRV out of the range of motion that causes seasickness to prevent further injury or illness. This range is approximately 0.2-0.5 Hz. Associated with the underwater parachute system are the attitude ring and mattress. The attitude ring is a buoyancy control device attached to the

ACRV to aid in flotation and stabilization. The attitude ring mattress is located under the hatch and acts as a stable platform for recovery operations.

### 1990-1991 UCF ACRV DESIGN, BUILDING, AND TESTING RESULTS

#### ACRV Model Construction

The ACRV Model Construction team designed, built, and tested a one-fifth-scale model based on the ACM derivative. Data for the weight and geometric dimensions of the ACM derivative were supplied by Rockwell International. Three design considerations were incorporated in the construction of the model. These were (1) shell construction, (2) center of gravity and mass moment of inertia of the system, and (3) hardpoint accommodations.

The shell for the ACRV model was constructed in two parts. The first part consisted of developing two molds that represent the upper and lower halves of the model. Technical support during this phase of the construction was supplied by Guard-Lee, Inc. located in Apoka, Florida. The molds were constructed using wood frames with PVC foam inserted to form the outline of the two halves. Resin and bondo material were then applied to arrive at the smooth shape required for shell lay-up. The second part of the construction process was the shell lay-up. The lay-up of the fiber-glass composite shells was contracted out to Guard-Lee, Inc. The upper and lower halves of the model were attached using a four-bolt/T-nut system with a weather stripping material for the sealing gasket.

The center of gravity and mass moment of inertia were modeled using a system of flat circular plates located in the model. The size and weight of the plates required were determined from pendulum tests performed on the empty shell, from which the mass moment and c.g. location could be found. As a result, three 19-in diameter steel ring plates were affixed to the bottom of the model floor, two 5.25-in steel plates were affixed to the inside top, and three to the inside bottom of the model. The c.g. was varied by attaching the large ring plates to slots cut in the floor. Also incorporated in the model was a point mass system to duplicate the motion of the egress mechanism. This system will allow for measuring the pitch angles caused by the operation of the egress mechanism.

To incorporate the egress and stabilization systems, the model was designed and built with the necessary hardpoints and attachments. A series of eye hooks were positioned around the periphery of the model just above the breakline, which were used for attachment of the stabilization systems during testing. To distribute the load caused by the stabilization systems, hardpoints were installed at the eye hook locations. The hardpoints consisted of 4 × 4 × 4-in blocks of wood located on the interior of the model into which the eye hooks were drilled. The wood blocks were reinforced by a fiberglass encasement. The hardpoints for the egress mechanism required only holes drilled into the floor of the model.

A test plan was developed to verify the fidelity of the ACRV model as an operational testbed. The test included size and weight verifications, seal integrity, inspection of hardpoint ac-

commodations for the egress and stabilization systems, c.g. variability, and mass moment verification.

Test results indicate small deviations from the size and weight specifications provided by Rockwell International. Hardpoint accommodations and seal integrity were maintained throughout the approximately 30 hr of water testing on the egress and stabilization systems.

#### Water Test Facility Identification

The Water Test Facility Identification team researched test facilities where stabilization tests on the ACRV model could be performed. This research included examining existing facilities and developing designs for a permanent facility at the University of Central Florida.

As a result of this investigation, stabilization testing with the ACRV model was performed at the O.H. Hinsdale Wave Research Laboratory (WRL) at Oregon State University in Corvallis, Oregon. O.H. Hinsdale WRL satisfied a majority of the requirements needed for testing. The facility was available during the planned testing period from April 1-5. The dimensions of the wave pool (342 × 12 × 15 ft) supported testing of the ACRV model in all configurations. Regular and irregular waves of periods from 1.0 to 10.0 s and wave heights up to 5.0 ft could be generated. A moveable carriage equipped with a platform and a 5.0-ton hoist moved the model into and out of the water. Visual records were made using two underwater video cameras and a video camera located in the elevated control room. Instrumentation such as accelerometers was connected to a computerized data acquisition system. The full-time staff of ocean engineers provided excellent technical support throughout the testing period. Financial support for travel, lodging, and facility fees was provided by a grant from Rockwell International.

#### Rapid Egress Systems

The Rapid Egress Systems team designed, built, and tested a one-fifth-scale working model of the Four Link Injured Personnel Egress Mechanism (FLIPEM) optimized in the previous academic year. FLIPEM consists of three parts: the lift mechanism, the extension support mechanism, and the restraint mechanism.

The lift mechanism employs two compressed air cylinders each capable of lifting the entire system. When activated by radio control the cylinders located beneath the couch platform extend the FLIPEM the required horizontal and vertical distance from the model floor to the hatch location. Built-in ratchets ensure one way motion and can be released to allow for manual retraction. The Two-Slider Support Mechanism (TSSM) provides the extension support of the couch platform through the hatch to a distance away from the model. The sliders, similar to those used on a tool box, are extended by a means of a reversible electric motor and a cable-pulley system. The restraint mechanism employs a spring-loaded hook, activated by radio control, to maintain the FLIPEM in the stowed position, and a series of locking pins to prevent movement of the couch platform during FLIPEM operation. The FLIPEM is shown in Fig. 1.

Operational and visual testing were performed at UCF. Testing was conducted in the areas of lifting force with nominal and off-nominal loads, vertical and horizontal travel distances,

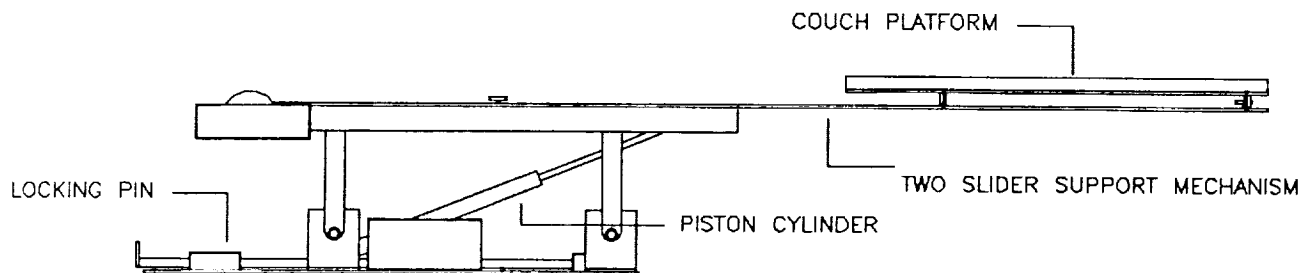


Fig. 1. Four Link Injured Personnel Egress Mechanism.

redundancy characteristics of the FLIPEM and extension force, travel distance, and redundancy characteristics of the TSSM. Test results indicate the design specifications for both systems were met or exceeded and without interference to other systems.

#### Stabilization Control Systems

The Stabilization Control Systems team designed, built, and tested one-fifth scale models of the attitude ring and underwater parachute stabilization system optimized during the previous year. The attitude ring proposed for the actual ACRV is composed of six inflatable spheres. The inflatable spheres were modeled using 8-in-diameter tether balls. The tether balls are connected to eye hooks located around the periphery of the model. The underwater parachutes, with diameters from 1 to 2.5 ft were constructed using nylon fabric and string. The parachutes were attached to eye hooks located on the model with stiff and elastic cables of 3-ft length. Fishing weights were attached to the parachute assemblies to aid in deflation of the chutes on the downstroke. Devices were designed and built to be attached to the parachute openings to decrease the amount of distance required to inflate the chutes on the upstroke. Three mechanical accelerometers were attached to the model floor to measure heave, surge, and pitch.

Wave testing in simulated sea states 2 to 4 at the O.H. Hinsdale WRL yielded results that indicate that the six-attitude sphere configuration produced minimal stabilizing effects on the ACRV model. The spheres did have the effect of enhancing the flotation characteristics of the model.

Pretesting at UCF on the inflation distances of the parachutes showed that the 1-ft-diameter chutes would open almost immediately and the 1.5-ft diameter chutes required nearly 3 ft of stroke to open. The larger diameter parachutes would not open in the 6-ft stroke tested. As a result of this inflation testing only the 1- and 1.5-ft-diameter parachutes were tested in the simulated sea states at O.H. Hinsdale WRL. Numerous parachute arrangements, including single and multiple chutes per cable, increasing the weight attached, using stiff and elastic cables, and devices to partially and totally open the chutes, were tested. Results indicate that the parachutes did affect the motions induced on the model, but did not reduce or increase the frequencies out of the range that causes seasickness.

#### SUMMARY

The 1990-1991 senior-level Mechanical and Aerospace Engineering Design class completed the one-fifth-scale design, building, and testing of the postlanding egress and stabilization systems for an Apollo Command Module-based ACRV. The objective was to determine the feasibility of (1) stabilizing the ACRV out of the range of motions that cause seasickness and (2) the safe and rapid removal of a sick or injured crewmember from the ACRV. Work was conducted in the following areas: ACRV model construction, water test facility identification, and stabilization control systems.

A one-fifth-scale working model of an Apollo Command Module (ACM) derivative that accommodates the egress and stabilization systems was designed and built by the ACRV Model Construction team. The fidelity of the model was established from geometric and dynamic characteristic tests performed on the model. Results indicate small deviations from the specifications provided by Rockwell International.

Stabilization tests on the ACRV model were conducted at the O.H. Hinsdale Wave Research Laboratory (WRL) at Oregon State University as recommended by the Water Test Facility Identification team. The testing period was April 1-5, 1991. The facility accommodated all testing configurations and the staff provided excellent technical support.

The Rapid Egress Systems team designed, built, and tested one-fifth-scale working models of the Four Link Injured Personnel Egress Mechanism (FLIPEM) and the Three Slider Support Mechanism (TSSM). Operational and visualization tests confirmed that the lifting force, travel distances, and redundant characteristics of both systems met or exceeded the design specifications for their operation.

The ACRV attitude ring and stabilization system models were designed, built, and tested by the Stabilization Control Systems team. The responses of the attitude ring/model and the parachute/model combinations when compared to the baseline dynamic response of the model itself show they had no effect on reducing the oscillations of the model in the simulated sea states 2, 3, and 4.

A concept employing Rocker Stoppers was built and tested at the water test facility to determine the effect a rigid system would have on reducing the oscillations. Two Rocker Stoppers

were connected, nose-to-nose, at one end of a long threaded rod. The other end of the rod was connected to a metal plate attached to the model above the breakline. Four of these arrangements were connected to the model. Since the Rocker Stoppers (Fig. 2) are made of rigid plastic, they perform the same work on the upstroke as on the downstroke. This configuration was tested in a simulated sea state 4 (1.2 ft amplitude, 0.45 Hz) and the response compared with that from the clean model in the same sea state. The results indicate that a rigid system in this configuration does reduce the oscillations the model experiences. The frequency of the pitch motion dropped from 0.45 Hz to 0.40 Hz with the Rocker Stoppers attached. This reduction is below the simulated range (0.45-1.1 Hz) associated with seasickness.

Several recommendations are suggested for future design projects in the area of postlanding operations associated with the ACRV. Integrated wave testing involving the egress system and the attitude ring spheres and mattress needs to be examined.

Another project would entail building and testing a full-scale egress system based on the FLIPEM design. Examining the flotation and wave motion characteristics of other ACRV configurations, such as the SCRAM and HL-20, and comparing them to a mathematical model is suggested. Finally, testing rigid stabilization systems using the Rocker Stopper concept for motion reduction shows potential for developing a damping system capable of moving the ACRV motion out of the range of frequencies associated with seasickness.

#### ACKNOWLEDGMENTS

The authors of this design synopsis are Kenneth C. Hosterman, Graduate Teaching Assistant, and Loren A. Anderson. Appreciation is expressed to the senior design students in Aerospace and Mechanical Engineering who contributed to this work. A special note of appreciation is due to NASA, USRA, and Rockwell International whose sponsorship made this work possible.

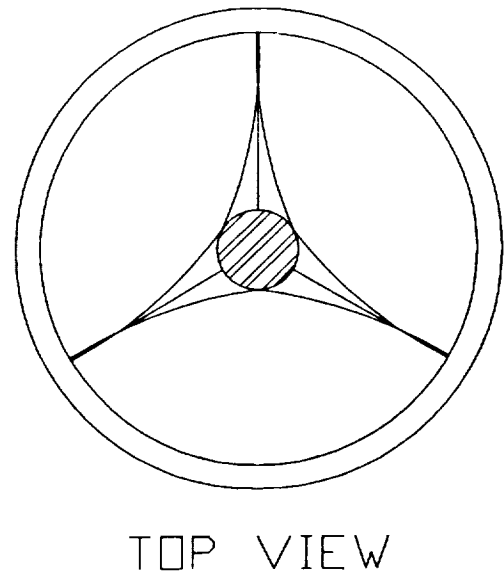
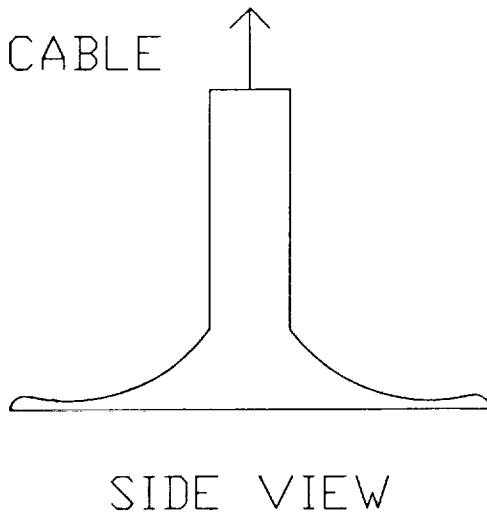


Fig. 2. Rocker Stopper Option.



## EARTH TO LUNAR CELSS EVOLUTION

UNIVERSITY OF COLORADO

S15-54

160591

p. 10

## INTRODUCTION

Three decades ago, humankind first glimpsed the Earth from space. Since that day, the space programs of a growing number of nations have served not only as the means by which our universe may be explored, but also as platforms from which to view the complex planet we call home. Undoubtedly, the U.S. space program under the direction of the National Aeronautics and Space Administration (NASA) has provided key leadership in this odyssey. NASA has completed close observations of seven of the planets, including robotic landers on Mars and has launched, retrieved, and repaired satellites with the world's first reusable space vehicle. Perhaps NASA's most difficult and best known challenge was landing the first humans on the Moon. As space author Joshua Stoff stated, "The Apollo program was a bargain. It cost the taxpayers a sum amounting to only one-third of one percent of the Gross National Product in 1970, yet the technical and scientific knowledge gained from it was immeasurable. The Apollo flights gave man a new sense of who he was and where he was, and the views of Earth from space dramatically portrayed the planet's fragility." In addition, the height of the U.S. space program coincided with the height of the United States' industrial prowess, and served as a catalyst for student enrollment in the fields of math and science.

## THE CURRENT STATE OF THE SPACE PROGRAM

NASA has begun several new space initiatives since the Apollo era, despite the tragic loss of the Challenger. The fourth shuttle and forty-first shuttle mission in 10 years have just been completed. This accounts for 249 days in space, 128 days more than the total of the three Skylab missions (Garret, personal communication, 1991). Two scientific observatories, the Hubble Space Telescope and the Gamma Ray Observatory, have begun making observations, and the Magellan spacecraft is completing its mapping of Venus. The Galileo and Ulysses spacecraft are currently en route to their planetary and solar destinations. However, over the years, the technical base from which these initiatives were spawned has experienced incohesive growth. Some areas, such as launch systems and communications, have seen massive strides over the past 30 years. The payload of the Saturn V was 120 tons, 60 times greater than the payload of the first Mercury Redstone only eight years earlier, and the shuttle has the best reliability record of any man-rated vehicle (97.6%). In contrast, life support system technologies have been nearly stagnant, with early space shuttle food packages being basically identical to those used in Apollo and the Gemini missions. Therefore, underdeveloped areas such as life support, provide

great potential for rapid technical advance with little initial cost. For NASA to meet these technical challenges, it must have an efficient personnel base and a consistent funding base.

In 1970 NASA had a total of 31,223 employees, a number that had dropped to 22,613 in 1980, and currently stands at 23,625. The percentages of scientists and engineers among NASA employees has risen and fallen with the same dynamics, beginning with 58.4% in 1970, 49.6% in 1980, and currently 55.6%. Both these patterns are indicative of the space program's funding (funding peaked at 0.8% of the GNP in 1969, and fell to 0.2% of the GNP in 1975, where it has leveled off since), which is creating an unbalanced personnel base. Therefore, the passage of knowledge from the more senior engineers to the newer employees is imperative to the ongoing synthesis of space technology. Although NASA still enjoys general public support, recent events in the budget process show that this support is not a guarantee of consistent funding, and publications such as the Augustine report have not only recognized these situations, but have also expressed concern over NASA's goal setting and scientific base.

Many of the above problems can be remedied using a "phased" design approach. Phasing allows new technology and personnel bases to be built upon the reliable foundation of past experience, while providing returns at each step. This allows more flexibility to political and financial discontinuities, and shows a visible track record of accomplishments. Lastly, for each step in the design process, spin-off technologies can be easily identified, amounting to wider support for space initiatives because their global benefits are showcased. The research effort outlined in this paper was designed to be reflective of these conclusions, categorized as cost effective, safe, and credible.

## DEFINITION OF CELSS AND ITS BENEFITS

The comprehensive results of human activities on the environment, such as deforestation and ozone depletion, and the natural laws that govern the global environment have yet to be determined. Closed Ecological Life Support Systems (CELSS) research can play an instrumental role in dispelling these mysteries, as well as have the ability to support life in hostile environments, which the Earth one day may become. CELSS conclusions, such as the timescales in which plants fix carbon dioxide (CO<sub>2</sub>), will be the key to understanding each component and how it affects the ecological balance between plants and animals, the environment, and the biological engines that drive Earth's system. However, to understand how CELSS can be used as an investigative tool, the concept of a CELSS must be clearly defined.

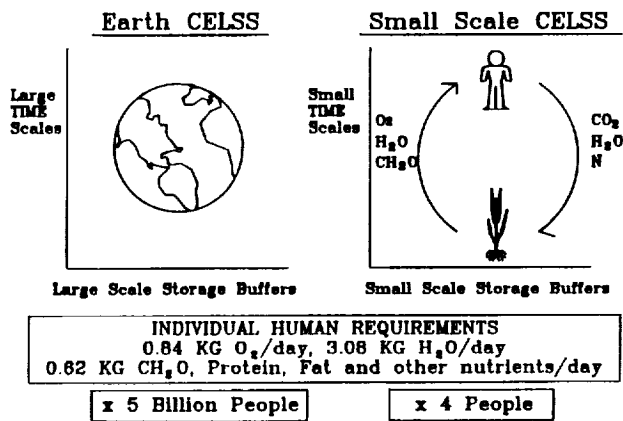


Fig. 1. Artificial ecosystems for space travel would operate on much shorter timescales and with much smaller buffer volumes than the only true closed ecological life support system, our planet Earth.

The best example of a CELSS is the one on which we live, Earth. The Earth, however, is not a true closed system because it receives inputs via energy from the Sun, and mass from contact with stellar and interstellar materials. However, for the most part, the Earth is an isolated system, where the requirements for its many life forms are met by the ecological balance between all terrestrial organisms. This balance is formed by the natural matching of net products of some life forms to the consumption needs of other life forms, and vice versa (Fig. 1). The "inputs" and "outputs" of these life forms can be broken down very simply into gas, liquid, and solid loops. They are called loops because the matching of consumptions (inputs) to productions (outputs) initiates a recycling of the initial foundation of resources, allowing the system to be closed, and thus self-sufficient. Plants and animals affect all three loops simultaneously. For example, animals consume oxygen and carbohydrates (food), breathe out carbon dioxide, and have nitrogenous compounds present in their feces. Through photosynthesis, plants utilize the carbon dioxide and nitrogen compounds to produce oxygen and carbohydrates. All CELSS have balances composed of these reactions, although the Earth enjoys the advantage of tremendous timescales and large available storage buffers.

Humans share the same life enabling environment with plants, but the baseline means of supporting life in hostile environments like space have utilized storage or physical/chemical (P/C) systems. P/C systems use nonbiological processes to support human life. The lithium hydroxide scrubber is an example of how P/C systems are used on the space shuttle to store excess CO<sub>2</sub>. However, this system is neither "regenerative" nor "recycling," as it uses up the LiOH and the carbon dioxide is lost. An example of a regenerative system is the molecular sieve that was used on Skylab to remove the CO<sub>2</sub> from the atmosphere. If biological elements are implemented into a system to initiate recycling, the system is termed "bioregenerative."

Understanding the interactions in bioregenerative recycling systems leads to numerous benefits: improved recycling of water can be provided through advances in water treatment with

bacteria or plants; longer-lasting light sources, such as LEDs, will be pioneered to decrease the cost of running greenhouses; high-yield agricultural techniques increase the net production of biomass; and higher yields for starving nations can be obtained just by better utilizing available resources. It is also conspicuous that such a system would benefit the human habitation of space in the ways categorized as important earlier. This system is *cost effective* because resupply mass can be reduced (lunar base: 453 kg/person/2 weeks in resupply mode; only 61 kg/person/week with biological waste water treatment). In addition, a CELSS does not involve many of the *safety* problems that are currently inherent in some baseline P/C systems. Both the Bosch and Sabatier process have the potential to release harmful gases such as carbon monoxide, hydrogen, or methane and have high operating temperatures. For example, the Sabatier process releases 9152 kJ of heat for every kilogram of CO<sub>2</sub> reduced. Lastly, CELSS technology has an innate *credibility* in that it is building on the oldest, most proven life support system ever, the Earth's own ecological balance.

### CELSS: AN ENGINEERING PERSPECTIVE

The working composition of a CELSS may be characterized by how it makes use of the "functions" involved in each of the gas, liquid, and solid loops (Fig. 2). These functions can be defined as storage, monitoring, treatment, transport, collection, and use. For example, to maintain a chicken in CELSS, its gas, liquid, and solid inputs must be "transported" to it for "use" in consumption. Then the outputs from the use function, such as feces, can be "collected" and transported to "storage." In storage, the nitrogen compounds in the feces can be extracted through a "treatment" function, and then be used as fertilizer for the plants. Together, these functions perform all the tasks needed for the operation of a CELSS.

Certainly, challenges remain before biological elements can be implemented with the same level of integration experience characteristic of P/C systems. Problems such as water recycling,

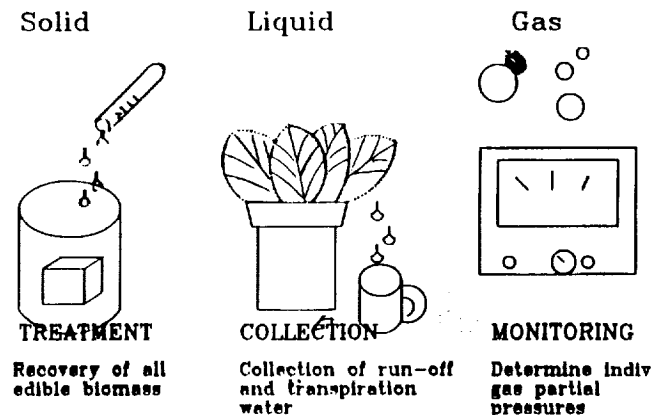


Fig. 2. Mass flows in a CELSS may be broken down into gaseous, liquid, and solid matter. For each loop, forcing functions move the matter between storage, treatment, collection, use, and monitoring locations.

contamination control, and conversion of all biomass into edible form must be overcome. But it is obvious that CELSS research has a tremendous potential to impact positively both how life is lived on Earth and in space.

### MISSION STATEMENT AND RATIONALE

The evolutionary establishment of a lunar base with a bioregenerative life support system in a Space Station *Freedom* (SSF) module to support a crew of four for two weeks duration was chosen as the design topic. Not only is the base the first step in the development of a proving ground for enabling technologies for the long-duration stay of humans in space, but the CELSS research will have an immediate and positive impact over a broad scope of Earth needs. In the U.S., it will also serve as a catalyst for the nation's economy and education. Advances in "space technology" such as robotics and CELSS can provide increased manufacturing competitiveness or "smarter" environmentally controlled homes. Currently the U.S. ranks behind other industrial nations in the average facility citizens have in mathematics and sciences. As during the Apollo program, this new initiative can inspire students to take an interest in these critical foundations of American education. Through development of a lunar base, a number of benefits will be experienced here on Earth long before a single piece of equipment is transported to the surface, or a single byte of scientific information is transmitted back to Earth.

Since the transport of mass is the primary cost driver for a lunar initiative, the integration of a CELSS into the base is a prudent decision because eventually the initial cost of the original CELSS mass will be paid for in resupply cost savings. This break-even point has been estimated by Lockheed for a very similar Lunar CELSS (LCELSS) scenario at 2.6 years for a crew of four. By using an average Earth to low Earth orbit (LEO) cost of \$10,000/kg and multiplying by a factor of five for the cost from LEO to the lunar surface, the cost per kilogram to the Moon can be estimated. Implementing a biological waste water treatment into an existing P/C resupply system alone reduces the cost from \$22.6M to \$3M for one person for two weeks.

Because of the merits of phasing described earlier, a phased implementation of biological elements was used, and a CELSS design group examined the strategy of phasing organisms into a baseline P/C system. All the design groups followed the same methodology for solving their design problems: Identify requirements and the options to meet them; perform a trade study and pick the best option; examine critical technologies and their spin-off applications. For the *CELSS* group, reducing resupply mass and optimizing the rate of movement towards a closed, balanced system were the primary objectives. A phasing strategy that concentrated on the most mass-intensive loop, liquid, was employed, and critical technologies such as hydroponics and lighting were investigated. An *Infrastructure* group examined implications of such a CELSS system and performed sanity checks on the power, mass, and volume requirements that such a system would have. The extent to which these would impact site location, transportation, power, navigation, communications, thermal control, and safety were also determined. Based on the results of these two groups, a

list of labor requirements was made. Since robotics can be employed to eliminate these tasks from astronauts' duties while increasing safety and decreasing mission cost, a *Robotics* group was formed. Referencing the labor requirements, the Robotics group was able to make recommendations for a robot with a power source as its design foundation, and work packages for different tasks. The results of these design groups provide a believable, cost-effective, and safe bioregenerative life support system design inclusive of the robotic and infrastructure needed to shelter and maintain it on the lunar surface. The first step is a CELSS for Earth- and space-based needs like recycling and regeneration of resources.

### CELSS

As the population of the world continues to increase, the conservation of our vital resources becomes ever more important. For example, California, the state with the largest population growth, has suffered recent droughts, leaving its water reserve at less than 20% of capacity. California's need for water is further compounded by a large agricultural industry that uses 90% of its fresh water for irrigation. The need for additional water is currently being met by "mining" groundwater, but most of the underground supply is a one-time usage that will eventually run dry. Therefore, because of the limited supply of potable "drinking" water, there is an urgency to find a way to conserve or replenish it. In Irvine this problem is already being addressed by a system that reuses all of the town's wastewater for municipal irrigation<sup>(1)</sup>. Currently, this critical area is being studied at Stennis Space Center: plants are used to recycle water and to remove air pollutants in the "BioHome" research project. A company in Boulder, Colorado, has already marketed and installed biological wastewater treatment systems (Purecycle) that recycle water in people's homes and have proven that the technology is achievable.

The major stumbling block for attaining a CELSS is closure. It is essential to CELSS research to be able to perform experiments without any outside influences in order to exactly quantify all the parameters governing plant and animal growth. The current baseline in closed experiments consists of closed growth chambers at Kennedy and Johnson Space Centers, as well as initial research and breadboard testing at Ames and Marshall Space Centers, respectively. Ninety days for a wheat experiment is the longest amount of time that closed experiments have been run. Other experiments such as Biosphere II may provide only limited data because the multiple variables present prevent a specific understanding of any particular component. When one considers the large number of organisms that need to be investigated, as well as the required iterations for each experiment, current facilities fall short of the ones required.

Currently, P/C systems are the technology used for total resupply missions such as the space shuttle. Regenerative systems have been examined on Earth, but have not been widely used in space except, for example, the molecular sieve used for CO<sub>2</sub> removal on Skylab. System selections are generally based on trade studies between system mass, resupply requirements, and mission duration. These P/C systems fall short when considering safety and compatibility issues. For instance, the Sabatier CO<sub>2</sub>

reduction process creates 0.33 kg of methane, a hazardous byproduct for plants and animals, per person/per day. P/C systems also become expensive in the long term because they require periodic replacement and repair. Operating parameters, such as high temperatures up to 1500 K for a Sabatier with methane cracking, and pressures up to 1.2 MPa for a Static Feed Water Electrolysis System for O<sub>2</sub> and H<sub>2</sub> generation require massive containment vessels to avoid potentially dangerous conditions. Therefore, even though physical/chemical systems have the advantage of being predictable and autonomous, their disadvantages outweigh their effectiveness for long-duration stays. Hence, they become only a building block on which a CELSS can be implemented and provide an eventual buffer for the working CELSS.

On Earth, bioregenerative technology is already being used to reduce wastes in sewage treatment. For example, municipal sewage plants used bacteria to consume waterborne wastes and purify water, but they produce large amounts of sludge. In open systems like these, however, the efficiencies are hard to calculate. It is imperative to a CELSS that bacteria, microorganism food chains, and advanced anaerobic treatment be better understood to prevent mass from being locked up within the system. The spin-offs attained can be directly applied to increasing the turnaround of recycled water from sewage treatment plants in addition to closing the water loop for a lunar base.

A major stumbling block associated with a CELSS is the basic lack of understanding of bioregenerative systems. The previous classes have addressed this issue and determined a way to depict organisms using a systems engineering approach. The first step of this characterization was to simply consider each organism as a black box, in which all the complexities inherent to an organism occur, allowing simple handling of its inputs and outputs. This black box can then be broken down into three levels: functional, process, and operational (Fig. 3). The *functional* level considers the inputs and outputs over an organism's lifespan in terms of mass. This allows a proper mass balance to be determined by correctly matching the inputs and outputs of the organisms. The *process* level allows one to consider the temporal aspect associated with these inputs and

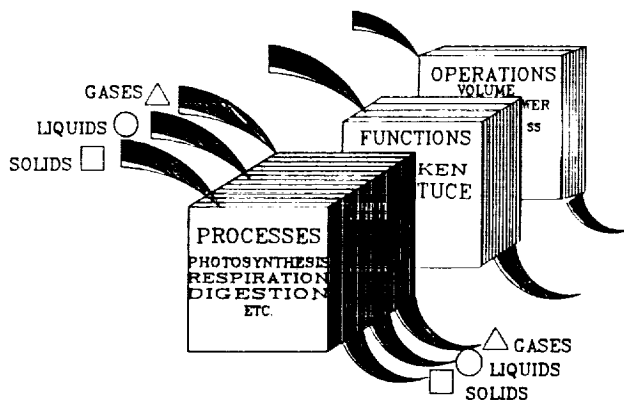


Fig. 3. A systems engineering approach, treating each organism as a "black box", has been chosen to describe and characterize possible candidates for a controlled ecological life support system.

outputs derived from the organism's growth curve, enabling one to determine the correct phasing/harvesting of the organisms. In addition, the *operational* level considers the power, mass, and volume support requirements attributed to each organism.

Using this systems approach, a mass balance was arrived at by writing a computer program, which then provided us with numerous possible combinations of organisms for a closed system. However, to verify this mass balance, an accurate characterization of organisms in closed growth chambers remains a stumbling block. To further understand these biological systems, research into critical technologies and bioregenerative performance depends on metric characterization.

There is an immediate market for the spin-offs gained from CELSS research. Greenhouses for example would directly benefit from any work done in reducing their staggering energy requirements. As a rule of thumb a greenhouse uses 100 times more fuel than field crops for producing plants like tomatoes. Furthermore, research into lighting systems such as LED that last five times longer than current lighting systems would significantly decrease the replacement costs and directly benefit the greenhouse industry. Therefore, research into improving energy and maintenance efficiencies has direct applications to greenhouses. In addition to plant lighting there are many options for current critical technologies such as hydroponics, monitor and control, harvesting, and processing. Therefore, trade studies need to be performed in these areas to ascertain the best candidate based on parameters like mass, power, volume, safety, cost, and reliability.

To achieve the goal of a lunar base with a CELSS there must be a realistic and flexible plan to implement it. The Apollo program for example, had a phased plan to put man on the Moon. They did not just jump into the unknown, but instead they developed the technology in progression with such programs as unmanned Vanguard, Redstone, Atlas, and Saturn. In manned spaceflight they also implemented proven technologies, as well as using a phased approach with the Mercury and Gemini programs before the actual Apollo capsule was used. This evolutionary approach not only builds on previous technological steps, but is flexible to variable economic and political support. The approach that was determined for a lunar base was also a phased approach that broke the research down into three phases: a ground-based phase, a space-based testing phase, and an operational phase. The basic rationale behind this particular phased approach is that CELSS research is so important to the understanding of the Earth as an ecosystem and contains so many industrial applications, that if the mission is scrapped after the ground-based phase, numerous benefits would still be attained. Similarly, the space-based and operational implementation phases have direct and immediate returns that make each step worthwhile whether if the entire mission is realized or not.

In order to have a successful plan it is necessary to have a step-by-step method in which spin-offs and Earth applications are realized at each phase (Fig. 4). Additional returns from the ground-based research of organisms are as follows: methodology to characterize organisms, optimal performance characteristics determined, organism database, robust new hybrids, waste water treatment technology, phased implementation determined. Spin-

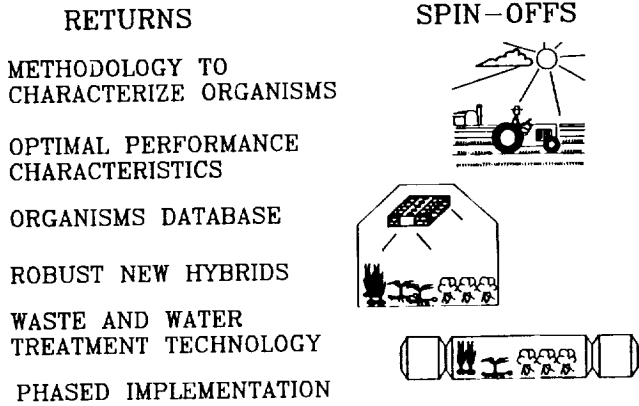


Fig. 4. Numerous spin-offs for Earth applications may be derived from CELSS research.

offs that would be realized are better resource usage, increased crop/livestock production, better yield predictions, understanding of individual contributions to the ecosystem, benefits from waste water treatment improvements, efficient food production procedures, and a transportable phased ecosystem to reduce resupply to remote terrestrial bases such as the Antarctic, desert and underwater. The main focus of the CELSS group was to determine the phased implementation of a bioregenerative system for a lunar base. After examining a number of possible strategies such as establishing a full-scale system right from the start, building a system by integrating organism pairs until a full-scale system is reached, or introducing one organism into the system at a time, the latter method was chosen. This method has less initial mass costs, has an evolutionary progression, is flexible to programmatic concerns like funding, is less complicated, is easy to implement, and provides returns and benefits at each stage.

The initial lunar base would use a P/C system with an integrated waste water treatment system for water recycling. This water loop becomes very important in long-term stays

because water represents over 90% of the total resupply mass. Plants were chosen to be the next component added to the system because of their impact on resource recycling and because they are less complicated to integrate with existing P/C systems and other organisms. Lastly, animals will eventually be phased in until a full scale system is achieved. The optimal phased approach that was determined is presented in Fig. 5.

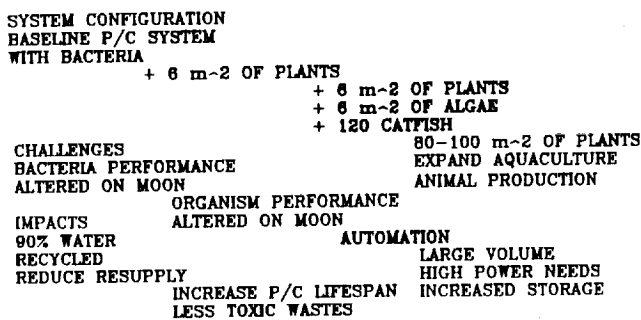
In a previous design effort<sup>(2)</sup> a systems engineering approach successfully characterized organisms. Employing this convention, a balanced bioregenerative life support system was designed with 120 m<sup>2</sup> of plant growth area per person. This compares to the 279 m<sup>2</sup> of intensive agriculture area in Biosphere II and the estimated 6-25 m<sup>2</sup> from the NASA-CELSS research. A methodology for a phased implementation of such a mass flow balanced system is presented in this paper. Furthermore, returns and spin-offs have been determined, stemming from ground-based research to space-based testing, and finally lunar operation.

Many tasks must be performed daily for CELSS research to bear fruit. For instance, care of plants and efficient volume control ensures the longevity of bioregenerative experiments. Robots must be used to partially tend the CELSS, freeing astronauts to further pursue CELSS research. Also, a number of support requirements including power, mass, and volume must be met.

**INFRASTRUCTURE**

An infrastructure is the basic foundation or underlying framework that supports a mission and supplies its fundamental needs. Ideally, once in place, this infrastructure can be taken for granted, like a highway system or a telephone network in today's society. Also, although the primary mission of the infrastructure is to enable a lunar base, each element should have specific returns and Earth applications. There are two distinct phases to the development of an initial lunar base with a CELSS, the ground-based and space-based phases. Since the ground-based phase serves as a stepping stone into space, it must be developed first. The ground based elements needed are a closed volume capable of supporting plant and animal life, facilities to allow human integration into the CELSS, a power system, and a thermal control system.

**PHASE I    PHASE II    PHASE III    PHASE IV**



**PERCENT OF REQUIREMENTS FULFILLED FOR A CREW OF FOUR**

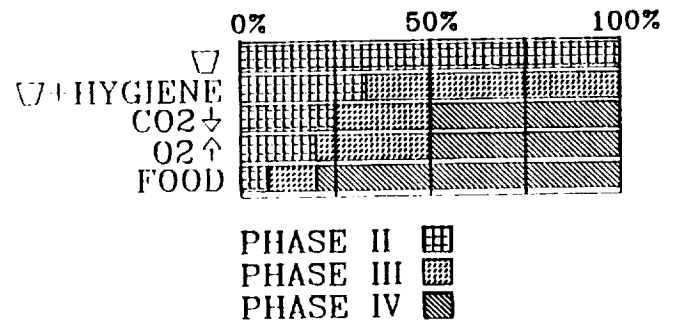


Fig. 5. Phased evolution of a balanced bioregenerative life support system. For each integration step, impacts on the existing life support system, as well as challenges, can be derived. The amount of consumables provided by the bioregenerative part of the life support system are shown for each phase.

The first segment of the ground-based infrastructure to be developed is a life-enabling closed volume capable of supporting the CELSS organisms. This support structure must be capable of maintaining the proper temperature, humidity, and gas concentrations needed for the growth of each organism. It must also provide the proper lighting, nutrient delivery, and waste handling systems, and should be of sufficient volume to allow for a phased implementation. It was estimated that 1 m<sup>3</sup> will be required to support 1 m<sup>2</sup> of growth area for lettuce, and a volume of 3.2 m<sup>3</sup> is sufficient for 120 catfish and an algae system. Therefore, a total volume of 15.2 m<sup>3</sup> will be sufficient to allow expansion through CELSS phase III. Since a Space Station *Freedom* module is to be used for the lunar structure, it should also be used for the ground-based CELSS research, allowing for the development and testing of the same facilities and systems that would be required on the lunar surface.

There are many Earth-based applications of the CELSS infrastructure. For instance, small reliable gas sensors could be used by the materials processing industry and others in which gas purity levels are important. The attainment of complete closure could also benefit these same industries by improving and lowering the cost of clean-room technology, thus facilitating the production of cheap, yet high-quality, medical products, computer chips, and aerospace components.

Once the CELSS has been tested using plants and animals, humans will be integrated into the system. While technically humans are animals, they require different, although mostly analogous, support facilities. As stated earlier, a crew of four was chosen for the initial lunar base. This allows for a large enough skill base among the crew, redundancy for critical skills, and the ability to complete labor intensive tasks with the initial crew while minimizing the initial lunar base mass. A list of the required facilities and their volumes for a four-person crew is given in Table 1.

The third ground-based element needed is a small, self-contained power system to generate the electricity for the CELSS and human support systems. The primary requirements for a lunar power system are that it be safe, reliable, and capable of generating the baseline lunar power requirement of 100 kW. Several options are available for lunar implementation, including radioisotope thermoelectric generators (RTG), nuclear reactors, solar dynamic and photovoltaic systems, and advanced methods

such as solar windmills and the use of thermal gradients. Although RTGs have been used extensively for other purposes, the integration of hundreds of 500-W RTGs into a single power system would present a formidable challenge. The advanced methods are ruled out because there are insufficient data available on either, although they could be viable options for power system expansion. Consequently, nuclear reactors, solar dynamic, and photovoltaic systems are the choices available to provide power for a lunar base. The current power-to-mass ratio for a photovoltaic system (without an energy storage system) of 66 W/kg is clearly superior to that for solar dynamic (2.5 W/kg) or nuclear (10-28 W/kg). The main drawback of using photovoltaic systems for most lunar applications is the mass of energy storage batteries to provide power during the lunar night. However, if the solar arrays could be placed at a site where continuous or near-continuous sunlight is feasible, such as on a mountain near a pole, a high power-to-mass ratio could be realized while avoiding the safety problems of using nuclear power. If not, a nuclear reactor, like the SP-100, is the best alternative.

The development of either a nuclear or solar power system would have definite, near-term Earth applications. Currently, nuclear power is viewed as unsafe by the general public, and solar cells are not efficient enough to make solar power commercially attractive. Both these problems would need to be addressed in the power system development. If solved, then either nuclear or solar would become a viable alternative to using environmentally damaging and increasingly scarce fossil fuels as our primary energy source.

Since much of the power supplied to the module's electrical and mechanical systems will be converted into heat, it is necessary to use some sort of heat rejection system to maintain an acceptable thermal environment. The system should be sized to handle the maximum power level (100 kW) and be capable of sustaining the optimum temperature range for each individual organism. Several methods are available to accomplish this task, including heat pipes, new techniques like a liquid droplet or moving belt radiator, or by using the Moon as a heat sink. The final method is not desirable due to the low heat capacity of regolith. However, either of the advanced methods could realize significant mass savings of up to one-fifth of a comparable heat pipe array.

Many heat rejection systems used today use chemicals such as Freon that have been proven to damage the environment. Therefore, one benefit of the CELSS heat rejection technology would be to provide a small, lightweight, yet environmentally safe, thermal control system for use on Earth.

Once the ground-based phase has been completed (Fig. 6), a substantial building block will be in place for the space-based phase, the development of a lunar base. Nevertheless, modifications must be made to adapt the ground-based elements to the different thermal, gravity, and radiation constraints of the lunar surface. Also, several additional elements are needed for the space-based phase: a lunar site, a communication network between the Earth and Moon, and a transportation system capable of transporting all the lunar base components to the chosen site. During this phase, safety also becomes a critical issue for all designs since help is approximately 380,000 km away.

TABLE 1. Approximate volumes and facilities for a human habitat on the lunar surface for a crew of four.

| Facilities                | Volume (m <sup>3</sup> ) |
|---------------------------|--------------------------|
| Personal quarters         | 18.8                     |
| Galley                    | 6.4                      |
| Hygiene/waste             | 4.5                      |
| Health maintenance        | 4.5                      |
| Dining/recreation         | 4.8                      |
| Data management/ com.     | 2.7                      |
| Exercise                  | varies                   |
| Maintenance               | 2.7                      |
| EVA storage               | 12.0                     |
| ECLS                      | 9.5                      |
| Storage (90 days)         | 22.6                     |
| CELSS (through phase III) | 15.2                     |

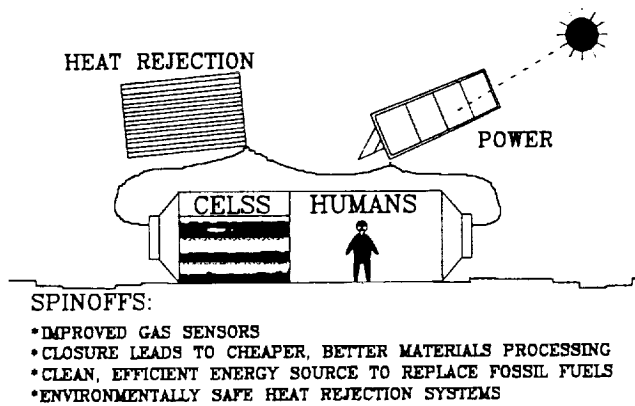


Fig. 6. Possible spin-off technologies from the ground-based research in CELSS infrastructure.

Some of the major threats to crew safety on the lunar surface include radiation, meteorite strikes, fires, loss of power, and illness or injury. For instance, since radiation doses above 25 rem can have adverse effects on human beings, the module must either have adequate shielding to protect its inhabitants or be placed in an area sheltered from solar radiation. Dual ingress/egress is an extremely important safety feature for the lunar base. This allows the crew to escape from the module in the event of a catastrophe, such as a major fire, even if one of the exits is blocked. A second important safety feature is an escape vehicle capable of transporting the crew from the lunar surface back to Earth. This would be necessary if something were to render the module uninhabitable or if a crew member should become critically injured or ill. Also, although the module is to be designed with redundant critical systems, secure storage must be allotted for all important life support elements, such as power, food, water, and air. A 90-day supply of each will be provided to allow the crew to fix the system malfunction, if possible, or sustain them long enough for evacuation or rescue to be possible.

The first lunar element that will be needed is a site for the base. There are several qualities that are desired of a lunar site, including a large relatively flat area; good transportation, communication, and solar access; and protection from meteorites and harmful solar radiation. A polar site in the shadow of a large mountain or crater would fulfill all these requirements and provide a constant thermal environment for the base, eliminating the expansion and contraction associated with thermal fluctuations. Since approximately 2% of the lunar surface (760,000 km<sup>2</sup>) is in permanent shadow, it should be possible to find such a site. Since there is a very limited amount of information available about the polar regions of the Moon, detailed remote sensing and mapping will be necessary to identify possible sites. Then robotic lander/rovers will further investigate each site and provide additional data so a site best meeting the above criteria may be chosen.

A communication network is needed to allow audio/visual data transmission between the Earth and the lunar base, enable robotic teleoperation, and provide system housekeeping and

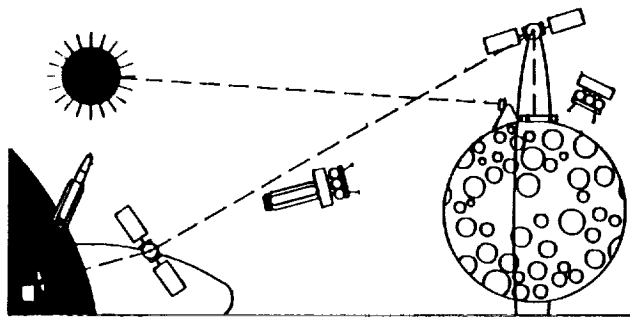
evaluation during non-man-tended periods. The maximum data rate of 20 Mbps (compressed) with a bit error rate of  $1 = 10^{-9}$  needed for telerobotics is within the capability of current technology, either through the use of spread spectrum millimeter wave technology or optical techniques. A more important consideration is the placement of satellites to ensure near-continuous contact with a polar base. Also, low lunar orbits are very unstable, requiring smart satellites capable of continuously evaluating their orbital status and making needed corrections. Several of these satellites in a highly eccentric polar orbit would maximize contact time with the base. The signal will then be relayed to a network of geosynchronous satellites that will in turn send the signal to an Earth receiving station.

One spin-off of the communication technology is the use of low-level expert systems and artificial intelligence employed by the smart satellites. This could be used for a number of applications including making buildings more energy efficient by enabling them to use not only the heating system but also drapes, blinds, window tinting, and solar energy to control temperature.

The final infrastructure element needed for the space-based phase is a transportation system capable of transferring all the base elements to the lunar surface and placing the communication satellites in orbit. The most efficient method to achieve this is the use of a three-part system, using a heavy lift vehicle (HLV), an orbital transfer vehicle (OTV), and separate cargo and lunar landers. Since a heavy lift vehicle is not currently in the U.S. launch vehicle inventory, the lunar lander should be designed first, thus defining the payload requirement for the OTV, and subsequently the HLV. The cargo lander must be capable of landing one module and node, approximately 20,000 kg, while the manned lander must provide transportation to and from the lunar surface for a crew of four. The payload requirement for the OTV is simply the largest lander, or 48,500 kg for the cargo lander. The HLV to be used is an inline shuttle-derived vehicle capable of delivering 95,000 kg to LEO, allowing an entire lunar mission to be delivered to LEO with only two HLV launches.

One of the critical technologies of the transportation system is the development of cryogenic handling, pumping, and bulk long-term storage methods. The resolution of these problems would allow hydrogen to be used in place of fossil fuels for many Earth applications, such as in automobiles. Since hydrogen is a clean, efficient, and abundant source of energy; this would not only benefit the environment, but would provide a cheap source of energy as well. A second critical technology with Earth applications is the terrain-following radar navigation system to be employed by the landers. Not only would safe lunar landings be possible, but the system could also be used by the commercial aviation industry to improve landing safety at night and during bad weather.

Once the transportation system and communication network are operational and a lunar site has been chosen, the ground-based elements will be transported to the Moon and base construction and assembly begun (Fig. 7). Due to workload and safety concerns, robots will be used for many of these tasks. Some of the infrastructure support requirements are the ability to clear an area of large obstacles, such as boulders; transport up to 20,000-kg payloads to their proper locations and place them in their desired orientation; and be capable of performing



**SPINOFFS:**  
 \* AI LEADS TO MORE ENERGY EFFICIENT BUILDINGS  
 \* HYDROGEN COULD REPLACE FOSSIL FUELS AS EARTH'S MAIN ENERGY SOURCE

Fig. 7. The required lunar base infrastructure elements show high potential for Earth-based spin-offs.

simple construction and assembly tasks. Since robots will also be utilized during the site preparation process and for CELSS maintenance, it is clearly a critical technology requiring more in-depth study.

**ROBOTICS**

Establishing a lunar infrastructure is vital, but it may require endless hours of labor-intensive extravehicular activity (EVA). In space or on the Moon, EVA presents considerable health concerns. For example, the puncture in Jay Apt's glove on space shuttle mission STS-37 could have been fatal in the cold vacuum of space. Moreover, harmful solar radiation and meteorite barrages add even greater risk to the hostile environment. The degree of risk is directly proportional to the time spent exposed to it. A major driver for redesigning Space Station *Freedom* was to decrease astronaut EVA time for assembly from 36 to 6 hours and reduce the thousands of hours required per year for maintenance activities. EVA preparation itself takes 2-4 hr of prebreathing and gearing. This time can be better used to accommodate more experiments at the same launch price. A system of robotics can meet these labor needs to reduce human risks and mission costs. By working with industry to codevelop robotics, costs can be further reduced, and benefits can be brought back to Earth.

Automation and robotics are a mechanical workforce designed for a wide array of tasks. In the last decade, the robot population has exploded to approximately 350,000 units worldwide<sup>(3)</sup>. Machine production industries control the largest share, with some automobile manufacturing corporations employing more than 300 robots per plant. A much smaller share find their way into a wide variety of industries ranging from fashion to space.

NASA has historically exploited automation and robotics to ensure safe and cost-effective flight control systems and surface surveying probes. Launch and guidance systems from Vanguard to the space shuttle have been automated to enhance flight control performance and free astronauts for orbital tasks. Furthermore, Apollo lunar probes, Viking planetary probes, and

the shuttle's remote manipulator arm have all applied robotics. However, these transportation and surveying systems differ greatly from industry's focus on construction.

As the scope of space missions continues to grow, so does the need for larger and more mass-intensive structures in space. Current launch systems cannot transport them, and the progression of heavy launch vehicles may never catch up to future space station upgrades and extraterrestrial outposts. NASA must endeavor to work with industry to improve current robotic construction and design robotic systems for the benefit of both. The time to act is now as Japan owns an overwhelming 63% of the world's robots to America's 12%<sup>(3)</sup>.

The Earth-to-Lunar CELSS mission elucidates the needs discussed above. Both areas of the mission, CELSS and infrastructure, require a number of labor-intensive tasks be completed. A partial general list of requirements is given in Table 2. Each general task has a set of very specific procedures. For example, one of the most meticulously labor-intensive CELSS activities, changing burnt-out LEDs, is detailed in Table 3. Likewise, a vital infrastructure requirement, retrieving cargo from a lunar lander, is developed in Table 4. These two lists represent completely different activities requiring not so different means. Though changing LEDs prescribes precise sensing and hauling cargo requires a stake driver, both activities need a power source, an automated control system, and a system of robotic motors and arms. Beyond the tasks described above, LED heat sensors will detect thermal abnormalities in the module hull, and the stake driver will take core samples of lunar regolith. In this respect, a small yet complete set of required components is capable of accommodating most of the CELSS and infrastructure

TABLE 2. Establishing a lunar base and maintaining a lunar CELSS requires many labor intensive tasks.

| CELSS                 | Infrastructure        |
|-----------------------|-----------------------|
| LED replacement       | Cargo Transportation  |
| Crop transportation   | Construction/Assembly |
| Crop harvesting       | Lunar surveying       |
| Growth/Volume control | Site raking           |
| Etc. . . .            | Etc. . . .            |

TABLE 3. Replacing a failed LED breaks down into specific labor and technology needs.

|  |
|--|
| Scan LED with light sensor for failure |
| Remove burnt LED                       |
| Transport LED to disposal              |
| Transport new LED from storage         |
| Insert new LED                         |

TABLE 4. Retrieving cargo sent from the Earth is a very labor-intensive, yet simple task.

|                             |
|-----------------------------|
| Locate cargo                |
| Attach cable to cargo       |
| Drive stake into regolith   |
| Position cable around stake |
| Attach cable to winch       |
| Operate winch               |

needs. For redundancy and costeffectiveness, the components will be modular with respect to a central power and control unit, much like a tractor. So, in the tradition of Mr. Potatohead, the innovative MPH lunar robot (Fig. 8) was conceived.

The MPH is an autonomous corporal power unit that enables variable component configurations. Electric power is generated by a dynamic radio-isotope power system (DIPS) and stored by zinc-air batteries. These were chosen primarily for their high specific efficiency and storage capability, respectively (the trades are shown in Tables 5 and 6). Most activities in the vicinity of the module will be powered by an umbilical cable to the main generator, but the power systems give autonomy away from the module and general redundancy. Also in the corporal unit, a computerized neural network controls all robotic actions. The components, listed in Table 7, will be arranged according to task needs. Current technology, however, is not up to tackling the lunar environment and other mission-related limitations. For instance, lunar dust may inhibit optics, and mass-intensive hardware raises launch costs.

Ongoing research and development will not only overcome some of these roadblocks, but will accrue benefits stemming from technology improvements. For example, overcoming the problem of lunar dust on camera lenses may lead to a particle-repelling glass. The development of stronger, lighter materials has considerable implications for auto and aerospace industries. Developing titanium-aluminum alloys will reduce the mass of aircraft by 60%<sup>(6)</sup>. Beyond industrial spin-offs, medical implications are pacemakers with efficient long-term batteries, durable cybernetics with strong efficient motors, high-resolution internal cameras, and teleoperated subdermal probes. Cleaner,

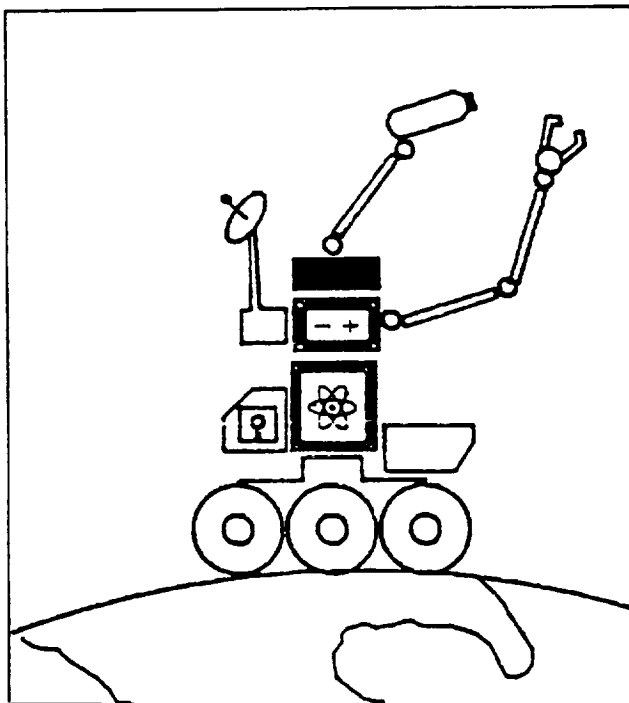


Fig. 8. The MPH lunar robot (Mr. Potatohead).

TABLE 5. The trade study of nuclear power generators<sup>(4)</sup> reveals DIPS as the economic technology choice. RTG: =Radio-Isotope Thermal Generator; DIPS = Dynamic Radio-Isotope Thermal Generator;  $P_{max}$  = peak electric power output.

| Generator Type  | $P_{max}$ (kW <sub>e</sub> ) | $P_{spec}$ (W <sub>e</sub> /kg) | Efficiency (W <sub>e</sub> /W <sub>th</sub> ) | Lifespan (years) |
|-----------------|------------------------------|---------------------------------|---|------------------|
| RTG             | 0.5-5                        | 5.2                             | 4.2-6.6%                                      | 10               |
| DIPS            | 1-10                         | >6.5                            | 18-24%  | 7                |
| Nuclear Reactor | 0.5-1                        | 80                              |   |                  |

TABLE 6. Though lifespans may be roughly the same, zinc-air batteries can store twice as much electric power as the next best battery or regenerative fuel cell (RFC). Sulfur-sodium and zinc-air battery data<sup>(5)</sup>. All other data<sup>(4)</sup>.

| Storage Type              | $P_{spec}$ (W <sub>e</sub> -hr/kg) | Lifespan (years) |
|---------------------------|------------------------------------|------------------|
| RFC                       | 20-35                              |                  |
| Ni-Cd Battery             | 20                                 | 15-20            |
| Ni-H <sub>2</sub> Battery | 30                                 | 10-20            |
| Pb-acid Battery           | 25                                 | 10-20            |
| S-Na Battery              | 100                                |                  |
| Zn-air Battery            | 200                                |                  |

TABLE 7. The MPH lunar robot can accomplish a variety of tasks with a small set of utility components.

|  |
|--|
| Remote camera to view tasks and site objects                           |
| End effectors for object manipulation, fastening, and sensing          |
| Winch for heavy towing   |
| Pump for fluids handling   |
| Software to enable different tasks                                     |
| Cable for heavy towing   |
| Bones are mechanical limbs for extension                               |
| Teleoperations/relay to enable camera transmissions and teleoperations |
| Basket for light storage during transportation                         |
| Motors to run all mechanical joints and hardware                       |
| Stake driver to embed stakes into regolith                             |
| EVA locomotion unit for mobility on lunar surface                      |
| Rail locomotion for mobility and power inside module                   |

more efficient power systems have global economic and environmental impacts. The applications need not stop with the separate MPH components. In Japan, robots have raised industrial productivity and improved work safety and health with just a 0.02% increase in unemployment<sup>(7)</sup>. Currently, teleoperated robots are being employed for nuclear plant maintenance, offshore mining, underwater dam maintenance, and orange picking to name a few. MPH spin-offs may be prototypes for future life-saving fire fighters, blood-handling sterile nurses, time-efficient home constructors and painters, and space station builders. In all cases, the MPH program offers immediate and continual benefits whether it is completed or not.

A comprehensive Earth-based R&D program will help overcome technology roadblocks and provide constant returns. The first stage consolidates the safest and most reliable existing technologies with the most desirable mass, volume, power, and resupply constraints. This primary MPH will be tested both in the Earth-based CELSS module and in reduced gravity KC-135

and space shuttle environments to provide improvements during the second stage. The MPH will aid in the lunar site selection process, and three MPHs will be used for site preparation and construction. The phased robotics mission advances current technology and is a feasible approach that will yield returns both immediately and continually, on the Earth and in space.

### CONCLUSIONS

This paper has compiled both the space- and ground-based benefits for a lunar base with a CELSS, and incorporated them into the overall rationale for a sustained lunar mission. The necessary steps to achieve this endeavor were outlined, with an emphasis on the phased implementation of biological elements into an initial P/C life support system. The implications of such a system on a lunar mission infrastructure were also investigated, thereby providing a sanity check for the CELSS requirements. Recommendations of designs were made for shelter, site location, transportation, navigation, power, safety, and thermal regulation. Lastly, because a CELSS will increase generic labor demands, there are numerous opportunities for robots to accomplish not only CELSS tasks, but other lunar base work assignments. This research resulted in several design conclusions for not only a CELSS or lunar robot, but for many number of Earth-based robotic applications.

Although there remain roadblocks in the path of demonstrating that a controlled environment can be optimally designed, closed, and maintained, some of these challenges are already being met by innovative solutions. Through a continued and expanded commitment to CELSS research and development, the necessary technologies can be produced for a number of applications including those for a lunar base. In addition to maintaining the nation's lead in space technology, and increasing our industrial strength with improved robotic capacity, a lunar mission can benefit the world as a whole. In fact, the most

compelling argument for CELSS research is not in decreased resupply for lunar, deep-sea, or polar missions, but in providing a comprehensive ecological database. From this knowledge, we may tackle a variety of other problems, such as using biological means to increase waste treatment in Third World countries, thus decreasing the spread of disease. On a global level, satellite observations, combined with ecological models based on CELSS research, can be integrated to observe the biological engines of the Earth. This will allow more accurate conclusions on organisms like the role of plankton in affecting the disputed consequences of the greenhouse effect and global warming. After all, it is the very result of space research on our planet and others that we are aware of such problems. This vital connection between space exploration and the citizens of the world is the heart of the justification for the space programs' continued existence. It is in this light that we should further pursue space exploration, and the multitude of returns it will continue to deliver to human kind, both on the Earth, and in space.

### REFERENCES

1. Englebert, Ernest A., Ann Foley Scheuring (1984): Water Scarcity—Impacts on Western Agriculture.
2. University of Colorado - Aerospace Engineering Sciences (1990): Methodologies for the Development of a Bioregenerative Life Support System.
3. North-Holland (1990): British Robot Association—Robot facts 1989, Robotics and Autonomous Systems.
4. Faller, W., A. Hoehn, S. Johnson, P. Moos, N. Wiltberger, M. Luttges (1989): Cis-Lunar Space Infrastructure Lunar Technologies.
5. Cook, Richard (1991): Electric car showdown in Phoenix. Zinc-air battery wins, Popular Science.
6. Brown, Alan S. (1991): Titanium is hot, but it can't stand the heat, Aerospace America.
7. Blumenthal Turia (1990): Economic effects of robotization in Japan, Robotics and Autonomous Systems.

## DESIGN OF BIOMASS MANAGEMENT SYSTEMS AND COMPONENTS FOR CLOSED LOOP LIFE SUPPORT SYSTEMS

UNIVERSITY OF FLORIDA

516-54  
160592

p. 5

The goal of the EGM 4000/1 Design class was to investigate a Biomass Management System (BMS) and design, fabricate, and test components for biomass management in a closed-loop life support system (CLSS). The designs explored were to contribute to the development of NASA's Controlled Ecological Life Support System (CELSS) at Kennedy Space Center. Designs included a sectored plant growth unit, a container and transfer mechanism, and an air curtain system for fugitive particle control. This report summarizes the work performed by the class members.

### SECTORED PLANT GROWTH UNIT (SPGU)

The goal of the Plant Growth group was to engineer the development of a plant growth unit in which planting, harvesting, and refurbishing would take place. The system that was designed, a Sectored Plant Growth Unit (SPGU), models a sector of the aeroponic plant growth unit conceptually designed for a Controlled Ecological Life Support System (CELSS), by the EGM 4000 Advanced Missions Space Design class, during the fall of 1990.

This unit, shown in Figs. 1 and 2, provides a growth promoting environment for all stages of crop development. Seed holders provide support as the individual plants grow. The roots receive a nutrient solution in the form of a mist (Fig. 3). The nutrient mist, along with separated plant particles (leaves, root pieces, etc.), are removed by the application of pressure and velocity gradients.

The SPGU is cleaned by a hydro-refurbishing system (Fig. 4) that cuts the plant at the root line, discharges all material in the seed holders, and liberates the edible and inedible parts of the plant from the unit. After the crop is harvested, the inedible biomass is removed from the SPGU with high-discharge water and air jets.

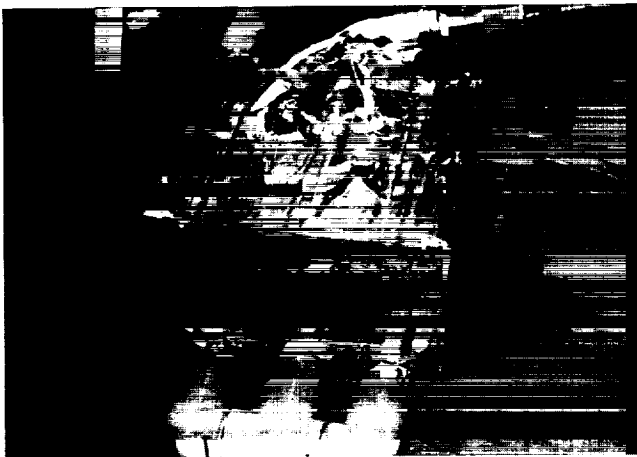


Fig. 1. Sectored plant growth unit (top view).

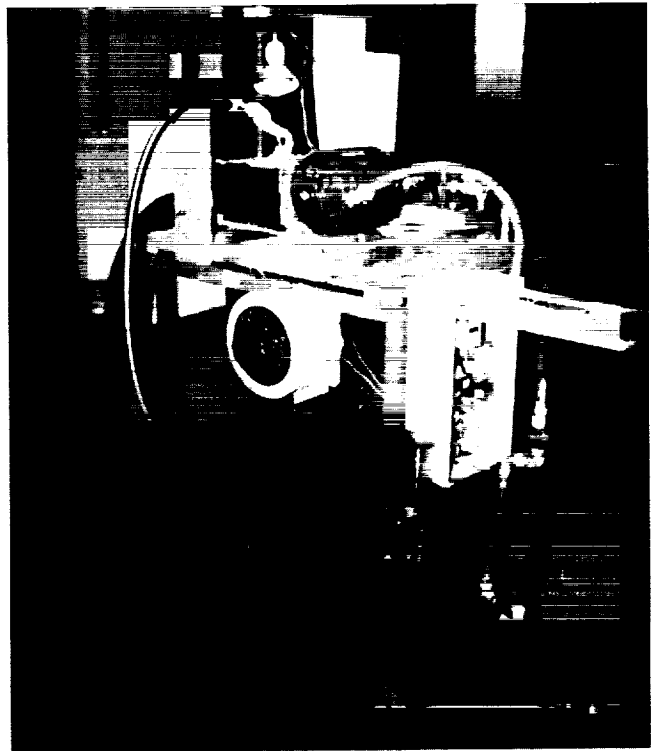


Fig. 2. SPGU and support systems.

As the CELSS research continues on the ceramic growth medium, several complications have arisen such as pore clogging. It was a goal of the Plant Growth group to avoid the problems that the porous tube and tray projects at Kennedy Space Center have encountered, while not overlooking other problems inherent to an aeroponic and hydro-refurbishing system, such as clogging of the misting and refurbishing nozzles.

During the conceptual design phase of the project (growing plants in a microgravity environment) the Plant Growth group took into account the planting, harvesting, and refurbishing activities, and how they apply in an integrated system. In the fall of 1990, the group determined some of the necessary criteria for a plant growth unit (PGU) and suggested a possible design.

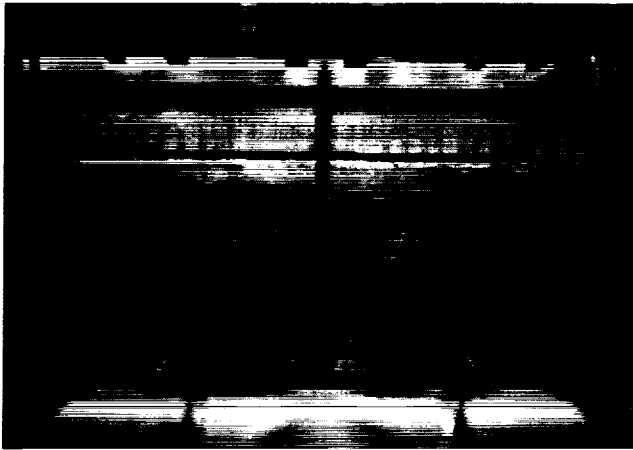


Fig. 3. Activated SPGU (side view).

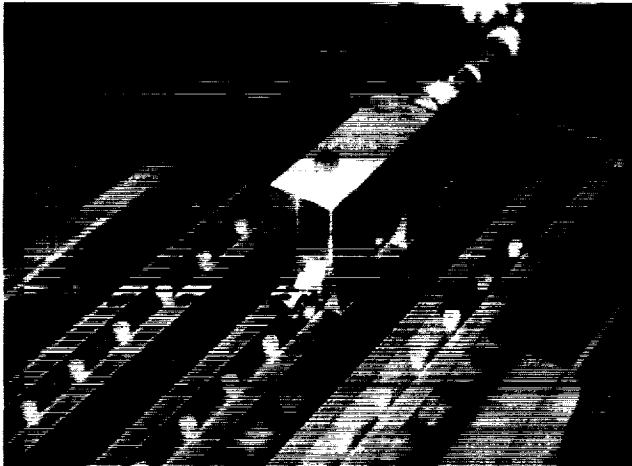


Fig. 4. Hydro-refurbishing block on SPGU surface.

In the spring of 1991, the design was revised, a prototype was built, and the concept was tested in an SPGU. Radishes were chosen as the SPGU crop because of their relatively small size and rapid growth rate.

Several methods are already in use for planting crops in nonsoil media, so little time was spent in designing a planting system for the SPGU. Likewise, harvesting, as an individual activity, received very little focus. By the design of the SPGU, harvesting is basically a continuation of the refurbishing process.

Although aeroponics is a proven method of plant nutrition, very little research has been performed using a vacuum system and pressure gradients to control the aeroponic mist flow. There are distinct differences between the SPGU and the Vacuum Oriented Nutrient System (VONS), currently being explored by Bill Cox at Kennedy Space Center. The SPGU is one unit containing many plants, rather than many units containing one plant each, which is typical of VONS. In a microgravity envi-

ronment, the vacuum may become important, providing a way to keep the mist in the nutrient delivery system. Also, little research has been performed on the use and effectiveness of water jets (knives) to clean organic and inorganic materials out of a plant growth chamber. Thus, considering the time constraints for the project design, the focus of the Plant Growth group was directed towards the unexplored aspects of a vacuum-oriented, aeroponic plant growth unit employing a hydro-refurbishing system. The Segmented Plant Growth Unit relates directly to the PGU conceptually designed for use in CELSS. The PGU is a complete system of stem and root chambers that are separated by coaxial cylindrical surfaces. These surfaces have fixed and moving nozzles that provide an aeroponic mist for plant nutrients, and precise, high-pressure sprays for refurbishing. By research and development, the final design of the SPGU should be large enough so that the data can be extrapolated to a full-size of PGU.

The placement of a seed prior to germination, and the orientation with which the plant grows after seed germination, are vital elements of a plant's growth and development. Many factors such as light, air, water, pressures, and forces, will affect how the plant develops. Because the design group intended to focus primarily on the relatively unexplored aspects of the system (the hydro-refurbishing and vacuum oriented aeroponic systems), no planting schemes were thoroughly investigated. However, several ideas were envisioned. Peat pellets, inflatable balloons, polymer funnels, and especially designed pieces of filter paper or perforated plastic were all ideas that may be used to hold seeds in specific orientations. With more research and testing, any of these ideas may be feasible for integration into a full-scale PGU.

The nutrient delivery system developed for the SPGU possesses the best aspects of aeroponics and VONS. The system allows the growth of many plants in one chamber, supplies the roots with nutrients by a misting action, and employs a vacuum for nutrient solution recovery. The system was developed for use in microgravity by designing the actual plant growth unit with certain specifications. For example, nutrient solution was not to escape from the root chamber, except through the vacuum, regardless of its orientation when being tested on Earth.

Cleaning the PGU is a serious problem. Currently, it takes a group of six people a week to clean out the area required to feed one astronaut. Thus, a major design requirement would be to drastically reduce cleaning time. It was proposed to use water jets to clean the entire PGU within a matter of minutes. These water jets would be required to run at a high pressure in order to concentrate a large force over the desired area. Attempting to keep the hydro-refurbishing system small, the volume flow rate was specified to be under 1 gpm. The water knife would be used to cut off the top portion of the plant while another jet would free the root mass and remaining stem from the PGU. Ultimately, a sensor-based, intelligent system would carry and selectively aim the nozzles.

The opposing gravity test was performed to observe the delivery and recovery of the nutrient solution in an opposing gravity field. This test was performed to confirm that the SPGU would work in a microgravity situation. The SPGU was oriented such that the nutrient solution entered from a lower potential energy state, with respect to gravity, than it was recovered from.

In other words, it was rotated such that the nutrient spray entered from the bottom, and the vacuum pulled it out of the top. In this orientation, the solution accumulated until an equilibrium water depth of about 1.5 inches was obtained. In this case, the vacuum was run at about 70% of the vacuum's maximum motor speed. As the vacuum's power was increased to 100%, the equilibrium water height decreased to approximately 0.5 in. In addition to increasing the vacuum power, supplying the nutrient recovery vacuum with more air helped decrease the equilibrium water level in the SPGU. By adding more holes between the top surface and the root chamber (in addition to the seed holder ports), more air was supplied to the vacuum. When this was done, the equilibrium water level in the SPGU completely disappeared; thus, the spray went straight from the misting nozzles to the recovery vacuum. Ideally, this would allow the roots to remain moist without being completely saturated. The tests performed on the SPGU, with respect to nutrient delivery in microgravity, showed that a vacuum-oriented nutrient solution recovery system could offer an alternative to current systems. Because the tests were performed under opposing gravity, it is conceivable that in microgravity, parameters such as vacuum pressures and flow rates could be reduced. Potential problems with separation of nutrient solution and vacuum fluid are foreseen.

A prototype SPGU surface was developed to perform refurbishing tests. The prototype surface has three rows of seed holder ports, with eleven ports in each row. Refurbishing tracks were milled exactly as in the actual SPGU. The main purpose of this refurbishing plate was to place mature radishes (or other small crops) into the port, and cut them with the refurbishing nozzles. It would not be necessary to wait for the plants to germinate and mature in this case. Because of the inability to find mature radishes with stems still attached, cutting tests were performed with celery. Celery has a very high percentage of cellulose, and is one of the strongest vegetable crops. Thus, it was hypothesized to be an optimal test for the refurbishing nozzles. At a water pressure of 500 psi, the fan nozzle was able to cut six celery pieces (1/4 in diameter each) in approximately 5 s. With increased pressures and a more efficient nozzle system, the refurbishing time may possibly be further reduced.

#### CONTAINER AND RECEIVING MECHANISM (CARM)

The Container and Receiving Mechanism (CARM) is a device designed to transport and store solid matter. In a microgravity environment, containment is a problem because of the tendency of particulate matter to disperse randomly about the crew compartment.

A canister system does not currently exist in CLLSS. Any research and development will prove highly beneficial to the BMS. Last semester two approaches were examined to develop a transport system. CARM could incorporate with either the pneumatic or magnetic belt ideas. In a CLLSS there is a need for the containment and storage of the edible biomass produced. The absence of a gravitational force necessitates the containment of all particles. In microgravity loose particles pose a unique problem since they disperse throughout the surrounding compartment. As a solution, a CARM that is multifunctional has been

proposed: its primary function is the sealed transport and transfer of food to a processing unit; the secondary function is the storage of food until further processing. CARM's use should not be limited to the transfer of edible biomass between the Plant Growth Unit and Food Management. It has numerous applications in the movement of mass between all compartments in a CLLSS.

Several different transfer systems were evaluated before final selection of the CARM. These included an L-channel device, a plunger system, and a roller method. After examining the different options, a final selection for a transfer mechanism was made. The CARM system chosen consists of a hard shell cylinder, a bag, and an interlocking mechanism (Fig. 5).

A cylindrical shape has several advantages: ease of transport, cleaning, and storage. This shape also adapts itself to the transport mechanism presented last semester in EGM 4000. For testing purposes a clear cylinder was chosen so that the internal environment could be observed. The hard shell construction allows air pressure to be used to move the contents. The 4" diameter by 12" length reflects the CARM's intended use in transporting a meal-size portion of edible biomass for a crew of four. The opening of the cylinder should be the same size as the container to prevent a backup of the contents at the opening.

A bag lining was needed to contain small particles. The contents of the bag were expelled by using air pressure within the cylinder to force the bag inside out. There were two important criteria for selection of the bag material: (1) flexibility for ease of transfer and (2) durability for a high number of cycles (1500 cycles/year). Several different options were considered for the bag's material: Flexiglass, polyurethane, and flexible PVC. The final selection of the polyurethane was determined by its flexibility and ease of inverting.

A vital component of the CARM is the closing of the bag attachment. This prevents particles from dispersing randomly during transport or transfer. Several different closing mechanisms were examined: a sphincter, an iris, and a hinge.

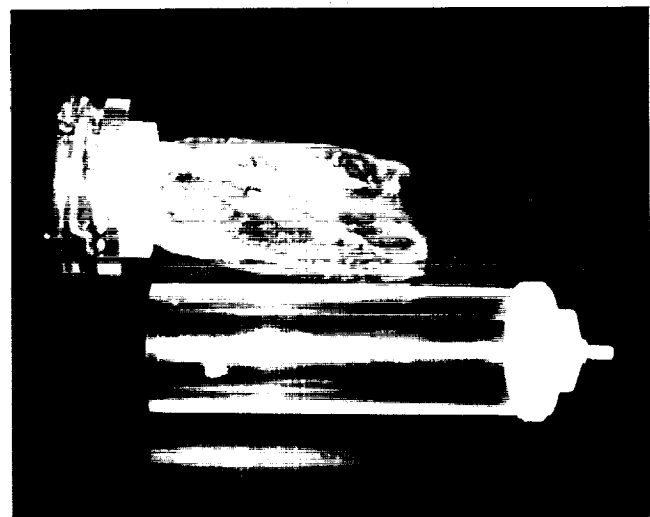


Fig. 5. Container and receiving mechanism (disassembled).

A modification of the iris is the snare end effector in the mechanical arm of the shuttle. This system consists of three wires arranged equidistant from each other on an outer ring attached transversely to an inner ring. The wires system works by rotating the outer ring while keeping the inner fixed. This twists the bag closed. This system has proved effective in containing small particles such as flour.

In order to substantiate the CARM working in a microgravity environment each test was run at multiple orientations. The use of multiple orientations assumes that if the CARM can work in opposition to gravity, then a microgravity environment will not adversely affect the CARM's performance. Testing of the CARM involved two separate procedures. The first experiment involved the complete sealing of a CARM unit without loss to the surroundings. The second, more challenging, experiment involved minimizing the loss to less than 1% during transfer from one CARM to another.

The first step was eliminating loss of the contents during transport from one area to another (Fig. 6). The zero-loss seal of the CARM unit was accomplished by using the modified iris design. Complete sealing was necessary to enable the CARM to be used as a storage unit. Without a tight closure to prevent the passage of air or moisture the food contents would spoil.

During transfer of the edible biomass from one CARM to another there are two specific types of loss: (1) the first loss introduced is from the junction of one CARM with the other and (2) the second loss introduced is from the residue left on the bag. Testing of the CARM prototype showed that there were no losses to the environment; however, when transferring small particles (i.e., flour) there was some residue left inside the bags.

CARM could prove a beneficial addition for long-term space missions. Its use should not be limited to transport and storage of edible biomass. With the development of CARM units in a variety of sizes, CARM has limitless possibilities. It can be used in planting and harvesting to deliver seeds and remove harvested

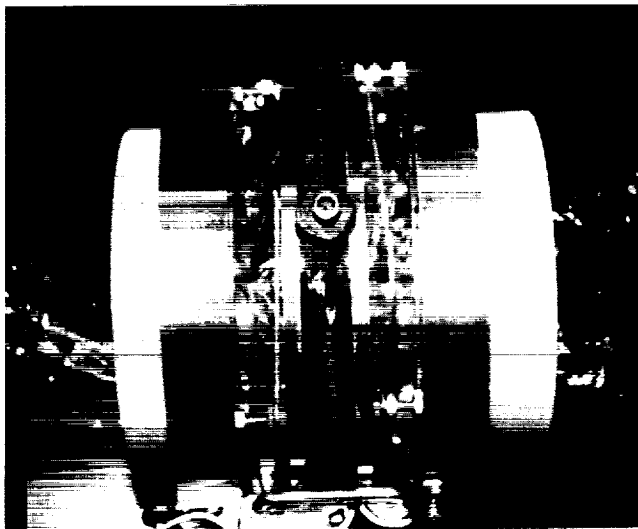


Fig. 6. CARM interlock with another unit for transfer.



Fig. 7. Air curtain device for fugitive particle control.

crops. CARM's applications extend to resource recovery where it can be used between bioreactors. CARM could be used to transport from the crew compartment throughout the BMS.

#### AN AIR CURTAIN SYSTEM FOR FUGITIVE PARTICLE CONTROL

In a microgravity environment fugitive particles from foodstuff, for example, can migrate and lodge on surfaces. Control of such debris plays an important role in the health of the crew and the functioning of equipment. In the Biomass Management System investigated by this class last semester, several subsystems could greatly benefit from the existence of fugitive particle control devices. For example, food preparation involves the transfer and processing of biomass that should be contained in specific regions.

Different systems to control fugitive particles were explored by this team. Of all the systems investigated, an air curtain (Fig. 7) was found to be the most promising solution for particle control. Air flow characteristics of different configurations were investigated and a system consisting of a single air curtain was selected for further development.

The main concern of this team was the effect of the arms through the air curtain, since it was suspected that this could disrupt the flow of air. To prevent debris from escaping or entering through the stagnation point created by the flow around the user's arms, a suction accessory was integrated at the bottom of the unit. The blowers and motor, which generate the air curtain, were installed behind the unit to allow frontal visibility. The sides and top are made of clear plexiglass to allow visibility into the device. To preclude the necessity of air separators, a plenum chamber was incorporated in the design. The nozzle was lengthened to create a more laminar flow. A method was designed to recycle the air back to the intake of the blowers. This method took advantage of the suction created by the blowers. A filtering system was incorporated into the design.

For testing of the device, small styrofoam particles of approximately 1/8 in (5 mm) diameter were put inside the unit

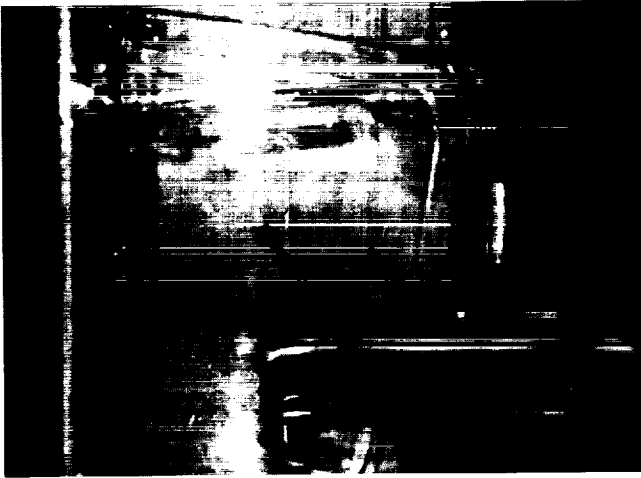


Fig. 8. Air curtain device in operation.

(Fig. 8). A hand-held fan placed inside the unit was used to disturb the particles. It was observed that the particles were successfully controlled by the device. These fugitive particles either (1) stayed in the working area or (2) were removed into the filtering system when attempting to escape. The nozzle output was 400 cfm at all points along its horizontal axis. The volume at the suction was 510 cfm. This volume increase was accomplished by increasing the area of the intake. The filtering system successfully trapped the fugitive particles for later disposal into the vacuum device.

Fugitive particle control is a major concern for long-term space missions. It was found that a single air curtain system would be effective in preventing particles from entering or exiting working areas. The prototype unit successfully controlled fugitive particles. The unit was found to successfully contain or expel low-density particles (i.e., bread crumbs) traveling at 218 ft/min (1.11 m/s) perpendicular to the curtain. The results suggest that the single air curtain configuration will be useful in containing fugitive particles from escaping or entering a work area in a microgravity environment. The unit was self supporting, i.e., the air curtain and the suction device were one single mechanism. The technology for the implementation of air curtains for fugitive particle control is readily available and units can be easily built to fit the desired function.

ORIGINAL PAGE  
OF BLACK AND WHITE PHOTOGRAPH



**LUNAR LANDER GROUND SUPPORT SYSTEM**  
**FLORIDA A&M UNIVERSITY/FLORIDA STATE UNIVERSITY**

517-14  
160593

P-4

**PROJECT BACKGROUND DESCRIPTION**

This year's project, like the previous Aerospace Group's project, involves a lunar transportation system. The basic timeline will be the years 2010-2030 and will be referred to as a second-generation system, as lunar bases would be present. The project design completed this year is referred to as the Lunar Lander Ground Support System (LLGSS). Not many projects have been attempted in this area because they involve the design of a system that is not nearly as glamorous as it is necessary.

Present plans for lunar colonization call for a phased return of personnel and materials to the Moon's surface (1). During the first phase, a base will be set up with power supplies, basic supplies, and various necessary equipment. The first base personnel would land at the base(s) and stay for a period of roughly 30 days and return to Earth. Shortly after that, a second group would land at the base(s) and stay for periods of 60 to 180 days and perform long term experiments to prepare for further explorations in the future. At these times, the lunar lander will be stationary in a very hostile environment and will have to be ready for use in a contingency plan in case of an emergency. Cargo and personnel will have to be removed from the lander and transported to a safe environment at the lunar base. This project addresses these systems and the problems encountered.

The interaction of the following three types of vehicles will have to be analyzed: a reusable lunar lander; a servicing vehicle; and a transportation vehicle.

The basic operational scenario is as follows: A lunar lander descends from a transportation node in low lunar orbit (LLO) to the surface and lands at a prepared area close to the base. The transportation node will be a stopover point for the lander delivering vehicle traveling from Earth to the Moon. A transportation vehicle will then bring out a servicing vehicle to be attached through umbilicals to the lander. The cargo or personnel would be removed and transported from the landing pad to the lunar base. Some of the transferral operations will be performed through the use of remotely operated cranes or robots, referred to as teleoperations. Once the personnel or cargo items have returned to the base, a "servicer" vehicle will keep the lander in a state of readiness.

The lander will be of a similar design to lunar landers of the Apollo era. It has been stated that a reusable lander that burns liquid hydrogen and liquid oxygen would be necessary for such missions. The lander will be able to perform standard docking functions with an orbital lunar node.

The servicer will provide several servicing functions to the lander, including: (1) reliquifying hydrogen and oxygen boil-off, (2) supplying power, and (3) removing or adding heat

as necessary. It has been observed that a drive system would be unnecessary for a "vehicle" that would be immobile most of the time.

The transport vehicle will be made to operate manually or through the use of teleoperations and robotics. It will serve the dual purpose of carrying the servicer out to the landing pad and transporting cargo or personnel back to the base. The basic configuration will be similar to that of a lunar roving-type vehicle.

A great deal of practical engineering was applied to the various systems and interactions of the project. Several NASA and contractor personnel showed interest in particular areas of our proposed project. None of the personnel contacted had seen a detailed design and analysis of a project involving many systems interacting between three vehicles such as ours. Specific areas of interest of industry personnel included (1) vehicle interactions, (2) vehicle interfaces and associated procedures, (3) heat rejection while on surface, (4) fuel storage and reliquification procedures, (5) radiation protection, and (6) dust problems in all systems. Practical knowledge of materials selection, heat transfer, electrical engineering, and structure design can be applied to most aspects of the project.

**EMPHASIS OF DESIGN**

The area chosen for analysis encompasses a great number of vehicles and personnel. The design of certain elements of the overall lunar mission are complete projects in themselves. The fundamental designs of bases, lunar landers, heavy moving vehicles, lunar nodes, and Earth-to-Moon transportation systems are extensive projects in their own right. For this reason the project chosen for the Senior Aerospace Design is the design of specific servicing vehicles and additions or modifications to existing vehicles for the area of concern involving servicing and maintenance of the lunar lander while on the surface.

The design of certain vehicles and structures not directly related to but interfacing with the servicing system was assumed. Examples of the vehicles and structures that were considered as outside design parameters that the lander servicing system depended on are as follows: lunar lander, lunar orbiting node, space transportation system, central lunar base systems, and lunar heavy moving vehicles.

The most plausible design for a lunar lander for the years 2010-2030 was found in a conceptual lunar lander report by Eagle Engineering (2). The report describes a second-generation single-stage lunar lander and the related physical parameters. The lander is a reusable vehicle powered by liquid hydrogen and liquid oxygen chemical rockets. The basic design is shown in Fig. 1. All other significant parameters are assumed as given

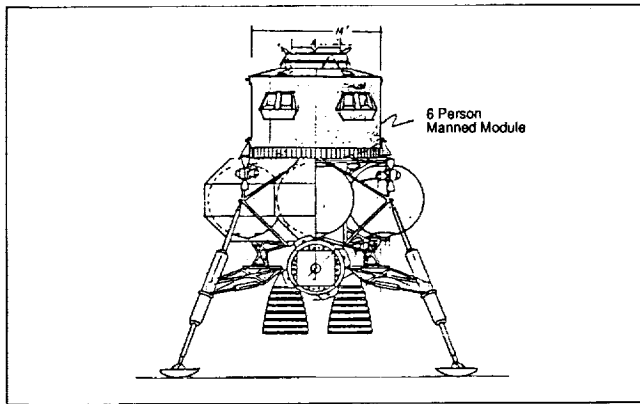


Fig. 1. Basic configuration of a lunar landing vehicle.

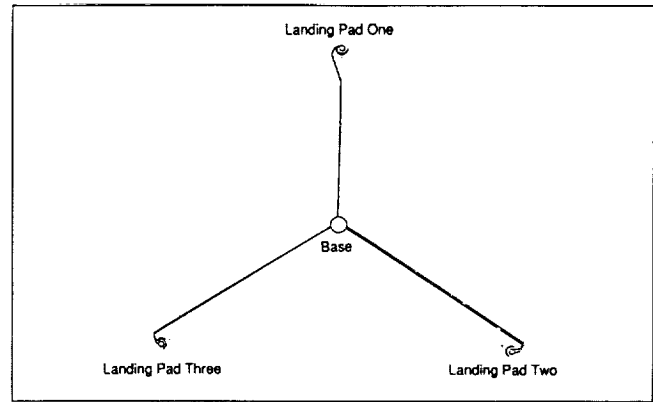


Fig. 2. Configuration of a lunar base

from this and similar reports. A large number of reports on base designs exist. The general layout varies a great deal from one report to the next, but the content and ideas are the same. The lunar bases previously designed exist across a broad spectrum, ranging from exposed rectangular structures to completely buried cylindrical structures. A typical design used for the servicing system project is one found in a second Eagle report (3). The basic structure is one of a series of cylindrical pressurized structures attached together (see Fig. 2) and partially buried under regolith.

The current examples of space transportation systems (STSs), or space shuttles, were extrapolated or used without modification for design parameters to consider during the synthesis of a lunar lander servicing system. The particular STS configuration considered dictates the aspects of any lunar surface design through limitations on geometry, mass, and safety issues.

Many examples of predicted designs for second-generation lunar surface vehicles exist. The basic operations are modified for operations pertaining to lunar lander servicing. The vehicles designed in this project take advantage of existing vehicles when possible, and involve heavy modification where necessary. A primary concern in the design of any lunar system is the commonality of both components and complete vehicles when necessary.

### Design Project Components

The Senior Aerospace Design Group project concentrates on the specific design of the servicing vehicle, various transport options for travel from the lunar base to the lunar lander, and the landing sites. The following vehicle and component designs are discussed in this report: servicer, heavy mover (tractor), large cargo/servicer trailer (including teleoperated crane), small servicer trailer, interface connections, and various modifications to existing equipment.

**Landing sites.** The landing sites are designated to be at a distance of 1000 m from the main central base structures, a restriction based on the blast damage caused by descending lunar landers (4). The lunar base has three separate landing pads that can have operations going on in any order. The landing sites are triangular, with the main base structures in the center

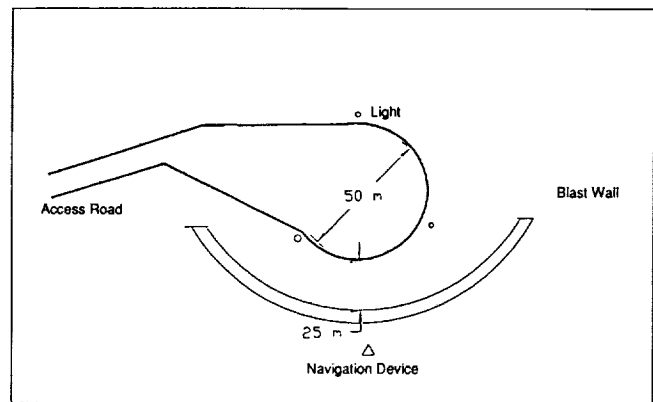


Fig. 3. Lunar base landing site layout.

(see Fig. 3). Graded regolith walls protect the lunar base and other landing pads from debris ejected upon landing. Graded travelways also connect the landing sites with the central base. A system of both electronic and visual landing aids would be present for aid in navigation to landing sites out of orbit.

**Servicer.** The servicer (see Fig. 4) is a stationary support vehicle placed next to the lunar lander while on the surface to provide basic functions of hydrogen reliquification, power supply, status communication, daytime cooling, and nighttime heating. The structure is a frame enclosing fuel cells, electronics, and spherical tanks. The exterior is covered with a rigid stand-off shield/thermal tile protection system. The upper surface consists of a fluid loop radiator for heat rejection of both fuel cell waste heat and waste heat from the lander during the day. Strip antennas are used for all communication with the base.

The loss of hydrogen fuel through boiloff due to heat conduction is generally not a large concern for short surface stay times. The boiloff becomes a real concern when the stay times are extended to 180 days, as is expected for third-phase lunar habitation. Simple calculations indicate that up to 50% of a lunar lander's liquid hydrogen can be lost to boiloff during

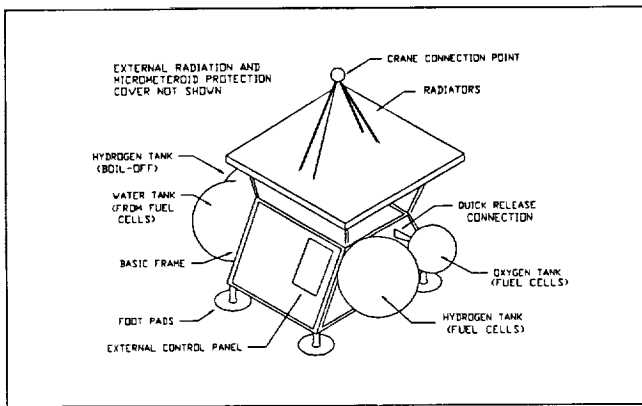


Fig. 4. Servicing vehicle for lunar lander.

a 180-day stay (2). This necessitates a system for storing H<sub>2</sub> boiloff and reliquifying it to pump back into the lander's tanks. The basic idea is to store the gaseous hydrogen that boils off during the hot lunar day in a large tank on the servicer. At nightfall the temperature drops to near absolute zero, allowing an extremely efficient helium cycle to be used to reliquify the hydrogen. The reliquified hydrogen would then be pumped back into the lander's tanks. Oxygen production is assumed during this time, making oxygen boiloff irrelevant, due to the availability of O<sub>2</sub> on the surface (5). Oxygen is also less susceptible to boil-off than hydrogen, due to its higher boiling point and lower heat conduction coefficient.

The power system for the lander would be designed for relatively short flight times, typically on the order of one hour. The additional system weight would be unwarranted for the 180-day stay times on the lunar surface. The servicer provides the additional power while the lander is on the surface, allowing the lander's power supply to be reserved for flight time only. The electronics and cooling system components would need power during the 180-day stay, along with controls testing to avoid seizing of components. The servicer fuel cell power supply would support the lander during the surface stay.

Communications would be provided through the servicer to the base concerning the status of both the servicer and the lander. This data would include all electrical and thermal aspects of both vehicles.

The additional daytime lander heat input from reflection from the lunar surface would require active heat rejection from the lander. The servicer would provide relief from this additional lander heat load by removing it through fluid loops to the servicer.

During the 14-day lunar night, the heat problem is completely reversed. The electronics and fluid loops of the lander must be kept in a state of readiness through heat input, otherwise the lander would cool down to the temperature of the lunar night. The electronics and fluid loops have to be kept warm in order to function at all, much less properly. The heat input from the servicer to the lander is through both electrical and fluid means.

A stand-off shield is necessary because of the increased probability of a meteorite impact during the 180-day stay time. Multilayer thermal tiles attached to the stand-off shields also provide protection from intense solar radiation on the servicer during the lunar day.

**Transport options.** The lander can deliver either cargo or personnel. When in cargo mode, the lander is assumed to be unmanned and is remotely piloted or computer guided. When in personnel delivery mode, the lander is expected to be piloted by a crew member. Each of these cases dictates different transport techniques upon landing. The simplified net result is that the lander is brought out to the landing site and cargo or personnel are retrieved to the base. Potentially confusing detailed descriptions of postlanding activities are described through diagrams and description in the following section. Alternative operations for some of the vehicles incorporated are also mentioned.

### LANDING SCENARIO

The scope of the Senior Aerospace Group design project can be demonstrated best through "cartoons" demonstrating the course of activities that are to take place at a lunar base after a lander descent. As mentioned above, there are two distinct scenarios for a lunar landing: cargo or personnel. Much of the equipment used in one case may be used in the other, with an emphasis on commonality and duality when possible.

Figure 5 depicts the course of operations at the base after an unmanned cargo lander has descended. Step 1 shows the prime mover vehicle towing the large cargo/servicer trailer out to the landing pad where the cargo lunar lander waits. The servicer can be seen on the trailer along with the cargo-moving teleoperated crane. Step 2 shows the servicer having been removed and the crane readying the removal of the cargo atop the lander. In Step 3, the cargo has been placed on the trailer.

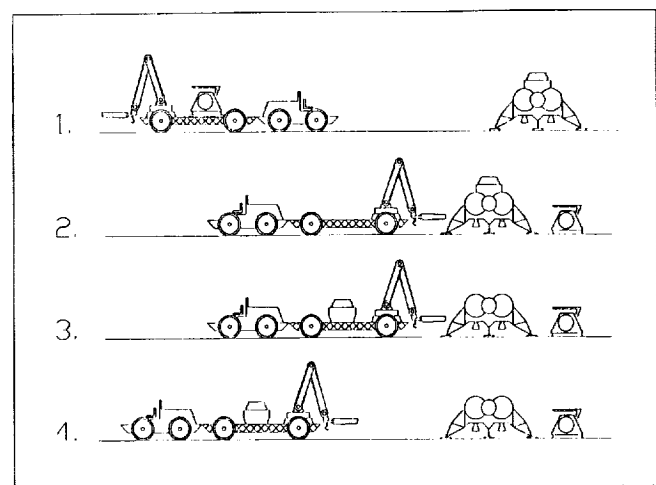


Fig. 5. Cargo mode post landing operations.

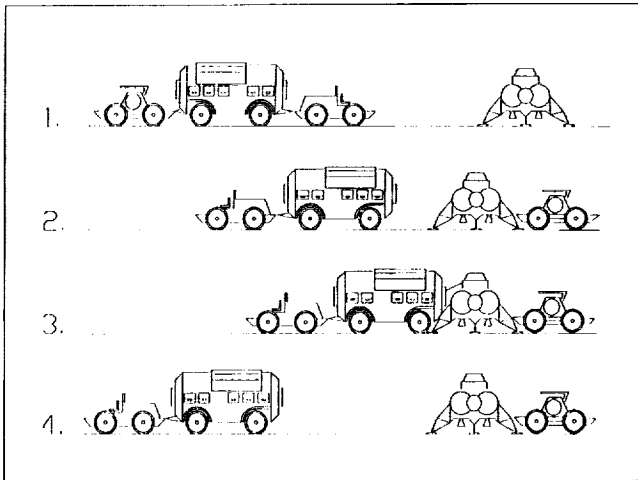


Fig. 6. Crew mode post landing operations.

by the teleoperated crane. Step 4 shows the prime mover vehicle towing the trailer with cargo back to the lunar base. It is possible that several trips may have to be made, depending on the size and weight of the cargo.

Figure 6 depicts operations after a human-piloted personnel lander has descended. Step 1 shows the prime mover towing a pressurized crew trailer out to the lander. The servicer can be seen atop a small trailer attached to the rear of the crew trailer. The trailer with the servicer is detached next to the lander, as shown in Step 2. Step 3 shows the crew trailer being attached to the crew hatch of the lander with personnel being evacuated. Step 4 shows the prime mover traveling back to the base. The crew trailer used in the personnel landing scenario is part of a pressurized long-distance exploration vehicle that would be present during a third-phase lunar inhabitation.

The crew trailer used in the personnel landing scenario would have its own drive system and steering, but would be controlled by the heavy mover via the power cart while on an exploration. Modifications or attachments would have to be made to the hatch on the rear of the crew trailer in order to attach directly to the lander. The crew trailer would already have been designed to mate with the base hatch system. This demonstrates a use of existing lunar equipment in the servicing project when possible.

In both landing scenarios, a crew in EVA suits will return to the landing site to finish connecting the servicer to the lander and to begin operations. A single or double EVA crew would return periodically to the site to perform maintenance activities and basic physical checks.

In both cases, the prime mover is piloted by a single EVA person. The existence of a teleoperated crane and EVA person on the same mission allows for parallel processing techniques to be used. While at the base, the crane is operated through IVA activities while the EVA person performs other activities.

There are several alternative operations for the prime mover vehicle used in the servicing activities. These include lunar soil mining and moving for oxygen production plants, base site construction, landing site construction and maintenance, and roadway grading. The large servicer/cargo trailer could also be used in some of these activities.

#### REFERENCES

1. Lunar Surface Operations Study, Eagle Engineering, *NASA Report N88-25415*, Dec 1, 1987.
2. *The Design of a Conceptual Lunar Lander*, Eagle Engineering, 1988.
3. *Conceptual Lunar Base Design*, Eagle Engineering, 1988.
4. Lunar Base Launch and Landing Facility Conceptual Design, Eagle Engineering, *NASA NAS9-17878*, March 25, 1988.
5. Briggs R. A. and Sacco A. Jr. Oxidation and Reduction of Ilmenite: Application to Oxygen Production on the Moon, Worcester Polytechnic Institute.

## 1990-91 PROJECT SUMMARIES

160594

P-2

## GEORGIA INSTITUTE OF TECHNOLOGY

**A LUNAR SURFACE VEHICLE MODEL**

To facilitate the future exploration and possible colonization of the Moon, a remotely operated vehicle is needed so that materials and supplies can be easily transported. This vehicle must be able to pick up a specified payload, transport it over the rough lunar surface, and then unload the payload at a desired location. We have designed a model of such a vehicle to permit the evaluation of its performance in an Earth environment. The layout of the model consists of a six-wheel drive, four-wheel steering, remote-radio-controlled vehicle.

The chassis design consists of an aluminum two-tier arrangement to provide adequate space for the components and systems of the vehicle. The lower tier contains the powertrain components while the upper tier contains the steering mechanism, the speed controller, and the payload lifting mechanism.

The vehicle's independent suspension uses a nylon fiber reinforced composite upper and lower control arm for each wheel and a plexiglass transverse leaf spring for each axle. The upper control arm contains a turn buckle to allow for camber adjustment of each wheel. The leaf spring is a simple design that has an adjustable spring rate.

The powertrain consists of a 20,000-rpm, 0.16-hp, DC motor powered by a 7.2-V, six-cell battery pack. The motor is controlled by a resistor-type speed controller with variable braking and reverse, and provides power to a 65:1 gear reduction unit that, in turn, powers three belt drives for the three differentials. The differentials are of a limited slip "ball" type used in model RC cars. This type of differential will allow better traction in loose soil. The differentials provide torque to the driveshafts, which are connected with universal joints at both ends.

The wheels for the vehicle are made of polystyrene foam for weight optimization and have an ellipsoidal shape. A custom, paddle-type tread design is epoxyed to the wheel before the outer surface of the wheel is dipped in a rubber compound to give a uniform coating. The ellipsoidal shape provides a large contact patch, which in sand gives maximum traction and also allows point contact on hard surfaces, which requires less steering force.

The steering system uses the Davis design, which allows for the correct turning angles of the inside and outside wheels such that each wheel has the same center of rotation giving no "scrub." A maximum inside wheel turning angle of 30° requires an outside wheel turning angle of 16°. These angles provide for a small turning radius of 23.3 in. The design uses a linear servo-controlled moving slider bar connecting two slotted members, one for each wheel. The movement of the slider bar causes the slotted members to rotate through different

angles of rotation giving the necessary wheel angles. The vehicle design uses four-bar linkage to connect the rear steering angle with the front steering angle with the aid of two spur gears to change the angle of rotation from rear to front.

The payload is an aluminum spool with a mass of 0.5 kg. The bottom lip of the spool contains more mass than the upper lip to prevent it from being tipped over easily. The lift mechanism consists of a chassis-mounted track, a sled that slides along the track, a pair of forks hinged to the front of the sled, a servo mounted to the chassis underneath the track, and a lifting arm mounted to the servo. The arm is connected to the forks through a cable; the end of this cable slides on the arm to prevent binding. The lift operates by approaching the payload with the sled in its lowest position with forks extended. After the payload is positioned within the forks, the lift arm, riding in a vertical slot through the center of the sled, pulls the forks into a vertical position so that the payload then rests within a round depression in the face of the sled. At this point, the lift arm makes contact with the end of the slot. A roller is mounted at the point of contact to minimize friction. The lift arm now pushes the sled up along the track, to a horizontal position behind the front wheels. The payload is held by gravity within the depression in the top of the sled. To unload the payload, the lift arm pushes the sled back down the track, then lowers the forks down to vertical position such that the payload is resting on the ground. The vehicle then backs away from the payload.

**LUNAR LOADER/TRANSPORTER**

With the increasing possibility of inhabiting the Moon, researchers are exploring feasible modes of lunar transportation. This paper researches one such transportation vehicle. The lifting mechanism offers several degrees of freedom. The additional degrees of freedom assist the operator in the loading and unloading of cargo in most regions of the Moon terrain. The vehicle's tires and body were both designed to efficiently operate on the Moon's rocky surface. The lunar transporter, specified within, may offer researchers some answers and incentives for future space exploration.

**TRENCHING AND CABLE-LAYING DEVICE  
FOR THE LUNAR SURFACE**

This paper details the design of a trenching and cable-laying machine for use on the Moon. Lunar bases will require exterior cables for power and communication. Burying these cables 1 m below the lunar surface shields the cables from radiation, meteorites, and surface traffic. The cable-laying device described

in the paper excavates a narrow trench 1 m in depth and lays a cable (2.5 cm maximum diameter) over a distance of 1 km. The trench is formed by a vibratory dual-plow system. The first plow digs a trench 0.5 m in depth and 10 cm wide, and the second plow deepens the trench to a depth of 1 m and width of 5 cm. The two-pass configuration of the plow greatly reduces the draw-bar force of the plowing action. Additionally, each plow blade is vibrated to further decrease the force needed to shear the soil. The drive system for the cable-laying plow consists of an auger mechanism. The auger drive system overcomes the traction problems associated with plowing in the low-gravity environment of the Moon. Since the traction is not gained through the weight of the vehicle itself, pulling the plow by the auger allows the cable-laying machine to remain small and light-weight.

#### **A LUNAR VEHICLE SYSTEM FOR HABITAT TRANSPORT AND PLACEMENT**

This paper addresses the need for a piece of machinery to unload, transport, and place a lunar habitat on the Moon's surface. Since NASA intends to carry out mining operations, as well as prepare the Moon for future colonization, habitats are needed to accommodate the astronauts on the extended lunar missions. Therefore, NASA must find a way to relocate these habitats once they are delivered to the Moon by a lunar lander. The design solution recommended by this paper is the use of two track vehicles containing scissors-lifts with cradles located on top. Each vehicle will be aligned under one end of the habitat. The scissors-lift will extend and the cradle will be adjusted to line up with the coupling neck of the habitat. Each scissors-cradle

mechanism will extend to a height in excess of 10 m to lift the habitat off the lander. The vehicles will be turned parallel to one another and moved until the habitat is clear of the lander. The scissors-cradle mechanism will then collapse, and the vehicles will be aligned and driven to the desired habitat location. At this point the scissors-cradle mechanism will fully compress to a vehicle height of 2.5 m, placing the habitat on the lunar surface. The vehicle will then drive out from under the habitat. This design solution takes into account power requirements, torque requirements, and the dimensions of the lander and shuttle bay.

#### **LUNAR STORAGE FACILITY**

Before the construction of a manned lunar base can begin, a storage facility must be set up. The purpose of this facility will be to store electronic equipment and small containers of other miscellaneous equipment, while protecting it from radiation. The goal of this project was to assess the need and then to find the optimal design by considering many performance objectives and constraints.

The proposed lunar storage facility is self-erecting, uses material (regolith) from the lunar surface, and can store objects of variable geometry, up to 3 m high. During shipment in the space shuttle cargo bay, the shed will be reduced to a basic cylinder shape whose outer dimensions will be 4 m in diameter by 15 m in length. Set-up of this shed will consist mainly of releasing a locking mechanism, after which the release of potential energy will cause the shed to erect itself. Radiation protection will be provided by filling an outer bladder with 2 m of regolith using a regolith slinging mechanism.

1990-91 PROJECT SUMMARIES

GEORGIA INSTITUTE OF TECHNOLOGY

S19-12  
160595  
P-4

Georgia Tech's School of Textile & Fiber Engineering and School of Mechanical Engineering participated in four cooperative design efforts this year. One group designed a thermal shield for a lunar telescope. The second group designed a selenotextile habitat shielding structure. The third group designed a pneumatically assisted elbow joint for the NASA zero-prebreathe suit (ZPS). The final group designed an electromechanical system to power an astronaut's finger joints. Following are summaries of these projects.

DESIGN OF A THERMAL SHIELD FOR A LUNAR TELESCOPE

The goal of this project was to design a shield to provide thermal protection for a lunar telescope. This design was required to meet specific objectives, including the ability to (1) retract during nighttime viewing; (2) close during lunar day; (3) reflect infrared radiation; (4) minimize temperature fluctuations; (5) cover the entire telescope; and (6) last 30 years.

In addition, the design was subject to a number of constraints related to lunar conditions and shuttle cargo space; some of these include (1) 50-man-hour assembly time; (2) launch mass  $\leq 4000$  kg; (3) transport length  $\leq 27$  m; (4) transport diameter  $\leq 7$  m; (5) efficacy within lunar temperature range; (6) tolerance of vacuum; and (7) tolerance of severe solar radiation ( $\beta$  and UV).

The final design has been dubbed "The Rising Cylinder." The proposed structure will consist of two concentric cylinders 9.75 m high and a 10-m-high third cylinder that will carry the cover. Figures 1 and 2 are schematics of the structure in the open and closed positions, respectively. The top two cylinders will be lifted into place using a bootstrap reeving system located in the support members of the cylinders. The cover will consist of two disk halves that open and close using a rack and motor system.

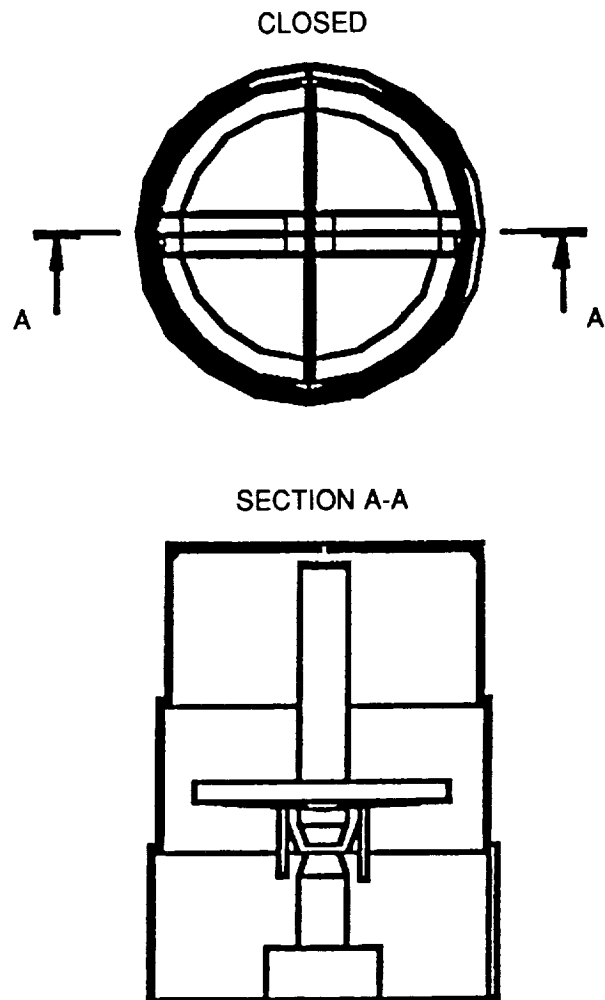
The primary thermal protection system will be gold-coated fiberglass woven fabric attached to the support frame. Specifications of this fabric are as follows: (1) 5.5 tex continuous filament fiberglass yarn; (2) 22 ends/cm; (3) 22 picks/cm; (4) plain weave; and (5) coated weight 194 g/m<sup>2</sup>.

Gold will be vacuum deposited onto a polyester film that will then be adhesively bonded to both sides of the fiberglass substrate. The purpose of this double-sided coating is to prevent "curling" caused by the differential between thermal properties of the coating and substrate. Gold was selected because of its reflectivity and because it does not oxidize.

This design has many advantages. The rigid structure will prevent folding and abrasion of the fabric. The structure will completely enclose the telescope, and the lifting mechanism technology already exists. There are, however, some disadvantages to this design. Opening and closing of the cover will be clumsy, and supporting the open cover will be difficult.

When the shield is closed, the telescope will be vertically positioned. When the shield is opened, the telescope can move

away from the vertical position by a maximum of 15° (see Fig. 2). The proposed shield is designed to have a lifetime of 30 years with a two-year maintenance schedule.



NOTE: GOLD PLATED FIBERGLASS REMOVED

Fig. 1. Schematic of Closed Lunar Telescope Shield.

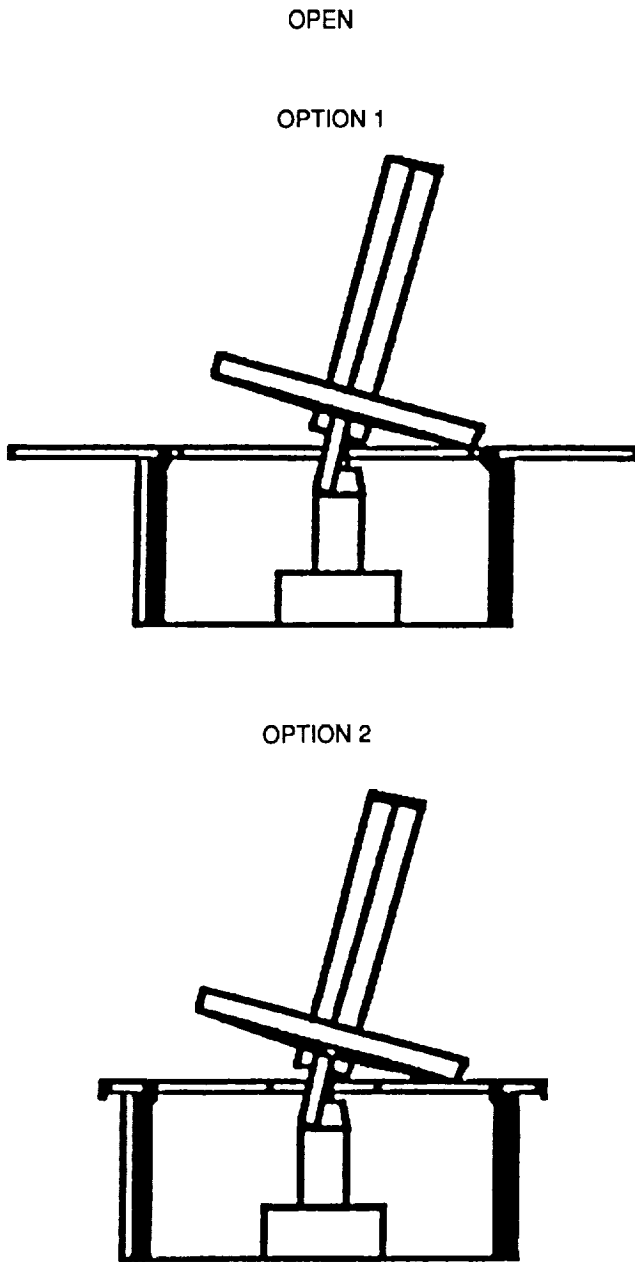


Fig. 2. Schematic of Open Lunar Telescope Shield.

**Selenotextile Shielding Structure**

The objective of this study was to design a structure to protect a lunar habitat from intense solar radiation. Included in the design is equipment for construction of the structure. The proposed protective structure is designed to withstand the extreme conditions of the lunar environment and to provide a 2-m maintenance space around the habitat. The construction equipment is designed to operate on less than 13 hp. Packaged, the structure and construction equipment will fit into a space shuttle cargo bay.

The shielding structure will be 26 m in length, 12 m in width, and 9.5 m in height. The structure will consist of 26 tubes, rectangular in cross section (1.5 m × 1.0 m), leaned like horseshoes at a 45° angle against a bank of regolith (see Fig. 3).

The individual tubes will be made of woven polytetrafluoroethylene (PTFE)-coated fiberglass fabric. Fabric specifications include (1) plain weave; (2) 22 ends/cm; (3) 25 picks/cm; and a (4) coated weight 240 g/m<sup>2</sup>.

Fabric sections (from which the tubes will be made) will be heat-sealed together to form airtight seams and thus prevent escape of regolith from the filled tubes. Each tube will have a top opening supported by a fiberglass hoop. Individual tubes will also be connected with an airtight joint to form the final structure.

The textile structure will be held in shape prior to and during filling by an interior cavity filled with compressed gas. Regolith will be supplied to the structure via the fiberglass hoops and a conveyor system. The primary conveyor system will be supported by a series of telescoping legs and will be fed regolith by a second conveyor resting on the support mound. The conveyors are shown in Fig. 4.

**Pneumatically Assisted Elbow Joint Design for the NASA Zero-Prebreathe Suit**

In the near future it is expected that NASA will establish a lunar colony. To assemble and operate this lunar base it will be necessary for astronauts to spend a significant amount of time working outside the base. The existing procedure for adjustment from cabin pressure to suit pressure takes 13 hours and 30 minutes. The proposed suit design will allow astronauts to make the transition from a high-pressure internal environment to a lower-pressure suit without spending time in an air lock. This suit, the Zero-Prebreathe Suit (ZPS), is pressurized to 57

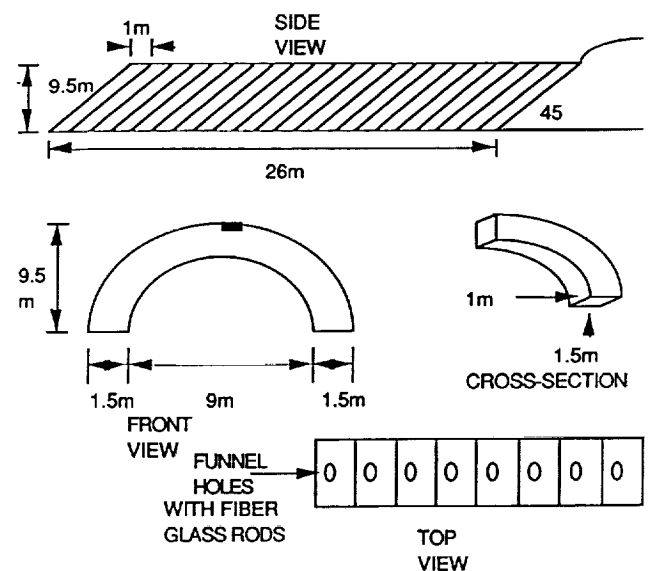


Fig. 3. Structure Schematic.

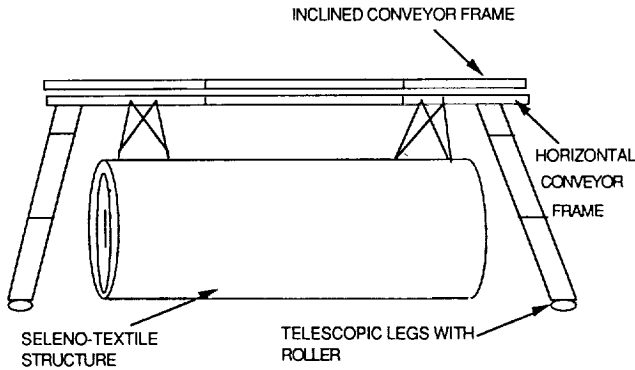


Fig. 4. Conveyor Structure.

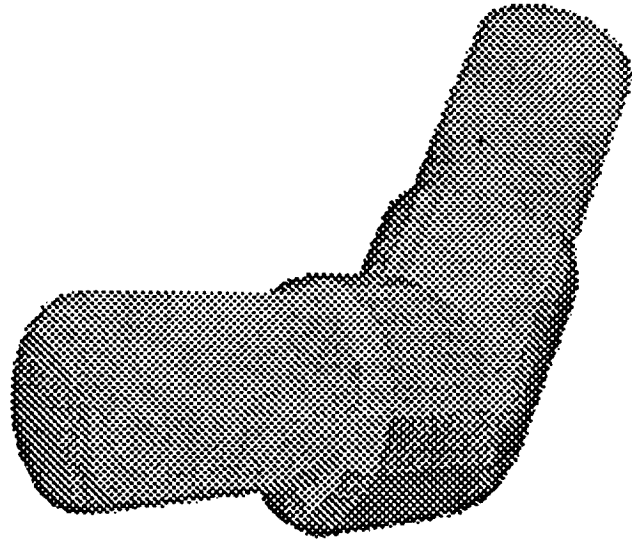


Fig. 5. Rendering of Elbow.

kPa, compared to the current shuttle suit, which is pressurized to 29 kPa, and the shuttle's atmosphere, which is pressurized to 101 kPa.

The current ZPS design uses a toroidal joint to provide flexibility and has a bending resistance of 3.0 Nm. When used with a micrometeoroid shield, the resistance to bending increases to 5.4 Nm. This resistance, in conjunction with deconditioning caused by prolonged exposure to low gravity or weightless conditions, accelerates the onset of fatigue and can artificially limit the amount of work that an astronaut can do. The proposed design will counteract the resistant forces to regain some lost work time and to help optimize the astronauts' performance.

The assist mechanism to overcome the resistance of the elbow joint uses an inflatable structure that deforms asymmetrically to match the path that the elbow travels through. A rendering of the proposed solution to the problem of overcoming the resistance of the ZPS suit is shown in Fig. 5. Figure 6 shows sectional views of the design. The components of the assist mechanism are shown in Fig. 6. The expansion pattern is shown in Fig. 7. The outer edge is exposed to a very high deformation, with approximately a 120% change in length. The inner edge expansion is relatively smaller, with a total elongation of approximately 70%. Note that the total angular rotation is 130°, as specified by NASA requirements. The upper sealing joint must be able to accommodate 15° of angular rotation. The proposed design meets this requirement by being compatible with the existing joint. Note that a 0.635-cm ring thickness has been included in the sealing joint design to accommodate any later adaptation of the design. Similarly, the lower sealing joint must accommodate 180° of rotation.

The total cross-sectional area of the structure is approximately 7.9 cm<sup>2</sup>. The area is approximate because the segmented form has an area that varies slightly between the large and small diameters. The torque exerted by the structure is constant at 5.4 N because the ends of the structure occur at the large diameter.

The assist mechanism is made from a plain woven polyester fabric cut with a saw-tooth pattern. In order to make the chamber deform, as shown in Fig. 7, filling yarns of varying linear densities should be used to weave the fabric. Fine filling yarn should

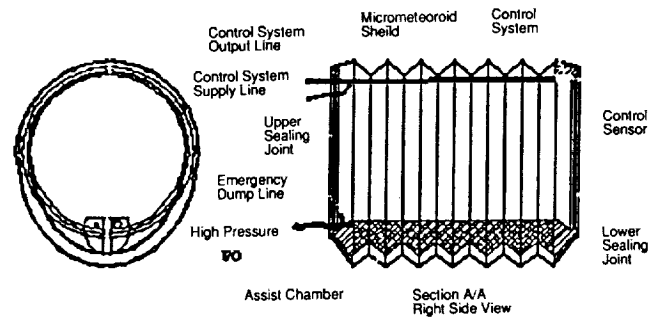


Fig. 6. Cross-Sectional View.

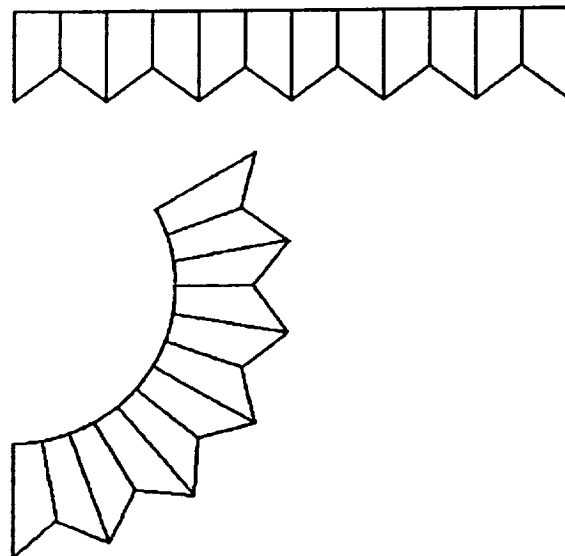


Fig. 7. Deformation Pattern.

be inserted for flexibility (and chamber elongation) along the outer side of the fabric pattern, and coarser filling yarn is used to weave stiffer fabric along the inner axis of the fabric pattern. When the fabric is folded and assembled, the fine yarns meet at the saw-tooth seam, where greater elongation takes place. The chamber should be assembled to achieve the necessary response of the chamber upon inflation.

Fabric specifications are (1) plain weave; (2) 14 ends/cm; (3) approximately 14 picks/cm; and a (4) nominal yarn diameter of 0.013 cm.

The finished, cut fabric should be impregnated with urethane before assembly of the structure.

This joint is designed to be incorporated with the NASA ZPS and to have a lifetime equal to that of the ZPS.

### Electromechanical System to Power Assist in Astronaut's Finger Joints

The proposed design is an electromechanical system to power-assist the movement of an astronaut's distal and proximal interphalangeal finger joints. Figure 8 shows these joints and their desired range of motion. The objectives of this project were to reduce astronaut fatigue and provide greater ease of movement.

The design was subject to a number of constraints, including the need to (1) allow 90° range of motion at proximal interphalangeal joint; (2) allow 45° range of motion at distal interphalangeal joint; (3) compensate for 75% of suit's bending resistance; (4) integrate with current suit; (5) weigh  $\leq 5$  lbs/arm; (6) not generate excessive heat; (7) require little or no maintenance; (8) have a lifetime comparable to that of a suit; and (9) not hinder hand operation in event of failure.

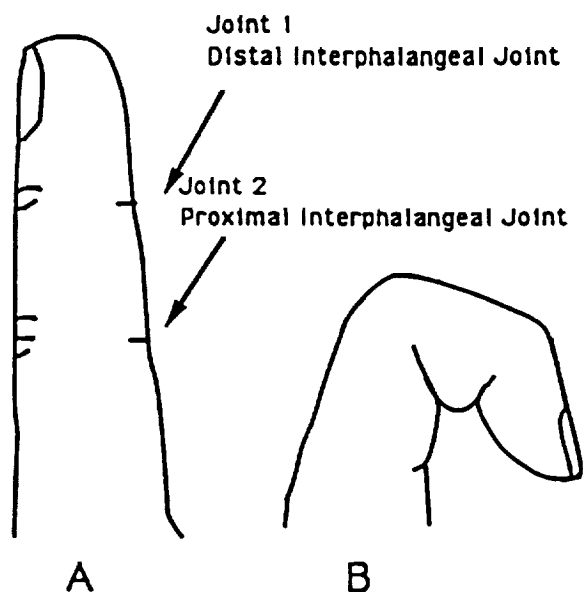


Fig. 8. Range of Motion Desired in Electromechanical System.

The approach taken is called the "Stacked Triangle" method. It includes design and selection of a force sensing system, electromechanical actuator, glove finger bending mechanism, actuator controls, and materials for the bending mechanism and motor mount construction. Figure 9 is a rendering of the design. The force sensing system will consist of a polyvinylidene fluoride (PVDF) piezoelectric pressure-sensing grid, which will relay electrical voltage to an amplifier per unit of force. The proposed electromechanical actuator is an advanced linear electric motor with a rare-earth magnetic core. The linear motor will move the finger apparatus by displacing a Kevlar cable. This cable will force the aluminum structure to actuate due to off-center force-derived moments about the distal and proximal interphalangeal joints. The automatic controls for the system will consist of sensor, amplifier, and motor transfer functions. The feedback loop will consist of an adjustable feedback gain. The entire system will be incorporated into the spacesuit between two Teflon-coated textile layers. All components will be integrated into the suit with appropriate textile materials.

The electromechanical system will overcome the suit's bending resistance and provide force to achieve a range of motion of 45° for the distal interphalangeal joint and 90° for the proximal interphalangeal joint. Required operations will be power assisted as necessary. The system is designed to have a lifetime comparable to that of the spacesuit.

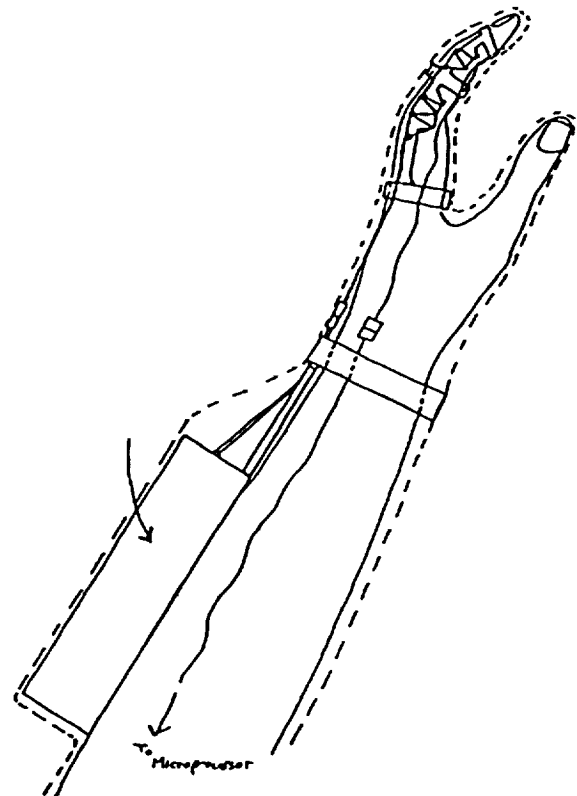


Fig. 9. Artist's Rendering of Electromechanical System.

**SOLAR ENERGY EMPLACEMENT DEVELOPER**

UNIVERSITY OF HOUSTON

S2044  
160596  
P. 6

A preliminary design has been developed for a Lunar Power System (LPS) composed of photovoltaic arrays and microwave reflectors fabricated from lunar materials. The LPS will collect solar energy on the surface of the Moon, transform it into microwave energy, and beam it back to Earth where it will be converted into usable energy.

The Solar Energy Emplacement Developer (SEED) proposed in this report will use a similar sort of solar energy collection and dispersment to power the systems that will construct the LPS.

**INTRODUCTION**

As we near the 21st century a critical need for alternate power sources becomes more and more apparent. Reliance on primary fossil fuel and nuclear sources in use today subject us and our planet to dangerous consequences including pollution and radioactive waste materials. Solar energy is an alternative that is clean and free, except for the cost of developing the technology and the initial setup of equipment. Solar energy can be collected from any point where the sun is visible, opening the possibility for off-world collection. This possibility will be most feasible if the equipment can be fabricated using materials gathered and processed on the Moon or other planets. All of the component substances necessary for production of solar power facilities exist in the resources of the Moon.

This paper proposes a design for a mobile facility to process lunar materials and construct these necessary components. The system will also use solar energy for component fabrication and operation power.

In 1968 Peter Glaser introduced the concept of using satellites to collect power and transmit it back to earth in the form of microwaves<sup>(1)</sup>. Since this innovative idea was introduced, many other related concepts have been proposed that use power-beaming to support lunar operations and send power back to the Earth from lunar-based arrays. This project applies some of these ideas and introduces new elements into a comprehensive design.

**LUNAR POWER SYSTEM**

The Lunar Power System (LPS), described in a 1990 study by David Criswell at the University of Houston, makes use of solar energy gathered on the surface of the Moon as an alternate power source for the future<sup>(2)</sup>. In its simplest form, the LPS is comprised of four components: Moon-based photovoltaics; microwave reflectors; microwave converters; and Earth-based rectifying antennae. It is constructed using silicon and iron which are common in the lunar soil. Solar arrays are set into a triangular arch shape and placed on the surface of the Moon in parallel rows. These rows of photovoltaics form plots connected to one another by underground wires that lead to a microwave converter box, where electrical energy is transformed into microwave energy and beamed back to Earth.

Silicon will also be used to form glass tubing utilized as structural support for microwave reflectors. The overall system, once on-line, consists of thousands of plots spread over the surface of the Moon. These plots can be located along the lunar limbs to collect sunlight over a 28-day period.

Reflectors can also be placed in orbit around the Moon and Earth. Around the Moon, the reflectors would serve to illuminate the surface during periods of darkness to eliminate power loss. Around the Earth, reflectors will redirect the beams of microwave energy during periods when the plots are not directly on line with the point of reception, enabling power to be transmitted continuously<sup>(3)</sup>.

**SEED SCENARIO**

The Solar Energy Emplacement Developer (SEED) is a set of components which, in the most basic form, use solar energy to accomplish lunar site work. The overall purpose of the SEED is to completely emplace the LPS. The first step in this emplace is to deliver the SEED elements to LEO by a heavy lift launch system. The components are then manifested into a lunar lander containing two habitat modules, two processing modules, a command/control unit, an escape vehicle, and eight rovers described in Table 1<sup>(4,5)</sup>. The lander is essentially a frame designed to serve multiple functions (Fig. 1). After landing, for example, it can be disassembled and reconfigured to provide a support structure for lunar regolith. Regolith will be used to cover the habitation modules for radiation protection.

The flight-ready lunar lander would be set on a trajectory for an equatorial landing on the Moon. Once the lander nears lunar orbit, solar sails are released and deployed. After deployment of the sails, the lander is automatically guided to an optimum landing site. The rovers then transfer themselves to the surface. Next, the lander is separated into three segments, two of which contain a habitation and processing module and the third, the command/control unit. Upon completion of the separation, the two segments containing modules are loaded onto the rovers. This completed, the components necessary for two LPS operational units are transported to their respective construction sites. The command/control unit is left behind as a communication depot and also serves as a safe haven and emergency takeoff site.

TABLE 1. Element Summary.

| No.                 | Element   | Power req. (kW <sub>c</sub> ) |       | Mass (T) | Volume (m <sup>3</sup> ) |
|---------------------|---|-------------------------------|-------|----------|--------------------------|
|                     |   | Day                           | Night |          |                          |
| 8                   | Rovers  | 20                            | 20    | 2.5      | 17.58                    |
| 2                   | Habitat Modules   | 40                            | 20    | 14.0     | 200.00                   |
| 2                   | Processing Modules  | 40                            | 40    | 14.0     | 200.00                   |
| 1                   | Unpressurized Rover   | 4                             | 20    | 1.7      | 15.0                     |
| 1                   | Command Module  | 40                            | 20    | 9.0      | 128.00                   |
| 1                   | Escape Vehicle  |                               |       | 3.5      | 30.00                    |
| Total               |   | 144                           | 120   | 90.2     | 590.58                   |
| Elements            | Description   |                               |       |          |                          |
| Rover               | Loads and unloads lunar regolith at the processing module. The rover's hopper (17.58 m <sup>3</sup> ) is capable of transporting 2.93 lunar metric tons of regolith. At 3.2 km/hr, the rover gathers 17.58 m <sup>3</sup> of regolith over a distance of .369 kilometers approximately ten minutes. |                               |       |          |                          |
| Habitat Modules     | Provides safe accommodations for a crew of two for 365 days.  |                               |       |          |                          |
| Processing Module   | Provides full production capability of solar arrays.  |                               |       |          |                          |
| Unpressurized Rover | Provides means of local transportation.   |                               |       |          |                          |
| Command Module      | Provides safe accommodations for a crew of two for 365 days. It provides a central facility to regulate base communications.  |                               |       |          |                          |
| Escape Vehicle      | Provides the capability to transport a crew of six to lunar orbit in the event of an emergency.   |                               |       |          |                          |
| Truss               | The space frame provides stability during lunar landing. The frame also can be disassembled and reassembled into different configurations.  |                               |       |          |                          |

After the habitation modules and the processing plants are placed on the surface at each LPS site, the rovers begin gathering regolith for processing. Rovers at each site deliver material to be processed and take the finished products and place them in an orderly fashion around the plot. When the process is completed at a site, the habitation module and processing plant are reconnected and transported by the rovers to begin construction at the next site.

The SEED project is based on several important assumptions: (1) a heavy lift launch vehicle will be necessary to carry all components to LEO and (2) extensive terrain mapping has been performed on the surface of the Moon to survey candidate sites. Implementation will also require advanced automation and robotic systems with a high degree of reliability. Finally, power beaming, which is still in its infancy, must be advanced to a point that transmitters and receivers can be sufficiently miniaturized to fit into small mobile units.

### SOLAR SAILS

The solar sails proposed for this design are helio-gyro configuration (Fig. 2). This configuration is chosen because of its high degree of maneuverability and failure resilience<sup>(6)</sup>. The sails are used to perform many functions during the construction and operations phase of the LPS.

During the construction phase, at least three sails would be in orbit around the Moon. These would be used to collect and beam power to the SEED components. With three sails in orbit, spaced equally distant from one another, contact with the entire surface of the Moon can be maintained<sup>(1)</sup>.

During the operations phase of the LPS, the sails will serve to illuminate the surface of the Moon where plots are located. To achieve this reflectivity, the sails would be fabricated with an aluminum thin-membrane surface. Also, the reflective area of the sails must be equivalent to the area being illuminated. Similar versions of the sail would also be in orbit around the Earth to reflect microwave beams to receiving antennae.

### ROVERS

The rovers are the workhorses of the SEED project (Fig. 3). Each rover is proposed to be approximately 2.5 m × 5 m × 2 m with a weight of approximately 2.5 metric tons and a carrying capacity of 3 lunar metric tons of regolith. The functions of the rover include transportation, material collection, and LPS assembly.

After the rovers transport the habitation modules and processing modules to their selected sites, they must disassemble the frame that supports the modules and reassemble it as shielding over the habitation module. Regolith will be placed on top of the frame to provide radiation protection (Fig. 4).

Next, the rovers begin collecting regolith for processing by deploying a drum device that loosens the regolith and places it on a conveyor system. After sufficient raw material has been collected, the regolith is taken to the processing module where it is unloaded. When processing is complete, the finished solar arrays are placed onto the back of the rover for positioning on the surface of the Moon.

The last step entails assembly of the LPS plot. Arrays are placed on the surface by angling the bed of the rover so that the "heel"

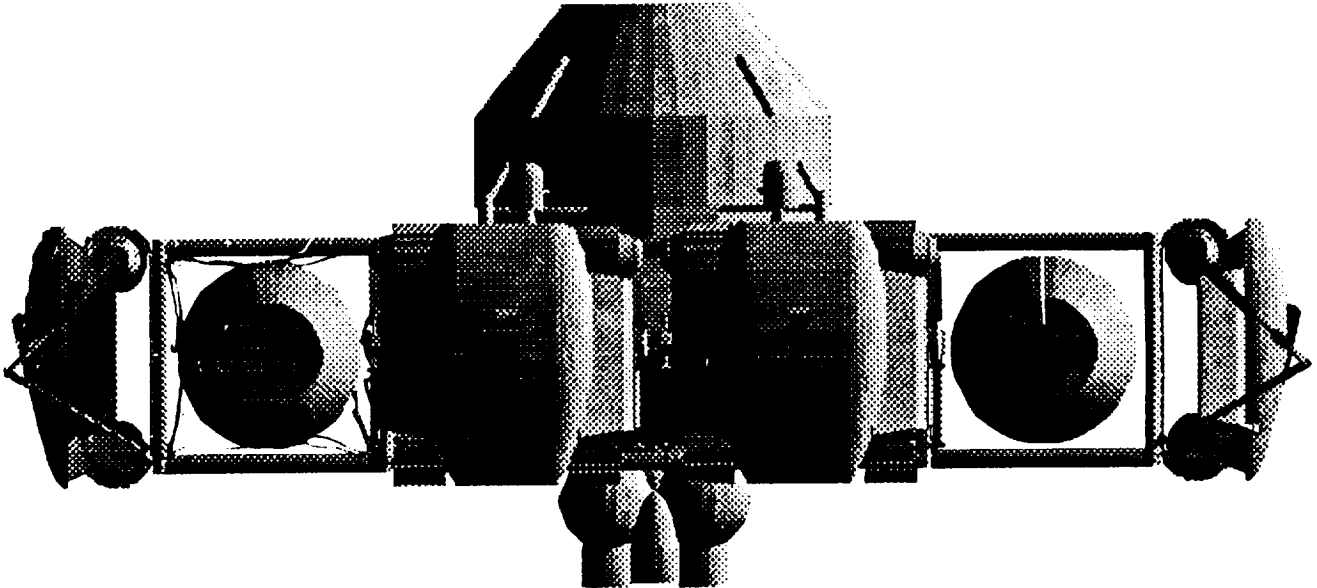


Fig. 1. Lander Configuration.

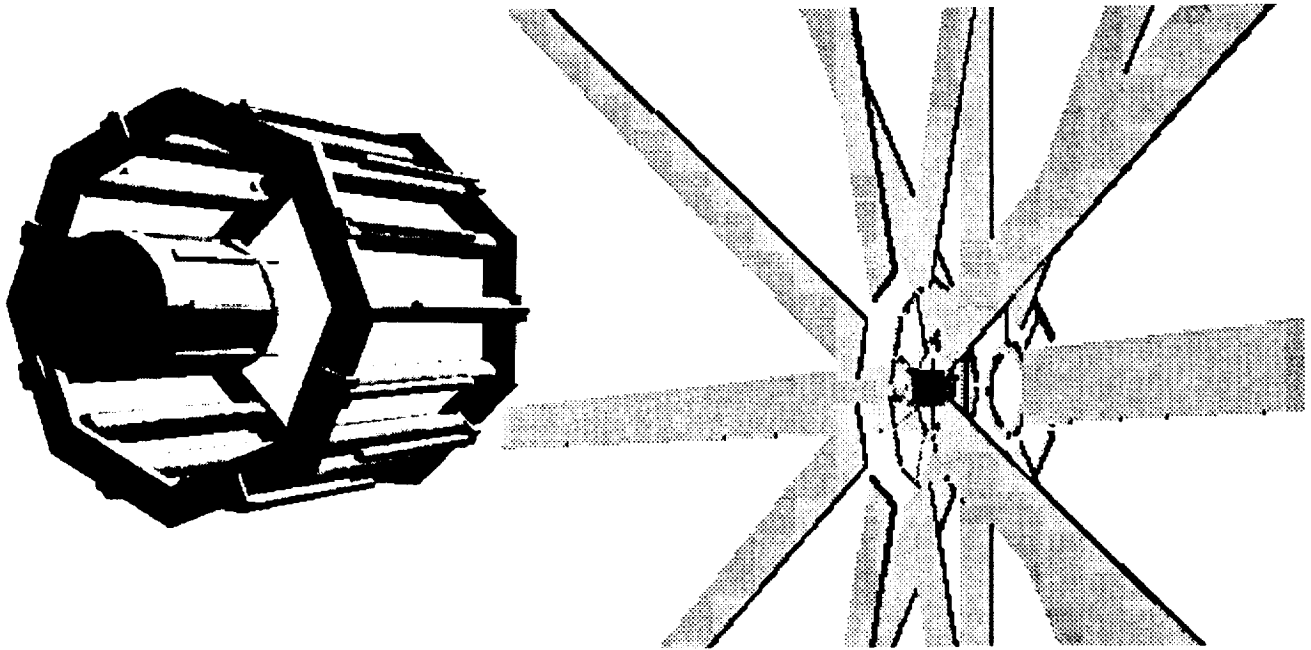


Fig. 2. Solar Sails.

ORIGINAL PAGE  
BLACK AND WHITE PHOTOGRAPH

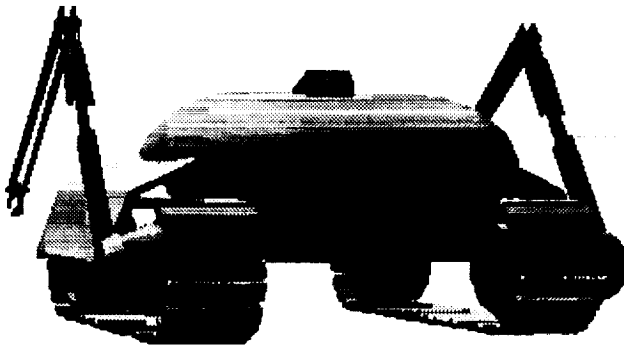


Fig. 3. Rover.

of the arrays is only a few inches from the surface. A manipulating arm then places the "heel" of the arrays, now located on top, onto the surface of the Moon. The rover then moves forward, leaving the array to slide into place. When the end of one set of arrays is reached, the set located directly beneath it is connected by the ends to the previous set. This process continues until the complete set of arrays and reflectors have been deployed. On completion of this operation, the rover moves to a new area and begins collection of regolith.

The rovers can be reconfigured in different ways, according to the functions they are serving. During the collection phase, the bed of the rovers can be completely closed to keep lunar dust from escaping. During the assembly phase, the cover of the rover can be opened to increase the cargo carrying length of the bed and provide a platform for the completed solar arrays.

The power requirements of each rover are estimated at approximately 20 kW based on previous models. This power would drive one motor per track and one motor for the conveyor system to move material in and out of the rover's storage.

### COMMAND/CONTROL UNIT

The command/control unit provides surface-to-surface communications for extra vehicular activity, rovers, habitat modules, and processing modules. The unit is designed to support a crew of two in a vertical, stacked configuration unlike the horizontal configuration of space-station-type modules. A lower unit (6.7 m diameter and 3.6 m high), contains a health maintenance facility, waste management facility, galley, wardroom, storage, crew quarters, environmental control, and life support systems. An escape vehicle is located on top of the command/control unit with accommodations for a crew of six in the event of an emergency.

### HABITATION MODULES

These aluminum modules are based on approximate space-station module dimensions. The modules provide an airlock and dust-off facility and are outfitted with equipment and supplies to support a crew of two for a duration of 365 days. During this stay, the crew would conduct local geologic investigations, undertake experiments in mining the lunar soil, and service and maintain equipment. Each habitation module provides a health maintenance facility, waste management facility, galley, wardroom, laboratory, storage, crew quarters, and environmental control and life support systems.

### PROCESSING MODULES

The LPS is a potential solar energy conversion system for terrestrial use. Processing modules support a manufacturing process sequence for the production of the LPS components. The primary function of these modules is to produce photovoltaics, glass fibers, and foamed tubular glass. The process will be expected to operate continuously during the construction of the LPS plots.

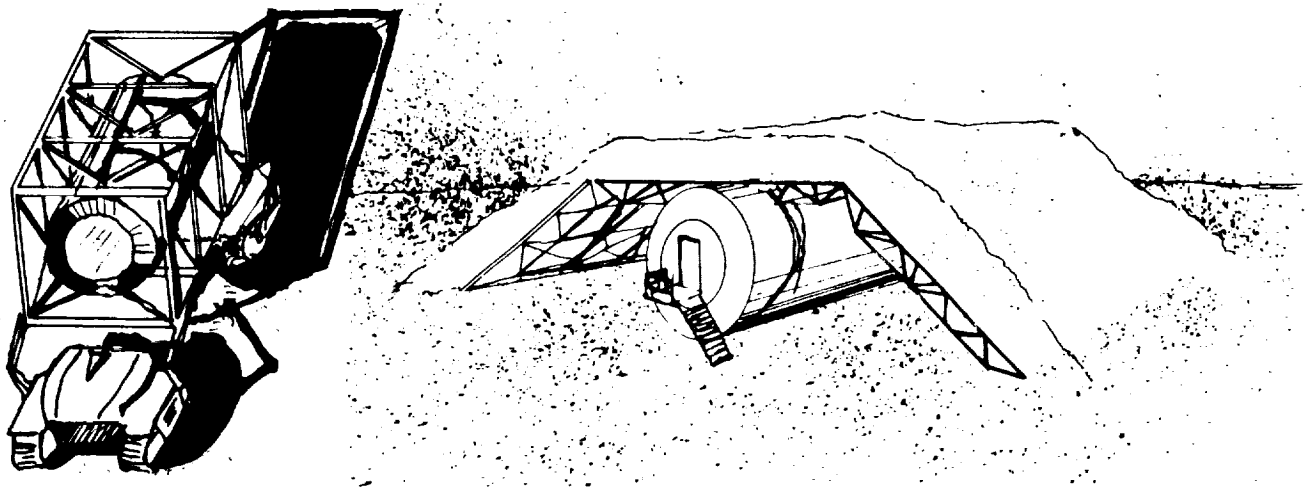


Fig. 4. Module disassembly and habitat shielding.

In order for the production to proceed effectively, the environment under investigation must produce solar cells with the capability to withstand thermal cycling, reduce the percentage of cell degradation, and produce high-strength structural components. Silicon was selected for the solar cells because of its abundance in the lunar regolith. These solar cells are ultra thin, moderate-efficiency cells.

The following steps are necessary for the production of the silicon cells. Lunar regolith will be unloaded at the processing module where materials needed for solar cell production are separated and extracted within the module. Silicon is then separated and purified to a degree appropriate for producing the solar cells. After being heated, the molten silicon is cooled to form a triangular arch. Due to the absence of moisture in the lunar environment, the strength of silicon may be as high as several million psi allowing the triangular arch structure to be self supporting. Iron is magnetically extracted from regolith and applied to the surface of the solar cell. The solar arrays are then cut to the appropriate length. Measurements will vary depending upon the location of assembly. Upon completion, the solar arrays are transported by rovers to a specified location and interconnected with a wire buried approximately 10 centimeters below the lunar surface. Buried wire avoids stresses on the interconnecting system caused by extreme temperature variations from the lunar day/night cycles<sup>(2)</sup>. The wires are then attached to a microwave transmitter that will convert the solar energy into microwaves. This system is assembled so that in the event of photovoltaic cell damage, remaining undamaged cells continue to generate power.

For the solar arrays to maintain efficiency during solar collection, accumulation and adhesion of lunar dust to equipment experienced in Apollo missions, must be eliminated. Lunar dust supports an electrostatic charge under ultraviolet irradiation<sup>(7)</sup>. A solution may be to form solar arrays with the same charge on the surface as the charge of the dust, causing the dust to be repelled.

Silicon is also used in the production of glass tubing and glass fibers for the construction of reflectors. Glass tubing will serve as structural support for glass fibers covered with a reflective aluminum surface and woven into a cross-grid of strands placed at intervals of 10 cm. The grid will allow light to pass through to the solar arrays and at the same time reflect microwaves toward Earth. Setup of the reflectors as well as the arrays is performed by the manipulating arms of the rovers.

#### SITE SELECTION

The site is best located in a relatively flat area, away from major surface variations such as craters. The total surface area proposed for this example is an ellipse measuring 16.25 km by 105.6 km. The reflectors must be aligned so that when viewed from Earth, the components converge to form the aperture or "spotlight."

The site must also contain the necessary resources for the production of components used for power generation. Materials critical for production of solar arrays and microwave reflectors are silicon, aluminum, and iron. These elements are common in many lunar minerals located in the maria. Statistical data from previous Apollo missions concerning the location and abundance

TABLE 2. Resource Utilization.

|                                | Lunar Highlands Soils (%) | Lunar Low-Titanium Mare Soils (%) | Lunar High-Titanium Mare Soils (%) |
|--------------------------------|---------------------------|-----------------------------------|------------------------------------|
| SiO <sub>2</sub>               | 45.0                      | 46.4                              | 42.0                               |
| TiO <sub>2</sub>               | 0.5                       | 2.7                               | 7.5                                |
| Al <sub>2</sub> O <sub>3</sub> | 27.2                      | 13.5                              | 13.9                               |
| FeO                            | 5.3                       | 15.5                              | 15.7                               |
| MgO                            | 5.7                       | 9.7                               | 7.9                                |
| CaO                            | 15.7                      | 10.5                              | 12.0                               |
| Total                          | 99.3                      | 98.3                              | 99.0                               |

TABLE 3. Demo — LPS Base.

| Base Parameters                                 | Value   |
|---|---------|
| Base area of PV cells per MW <sub>c</sub>       | 0.01    |
| Diameter of transmitter (km)                    | 16.25   |
| Area of one reflector segment (m <sup>2</sup> ) | 217.00  |
| Number of plots and reflectors                  | 1000.00 |
| Surface area of transmission (km <sup>2</sup> ) | 5644.00 |
| Surface area of power plots (km <sup>2</sup> )  | 68.60   |

of major elements located in the highlands and the maria is summarized in Table 2. David Criswell has estimated the size of a demonstration base facility computed from a previous model of the LPS summarized in Table 3.

In order to minimize stay-time for a crew in the event of an emergency, the site should be located along the equator of the Moon. The equatorial trajectory allows for ascent and descent opportunities every two hours<sup>(8)</sup>. The SEED, therefore, is proposed to be located along the equator at the limb.

#### CONCLUSION

Our society needs to develop new means of providing energy and our options are limited. Current approaches are damaging to society, both economically and environmentally. Solar energy may provide an answer to these problems in the future. It is important to begin to create new solutions for collecting the vast source of energy available from space for use on Earth. The SEED is proposed as a possible way to meet energy requirements of the 21st century.

#### ACKNOWLEDGEMENTS

Summary report prepared by Michael Mortensen and Bob Sauls, SICSA.

#### REFERENCES

1. Cull R.C., Power for the Moon: is microwave power beaming an option?, Second Beamed Space Power Workshop, NASA Conference Publication, CP-3037, pp. 329-342: 1989.
2. Criswell, David, R. and R.D. Waldron, Lunar System To Supply Electric Power To Earth. Paper #900279. Accepted for publication and presentation at 25th Intersociety Energy Conversion Engineering Conference, Reno, Nevada, August 12-17, 1990.
3. Criswell, David R., Extraterrestrial Materials Processing and Construction. Lunar and Planetary Institute. Houston, TX. Final report (30 September 1978) NSR 09-051-001 Mod. No. 24. 1978.

4. National Aeronautics and Space Administration, Lunar Energy Enterprise Case Study Task Force, NASA Technical Memorandum #101652: 1989.
5. National Aeronautics and Space Administration, Exploration Studies Technical Report, Volume III: Planetary Surface Systems, The Office of Exploration, FY 1989 Annual Report, Technical Memorandum 4170, pp. 5-49: March 1989.
6. Mallove, Eugene F and Gregory L. Matloff, *The Starflight Handbook*, John Wiley and Sons, Inc., New York: 1989.
7. Heiken G. Vaniman, D. and B. French., *The Lunar Sourcebook*, Cambridge University Press, Cambridge Mass., pp 27-34: 1991
8. Hoffman, S., Lunar and Mars Trajectories (and some other stuff), SAIC Space Sciences, Technical Memorandum: 1990.

## EXERCISE/RECREATION FACILITY FOR A LUNAR OR MARS ANALOG

UNIVERSITY OF IDAHO

S21-54  
160597  
p. 4

The University of Idaho, NASA/USRA project for the 1990-91 school year is an exercise/recreation station for an Earth-based simulator of a lunar or martian habitat. Specifically, we designed a stationary bicycle that will help people keep fit and prevent muscular atrophy while stationed in space. To help with motivation and provide an element of recreation during the workout, the bicycle is to be enhanced by a virtual reality system. The system simulates various riding situations, including the choice of a mountain bike or a road bike. The bike employs a magnetic brake that provides continuously changing tension to simulate actual riding conditions. This braking system is interfaced directly with the virtual reality system. Also, integrated into the virtual reality display will be a monitoring system that regulates heart rate, work rate, and other functions during the course of the session.

### INTRODUCTION

With the proposed plans to have permanent manned stations on the Moon or Mars, it is vital to have facilities that help keep the crew members in shape both physically and psychologically. Serious muscle atrophy results from living in microgravity for long durations, and ill psychological effects due to isolation and confinement can occur. The scope of this project is to develop a facility to overcome these problems that will be tested in an Earth-based simulator of a lunar or martian habitat. Several types of entertainment and exercises could be incorporated into the exercise/recreation facility to maintain the crew members' wellbeing. This paper gives a summary of research, and describes an exercise bike with a virtual reality system, which combines recreation with exercise.

### RESEARCH

#### Psychological and Physical Effects of Isolation and Confinement in Long-Duration Space Flight

This exercise/recreation station is for use in an Earth-based habitat, but it needs to be adaptable to a lunar or martian habitat. Since the lunar or martian habitat will be in a harsh environment without outdoor access, it is possible for the crew members to feel confined and isolated. This feeling affects people in several ways. In an isolated and confined environment, crew members can often feel that the area they occupy is smaller than it actually is. It is also common for the crew to become short-tempered with one another, especially in high stress situations. This is due, in part, to the fact that these crew members have been separated from their original social groups and placed together for a long period of time in a dangerous environment with limited living space. Provisions for the crew member who wants to "get away from it all" also need to be considered during the station's design phase. Chris McKay, senior scientist at Ames Research Center, who has "wintered over" in Antarctica and is familiar with isolation and confinement, emphasized this point. During his expeditions, there were many instances when he would go to his tent in an effort to be alone. Even though he could not see anyone, he still heard the voices and radios

of the rest of the crew. In order for the crew to maintain a healthy attitude in this harsh environment, some form of entertainment must be provided. Exercise, as active entertainment, can supply a physical and mental release not present in other forms of recreation. Studies of Navy crewmen show that exercise can help maintain a better attitude in isolated and confined environments.

In addition to the psychological reasons for exercise, two physical purposes are accomplished: (1) minimizing the deconditioning effects of reduced gravity and (2) ensuring that the crew members will be fit enough to perform their required duties, both at the station and when they return to Earth. The deconditioning effects from reduced gravity are the most important. At reduced gravity, a person's body is not "strained" as much as in Earth's gravity, so the body tends to deteriorate and lose what it does not need or use. This loss affects the physiological and cardiovascular characteristics of the body. The primary physiological effects that are seen include decreased muscle mass (atrophy), strength loss in both the skeleton and muscles, a decrease in bone density, and a decrease in overall mobility. The primary cardiovascular effects are a decrease in oxygen intake during normal breathing, an elevated resting heart rate, and an overall decrease in the flow of blood to all parts of the body.

#### Entertainment

The equipment in the facility must be durable, safe, and compact. It should also be entertaining enough for the crew members to enjoy exercising. If crew members enjoy using the equipment, they will be more likely to stick to a stringent exercise plan. The equipment should also be realistic enough to allow the crew members to temporarily "escape" from their confined quarters and reduce the effects of isolation and confinement. Entertainment can be supplied in a number of ways such as windows, photographs, books, communication with Earth, and television.

One way to accomplish all of these is with a virtual reality (VR) system. Virtual reality consists of computer-generated "worlds" displayed to the viewer through binocular goggles. The viewer is actually an active participant of the generated

world, and since the images are generated continuously, the viewer is given the opportunity to change the scene by physical actions. This is accomplished by placing motion sensors on the equipment or body. One advantage of VR is that it is not limited to reality, as the participant can enter the realm of fantasy by causing things to occur in the computer world that cannot actually happen in the real world, such as walking through walls or flying.

Auditory signals accompanying a visual display will increase the entertainment value. Possibilities range from loudspeaker systems to personal sound systems transmitted monaurally, in stereo, or through 3-D sound imaging. Three-dimensional sound imaging is a way that sound can be more realistically transmitted. As the listener's location changes with respect to the source, sensors mounted to the head allow the sound that is heard to vary in location. So if a plane is up and to the right, that is where the sound would appear to come from. In other words, this allows the listener to hear the position of the sound source.

### Equipment

The equipment in the exercise facility is primarily designed to prevent, or slow down, the deconditioning effects of reduced gravity. As stated earlier, reduced-gravity conditions affect both the physiological and cardiovascular aspects of the body. The equipment is designed to improve both muscle and skeletal strength and to maintain certain endurance requirements. Muscle strength must be improved so that the muscles do not experience atrophy when exposed to reduced gravity, and usually isometric, isokinetic, or isotonic exercises are sufficient for this. The body needs to improve its skeletal strength, which is accomplished through impact due to exercises such as normal walking. However, walking in reduced-gravity does not impose as much stress on the body as walking in Earth's gravity, so the exercise machine is designed to simulate the impact one would feel on Earth during exercise.

Physical endurance obtained through constant exercise must also be maintained to ensure that crew members can perform their required duties. The equipment should be designed to provide an adequate cardiovascular workout. One of the indicators of aerobic workload is the amount of oxygen intake during breathing. A high oxygen intake, which is an indication of a good workout, must be accomplished during exercise to make sure that the crew members are experiencing a complete workout. Also, the heart must be exercised extensively so that it can maintain proper blood flow to all parts of the body.

Various types of exercises were investigated in order to determine which were best for physiological and cardiovascular workouts. Resistance and impact exercises were found to be the best for the physiological workout, and aerobic exercises were found to be the best for the cardiovascular workout. Studies have shown that the tension developed and the stretch maintained by muscle fibers during resistance exercises are key factors in maintaining muscle mass. Also, aerobic exercises maintain a strong heart and keep up the oxygen intake to the lungs. A combination of a treadmill, exercise bike, rowing machine, and Nautilus-style resistance machine would be the most effective for minimizing deconditioning effects and maintaining

the body at its proper physical condition. The selection of the exercise machines in the facility is based upon a correct balance between the cardiovascular and physiological conditioning.

## FINAL EQUIPMENT SELECTION

### Exercise Bike

The objective of this project is to incorporate exercise with recreation so an exercise bike with a VR system was chosen. The exercise bike was chosen for several reasons. It provides an excellent physiological and cardiovascular workout, while keeping the entertainment aspects diversified. The rider is in a stationary, upright position most of the time, and is therefore able to do many things, such as watch a television screen, read a magazine, or look out of a window. Biking is a form of exercise that will give the rider more enjoyment and a more realistic feeling. It will also be easier to incorporate VR in the design to give the rider a larger variety of exercise experiences.

### Virtual Reality System

A VR system with 3-D audio imaging was selected to satisfy the entertainment criteria of the exercise bike. As described in the background portion of this report, VR allows us to simulate a realistic biking experience on a stationary bike in a confined area. Virtual reality is a relatively new technology that restricts a detailed design for our bike. The main components that are needed are a set of viewing goggles, ear phones, motion sensors, and an appropriate software and hardware package. With the VR system, the user will be able to create whatever course is desired for the ride. It can be a mountainous terrain, a street course, or one of many other choices. The 3-D sound adds to the realistic effect in that if a plane flies overhead from right to left, the rider would hear that plane passing overhead in that direction.

The user's input to the VR system will be accomplished through turning the cranks, steering the bike and using the brake levers and shifters in accordance with what is seen through the goggles. The system will be preprogrammed for each rider according to an exercise physiologist's prescribed work rate. If the rider falls below the necessary intensity, the VR may show an approaching hill in his riding world that must be climbed. A stronger current would then be signaled into the eddy brake, thus increasing the workload. If the rider is above the desired work rate, a gradual downhill stretch may appear on the VR screens. A weaker current could be signaled to the eddy brake and the rider's workload would decrease. The same thing can be accomplished by having the rider simply shift up or down. Shifting up would signal the computer to decrease the current in the eddy brake and increase the current when shifting down.

## RIDING SYSTEM

The riding system consists of four major components: a bike, a tilting mechanism, a braking system, and a harness. A riding system was developed that could simulate all possible riding situations, such as going up hills and banking around corners.

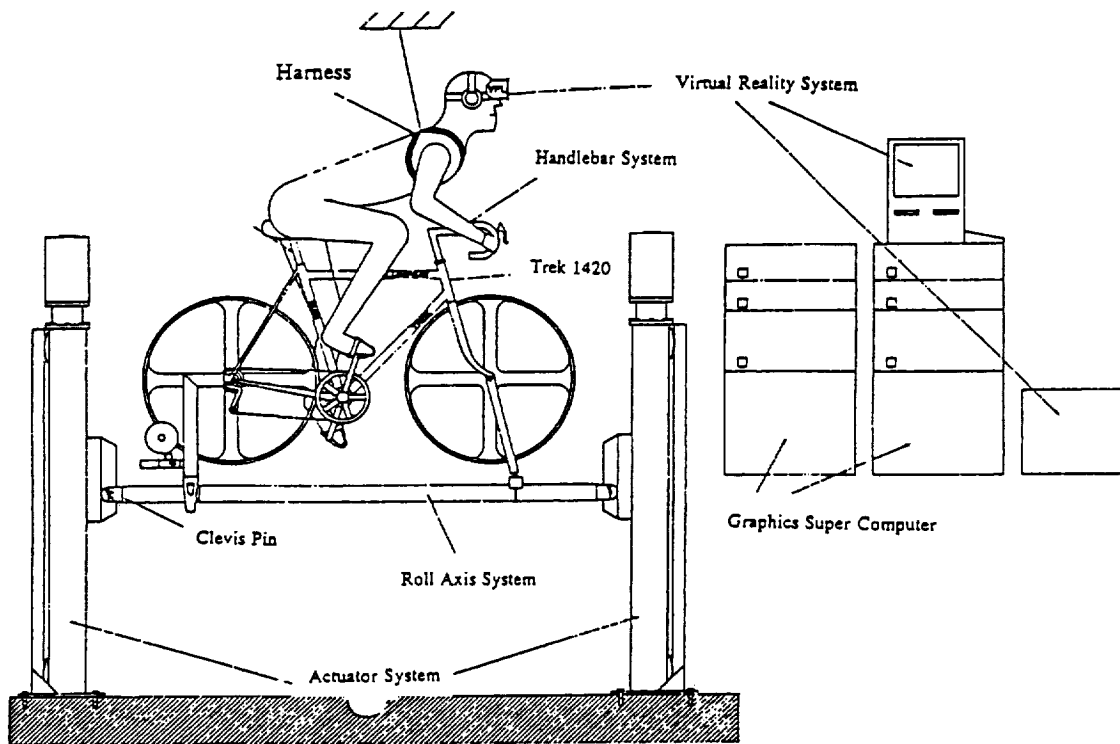


Fig. 1. Riding system.

The system was designed to have both pitch and roll, as well as a variable rolling resistance. The riding system is shown in Fig. 1.

### The Bike

A nonferrous bike, constructed of aluminium, was selected because the magnetic properties of ferrous materials interfere with the tracking mechanism used by the VR system. In order to simulate varied riding conditions, the bike needs to be versatile. The bike that was selected combined the performance qualities of a racing bicycle with the comfort of a touring cycle. The geometry of the bike was selected according to Military Standard 1472 to fit the height range requirement for the 95th percentile man to the 5th percentile woman. A Trek 1420, Aluminium size 50 combination bicycle was selected because it fulfills the above requirements. In order to fit the 5th to 95th percentile, adjustable handlebars and an adjustable seat are incorporated into the design.

### Handlebar Assembly

A handlebar assembly that simulates both a mountain bike and a road bike will replace the handlebar assembly that comes with the Trek 1420, as shown in Fig. 2. This handlebar assembly will have brake levers and gear shifters that will be tied into the VR system. The handlebar stem will be inserted into the bicycle headset of the Trek 1420. This will provide the typical

steering rotation of the handlebars giving the user a very realistic feeling from a stationary bike. An adjustment feature will be added to the handlebars, since the bars must slide forward 20 cm to meet the anthropometric data requirements of the different crew member sizes.

### Tilting Mechanism

The bicycle is mounted on a tilting mechanism that provides both pitch and roll for the bicycle. The tilt mechanism consists of two actuators, a connecting bar, and supports. The actuators provide pitch by adjusting the height of the roll bar. The actuator system consists of two electric linear actuators mounted vertically. The actuators are driven by a 1-hp DC motor that will be mounted on the top of each actuator column. These actuators have a maximum throw of 3 ft, which allows the bicycle to reach a maximum pitch of 25°. A maximum speed of 10 in/s can be obtained by the actuators, which will facilitate the simulation of hills and dips commonly encountered while riding.

The roll bar acts as the rolling mechanism for the bicycle and is connected between the two actuators. The roll bar is constructed of two pieces of aluminium tubing coupled to a telescoping section. This telescoping section allows the roll bar to elongate so that binding does not occur during pitch changes. Aluminium tubing is used because it is easy to machine, nonferrous, and lightweight. The telescoping section is made of a heavy-load spline nut, press fit into the aluminium tubing so that the bearing is fixed in one part of the tubing and the

|   |                             |
|---|-----------------------------|
| 1 | CAMPAGNOLA C-RECORD HEADSET |
| 2 | MOTION SENSOR               |
| 3 | QUICK RELEASE               |
| 4 | GRP SHIFT PROLINE 1990      |
| 5 | RITCHIEY TRUE GRP           |
| 6 | DIACOMPE XCE SHORT STOP     |
| 7 | MOODLO 8/X-TENOS            |
| 8 | DURA-ACE BRAKE/SHIFT LEVERS |

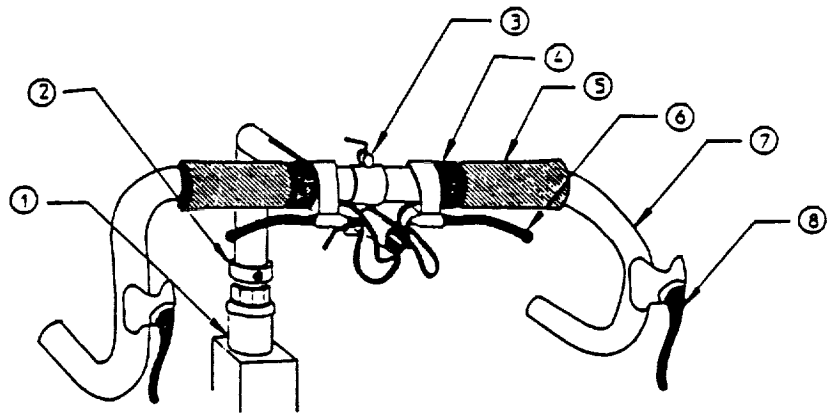


Fig. 2. Handlebar assembly.

shaft is free to slide within it. The bike is attached to the roll bar using a pillow block on the rear assembly. A ball-joint assembly attaches to the front hub allowing a full range of motion for the crankset. This is desirable for both gyroscopic stability and riding simulation. The pillow block assembly attached to the rear hub allows the bike to roll about the roll bar axis, enabling the rider to lean the bike to simulate cornering in a more realistic manner. The bike is stabilized by supports on the ground when the wheels are not rotating and by the gyroscopic effects of the wheel when they are spinning, as on a real bike. A small motor will be attached to the front wheel to rotate it at the same speed as the rear wheel.

The support system holds the actuators in place. These are attached to the floor to provide the bike with a solid foundation, preventing any flex from occurring between the bicycle and the actuator system.

### Resistance Mechanism

The resistance mechanism is designed to replicate the rolling resistance of the bicycle as it travels over varied terrain, such as hills, dips, corners, etc. This is accomplished by attaching a permanent magnet braking system, which provides a smooth, quiet, and efficient resistance. This is attached to the roll bar mechanism and a spring-loaded link holds the braking system against the rear tire of the bicycle. The resistance of the bike can be adjusted depending on the riding condition that is simulated during the VR session. This particular resistance mechanism was selected because of its low magnetic flux output and because it is easily controlled using an analog signal.

### Harness

The function of the harness (Fig. 3) for the riding system is to protect the rider from any accidents. If the crew member becomes overexerted and loses consciousness, no injury will occur. The main function of the harness is to prevent accidental falls from the bike. The harness was designed to be easily adjustable, comfortable, nonrestrictive, easy to put on and take

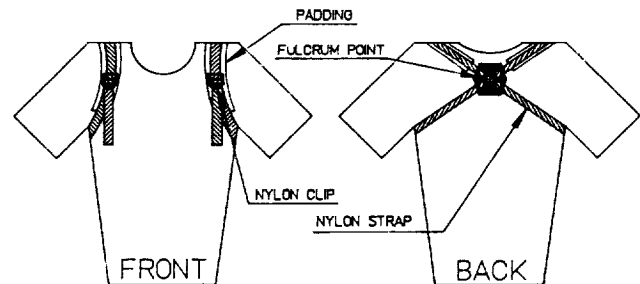


Fig. 3. Upper restraint harness.

off, and strong enough to protect the rider. Therefore, a harness similar to a rock climbing safety strap was selected because of its unique quality of high strength without being restrictive and heavy. The harness is very easy to adjust to various body sizes and is not gender specific. The harness is attached to a point above the rider by a cable fixed to the back of the harness. This will protect the rider from falls in the forward and lateral directions.

### CONCLUSION

This design accomplishes the purposes of having both an exercise and a recreation facility. It will reduce the effects of deconditioning and also the ill effects of isolation and confinement. With the VR system and the tilt and roll feature of the riding system, the bike will be entertaining and realistic enough that the crew members should want to stick to their exercise plan.

Since gyroscopic effects are not completely understood, tests will have to be performed to determine the stability of the bike. Once this is determined, the design may need some adjustments to maintain a realistic feel and to ensure the safety of the rider. Also, virtual reality is only in its beginning stages. As the technology in this field increases, the entertainment value and the capabilities of the system will also increase.

# AUTOMATION OF CLOSED ENVIRONMENTS IN SPACE FOR HUMAN COMFORT AND SAFETY

KANSAS STATE UNIVERSITY

522-54  
160598  
p. 5

## INTRODUCTION

### Project Description

The development of Environmental Control and Life Support Systems (ECLSS) for Space Station *Freedom*, future colonization of the Moon, and Mars missions presents new challenges for present technologies. ECLSS that operate during long-duration missions must be semi-autonomous to allow crew members environmental control without constant supervision. A control system for the ECLSS must address these issues as well as being reliable. The Kansas State University Advanced Design Team is in the process of researching and designing controls for the automation of the ECLSS for Space Station *Freedom* and beyond.

The ECLSS for *Freedom* is composed of six subsystems. The temperature and humidity control (THC) subsystem maintains the cabin temperature and humidity at a comfortable level. The atmosphere control and supply (ACS) subsystem insures proper cabin pressure and partial pressures of oxygen and nitrogen. To protect the space station from fire damage, the fire detection and suppression (FDS) subsystem provides fire-sensing alarms and extinguishers. The waste management (WM) subsystem compacts solid wastes for return to Earth, and collects urine for water recovery. The atmosphere revitalization (AR) subsystem removes CO<sub>2</sub> and other dangerous contaminants from the air. The water recovery and management (WRM) subsystem collects and filters condensate from the cabin to replenish potable water supplies, and processes urine and other waste waters to replenish hygiene water supplies.

These subsystems are not fully automated at this time. Furthermore, the control of these subsystems is not presently integrated; they are largely independent of one another. A fully integrated and automated ECLSS would increase astronauts' productivity and contribute to their safety and comfort.

### Three-Phase Design Plan

A three-phase approach was implemented by the Kansas State University Advanced Design Team to design controls for the ECLSS. The first phase, completed within one year, researched the ECLSS as a whole system and then focused on the automation of the atmosphere revitalization (AR) subsystem.

During the second phase, the system control process was applied to the AR subsystem. To aid in the development of automatic controls for each subsystem and the overall ECLSS, mathematical models have been developed for system simulation on a computer. Expert system control as well as conventional

control methods are being tested on the models. Using the AR subsystem control system as a "proof of concept," the other ECLSS subsystems will be automated.

Finally, during phase three, the control system of the six subsystems will be combined to form a control system for ECLSS. The expert system developed for the AR will be expanded to control the ECLSS, as well as provide fault diagnosis and isolation to the astronauts.

The Kansas State University Design Team has completed phases one and two. Mathematical models for the CO<sub>2</sub> removal assembly, CO<sub>2</sub> reduction assembly and oxygen generation assembly, as well as an expert system, have been developed for the AR. The mathematical models are written in the C-Language. At this time, the models function independently at the assembly level. The expert system, using an expert system shell called CLIPS, monitors and controls the AR subsystem assemblies in a hierarchical manner.

### Design Team Description

The Kansas State University Advanced Design Team is composed of engineering students from several disciplines, a student from general science and education, two graduate student assistants, and engineering faculty members. Architectural, chemical, computer, electrical, and mechanical engineering disciplines are represented by both students and faculty.

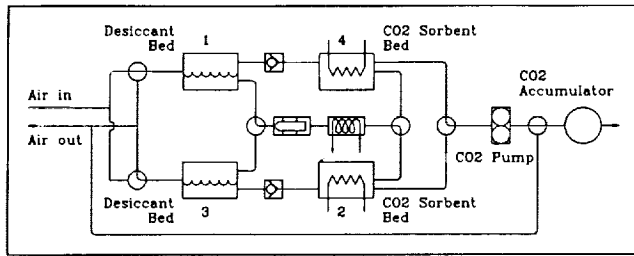
### Document Organization

This document presents a portion of the work done by the design team during the 1990-91 academic year. First, part of the CO<sub>2</sub> removal assembly model is presented. Then a portion of the removal assembly's expert system is discussed. Complete details for the three models and the experts system can be found in the final report.

## MATHEMATICAL MODELING

### CO<sub>2</sub> Removal Assembly Model

**Description.** The CO<sub>2</sub> removal assembly is part of the (AR) Subsystem. Its purpose is to remove CO<sub>2</sub> from the cabin atmosphere, deliver CO<sub>2</sub> to the CO<sub>2</sub> reduction assembly and return humidified air to the cabin. This is done using a four-bed molecular sieve consisting of two desiccant beds to remove water vapor from incoming air, two CO<sub>2</sub> adsorption beds, a

Fig. 1. CO<sub>2</sub> Removal Assembly.

blower to force air through the system, a CO<sub>2</sub> pump, a CO<sub>2</sub> accumulator, a precooler and five multiple-flow selector valves. Figure 1 illustrates these major components.

**Math Model.** This physical system is modeled using the following simplifications: (1) all beds are modeled as lumped systems; (2) adsorbing/desorbing processes along the bed are averaged; (3) thermal equilibrium is assumed (which negates the dependence on bed length); and (4) the CO<sub>2</sub> desorbent bed is in thermal equilibrium.

All four beds have been modeled as lumped systems. For simplicity, we have neglected the fact that the adsorbing/desorbing processes vary as a function of distance through the bed. In our model, we have assumed instantaneous thermal equilibrium, which, in effect, negates the dependence on bed length. We intend to improve the model by subdividing each bed into many smaller beds. To implement this scheme, the overall bed volume and sorbent mass will be divided by the number of "plugs." The simulation will be modified using 2-D arrays.

The following are the equations that model the CO<sub>2</sub> desorbent bed, incorporating the assumptions listed above.

$$P_b = K_1 \left( \frac{m_d}{m_b} \right) (T_b - T_{ref}), \quad (1)$$

$$T_b = T_g, \quad (2)$$

$$P_g = \frac{m_g R T_b}{V_g}, \quad (3)$$

$$\frac{dm_d}{dt} = (P_b - P_g) k_2, \quad (4)$$

$$\frac{dm_g}{dt} = (P_b - P_g) k_2 - m_o, \quad (5)$$

$$\frac{dT_b}{dt} = \frac{\left( \frac{dm_d}{dt} S_c + \text{Power} \right)}{m_b C_{vb}}, \quad (6)$$

The required definitions are given by

- $P_b$  = CO<sub>2</sub> equilibrium pressure of bed (kPa)
- $K_1$  = constant (picked to be  $0 \leq K_1 \leq 1$ )
- $m_d$  = mass of CO<sub>2</sub> in sorbent material (kg)
- $m_b$  = mass of sorbent in bed (kg)
- $T_b$  = temperature of the bed (K)
- $T_{ref}$  = reference temperature (K)
- $T_g$  = temperature of CO<sub>2</sub> gas (K) (substitute  $T_b$ )
- $P_g$  = pressure of CO<sub>2</sub> gas in bed void space (Kpa)
- $m_g$  = mass of CO<sub>2</sub> gas in void space (kg)
- $R$  = CO<sub>2</sub> gas constant (kPa.m<sup>3</sup>/kg.K)
- $V_g$  = void space of bed, also volume of CO<sub>2</sub> (m<sup>3</sup>)
- $k_2$  = transfer coefficient ( $0 \leq K_2 \leq 1$ )
- $m_o$  = CO<sub>2</sub> gas mass flow rate, determined by pump (kg/s)

$S_c$  = heat of sorption of CO<sub>2</sub> (J/kg CO<sub>2</sub>)

Power = power applied to bed (J/s)

$C_{vb}$  = heat capacity of sorbent material (J/kg.K)

$dm_d/dt$  = rate of CO<sub>2</sub> desorbed (kg CO<sub>2</sub>/s)

$dm_g/dt$  = change in mass of CO<sub>2</sub> in void space (kg CO<sub>2</sub>/s)

$dT_b/dt$  = change in temperature of bed (K/s).

**Sample Output.** Several simulation runs were conducted, altering a single parameter each time. The model seems most sensitive to pump speed ( $w$ ) and reference temperature ( $T_{ref}$ ). Figure 2 shows the temperature of the desiccant bed for the model running with the following conditions:

- Mass flow rate of air into model = 0.2 kg/s
- H<sub>2</sub>O concentration into model = 0.01 kg H<sub>2</sub>O/kg air
- CO<sub>2</sub> concentration into model = 0.001 kg CO<sub>2</sub>/kg air
- Temperature of air into model = 300 K
- Angular velocity of CO<sub>2</sub> pump = 200 rad/s
- Reference temperature of model = 250 K

### CO<sub>2</sub> Removal Assembly Expert System

Conventional control systems like those required by an ECLSS can quickly become unmanageable and even unstable; expert systems allow more freedom to design the control system using

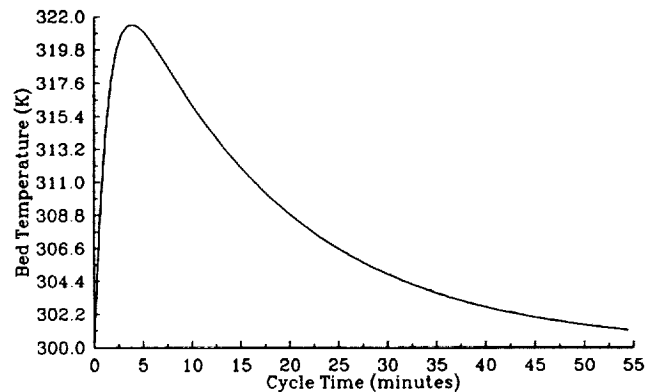


Fig. 2. Temperature of Desiccant Bed.

and implementing rules of thumb and heuristic reasoning. Therefore, an expert system allows development of control without complete characterization of the component. In this manner, the mathematics of expert systems allows inexact reasoning or fuzzy logic. In other words, expert systems allows implementation of expertise or rules directly, much like the human thought process. For these reasons, an expert system was developed to control the atmosphere revitalization assembly.

The atmosphere revitalization expert system (ARES) was created using the CLIPS expert system shell. ARES consists of mathematical models of the AR and a control system, Savant.3. Savant.3 contains a knowledge base for each of the three assemblies in the AR. These knowledge bases contain expert knowledge for each assembly in the form of rules, and represents this in English conditional statements. Savant.3 also converts sensor values into English statements, makes inferences using the knowledge base, generates commands based on the inferences, and provides an explanation of conclusions. Each time ARES is activated it provides one command for each assembly.

### Knowledge Base

The knowledge base of ARES consists of three smaller knowledge bases. The assembly knowledge bases together contain rules used to identify current operation conditions and diagnose problems in the AR.

The knowledge base incorporates fuzzy membership functions for the sensor data used. In this way, decisions are made by assignment of weights between zero and one that correspond to the assurance of how "true" a decision provided by the inference engine. This allows the expert system to arrive at two or more conclusions that may conflict due to the inexact mathematics of expert systems. The response that has the greatest weight or has the higher confidence rating is selected to be executed by the inference engine. The following section discusses, in part, the rules and expertise of the CO<sub>2</sub> removal assembly knowledge base.

### CO<sub>2</sub> Removal Assembly

The main function of the expert system is to monitor the components of the CO<sub>2</sub> removal assembly. Different sensor values are read and compared to certain parameters, and the expert system makes a decision based on those sensor values. The focus of the rules was to detect component failures. Currently, the rules do not include any valves or the four beds.

**Rule #1.** The expert system monitors the temperature sensor at the output of the precooler. If the value is not within acceptable parameters, the expert system decides if failure has occurred. If a failure decision is reached, the expert system instructs the removal assembly to shut down.

**Rule #2.** The expert system monitors the two pressure sensors located on either side of the blower and checks the differential pressure. If the pressure differential is unacceptable, the removal assembly is instructed to shut down.

**Rule #3.** The expert system monitors the power sensor on the CO<sub>2</sub> pump. If the value is unsuitable, then the removal assembly is instructed to shut down.

**Rule #4.** The expert system monitors the pressure sensor located on the CO<sub>2</sub> pump. If the value is not within the established parameters, the removal assembly is instructed to shut down.

**Rule #5.** The expert system monitors the gas flow at the CO<sub>2</sub> accumulator through two gas flow sensors located on either side of the accumulator. If a failure decision is reached, both the CO<sub>2</sub> removal and the CO<sub>2</sub> reduction assemblies are instructed to shut down.

### Savant.3 (Decision Mechanism)

This section is a summary of the program sections of Savant.3. Savant.3 is the decision mechanism of ARES. It consists of five sections of which the knowledge base has been discussed. The other four sections are the inference engine, the operations resolver, the response selector and implementator, and the explanation facility.

The inference engine of Savant.3 is a shell above CLIPS. First, the inference engine interprets the rules of the knowledge base. Next, it evaluates the fuzzy membership functions by assigning a weight (confidence value) to the sensor values given by the mathematical models of ARES. Finally, it selects the best response for each assembly.

The second section titled Resolve Operations, is used to locate and resolve linguistic statements using functions such as "and," "or," and "is not". This is necessary since the knowledge base was written in standard English statements, allowing ease in interpretation. At this point in the program, all rules that are true with any confidence factor are placed on a "fired" rule list inside CLIPS.

The next step is to select the proper response from the list of "fired" rules. The Response Selection and Implementation section of Savant.3 is responsible for selection. This section selects the response with the strongest confidence factor from among the conflicting responses on the "fired" rule list, and this response is then constructed into a command for each assembly.

The final section of Savant.3 is the Explanation Facility. This section is not necessary for operation of ARES, but is very important. ARES is only as accurate as the experts of each assembly. It is no smarter than its programmers and therefore is susceptible to incorrect conclusions. The Explanation Facility allows the user to see the steps taken by ARES in making decisions for each assembly. It does this by retracing the paths used to determine the selected responses, and generates a dialogue explaining the responses arrived at, allowing the user to revoke the decision.

### Verification and Testing of Expert System

A simple expert system was designed to help monitor and control the ECLSS for a space station. Currently, the system has control over only portions of the air revitalization system. After rules that govern the system's behavior are written and placed into the knowledge base, the expert system was tested to discover programming errors. The final stage of the expert system's development is verification—applying a series of inputs and insuring the resulting decisions are correct. Even though

the current system contains only four components that may be varied, verification is a difficult task. To verify all possible conditions, combinations would require around 300 individual tests. The complete expert system to govern the entire ECLSS will be nearly impossible to verify completely. A number of different sets of conditions were tested and checked. These condition sets fall into nine cases, six of that are described below. For each case, the conditions are stated first, then a brief description of the system response is given. The four conditions which can be varied are

1. Cabin-O<sub>2</sub>—Used to determine amount of breathable air currently available to the astronauts. Helps control oxygen generation assembly (OGA).

2. Inlet-CO<sub>2</sub>—Indicates amount of CO<sub>2</sub> present in the cabin atmosphere. Helps control CO<sub>2</sub> removal assembly.

3. CO<sub>2</sub>-Accumulator—Indicates level of CO<sub>2</sub> storage tank located between CO<sub>2</sub> removal and CO<sub>2</sub> reduction assemblies. Helps control these same two assemblies.

4. H<sub>2</sub>O-Accumulator—Indicates level of water in storage tank located between CO<sub>2</sub> reduction and OGA assemblies. Helps control these same two assemblies.

#### CASE 1:

Condition: All values in normal operating range.

#### Response:

OGA—Commanded to turn on (if currently off) or to continue in normal operating mode.

CO<sub>2</sub> Reduction—Commanded to turn on (if currently off) or to continue in normal operating mode.

CO<sub>2</sub> Removal—Commanded to move to an efficiency mode. Since no supplies are low and cabin CO<sub>2</sub> is normal, CO<sub>2</sub> removal assembly can reduce power requirements by decreasing production slightly.

#### CASE 2:

Condition: Both accumulators are empty, all other values in normal operating range.

#### Response:

OGA—Commanded to turn on (if currently off) or to continue in normal operating mode. This system will not, however, be able to operate if no water is available. This system should turn off until water is available.

CO<sub>2</sub> Reduction—Commanded to turn on (if currently off) or to continue in normal operating mode. This is to refill the empty H<sub>2</sub>O accumulator.

CO<sub>2</sub> Removal—Commanded into high removal mode. This will help to replenish the CO<sub>2</sub> accumulator and provide resources needed by the CO<sub>2</sub> Reduction assembly to refill H<sub>2</sub>O accumulator.

#### CASE 3:

Condition: Both accumulators at a low level, all other values in normal operating range.

#### Response:

OGA—Commanded to turn on (if currently off) or to continue in normal operating mode. This system will not, however, be able to operate if no water is available. This system should perhaps turn off for a while until water is available. This is the correct response as programmed although not really the correct way to handle the given situation.

CO<sub>2</sub> Reduction—Commanded to turn on (if currently off) or to continue in normal operating mode. This is to refill the empty H<sub>2</sub>O accumulator.

CO<sub>2</sub> Removal—Commanded to move to high production mode. This will help to replenish the CO<sub>2</sub> accumulator and provide resources needed by the CO<sub>2</sub> reduction assembly to refill H<sub>2</sub>O accumulator.

#### CASE 4:

Condition: Both accumulators at a high level, all other values in normal operating range.

#### Response:

OGA—Commanded to turn on (if currently off) or to continue in normal operating mode.

CO<sub>2</sub> Reduction—Commanded to turn on (if currently off) or to continue in normal operating mode.

CO<sub>2</sub> Removal—Commanded to move to an efficiency mode. Since no supplies are low and cabin CO<sub>2</sub> is normal, CO<sub>2</sub> removal assembly can reduce power requirements by decreasing production slightly.

#### CASE 5:

Condition: Inlet CO<sub>2</sub> at a high level, all other values in normal operating range.

#### Response:

OGA—Commanded to turn on (if currently off) or to continue in normal operating mode.

CO<sub>2</sub> Reduction—Commanded to turn on (if currently off) or to continue in normal operating mode.

CO<sub>2</sub> Removal—Commanded to move to a high removal mode. This is an attempt to remove the excess CO<sub>2</sub> from the cabin and restore a proper CO<sub>2</sub>-O<sub>2</sub> balance for the astronauts.

#### CASE 6:

Condition: Inlet CO<sub>2</sub> at a low level, all other values in normal operating range.

#### Response:

OGA—Commanded to turn on (if currently off) or to continue in normal operating mode.

CO<sub>2</sub> Reduction—Commanded to turn on (if currently off) or to continue in normal operating mode.

CO<sub>2</sub> Removal—Commanded to turn off. This is done to avoid overfilling the CO<sub>2</sub> accumulator before the need to remove CO<sub>2</sub> becomes important. This also conserves power at times when the system is not needed.

### Limitations

The biggest limitation at present is the number of rules on which the system can operate. With only four pieces of data with which to make decisions, those decisions will be limited in scope and accuracy. Next, the system produces confidence factors because of the narrow scope of the current expert system. Finally, the expert system does not always produce the best decision. As noted in cases 2 and 3 above, the OGA is commanded to turn on even though adequate resources for operation may not be available. It is evident that further options need to be considered and tested before a final decision is made as to the operation of the system.

### CONCLUSIONS

Because of the complex nature of the conditions that may affect operation of the ECLSS, standard control schemes do not provide an adequate means for system maintenance. The expert system, on the other hand, is more tolerant of inexact data and does not need constant supervision. For these reasons, an expert system makes a better choice for ECLSS control.

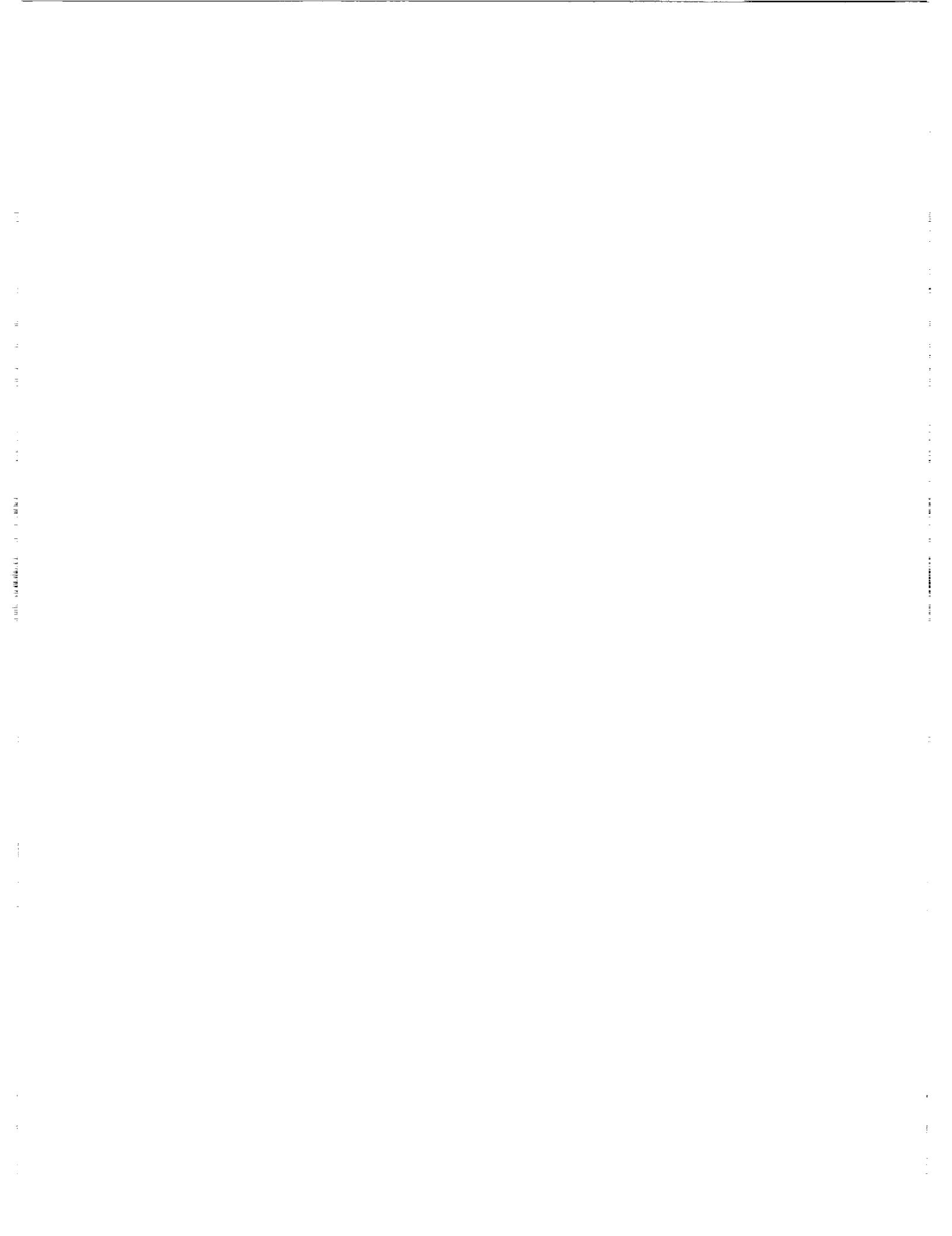
The expert system designed this semester used the CLIPS expert system shell. This shell program proved to be cumbersome and difficult to implement, and should be avoided in future design if possible.

The rules defined in the previous sections obviously do not represent a set that will completely control the assembly. Rather, these rules are a beginning set that defines the overall or general

operation of the assembly's main components. Many other, more detailed rules will be needed to complete the knowledge bases for the expert system and to provide an adequate control system for the ECLSS. Further information about the operation and interaction of the various subassemblies will be required before such rules can be defined.

The Savant.3 decision mechanism is the most complete portion of the current expert system design. The inference engine, which interprets knowledge base data, and the response selector, which chooses an action based on the number of conclusions and their associated confidence factors, will not be affected by the addition of new rules. In fact, these sections could be used with no alteration in an expert system for control of the entire ECLSS. The only section of Savant.3 that will need to be altered will be the operation section. Because this section depends on the rules in the system, it will not be able to be completed until all rules have been entered into the system.

Currently, the system testing shows correct operation based on the available rules. However, because of the small number of rules available to test at this time and because of the general nature of those rules, the decisions reached are not necessarily the best or even the correct ones. It should be restated, however, that the responses gained at this time are the correct ones for the system programmed.



**DELTA ADVANCED REUSABLE TRANSPORT (DART)  
AN ALTERNATIVE MANNED SPACECRAFT**

**UNIVERSITY OF MARYLAND**

*S23-18  
160599  
P-11*

**INTRODUCTION**

Although the current U.S. Space Transportation System (STS) has proven successful in many applications, the truth remains that the space shuttle is not as reliable or economical as was once hoped. In fact, the Augustine Commission on the future of the U.S. Space Program has recommended that the space shuttle only be used on missions directly requiring human capabilities on-orbit and that the shuttle program should eventually be phased out. This poses a great dilemma since the shuttle provides the only current or planned U.S. means for human access to space at the same time that NASA is building toward a permanent manned presence.

As a possible solution to this dilemma, it is proposed that the U.S. begin development of an Alternative Manned Spacecraft (AMS). This spacecraft would not only provide follow-on capability for maintaining human spaceflight, but would also provide redundancy and enhanced capability in the near future. Design requirements for the AMS studied here include:

- Capability of launching on one of the current or planned U.S. expendable launch vehicles (baseline McDonnell Douglas Delta II model 7920 expendable booster).
- Application to a wide variety of missions including autonomous operations, space station support, and access to orbits and inclinations beyond those of the space shuttle.
- Low enough costing to fly regularly in augmentation of space shuttle capabilities.
- Production surge capabilities to replace the shuttle if events require it.
- Intact abort capability in all flight regimes since the planned launch vehicles are not man-rated.
- Technology cut-off date of 1990.
- Initial operational capability in 1995.

In addition, the design of the AMS would take advantage of scientific advances made in the 20 years since the space shuttle was first conceived. These advances are in such technologies as composite materials, propulsion systems, avionics, and hyper-sonics.

**DART AMS OVERVIEW**

In response to the demonstrated need for an AMS, the Delta Advanced Reusable Transport (DART) was designed by students in the ENAE 412 Space Systems Engineering class at the University of Maryland. As seen in Fig. 1, the DART spacecraft design centers on a semiballistic capsule concept similar in many respects to

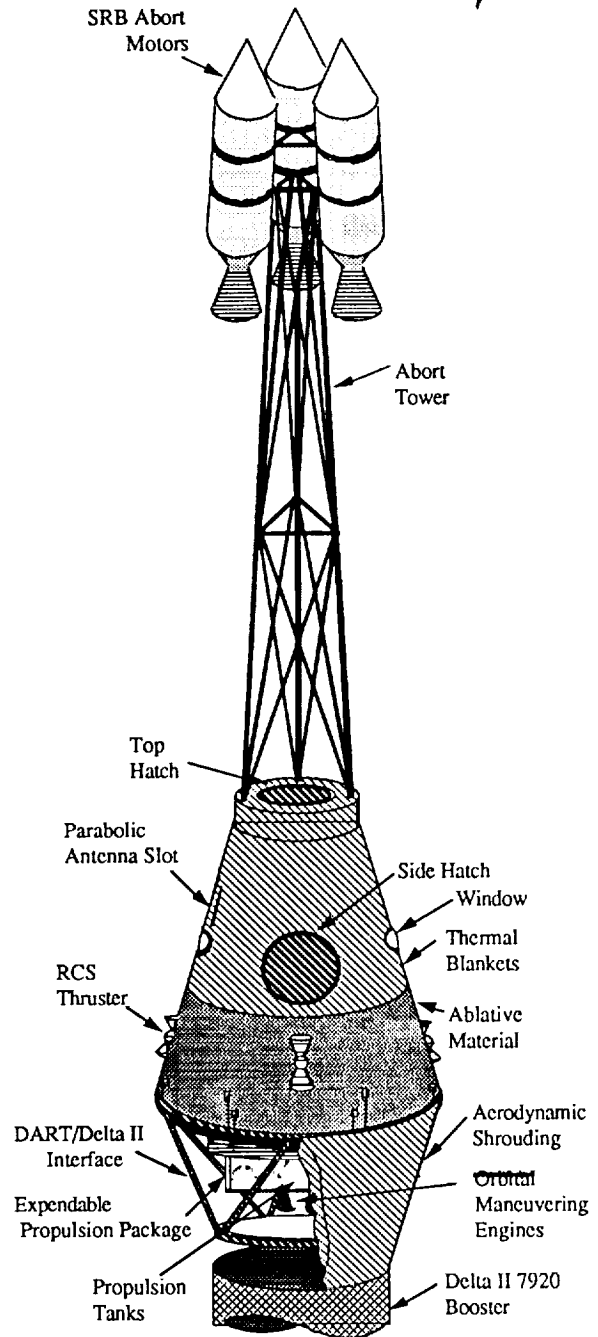


Fig. 1. DART AMS concept.

*FIG 164 INTENTIONALLY BLANK*

the U.S. manned spacecraft of the 1960s, but employing more advanced structures, propulsion, and avionics technologies. The proposed baseline design features are summarized in Table 1.

TABLE 1. DART baseline design features.

|                |   |
|----------------|---|
| Mass           | 4772 kg at launch                                       |
| Size           | 3.5 m diameter, 4.5 m length                            |
| Crew           | 2 to 5  |
| Payload        | 52 to 292 kg  |
| Mission Length | 1 to 5 days   |
| Recovery       | Semiballistic reentry;<br>parachute to ocean splashdown |

With 96% reliability, the Delta rocket's launch program supplies the DART spacecraft with the cost-effective and readily available launch capabilities required of an AMS. This includes the use of existing launch facilities at Complex 17, Cape Canaveral Air Force Station (CCAFS), Florida. The 1990 technology cut-off date was imposed to both cut development and research costs, as well as to insure that the 1995 initial operation capability requirement is satisfied.

The DART spacecraft's mass and size constraints are defined by the Delta II's maximum payload mass capability for a designated orbit. DART's baseline mission is a low Earth orbit (LEO) satellite servicing operation, although a nominal orbit of 500 km and 28.5° inclination was chosen for calculation purposes to allow for space station capabilities. This 500 km orbit can be achieved with a maximum payload of 4824 kg. The DART mass breakdown is shown in Table 2.

TABLE 2. DART mass breakdown.

| System        | Subsystem                          | Mass (kg) |
|---------------|------------------------------------|-----------|
| Structures    | Main Structure                     | 237       |
|               | Docking Module                     | 28        |
|               | Thermal Protection System          | 318       |
|               | Abort Tower/Motors                 | 195*      |
|               | Impact Attenuation System          | 129       |
|               | Parachutes                         | 200       |
| Systems       | Interface                          | 7         |
| Integration   | Propulsion                         | 3         |
| Propulsion    | Main Engines                       | 136       |
|               | Main Propellant Tanks and Plumbing | 80        |
|               | Reaction Control System            | 491       |
|               | Fuel                               | 767       |
| Avionics      | Data Processing                    | 96        |
|               | Attitude Sensors                   | 10        |
|               | Sensors                            | 150       |
|               | Radar                              | 75        |
|               | Guidance and Navigation            | 29        |
|               | Communication                      | 82        |
|               | Power Generation                   | 131       |
| Human Factors | ECLSS                              | 634       |
|               | Food and Water                     | 574       |
|               | 5 Astronauts                       | 400       |
| Total         |                                    | 4,772     |

\* Effective mass = 1/4 actual mass.

The DART capsule consists of an inner pressure vessel and an outer honeycomb structure, both constructed out of aluminum. In addition, a thermal protection system (TPS) utilizing

a combination of ablative material and thermal blankets is applied to the external surface of the capsule. The TPS maintains acceptable skin temperatures during all phases of the mission.

The AMS design requirements specify the necessity of intact abort capability in all flight regimes. During launch, an abort tower is attached to the top of the capsule and an aerodynamic shroud cover the DART/Delta II interface ring truss. The shroud and abort tower are jettisoned before reaching desired orbit. Situated within the ring truss is an expendable hypergolic propulsion system utilizing hydrazine and nitrogen tetroxide propellants; it is strapped onto the capsule and jettisoned during re-entry.

During a mission, the DART spacecraft will experience a variety of forces tending to rotate and/or translate the capsule. Thus, the DART is equipped with a reaction control system (RCS) to measure, correct, and counteract any adverse motion. In addition to the main engine and RCS propulsion systems, DART requires a power generation system. Solar cells provide the primary electrical power with rechargeable batteries as the secondary power source.

The DART avionics systems provide navigation, attitude control, data processing, sensors, and communications. The LTN-90 ring laser gyro inertial navigation system (INS) will serve as the primary attitude and position reference. A data processing system is required for navigation, attitude, and flight control computations. This system uses sensors to keep the astronauts informed about the status of all DART systems. Communications are needed for video and voice contact, navigation and rendezvous transmissions, and for conducting experiments. To insure reliable communications, two different paths have been chosen: one through the Tracking Data Relay Satellite System (TDRSS) and the other directly to Earth stations.

DART's manned-rating requires thorough investigation of human factors. The interior of the capsule will be held at standard atmospheric conditions with metabolic carbon dioxide removal by means of solid amine. Spacesuits are similar to those worn by shuttle astronauts. Food and water must be carried in full due to the large mass and volume requirements of a water recycling system.

Figure 2 details the internal layout of the DART AMS. Included are the dimensions of the habitation environment as well as controls and monitors needed during the mission. Note that there are three couches in addition to the pilot and copilot seats. These couches can be removed, allowing for two, three, four, or five crew members or payload and experiment lockers. Storage bins in the crew compartment will hold such items as tools, schedules, clothing, and personal items.

As stated in the overview, the baseline mission proposed for DART is a LEO satellite servicing operation. Three astronauts will be launched from the Kennedy Space Center (KSC) to a rendezvous orbit with the satellite requiring servicing. Microgravity experiments will be performed during the three-day Earth orbit wait period required for astronaut adaptation to the microgravity environment. The next phase of the mission involves an extravehicular activity (EVA) that could include routine satellite maintenance, component replacement, and repair. The mission duration varies from three to five days.

The DART spacecraft can be utilized as a "taxi," a "tug," or as an emergency escape vehicle for Space Station *Freedom*. The

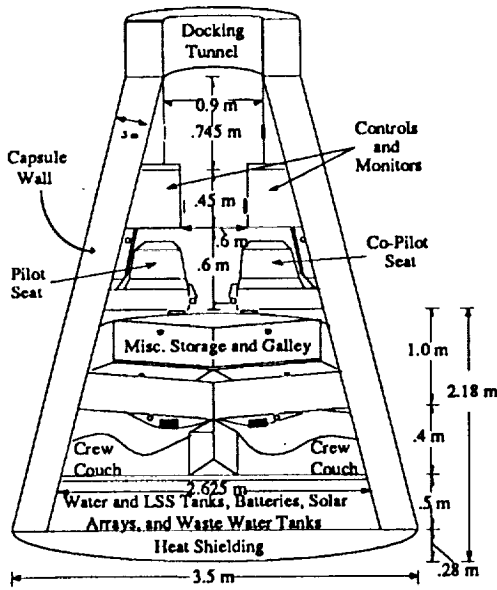


Fig. 2. DART AMS internal layout.

“taxi” concept entails the delivery of new astronauts to the space station and the return of current station personnel to Earth; as a “tug,” vital supplies will be delivered to *Freedom*. The length of these missions varies from one to three days. Should an emergency arise, evacuation may become necessary. Special DART spacecraft could be configured and ready at all times to provide an emergency “lifeboat vehicle” for station personnel.

In order to complete other missions, alternative launch vehicles such as the Atlas IIA and Titan III were considered. Assuming launch trajectories are approximately Hohmann transfers, the vis-viva equation was used to calculate the required launch  $\Delta V$ s. Table 3 shows these  $\Delta V$ s and maximum altitudes of the launch vehicles with the 4772-kg DART. The Titan III launch vehicle was found to hold the most possibilities for DART. The large  $\Delta V$  allows for missions to very high inclinations and altitudes almost four times that attained with the Delta II.

TABLE 3. Alternative launch vehicle capabilities.

| Launch Vehicle | $\Delta V$ with 4772-kg DART (m/s) | Max. Alt. with 4772-kg DART (km) |
|----------------|------------------------------------|----------------------------------|
| Delta II       | 9,314                              | 500                              |
| Atlas IIA      | 9,558                              | 1,000                            |
| Titan III      | 10,164                             | 1,900                            |

All the missions described require rendezvous capability—either with a satellite or the space station. Space Station *Freedom* was chosen as the baseline for the rendezvous analysis, although the equations can be applied to many other scenarios. The vis-viva equation was used to calculate necessary velocity changes for Hohmann transfers in the rendezvous sequence. The Clohessy-Wilshire equations<sup>(1)</sup> were solved for the final approach to the target vehicles. To account for in-flight deviations and errors due to navigation instrumentation, human error, or the Delta II launch vehicle, a rendezvous sequence was created.

This sequence utilizes specific points where corrective maneuvers will be made, so that a much slower and safer approach can be achieved.

A maneuver with the distance vector in  $x$  (termed an  $r$ -bar maneuver) was chosen for final approach to minimize exhaust plume impingement upon the target vehicle. To insure that the final approach is made slowly, a rule was implemented that no burns will be made over 1% of the distance from the vehicle to the target. Consequently, many short burns must be made, each with decreasing strength. At the onset of the final maneuver proximity operations, the DART spacecraft is 1000 m from its target. The rendezvous burn sequence is

- (1) 1000 m  $\geq$  500 m
- (2) 500 m  $\geq$  100 m
- (3) 100 m  $\geq$  50 m
- (4) 50 m  $\geq$  25 m
- (5) 25 m  $\geq$  10 m
- (6) 10 m  $\geq$  5 m
- (7) 5 m  $\geq$  0.5 m

The Clohessy-Wilshire equations were used to solve for impulse velocity components and the time to complete each maneuver.

A 4-minute transfer was chosen for each of the maneuvers making the total final approach a 28-minute maneuver. Summing the  $\Delta V$ s for the rendezvous and proximity operations, the total  $\Delta V$  is approximately 20 m/s without a plane change maneuver, and 85 m/s with a 0.5° plane change correction. Allowing for in-flight deviations, a  $\Delta V$  of 100 m/s is required for the orbital maneuvering system (OMS), which will perform the rendezvous sequence, and a  $\Delta V$  of 6 m/s is required for the RCS engines, which will perform the final approach.

### STRUCTURES

The main shell of the DART capsule is made from 5052 alloy aluminum honeycomb sandwich sections bonded together to form the external cone structure. Graphite epoxy hat-section stringers located 20° apart will serve as load frames. Using the symmetrical bending formula, the individual cross-sectional areas of the stringers were calculated (see Fig. 3). The shear flow of this external shell could then be determined with the results

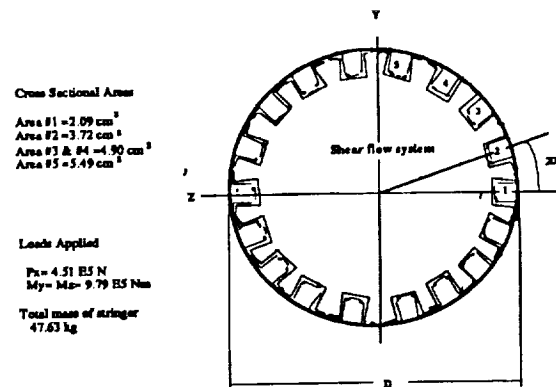


Fig. 3. Hat-section stringer attachment and cross-sectional areas.

shown in Fig. 4. Based on the maximum shear flow of 1.02E6 N/m, the honeycomb facing thickness was calculated to be 0.119 cm. A core density of 354 kg/m<sup>3</sup> was chosen for the aluminum honeycomb because it provided the lowest mass able to withstand a maximum compressive stress of 37.3 MPa. The total mass of the external honeycomb shell is 192.73 kg, and the total mass of the stringers is 45.0 kg.

The inner pressure vessel was designed to maintain a pressure 0.1034 MPa greater than the outside pressure. Assuming a factor of safety of 1.5, the thickness of the pressure vessel was determined using the pressure cabin thickness equation<sup>(2)</sup>. 2024-T4 aluminum will be used for this wall due to the low stresses created by the internal pressure. Discussed later in the "Reentry Studies" section is the TPS that will be applied to the outer structural skin of the DART spacecraft.

An abort tower was designed for intact abort capability in all flight regimes. Three motors 120° apart and capable of 113.8 kN of thrust each, are located at the apex of the tower. A computer program was written to optimize the abort tower height with the angle of the solid rocket motors. The design is for the flow to impinge on the bottom of the capsule. The place where this impingement occurs will be protected by the TPS in order to provide a safe means of abort. The tower mass was assumed to be 5 kg/m. As the motor angle increases, so does the motor mass. An optimum gimbal angle of 8° with an abort tower height of 4.8 m was determined to provide the lowest mass for the abort tower/motor system.

A structural interface is required to integrate the DART capsule with its Delta II launch vehicle. A ring truss made of 6016-T6 aluminum alloy was designed (see Fig. 5) to hold the 4772-kg DART spacecraft statically stable under the maximum loadings

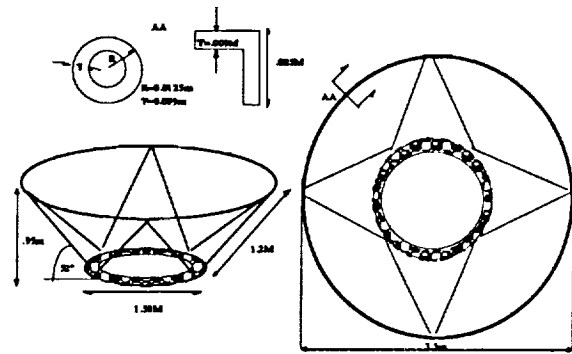


Fig. 5. DART/Delta II interface dimensions.

of the Delta II launch profile. Vibrational side loading will produce a maximum 0.7 gs along the lateral axis, and the longitudinal thrust axis will experience a maximum 5.86 gs during launch. Also, the interior volume of the truss must allow enough room for the strap-on propulsion package.

The DART capsule is secured to the truss by four steel cables. Applying the maximum loadings for the Delta II booster to the DART center of gravity, the ultimate force for the steel cables was found to be 22 kN. Using the method of sections and joints, and the definition of static stability, the forces in each member were isolated as a statically determinate system. The critical members were those on the 52° side angle; they bear a maximum force of 169.1 kN, which generates a maximum stress of 242 MPa. Using this value, a cross-sectional area of 7.0E 4 m<sup>2</sup> was obtained for the truss members. From the final dimensions and the minimum cross-sectional area, the volume of each member was calculated and summed over the entire structure. The total volume of the interface is 0.0107 m<sup>3</sup>, which produces a ring truss mass of 29 kg.

The DART strap-on propulsion package (shown in Fig. 1) is basically a box truss and ring fitting of 6016-T6 aluminum. The box forms a structural basket to hold the fuel, oxidizer, and pressurant tanks as well as necessary plumbing and regulators. The ring functions to diffuse the 17.8-kN force of the engines over an area of 0.178 m<sup>2</sup>. These conditions are acceptable to maintain heat shield and main structure integrity.

Each engine is connected to the cross members of the box truss using a conical cuff. These cuffs fit around the heat sink material used to cool the nozzle, and are secured with three arms bolted to the box truss. They hold the engine nozzles 5 cm apart to avoid nozzle impingement and are fastened together with 10 steel side bolts. Bolt stresses were found to be 185 MPa, requiring a cross-sectional bolt area of 4.51 mm<sup>2</sup>. The entire strap-on propulsion system is connected to the DART spacecraft with steel cables and is designed for a safety factor of 1.2.

### PROPULSION AND POWER SYSTEMS

The requirements for the OMS of the DART spacecraft are reliability, low mass, and the capability of performing all necessary orbital maneuvers such as rendezvous and deorbit. The thrust required for reentry was determined by using the

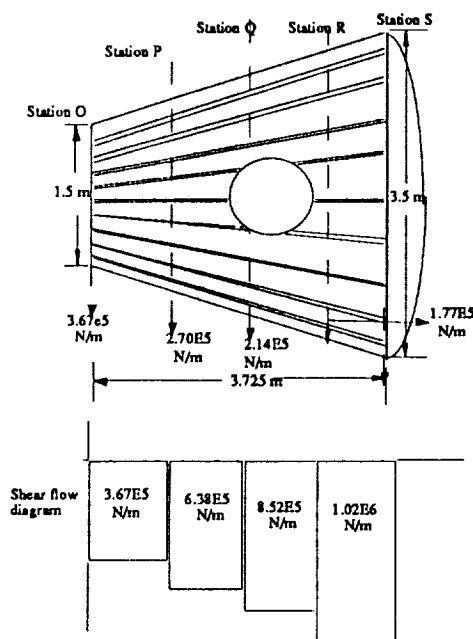


Fig. 4. Shear flow diagram.

re-entry  $\Delta V$  and the time for the maneuver to be executed. The re-entry  $\Delta V$  was found to be 240 m/s and the time for the maneuver was approximated as 1 min. This approximation was made so that there would be less than  $1^\circ$  of rotation about the Earth for the duration of the reentry burn, resulting in an impulsive maneuver. The required reentry thrust was found to be 18 kN.

Three major factors influenced the DART main engine propellant selection. Liquid propellants were chosen over solid propellants so that the OMS would be capable of several restarts. The second factor involved ignition systems. The two choices for ignition were to use a traditional ignition system or to use hypergolic propellants, which ignite on contact. Hypergolic propellants were chosen due to their low masses and simplicity. A trade-off study was undertaken to examine the properties and characteristics of several propellant combinations. The combination of hydrazine and nitrogen tetroxide was chosen due to ease of storage and more desirable physical characteristics.

The propellant feed system choice was made by examining two types of systems: pressure fed and turbopump fed. The turbopump system is a complicated one that provides high pressures for the chamber. Although the pressure-fed system delivers a lower pressure to the chamber (usually less than 5 MPa), it was chosen because the system has a minimal amount of moving parts, making it lighter, less expensive, and more reliable.

Because of volume constraints set by the DART/Delta II interface, a design configuration with four engines will be implemented. With four smaller engines (instead of one or two larger engines), the available volume can be maximized more easily. Having four engines also provides redundancy if one of the engines should fail. A bolt-on engine configuration was also developed for DART. However, the choice was made to use the strap-on engine system since it is entirely exterior to the spacecraft, leaving more room available for cabin use.

The optimum chamber pressure was determined by taking the minimum thrust required and determining the smallest exit diameter that is capable of providing that thrust. Results from this analysis are shown in Fig. 6, from which the smallest exit

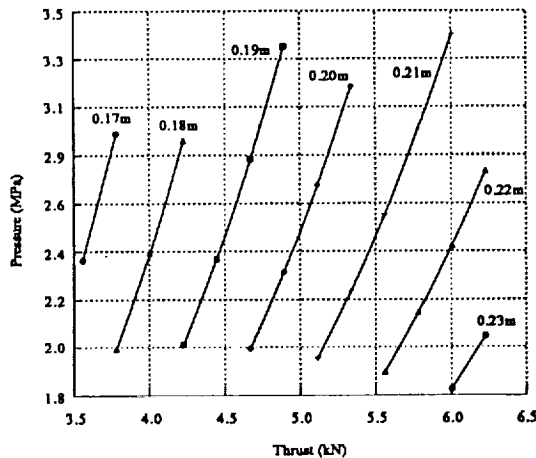


Fig. 6 Chamber Pressure vs. Thrust (Varying Exit Diameter)

diameter was found to be 19 cm. A thrust of 4.45 kN was used for this calculation. Applying this information, a computer program was written to determine the main engine specifications. Results from this analysis are summarized in Table 4. Figure 7 shows main engine dimensions.

TABLE 4. Main engine specifications.

|                       |                    |
|-----------------------|--------------------|
| Fuel                  | Hydrazine          |
| Oxidizer              | Nitrogen Tetroxide |
| Avg. Molecular Weight | 19 kg/mol          |
| Cp/Cv                 | 1.26               |
| Thrust/Engine         | 4.45 kN            |
| $I_{sp}$              | 305.6 s            |
| Flow Rate             | 1.48 kg/s          |
| Nozzle Mass           | 28.6 kg            |
| Chamber Mass          | 2.3 kg             |

Two different types of nozzles were compared for use in the main engine: bell and conical. The necessary length of the nozzle was determined to be 28.6 cm for the conical and 43.8 cm for the bell. The cost of the nozzles is also important since the engines are not reusable. The cost of constructing a conical nozzle is much less than the cost of manufacturing a bell nozzle. The main disadvantage of the conical nozzle is that there are more losses than in a bell. The losses, though, are small, and the conical nozzle was determined to be the best choice for the DART propulsion system.

When the engines are operated, they generate great amounts of heat. If the engine walls are not designed properly they will begin to melt and send particulates into the flow. The proper thickness of the wall was determined by using heat conduction equations. The thickness of the wall was determined to be 3.7 cm, tapering to 1.0 cm at the nozzle exit. The material that was used to make the walls into a heat sink was a high-grade nickel alloy. The masses of the nozzle and chamber were found to be 28.6 kg and 2.3 kg, respectively.

The engine performance of the DART spacecraft was mainly determined by the specific impulse ( $I_{sp}$ ) of the OMS. A program was written to iteratively determine the  $I_{sp}$  of the OMS. The  $I_{sp}$  was determined to be 305.6 sec. The fuel necessary for the mission was then determined using the rocket equation that relates mass and  $I_{sp}$  to  $\Delta V$ . With a  $\Delta V$  of 340 m/s, the total

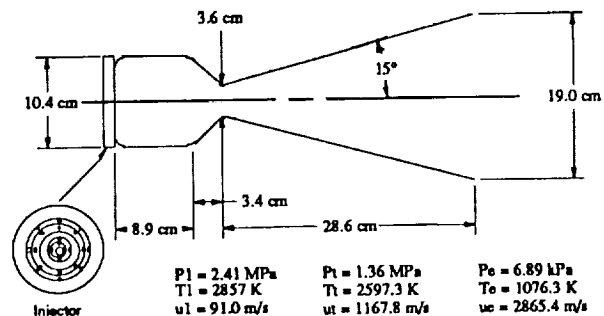


Fig. 7. Main engine dimensions.

propellant mass was determined to be 493.3 kg. The mass of the fuel and oxidizer was found using the mass ratio of oxidizer to fuel required for shifting equilibrium of hydrazine and nitrogen tetroxide, which is 1.08. The mass of hydrazine required for a  $\Delta V$  of 340 m/s is 237.2 kg and the mass of the oxidizer is 256.1 kg.

As mentioned above, the propellant tanks and the main engines will be contained within the strap-on propulsion package, as shown in Fig. 8. The fuel and oxidizer tanks must remain a constant 3.10 MPa, and the highly pressurized gas to feed the system will be helium at 27.58 MPa. An isentropic process was assumed in order to calculate the 12.7 kg of helium necessary for the pressurant. There will be two sets of tanks for all four engines. A total of six tanks (two fuel, two oxidizer, and two helium) will be connected across from one another in parallel so that if one set failed, the second set, along with the RCS, could safely stabilize the craft.

For the DART vehicle, the module containing the propellant tanks has a relatively large length-to-diameter, so cylindrical tanks will be used for the fuel and oxidizer. Due to the very high pressure required, spherical tanks are used for the helium. The most important factor in the selection of construction materials for propellant tanks is strength-to-density ratio. Comparing this ratio for tanks made of aluminum, stainless steel, and fiberglass, it was found that the best ratio can be achieved with a fiberglass-wound tank containing an aluminum-alloy liner. The liner will be corrugated to extend pressure cycle life.

The DART RCS has two major functions: to counteract adverse motion due to forces and moments, and to maneuver the vehicle for attitude control purposes and reentry. Besides perturbations due to nodal regression and apsidal shifting, other principal forces that the spacecraft will experience during its mission include aerodynamic drag and internal acceleration. Internal acceleration can be attributed to propellant shifting, astronaut movement, and the deployment of solar array panels.

The RCS thruster system will be pressure fed, with the thruster locations shown in Fig. 9 and the specifications given in Table 5. The required thrust was calculated from the maximum rotational angular velocity of the DART capsule. The thrust must adequately counteract the angular moments about all major axes. Again, a combination of hydrazine and nitrogen tetroxide was chosen with helium as the high pressure gas. Spherical tanks are used due to their small surface-to-volume ratio. The fuel and oxidizer

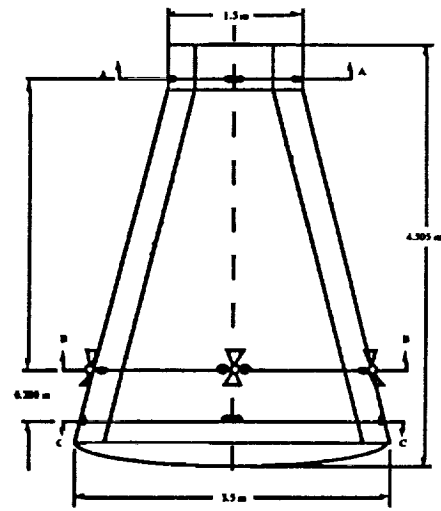


Fig. 9. RCS thruster locations.

tanks will have a pressure of 1.034 MPa, while the helium will be stored at a pressure of 10.0 MPa. Since nitrogen tetroxide is very corrosive and explosive, the tank material chosen is Ti-6Al-4V ELI. The helium and fuel tanks will be made of composites lined with aluminum.

TABLE 5. Thruster specifications.

| Section     | Thrust (N) | Mass (kg) |
|-------------|------------|-----------|
| A-A Vernier | 100.0      | 1.090     |
| B-B         | 351.0      | 2.260     |
| B-B Vernier | 42.0       | 0.634     |

The DART spacecraft's power generation requirement is set at 1500 W of continuous electrical power. A solar array was chosen as DART's primary power supply. Depending upon the solar angle of incidence, the time of direct sunlight will be approximately 60.4%. The mass of the assembled solar cells will be 12.44 kg, and the mass of the flexible roll-up blanket that will be used to deploy the solar array is 25.05 kg. The solar cell and blanket assembly will be rolled up into a 0.25-m-diameter cylinder that will be stowed inside the spacecraft until it is safely delivered to orbit. At this point, small motor will unroll the blanket and will keep it taut throughout the mission.

The solar array will be backed up by a secondary system consisting of silver-zinc rechargeable batteries. The battery system will be turned on automatically when the power demand increases or during solar eclipses. The baseline LEO that DART will maintain has a period of 94 min. This means that the spacecraft will be in shadow 39.6% of the time, or 47.52 hours. The batteries will supply the same amount of power as the solar array so that the total energy required during the 47.52 hours is 71.28 kw-hr.

Since silver-zinc batteries have a lifecycle of 20 to 200 cycles, they can constantly be recharged using solar cell electrical output. At a discharge rate of 10 hours the batteries will be

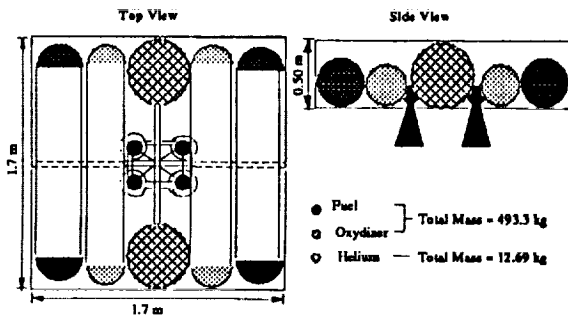


Fig. 8. Propulsion package configuration.

recharged five times during the mission, reducing the total weight of the batteries to 93.76 kg. Four batteries will be used to add redundancy; three batteries will be charged and discharged to supply the power needed and the other battery will be reserved for possible emergencies, with enough power for three hours.

## AVIONICS

The DART spacecraft uses the LTN-90 ring laser gyro inertial navigation system (INS) as both the primary attitude source and as the sensor for position, velocity, rotation rate, and acceleration. The LTN-90 is composed of an inertial sensor display unit, a mode selector, and an inertial reference unit. In the inertial reference unit are the ring laser gyros (RLG), which measure rotation accelerations and rates about the three spacecraft axes, and three single axis accelerometers, which measure accelerations and rates.

Because the positional error of the LTN-90 increases every hour, it will have to be updated by another navigation system. The primary satellite navigational system considered for updates is the Global Positioning System (GPS). GPS is a satellite-based navigational system that will give continuous worldwide coverage by 1992, when 21 operational satellites are scheduled to be in orbit. The satellites orbit once every 12 hours ensuring that at least 4 satellites will be in view at all times.

Attitude determination and control of the DART spacecraft requires an accuracy of better than  $0.25^\circ$ . Five different systems were studied for the DART attitude control system. These five systems include reaction wheels, momentum wheels, reaction thrusters, control moment gyros, and magnetic torquers. As previously discussed in the "Propulsion and Power Systems" section, reaction thrusters were chosen for the DART spacecraft's attitude control system because of their accuracy and quick response capability.

The primary function of the data processing system is to monitor all equipment on the capsule. Through the use of sensors and output devices, this system will keep the astronauts informed about the status of all DART systems. The processing of this information involves reading in the sensor data and comparing the value with limits set for that sensor. If the value is not within the specified range, a warning light is activated and action is then taken to correct the problem.

Another function of the data processing system is to make the necessary computations for the OMS and the RCS. These computations involve determining the directional vector to the target position, number and duration of the OMS engine burns, and the required thruster firings for the attitude control. The data processing system is also required to interact with other external systems on the spacecraft. For example, the communication system must be linked to the processors to allow for data uplink and downlink.

Three major types of architectures were studied for the data processing system: centralized, federated, and distributed. A centralized system was chosen for DART. The configuration entails four general-purpose processors for guidance, navigation, and control. From these central processors will be links to main memory, the sensors, display controls, engine interfaces, and other external surfaces. These four processors will perform

synchronized computations, and intercomputer comparisons will be done to check for computational errors. In the event of a disagreement, the outvoted processor removes itself from the loop and attempts self-correction.

Each processor will have its own 16 Mbytes of RAM. This size allows for an estimated 1 Mbyte of software, 8 Mbytes reserved for runtime memory, and 7 Mbytes for temporary data storage and uplinked code, if needed. The design of the data bus consists of a two-way linear bus configuration. Fifteen busses will be used on DART: four between the four processors, two for sensors, two for mass memory, two for displays and keyboards, two for engine interfaces, and two for external interfaces and communications.

The choice of display equipment involved three types: CRTs, liquid crystal displays (LCD), and luminous flat panels. LCDs will be used for the DART's three displays. One of these displays will be used for the video camera needed for rendezvous and inspection; the other two are for the pilots.

Sensors return information concerning all operational systems on DART to the astronauts. These sensors will be applied to the following DART vehicle systems: propulsion, life support, reaction control, and abort. For the propulsion system, 172 sensors will be necessary to monitor the fuel, oxidizer, and pressurant tanks. Conditions that will be monitored include temperature, pressure, flow rate, and valve openings. For the life support system (LSS) 179 sensors will be necessary to measure the conditions of the nitrogen and oxygen tanks as well as the cabin atmosphere. Ninety-eight sensors are required to measure RCS tank and thruster temperatures. In addition, sensors are also needed for hatch closure, docking, and abort system confirmation. In all, 469 sensors with a total mass of 30 kg will be used on the DART spacecraft. An additional 120 kg has been allocated for wiring and digital/analog convertors.

Since the DART spacecraft will be performing rendezvous and docking maneuvers, a radar system is required. A trade-off study was performed that compared the Lunar Sounder, SEASAT Synthetic Aperture, OMV, and the Integrated Radar and Communications Subsystem (IRACS) radar systems. The IRACS system was chosen because it not only functions as a rendezvous radar, but can also operate as a communications system capable of a two-way link between orbiter and ground tracking stations. The system is compatible with TDRSS and can be used as a backup in case of navigation malfunctions.

DART's communication needs include video, audio, data, EVA, radar, and navigational transmissions. The primary receiving station will be TDRSS, which currently consists of two satellites that will enable communications for 80 minutes of the DART spacecraft's 94-minute orbit. If communications cannot be made through TDRSS, the second choice will be direct transmission to Earth. The number of Earth stations is limited, but there could be three or more used per orbit, which would account for about 30 minutes of transmission per 94-minute orbit.

As stated above, the DART capsule will receive transmissions from the GPS for navigational updates. An antenna and receiver are required and the system operates on two frequencies, one at 1.575 GHz and the other at 1.228 GHz. The bandwidth for these base frequencies was determined from the amount of data that must be transmitted each second and the clarity that the data must have in order to be receivable. The link budgets

are used to determine whether or not a signal will be receivable. The overall qualifying figure in the link budget determination is the carrier-to-noise ratio. This ratio must be positive and be at least 10.0 to 12.5 dB in order for the signal to have good reception<sup>(3)</sup>. The weakest link is the downlink to TDRSS. In this link, the carrier-to-noise ratio has been reduced to the minimum needed for good reception.

Different antennas are needed in order to transmit and receive the desired frequencies. For the S-band a dipole antenna will be housed under a skin blemish to avoid the need for mechanical deployment. There will be two such antennas, one facing the Earth and one 180° around the spacecraft so that it is facing space. The UHF band will use a helical coil antenna because of its suitability to EVA communications applications. It will be located on the egress face of the capsule, so as to face the astronauts as they perform EVA. The Ku-band is appropriate for the high data rate requirements of the video link, which infers a very wide bandwidth. To fulfill these requirements, a deployable parabolic antenna of 0.5 m diameter will deploy out of a slot on the pilot's left side through the exterior skin of the capsule. Its location was chosen to allow the antenna to point toward both TDRSS and Earth during orbit. The L-band antenna will be mounted in the same fashion as the S-band antennas, but only on the surface facing GPS satellites.

## HUMAN FACTORS

The internal layout of the DART capsule can be seen in Fig. 2. At the top of the capsule is the front hatch, which has a video camera on the outside to aid in rendezvous and docking. Moving into the capsule through the docking tunnel, control panels are encountered. Behind these control panels are the avionics systems, with extra space for avionics and control packages in the 0.3-m-thick capsule wall. Included in this total wall thickness is the heat shielding, external honeycomb shell, load frames, internal pressure vessel wall, and RCS thruster tanks.

At the end of this passageway are the pilot and copilot seats. Three-point harnesses will be used for all the crew to ensure maximum mobility while effectively securing the astronauts to their seats. However, since the pilots will be on their backs during launch and reentry, foot restraints are necessary to keep their legs from coming up into their chests. These restraints are located underneath the console directly in front of them. A small window is located on either side of the capsule, allowing the pilots limited outer visibility. A window was found to be needed, even if small, to give the astronauts a better sense of attitude and direction.

Moving through the 0.5-m passageway between pilot seats towards the back of the capsule, there are three couches for passengers and a side hatch for crew ingress/egress (see Fig. 10). Specifications of the seating facilities dictate that the maximum height and mass of the astronauts be 1.8 m and 80 kg, respectively. This crew seating configuration achieves an effective center of mass as well as 2.44 m<sup>3</sup> of storage compartment volume around the couches. Another added feature of the couch design is the ability of the couches to be easily removed. According to mission needs, as many as three couches can be removed either on the ground or at the space station to allow more room for

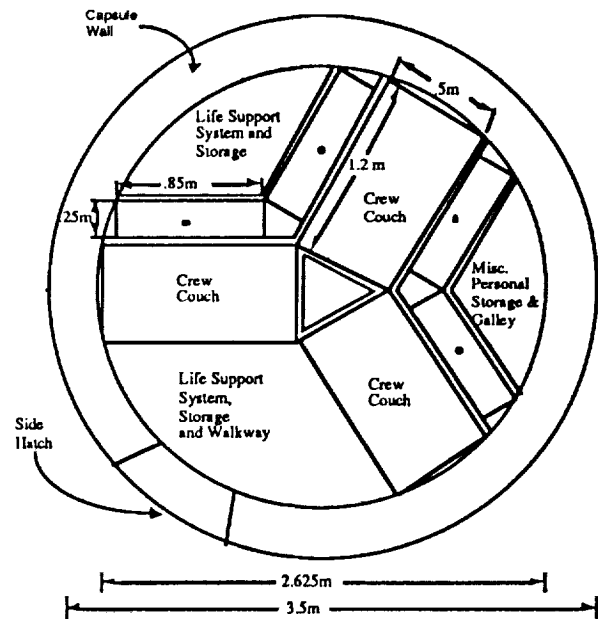


Fig. 10. Crew seating diagram.

storage and/or experiments. The volume attainable with three couches removed is 3.16 m<sup>3</sup>. Below this level are the water and LSS tanks, solar arrays, and batteries.

The radiation environment that the DART spacecraft will be exposed to during its proposed missions will not be a problem for the astronauts. In LEO at an inclination of 28.5°, the predominant source of radiation are the protons from Earth's Van Allen belts. It was calculated that the daily exposure to the crew would be about 185 mrem. At this daily dosage level, it would take 270 days to reach the NASA recommended annual exposure limit of 50 rem. Thus, the shielding provided by DART's honeycomb external shell and inner pressure vessel is adequate to protect the astronauts from dangerous radiation levels. As a precaution, passive radiation dosimeters (PRD) will be employed to measure the exact amount of radiation encountered by the astronauts.

The interior of the DART capsule will be held at standard atmospheric conditions. The metabolic oxygen requirement is an average of 1.0 kg per person-day; the amount of waste metabolic carbon dioxide produced will also be 1.0 kg per person-day. The carbon dioxide will be removed from the atmosphere using solid amine, which consists of small microporous beads whose surface is covered by amine. The beads themselves are composed of a polymeric acrylic ester. Since solid amine absorbs carbon dioxide at room temperature, it is easy to use and economical. The cabin air will be passed through an inlet filter to remove any trace elements or particles, then into a chamber where one of three amine canisters will be located. When the amine canister becomes saturated with carbon dioxide, the inlet flow will be switched to another canister. The saturated canister is then heated and the desorbed carbon dioxide is sent through a compressor and stored. The system will operate at a rate of 3600 lt/hr, have a total mass of just over 50 kg, a volume

of under 0.4 m<sup>3</sup> and requires 300 W of power for the compressor, pumps, and heaters.

The necessary elements for fire are fuel, oxygen, and a means of ignition. Ionization smoke detectors will be placed where trouble spots are expected (i.e., oxygen tanks, electronics, etc.). Fire extinguishment will be accomplished using Halon 1301, a chemical that inhibits the combustion reaction. Unreacted halon 1301 is harmless to humans for short exposures; however, when used on a fire, both hydrogen fluoride and hydrogen bromide (which are toxic in an enclosed atmosphere) result. This requires that the DART capsule be returned to Earth immediately in the event of a fire.

When the DART astronauts suit-up at KSC, they will be donning virtually the same suits worn by the crew of the space shuttle. The only difference is that they will not have a self-sustaining LSS permanently attached to their backs. The suit will be totally dependent on the capsule's LSS during launch, reentry, and depressurization. During the mission, a shirt-sleeve environment will be available. This enables the astronauts to wear cotton pants, shirts and jackets if desired.

Sufficient food and water must be available to supply the required 2500-3200 daily calories for a male crew member and 2200-2900 daily calories for a female crew member. The two types of food rations chosen for the DART spacecraft are the standard shuttle ration and the Meal Ready to Eat (MRE) ration. The shuttle ration offers over 23 menus, all of which are thermostabilized and dehydrated. If any heating of the food is required, a chemical heat packet is included in the packaging.

Each shuttle ration packs 2750 calories in it, and has a dry weight of 1.5 kg. To this, 1.9 kg of preparatory water must be added. Each meal takes up a volume of 0.004 m<sup>3</sup>, increasing to 0.005 m<sup>3</sup> when the preparatory water is added. The shuttle ration will be used for all planned meals, with the MRE ration relegated for the one-day emergency reserve. The MRE ration was originally developed for U.S. special forces field use. As such, it is very compact, needing no preparation to eat. The MRE packs 2600 calories per meal, has 12 different menus currently available, weighs 3.1 kg, and fits into a volume of 0.004 m<sup>3</sup>.

The potable water requirements for each crew member are approximately 1.2 kg per person-day. This will have to be carried in full, because the mass and volume requirements of a water recycling system will be too great for the short duration of the planned mission.

Waste solids and liquids require special handling in a micro-gravity environment. Each crew member will, on average, produce 4.0 kg of waste per person-day. This waste includes exhaled carbon dioxide, perspiration, food packaging, urine, and fecal solids. A diaper-like undergarment made of rubberized nylon will be worn to collect urine. The urine will then be transferred by hose to a holding tank and eventually ejected into space. Feces are stored in "blue bags" similar to early U.S. space missions.

Hygiene washing will not be needed for mission durations of less than four days. For the longer missions, washing can be accomplished using a sponge in a water-tight cocoon. The cocoon can be folded up when not in use, with the excess water evacuated by pump. A shower using the cocoon will use approximately 2.0 kg of water. The life support mass breakdown, exclusive of consumable food and water, is given in Table 5.

TABLE 5. Life support mass breakdown.

| Parameter                      | kg per Person-Day |
|--------------------------------|-------------------|
| Metabolic Oxygen               | 1.0               |
| Metabolic CO <sub>2</sub>      | 1.0               |
| Potable Water                  | 1.2               |
| Perspiration/Respiration Water | 1.8               |
| Trash Solids                   | 0.05              |
| Trash Liquids                  | 0.12              |
| Fecal Water                    | 2.0               |
| Fecal Solids                   | 0.09              |
| Hygiene Water                  | 4.0               |

REENTRY STUDIES

The DART spacecraft's reentry is modeled as semiballistic with a L/D ratio of 0.25. The reentry scenario begins with an impulse thrust maneuver at an altitude of 500 km. The ΔV from this thrust will produce a change in altitude by altering the orbit of the vehicle to that of an ellipse with apogee at 500 km. The intermediate phase of the reentry will begin at about 120 km where the deceleration of the DART capsule will become significant due to Earth's atmosphere. The trajectory to this altitude is calculated by using the vis-viva equation for Keplerian ellipse geometry.

The reentry equations of the intermediate and gas dynamic phases can be derived by summing the forces in two dimensions and making the lift vector normal to the capsule. These equations can then be utilized in a second-order differential equation. The Z-function method by Chapman<sup>(4)</sup> is applied to solve this differential equation using a computer program that was written for this DART reentry analysis. Fig. 11, a plot of altitude vs. velocity for different initial flight path angles, is a result of this analysis. Besides velocity, variations in deceleration, flight angle, and density were also calculated vs. altitude.

The reentry aerodynamic and thermodynamic properties of the DART spacecraft are dependent upon the flight trajectory, the orientation of the spacecraft, and the shape of the outer shell. The reentry trajectory calculated above is utilized in the analyses described below. A radius of curvature of 5.6 m was determined for the aft heat shield portion of the DART capsule.

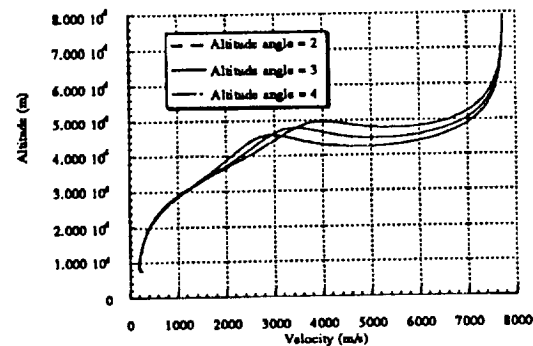


Fig. 11. Velocity vs. altitude for various initial flight path angles.

Given this symmetrical, spherical aft heat shield, a L/D ratio of 0.25 can be achieved by changing the trim angle of attack. This is accomplished by designing the DART center of gravity to be in a location where no resulting moment can occur. From Fig. 12, it is seen that given a radius of curvature of 5.6 m and a L/D ratio of 0.25, the corresponding angle of attack is approximately 15°. The required center of gravity offset from the capsule centerline (0.064 m) was then found from force coefficient results.

In addition, the pressure distribution across the aft heat shield was also calculated assuming modified Newtonian flow. At the maximum heating conditions, the pressure ratio was found to be 500 and the maximum pressure 5E7 N/m<sup>2</sup>.

To protect the DART spacecraft from the high aerodynamic heating loads seen during reentry, a TPS will be applied to the outer structural skin of the vehicle (see Fig. 13). A detailed aerodynamic heating analysis was conducted to calculate the heat distribution on the vehicle during reentry. For this analysis, the TPS was divided into two parts: (1) the aft heat shield and (2) the conical heat shield. It was determined from the DART reentry trajectory study that the peak heating rate occurs at an altitude of 53,555 m. Standard atmospheric conditions at this altitude were used in the convective heat flux equations<sup>(5)</sup>. Therefore, the heating results shown in Fig. 14 represent the highest temperatures and convective heat fluxes that will be seen by the DART capsule during reentry.

Using these results, a trade-off study was conducted to determine the most appropriate material(s) for the DART TPS. Materials under consideration included ablative, ceramic tiles, carbon carbon, cork, and thermal blankets. The results of the heating analysis support the use of a combination of ablative material and thermal blankets as seen in Fig. 13. The ablative material will cover the aft heat shield and the lower portion of the conical heat shield. Low-density phenolic epoxy resin was chosen for its low mass, low material cost, and thermal characteristics. The phenolic epoxy resin can be applied to the DART vehicle in the form of spray-on foam and can be stripped during refurbishment with a water cannon. Thermal blankets consisting of low-density fibrous silica batting protect the upper conical section of the capsule during reentry. The reusable blankets dissipate heat by radiating it away from the capsule. The baseline method for ablator and thermal blanket attachment will be direct bond as opposed to subpanel methods.

The DART spacecraft will use a parachute recovery system. A paraglider landing system was also researched, but the parachute was chosen due to mass and volume constraints. Two parachutes were chosen because larger chutes are more difficult to manufacture and take longer to deploy. Note that each parachute will require a diameter of 41 m in order to give the capsule a descent rate of 7.62 m/s. Also, in the event of a single parachute failure, the other will safely recover the DART capsule with a descent rate of 10.79 m/s.

The parachute deployment sequence begins at an altitude of 4000 m with the extraction of the pilot parachutes by mortars. The pilot parachutes, in turn, deploy the main parachutes, which fully inflate in 6 s. After the parachutes have been deployed and stabilized, a simple mechanism will release the aft heat shield, which is connected to an air bag. The air bag functions to soften the water impact and will be filled with helium.

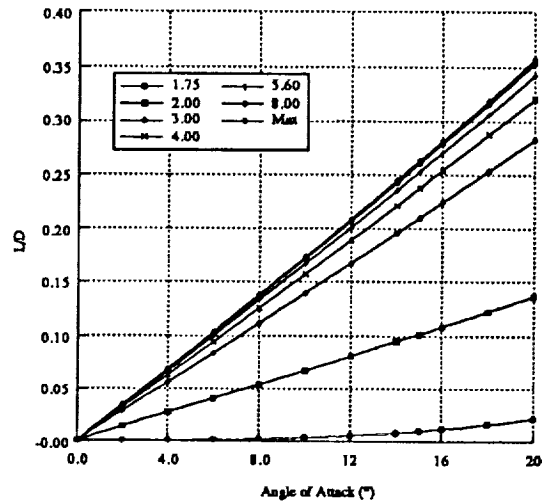


Fig. 12. L/D vs. angle of attack for different radii of curvature.

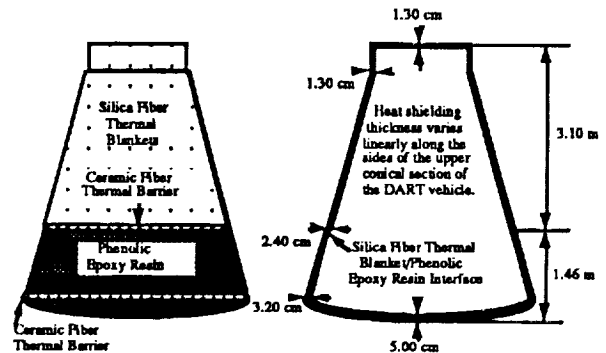


Fig. 13. TPS configuration and thickness.

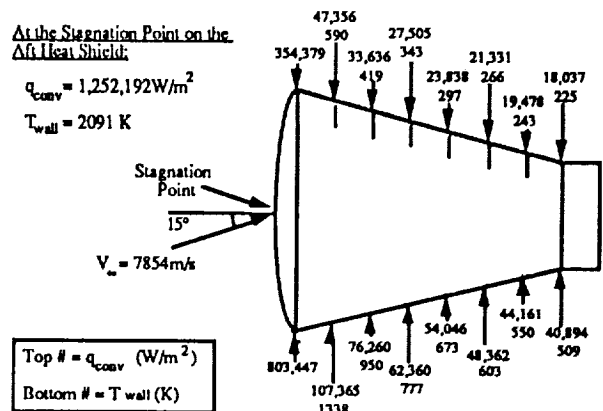


Fig. 14. Aerodynamic heating analysis results.

Constructed of nylon cloth covered with a thin coating of rubber, cables will be added to the outside surface of the bag for reinforcement. Note that the aft heat shield remains attached to the bottom of the bag and serves to stabilize the capsule in rough waters by lowering its center of gravity.

### REFURBISHMENT AND COSTING

The refurbishment fraction,  $f$ , is a percentage of the initial cost used to project the reuse and refurbishment cost for a system over its mission model. Historically, the fraction ranges from 0.03 for the X-15 to 0.10 for the space shuttle. The minimum mission model for the DART AMS is 10 flights per year for 20 years.

The refurbishment fraction is really the sum of two parts: the refitting of the capsule per year of the model with new systems (based on the original unit costs), and the refurbishment of the system per year over the model. A mathematical model that estimates the lifespan of DART components and uses a power law to increase the percentage of systems needing refitting per year is applied. Using this model, the refitting portion of the refurbishment fraction was found to be 0.05 while the refurbishment part was calculated at 0.02, resulting in a refurbishment fraction of 0.07.

An accurate and detailed costing analysis for the DART spacecraft is necessary for many reasons. One reason is to show that the spacecraft is an affordable addition to the U.S. Space Program. Another reason is to demonstrate the economical advantages of DART's partially reusable design.

The main costs were broken down into two categories: recurring and nonrecurring. Recurring costs include the cost of the craft itself, transportation, launch vehicle costs, launch preparations, ground support, recovery, and refurbishment. Nonrecurring costs include the cost of preparing to produce the spacecraft and the cost of adapting the existing infrastructure to accommodate the operation of the craft. The total program cost is found by adding together the recurring and nonrecurring costs, and then adding the cost of ground support equipment, subsystem development tests, and project management. For a flight model of 150 flights (10 per year for 15 years) and a refurbishment factor of 0.07, the cost model projects the total DART project cost will be 20.4 billion dollars or an average of 102 million dollars per flight (FY91 dollars).

A trade-off study compared the total program cost of a semireusable craft to that of an expendable one over constant mission model. This model set the number of missions per year at 10 a year for 20 years starting in 1995. Inflation was purposefully not accounted for so that the total program cost could be seen as an initial investment in 1991 dollars with interest yield the same as the inflation rate. The results of this study demonstrate that if more than 90 flights are expected, a semireusable spacecraft becomes more economical than an expendable one.

### CONCLUSION

This summary outlined the advantages of DART as an alternative manned spacecraft. With the use of the Delta II 7920 commercial booster, DART will have a 96% reliable launch system if existing ground support facilities at Cape Canaveral, Florida, are utilized. The DART design team has refit a capsule-based manned space vehicle with current technology. The capsule has a launch weight of 4772 kg, a base diameter of 3.5 m, a height of 4.5 m, and a cone side angle of 15°. In orbit, propulsion is generated using a hypergolic, expendable propulsion package. The craft uses the Tracking Data Relay Satellite System in addition to the Global Positioning System for communications and positioning. DART's reentry will be semiballistic, with a parachute recovery to an Atlantic Ocean splashdown.

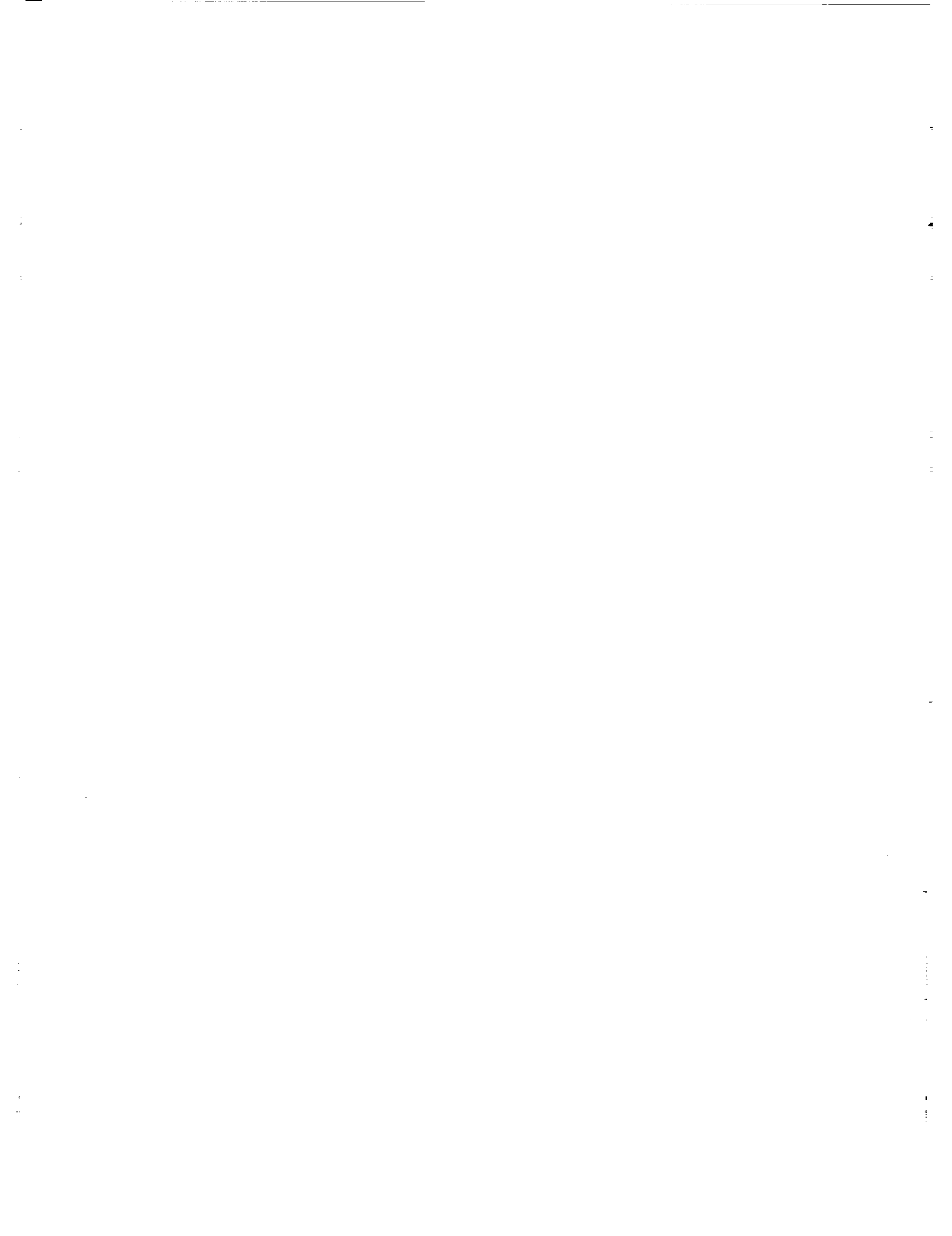
When integrated into the U.S. Manned Space Program, DART will provide flexible, reliable, and cost-effective access of crew and cargo to specific space destinations. This added capability will further microgravity experimentation and aid in the achievement of a permanent manned access to space. The DART program is designed for a mission model of 10 flights per year over 20 years, has a refurbishment fraction of 0.07, and a cost of \$102 million dollars per flight.

### ACKNOWLEDGMENTS

This work was conducted with the support of the Advanced Space Design Program of the Universities Space Research Association. This support is gratefully acknowledged. Principal author T. Lewerenz and co-authors M. Kosha and H. Magazu summarized the work of O. Bello, R. Bennett, F. Carreon, R. Cunningham, T. Foor, M. Gates, A. Harrison, M. Kaczmarek, Z. Kahn, M. Kosha, K. Le, T. Lewerenz, D. Loveless, H. Magazu, D. Matthews, J. Travisano, E. Villacis, D. Vine, A. White, and C. White. Faculty advisors were D. Akin, M. Lewis, and C. Lind.

### REFERENCES

1. Kaplan, Marshall, *Spacecraft Dynamics and Control*. New York: John Wiley & Sons, 1976.
2. Megyesy, Eugene F., *Pressure Vessel Handbook*. 1973.
3. Morgan, Walter I., and Gordon, Gary D., *Communications Satellite Handbook*. New York: John Wiley & Sons, 1989.
4. Chapman, D., "An Approximate Analytical Method for Studying Entry into Planetary Atmospheres." *NASA TR-11*, 1959.
5. Anderson, J. D., Jr., *Hypersonics and High Temperature Gas Dynamics*. New York: McGraw-Hill, Inc., 1989.



**TAURUS LIGHTWEIGHT MANNED SPACECRAFT  
EARTH ORBITING VEHICLE**

**UNIVERSITY OF MARYLAND**

524-18  
160600  
p-10

**INTRODUCTION**

The Taurus Lightweight Manned Spacecraft (LMS) was developed by students of the University of Maryland's Aerospace Engineering course in Space Vehicle Design. That course required students to design an Alternative Manned Spacecraft (AMS) to augment or replace the Space Transportation System and meet the following design requirements (1) Launch on the Taurus Booster being developed by Orbital Sciences Corporation; (2) 99.9% assured crew survival rate; (3) Technology cutoff date of January 1, 1991; (4) Compatibility with current space administration infrastructure; and (5) First flight by May 1995.

The Taurus LMS design meets the above requirements and represents an initial step toward larger and more complex spacecraft. The Taurus LMS has a very limited application when compared to the space shuttle, but it demonstrates that the U.S. can have a safe, reliable, and low-cost space system. The Taurus LMS is a short mission duration spacecraft designed to place one man into low Earth orbit (LEO). The driving factor for this design was the low payload carrying capabilities of the Taurus Booster—1300 kg to a 300-km orbit.

The Taurus LMS design is divided into six major design sections. The Human Factors section deals with the problems of life support and spacecraft cooling. The Propulsion section contains the Abort System, the Orbital Maneuvering System (OMS), the Reaction Control System (RCS), and Power Generation. The thermal protection systems and spacecraft structure are contained in the Structures section. The Avionics section includes Navigation, Attitude Determination, Data Processing, Communication systems, and Sensors. The Mission Analysis section was responsible for ground processing and spacecraft astrodynamics. The Systems Integration Section pulled the above sections together into one spacecraft, and addressed costing and reliability.

**TAURUS SYSTEMS OVERVIEW**

The Taurus Lightweight Manned Spacecraft (LMS) is a single-crew, short-mission spacecraft. The spacecraft is configured with a reentry capsule and a service module that is disposed of before reentry. The capsule will carry the pilot, main and secondary life support systems, avionics, back-up power supply, and parachute recovery system. The service module will carry the Orbital Maneuvering System, the main Reaction Control System and the Primary Power Generation System (see Fig. 1).

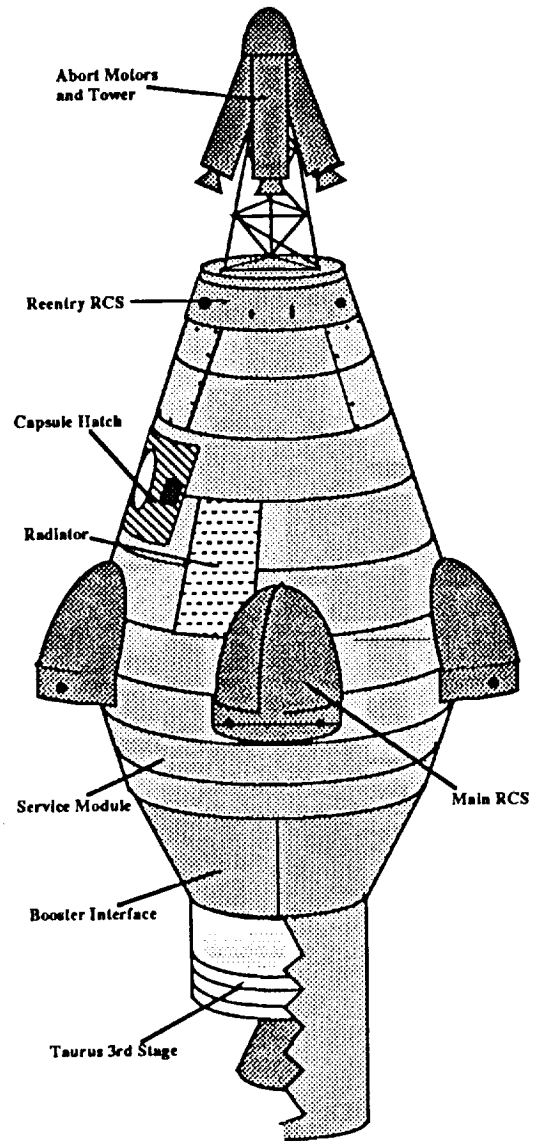


Fig. 1. Taurus LMS atop the booster.

The configuration of the service module/capsule design was chosen for two reasons. First, the spacecraft needed minimal mass on reentry to meet the required control characteristics.

176 INTENTIONALLY BLANK

This is accomplished by disposing of all unnecessary mass such as the propulsion system. Second, a stepdown from 2.0 m to 0.9 m was needed to place a capsule onto the booster.

The size of the Taurus LMS was chosen predominantly by the constraints imposed by the Human Factors group to place one man into a space capsule. The base of the capsule (above the heat shield) is 2.1 m in diameter, which is the smallest possible dimension to put one man into the capsule. The top of the capsule is 0.74 m, which is the minimum dimension required by the Propulsion group to attach the abort system. The height is fixed at 2.1 m to allow the sides of the capsule to be straight.

The top dimension of the service module is fixed by the bottom dimension of the capsule at 2.1 m in diameter. The height is 0.75 m. This dimension is selected because of the need to have the propulsion system in the service module. The bottom dimension is fixed at 1.6 m in diameter for attaching the Taurus booster structural interface (see Fig. 2).

The major constraint on the design of the Taurus LMS is the mass of the spacecraft. The maximum payload mass of the Taurus Booster is 1300 kg to a 300-km LEO. The systems masses are kept to a minimum, and are presented in Table 1. The total mass for the Taurus LMS is 1168.21 kg. This figure includes a budget margin of 50 kg for miscellaneous hardware. This launch mass is under the maximum payload allowable for the booster, thereby making the Taurus LMS a viable program.

The mass budget listed in Table 1 is corrected to show the mass gains from ejecting the abort system and the booster interface before the low Earth orbit is achieved.

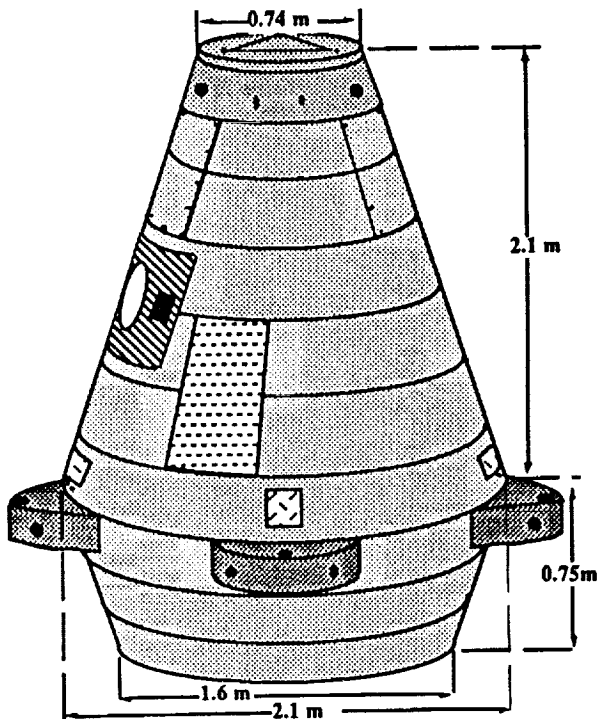


Fig. 2. Taurus LMS dimensions.

TABLE 1. Systems mass budget.

| System                        | Mass (kg)      |
|-------------------------------|----------------|
| Capsule structure             | 133.88         |
| Life support system           | 120.00         |
| Crew cabin                    | 112.50         |
| Abort system (effective)      | 40.00          |
| RCS capsule                   | 9.00           |
| RCS fuel and tank             | 0.54           |
| RCS oxidizer and tank         | 0.86           |
| RCS helium and tank           | 1.29           |
| Batteries                     | 21.05          |
| Thermal control               | 40.00          |
| Communications                | 11.50          |
| Sensors                       | 40.00          |
| Data processing               | 45.00          |
| Guidance and control          | 15.20          |
| Parachute system              | 60.00          |
| Service module structure      | 150.00         |
| Interface to capsule          | 20.00          |
| RCS main                      | 20.00          |
| OMS engine                    | 20.00          |
| Fuel and tank                 | 85.64          |
| Oxidizer and tank             | 106.52         |
| Helium and tank               | 4.73           |
| Power generator               | 25.20          |
| Booster interface (effective) | 31.30          |
| Misc. Hardware                | 50.00          |
| <b>Total</b>                  | <b>1168.21</b> |

The crew capsule will be the primary component of the Taurus LMS. It contains the pilot, the dual life support systems, the avionics systems, and the emergency/reentry power systems. Mounted to the exterior of the capsule will be the Reentry Reaction Control System, the Abort System (during launch), the Guidance and Navigation Sensors, and the Communications Antennas. The major components of the capsule are shown in Figs. 3 and 4.

The service module carries the orbital maneuvering engine, the power generation system, and the main reaction control system. All three of these systems feed off a central fuel and oxidizer system. The size of the propulsion system determined the height of the service module. The placement of the propulsion system is shown in Figs. 5 and 6.

#### MISSION ANALYSIS

The limited mass capability of the Taurus booster restricts the orbital maneuvering abilities of the Taurus LMS. With a total  $\Delta V$  of approximately 270 m/sec available for the OMS, the Taurus LMS is not capable of performing a rendezvous mission, which would require a  $\Delta V$  of at least 400 m/sec. Consequently, the baseline mission for the Taurus LMS is a single manned launch and return. The spacecraft is designed to be launched due east from Cape Canaveral at an inclination of 28.5° and with an orbital altitude of 300 km.

#### HUMAN FACTORS

The life support system of the Taurus LMS has been designed around a single astronaut on a 24-hour mission to LEO. The main life support system (MLS), as outlined in Fig. 7, consists

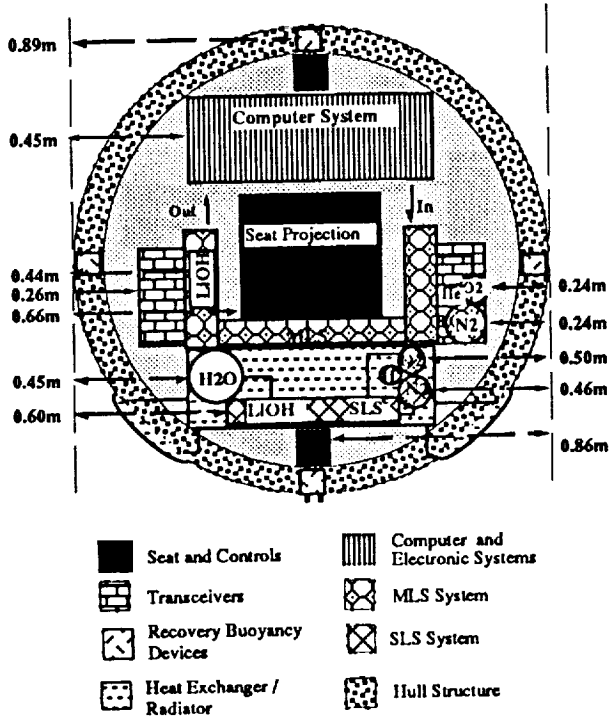


Fig. 3. Capsule internal cross section 10% from bottom.

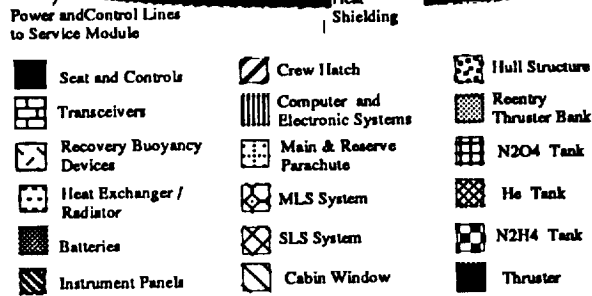
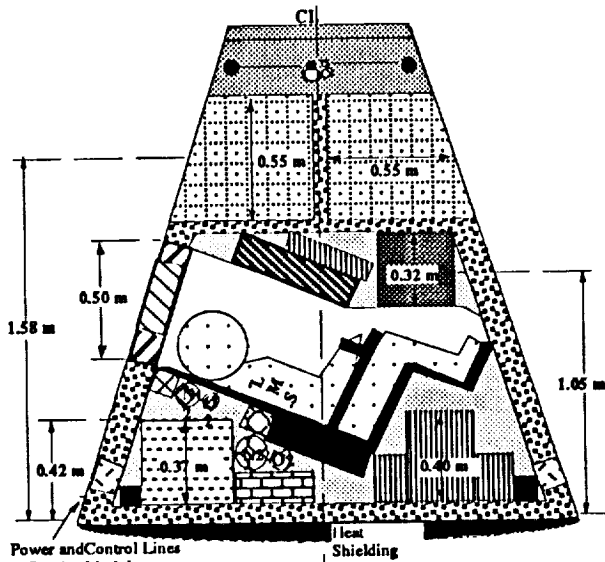


Fig. 4. Capsule internal side view.

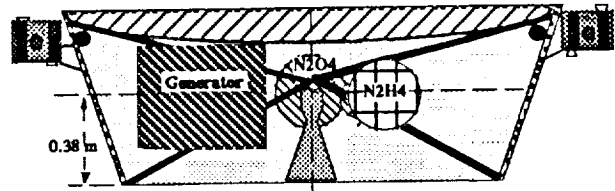


Fig. 5. Service module internal side view.

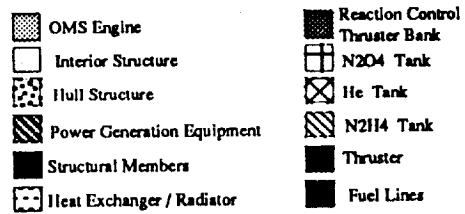
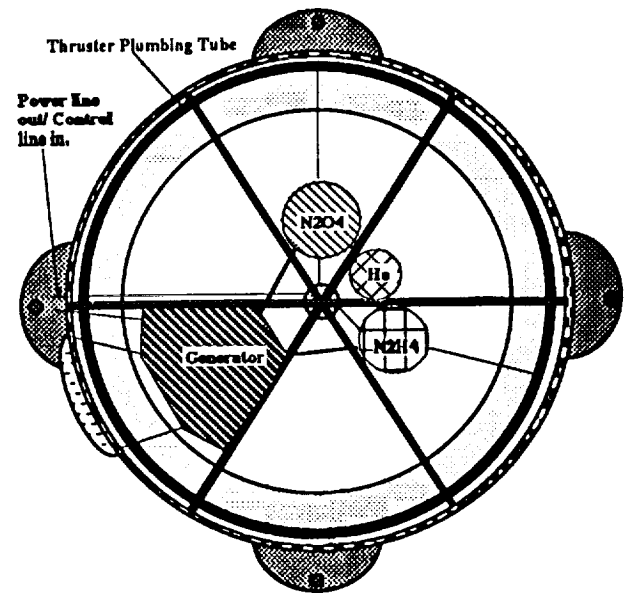


Fig. 6. Service module internal top view.

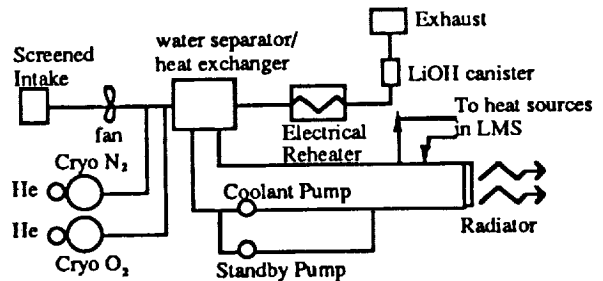


Fig. 7. Main life support system.

of a pressurized crew compartment held at 21°C and 50% humidity<sup>(1)</sup>. Continual recirculation of the cabin atmosphere (80% of which is nitrogen and 20% of which is oxygen at a total pressure of 101.3 kPa) is achieved through a single duct that will contain scrubbers to remove excess water vapor, carbon dioxide, and trace contaminants. The MLS air supply is stored cryogenically in two tanks, one for oxygen and one for nitrogen. Enough air is stored on liftoff to allow for repressurizing the cabin during orbit in the event of contamination or loss of cabin air, while allowing for an average astronaut metabolic consumption value of oxygen of 0.91 kg per 24 hours. A cabin volume of 4.08 m<sup>3</sup> is estimated in the calculations of the required mass of gas to repressurize the cabin.

One cryogenic tank contains 4.055 kg of liquid nitrogen, the other contains 2.066 kg of liquid oxygen. Electrical reheaters supply the energy to vaporize and heat the cryogenic fluids to a cabin temperature of 21°C. The computer regulates the pumping of the gas on a need basis, determined by its sensors.

A water separator serves as a heat exchanger. The separator is composed of a bank of four hundred aluminum tubes with an overall mass of 16.12 kg. Ethylene glycol will flow through these tubes, entering the bank at 0°C and leaving it at 5°C. Air will enter the heat exchanger at 21°C and will be cooled down to 10°C by the ethylene glycol, which in turn will flow to two radiators located on the exterior skin of the spacecraft<sup>(2)</sup>. These radiators will be oriented towards deep space during the mission and will radiate to space a total of 383 W of heat. The radiator is a tube-and-fin type, in which the coolant tubes have fins attached to them to increase the radiating area. Each radiator is constructed of aluminum and weighs 3 kg.

Once the air is reheated, it will pass through a lithium hydroxide (LiOH) canister that will chemically remove excess carbon dioxide. Each LiOH canister is cylindrical, with a diameter of 12 cm and a length of 0.26 m. One canister contains enough LiOH for 12 hours of carbon dioxide removal. Three (rather than two) canisters are used in the 24-hour mission for safety reasons.

The secondary life support system (SLS), as shown in Fig. 8, consists of a 10-kg pressure suit. This suit is worn by the astronaut throughout the mission, but is not pressurized unless there is an MLS malfunction. The SLS provides a self-contained

environment for the astronaut until successful deorbit and landing is achieved. The pressure suit is composed of the helmet and the body. A special seal separates the two parts, allowing for a one-time pressurization of the body by pure nitrogen gas, while continually circulating 50% oxygen and 50% nitrogen at a total pressure of 55.16 kPa inside the independent helmet. The SLS gasses are carried in a pair of separate cryogenic tanks that contain 1 kg of oxygen and nitrogen, respectively. The gasses are heated electrically before being injected into the SLS loop. A water-cooled undergarment, with tiny tubes woven into the fabric through which cooling water flows, provides thermal control for the astronaut. There are three attachment points on the pressure suit for hookups into the communications system, the atmospheric filtering system, and both the liquid-cooled undergarment and the pressurizing line from the cryogenic nitrogen storage tank.

The mission duration is short enough that only 5 kg of weight is used to supply the necessary rations. A large plastic squeeze bottle will be filled with drinking water and placed aboard the capsule for the astronaut, along with several freeze-dried food bars. Additional life support equipment include a 4.5 kg CO<sub>2</sub> fire extinguisher, a firstaid kit, and a 17.7 kg survival pack similar to the ones carried by U.S. military pilots.

There is no waste removal from the spacecraft. The astronaut will use catheters and plastic bags for liquid waste, and will wear a diaper-like undergarment for solid waste collection.

Two major requirements influenced the design of the pilot seat: it had to be conducive to large accelerations and it had to occupy a minimal cross-sectional area and volume inside the capsule due to the weight restriction. The mass of the seat is 16 kg.

## PROPULSION AND POWER

The abort system will insure crew survival in case of a critical failure of the Taurus booster system, such as an explosive detonation of the booster fuel or a critical malfunction. Assuming a 5-s detection time before the fuel in the booster detonates, the abort system would have to place the Taurus LMS crew capsule at a distance of 805 m from the launch site or moving booster, and place the capsule at a minimum of 500 m in altitude for recovery parachute deployment. The 805 m radial distance represents the typical danger radius of a detonating solid rocket booster system.

Thrust termination ports are required hardware additions to the Taurus booster. The thrust termination device, or "blow out" ports, would almost instantaneously vent the pressure and extinguish the flame within the thrust chamber, thereby dropping the acceleration of the Taurus booster to zero and allowing the abort system to function well within the required acceleration limits set by the human factors division for human pilots.

Solid abort rockets will be used in the Taurus spacecraft because of their (1) high thrust-to-weight ratios, (2) simple design, (3) high reliability, (4) lower volume requirements, and (5) ease of storage. A combination of three solid abort motors, placed 120° apart, will reduce the hardware mass and increase reliability by decreasing the number of failure and heating points on the Taurus capsule during an abort sequence.

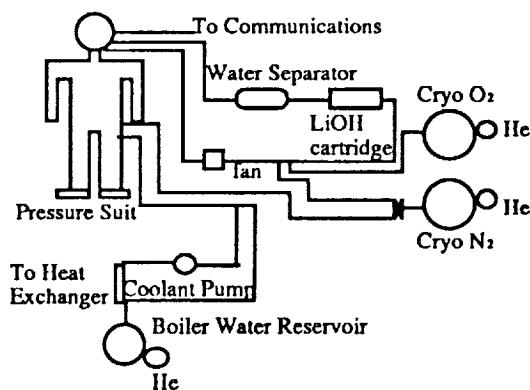


Fig. 8. Secondary life support system.

A tower structure was designed for the abort rocket placement, providing a mass savings by discarding the entire abort system at a predetermined altitude (40-50 km) past the point of maximum dynamic pressure. Other advantages of this tower structure are minimal heating of the upper stages of the Taurus booster and capsule by the exhaust plume of the motor, and good directional control characteristics. The motor top is an aerodynamically designed fairing to reduce drag.

To reduce the mass of the system, a high-energy, solid double fuel DB/AP-HMX/AL has been selected based on the need for an energetic solid propellant with a high specific impulse of 270 s<sup>(3)</sup>. The HTS organic (graphite) composite was selected for the motor casing and nozzle assembly, due to its high tensile strength and low density when compared to current metal alloys and other composite materials. This casing material will be protected from the hot gasses and the solid fuel's chamber temperature of 3707°C by a layer of ablative asbestos phenolic 2.54 mm thick. At the motor throat, thermal protection heat transfer consists of an 0.8-mm-thick layer of ablative pyrolytic graphite covering a back-up 2.0-cm layer ATJ molded graphite (see Fig. 9). The 0.8-mm layer of pyrolytic graphite will extend from the throat to the tip of the nozzle to protect the structural HTS graphite.

The abort initiation can be controlled manually and by ground. The manual abort system is located in the crew cabin. The abort command can be initiated by launch control in the event of a detected malfunction of the Taurus booster or other critical subsystem. The ignition system for the solid motors consists of a pyrotechnic igniter mounted at the top of the abort motor solid fuel.

The orbital maneuvering system (OMS) consists of a non-reusable main liquid propellant rocket engine, two tanks (one for the fuel and one for the oxidizer), an injector, and a pressurized gas system. The OMS must be reliable and have a low mass. It also must be capable of restarting numerous times, and of operating in the vacuum conditions of space with a thrust

level of 3158 N. This value was determined by assuming a  $\Delta V$  of 270 m/s and an impulsive maneuver of 1', which is approximately 1° of distance around the Earth's orbit.

The main engine is a liquid propellant type. The advantages of this type of engine over a solid one are high performance, repeated restarts, and randomly variable duration for each start. Hypergolic propellants are used to allow for a greatly simplified ignition system. Moreover, since hypergolic propellants ignite smoothly upon contact, accumulation of the mixture of fuel and oxidizer in the combustion chamber does not occur in large quantities, and the danger of explosion is minimized. The combination of nitrogen tetroxide and hydrazine is used due to its high specific impulse, ease of storage, and material compatibility for the tank design.

The engine specifications and the properties in the combustion chamber were determined assuming a one-dimensional compressible flow and an isentropic nozzle region. A study of the variation in chamber pressure vs. thrust coefficient was undertaken to obtain the optimum chamber pressure. The effects of increasing the chamber pressure above 2.069 MPa on the thrust coefficient were slight. The optimum chamber pressure, therefore, was determined to be 2.069 MPa. The specific impulse ( $I_{sp}$ ) of the main engine was found to be 292.3 s. Using this  $I_{sp}$  and a total  $\Delta V$  of 270 m/sec in the rocket equation, the total propellant mass was found to be 48.08 kg of fuel (hydrazine) and 51.92 kg of oxidizer (nitrogen tetroxide). A summary of the combustion chamber parameters and engine specifications is presented in Fig. 10.

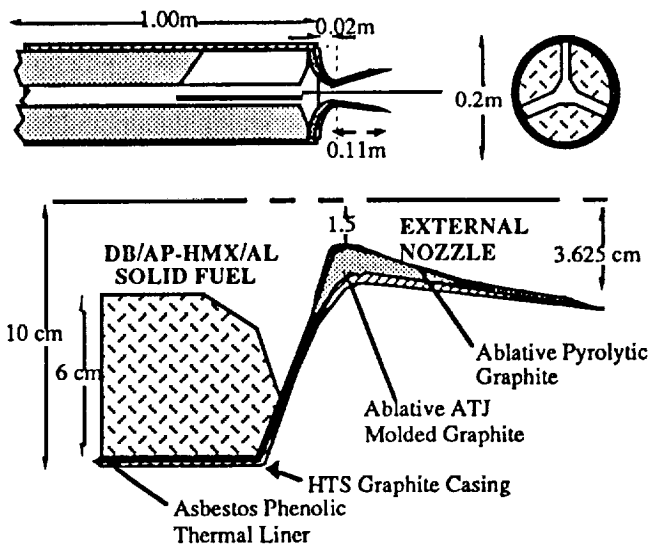
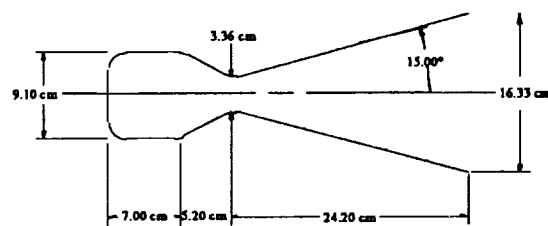


Fig. 9. Solid abort motor internal layout.

|                       | Chamber | Throat  | Exit  |
|-----------------------|---------|---------|-------|
| P (MPa):              | 2.069E6 | 1.144E6 | 6894  |
| T (K):                | 2857    | 2528    | 1880  |
| A (cm <sup>2</sup> ): | 65.1    | 8.9     | 209.3 |



|                       | Chamber | Throat  | Exit  |
|-----------------------|---------|---------|-------|
| P (PA):               | 2.069E6 | 1.144E6 | 6894  |
| T (K):                | 2857    | 2528    | 1880  |
| A (cm <sup>2</sup> ): | 65.1    | 8.9     | 209.3 |

Mass = 16 kg  
 Thrust = 3158 Nt  
 Isp = 291.3 sec  
 Propellants = N<sub>2</sub>H<sub>4</sub>/N<sub>2</sub>O<sub>4</sub>  
 Mixture Ratio = 1.08

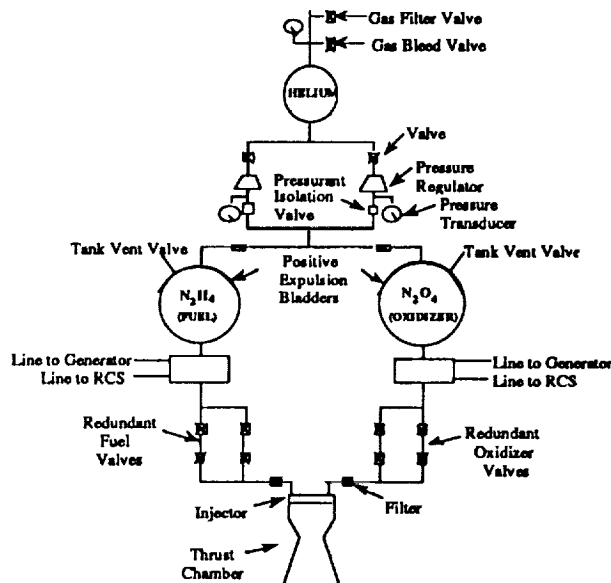
Specif Heat Ratio = 1.26  
 Chamber thickness = 1.54 cm  
 Throat thickness = 1.54 cm  
 Nozzle Thickness = 0.71 cm

Fig. 10. Engine specifications.

Thermal protection using ablative cooling is effective for longer firing durations without significant weight penalties. Although this technique was initially used for solid propellant systems, it has since proved to be quite successful for liquid engines with chamber pressures of 2.069 MPa or less, and pressure-fed systems<sup>(4)</sup>. The char depth or thickness of the thrust chamber will increase at the combustion chamber and throat, and decrease to a constant thickness along the rest of the nozzle. Using a Refrasil phenolic ablative thrust chamber, the thickness at the combustion chamber and throat is 1.54 cm, and 0.71 cm for the rest of the nozzle.

To introduce and meter the flow into the combustion chamber, an impinging stream-type injector has been selected. The propellants are injected through a number of separate orifices so that the fuel and the oxidizer streams impinge upon each other aiding in the break-down of the liquid.

The OMS is located in the service module of the Taurus LMS, and will use a simple and reliable pressurized gas feed system. The oxidizer and fuel are fed into the combustion chamber by the displacement of helium gas stored at a pressure of 27.58 MPa. The tanks for the propellants are kept at a constant pressure of 3.45 MPa. They contain all the propellant needed to operate the OMS, Reaction Control System, and Power System. This design enables any one of the aforementioned systems to draw more propellant from the common tanks in the event of an emergency. The plumbing in the OMS is designed so that active systems are double-strunged to provide redundancies, while passive systems are single strunged. A schematic diagram of the OMS is shown in Fig. 11.



**Tank Dimensions, Mass and Pressure**

|            | He        | N <sub>2</sub> H <sub>4</sub> | N <sub>2</sub> O <sub>4</sub> |
|------------|-----------|-------------------------------|-------------------------------|
| Radius :   | 18 cm     | 27 cm                         | 26 cm                         |
| Mass :     | 4.73 kg   | 85.64 kg                      | 106.58 kg                     |
| Pressure : | 27.58 MPa | 3.45 MPa                      | 3.45 MPa                      |

Fig. 11. Schematic diagram of the OMS.

The RCS measures, corrects, and counteracts adverse motion due to forces and moments that cause the spacecraft to rotate or translate. It also maneuvers the Taurus LMS in attitude control, position keeping, and reentry. The spacecraft will experience two types of perturbations depending on the inclination of the orbit plane to the equator. These are nodal regression and apsidal shifting. Other principal forces that the spacecraft will experience include aerodynamic drag and internal accelerations produced by propellant shifting and astronaut movements.

The RCS was divided into a reentry control, located at the top of the Taurus LMS capsule, and a main reaction control, located at the top of the service module. The reentry system will be used during deorbit when the service module is detached and the capsule begins to reenter the Earth's atmosphere. Its primary purpose is to allow for cross-range maneuvering and reentry oscillation dampening.

The main reaction control system provides the Taurus LMS with three degrees of freedom control at all times with two to three redundant thruster directions. The thrusters will be covered by an aerodynamic shroud, which is blown off when separation from the Taurus booster occurs.

The primary power supply is a single reciprocating hydrogen-nitrogen tetroxide engine<sup>(5)</sup>. The mass and size of the engine has been scaled down from an existing engine used in missions similar to the one performed by the Taurus. For the required energy of 19.2 kWhr, the weight of the engine was scaled down to 25.2 kg. This includes the weight of the compressor, alternator, cooling system, and plumbing. The engine has dimensions of 0.519 m by 0.405 m by 0.463 m, which results in a volume of 0.0973 m<sup>3</sup>.

The secondary power supply is a system of silver-zinc rechargeable batteries. They are lightweight and compatible with the other systems. The batteries will be used for reentry power after the service module containing the primary power system is detached, and whenever the demand for power rises above the primary power supply's output capability. The batteries have a cycle life of 20 to 200 cycles, and can be recharged using the primary system's electrical power output. For a discharge rate of four hours, the total weight of the batteries will be 21.05 kg. The batteries, therefore, can be recharged six times during the entire mission.

The silver-zinc batteries are composed of 45 to 50 cells or plates that are connected and stored inside two separate sealed boxes to prevent leakage and protect them against the space environment. Selecting two batteries adds redundancy and reduces the risk of a malfunction. When the mission is completed and the spacecraft is ready for reentry, the batteries will provide the primary power.

## AVIONICS

The initial navigation system on board the Taurus LMS is the LCINS (Low Cost Inertial Navigation System). The LCINS is a strapdown configuration with two degrees of freedom gyros. The inertial reference assembly is reduced in size, and a digital microprocessor performs all of the measuring, data processing, instrument torquing computation, scaling, attitude, and navigation functions. With dimensions of 152 by 152 by 215

mm, weight of 3.0 kg, and power of 35 W, the LCINS is the ideal system to use in a heavily mass-constrained spacecraft such as the Taurus LMS.

Since the positional error of the LCINS increases every hour, it is updated by another navigation system. The primary satellite navigational system considered for the updates is the Global Positioning System (GPS). GPS is a satellite-based navigational system that will give continuous worldwide coverage by the year 1992, when there will be 21 operational satellites in orbit. The satellites orbit every 12 hours and transmit two L band signals: L1 at 1575.42 MHz and L2 at 1227.60 MHz. This system of orbits ensures at least four satellites in view at all times.

An accuracy of better than  $0.25^\circ$  is required for altitude determination and control of the Taurus LMS. Sun, horizon, and laser fiberoptic gyroscopes are used to determine the spacecraft's attitude. Reaction thrusters are used in the Taurus LMS attitude control system (previously discussed in "Propulsion and Power Systems") for their high force and accuracy.

The primary function of the data processing system is to monitor all equipment on the Taurus LMS. Through the use of sensors and output devices, this system will keep the astronaut informed about the present condition of all aspects of the spacecraft. Another function of the data processing system is to perform necessary navigation and flight control computations. The goal of this system is to allow for as many onboard processing capabilities as possible, thereby relying less on ground-based computations.

The data processing system will also make the necessary computations for the OMS and the RCS. These computations involve determining the directional vector to the target position, the number and duration of OMS engine burns, and the required thruster firings for attitude control. The data processing system must also interact with other external systems on the spacecraft. For example, the communication system must be linked to the processors to allow for data uplink and downlink. This computer system has been designed to control all systems of the spacecraft in case the astronaut is unable to perform his/her duties, allow for dual control when both the computer and astronaut are functioning, and allow for manual control if the computer malfunctions.

Three major types of architecture were studied for the Taurus LMS design: centralized, federated, and distributed. A centralized system has been selected (see Fig. 12). This design consists

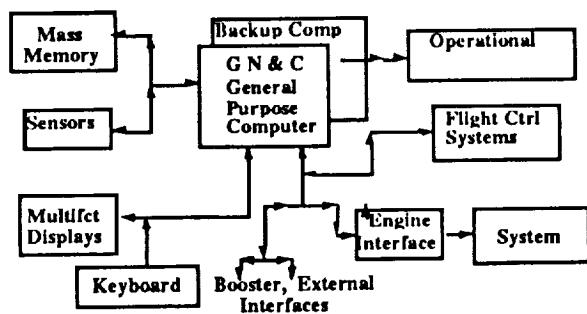


Fig. 12. Schematic diagram of centralized system.

of two general-purpose processors (one as the primary processor, and one as a backup computer) for guidance, navigation and control<sup>(6)</sup>. These central processors will be linked to the main memory, sensors, display controls, engine interfaces, and other external interfaces.

Each processor will have its own RAM associated with it. The size of the RAM will be 16 Mbyte. This size allows for an estimated 1 Mbyte of software, 8 Mbytes reserved for runtime memory, and 7 Mbyte for temporary data storage and space for uplinked code if needed. In case this memory gets corrupted, the capability to reload the software from the mass memory will exist. The decision to go with individual RAM is made to allow quicker and more independent execution. The design of the data bus consists of a two-way linear bus configuration. Six buses are used in the Taurus capsule, two for sensors and mass memory, two for engine and external interfaces, and two for displays and keyboard (all connected to the CPUs). Two liquid crystal displays (LCD) are used in the Taurus capsule<sup>(7)</sup>. They require little depth (approximately 2.0 cm) and power, and are digitally compatible. They do, however, require some type of external back light.

Sensors are required for the Taurus LMS to operate through computer and/or manual control. The sensors return information concerning capsule operational systems to the astronaut for updates and corrections. Consequently, sensors are applied to the propulsion, main life support, secondary life support, reaction control, and abort systems. For the propulsion, it is necessary to measure the conditions of the pressurant, oxidizer, and propellant tank, as well as the conditions of the plumbing and rocket combustion chamber. A total of eight temperature sensors ranging from 20 to 3000 K are required in the system.

With respect to the main life support system, it is necessary to measure the conditions of the pressurant, nitrogen and oxygen tanks, as well as the heat exchanger and cabin conditions. The total number of pressure sensors needed is 18. The sensors for the secondary life support system are similar to those in the main system due to their similar design; the only difference is the addition of a water tank. The total number of sensors required is 134. The total number of sensors required in the reaction control system is 98. Abort control sensors are placed on the system to guarantee that the tower has been armed before launch. Ten solid solid fuel motor sensors are used. Eight extra sensors are added to the Taurus system for hatch and ejection determinations. In total, there are 428 sensors on the Taurus LMS to check all systems for proper functioning, and to permit necessary changes if malfunctions occur. Because of the weight constraint on the Taurus system, only those sensors necessary for proper operation are used. The total weight of the sensors is approximately 25 kg. Using optical fiber wiring minimizes the amount of heat and radiation shielding. The entire mass of the sensors system on the Taurus service module is 50 kg. All sensors have been made double redundant and are 99.999% reliable.

Two modes of communication have been chosen to ensure reliability. The primary receiving station will be the Telemetry Data Relay Satellite System (TDRSS). It consists of two satellites that enable communications for 80 min of the 95-min orbit. To communicate through TDRSS, frequencies must be chosen for their few atmospheric losses in transmissions to Earth. The

range of 1 to 10 GHz is the only range that meets this requirement. In the event communications cannot be made with TDRSS, a second choice for a receiving station will be direct transmission to Earth. Although the number of Earth stations is limited, there could be at least three used per orbit, which would account for about 30 min of transmission time per 95-min orbit. The capsule will also receive transmissions from the Global Positioning System (GPS). These communications are used for navigation purposes, and operate on two frequencies, at 1.575 GHz and 1.228 GHz. The antenna is placed on the capsule's surface facing outward to GPS. The frequency assignments are based in the S band and are spaced so that not more than 500 MHz will be assigned for any one transponder. The bandwidth for these frequencies is determined from the amount of data that must be transmitted each second, and the clarity that the data must have in order to be received.

Link budgets are used to determine whether a signal will be receivable. The overall qualifying figure in the link budget determination is the carrier-to-noise ratio. This ratio must be positive, and at least 10 to 12.5 dB in order for the signal to have good reception. The weakest link is the downlink to TDRSS. In this link the carrier-to-noise ratio has been reduced to the minimum needed for good reception.

To transmit and receive the desired frequencies, different antennas are needed to cover the gaps in the bands used. Each band requires a different type of antenna based on the necessary bandwidth. A dipole antenna will be implemented for the S-band, and housed under a skin blemish to avoid the need for mechanical deployment. There will be two of these antennas, one facing Earth, and one facing space. The two antennas supply a mode of redundancy, and make serving Earth stations and TDRSS efficient during orbit. The L-band antenna will be mounted on the skin in the same fashion as the S-band antennas, but only on the surface facing GPS satellites.

### STRUCTURES

A tower or truss acts as the connection between the abort system and the capsule. It consists of a 3-sided structure with a total of 24 members made of 6061-T6 aluminum. The abort engines are covered in a graphite/epoxy casing that is bolted directly to the top of the tower. Each longitudinal member of the tower is connected to the capsule by two short members fastened to the capsule by explosive bolts. The tower and abort system, therefore, can be jettisoned so that extra mass is not carried into space.

The structural framework of the capsule consists of 14 stringers and a skin thickness of 4.8 mm. I-beam stringers were chosen for two reasons: they are extremely resistant to bending, and flanges on each side make for easy fastening of the skin and pressure vessel. Each stringer will carry an axial loading of 5 kN with a cross-sectional area of 0.00012 m<sup>2</sup>. The hatch is designed to hold a small navigation window.

The service module structures are divided into four categories: explosive bolts for the capsule and service module, longitudinal stringers and transverse rings, shear flow, and a capsule-supporting truss. These structures are designed to sustain a 10-g axial acceleration, and a 1-g sideways acceleration. A safety factor of 1.2 was used throughout the analysis.

Four equally spaced explosive bolt joints connect the capsule and the service module. A riveted-type butt joint was designed so that the bolts are of equal strength in shear, tension, and compression. There are four joints with two 225-mm explosive bolts on each joint.

Eight longitudinal stringers (I-beams with cross-sectional areas of 330 mm<sup>2</sup>) were chosen to carry the axial load. Two stiff end rings provide rigid support against lateral displacement, while three relatively flexible intermediate rings give elastic lateral support. The five transverse rings are shown in Fig. 13. The stringers and rings are made of 6061-T6 aluminum. The loading acting on each stringer is 11.587 kN.

The shear flow is only carried by the skin and has a maximum value at the bottom of the service module. The skin is also made of 6061-T6 aluminum, and has a thickness of 2 mm. Figure 14 presents the values for the forces and shear flow carried by the stringers and skin.

A truss structure will interface the Taurus LMS and the Taurus booster. The design constraints of this structure are prescribed by the dimensions of the service module and the mechanical interface of the Taurus booster. These dimensions are shown in Fig. 15. In addition, the structural interface is designed to take a vertical force of 8 g and a horizontal force of 1.7 g.

The truss structure will be made of 60601-T6 aluminum and will weigh approximately 31 kg. The axial stresses in each member of the truss are below the yield stress of this material (542 MPa). The design loads with a margin of safety are 108 kN in the vertical direction and 23 kN in the horizontal direction. The volume of the material used is 0.0112 m<sup>3</sup>. The interface will be equipped with explosive bolts around both the upper and lower circular perimeter. The bolts will be equipped with springs to allow separation from the service module once the orbit is circularized.

### REENTRY AND RECOVERY

The first portion of the reentry trajectory is a free-flight phase that takes the spacecraft from its orbit to the atmosphere (assumed to begin at 120 km). The second portion is the

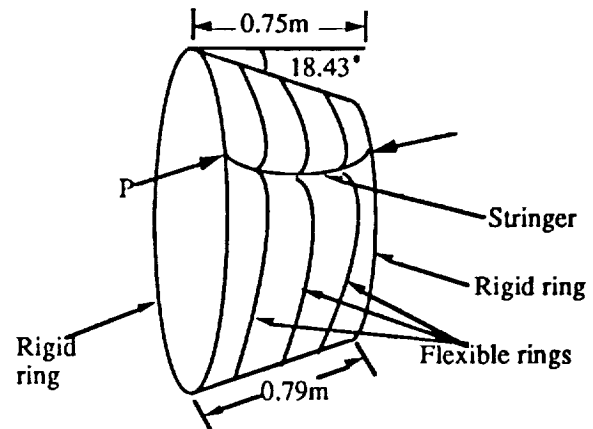


Fig. 13. Stringer under compressive load.

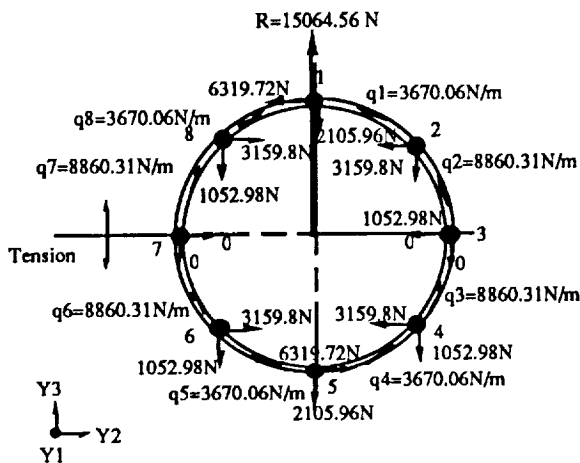


Fig. 14. Forces and shear flow carried by the stringers.

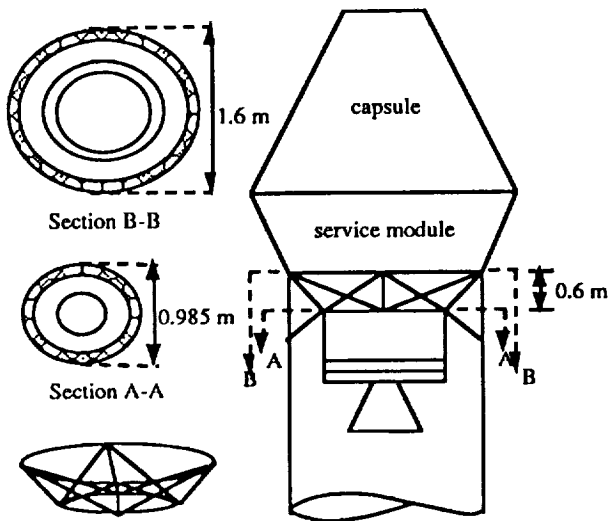


Fig. 15. Capsule configuration and interface dimensions.

atmospheric flight phase, during which the spacecraft flies through the atmosphere to land. A deorbit burn is necessary to slow the spacecraft down so that it falls from its orbit to a transfer orbit that brings it down into the atmosphere. Upon reaching the atmosphere, aerodynamic forces will overcome orbital mechanics and control the trajectory. The burn determines the spacecraft's new orbit, which sets its flight angle and velocity at atmospheric interface. The  $\Delta V$  required to deorbit is 140 m/sec from an altitude of 300 km. This corresponds to having a reentry flight path angle of  $2.0^\circ$ . Time of flight and angular distance traveled in the free-flight portion were computed by the method of Eccentric Anomaly<sup>(8)</sup>. It will take 18 min and 52 sec to fly from the deorbit burn altitude of

300 km to 120 km. During this time the spacecraft will fly  $77.14^\circ$  around the Earth. This will allow the location of the deorbit burn performance to determine a selected touchdown site.

A computer program was written to predict the atmospheric flight reentry trajectory. The time of flight between crossing 120 km and Earth impact is 775 s. The spacecraft gains altitude for 50 s at an altitude of approximately 59 km before continuing to fall. The velocity does not change significantly until 150 s into this portion of the flight, at which time the craft has reentered to 80 km and aerodynamic forces begin to influence the spacecraft's trajectory. The maximum spacecraft deceleration is 3.07 g. The craft will have slowed down to 63 m/s (0.19 Mach) by the time 3 km is reached so that the parachutes can be deployed.

The Taurus LMS will use a phenolic-nylon ablative heat shield with a heat combustion of 12 MJ/kg to protect the capsule from the aerodynamic heating loads upon reentry. The thermal protection system is composed of a carrier support panel, mounted to the capsule structure via channel beam panel supports, with a layer of insulation between the panel and the skin at the capsule<sup>(9)</sup>. The capsule will undergo a maximum wall temperature of 1606 K and a maximum heating rate of 563.4 KW. The TPS for the walls of the capsule will be the same as for the heat shield, but bonded directly to the skin of the spacecraft.

The Taurus LMS recovery system consists of two round parachutes deployed simultaneously at a reentry speed of Mach 0.19. The deployment sequence will begin at 3 km above sea level, at which point a computer command will fire explosive pilot bolts on both parachute hatches, allowing the mortar-deployed pilot parachutes to pull the two canopies out into the wind-stream. Once the parachutes are inflated, the capsule will begin a 10-min canopy descent to the ocean, inflating its pontoon before splash down. Upon splashdown, the canopies will be released and dye markers will be ejected through the parachute hatches. A radio beacon will help guide the recovery aircraft and vessels to the Taurus LMS.

**COSTING**

The costing of the Taurus LMS was done as an expendable vehicle that will become operational with one mission in May 1995. The Taurus LMS will have three missions in 1996. The project will be disbanded at the end of the fourth mission to allow the space administration to proceed with the application of the Taurus LMS technologies.

The costing of the Taurus LMS was divided into two parts, nonrecurring and recurring. Nonrecurring costs are the costs of design, development, testing and engineering of the spacecraft, as well as the project management and integration costs. Recurring costs are the costs of the individual spacecrafts as well as the integration, assembly, and checkout of the spacecraft, as well as booster and launch/recovery costs<sup>(10)</sup>. The Non-recurring costs of the project will be \$1148.3 million in 1991 dollars. The total project costs would be \$1491.31 million. This results in cost of \$372.83 million per flight.

### GROWTH POTENTIAL

Growth potential for the Taurus LMS takes two forms. The first would involve an increase in the Taurus booster capabilities. The second would entail launching on a different booster. Assuming the former occurs, the ability to launch with an additional 300 kg of fuel would provide for the necessary  $\Delta V$  to enable a rendezvous and docking with the Space Station *Freedom*. In this scenario, the Taurus LMS could be used for small-scale emergency supply deliveries, space station crew rotation, or as an emergency lifeboat docked at the space station. Moreover, it could perform a visual satellite inspection to determine the cause of failure and evaluate the feasibility of in-orbit repair.

The second option would be to launch the Taurus LMS on a Delta booster. This would permit nearly four times the mass to be launched into orbit, making the aforementioned missions possible.

### CONCLUSION

The Taurus Lightweight Manned Spacecraft is a stepping stone for the Alternative Manned Spacecraft program that offers a foundation to build a new space program. The use of the Taurus Booster results in the design of a limited mission vehicle that is capable of putting one man into low earth orbit for a 24-hour mission with minimal life support and minimal crew member comfort. The purpose of the LMS project was to prove that a man can be put into space using a low payload booster.

### ACKNOWLEDGMENTS

This work was conducted with the support of the Advanced Space Design Program of the Universities Space Research Association. This support is gratefully acknowledged. Principal

author M. Bosset was assisted by K. A. Chase and J. Clegern. This paper summarizes the work of M. Bosset, G. Bulla, K. A. Chase, J. Clegern, M. S. Connelly, A. Est, C. Henry, M. Kaczmarek, B. Kelm, K. Le, D. Loveless, C. Neidhart, T. H. Peng, J. Plotkin, J. A. Sandusky, D. Sewell, J. Travisano, E. Vandersall, E. Villacis, and A. G. White. Faculty advisors were D. Akin, M. Lewis and C. Lind.

### REFERENCES

1. Purser P. E., Faget M. A., and Smith N. F., eds., *Manned Spacecraft: Engineering Design and Operation*, Fairchild Publications, Inc., New York, 1964.
2. Singh Jasbir: *Heat Transfer Fluids and Systems for Process and Energy Applications*, Marcel Dekker, Inc., New York, 1985.
3. Sutton, G. P., *Rocket Propulsion Elements*, John Wiley & Sons, Inc., New York, 1986.
4. Huzel, K. Dieter and Huang, H. David, "Design of Liquid Propellant Rocket Engine," NASA Scientific and Technical Information Office, Washington, DC, 1971.
5. Morgan, N. E. and W. D. Morath, "Development of a Hydrogen-Oxygen Internal Combustion Engine Space Power System."
6. Adapted from Rockwell's block diagram for the Shuttle's Data Processing System.
7. Spitzer, C. R., *Digital Avionics Systems*, Prentice Hall Inc., New Jersey, 1987.
8. Bate, R. R., Mueller D. D., and White J. E.; *Fundamentals of Astrodynamics*, Dover Publications, New York, 1971.
9. Dow, M. B., and Thompkins, S. S., "Materials and Design for Ablative Heat Shields," NASA TM X-2570, 1972.
10. National Aeronautics and Space Administration, "JSC Cost Model Summary" 1991 (converted by D. Akin).

**WALKING ROBOT: A DESIGN PROJECT FOR  
UNDERGRADUATE STUDENTS**

**UNIVERSITY OF MARYLAND, MECHANICAL ENGINEERING**

525-37  
160601  
P-4

The objective of the University of Maryland walking robot project was to design, analyze, assemble, and test an intelligent, mobile, and terrain-adaptive system. The robot incorporates existing technologies in novel ways. The legs emulate the walking path of a human by an innovative modification of a crank-and-rocker mechanism. The body consists of two tripod frames connected by a turning mechanism. The two sets of three legs are mounted so as to allow the robot to walk with stability in its own footsteps. The computer uses a modular hardware design and distributed processing. Dual-port RAM is used to allow communication between a supervisory personal computer and seven microcontrollers. The microcontrollers provide low-level control for the motors and relieve the processing burden on the PC.

### INTRODUCTION

Special-purpose robots are commonplace today in manufacturing and other controlled environments. Current technology is sufficient to build walking machines capable of traversing rugged terrain. However, few robots of this type have been built. The University of Maryland's walking machine, PredaTerp, is a six-legged robot designed to be able to walk over uneven ground, clear small obstacles, climb stairs, and autonomously navigate any desired path.

The robot's design evolved to be a novel application of existing technologies. The six legs were designed by combining well-understood mechanisms and optimized for performance, flexibility, and simplicity. The body design used two tripods for walking stability and ease of turning. The electrical hardware design employed modularity and distributed processing to drive the many motors. The software design used feedback to coordinate the system.

The robot is designed to be easily enhanced. Minor modifications would enable the machine to perform useful tasks with high precision and reliability. The walking machine may be easily adapted to hostile environments such as high radiation zones and alien terrain.

### LEG DESIGN

It was desired to design a leg with an ovoid walking path to minimize the "slamming" effect caused by a robot's inertial forces during normal walking. This effect is highly pronounced in designs employing a circular kinematic path. The leg consists of three mechanisms. The ovoid path is generated by a modified crank-and-rocker mechanism; it is magnified by a pantograph mechanism and can be raised and lowered by a leg-lift mechanism.

The four-bar mechanism consists of a crank link, coupler link, rocker link, and fixed (ground) link. In this design, the traditional straight bar coupler was replaced with an oblique triangular link. The internal angles of the modified coupler can be varied to create an array of continuous, oblique circular paths at the disjointed vertex of the triangle. The constraints required the

leg to have an ovoid path in order to prevent the inertial "slamming" effect during walking motion. In addition, the constraint on the number of motors required this motion to be carried out by one motor.

The four-bar, crank-and-rocker mechanism (Fig. 1) is defined by links AP (crank), BQ (rocker), ABC (coupler), and PQ (ground). The motor turns the crank through a worm gear combination. As the crank rotates, a pendulum path is created by the rocker link. The stride length of the path at point C, (Fig. 1) is 3.5 cm, with a stride height of 0.68 cm.

The desired stride length was 15 cm. In order to achieve this, the 7.5-cm path produced by the crank-and-rocker mechanism is amplified by a pantograph mechanism (the remaining four links of Fig. 1). The ovoid path at point C has been translated, inverted, and magnified by a factor of 2 at the foot (point H).

The leg-lift mechanism is capable of changing the leg height as well as the stride length. The leg-lift mechanism is the pinion gear and lifter gear-link attached to point F (Fig. 1). The lifter motor rotates the lifter gear, causing the pantograph mechanism to compress or expand. The leg was designed to extend and compress 7.5 cm from the position of the foot during normal walking. This results in a total lift range of 15 cm, sufficient to clear small obstacles and climb stairs.

The crank-and-rocker, pantograph, and leg-lift mechanisms are supported between two rectangular plates. These plates provide the ground attachments for the crank-and-rocker at points P and Q, and also for the lifter mechanism at points R and S. The plates also provide a convenient means for mounting the entire leg assembly to the robot body, and protect the leg links from external objects that could damage or bind the moving links during operation. The motor and gearbox combinations of the lifter and four-bar mechanisms are mounted outside the plates to avoid mechanical interference. Motors and gearboxes can be mounted on either of the two plates, depending on their orientation on the robot body. Three legs have a right-hand orientation and the remaining three have a left-hand orientation for this design.

Dynamic engineering analysis using DADS computer software provided insight into link forces, torques, displacements, velocities, and accelerations during normal walking as well as during

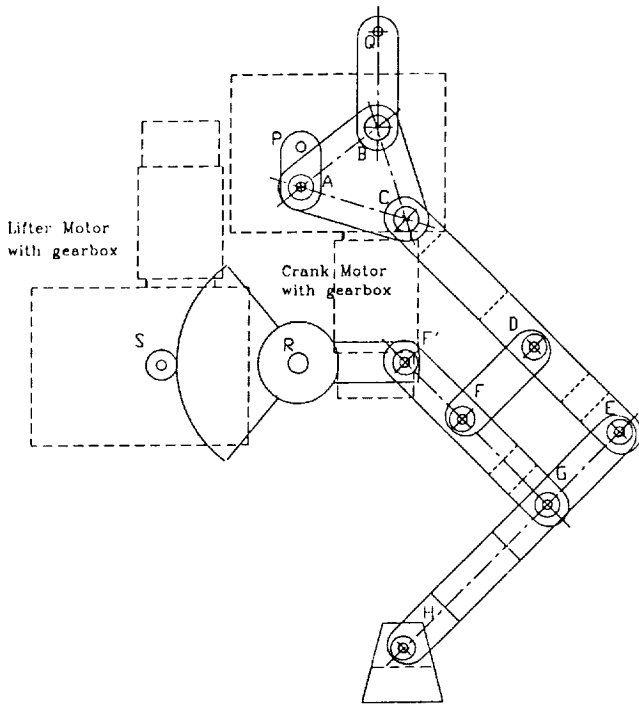


Fig. 1. Leg mechanism.

stair climbing. These data were used to design against stress failure and to select appropriate motors and bearings for the legs. This analysis also prompted an idea to connect a torsion spring to point Q on the rocker link. During the DADS analysis it was discovered that a torsion spring attached to the rocker would lower the maximum required torque by approximately 40%. This resulted in a smoother torque vs. time curve (smoother walking motion) and allowed the use of a smaller and lighter motor.

All the links for the leg mechanisms were machined by numerical control (NC). An NC machining center was programmed to cut the aluminum and steel leg links and modify the lifter gear. This highly precise machine cut complex shapes and drilled critical holes quickly while maintaining tolerances within 0.0002" (0.00051 cm). The aluminum support plates were punched by an NC turret punch. It was important to maintain tight tolerances for the hole positions, relative to one another, in the support plates because they provide the ground link for the lifter and four-bar mechanisms. The machine holds tolerances to within 0.001" (0.0025 cm).

**BODY DESIGN**

The main goal of the body design was to produce a frame capable of providing maximum flexibility and agility for the walking robot. The general design is of two concentric triangles, 180° out of phase, but able to rotate with respect to one another. The frame was designed to be inexpensive, lightweight, and to accommodate the electrical hardware and leg assemblies.

It also needed to allow a minimum of 30° free rotation between body planes. It was decided that the foot paths must be 15 cm long, creating a stride of 30 cm. The front-to-back distance between adjacent foot centers on opposite frames is 15 cm, and the front-to-back distance between feet on the same frame is 45 cm. This causes the robot to walk in its own footsteps.

The main part of the frame was made of 1" (2.5 cm) steel electrical conduit (Fig. 2). Cold rolled 0.125" x 1" (0.3 cm x 2.5 cm) steel bar was bent into U shapes and welded between the two side pieces of each frame to hold them in place. The bars also serve as attachment points for the front and back leg assemblies. Supporting arcs were welded to the side pieces to hold them apart, and to provide rigidity and resistance to the moment of the side legs. An 18-gauge steel sheet was riveted to both sides of each frame. The sheet added rigidity to the frame, but its main purpose was to provide a place to install the hardware, and to improve the appearance of the machine.

The robot body employed a turning mechanism to rotate one body plane relative to the other. Plates of 3/16" (0.5 cm) steel were cut to fit between the support arcs of each frame to hold up the turning column. This was necessary because the turning column supports half the body weight at all times. Two tapered roller bearings were used in the turning mechanism. Four gussets were welded to the bottom of the turning shaft to add resistance to moment. An aluminum bearing hub was

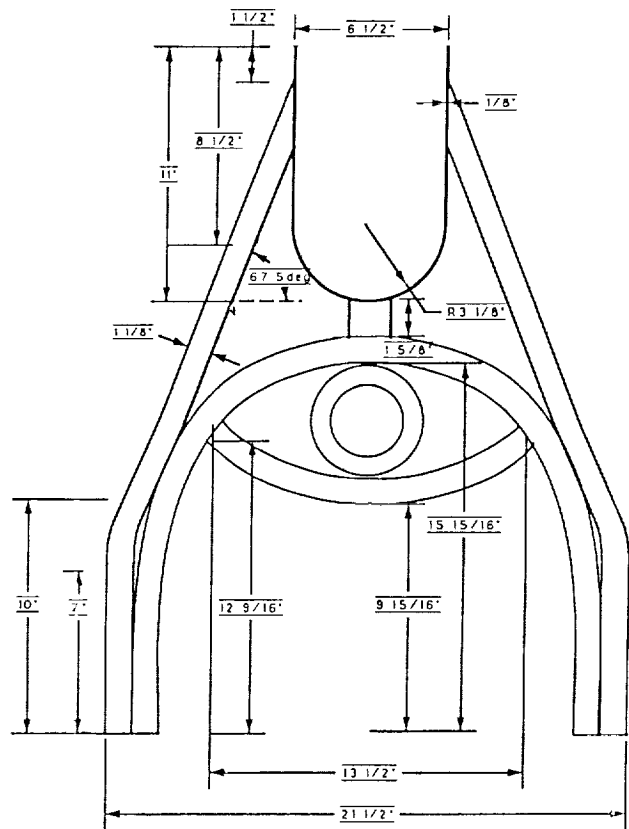


Fig. 2. Body frame.

constructed to separate the two bearings on the shaft. Bearings were press-fit into the hub. The topmost part of the turning shaft was threaded and a retaining nut was used to hold the frame assembly together and constrain the bearings. The motor torque was magnified through a worm gear combination. This was mounted rigidly to the upper body frame.

### ELECTRICAL HARDWARE DESIGN

Although the mechanical hardware is quite flexible, the number of motors it requires leads to a quite formidable problem: the simultaneous monitoring and controlling of 13 motors. The electrical hardware performs this task by having seven identical microcontroller circuits, each controlling one leg or the turning motor and an IBM PC-compatible computer as the supervisory processor (Fig. 3). All the subsystems of the computer control system of the robot contain identical elements. This modularity simplifies construction and troubleshooting. Once a prototype module is perfected, it only need be replicated to complete the entire subsystem.

Each microcontroller circuit is designed around an 87C196KB, a 16-bit embedded controller with many on-chip peripherals, including 8 kbytes of EPROM, pulse-width modulation, and high-speed IO functions.

Communication between the microcontrollers and the PC is accomplished with dual-port static RAMs. Each microcontroller shares a 2-k block with the PC. Each microcontroller will control, at most, two motors at a time. These microcontrollers are supervised by a personal computer, which oversees and coordinates the individual processors. The supervisory processor provides long-term system control over the navigational functions, as well as periodically checking up on each leg as needs dictate.

The motor power circuitry is able to handle a very wide current range very efficiently. All the power transistors are generously heat-sinked to quickly dissipate heat and thus maintain a safe operating temperature range. Motor speed is controlled by pulse-width modulation, in which peak current remains constant and average voltage is adjusted. This is an efficient

method of speed control, ideally suited to computer control. Power to the motor is switched on and off rapidly, the duty cycle determined by the processor.

Onboard batteries power the robot, with a switching voltage regulator controlling the voltage supplied to the computer. In order to maximize the robot's length of service per charge, the most efficient available regulator was used. The chosen switching regulator rapidly switches the unregulated power through a coil, efficiently providing a constant voltage.

All motors incorporate optical encoders that provide precise data concerning the position of the motor shaft. Simple circuits were used to decode phase data from the encoders into a form easily utilized by the microcontrollers. This provides the microcontroller with the direction and velocity of the motors.

The robot must protect itself from damage. In certain situations, if a motor does not turn off, the various mechanisms may be destroyed. Fail-safe switches were incorporated in the design to prevent such occurrences. If a motor reaches a certain point, the power driving the motor in that direction is shut off, and a signal is sent to the microcontroller. The microcontroller can still turn the motor in the opposite direction. Fuses are located throughout the robot to avoid electrically over-stressing components and risking fires. Each motor has its own fuse. If a fuse should blow, an LED would provide a visual indication of the bad fuse.

### SOFTWARE DESIGN

The primary design goal of PredaTerp's software was to implement an optimal solution to control the mechanical and electrical systems. The software engineering was split into three separate but interdependent tasks. The high-level code, written on the supervisory PC, coordinates the leg and turning motor actions to complete the events. The low-level task is that of driving the motors with the 80C196KB microcontrollers. The communications protocol provides the means of communication between the PC and the microcontrollers through the dual-port RAM.

The use of the PC allowed the utilization of established programming tools and techniques to write autonomous programs. The use of the PC also afforded a simple and flexible solution for tether design: a standard keyboard.

The PC is also able to assure that the commands passed to the legs and body are performed as desired. The PC does not necessarily oversee operations continually while in tether control mode, but the ability to do so is vital for autonomous operation. Rather than being required to repeatedly look at positional information, the PC is able to view this data only as the need arises. This ensures that the PC is kept free for decision making tasks, and only concerns itself with the microcontrollers if problems occur. Examples of such problems are leg timing during walking and turning and ensuring that a minimum of three legs are on the ground for stability. The PC also monitors the "environmental" sensors that return feedback from the robot's surroundings. Presently, these consist of embedded foot switches and a simple voice recognition circuit. The foot switches sense the presence of solid footing or the lack thereof.

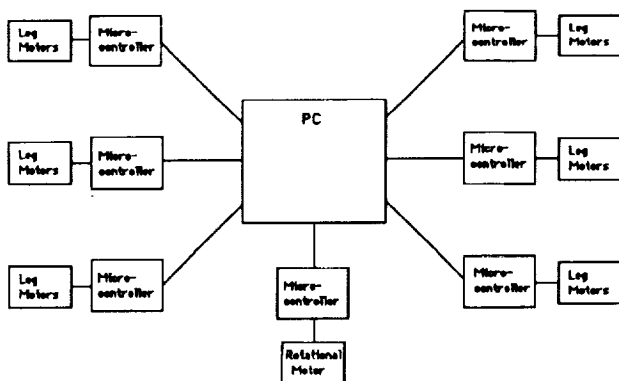


Fig. 3. Electrical hardware design.

The PC can generate commands autonomously or it can receive them through the tether. The commands available are "Stop," "Reset," "Quit," "Update Display," "Set Velocity," "Autonomous Program," "Walk," "Set Height," and "Turn." The "Stop" subroutine executes a code that halts any actions being performed by the microcontrollers. "Reset" executes a code that sets the robot to a known initial state. "Quit" halts all program execution. "Update Display" rewrites the graphics screen to the monitor. "Set Velocity" specifies a walking or turning speed. The "Autonomous Program" command puts the robot into a state in which it is able to operate on its own in an unknown environment. "Walk" executes a code that causes the microcontrollers to engage the walking motors, and "Height" engages the lifter motors for the stair event. "Turn" specifies the angle and direction required of the turning motor. The user specifies which leg a specific command refers to via a sequential leg number protocol.

Upon initially receiving power, the microcontroller sits idle until it receives a "Reset" command. The "Reset" commands are "XReset," "YReset," and "TurnReset." Their purpose is to bring the mechanical systems to a known state, a "home" position, and thus gain control over the machine.

In addition to executing commands from the PC, the '196 is responsible for maintaining motor control within error limits deemed acceptable by the PC. To accomplish this, the '196s execute a proportional integral differential (PID) control algorithm, which is set to run on an interrupt to ensure execution at precise time intervals. The PID routine receives feedback from the encoders and determines the power necessary to keep the motor at the desired position and velocity. This value is passed to the pulse-width modulation hardware.

Commands and data are passed between the PC and the '196 microcontrollers by the dual-port RAM (DPRAM). The commands sent are "Walk," "Set Velocity," "Turn," "XReset," "YReset," "Height," "Stop," and "TurnReset." Data passed to execute these commands are velocity, direction, height, step number, and turn angle. The microcontrollers send a signal back to the PC after completing a given command. This signal causes an interrupt.

## DISCUSSION AND CONCLUSION

The design and manufacture of a walking machine was completed by 40 students in 7 months. The responsibilities were divided into leg, body, hardware, and software tasks.

The leg design combined a modified crank-and-rocker mechanism with pantograph and leg-lift mechanisms. The six legs each operate with two degrees of freedom, providing great flexibility. Structural integrity was maintained through computer engineering analysis and numerical control machinery.

The body design provided an additional degree of freedom for the robot. This was achieved with a turning mechanism. This mechanism controls the relative position of the two body frames. The rigid tripod frames provide a means to mount the six legs.

The electrical hardware design employed distributed processing and modular components to control and power the walking machine. A supervisory personal computer accepts commands, oversees control, and runs autonomous programs. Microprocessors were used to directly control the 13 motors. Communication between the PC and microprocessors is performed with dual-port RAM.

The software design coordinates the robot's actions. A low-level code written to the microcontrollers controls the motor positions. A high-level code written to the PC processes programs and commands. A communications code breaks down PC commands into smaller microcontroller tasks and coordinates timing of data.

The machine is easily adapted to almost any terrain because of the design's flexibility. The leg design emulates a human stride, allowing a modified system to serve in functions hazardous to humans. The feedback control design allows the robot to be adapted to perform repeatable precision tasks. The PC-based master processor allows for easy expansion of hardware and software capabilities in the future.

**PROJECT COPERNICUS: AN EARTH OBSERVING SYSTEM**

**MASSACHUSETTS INSTITUTE OF TECHNOLOGY**

526 43  
160602  
P-6

"Fifteen years will mean forever," the mission slogan for Project Copernicus, conveys the belief of the Hunsaker Aerospace Corporation and the Bush administration that sustained global observation for over a decade will benefit the Earth and its inhabitants for centuries to come. By examining the Earth's systems for only 15 years, scientists will develop a much better understanding of the global environment.

The Earth's system is in a constant state of change. Many of the processes that are creating this change are natural, while others are human induced. It is imperative that we reduce the scientific uncertainties associated with global change issues. Scientists need to be able to quantify human-induced changes in order to act as the catalyst for a major behavioral alteration within society. These changes not only affect biological, climatological, and hydrological processes, but they will also affect our society and the world economy.

Unexpected global change can be devastating. Changing weather patterns could affect the food supply of billions of people. Droughts or floods induced by global change can destroy countless acres of crops, destabilizing national and worldwide economies. Ozone deterioration is another significant change that will have ramifications for human civilization.

Society needs to understand how changes such as global warming, El Niño, and ozone depletion affect its current and future existence. With a better understanding of how the Earth system is changing, we can help stop the human-induced alterations. If scientists are capable of predicting global change, society will be able to reallocate resources to compensate for environmental changes.

President George Bush has recently recognized the need for this reallocation. As a first step, he has charged the U.S. Global Change Research Program (USGCRP) with examining the changes in the global Earth system. A major initiative of the USGCRP is the Mission to Planet Earth.

The Mission to Planet Earth will characterize the state of the entire planet and also quantify the regional variations in the environment. The regional variations are best studied with *in situ* measurements on land, in the oceans, or in the atmosphere. But, in order to achieve a global perspective, the observations must be conducted from outside the region of influence; thus they need to be made from space.

The Earth Observing System (EOS) is a space-based portion of the Mission to Planet Earth. EOS has been conceived to provide observations from vehicles in low Earth orbit. The objective of EOS is to provide an information system that will acquire data on geophysical, biological, and chemical processes. These data can then be examined in a comprehensive study of the entire planet. A large component of the EOS is the Data and Information System (EOSDIS). EOSDIS is intended to provide computing and networking to support EOS research activities.

Hunsaker Aerospace Corporation is presenting this proposal for Project Copernicus to fulfill the need for space-based remote sensing of Earth. Hunsaker is primarily a spacecraft design firm. The company therefore will concentrate on the means of data acquisition, rather than with the interpretation, modeling, distribution, archiving, and processing of EOS data. Hunsaker Aerospace Corporation is committed to designing and manufacturing this revolutionary space science mission. Copernicus is designed to be a flexible system of spacecraft in a low near-polar orbit. The project will be capable of accommodating continuously developing scientific mission requirements. Copernicus is an essential element of EOS and of the Mission to Planet Earth (see Fig. 1).

Hunsaker's goal is to acquire data so that the scientists may begin to understand many Earth processes and interactions. Table 1 shows these processes. They are classified into the science areas of Climate and Hydrological Systems, Biogeochemical Dynamics, and Ecological Systems and Dynamics. The importance of these priorities increases going up and to the left on the table. Hunsaker has adopted these scientific priorities from the questions that the USGCRP has posed in its assessment of the 1991 fiscal year plans.

The mission objective of Copernicus is to provide a space-based, remote-sensing measurement data acquisition and transfer system for 15 years. Many Earth processes are rapidly changing; others take over decades to complete their cycles. Project Copernicus must have continuity over the shorter timescales to provide data on rapidly changing processes. Copernicus must also last for 15 years in order to acquire data on slowly changing cycles.

The Hunsaker Corporation, after a detailed review of the scientific priorities, chose NASA's EOS-A instruments for the baseline design of the Copernicus-A mission. The instruments selected for Copernicus-A not only measure a majority of the

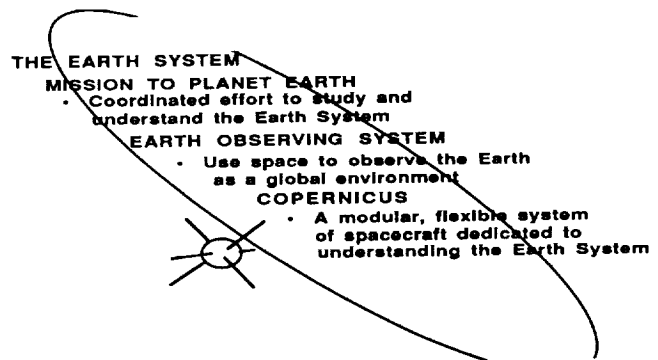


Fig. 1. Mission Flow-Down and Goals

|                               |   |   |  |
|-------------------------------|---|---|--|
| ↑<br>INCREASING PRIORITY<br>↓ | <b>Climate and Hydrological Systems</b>   | <b>Biogeochemical Dynamics</b>  | <b>Ecological System and Dynamics</b>  |
|                               | <ul style="list-style-type: none"> <li>• Role of Clouds</li> <li>• Ocean Circulation and Heat Flux</li> <li>• Land/Atm/Ocean Water and Energy Fluxes</li> <li>• Coupled Climate System &amp; Quantitative Links</li> <li>• Ocean/Atm/Cryosphere Interactions</li> </ul> | <ul style="list-style-type: none"> <li>• Bio/Atm/Ocean Fluxes of Trace Species</li> <li>• Atm Processing of Trace Species</li> <li>• Surface/Deep Water Biogeochemistry</li> <li>• Terrestrial Biosphere Nutrient and Carbon Cycling</li> </ul> | <ul style="list-style-type: none"> <li>• Long-Term Measures of Structure/Function</li> <li>• Response to Climate and Other Stresses</li> <li>• Interactions between Physical and Biological Processes</li> <li>• Models of Interactions, Feedbacks, and Responses</li> <li>• Productivity/Resource Models</li> </ul> |
|                               | ← INCREASING PRIORITY →   |   |  |
|                               | (Empty space for diagram completion)  |   |  |
|                               | (Empty space for diagram completion)  |   |  |
|                               | (Empty space for diagram completion)  |   |  |

TABLE 1. Science Priorities

climatological variables (listed in Table 2), but they also provide a representative sampling of the sizes, data rates, and power requirements of other remote sampling instruments that could be mounted on present or subsequent Copernicus platforms as science priorities change. The Copernicus-A instruments, therefore, not only achieve scientific goals, but they also add flexibility to the Copernicus design. The constraints placed on the project by this representative sampling of instrument specifications define the requirements for the baseline Copernicus bus designs.

TABLE 2. Candidate Climatological Variables

|                           |                          |                       |
|---------------------------|--------------------------|-----------------------|
| Stratospheric Gases       | Tropospheric Water Vapor | Ocean CO <sub>2</sub> |
| Tropospheric Gases        | Precipitation            | Biomass Inventory     |
| Atmospheric Aerosols      | Cloud Cover/Height       | Ocean Chlorophyll     |
| Atmospheric Particles     | Vegetation Cover/Type    | Sea Ice Cover/Depth   |
| Surface Emissivity/Albedo | Soil Moisture            | Surface Roughness     |
| Solar Spectral Radiation  | Snow Cover Depth/Wetness | Sea Level Rise        |
| Atmospheric Temperature   | Surface Temperature      | Volcanic Activity     |
| Wind Fields               | Solid Earth Motion       | Forest Fire Evolution |

The driving force behind the design of Project Copernicus is simultaneity. Simultaneity, simply defined, is two or more instruments looking at the same ground pixel at the same time. There is a more stringent form of simultaneity, called congruency, that requires spatial and temporal coincidence. For example (see Fig. 2), if one instrument is measuring a process on the Earth, its data may be incorrect because of some disturbing phenomenon such as water vapor in the atmosphere or radiation emitted from Earth. A second instrument could be flown with the first instrument or on another bus in formation with the first. This second instrument would measure the disturbing phenomenon and allow the data for the first instrument to be corrected.

If any type of simultaneity is required, it is preferable to fly the simultaneous instruments either on the same bus, or on buses that are flying in formation. The simultaneity requirements

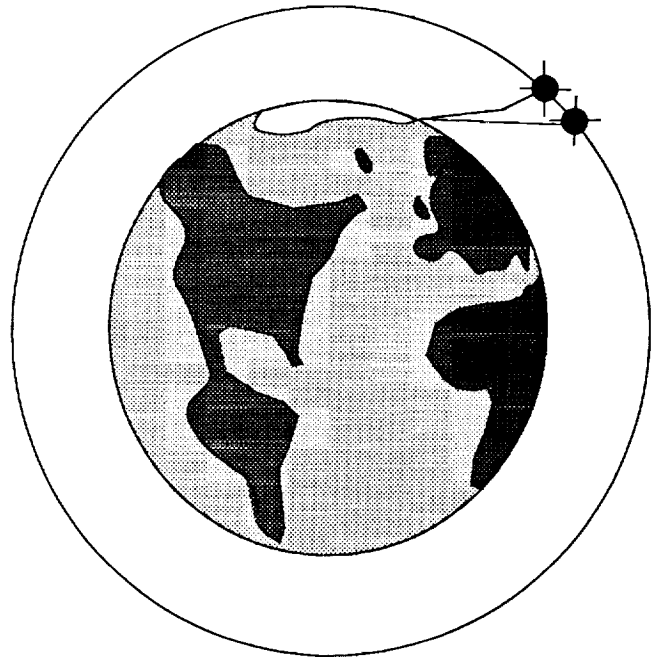


Fig. 2. Simultaneity Example for Atmospheric Correction

of the instruments selected for Copernicus-A have yielded two designs. The instruments are either all grouped together on a single large bus, or are placed in congruent groups on a series of small buses. For the Copernicus-A design, formation flying was not implemented. The small bus design was able to accommodate entire groups of congruent instruments, thereby eliminating the necessity of formation flying and the complications associated with it.

In addition to stipulating requirements for the vehicles themselves, the instruments also require a certain orbit for functionality. The orbit, in turn, dictates a large portion of the spacecraft design for stationkeeping requirements. For the Copernicus-A design Hunsaker has selected a near-polar, Sun-synchronous circular orbit at an altitude of 727.5 km with a 98.3° inclination. This orbit provides coverage of the entire globe with constant resolution. At the selected altitude, coverage of the entire Earth is accomplished every two days.

To enter this orbit, Copernicus will be launched on a Titan IV launch vehicle to a 185-km × 727.5-km orbit. The small bus vehicles will then be circularized by periapsis firings of onboard thrusters (see Fig. 3). The large bus vehicle will circularize by an impulse burn of its onboard thrusters. By using the onboard thrusters for circularization, a kick stage does not need to be implemented into the launch system. By eliminating the need for a kick stage, Hunsaker is eliminating a source of space debris.

Hunsaker recognizes that space debris is becoming a monumental problem for space missions. In keeping with the environmentally conscious theme of Project Copernicus, Hunsaker has made every effort to eliminate space debris from the project. This requirement not only results in onboard thrusters being used for orbital insertion, but it also results in

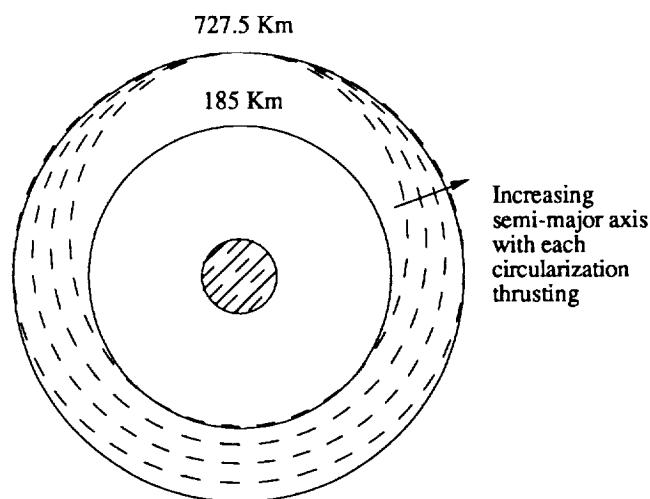


Fig. 3. Small Bus Orbital Insertion

a spacecraft deorbit requirement. At the end of the mission, the vehicles themselves will be deorbited and break up safely over the ocean.

The mission profile consists of launching a selected number of remote-sensing measurement instruments on a modular bus system. This bus(es) will be inserted into a low Earth, near-polar orbit. To achieve the polar inclination, Copernicus will be launched from the Western Test Range at Vandenberg, California. If several satellites are used to carry the instruments, the vehicles need not be constrained to the same orbit. The instruments will perform measurements, and the satellite(s) will transmit the data down to the EOSDIS center at NASA's Goddard Space Flight Center. Additional operations will be performed as commanded by groundbased operators. When the spacecraft system is nearing end of life, the existing vehicles will be deorbited as per the deorbit criteria. The vehicle(s) will break up and fall into the ocean. Prior to deorbit, another satellite will be launched. Once adequate data is no longer being received from one system, the next bus(es) in the series will be launched.

Hunsaker's design philosophy consists of program priorities and design ground rules for the spacecraft design. The design considerations are prioritized in the following order: (1) reliability, (2) system performance, (3) flexibility, (4) cost, (5) manufacturability, (6) supportability, and (7) schedule.

The mission of Project Copernicus, the study of the Earth's environment, gives the scientific goals of the mission with the utmost priority in every aspect of the design process. These goals are balanced with engineering capability to produce a feasible design.

The design priorities are closely interrelated with the ground rules. The ground rules are selected to ensure that Project Copernicus meets the scientific requirements placed upon it. The ground rules include design to ensure continuity, to achieve unprecedented scientific results, and for maximum flexibility.

Hunsaker recognizes that data continuity is essential to the principal investigators of the instruments. Data continuity on short timescales of days or weeks is important since many Earth

processes are rapidly changing. Continuity is also equally important on longer timescales of years or decades. Any interruption in the data flow for either timescale would jeopardize the scientific understanding of these phenomena.

Hunsaker is also concerned with integrating Project Copernicus with other EOS projects. This will increase the available data on many of the Earth processes that Copernicus is to examine.

The continuity ground rule affects a large portion of the spacecraft design. Issues such as reliability levels and redundancy levels flow directly from the continuity ground rule. If the spacecraft becomes dysfunctional or loses a primary instrument, it must be serviced in orbit or another satellite must be launched. For the Copernicus program, serviceability will not be employed. Instead Hunsaker will rely on the programmatic flexibility built into the system and launch another spacecraft. Continuity also raises concerns about orbit maintenance. The orbit of the Copernicus satellites must be maintained to sustain the appropriate viewing altitude and inclination. This results in requirements on the onboard thrusters, guidance, and navigation systems. The space environment also provides unique challenges: Micrometeorites, radiation, and thermal effects all affect the spacecraft and must be compensated for in the design of Copernicus to ensure continuity.

Continuity is needed for the mission lifetime of 15 years. Hunsaker considered whether a single vehicle should be launched, or similar satellites should be relaunched periodically. If the relaunch option is chosen, the redundancy and amount of consumables aboard can both be reduced substantially.

Hunsaker's costing analysis indicated that if the large bus option was selected, a new bus should be relaunched after seven and a half years. If the small bus option is launched, a new set of buses will be launched after five years. This relaunch schedule requires that there be an extra, large bus produced in case of catastrophic failure of the large bus. There will be enough small buses produced so that if one fails, the next in the launch series can be launched earlier.

The second ground rule is to design for excellent scientific results. This groundrule includes such issues as simultaneity and orbital selection and orbital maintenance (stationkeeping).

The third ground rule is to design to ensure flexibility. Copernicus must have sufficient programmatic flexibility so that if a budget cut or unexpected scientific priority change confronts the project, it will rapidly and efficiently adapt. The spacecraft of Project Copernicus must also be flexible. If there is an instrument change or modification because of continuously changing scientific priorities, the spacecraft should be able to easily accommodate this change.

To facilitate the design of the two buses, Hunsaker created the organization seen in Fig. 4. The systems integration group and the program planning group set the scientific and programmatic requirements to achieve Copernicus' goals. These requirements were then communicated to the small and large bus groups who were responsible for designing a system of spacecraft capable of meeting them. The bus groups used a number of subgroups to design the subsystems. The subgroups included Power and Propulsion; Command, Control, and Telemetry; Structures and Thermal Control; and Guidance, Navigation, and Control.

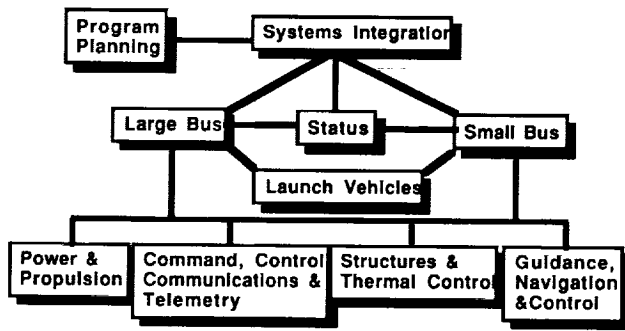


Fig. 4. Hunsaker Organizational Chart

The status group was responsible for monitoring the spacecraft's systems for the duration of the mission and communicated primarily with the bus groups and systems integration.

Finally, the launch vehicle group communicated with the bus groups to determine which launch vehicle would meet the bus group's needs. The launch vehicle group then helped interface the satellite with the selected vehicle.

The Hunsaker Corporation was responsible for two bus designs, each of which could achieve the goals of Project Copernicus. The Large Bus design was created as a single satellite that would contain all of the chosen EOS-A instruments and their associated support equipment. The Small Bus design would consist of several smaller satellites, each of which would carry a specified group of the EOS-A instruments.

Both bus designs had to meet the primary mission objectives: continuity, flexibility, and scientific results. From these three objectives come the primary design issues. Continuity raises issues of complexity of design and manufacture, hardware reliability, and levels of system redundancy. Flexibility poses the problem of design for modularity and adaptability to future instruments and requirements. Scientific results translate to level of system performance, instrument support, and maintenance of proper orbit. These issues were reflected in the mission priorities of reliability, performance, and flexibility, as laid down by Hunsaker.

In designing a superstructure for the Large Bus, these and additional, more specific issues had to be addressed. To contain all 15 of the baseline EOS-A instruments, the bus would require a large area on which to mount them, while restraining the mass and dimensions of the bus to the abilities of launch vehicles in production or under design. Because of its large size the superstructure of the Large Bus could become increasingly difficult to manufacture maintaining tolerances over many components. In terms of reliability, such a structure should be simple enough in design to avoid single-point failure during operation, as such a failure could jeopardize the entire mission. In addition, size constraints may limit the flexibility of moving or replacing instruments on the bus.

Hunsaker proposed several Large Bus structural designs, two of which were deemed suitable in terms of maintaining all instruments and equipment within launch vehicle constraints. The first was a folding plate design that would support the instrument packages on one face while carrying the support

equipment on the other. Folded into three sections within the launch vehicle, the structure would be deployed in orbit. The second design was a simple box truss, one face of which would carry all the instruments, while all the support equipment would be internalized within the body of the truss (Fig. 5).

After close comparison of the two designs, the box truss design was deemed superior in its abilities to meet the mission requirements. In terms of structural strength, instrument stability, and complexity of operation, the box truss was clearly the superior design. The major drawback was its compact size, which reduced the effective area for instrument placement.

The final design, although still a box truss, was modified somewhat to accommodate MIMR, the largest instrument of the EOS-A package, and the power generating solar arrays. All the EOS-A instruments, with the exception of MIMR, are suspended from the lower face of the truss, which will face the Earth at all times. The construction consists primarily of 2-in-diameter aluminum truss members, with aluminum plates used as instrument attachments to the truss. The overall structural dimensions are 7.0 m long, 3.2 m wide, and 1.5 m high. The mass is approximately 1000 kg. Figure 6 illustrates the structure.

In designing the structures for the Small Bus design, Hunsaker had to optimize not only the satellite structure, but also the number of satellites in the system. Four distinct designs were proposed, each with a particular design criterion as its primary

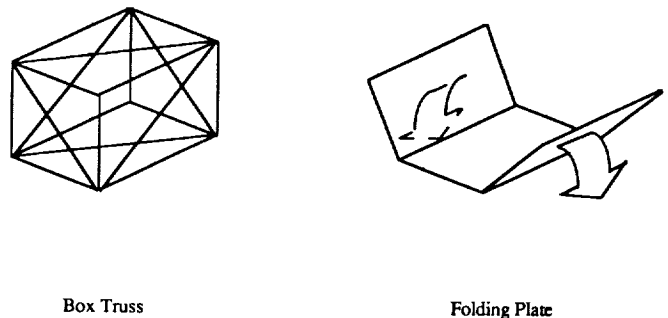


Fig. 5. Large Bus Configurations

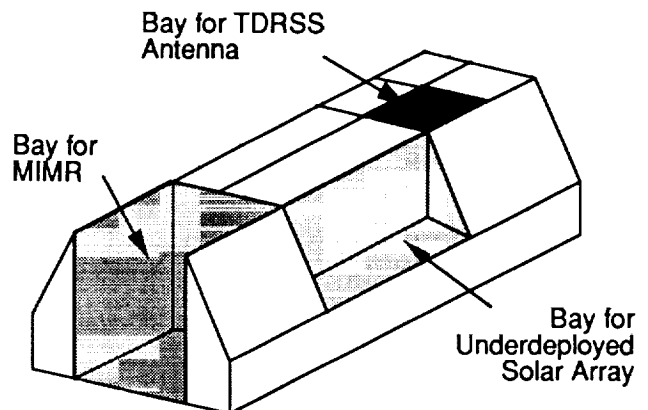


Fig. 6. Large Bus Truss Structure

target. The first, Synchronious, consisted of five satellites aimed at maintaining simultaneity in measurement. The second, Modularious, was composed of six satellites designed around maximizing instrument flexibility. The third, Pointious, had five satellites designed to meet and exceed instrument pointing requirements. Lastly, Mixious consisted of nine satellites carrying multiple versions of each instrument to maximize system redundancy. The final configuration chosen was none of the above, but rather a modification of Synchronious, named Phoenix, consisting of four slightly larger satellites. Each satellite carries two to four instruments, each group of instruments satisfying simultaneity requirements on a single satellite.

The issues facing the Small Bus design were similar to those of the Large Bus. With a reduced number of satellites, the bus needed to maintain flexibility in moving instruments on a given platform or from one satellite to another. This also required a simple design that could adapt to instruments of varying shape and size.

The final structural design of Phoenix consists of four identical octagonal trusses with an open center for support equipment (Fig. 7). Of the two larger faces of the truss, one is used as a platform for up to four instruments. This face is fitted with a sandwich plate consisting of two aluminum plates encasing a honeycomb core. The overall structure has a diameter of 3.6 m, and is 1.0 m thick.

Other technical issues that affect both bus designs, such as system redundancy, partial mission success, and formation flying cannot be answered by the structure alone. The additional subgroups of Thermal Control, Power, Guidance, Control, and Communications and Data Handling provide the needed support to achieve the mission objectives. Because the subgroup designs are nearly identical in concept on both buses, they will each be treated as a single design.

Thermal control, the means by which the spacecraft dissipates heat and maintains the operating temperatures of the instruments within narrow margins, was designed as a passive system on

a component level. Each instrument and power-consuming device onboard each satellite is mounted onto a Freon-filled cold plate that is connected to a heat pipe. The Freon is circulated through the cold plate, then fed through the heat pipe via capillary action to the external end of the pipe, where the heat is dissipated into cold space. In addition, each instrument is insulated by MLI Mylar and polished metal sheets that cover its exposed surfaces.

The Power subgroup, whose purpose was to design a system to generate and store sufficient power to operate a satellite's instruments and support equipment, proposed the use of photovoltaic solar arrays and nickel hydrogen batteries. The systems onboard the Large Bus operate at 120 V, whereas the Small Bus operates at 28 V. The solar arrays of the Large Bus are 130 sq m in area, generating 10,500 W of power at mission start. Each Small Bus requires about half as much power, and has proportionately smaller arrays. The batteries can store sufficient energy to operate each satellite for the 40 min the spacecraft is out of the Sun's view. Figure 8 illustrates the power flowdown for the Large Bus.

The Guidance & Control subgroup is composed of four major divisions: attitude determination, attitude control, position determination, and position control. Attitude determination is required to orient the spacecraft and instruments in orbit with great accuracy. The pointing requirements are particularly stringent for Project Copernicus because of the presence of several instruments that are designed to resolve climatological and surface changes on a scale of hundreds of meters. This sets accuracy requirements as low as 60 arcsec for control and 100 arcsec/sec for stability. Therefore, the Large Bus and two of the four Small Bus satellites implement two Ball Brothers Star Mappers each. The secondary system is the Microcosm Autonomous Navigation System (MANS). Attitude control is performed by two sets of three-axis reaction wheels and copper coil magnetorquers. Position determination, necessary to maintain the correct global coverage and equatorial crossing

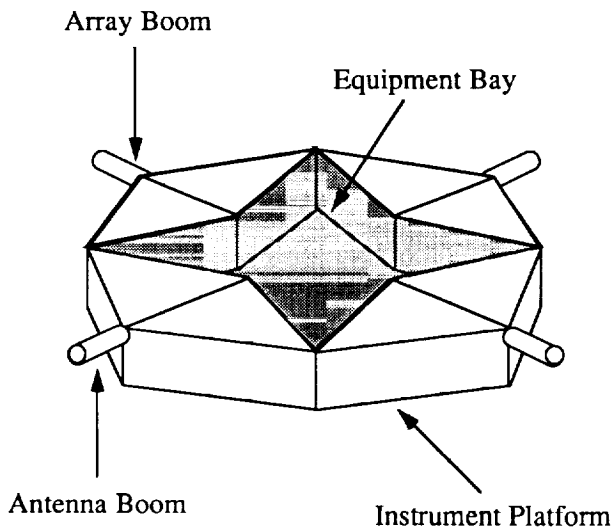


Fig. 7. Small Bus Structure

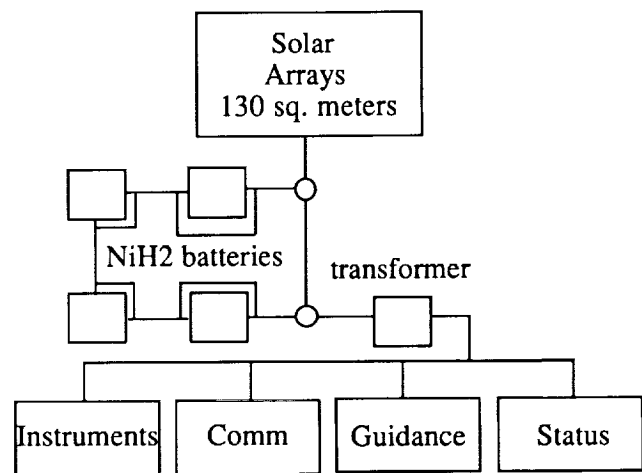


Fig. 8. Large Bus Power Flowdown

time of 1:30, is performed primarily by a Motorola Global Positioning Receiver operating at 10 Hz. The optimal position accuracy is within 0.6 m. Position control is controlled by two pairs of 46-N hydrazine thrusters, conducting stationkeeping maneuvers through Hohmann transfers.

The Command, Control, Communications, and Telemetry group had three major areas of concern: data handling, communications, and command and control. The data handling system is the same for the Large and Small Bus. Each instrument sends information to a Hunsaker-designed data handling computer, distinguished by its low speed of 6 MHz and wide data path of 48 bits, allowing the computer to handle 300 megabits per second. The data is then transmitted or stored on optical disks. Data transmission will take place primarily via a Ku-band downlink through the high-gain Tracking Data Relay Satellite System (TDRSS) antenna. Commands from the ground will be uplinked through the Ku-band or the multiple-access S-band. On each bus there are two omnidirectional antennae to relay commands if the high-gain antennae fails, or if the guidance and control system fails and the antennae cannot be aimed at a TDRSS satellite. The commands uplinked from the ground are processed by the command, control, and telemetry system consisting of sensors, Built-in-Test Managers (BIT), and On-Board Computers (OBC).

Once the designs of the two bus systems were complete, Hunsaker was able to choose which system could more easily

meet the programmatic priorities. Hunsaker recognized that the scientific goals of Copernicus had the highest priority, but these goals had to be balanced with rational design.

Both Large and Small Bus systems were similar in terms of the reliability and performance priorities. The next two design priorities are flexibility and cost. The Small Bus System is significantly more flexible. Small Bus is a more robust system which could more easily adapt to changes in instrument payloads. Small Bus could also more easily accommodate a change in launch vehicle. Additionally, if the program's budget is unexpectedly cut, Small Bus can scale back the system. Large bus, alternatively, would have to be cancelled if confronted with significant budget cuts. Small Bus is also much less costly. Furthermore, the Small Bus is much more manufacturable than the Large Bus because of the smaller number of parts and connections.

Hunsaker Aerospace Corporation has selected the Small Bus design for the Project Copernicus mission. The flexibility of the Small Bus is very attractive not only for Copernicus-A instruments, but also for Copernicus-B instruments. Small Bus is a more robust design; it can more easily accommodate unexpected changes in instruments, instrument usage, or budgetary alterations. Hunsaker is confident that the Small Bus design will be capable of achieving the lofty goals of Project Copernicus.

160603

P- 7

**PROJECT MEDSAT**  
**THE UNIVERSITY OF MICHIGAN**

**INTRODUCTION**

During the winter term of 1991, two design courses at the University of Michigan worked on a joint project, MEDSAT. The two design teams consisted of the Atmospheric, Oceanic, and Spacite System Design" and Aerospace Engineering 483 (Aero 483) "Aerospace System Design." In collaboration, they worked to produce MEDSAT, a satellite and scientific payload whose purpose was to monitor environmental conditions over Chiapas, Mexico. Information gained from the sensing, combined with regional data, would be used to determine the potential for malaria occurrence in that area. The responsibilities of AOSS 605 consisted of determining the remote sensing techniques, the data processing, and the method to translate the information into a usable output. Aero 483 developed the satellite configuration and the subsystems required for the satellite to accomplish its task. The MEDSAT project is an outgrowth of work already being accomplished by NASA's Biospheric and Disease Monitoring Program and Ames Research Center. NASA's work has been to develop remote sensing techniques to determine the abundance of disease carriers and now this project will place the techniques aboard a satellite. MEDSAT will be unique in its use of both a Synthetic Aperture Radar and visual/IR sensor to obtain comprehensive monitoring of the site. In order to create a highly feasible system, low cost was a high priority. To obtain this goal, a light satellite configuration launched by the Pegasus launch vehicle was used. The Pegasus is a recently developed launch vehicle designed by Orbital Sciences Corporation and the Hercules Aerospace Company. It uses the advantages of unique air launch to lift small payloads into orbit for a cost of approximately \$8 million.

**THE PEGASUS LAUNCH VEHICLE**

Produced by the Orbital Sciences Corporation and the Hercules Aerospace Company, the Pegasus is a small launch system designed to place small payloads (136 to 410 kg) into orbit. Using the unique approach of an air-assisted launch, the system is able to accomplish its mission relatively inexpensively, at \$8 million for the entire launch cost. The Pegasus is fired from a special pylon under the wing of a B-52 or other similar size airplane. At launch, the airplane is in cruise flight conditions, flying at about Mach 0.8 and at an altitude of 12,000 m. The first stage ignites about 90 m below the B-52 and lasts 75 s. During this stage, the vehicle quickly accelerates to supersonic speed and then undergoes a 2.5-g pull-up maneuver. After coasting for a short time, the second stage burns for 75 s. The third-stage burn completes the orbital insertion. This occurs approximately 530 s after launch, 2200 km downstream.

**GROUND SEGMENT**

The ground segment activities of the MEDSAT project have involved consideration of characteristics of malaria, site selection, data types, plans for ground station development, and the potential MEDSAT output.

Malaria is a generic term used to describe the pathological manifestations of a group of protozoan parasites of the genus *Plasmodium*. These parasites are known to cause a unique etiology in human hosts with distinct case fatality rates and patterns of symptoms. Aside from the human hosts, malaria parasites require an extrinsic period within a mosquito host in order to complete their life cycle successfully. The most common of these insect hosts are mosquitoes of the genus *Anopheles*. Although there exist approximately 400 species within this genus, only about a fifth of these are capable of actively transmitting malaria between human hosts. These vary widely in their geographical distribution, length of life cycle, and reproductive and feeding habits. A detailed study of the environment and life cycle of these vectors is essential to any program that seeks to reduce the incidence of malaria. The density of the insect vector population and their pattern of contact with infected and noninfected individuals are the main factors in determining the severity of the malaria problem in a specific area.

To select a primary site for the MEDSAT project, first a country was selected and then a specific site inside the country was chosen. The ideal country would be one with a stable government that would not only be receptive to the idea of participating in a project with NASA, but also one that possesses the necessary resources to enable both the collection of ancillary data and the useful application of the project output once it is produced. Of the nine countries selected for final evaluation, Mexico was the one that came closest to fulfilling the conditions stated above. Mexico currently accounts for 14% of all the malaria reported in the Americas. According to 1986 estimates, approximately 43 million people in Mexico live in malarious areas, resulting in 131,000 new cases annually.

To select our primary research site, a more detailed evaluation of the pattern of malaria incidence and prevalence within the selected country was completed. The final decision to select the county of Soconusco in the state of Chiapas was based upon several factors that determine a unique and urgent malaria problem in this region. Soconusco is located along the Pacific ocean, at the southernmost tip of Mexico, along the Guatemalan border. A demand for labor in this area has resulted in the large-scale influx of Guatemalan migrant workers into the region. The high number of cases of malaria in this area is most likely due to this population of migrant workers. By concentrating

surveillance and control efforts on the localities in Soconusco where these migrants are concentrated, the foci of this growing problem can be effectively targeted. In this particular study, it is hypothesized that there may be correlations between mosquito habitats and human population areas, particularly regarding vegetation and regions of standing water. However, such hypotheses need to be tested. In the research phase, ground data in the form of known mosquito habitats and actual malaria cases will be collected and used in collaboration with remotely sensed data to generate a model that can be used to map and predict those areas that are most prone to malaria outbreaks. A mobile ground station requires that only the most pertinent data be received and directly applied towards the production of a malaria risk map. Hence, the application phase will involve combining very specific predetermined data types, both ground and remotely sensed, and feeding them into the MEDSAT Geographical Information System (GIS) to be modeled and mapped. The output is envisioned as an accurate prediction device supplied to public health officials in Mexico as often as every day. The malaria risk map may for instance provide the ability to predict where and when mosquito populations will reach their maximum density allowing for the effective allocation of malaria control measures. In the long term, more and more data will be gathered and mathematically manipulated. From this process we will learn more about the behavioral and habitational characteristics of malaria transmitting mosquitoes as well as the people they infect.

#### THE SYNTHETIC APERTURE RADAR SENSOR

In order for MEDSAT satellite to be an effective tool used in determining areas of high malaria risk in the region of Chiapas, Mexico, it must possess a sensor capable of remotely sensing mosquito habitats and human habitation through rain and clouds independent of solar illumination conditions. The all-weather and day/night operational attributes of a Synthetic Aperture Radar (SAR), coupled with the ability to utilize the output imagery in identifying, classifying, and measuring the terrain parameters that are of key importance to this project, make the SAR ideal for the MEDSAT sensing platform.

Fundamental to the success of the MEDSAT project is a detailed knowledge of the spatial distribution of population densities of the malaria transport vector, the mosquito, to enable efficient implementation of appropriate disease control methods. The mosquito habitats of interest will consist primarily of wet grasslands in coastal regions to areas of partially or heavily shaded water in forest regions further inland. In addition to knowledge of the mosquito habitats, spatial distribution of migrant worker camps is also highly desirable.

#### Frequency Band

Ideally, one would like to combine the advantages of multiple frequencies into one instrument. However, due to the constraints of a small satellite, MEDSAT will employ only one microwave frequency band in the SAR design. Based on MEDSAT's remote sensing requirements, the optimum frequency band for the SAR has been determined to be the L-band (1.275 GHz/0.23 m). A radar system operating at a frequency below 5 GHz is necessary

to penetrate the crop canopy to measure soil moisture under a dense vegetation cover. L-band can accomplish that task, and can also be used to successfully identify and distinguish among various target classes such as crops, forests, swamps, and flooded forests. Another advantage of the L-band is that it requires an angle of incidence less than 20°. This is desirable for remotely sensing soil moisture to minimize both the backscattering by vegetation and the effective attenuation loss related to the two-way transmission through the vegetation canopy.

#### Geometric Imaging Requirements

Geometric imaging requirements consist of altitude and range to target, image ground-swath size, resolution cell size, incidence angle, and polarization of the transmitted microwave radiation. All these parameters are interrelated and all are ultimately constrained by the restrictive volume, mass, power, and data rate allotments of the MEDSAT project's small satellite design.

Because the antenna radiating power is directly proportional to the cube of the range to target, a substantial saving in power can occur by simply having as low an operational altitude and range to target as possible. The restrictions in power and data rate limit the SAR sensor's maximum ground-swath size range dimension, or width, to 50 km, and the maximum ground-swath azimuth dimension, or length, to 250 km.

The MEDSAT SAR design incorporates a ground resolution cell size of 75 m by 75 m. This cell size has been determined as a trade-off between achieving the maximum possible system resolution and keeping within the power and data rate constraints. Higher system resolution, and thus smaller resolution cell size, corresponds to better target detection and classification in the resulting images.

The MEDSAT SAR will employ a small incidence angle. The major reason for going to a small incidence angle radar system is the correspondingly lower antenna radiating power requirements as compared to larger incidence angle systems. Another advantage of a small incidence angle radar system is in the ability to discriminate various types of target classes, especially vegetation types. The only disadvantage of a smaller incidence angle radar system is the increase in amount of image layover for tall vertical targets like mountains and skyscrapers. Since the primary target area is the coastal plain area of Chiapas, Mexico, this disadvantage should be negligible for the present imaging interests of the MEDSAT project.

The MEDSAT SAR sensor will be fully polarimetric in order to gain an increased ability to distinguish various target classes from each other in the resulting imagery. A fully polarimetric SAR is a synthetic aperture radar system that has the ability to measure all the possible multipolar returns from the target/ground. The polarimetric information will help to fill the image interpretation gap created by having to use only one frequency band in the SAR design.

#### System Design Specifications

The determination of the SAR design parameters is not only influenced by the geometric imaging requirements and the power, size, and data constraints of the small satellite design, but also by the image quality requirements. The six design

specifications are: pulse repetition frequency, pulse length, system losses, noise temperature, signal-to-noise ratio, antenna area, and noise floor.

The pulse length was chosen as 20  $\mu$ s, and the pulse repetition frequency was determined to be 5047.95 Hz.

The MEDSAT SAR will employ burst mode operation, in order to reduce the operational data rate and power draw of the sensor. This technique works by simply turning the radar on and off in specific timed bursts during the imaging time over the target. The duration of the "burst on" time is calculated to create a synthetic aperture of sufficient length to satisfy the azimuth resolution specification. The reduction in the number of transmitted pulses for the MEDSAT SAR results in a lower operational power draw and a smaller amount of data per image.

The MEDSAT SAR will also incorporate an adaptive quantization scheme. This quantization scheme provides a data compression to complement the data reduction obtained by the burst mode operation. Applying these two techniques to decrease the amount of SAR data means that the system will operate at a much lower data rate and require substantially less memory than traditional SAR systems.

The small satellite design of this project places severe limitations upon the antenna's size and mass. Therefore, the overall size of the MEDSAT's SAR antenna will be by  $6 \times 1$  m. Drawbacks of such a small antenna include decreased antenna gain, increased power requirements and larger bandwidths. To meet the payload specifications of the launch vehicle, the antenna will be subdivided into 10 identical panels, each  $51 \times 100$  cm. These panels will be separated by 10 cm and will be supported by a foldable epoxy-graphite truss. The minimum number of transmit/receive (T/R) modules (at 12 W) needed on the antenna was determined to be 226. By using multiple T/R modules, the SAR gains advantageous beam steering capabilities. This will allow for the optimization of the main and side lobes of the antenna.

#### VISUAL AND INFRARED SENSOR

Since it is not yet possible to directly sense the regions of high mosquito density, it is necessary to indirectly infer how changes in vegetation may affect the mosquito population. Therefore, a visual and infrared sensing system (VIS/IR) will be included in the MEDSAT scientific payload. The VIS/IR sensor will have two main functions. First, to detect regions in Chiapas where habitats are ideal for mosquito production. Second, to track the location of migrant workers from Guatemala. In addition to these, other functions of the sensor will be to locate geographical indicators, both natural and man-made, which with ground truth observations can aid in specifying which portion of Chiapas is being portrayed.

Remote sensing of vegetation depends greatly upon reflectance characteristics over the solar spectrum. In order to determine the malaria habitat, one must use the relationships between the mosquito habitat and vegetation, moisture, and temperature on the ground. Thus, detectors in four wavelength bands (A,B,C, and D) were considered to sense the desired characteristics. Considering each of these wavelength bands, there are advantages and disadvantages regarding the amount of valuable information given, feasibility and cost. In Band A (0.62-0.69

$\mu$ m) the reflectivity of green vegetation is very low. In Band B (0.77-0.9  $\mu$ m) the reflectivity varies dramatically among different types of vegetation, as well as in different stages for a certain type of vegetation because the reflectivity of this band indicates leaf cell structure. From this information, we can classify different vegetations and therefore find the potential malaria habitat. From Band C (1.55-1.7  $\mu$ m) one can get the vegetation moisture content information. Band D (4.0-5.6  $\mu$ m) can remotely sense the temperature.

#### DATA MANAGEMENT AND PROCESSING

Data management and communication is integral to the operation of any satellite system. For the MEDSAT, large amounts of data must be collected from the SAR and the VI/IR sensors. To be of any use, these must be transmitted to a station where they can be decoded and processed into a final image. As a final step, these data may be distributed to the users and/or archived in some manner to be of further scientific use. Therefore, data management and communications must function in an efficient and timely manner.

Design constraints that limit the functionality of data management and communications are power requirements, size, weight, and time. Data management and communications must consume the least amount of power possible to afford the operation of the SAR and VI/IR sensors. Its size must be small to ensure available hardware space; its weight must also be limited to allow the maximum amount of scientific payload. Finally, the data management and communications hardware must operate quickly to ensure that data can be transmitted to a ground station. Given all these constraints, five subdivisions were considered: data handling, data processing, communications path, data compression, and data storage.

The data handling system is controlled by a customized microprocessor. This onboard computer will also control the scientific instruments and direct the flow of data collected. Raw SAR data needs to go through a great deal of processing to generate an image from the radar backscatter data. The best approach to this problem is to collect the sensor data, process the information for downlinking, and subsequently generate the image at a ground facility. The extent of onboard SAR data processing and handling would include conversion of the analog signal to digital signal, data compression, error correction coding, and storage prior to downlinking. The raw SAR sensor data is steered into an analog/digital conversion unit to be converted to a digital format. In the next step, the information is compressed by a data compression unit. After this has been completed, the error correction coding system adds correction bits to the bit stream and organizes the data into packets for transmission. The resulting data is stored by the optical disk storage system and awaits transmission to the ground receiving station.

The VI/IR data is converted into a digitized form when it is collected by the sensors. Hence, only compression and storage are required before transmitting the data to the ground for image registration. The VI/IR sensor data is handled in a similar way as that of the SAR. However, the analog/digital conversion is excluded since the sensor has already accomplished this step.

The sensor image generation and correction is performed on the ground. Once the data have been downlinked to the

receiving ground station, the information is transferred to two sites via the NASCOM system. One dataset will be transmitted to the NASA Ames Research Center while the other set will be sent to the field site in Mexico. NASA Ames will then be able to do extensive and more sophisticated imaging using the SAR data. Ames may also want to archive the generated images since the field station will be physically limited in its ability to store the large volume of information. The field station will be equipped with the hardware and software needed to process the SAR and VI/IR data.

An important aspect of MEDSAT is its data collection capabilities. In order to minimize the time required for the enormous amount of data to be transmitted, the collected data need to be compressed as much as possible. This will greatly increase the efficiency of the operation of MEDSAT. The compression method best for this design is the vector quantization method. The compression ratio of vector quantization can be specified by the designer, thus easing design constraints. The MEDSAT design team also suggests that vector residual vector quantization be used to reduce error. For decompression, the computer compatible tape is the method of choice because of the reduction in processing time required for a final image.

### COMMUNICATIONS

A satellite's communication subsystem is the link between Earth and the satellite. This allows new commands to be sent to the satellite for the sensors and the attitude control mechanism. In turn, the satellite can return the data collected by the sensors to stations on Earth where the data can be analyzed and sent to the appropriate authorities. The onboard equipment and the uplink/downlink sites make up this subsystem.

MEDSAT's onboard subsystem is made up of the offset-fed parabolic antenna, a diplexer, and two transponders for transmitting and receiving the information. The antenna dish is constructed of a 78 sq cm (2.5 cm thick) plate. It is made from a graphite composite and lined with a thin layer of reflective material. The feed is a corrugated circular horn 9.2 cm in diameter and 8.6 cm long. It is also made of graphite composite.

In determining the uplink/downlink capabilities of the satellite, the limited amount of power available was a large concern. The sites for uplinking and downlinking information with the satellite were also constrained by the inclination angle of the satellite's orbit. Hawaii was finally chosen as the site for the ground station because it fulfilled several criteria. First, it allows a sufficient amount of time between sending and the downlink to build up power. It also lies within the 21° inclination restraint and it is part of the U. States so that fewer political problems would be faced in establishing the site.

### MISSION ANALYSIS

The objective of the mission analysis group was to design the optimal orbit that would satisfy the sensing and launch vehicle requirements. The specific requirements that the orbit must satisfy are: daily sensing of Chiapas, a four-year life time, a low altitude, the ability to communicate with a suitable groundstation for efficient uplinking and downlinking, and good equatorial coverage.

The main concern for the design of MEDSAT is the payload weight capability of the Pegasus. As the weight is increased, the altitude that can be reached with the Pegasus decreases. Taking these limitations into account, the capabilities of the Pegasus launch system will enable the 340 kg MEDSAT to be inserted into a 477-km circular orbit with a 21° inclination. In calculating these parameters, the precession of the nominal orbit as a result of the oblateness of the Earth was taken into account.

A circular orbit was chosen over an elliptical orbit in order to prolong the lifetime of the satellite. The period corresponding to an altitude of 477 km is 94.1 min. This period and altitude will allow the satellite to cover the target site twice every day. This will allow almost continuous daylight sensing, thus obtaining the maximum benefit from the VI/IR sensor. However, because the precession was taken into account when determining the period, the time of day of coverage will vary. Each day, the satellite will pass over Chiapas 27.74 minutes before the previous day's pass.

One of the major effects on a low Earth orbit satellite during its mission is the atmospheric drag. The drag force acts in the opposite direction of the motion of the satellite and gradually lowers the satellite's altitude by decreasing its energy. As the energy decreases, the altitude will decrease and the orbit will decay until the satellite eventually reenters the atmosphere and burns up. As a result, thrusters will be employed to occasionally boost the satellite and offset the drag. By using thrusters, the required four-year lifetime is obtained. This will be accomplished through a Hohmann transfer maneuver consisting of two burns, one to transfer to the higher orbit and one to recircularize the orbit. This is the lowest energy transfer maneuver and consumes the least amount of fuel. The thrusters used for these maneuvers will be the same as those used for attitude control.

The airborne launch of the Pegasus from beneath a B-52 offers considerable flexibility without the launch window restrictions of ground-based launch facilities. The only restriction on the launch is that it must be over open water with a clear downrange to allow for reentry of the first and second stages. For the launch of MEDSAT the most advantageous launch site is the east coast of Florida. This will allow the Pegasus to be launched due east at 21°N, thus gaining the most advantage of the Earth's rotation.

### SPACECRAFT INTEGRATION AND STRUCTURES

The primary responsibilities of the spacecraft integration and structures group are developing the configuration and thermally controlling the satellite. The first and most important goal is to develop both the internal and external configuration that integrates various subsystems of the satellite into a single operating system. The basic subsystems are the SAR, the infrared sensor (IR), the power system, the attitude control, the launch interface, and the thermal control.

From a spacecraft integration standpoint of MEDSAT, the main design parameters taken into account are subsystem safety, volume, mass, and cost. There were four primary design constraints that shaped the design of the satellite. The first was the OSC/Pegasus launch vehicle, which has a total of 7.2 m<sup>3</sup> usable volume in its payload fairing. During launch, the satellite must fit within the dynamic envelope of the payload fairing

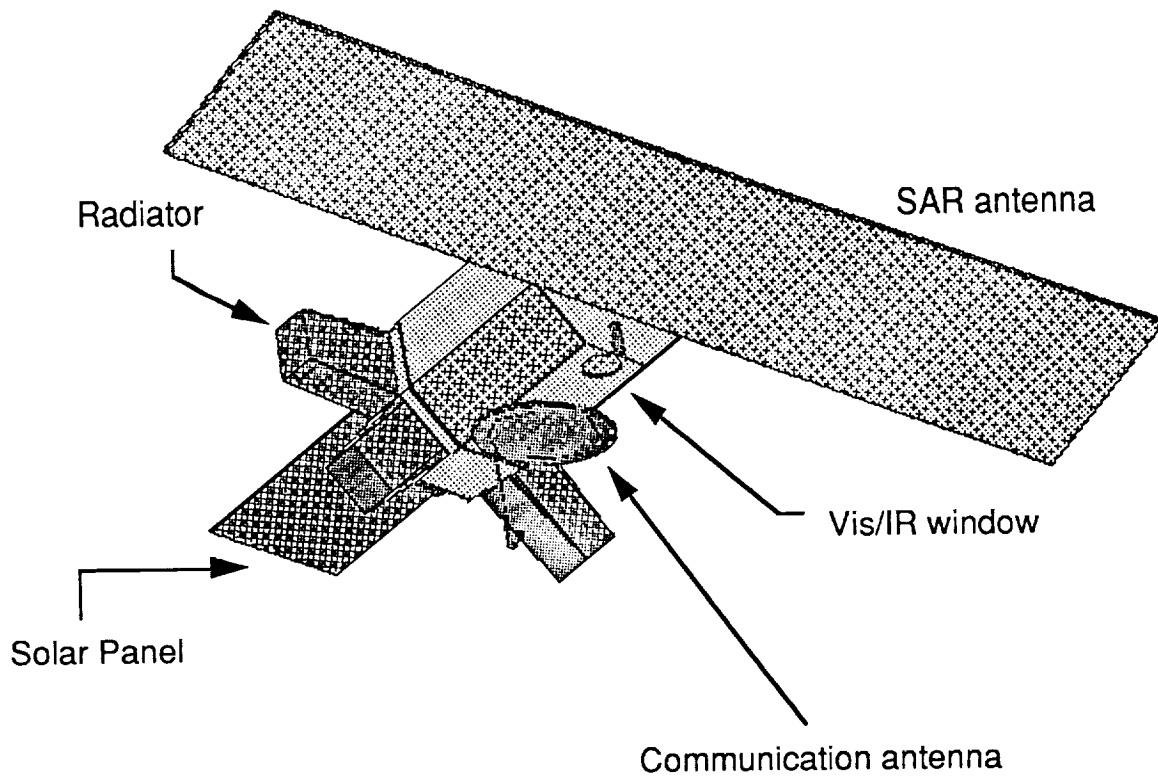


Fig. 1. Exterior shape of MEDSAT.

to avoid contact with the inner wall of the payload bay. Upon reaching orbit, subsystems will deploy into their operating configurations. Second, the combination of the orbit altitude and the launch capability of the Pegasus determines the mass of MEDSAT to be 341.8 kg. Since the total mass of the satellite is limited, the mass of each subsystem must be minimized. Due to the modern technology and the efficiency of the supporting subsystems, MEDSAT allows 28% of the total mass to scientific payloads. Third, each subsystem requires adequate safety, so that the malfunction or failure of any system does not hinder the performance of the other systems. Fourth, the low cost requirement of MEDSAT dictates that each subsystem be built with reasonable cost.

With the above design considerations and parameters, the final external configuration of the MEDSAT main body is an octagonal cylinder attached to a conical section. The satellite body is constructed with 8-mm-thick aluminum honeycomb with two 1-mm-thick aluminum face sheets. Aluminum honeycomb is chosen for its high strength-to-weight ratio. Once in orbit and separated from the Pegasus third stage, the satellite's attitude control system orients itself so that the cylindrical section points along the north pole axis of the Earth and the conical section points along the south pole axis of the Earth. The SAR consists of an antenna with deployed dimensions  $6.0 \times 1.0 \times 0.0254$  m and the supporting electronics. It is constructed with aluminum honeycomb and truss structures and it is mounted on the north

side of the satellite body. The antenna is stored in a box of dimensions  $1.0 \times 0.6 \times 0.38$  m in the octagonal section of MEDSAT. The exterior shape of MEDSAT is shown in Fig. 1.

When the satellite reaches the desired orbit and orientation, the SAR antenna slides out of the side of the satellite, unfolds its panels, and locks into a stable and rigid position facing the northern hemisphere of the Earth. All the supporting electronics are located inside the satellite body.

The IR sensor contains optical lenses, visual and thermal IR detectors, readout and interface electronics, and supporting frame. It utilizes a window opening positioned between the communication antenna and the SAR antenna allowing alignment with the axis of the SAR.

The power subsystem consists of two major components, the solar array and the battery. Driven by the power requirements of MEDSAT, the size of the solar array is 1 sq m in area and 1 cm thick. During launch, the solar array is folded and stored on top of the conical section of the satellite.

The 0.78-m-diameter communication antenna, which is constructed of graphite composite, is located on the cylindrical section of the satellite. During launch, the antenna is hinged at two points and wrapped around three sides of the satellite.

A thermal control system is used to regulate the temperature of each component. The main components that require cooling are the IR sensor and the batteries. The system includes three radiators and three heat pipes. Two radiators are used to maintain

the IR charged-couple device at 90 K. These radiators are located on each side of the communication antenna on the conical section. The third radiator is used to regulate the battery and the IR optical lenses. Because the radiating surface temperature of the radiator is higher, it is located on the trailing side of the satellite, which receives significant amount of solar radiation. All radiators will be folded during the launch. The deployed radiators will be normal to the satellite surface and point towards the south pole. Since the solar incidence angle varies with respect to the time of the year, the radiator must be shielded from both the Earth and solar radiation.

The interior components of the spacecraft also need to be insulated from the temperature extremes generated on the outer wall surface. The insulation consists of a 1-cm-thick blanket made up of 30 separate layers of Kapton. As the outer surface temperature of the satellite drops due to the Earth's shadow, the Kapton insulation is not sufficient. As a result, heaters need to be turned on to keep the payload within its operating temperature.

#### ATTITUDE CONTROL

The Attitude Determination and Control System (ADCS) of the MEDSAT satellite must correctly position the satellite upon orbit insertion, maintain the nadir orientation of the spacecraft, point the scientific instruments to within  $0.3^\circ$  of the target, and provide a reference to keep the solar array pointed toward the Sun. The ADCS will have to measure and counter disturbance torques while in orbit. For a satellite in low Earth orbit, these torques will consist primarily of gravity gradient, aerodynamic drag, and solar radiation. The two main jobs the system will perform are sensing changes in position, and correcting these changes. Accordingly, the main subsystems of the ADCS are the position sensing subsystem, the attitude sensing subsystem, and the actuator subsystem. The data from any of these systems will go through the microprocessor to the other subsystems that rely on it. The positioning subsystem plays two roles. It must determine when the satellite is positioned over a particular area to know when to turn on the scientific instruments and it must determine the attitude. The positioning subsystem will utilize the Global Positioning System (GPS).

The attitude sensing subsystem is necessary in order to determine the orientation of the satellite. These sensors have two jobs: to provide orientation information to keep the scientific instruments pointed accurately and to provide a reference to the Sun for the solar array. To perform these two duties, the attitude sensing subsystem will have an inertial sensor (TRILAG gyro) and a Sun sensor.

The attitude actuator system will consist of 3 reaction wheels, 1 along each axis, and a 10-thruster propulsion system. The reaction wheels will perform corrections as needed to maintain stability for the scientific mission. The thrusters will be used for orbit insertion, downloading momentum, providing redundancy for the reaction wheels, and performing the  $\Delta V$  maneuvers necessary to prolong the lifetime of the satellite. The thrusters will be positioned so that forces can be applied to cause rotation about each of the axes without causing translational motion, as well as a causing translational motion without rotational motion.

#### POWER

To achieve the project goal of low cost, the power system of MEDSAT is designed to use mostly standard satellite equipment such as gallium-arsenide solar cells and nickel-cadmium batteries. However, the system includes a modern microprocessor to increase the power system efficiency, prolong the life of the batteries, and reduce the overall weight of the power system. MEDSAT's power system is faced with the unusual task of providing high power levels to the scientific instruments for short durations in the low Earth orbit environment. This requires a battery with a large charge capacity, and also a pulse modulator to feed the SAR with the required short pulses of peak power. The first step in providing power for the satellite is to harness the energy of the Sun. A solar array generates electrical power to be used by the satellite to run various components. The solar energy is converted into electrical energy by the solar cells. The solar cells used on MEDSAT will be gallium-arsenide-based cells. The main reason why gallium-arsenide cells were chosen over silicon cells is that they offer a reduction in array area. This significantly reduces the aerodynamic drag on the satellite, which in turn reduces the fuel required during MEDSAT's lifetime. In addition, the smaller array reduces the disturbance torques on the satellite, easing the problem of attitude control. Since MEDSAT has a limited available surface area, and also due to the high power requirements, the solar cells will be panel mounted. The solar array structure itself will consist of an aluminum honeycomb core sandwiched between aluminum facesheets. A layer of insulation is located between the actual cells and the aluminum. The array will have orientation control in only the axis that is stable.

Satellites in low Earth orbit, like MEDSAT, spend a considerable portion of their orbital period in the shadow of the Earth. During this darkness, the solar array cannot produce power for the satellite subsystems. Consequently, electrical energy must be stored to provide power during this eclipse period. To do this, nickel-cadmium battery cells will be used. The battery chosen for the satellite must provide power at nearly 28 V, the satellite's bus voltage. To achieve this voltage, the battery will consist of 23 of the 1.2-V cells connected in series. One goal of the energy storage system was to be able to fully recharge the battery in one orbit after a sensing session. The battery system designed for MEDSAT is almost able to fully recharge the battery before the next orbit begins.

With the advent of lightsats and improved computer technology, power control systems are becoming more flexible and efficient. The power conditioning and control system of MEDSAT is based on an independent microprocessor that resides in the central satellite computer module. This microprocessor continually monitors the satellite power system, including the battery voltage, array current, and battery charging rate, and it can also carry out instructions received from the ground.

#### FIRST-ORDER COST ANALYSIS

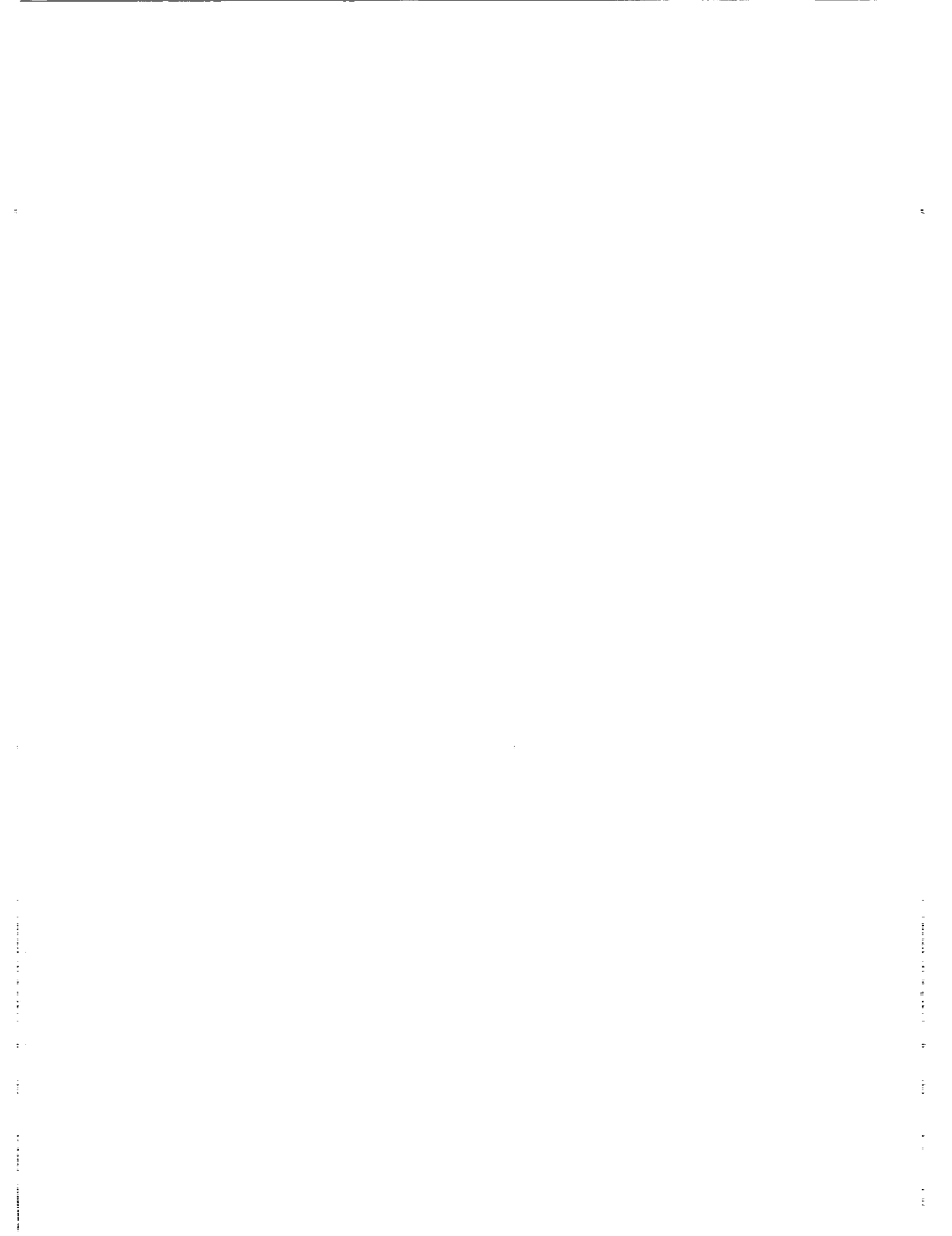
To address the first-order cost analysis, the satellite system was divided into subsystems. For each subsystem, actual industry estimations were used. The overall system cost was then computed by summing the subsystem component costs. The

total estimated MEDSAT project cost was \$35 million dollars (in 1991 dollars). The purpose of a first-order cost analysis is to give a general estimate of the costs over the lifetime of the mission. A degree of uncertainty is always involved in estimates. Cost overruns, schedule restraints, and the inherent speculative nature of estimating will contribute to errors.

To obtain funding for a costly space mission, it is important to be able to demonstrate the anticipated benefits. Such benefits can take two forms. Humanity can be benefited through improvements in the quality of living, and science can advance through the development of new technologies. With over half the world's population living in areas of malaria risk, the benefits

of a project like MEDSAT that could help control this disease would be very significant. The MEDSAT satellite will also be breaking new ground in the area of compact lightweight remote sensing. Never before has a satellite contained both a SAR and an IR system. In this way, the technology gained from the MEDSAT project could be used in future endeavors in satellite design.

The design team of the MEDSAT project has made a conscious effort to make this project cost effective by using the Pegasus launch vehicle and by using already developed and tested technology. The design team has realized that it is very important in these times of economic hardship to propose a project that satisfies the mission goal while being cost effective.



# PROJECT UM-HAUL: A SELF-UNLOADING REUSABLE LUNAR LANDER

UNIVERSITY OF MICHIGAN

528-18  
160604  
P-17

## INTRODUCTION

The establishment of a lunar base is technologically and financially challenging. Given the necessary resources and political support, it can be done. In addition to the geopolitical obstacles, however, there are logistical problems involved in establishing such bases that can only be overcome with the acquisition of a significant transportation and communications network in the Earth-Moon spatial region.

Considering the significant number of payloads that will be required in this process, the mass-specific cost of launching these payloads, and the added risk and cost of human presence in space, it is clearly desirable to automate major parts of such an operation. One very costly and time-consuming factor in this picture is the delivery of payloads to the Moon. Foreseeable payloads would include atmospheric modules, inflatable habitat kits, energy and oxygen plant elements, ground vehicles, laboratory modules, crew supplies, etc. The duration of high-risk human presence on the Moon could be greatly reduced if all such payloads were delivered to the prospective base site in advance of crew arrival.

In this view, the idea of a "Self-Unloading Reusable Lunar Lander" (SURLL) arises naturally. The general scenario depicts the lander being brought to low lunar orbit (LLO) from Earth atop a generic Orbital Transfer Vehicle (OTV). From LLO, the lander shuttles payloads down to the lunar surface, where, by means of some resident, detachable unloading device, it deploys the payloads and returns to orbit. The general goal is for the system to perform with maximum payload capability, automation, and reliability, while also minimizing environmental hazards, servicing needs, and mission costs.

Our response to this demand is UM-Haul, or the UnManned Heavy payload Unloader and Lander. The complete study includes a system description, along with a preliminary cost analysis and a design status assessment.

## Design Development

The specific design requirements and constraints adopted are those formulated in the 1991 AIAA/Industry Design Competition Proposal Request for the SURLL. They are

1. Descent from LLO to the lunar surface carrying a 7000-kg payload, the unloading mechanism, and propellant for ascent back to LLO.
2. Capability to refuel and reload in LLO for another landing.
3. Capability to carry the unloading mechanism back to LLO for later use at another landing site.

4. Return to LLO without the unloading device, and bring down a payload of mass equal to 7000 kg plus that of the unloading device.

5. Capability to perform 10 landing/unloading sequences before major servicing.

6. Modularized subsystems for easy maintenance.

7. Ability to handle a payload of the same diameter as Space Station *Freedom* (SSF) logistics module.

8. The payloads need not be supplied with power or thermal control.

Earth systems are not acceptable SURLL solutions for a variety of reasons, most of which can be ascribed to the adverse conditions of the lunar environment: extreme temperatures, abrasive soils, low gravity, intense radiation, and the absence of atmosphere. Thus, whereas Earth cargo handling systems may provide useful functional concepts, the design of a lunar cargo delivery system is subject to some very different requirements. This tends to necessitate a "build from scratch" approach.

The design effort was subdivided into six technical subgroups: Payload/Spacecraft Integration, Structures, Propulsion, Power, Controls and Communications, and Mission Analysis. The subsystem designs are described below.

## PAYLOAD AND SPACECRAFT INTEGRATION

Giving consideration to assembly, functionality, power, and thermal control needs, stability, and center of gravity locus, the Payload and Spacecraft Integration (PSCI) group integrated (i.e., placed and interconnected) the subsystem components within the spacecraft frames. External interfaces, including payload handling, were also addressed.

## System Overview

UM-Haul consists of two main components: lander and unloader. The lander is a low center of gravity platform with four main engines, propellant tanks, a centralized cargo bay with deployable ramps, and four shock-absorbing retractable landing legs. The unloader is a solar-powered, telerobotic, eight-wheeled carrier vehicle that fits in the Lander's cargo bay. It utilizes a special lift mechanism in conjunction with legs mounted on the payload unit to deploy cargo on the lunar surface. The unloader can remain on the surface while the lander returns to orbit for another payload. A visual impression of the system is given in Fig. 1; Table 1 briefly summarizes features of the lander and unloader systems.

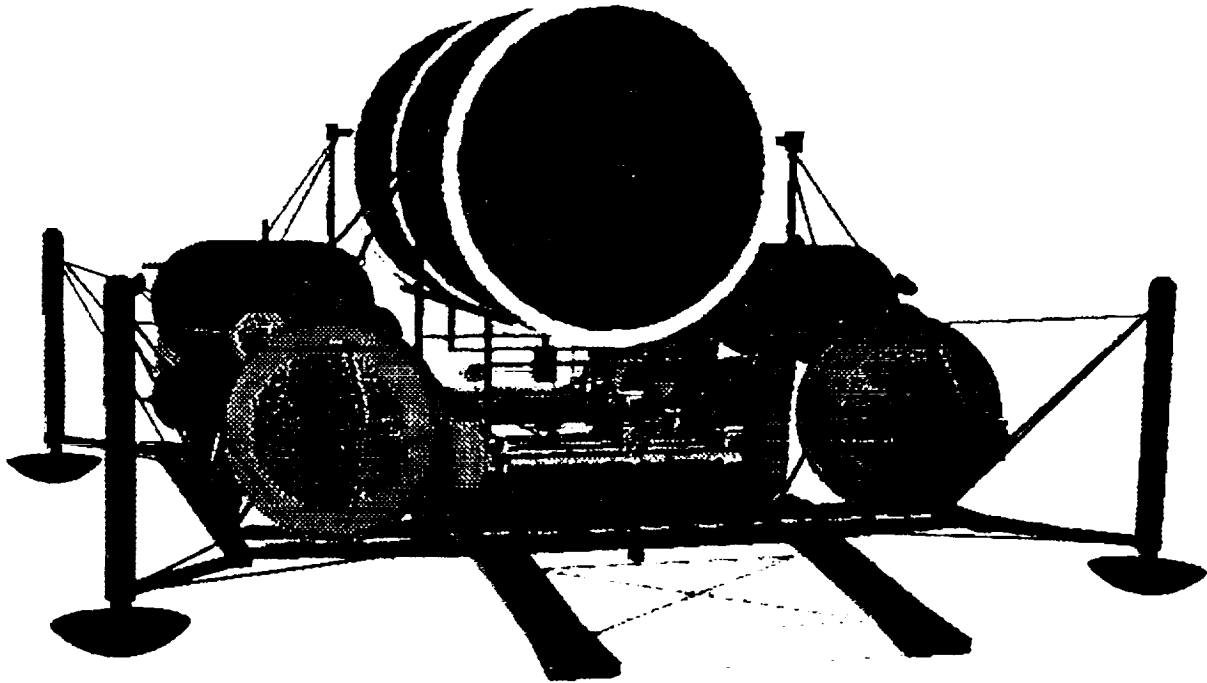


Fig. 1. The UM-Haul system.

TABLE 1. Summary of system features.

| Function                      | Lander                                    | Unloader                                  |
|-------------------------------|---|---|
| <b>Propulsion</b>             |   |   |
| Main Engine/Drive, Lift Motor | Pratt & Whitney RL10-IIIB (4)             | DC Motors: 746 W (8,4)                    |
| RCS Thruster/Steering Motor   | GH <sub>2</sub> /OX8911 Bell Textron (20) | DC Motors: 373 W (8)                      |
| <b>Power</b>                  |   |   |
| Primary Power System          | GH <sub>2</sub> GOX Fuel Cells (3)        | GaAs/Ge Solar Array (4.5 m <sup>2</sup> ) |
| Secondary Power System        |   | NaS Batteries (6)                         |
| <b>Structure</b>              |   |   |
| Structural Material           | Al-Li 2090-T841                           | Al-Li 2090-T841                           |
| Structural Mass               | 3,409 kg                                  | 448 kg                                    |
| Total Dry Mass                | 6,162 kg                                  | 1,438 kg                                  |
| Payload Capacity              | 8,438 kg                                  | 8,438 kg                                  |
| Landing Legs/Wheels           | Pads, retractable (4)                     | Wire mesh, indep. drive, steer (8)        |
| Suspension System             | Helium Gas Shocks                         | Rotational Springs                        |
| <b>Communications</b>         |   |   |
| Frequency (Primary, backup)   | Ka-Band, S-Band (Backup)                  | Ka-Band, S-Band (Backup)                  |
| Link to Unloader/Lander       | Beacon (1)                                | Receiver (1)                              |
| <b>Controls</b>               |   |   |
| Obstacle Avoidance System     | Laser Radar (1)                           | Television Cameras (4)                    |
| Guidance System Sensors       |   |   |
| Relative Frame:               | Star Trackers (3)                         | Wheel Odometers (2)                       |
| Body Frame:                   | Ring Laser Gyroscopes (6)                 | Gyrocompasses (2)                         |
| Position, Velocity, Acc.:     | Accelerometers (6)                        | Accelerometers (2)                        |

### OTV Interface

The lander refuels and receives new payloads regularly from a standard OTV. The OTV is fitted with a payload pallet/docking port for interface with the lander. The pallet arms hold the payload with four Light-Weight Longeron Latches (LWLLUs). A Payload Transfer Mechanism (PTM) sits in the middle of the pallet and guides the payload over to the lander when docked. Also on the pallet arms there are Docking/Fuel Ports (D/FP), which provide the fueling hookup with the lander.

### Payload Interface

The general size and shape of the payload is an important characteristic of a transport system. For the sake of simplicity it was therefore decided to interpret Design Criterion #7 in a narrow sense, by adopting the SSF logistics module as the standard payload. The logistics module is cylindrical, 7.4 m long and 4.6 m in diameter; it has three bulkhead rings and a set of trunnion points for easy handling. For UM-Haul purposes, it became necessary to further furnish this payload with four deploying legs.

The lander receives a payload with four motorized trunnion latches mounted on special bearing truss members along the central unloader bay. These will completely secure the payload during transport. The holders are high enough to give clearance for the unloader in the bay underneath. After landing, the unloader uses special lifting posts to clear the payload from the lander truss.

While aboard the unloader, the payload rests on a set of rails with rocker joints. A trunnion, located at the base of the standard payload, fits into a cylindrical hardlock suspended from the unloader's lifting structure. This prevents the payload from shifting in the rails when the unloader is on a slope. At the time of deployment, the payload legs are released with the aid of pyrom pins, and lock into "standing" position. Using its lifting mechanism, the unloader slowly lowers the payload to the ground until it rests fully on the four legs.

### System Launch and Assembly

The external dimensions of UM-Haul preclude integral launch with any existing or planned Earth Launch Vehicle (ELV). LEO assembly, at or near a permanently manned structure such as SSF, has therefore been envisioned. The space shuttle orbiter has the capacity to move the entire UM-Haul assembly kit to orbit in three launches, not including propellants. The modular design of the lander structure in particular helps contribute to the relative simplicity of in-orbit assembly.

## STRUCTURES

The structural components of the UM-Haul system were designed to serve certain basic mission functions, and to provide support for the other subsystems. Emphasis was placed on strength and durability, while also seeking to minimize the total structural mass. A static analysis with beam theory was used throughout for loading strength calculations. Reliability and

redundancy are essential considerations due to the rigorous system lifetime requirements. The vital elements of the Lander and Unloader have been designed with a factor of safety that will allow for continued operation after unforeseen contingencies. The Unloader structure has a safety factor of 3, the Lander structure a safety factor of 1.5. For all major structural components, the material chosen is the alloy Al-Li 2090-T841, due to its low density and high yield strength.

### Lander Structure

The Lander structure consists of the following main components: platform and unloader bay, engine shrouds, ramps, and landing legs. In the following, a brief description will be given of each component.

The platform is the "backbone" of the structure, with an area of  $8 \times 10$  m, and designed to withstand 1g of landing deceleration with full loading. The unloader bay is located in the middle section of the platform and is characterized by a set of runners traversing the length of the platform. The ramps run off both sides of the unloader bay, and fold up to a vertical position during flight.

The engine shrouds provide the housing and restraint for the main engines. They are located near the middle of the platform on either side of the unloader bay. The maximum single-engine thrust of 33,000 N is used for the maximum loading calculations. The landing legs are retractable to give a low ground clearance (and thus low ramp slope) during unloader operations. They are designed with a helium gas shock system to absorb the impact of landing. Located diagonally outward from the platform corners, they attain a maximum distance from the engine plumes during landing and takeoff burns. The temperatures and dust blasts generated from the engines have a deteriorating effect on the landing legs.

### Unloader Structure

The unloader structural system consists of a chassis, payload interface and handling system, suspension and steering systems, wheels, and subsystem support structures.

The chassis is the main support frame upon which all other unloader subsystems are attached. It is thus responsible for withstanding all stresses due to these subsystems and loads due to system operations. It consists of two longitudinal beams and four transversal spars assembled in a "block eight" configuration.

Inside the chassis frame there is a truss grid for support of various subsystem components such as radiators, instrument bays, solar arrays, batteries, etc. Of special importance is the solar array support, since the fragile semiconductor cells need protection from vibrations and dust kick-up. While the grid combines with the suspension for good vibration damping, the dust shielding is provided by a special "curtain."

Prominent on the unloader is the payload interface and handling system, which includes a set of threaded posts with housing rail posts, support rails, a set of rocker joints for the payload bulkheads, and a hardlock support. With the aid of four 746-W motors, this system performs the important task of securing and deploying (lifting/lowering) the payloads. Details of the system can be seen in Fig. 2.

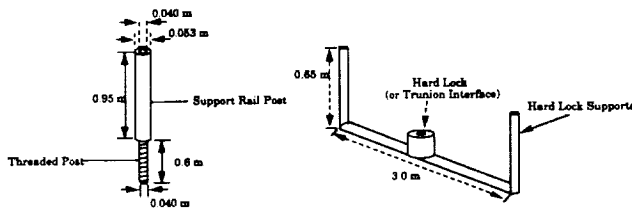


Fig. 2. Lifting posts and hard lock.

The unloader's eight wheels are of a wire mesh type, each independently driven and steered. The drive motors are 746 W each. The suspension consists of rotational springs. Details of the steering and suspension systems can be seen in Fig. 3.

**PROPULSION**

The focus of the propulsion design fell on selection of main engines and attitude thrusters (RCS). A design was conceived to integrate the primary propellant delivery system with the RCS and the fuel cell power system.

**Engine Selection**

After considering our mission's needs for thrust, throttability, durability, and cost-efficiency, the only viable candidates for main engines were the chemical liquid bipropellant (liquid oxygen and liquid hydrogen) rocket engines. Out of these, the cryogenic propellants took the edge over hypergolic propellants, having a high specific impulse ( $I_{sp}$ ) and the prospect of symbiotic propellant usage with future OTV's.

With this category firmly in mind, a scan of presently and near-future available engines began. The chosen engine was Pratt & Whitney's RL10-IIIB, a derivative of the already existing Centaur RL10A-3-3A. Although the RL10-IIIB is still in a developmental stage, its predicted merits are very good: It has a maximum thrust of 33,360 N, an  $I_{sp}$  of 470 s, and a mass of only 180 kg.

The thruster chosen for the Reaction Control System is the Bell Aerospace 8911 GOX/GH2. The reverse flow chamber feature of this engine aids in the combustion process of the reactant gases, and thus achieves a good thrust without the need for a combustor.

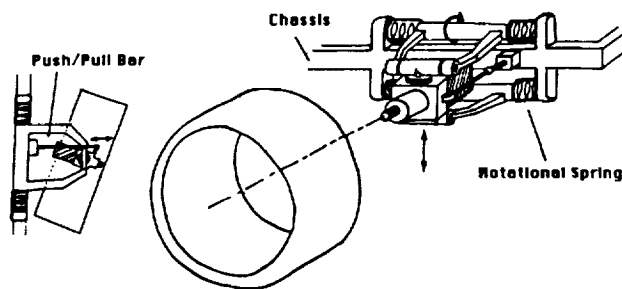


Fig. 3. Steering and suspension.

**Propellant Storage and Delivery**

The liquid oxygen (LOX) is stored in a set of big cylindrical tanks and the liquid hydrogen (LH<sub>2</sub>) is stored in a set of big tanks, embedded in the trusswork in the neighborhood of the main engine shrouds on the lander. The reactants must be protected thermally since the boiling point of LOX is 90.4 K, and that of LH<sub>2</sub> a mere 20.2 K. Additionally, it is desirable to provide protection from debris and meteoroid strikes that might rupture the tank membrane.

For this purpose, a multilayer insulation has been chosen with 3.8 cm of Double Goldized Kapton reflectors separated by Dacron net for a total of 20 layers, covered by a Nomex resined face sheet and tension membrane.

The UM-Haul main engines employ a turbopump-fed delivery system with regenerative turbines; the LH<sub>2</sub> is used first to cool the engine nozzle; in passing through the nozzle jacket the LH<sub>2</sub> is vaporized and thus pressurized to drive the turbopump. Finally, the gaseous hydrogen arrives in the combustion chamber where it reacts with vaporized LOX and produces thrust.

It turns out that the RCS thrusters and the lander's power system fuel cells run on roughly the same chamber pressure. Since they also use the same reactants—gaseous hydrogen and oxygen—integrating them with the main propellant delivery system came naturally. The result is shown in Fig. 4. With the aid of miniturbopumps (labeled R1S), the liquid propellants are vaporized (2), in the process pressurizing small accumulator tanks (3) to operational level for the RCS thrusters and fuel cells. Note that the minipumps are regenerately driven by combustors (4) bleeding off reactants from the accumulator tanks.

**POWER**

The power systems of UM-Haul had to meet very strict demands. Selection of the proper system for endurance, efficiency, mass, and output level was imperative. Power architecture was developed throughout. A thermal management system was conceived, relieving subsystem-generated heat buildup.

**Power Systems**

The needs of the UM-Haul system are unusual. The unloader may be required to stay on the lunar surface for weeks with

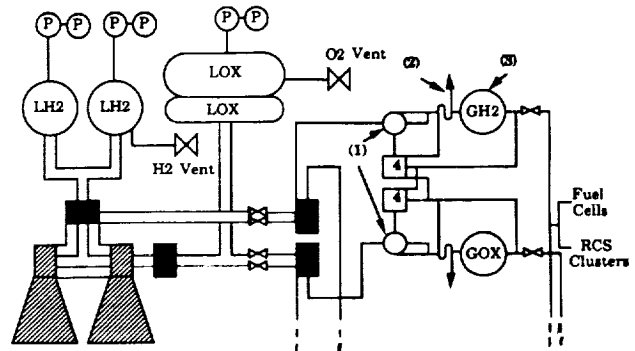


Fig. 4. Integrated propellant delivery system.

little or no activity, and suddenly called to duty with a big energy output. Although its cruise speed is only 0.1 km/hr, one must take into account that the unloader is carrying 5-6 times its own weight. The total energy estimate runs up to 7.2 kWhr for each unloader mission. Peak power is roughly 1200 W. For the lander, one sees a more modest, but steady consumption.

The primary and secondary power systems for the unloader are GaAs/Ge solar cells and NaS batteries, respectively. The lander power system consists of  $\text{GH}_2/\text{GOX}$  primary fuel cells, and since they feed off the generous supplies of the propulsion system, they can be used to charge the unloader batteries in special cases.

The GaAs/Ge solar array has 2800 cells, has an area of 4.5  $\text{m}^2$ , and gives 600-800 W over 29 V. The energy is stored in the NaS batteries during periods of inactivity. The batteries have a normal operating temperature of 350°C, and lose efficiency with lower temperatures. Left to the cold lunar night at low discharge rate, they could freeze without a thermal management system. This will be discussed later.

The lander's fuel cells draw energy from the reaction of gaseous oxygen and hydrogen. They are located with the RCS reservoirs on the lander, near the main hydrogen tanks.

### Thermal Management

The numerous power-driven units on the lander and on the unloader generate heat. This heat rapidly builds up unless it is led away; there is no atmosphere to conduct or convect heat, therefore one must radiate it through specially designed space radiators.

The thermal loads produced by the lander and unloader are 954 and 1480 W, respectively. Each heat generating unit will be connected with a heat pipe of aluminum (filled with mercury), thus transmitting excess heat through the pipe to the radiator. There is one radiator on each vehicle.

But not all systems want cooling; the NaS batteries on the unloader need heating, i.e., thermal insulation. The batteries will be put in a heat insulating box with a phase change substance, carbazole. This substance absorbs excess energy and releases it as it cools down and solidifies.

## CONTROL AND COMMUNICATIONS

The design of Guidance, Navigation, and Control (GN&C) systems for UM-Haul involved selecting attitude and positioning sensors, obstacle avoidance systems, and processing hardware. Features of a communications system were developed.

### Lander GN&C

The task of this system is to determine the position, velocity, and attitude of the spacecraft. Hazard avoidance (for landing) also plays an important role in this particular system. The four active components of the system are external referencing, inertial referencing, obstacle avoidance, and computer interaction/system integration.

The external (or "relative") referencing is achieved by a combining sensors (star trackers) with a vertically stabilized platform (the stars) to obtain an attitude reference. The inertial (or "body

frame") referencing is concerned with sensing changes in rotation and velocity. To this end it was decided to apply ring laser gyroscopes, one for each body axis. Ring laser gyroscopes are very sensitive, and accumulate less error than conventional momentum wheels and gyroscopes. The output from the laser gyroscopes is integrated by the onboard computer to give rotational changes. For the translational changes, an accelerometer is used.

An obstacle avoidance system is essential to safe landings by unmanned vehicles in the mostly unknown lunar terrain. A laser radar starts the scanning process approximately when the lander passes High Gate (880 m altitude) and continues to narrow its mesh as the lander approaches. Obstructed sites will be noted and avoided through careful interpretation by the onboard computer. The laser radar consumes 258 W of power.

The computer interaction and system integration is the process by which the onboard computers collect all the referencing data and digest it into position, attitude, velocity, and flight plan (commands from Earth). The Lander has three onboard computers, two of which are idle during most nonmaneuvering phases of the mission, but capable of taking over all functions of the other computer(s) should a malfunction occur.

### Unloader GN&C

The unloader's GN&C system is composed of four ingredients: hazard sensing, path determination, motion sensing, and integration.

For hazard sensing, television cameras are employed, two at each end of the vehicle. This gives stereoscopic imaging opportunities, of great use in path determination. Disadvantages include ineffectiveness during lunar night and the delay in data transmission, given the nonautonomy of the system.

Path determination is an interactive process between the onboard computers and mission control (humans). The motion sensing is still provided by body-mounted accelerometers, but is supplied also by wheel odometers for positioning and gyrocompasses for heading.

The UM-Haul unloader employs the Computer-Aided Remote Driving (CARD) method of semiautonomous travel. The system integration diagram for a CARD method is shown in Fig. 5.

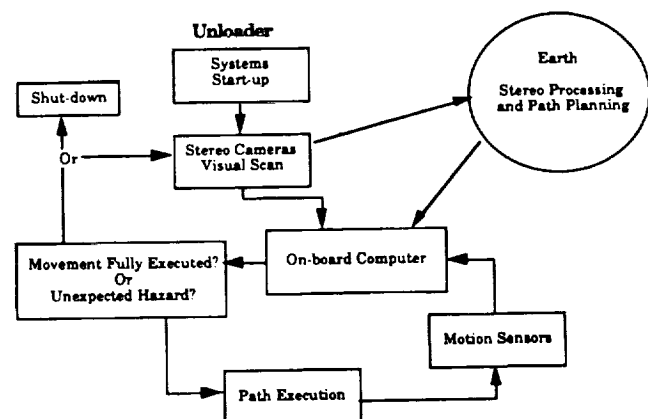


Fig. 5. Unloader CARD system.

To execute this system, the unloader employs two onboard computers, one of which is solely dedicated to the GN&C and CARD systems; the other is used for system resource management, troubleshooting, and back-up GN&C.

### Communications System

The items to be communicated in the UM-Haul system are countless. Propulsion system monitoring, power system data, flight data, guidance aspects, and system diagnostics are but some general areas. It is clear that communications are essential to the success of any SURLL mission, and UM-Haul in particular.

The optimum link configuration involves the ground terminal (GT) path, i.e., direct transmission of data between the lunar surface and one of three continuously listening Earth stations (initial deployment). The Ka-band (20-40 GHz) was chosen as primary carrier frequency, with the S-band (2-4 GHz) as a backup frequency range.

The communications hardware includes 2 Ka-band and 2 S-band antennas for both lander and unloader. Likewise, on each vehicle there is a set of transmitters/receivers and a set of filter/switches for both Ka-band and S-band.

Communications and operation of UM-Haul would be greatly enhanced by the establishment of a lunar communications satellite.

## MISSION ANALYSIS

Mission Analysis was chiefly responsible for obtaining a flight plan for the lander. A study was also done on mission timelines for selected landing sites, and on the line-of-sight conditions for various envisioned communications paths between the UM-Haul vehicles and other stations.

### The Mission Cycle

For a better understanding of the UM-Haul operational concept, it is useful to subdivide the typical mission into five segments: initial in-orbit operations, transit to lunar surface, lunar surface operations, launch to orbit, and concluding in-orbit operations.

Initial in-orbit operations for a mission include payload transfer, systems check, descent planning, separation, and descent countdown. Transit to lunar surface consists of the descent orbit burn and a touchdown burn, possibly with hovering. The lunar surface operations involve another complete systems check, ramp deployment, unloader activation, cargo securing and transit, unloading, and finally a clearance or reboarding maneuver by the unloader.

Preceding the launch to orbit phase, yet another systems check is performed. A rapid ascent burn takes the lander up to LLO. An orbit insertion burn is required upon obtaining the desired altitude. Finally, during the concluding orbit operations, the lander waits in orbit for the arrival of another OTV. Rendezvous, proximity operations, and docking follow. Once safely docked, the lander is refueled and checked by the OTV. If 10 mission cycles have been completed, the entire system is returned to LLO for maintenance; otherwise, it is ready to load another payload and begin the next cycle.

### Mission Planning

Mission analysis has been mainly concerned with the flight aspects of the mission cycle, insofar as they involve orbital mechanics and the preparation of a  $\Delta V$  budget.  $\Delta V$ s are velocity changes needed for a spacecraft to change its angular momentum and energy relative to a gravitating body and thus enter a new trajectory. It is the propulsion system(s) of the spacecraft that furnish these  $\Delta V$ s, so for thrust and fuel consumption specifications the  $\Delta V$  budget is of vital importance to the mission. Another budget of major significance is that of time.

Elements of the mission cycle with most direct bearing on the  $\Delta V$  budget can be roughly categorized in three phases: rendezvous, descent, and ascent. The two main parameters in these scenarios are the lunar surface and the LLO parking orbit.

The parking orbit chosen for the lander is a circular LLO with an altitude of 111 km. This height was chosen with consideration orbital instabilities occurring below 93 km, and the increasing  $\Delta V$  costs of higher orbits. The orbital period is 119', and the inclination angle (with respect to the lunar equator) is equal to the latitude of the next landing site.

The first (or last) event in the UM-Haul mission cycle is the rendezvous and docking between the lander and the OTV in LLO. It is clearly impractical to require a precise insertion of the incoming OTV in the close neighborhood of the waiting lander. (This would give narrow and infrequent launch windows in LEO.) Instead, the OTV is inserted into the 111-km orbit at some arbitrary phase angle away from the lander. The lander will now enter a 101-km chase orbit to catch up with the OTV. In the worst case, (i.e., when the initial phase angle is  $360^\circ$ ) the lander will spend 10 days catching up. When the OTV is in sight and at a determined phase of  $0.725^\circ$ , the lander performs an ascent burn followed by a braking burn to rendezvous with the OTV (terminal phase maneuvers). After rendezvous, proximity operations must be executed in order to dock with the OTV.

For descent, the lander first separates from the OTV and then executes an engine burn for a retrograde  $\Delta V$  of 21.8 m/s (descent orbit initiation), thus entering a Hohmann transfer ellipse to a perilune altitude of 15.24 km. At this point, the lander performs its powered descent initiation burn. The braking is considerable, as the total  $\Delta V$  reaches 1693.8 m/s. A slow, increasingly vertical descent to the surface results. Limited hovering time is allowed for in the  $\Delta V$  budget if the targeted landing spot turns out to be unfavorable.

After the surface operations are complete, the lander returns to LLO. This operation consists of three main parts: first, a rapid ascent burn ( $\Delta V = 81.7$  m/s) to acquire altitude (thus avoiding risk of collisions); next, a forceful horizontal orbit insertion maneuver ( $\Delta V = 1682.4$  m/s); finally, depending on the present orbital inclination, a dog-leg plane change maneuver will be required to poise the lander for its next mission.

### Prospective Landing Sites

Four possible landing sites were selected for UM-Haul, mainly based on their suitability as prospective lunar outpost sites. Such candidacy is heavily determined by scientific interest and industrial promise. Due to the presently inadequate communi-

cations support, it is necessary to confine UM-Haul to nearside landings; in any case, topologically ideal sites were hard to find on the farside. However, the farside is of particular interest for radioastronomy observatories, since the Earth radio waves are blocked out. Two of our sites are therefore near the 90° parallels (E and W) where they actually librate out of Earth view for parts of every month. The sites are:

Lacus Veris (87.5°W, 13°S): Scientific Interest; access to farside.

Taurus-Littrow (30°E, 20°N): Mare region - O<sub>2</sub> production. Apollo 17 site.

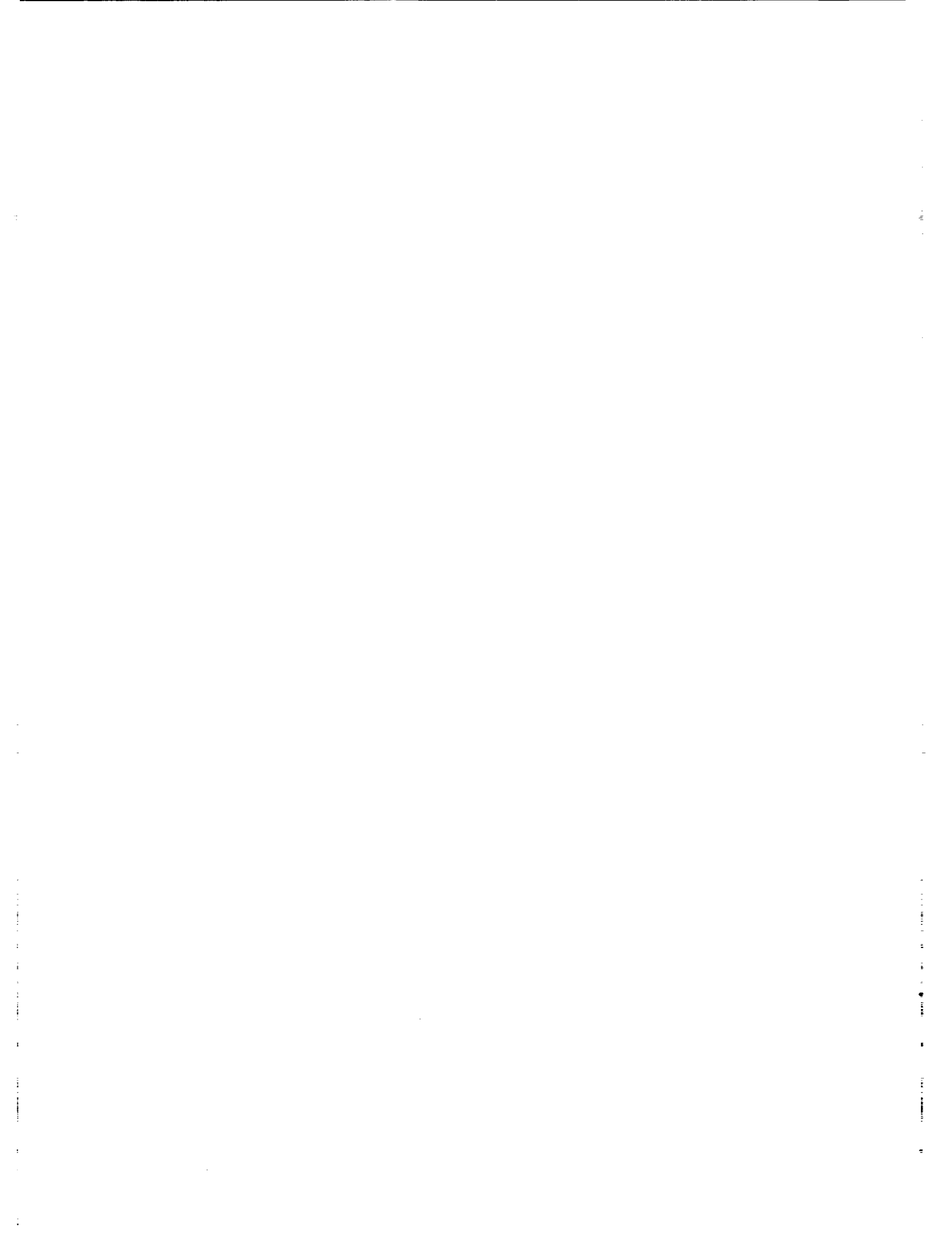
Mare Nubium (20°W, 10°S): O<sub>2</sub> production. Near Apollo 12 site.

Mare Marginis (92.5°E, 9.5°N) O<sub>2</sub> production. Technically on farside.

## CONCLUSION

A preliminary design has been developed for a Self-Unloading Reusable Lunar Lander, meeting the criteria stated in AIAA/Industry's Request for Proposal. The result, UM-Haul, comprises a lander/unloader system with capability to handle payloads up to 8438 kg. The hardware cost of one UM-Haul system is estimated at \$1.2 billion.

The following key areas need focus for the completion of the preliminary design: structural analysis (CAD, static, and dynamic), guidance system design, propellant delivery piping, engine power requirements, unloader AI implementation, telemetry design, system verification of margins, and cost analysis.



**MARS INTEGRATED TRANSPORTATION SYSTEM  
MULTISTAGE MARS MISSION**

**UNIVERSITY OF MINNESOTA**

529-18  
160605  
P. 6

In accordance with the objective of the Mars Integrated Transport System (MITS) program, the Multistage Mars Mission (MSMM) design team has developed a profile for a manned mission to Mars. The purpose of the multistage mission is to send a crew of five astronauts to the martian surface by the year 2019. The mission continues man's eternal quest for exploration of new frontiers. This mission has a scheduled duration of 426 days that includes experimentation en route as well as surface exploration and experimentation. The MSMM is also designed as a foundation for a continuing program leading to the colonization of the planet Mars.

**NOMENCLATURE**

|      |                                       |
|------|---------------------------------------|
| AFE  | Aero-Assist Flight Envelope           |
| DC   | Direct Current                        |
| HLLV | Heavy-Lift Launch Vehicle             |
| LEO  | Low Earth Orbit                       |
| MEV  | Mars Excursion Vehicle                |
| MHM  | Mars Habitation Module                |
| MITS | Mars Integrated Transportation System |
| MRV  | Mars Roving Vehicle                   |
| MSMM | Multistage Mars Mission               |
| MTV  | Mars Transfer Vehicle                 |
| NTR  | Nuclear Thermal Reactor               |
| TEI  | Trans-Earth Injection                 |
| TMI  | Trans-Mars Injection                  |

**INTRODUCTION**

Long-range plans for NASA have included the development of manned missions to the martian surface. The goal of NASA is to have the manned landing of the Mars mission coincide with the 50th anniversary of the landing of man on the lunar surface. This report is an outline of a design for a manned mission to Mars.

**Objectives**

1. To place a crew of trained astronauts from Earth on the surface of Mars close to the year 2020.
2. During this initial stay the astronauts are to establish a Mars outpost site and conduct local science and exploration.
3. Return the crew, surface samples, and useful hardware information back to Earth.
4. Accomplish the above tasks in a cost-effective manner with acceptable levels of safety in the design systems.

**General Assumptions**

1. A minimum configuration space station exists within the 2015-2018 timeframe.
2. A new HLLV will be available and operational.

3. No lunar base will be necessary for the commencement of a Mars initiative.
4. A series of robotic missions will precede a manned Mars mission.
5. Adequate communication facilities exist.
6. A reliable NTR propulsive engine is available.
7. No remarkable advances will be made in the human body's regenerative powers in a zero-gravity environment.

**MISSION PROFILE**

The mission developed consists of two main profiles with a number of smaller stages incorporated into each of the two larger stages. The two stages use two different types of vehicles. One vehicle has been designed around the mission's cargo and the other is focused on the mission's crew. The MHM is a cargo vehicle. The other main vehicle, the MTV, is the crew's transport vehicle. Each vehicle is launched at different stages throughout the mission. The chronological description that follows describes the mission, vehicles, and their combined purposes.

**MHM Mission Profile (Phases A-F)**

The MHM (Fig. 1) is the first vehicle/system that is prepared and sent to Mars. The MHM is to serve as the command and control center for the astronauts on the martian surface. It will carry the logistics equipment and supplies needed for the 30-day stay on the martian surface. The MHM does not carry any crew members on its journey; therefore, it can be sent prior to a crew-intensive system. The first step in the MHM flight profile is the launch of the MHM package on board a 200-300-Klb-class Inline ET-derived launch vehicle, (Phase A). Once in space, the MHM enters a specified parking orbit at an altitude of 300 km. Soon thereafter, a second 200-300-Klb-class rocket launches a ET-derived cryogenic booster to rendezvous with the MHM package. This trans Mars injection (TMI) booster docks with the MHM and awaits the proper launch window for reaching Mars. The window for launching the MHM is January of 2014. Once the window is open, the TMI booster fires, placing the MHM in a Mars-bound trajectory (Phase B). The MHM must develop a  $\Delta V$  of 3.60 km/s to accomplish the TMI burn. Three

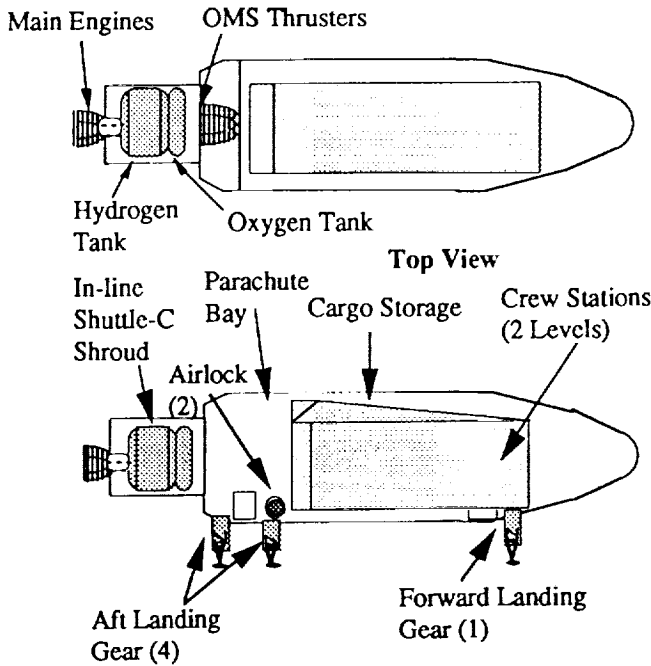


Fig. 1. Component diagram of the Mars habitational module.

space transportation main engines are used as the propulsion system for the MHM, which develops this  $\Delta V$  for TMI. The actual propulsive burn needed to develop this  $\Delta V$  is approximately 6 min. Once the TMI burn is completed the spent booster is jettisoned (Phase C).

En route, reaction and control system thrusters fire to perform course corrections as needed. The reaction and control system is used to keep the MHM on a Hohmann transfer path to Mars. The Hohmann transfer route is used because time is a critical factor in the MHM journey. The Earth-to-Mars transfer time for the MHM will be approximately 259 days. The launching of the MHM is approximately two years ahead of the scheduled launch date for the MTV and the mission's crew.

As the MHM approaches the martian atmosphere the MHM orientates itself for aerocapture. The MHM's straight biconic shape and thermal shielding allow it to successfully use the martian atmosphere to bleed off speed and enter a Mars orbit.

The MHM's 40.0-m straight biconic shell is designed with a lift-to-drag ratio of 1.0, and has an ideal velocity window of 4.0-9.5 km/s. The entry velocity of the MHM will be at a  $\Delta V$  close to 4.5 km/s. The relatively slow  $\Delta V$  for entry will limit the aeroheating that occurs during the atmospheric entry into Mars. Calculations show the aeroheating induced on the MHM's surface will develop temperatures close to 1600°C.

The outer skin of the MHM is an aluminum silicon-carbide composite and glass-reinforced polyimide honeycomb sandwich. This skin not only withstands the high temperatures developed from aeroheating, but it also exceeds the minimum allowable parameters for internal pressure. This outer skin has a safety factor of two, in reference to both the aeroheating temperatures and the internal pressure.

The MHM continues to use the reaction and control in a deorbit burn and descends to the martian surface (Phase E). After the MHM has slowed down to below Mach 1.0, parachutes will be released to slow the craft down further and guide it to the landing site, 20°N 150°W, just west of the Olympus Mons. Shock-absorbing structures on the base of the MHM are extended to protect the craft from the shock of impact. A secondary landing site has been chosen for contingency purposes. This site is located at 10°S 150°W and is known as Mangala Vallis.

After the MHM has landed, an extensive system check is performed on the MHM. When the MHM is verified intact and operational, the MTV is then cleared for launching. During this period the MHM's radiation protection system is being completed.

The MHM's surface radiation system is a regolith bag system (Fig. 2), whereby bags filled with the regolith of Mars provide radiation protection for the crew. A robotic filling system is used to complete this task. The robotic regolith filling system consists of three main components, each of which accomplishes one part of the task. A small roving vehicle, the gatherer, is used to collect the regolith from various areas near the MHM. The gatherer then dumps the regolith in the second component, the hopper. The hopper includes a swing arm that moves over to the regolith bags and fills them. Once the bags are filled and sealed, a pulley system moves them to their appropriate position on the MHM. Once this is completed the MHM is ready for use when the astronauts arrive.

**MTV Earth-to-Mars Mission Profile (Phases G-M)**

The actual manned mission of the journey begins with the MTV (Fig. 3). Once the systems in the MHM have been verified as safe and operational, the MTV is cleared to continue the overall mission. The mission continues with the assembly of the MTV in LEO, at an altitude of 300 km (Phase G). The various components of the MTV, including the MEV, are launched

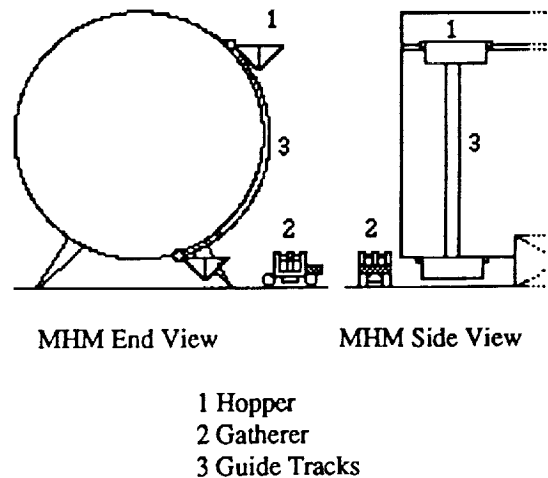


Fig. 2. Robotic regolith system.

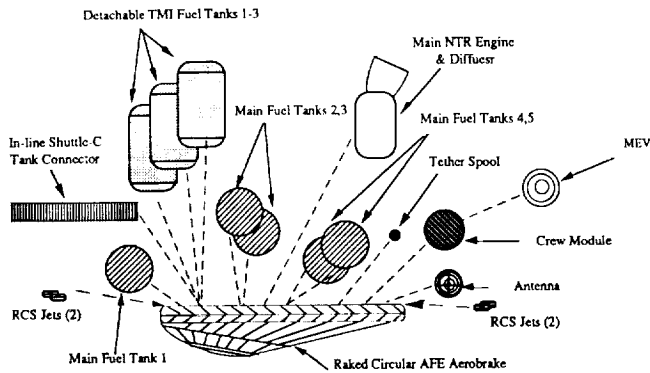


Fig. 3. Mars Transfer Vehicle, by components.

into space and assembled in the vicinity of the space station with the help of the space tug. Once the Earth-Mars transfer window opens (Phase H), during March 2016, final preparations for the mission are made. During this period final connections are made, as well as system checks and verification. The crew for the mission is delivered aboard a shuttle to the space station, and after a ceremonial send-off, the five astronauts are transferred to the MTV. After final systems verification, the MTV is positioned for the TMI burn. The optimum date for this TMI burn is March 21, 2016. This date has been determined with the aid of the SWISTO computer simulator.

The TMI injection burn for the MTV burn is performed using a fluidized particle bed reactor. The reactor must develop a  $\Delta V$  of 3.99 km/s for the MTV's TMI burn. The propulsive burn for the TMI lasts approximately five hours. During this burn the MTV will use all the fuel from three of its eight fuel tanks. The fuel tanks are all identical and have taken advantage of the space shuttle's manufacturing process. This was done by allowing the tanks to have a common size relationship with the space shuttle main fuel tank. The fuel used in the reactor is liquid hydrogen, which is also used by the space shuttle. Following the TMI burn the three empty fuel tanks are jettisoned (Phase I). Within 24 hours, the craft is beyond the Moon and progressing on a 150-day journey to Mars.

Three days after the TMI burn the artificial gravity system is deployed to develop a gravitational acceleration identical to the Earth's gravitational field (Fig. 4). The artificial gravity system is a tether system that spins two masses around a single point using centripetal acceleration to develop the gravitational field. Due to the effects that centripetal acceleration has on humans, some constraints were placed on the tether system. The tether system operates with a rotational speed of two revolutions per minute to promote safety and wellness for the crew, because the revolution rate allows for a relatively slow velocity, which minimizes the effects of variations in centripetal acceleration. When the tether deploys, the MTV separates into two sections, the Mars Excursion Vehicle and the MTV's crew module, and the aeroshell, remaining fuel tanks, and the reactor. With these masses on each end of the tether the lengths needed will be no more than 400 m and no less than 140 m. The values stated above are using a 0.06-m-diameter tether cable made of Kevlar 49.



Fig. 4. MTV deployed tether configuration.

Kevlar 49 is used because it has a very high tensile strength and a low density compared with other materials. The cable's configurations consists of irregularly bundled strands of Kevlar 49, combined to form the cable (Fig. 5). The irregularly bundled cable offers increased flexibility while maintaining the cable's strength. The tether is deployed and retracted using a winch that receives power from the MTV's power generator. The tether connects to the crew module in three places, so as to better distribute the stresses placed on the outer skin. The tether mount is also made out of Kevlar 49. Because of this it is possible for the tether and mounts to be fabricated as one piece of Kevlar.

Four days later, when the artificial gravity system is fully deployed, the crew starts its in-flight work schedule. The five-member crew is composed of the flight commander, a pilot, a flight surgeon, and two specialists. The crew's schedule during transit periods consists of a five-day work week. All crew members have Sunday off. During the rest of the week the crew staffing varies as each crew member has the second day off on a rotational schedule.

Throughout, the transit crew members will perform a variety of tasks ranging from astronomical observation to landing simulations, as well as some of their own research. A number of systems are needed during transit for research and life support (Table 1). These systems include the Environmental Control Life Support System, climate control, and various radiation control systems. The communication and navigation systems are two major systems needed for the crew's mission on the MTV.

The communication system in the MTV is provided by a KA band transmitter and receiver at a frequency of 32 GHz, with 10 Mbps audio/video transmission rate, and 200 kbps rate for engineering data. This communication will take place from either direct transmission signals with Earth or through the Tracking Data Relay Satellites. When the communications are sent through the satellite system, data will be relayed to Earth using an S band at 4 GHz. For direct communication there are three surface antenna stations: White Sands, New Mexico; Madrid, Spain; and Canberra, Australia. Primary communication for the mission is through these three stations. The navigation for the MTV is provided by the Star Tracker. The Star Tracker is an optical system that compares angles from 37 different stars to determine position. A back-up navigation system that uses Doppler shift is also provided for the MTV. Besides this communication and navigation equipment the MTV has a number of other systems that are power driven.

Upon arrival at the martian atmosphere, the MTV is oriented to begin the aerocapture maneuver (Phase L). Using a 45-m AFE-derivative aeroshell, it aerodynamically brakes through the

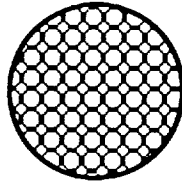


Fig. 5. Irregularly bundled cable.

TABLE 1. Life support power requirements.

| System                       | Power Required, W |
|------------------------------|-------------------|
| Temp. & Humidity Control     | 7900              |
| Atmos. Control, Supply       | 67.2              |
| Atmos. Revitaliation         | 2206              |
| Fire Detection & Suppression | 47.2              |
| Water Recovery & Management  | 804               |
| Waste Management             | 535.5             |

upper layers of the martian atmosphere, bleeding off enough speed to be captured into orbit by the gravitational force of Mars. The aeroshell has a lift-to-drag ratio of 0.30. This value seems quite low, but since the aeroshell only needs to sustain a parking orbit and not reach the surface, a high lift-to-drag ratio is not required. The 0.30 lift-to-drag ratio is necessary because of the entry flight corridor and entrance velocities. The MTV enters the atmosphere at an angle of attack of  $-18.6^\circ$  (Fig. 6). This helps the aerobrake enter the martian atmosphere with  $\Delta V$ s of approximately 5.4 km/s. Once the MTV has entered the martian atmosphere it establishes a circular parking orbit (Phase M). The orbit is at an altitude of 300 km, due to the entry velocity restrictions. With the MTV in orbit around Mars, the crew performs an extensive check on the MTV and the MEV.

**MEV Descent, Ascent, and Surface Operation Profile (Phase N-Q)**

After the verification of all systems, the crew transfers to the MEV (Fig. 7) for descent (Phase N). The MEV uses the same straight biconic shape as the MHM; the only difference is that the MEV is smaller, a 20-m straight biconic vs. the MHM 40-m straight biconic. A biconic shape is required because the MEV needs a relatively high lift-to-drag ratio to reach the MHM base from its specified range and parking orbit. The MEV uses three Pratt and Whitney RL-10 IIC engines in a traditional tripod configuration for retrothrusting in the propulsive descent. The combinations of the MEV's engines and cross-range, provided by its lift-to-drag ratio, will allow the MEV the accuracy to land within 30 km of the MHM base. As the actual touchdown

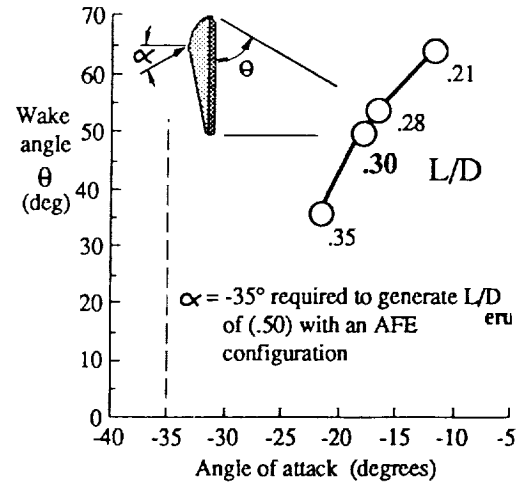


Fig. 6. Wake angle vs. angle of attack.

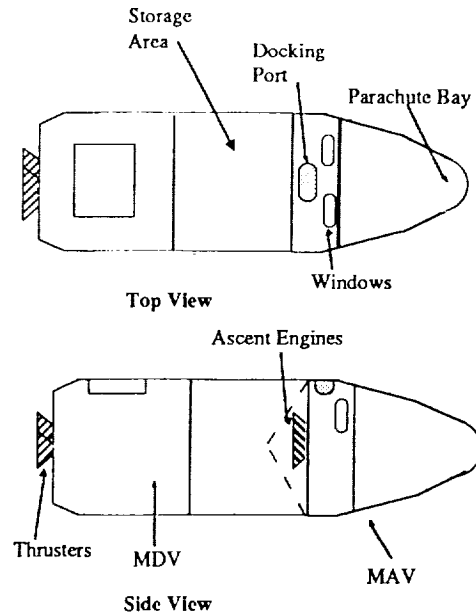


Fig. 7. Component diagram of the Mars excursion vehicle.

approaches, the MEV will extend landing legs and a parachute cluster will provide the MEV a gentle landing on the martian surface.

After the MEV has touched down on the martian surface, the crew perform a complete check on their gear in the MEV and the contained MRV. Once this system check is completed, the astronauts prepare to take their first steps on Mars (Phase O).

Once the astronauts are situated on the surface, they need to rendezvous with the MHM. The crew may need to travel up to 30 km to complete this rendezvous. The crew will travel this distance in the MRV (Fig. 8).

Because the MRV needs to carry the entire crew from the MEV to the MHM, it has a seating capacity for five astronautus in full gear. The MRV is designed to be very versatile while

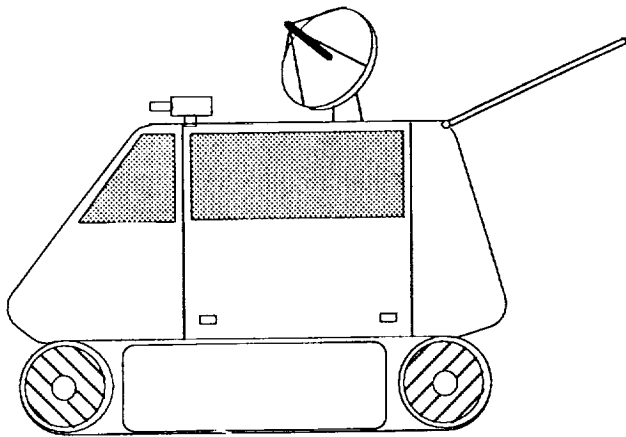


Fig. 8. Mars roving vehicle, side view.

also being very simple. The vehicle travels via a two-track system, which allows the rover to negotiate various terrains easily, while also allowing it to rotate without any forward movement. The power system for the MRV is provided by a conventional-fuel power cell system, which provides 4.5 KW<sub>e</sub>. This system allows the rover to have a power safety factor of 1.5. The power system is rechargeable, which will allow the MRV to be used numerous times throughout the surface stay. Interior power and accessory systems in the rover are powered by simple DC motors. This system provides power for the rover's communication, navigation, and lighting systems. The MRV is fully enclosed to protect the astronauts and sensitive equipment inside the rover.

The MRV is carried inside the MEV, and is driven down a ramp from the MEV to the martian surface. From here the crew boards the MRV and travels to the MHM to complete the surface stay. With the rover's maximum operational speed of 15 km/hr it will take no more than three hours for the rover to rendezvous with the MHM. Once this rendezvous is completed, the actual surface operations begin.

The tasks that the crew will perform while on the surface of Mars are wide ranging and include geological, geochemical, biological, and astronomical experiments and research. One area that the crew will spend a large amount of their surface time researching is *in situ* resource utilization. The primary focus of *in situ* resource utilization is extracting usable materials from the martian surface. On Mars this would be principally hydrogen, oxygen, and H<sub>2</sub>O. The crew on this mission would seek to verify the technology and possibly start an oxygen producing facility. This facility would then be used for follow-on missions.

This experimentation, completed on the surface, continues the mission's goal of not only putting humans on the martian surface, but doing surface experimentation that will set up a base for continuing missions (Figs. 9, 10). At the end of this 30-day stay the crew will again use the MRV to rejoin the MEV. Once the crew reaches the MEV, they will embark and prepare to leave the surface.

The MEV has a built-in section that will transport the crew from the surface back to the MTV, which is in a low Mars parking orbit. This section, the Mars Ascent Vehicle (MAV) is propulsively

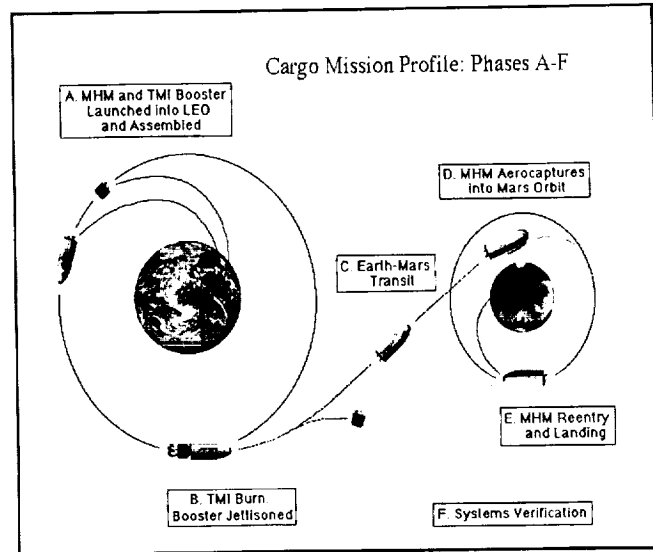


Fig. 9. Cargo mission profile, phases A-F.

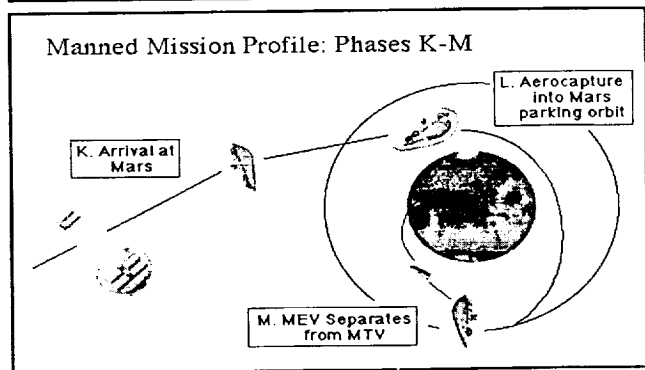
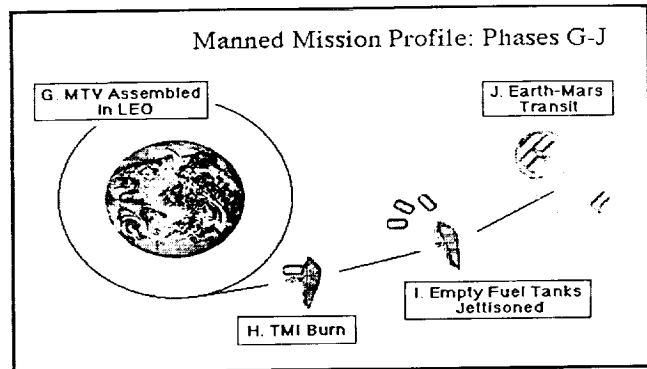


Fig. 10. Manned mission profile, phases G-M.

lifted into an orbit that coincides with the MTV. The MAV's propulsive unit comprises three Pratt and Whitney RL-10 IIC engines in a traditional tripod configuration. These engines will produce enough thrust to propel the MAV into a concurrent

orbit with the MTV (Phase P, Fig. 11). Once the orbit has been established, a docking maneuver is performed by the MAV to complete its rendezvous with the MTV.

**MTV Mars-to-Earth Mission Profile (Phases Q-T)**

Once the docking procedure is completed the crew will transfer back into the crew module of the MTV. The crew then finishes preparations for the trip back to Earth and jettisons the MAV before firing for the TEI (Phase Q). The TEI burn is again done by the fluidized particle bed reactor. The burn stage has a duration of approximately three hours, while developing the needed  $\Delta V$  to escape Mars's gravitational field. This is the beginning of the 240-day trip back to Earth. The artificial gravity system will continue to produce a gravity environment until the MTV approaches Venus approximately 110 days later. As the MTV approaches Venus the tether is retracted for the Venus swing-by, (Phase R, Fig. 12). The Venus swing-by stage of the mission will use the gravity of Venus to help develop a higher  $\Delta V$ , which will enable the crew to return healthier and at an earlier date. During the swing-by stage the crew will perform studies of Venus and observations of the Sun at a vantage point far closer than that of our own planet. Following this pass around Venus, midcourse corrections are made by the nuclear thermal reactor. Once the midcourse corrections have been completed, the tether system is redeployed, once again producing artificial gravity. The Venus-to-Earth transit will last

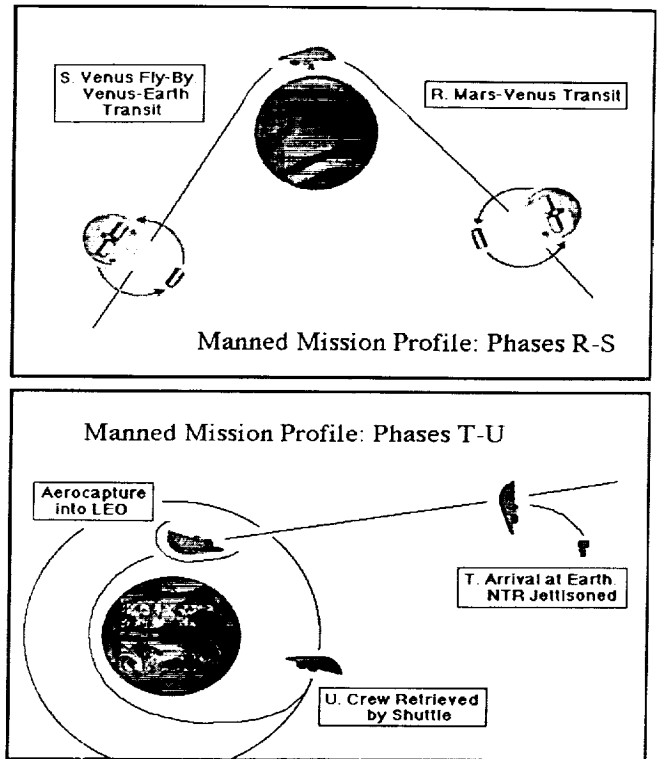


Fig. 12. Manned mission profile, phases S-U.

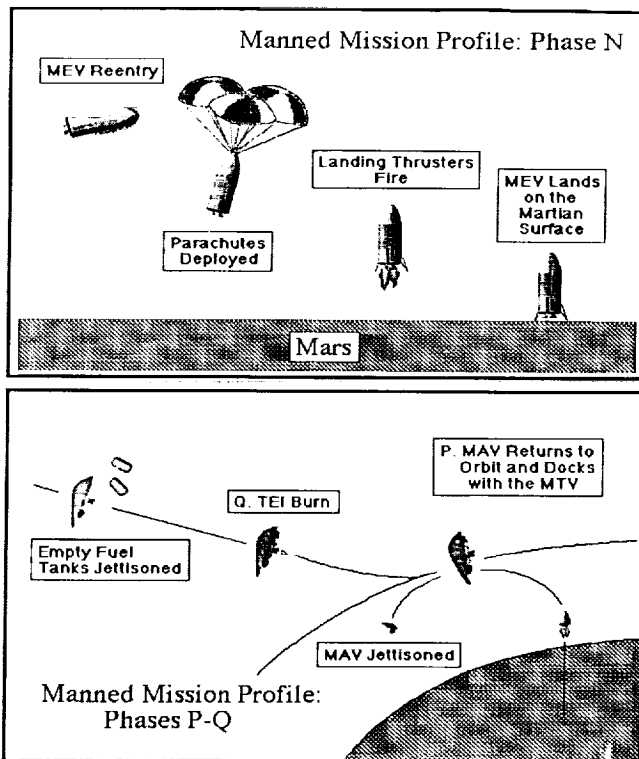


Fig. 11. Manned mission profile, phases N-Q.

approximately 130 days. Near the end of this stage the tether is retracted, in preparation for the entry into Earth's atmosphere (Phase S). The MTV will enter the Earth's atmosphere using the aerobrake in the same manner as it entered the martian atmosphere. After the MTV aerocaptures into Earth orbit, it then establishes the same LEO as used to start the mission. The MTV then rendezvous with the space station, where the astronauts will wait for the space shuttle. The space shuttle will return them to Earth for a hero's welcome, after a quarantine period of two weeks (Phase T). This period is used for testing and evaluation of the astronauts' mental and physical health.

## SINGLE-STAGE MARS MISSION

## UNIVERSITY OF MINNESOTA

S30-12

160606

P. J.

President Bush established a three phase Space Exploration Initiative for the future of space exploration. The first phase is the design and construction of Space Station *Freedom*. The second phase is permanent lunar base. The last phase of the Initiative is the construction of a Mars outpost. The design contained in this report is the concept of a single-stage Mars mission developed by the University of Minnesota Aerospace Design Course. The mission will last approximately 500 days including a 30-60 day stay on Mars.

## ACRONYMS

|       |   |
|-------|---|
| AM    | Ascent Module                                 |
| ECLSS | Environmental Control and Life Support System |
| ERV   | Earth Return Vehicle                          |
| EVA   | Extravehicular Activity                       |
| HLLV  | Heavy Lift Launch Vehicle                     |
| LEO   | Low Earth Orbit                               |
| MIT   | Mars Integrated Transportation System         |
| MOC   | Mars Orbital Capture                          |
| MTV   | Mars Transportation Vehicle                   |
| NTR   | Nuclear Thermal Rocket                        |
| SPE   | Solar Particle Event                          |
| SSF   | Space Station <i>Freedom</i>                  |
| TEI   | Trans-Earth Injection                         |
| TMI   | Trans-Mars Injection                          |

## INTRODUCTION

On July 20, 1990, President Bush established the direction for future U.S. space activities with his words, "... And then a journey into tomorrow, a journey to another planet, a manned mission to Mars." The Mars Integrated Transportation System (MITS) design project consists of the conceptual design of a system that will satisfy the following objectives:

1. Transport an expeditionary crew of trained astronauts from Earth orbit to Mars orbit, then descend to a preselected location on the martian surface. This mission will be planned for around the year 2020.
2. Establish a Mars outpost site and conduct local science and exploration investigations including local resource evaluations. The crew will be provided with a habitation module and surface rover and will stay for approximately 30 days.
3. Return crew, surface samples, and appropriate hardware/information safely back to Earth orbit.
4. Accomplish the above tasks in a cost-effective manner with acceptable levels of safety, and design systems that will provide the infrastructure for continued missions.

This report is the design proposed by a team in the NASA/USRA/University of Minnesota Mars Integrated Transportation System advanced design program.

The assumptions for this design are as follows:

1. Space Station *Freedom* (SSF) is in low Earth orbit (LEO) and is capable of supporting the construction and launch operations of the MITS, as well as the eventual recovery of the spacecraft. In its construction supporting role, SSF is expected to house the construction crew while the actual construction takes place near or at SSF.
2. Extensive robotic exploration of Mars has been conducted prior to the MITS mission. The data gathered would verify the landing site, finalize experiment designs, place communications satellites in Mars orbit, and determine available resources.

## MISSION OBJECTIVES

There are five main objectives for the first manned mission to Mars. All these goals, while having their own individual purpose, share the common purpose of increasing our knowledge of Mars and of how to get there in order to prepare the way for future missions and, eventually a permanently manned base on the planet. The five goals are

1. Verify the technology used for manned missions to Mars.
2. Approve the landing site for use as a permanent martian base.
3. Establish the necessary groundwork to ensure the success of future missions.
4. Test equipment and procedures that will be used to support and operate the permanent base.
5. Begin the detailed scientific research and exploration of the martian atmosphere, surface, and subsurface, as well as examination of the local space around Mars.

## MARS TRANSFER VEHICLE (MTV)

The MTV consists of six main components: the MEV, truss and support structure, propellant, NTR system, ERV, and the habitation area. All six of these subsystems are discussed below. Several considerations were necessary in developing the overall MTV configuration. The necessity of having artificial gravity required locating the habitation area at a distance of approximately 60 m from the center of gravity for the trans-Mars journey (resulting in a force of 1 g), and as far away as possible for

the trans-Earth journey. This need, coupled with the need to keep the truss as short as feasible, led to a need to keep as much of the mass as possible at a distance from the habitation area.

### Truss Design

The design of the truss that forms the nucleus of the MTV will feature a combination of tetrahedral elements. The truss will have a square cross-section of 3-m sides and an overall length of 90 m. The material used for the truss structure is assembled in parts on Earth and launched into orbit in pieces. The truss will be fully assembled near SSF.

### Propellant Tanks

The propellant tank layout can be seen in Fig. 1. The layout consists of eight tanks; four for the TMI maneuver and two each for the MOC and TEI maneuvers. All tanks use the 8.4-m-diameter of the current space shuttle external tank design. This provides some commonality in the design. The lengths of the tanks have been chosen to house the fuel required for each leg of the mission without allowing excess room for "sloshing" of the propellant. This sizing allows for the jettison of the TMI and MOC tanks immediately following their usage, thereby reducing the mass of the vehicle and required propellant.

### Nuclear Thermal Rockets

NTRs will be used for MITS propulsion. While nuclear propulsion has many advantages over chemical propulsion, the radiation given off is a problem. Radiation from the NTRs is a major safety risk in the design of the MTV. Several methods of reducing radiation have been considered.

Distance is one of the most effective radiation shields. Radiation falls off at a rate of the distance to the fourth power. This form of shielding was a driving factor for the design of the MTV.

In addition to distance, propellant is an effective and cost-reducing source of shielding. The problem with using the propellant as shielding was that as the propellant was used, the amount of shielding decreased. By the time the MTV starts

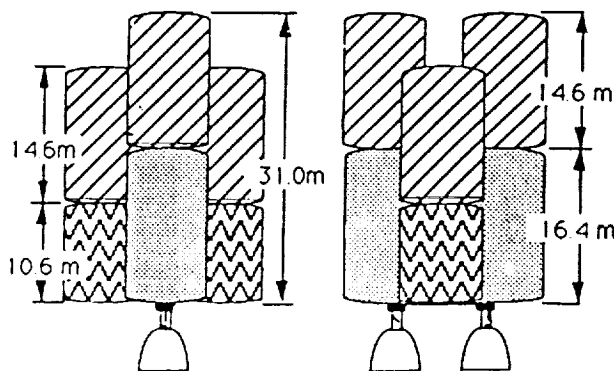


Fig. 1. Propellant tank configuration.

the trans-Earth portion of its journey (the longest phase of the mission), less than 10% of the initial propellant will remain. This is not an adequate shield. However, this concern will be incorporated in the design. The propellant used for the TEI will be placed between the habitation area and the NTRs to provide extra shielding for the first part of the mission.

A fourth method of increasing the radiation protection between the NTRs and the habitation area is the use of a massive shield. The amount of shielding depicted in the drawings is 30,000 kg of lead.

### Earth Return Vehicle (ERV)

The ERV will be the only part of the MTV to return to Earth. Upon arrival at Earth the ERV will consist of the Earth aerobrake, the AM, and the propellant for maneuvering into orbit with Space Station *Freedom*. The ERV will dock at Space Station *Freedom* and transfer the astronauts, soil samples, and data obtained from experiments along the entire mission to the laboratory modules on Space Station *Freedom* and ultimately back to Earth.

### HABITATION MODULE LAYOUT

There will be two cylindrical modules in which the crew will spend the majority of the trip. Both modules will have two floors. With access between the two modules on both floors, Fig. 2 shows the dimensions of the modules. The modules have been designed so that either one could provide living quarters for the crew in the event that one of them was rendered inoperable during a catastrophe.

There will also be two modules that will be brought down to the surface of Mars where the crew will spend approximately 30 days. These modules will be 5 m (16.4 ft) in diameter and 14 m (45.9 ft) in length. There will only be one floor on each of these MEV modules. The size of the MEV modules is smaller than the MTV modules because the crew will be spending less time on the surface of Mars than on the trip through space. Also, the astronauts will have the option to go outside the MEV modules, but they will be confined to the MTV for many months.

### MTV Hab Module

The Hab module of the MTV will contain most of the facilities the crew will use while eating, sleeping, or during recreation and relaxation times. Figure 3 shows the floor plans for the upper and lower floors of the MTV Hab module.

The crew quarters will include a fold-out bed so that space may be conserved and additional storage may be accessed. A desk will be provided as well as a personal computer networked to the ship's computer for personal use. The crew quarters should allow for privacy, so individual quarters are provided.

One personal hygiene center is located on each floor of the MTV. A galley for food preparation is located on the upper floor. It will contain storage for dishes, silverware, and pots and pans. The pantry, refrigerator, and freezer will store 3900 kg of food. Appliances will include an oven, a microwave, a mixer, and a hydrator.

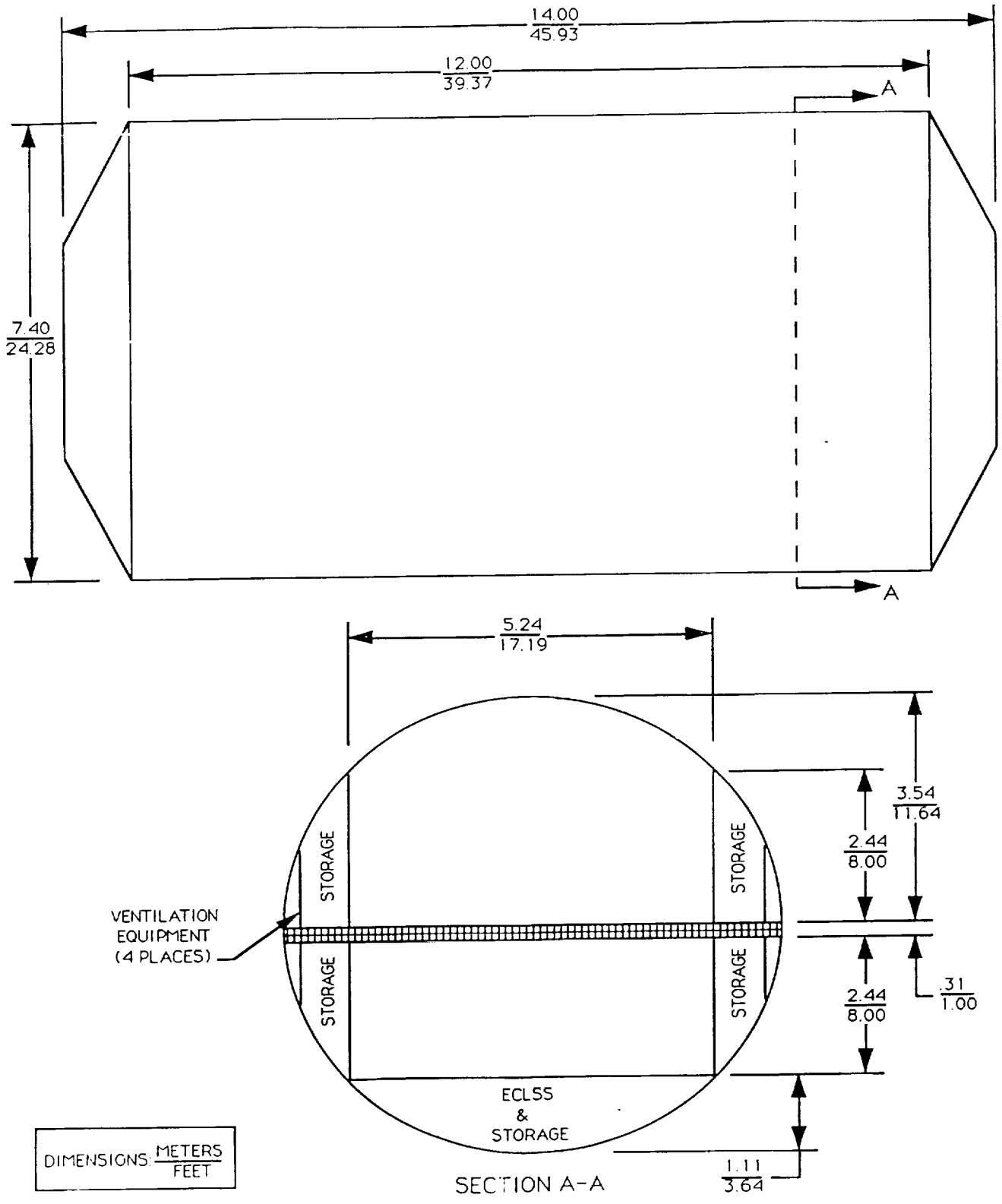


Fig. 2. MTV Module dimensions.

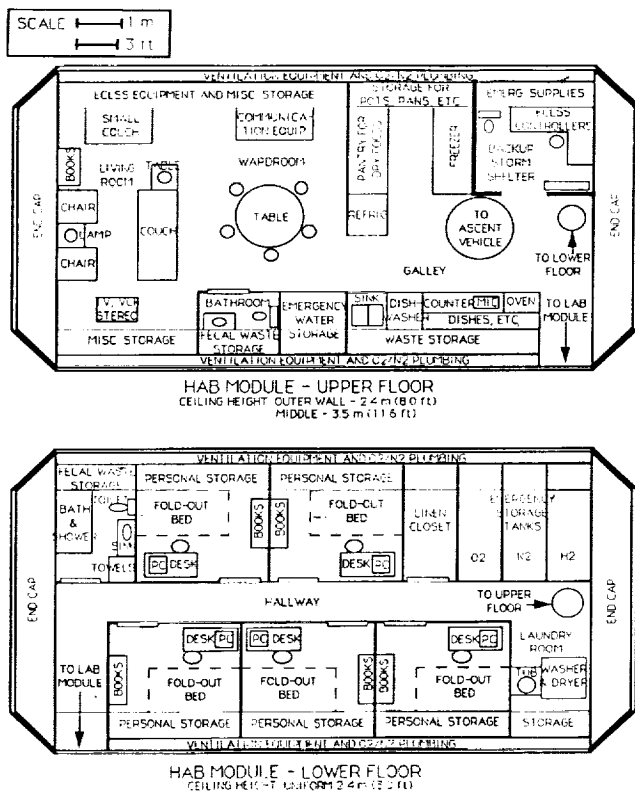


Fig. 3. MTV hab module floor plans.

A wardroom will consist of a dining area with table and five chairs, and video equipment for communication with Earth. The Hab module will also include a living room that the crew can use during recreation and relaxation. A backup radiation shelter will be included in the module that will double as the ECLSS control room. Also located in the Hab module will be emergency storage tanks for oxygen, nitrogen, hydrogen, and water.

#### MTV Lab Module

The Lab module contains most of the facilities involving work-related activities. Included will be the command/control center, the nerve center of the ship, which will provide access to all ECLSS systems, as well as to computers and communications equipment.

The lab maintenance facility will include the tools necessary to perform the required research and analysis of data acquired during the mission. Astronomy, biology, chemistry, physics, and geology are only a few of the kinds of research that can be performed. Additionally in this area, there will be a general shop with the tools necessary for the construction and repair of the ship's system.

A medical facility capable of surgical procedures will be needed. A general examination table, as well as the necessary tools and instruments will be accessible on racks in this area. Dental procedures will also be performed in this facility.

A physical fitness center will include variable resistance machines as well as aerobic machines. The medical facility will

have access to the physical fitness center so that the crew can be monitored during exercise.

A radiation shelter will be designed according to recommendations given in this report. It must be self-sufficient since the duration of a SPE may last from several hours to a day. Therefore, personal hygiene facilities, ship monitoring equipment, and food preparation and storage will be included in the storm shelter. A computer will allow access to the main computer for monitoring of the ship's functions during an SPE. Recreation may be had by means of books and games, which will be stored in the shelter.

The NTRs had to be kept as far away from the habitation area as possible to reduce radiation exposure of the crew. The propellant will serve as shielding from the NTRs. The loading of the vehicle must be as symmetric as possible to reduce the structural loads in the truss. If possible, all habitation areas (including those on the MEV and AM) should be located in the same area. This allows for alternate living areas in case of an emergency, and eliminates or reduces EVAs. The antenna system must be located near the center of gravity for uninterrupted communication with Earth. This resulted in a need to keep the center of gravity in a fixed location, or as close to the same location as possible for the trans-Mars and trans-Earth portions of operation.

Based on these requirements the MTV has been developed as shown in Figs. 4-6. Figures 4-6 also indicate the names of the major components of the MTV. The overall length of the vehicle is approximately 97 m. The design has a width of approximately 20 m across the propellant tanks, again needing support structure finalization, and 30 m across at the MEV.

#### The Mars Excursion Vehicle (MEV)

The MEV will be used to transfer the crew from the MTV to the martian surface. The design, as shown in Figs. 7-10, includes an AM having 19,000 kg of descent propellant dispersed into six spherical tanks, two habitation modules having a diameter of 5 m and a length of 11 m, and a martian rover. The total height of the vehicle is 11 m.

The inner space of the AM will consist of one chair for each astronaut and space for items that will be brought back to Earth (i.e., soil and data). The AM will be used only to transport the astronauts from Mars back to the MTV, and then from the MTV into LEO and ultimately Space Station *Freedom*. Other features of the MEV include multiple airlocks, a support platform and a tunnel system connecting the habitation module. The airlocks are located on each of the habitation modules and connect to a tunnel system extending between both the AM and the habitation modules. A passageway out of the tunnel leads to the rover, which is located between the habitation modules. A platform supports the entire descent vehicle.

#### MISSION PROFILE

There are many distinct stages to the MITS mission, and the vehicle changes drastically as the mission progresses from launching the vehicle components into LEO to docking with SSF upon return from Mars. Figure 11 depicts a sketch of the mission profile.

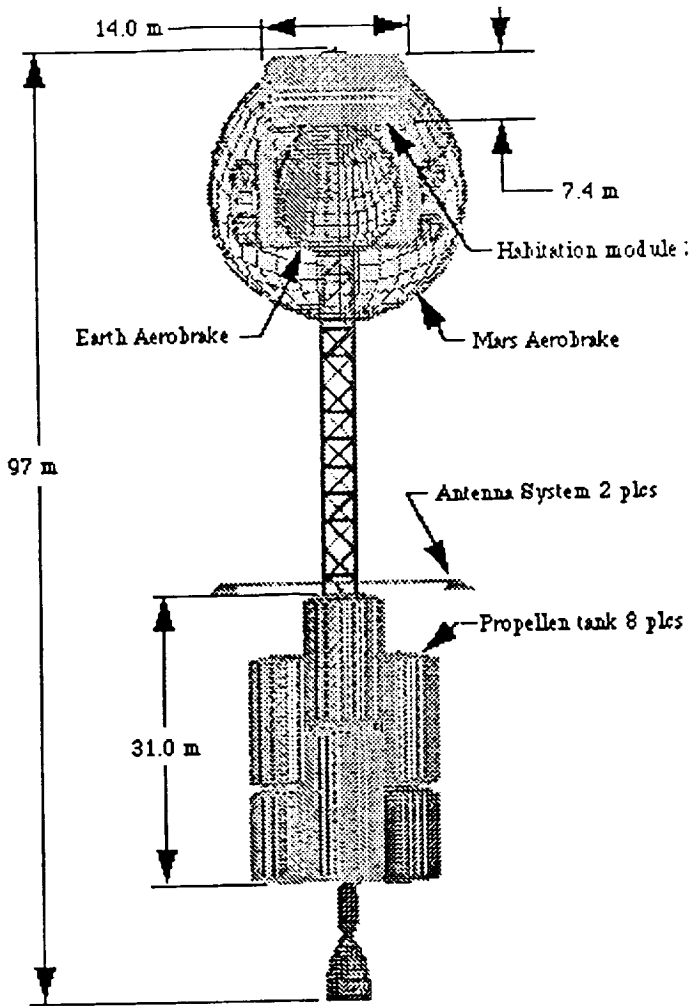


Fig. 4. MTV configuration front.

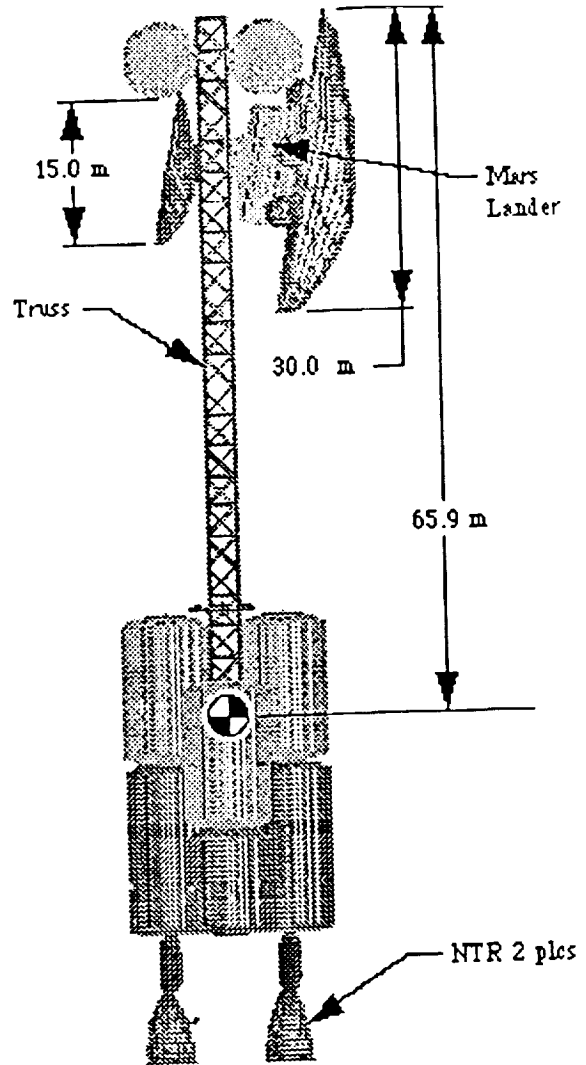


Fig. 5. MTV configuration—Side.

**I. Launch of Vehicle Components into LEO**

In this phase of the mission, the individual parts of the MITS are launched into LEO by an HLLV. The components are taken to construction facilities near SSF.

**II. Assembly of Vehicle near SSF**

This phase of the mission consists of the on-orbit assembly of the MITS at the appropriate facilities near SSF. At the end of this phase, the MITS crew is transferred from SSF to the Mars vehicle. The vehicle performs a maneuver to distance itself from SSF, then proceeds to phase III.

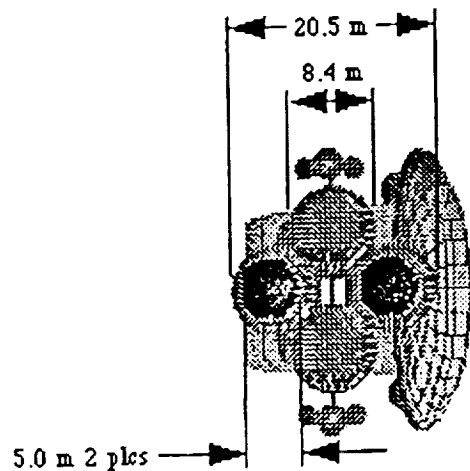


Fig. 6. MTV configuration—Bottom.

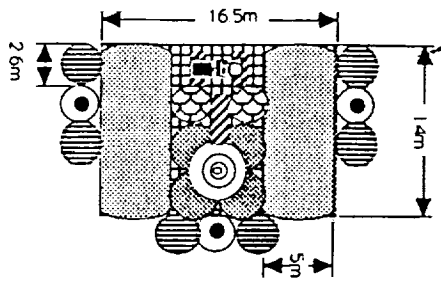


Fig. 7. MEV configuration—Top.

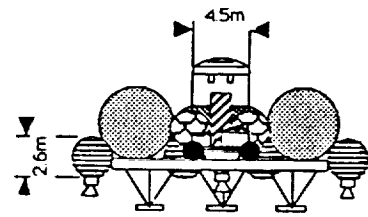


Fig. 9. MEV configuration—Back.

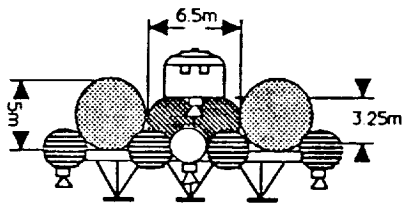


Fig. 8. MEV configuration—Front.

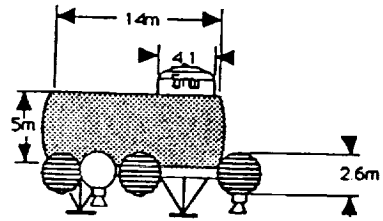


Fig. 10. MEV configuration—Side.

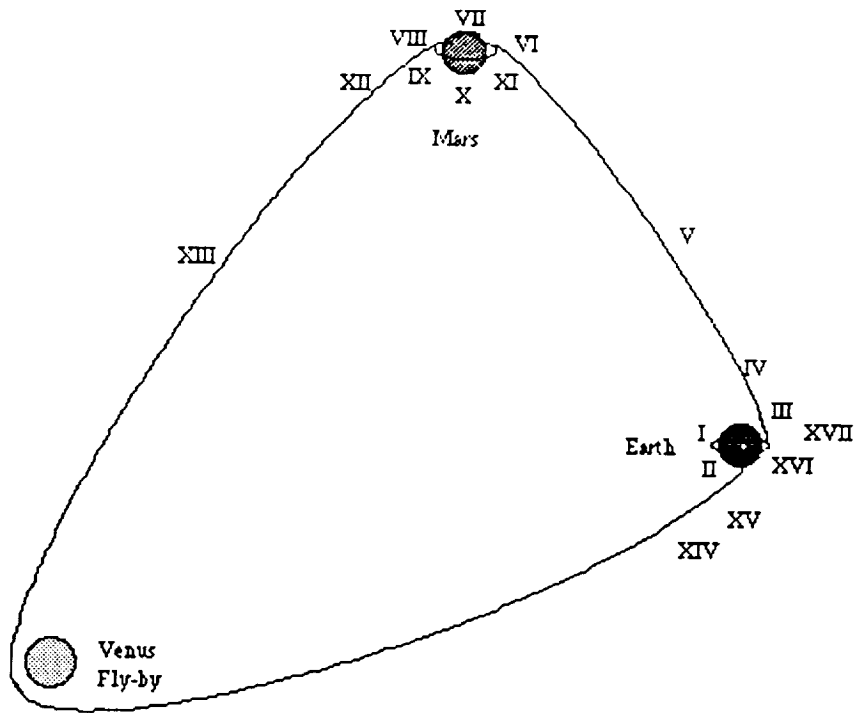


Fig. 11. Mission profile.

### III. Trans-Mars Injection Burn

At this point, the NTR engines of the MITS perform the necessary burn to take the vehicle out of Earth orbit and into a Mars-bound trajectory. After the burn, the engines idle to supply power to the vehicle for the rest of the trip.

### IV. Expend Used Fuel Tanks

After the trans-Mars injection burn, which will require an enormous amount of fuel, the empty tanks are expended.

### V. Earth-Mars Transit Phase

This is the second longest phase of the journey, lasting approximately 170 days. For most of this period, the MITS will be rotating, creating artificial gravity for the crew. However, this rotation will be stopped at least once, and possibly twice for periods of around one week. During these times, experiments and observations will be performed that require a zero-g, or nonrotating environment. Also during these times, course corrections are made if necessary.

### VI. Propulsive Capture at Mars

This phase of the mission involves the MITS entering Mars orbit by propulsive capture. The NTR engines will slow the entire vehicle into an equatorial or near-equatorial orbit. At this point, a number of scientific studies will take place including martian surface observations and studies of the martian moons Phobos and Deimos. The crew will make final preparations, testing the various systems and equipment on the MEV before embarking on the surface.

### VII. Separation of MEV from MTV

At this point, the crew boards the MEV and separates it from the MTV. All five crew members will be on the ground crew, leaving the MTV to orbit Mars unmanned.

### VIII. Landing of MEV

During this phase, the MEV enters the martian atmosphere and lands in the Tharsis volcanic region of Mars (see next section for more details on Tharsis). During the descent, the entire crew is in the AM, which also serves as a control center for the MEV. The crew remains on the surface for 30-60 days, conducting local science and exploration.

### IX. Ascent Module Launches Crew into Orbit

After the surface phase of the mission, the crew boards the ascent module and fires the ascent engines. The Mars habitation module, landing equipment and engines, rover, and other equipment are left behind for possible future use. The AM carries the crew into orbit.

### X. Ascent Module Docks with MTV

At this point, the AM performs the required maneuvers to rendezvous with the MTV, and docks with the Earth return aerobrake. The crew is transferred to the MTV habitation modules.

### XI. Jettison of Mars Capture Fuel Tanks

Before leaving Mars orbit, the fuel tanks that were emptied during Mars capture will be expended.

### XII. Trans-Earth Injection Burn

In this phase, the NTR engines fire, causing the MTV to leave Mars orbit and enter a trajectory that will ultimately carry it back to Earth, with a Venus swingby.

### XIII. Mars-Earth Transit

This is the longest phase of the mission, lasting approximately 270 days. As in the Earth-Mars transit phase, most of this time will be spent in artificial gravity, with some interruptions for experimentation and course corrections. When the MITS performs a Venus swingby, observations will be made, with possible probes sent to make more detailed studies.

### XIV. Separation of ERV from MTV

Before the MITS reaches Earth, the crew separates the ERV from the MTV. The ERV consists of the Earth return aerobrake and the AM.

### XV. MTV is Expended

This phase involves letting the MTV continue past Earth, as the ERV is captured. The rest of the MTV is discarded.

### XVI. ERV Aerobrakes into LEO

After separating from the MTV, the ERV performs an aerobraking maneuver to enter LEO.

### XVII. ERV Docks with SSF

Finally, the crew, data, and samples are transferred from the ERV to Space Station *Freedom* for return to the surface of Earth.

## LANDING SITE—THARSIS RIDGE

Although smaller than Earth, Mars is still a large planet with many interesting features. Picking a landing site was a difficult task. The criteria used to determine the best landing site were low altitude, low wind speeds, equatorial location (to assist in AM launch), moderate temperatures, smooth terrain for landing, and interesting geological and other scientific prospects.

The site that best fits the criteria is the Tharsis region, with Eden as an alternate site. Tharsis is located at 8°S, 84°W at an altitude of 10 km above zero reference. Wind speeds vary

from 14-40 m/s and temperatures range from 170 to 250 K. The terrain is mostly flat with a few craters. Several major volcanoes exist in the area. The soil consists of dune sand, loess, lag gravel, and young volcanic lava.

## CREW ACTIVITIES

### In Transit

The duration of the first mission to Mars will be roughly 488 days. Since over 90% of this time will be spent in transit, it is necessary to have a schedule for the crew to follow to use this time to its full potential. Each day has been divided into five periods. They are as follows:

- 8 hours of sleep
- 3 hours for meals
- 2 hours of personal/leisure time
- 8 hours of work
- 2 hours for exercise

The proposed activities for leisure are reading books and journals, watching movies, listening to music, exercising, receiving current news transmissions from Earth, and audio and/or video communication with family.

The hours of work have been divided into two groups: scientific activities and mission duties. Some of the scientific activities being considered include observations through a moderate-sized telescope, studies of X-ray and gamma-ray radiation, radio astronomy, cosmic-ray astronomy, and the collection of interplanetary dust particles. The mission duties include monitoring the computer control system for any possible

problems, monitoring the path of the MTV for any necessary course corrections, keeping a log of all activities onboard, maintaining audio contact with Earth on progress/problems, and preparations for landing on Mars.

### On Surface

During their surface stay, the astronauts will perform geologic sampling and surface drilling, petrology, geochemistry, and physical properties experiments. They will also spend time on rover missions deploying Surface Science Telemetry Stations (SSTS), which will transmit data on wind speed and direction, radiation seismic activity, and atmospheric composition for years to come.

In preparation for a future permanent base on Mars, several experiments will be performed on *in situ* resource utilization, though *in situ* resources will not be counted on to sustain the first manned mission. Since water and oxygen are the most important resources that may be obtained from Mars, these will be studied first.

## CONCLUSION

This proposed design for a Mars Integrated Transportation System meets all the objectives necessary to satisfy President Bush's long-range plans for the future of NASA as it reaches out for Mars.

This report is respectfully submitted with the hope that it will provide a meaningful contribution in the effort to place humans on Mars.

**MULTIPURPOSE SATELLITE BUS (MPS)**

**NAVAL POSTGRADUATE SCHOOL**

531-18  
160607  
P 10

The Naval Postgraduate School Advanced Design Project sponsored by the Universities Space Research Association Advanced Design Program is a multipurpose satellite bus (MPS). The design was initiated from a Statement of Work (SOW) developed by the Defense Advanced Research Projects Agency (DARPA). The SOW called for a "proposal to design a small, low-cost, lightweight, general purpose spacecraft bus capable of accommodating any of a variety of mission payloads. Typical payloads envisioned include those associated with meteorological, communication, surveillance and tracking, target location, and navigation mission areas." The design project investigates two dissimilar missions, a meteorological payload and a communications payload, mated with a single spacecraft bus with minimal modifications. The MPS is designed for launch aboard the Pegasus Air Launched Vehicle (ALV) or the Taurus Standard Small Launch Vehicle (SSLV).

**MISSION PAYLOADS**

Two payloads were furnished from the MPS bus design, each with distinct mission requirements. The first payload is the Advanced Very High Resolution Radiometer (AVHRR). The AVHRR is an operational radiometer that scans the Earth's surface 24 hours each day in the spectral regions from 0.7 to 12  $\mu\text{m}$ . The AVHRR can provide land, water, and cloud imaging; sea surface temperature; and ice concentration and coverage in either high- or low-resolution modes.

The AVHRR will be launched by the Pegasus Air Launched Vehicle (ALV) into a 833-km (450 n.m.), 0830 descending or 1530 ascending Sun-synchronous orbit at a 98.75° inclination. Orbit period is 101 min with worst case 37-min eclipse occurring during the summer. Average eclipse time is on the order of 33 min. The AVHRR is mounted on the Earth face so that the bus is nadir pointing. Solar array damage due to radiation and orbit altitude degradation are negligible at 833 km (450 n.m.). Figure 1 shows the AVHRR payload configuration.

The second payload considered in the design is the Extremely High Frequency (EHF) communication payload. The EHF payload will supplement existing communications of the operational forces in time of crisis. Communication is done at 2400 bps by means of 32 channels using frequency hopping over 255 frequencies. The signal bandwidth of a single channel is 245 kHz. Total bandwidth required is 2 GHz. The payload was designed to be quickly mated with the MPS bus. The antenna/feed horn arrangement was designed and provided by Lincoln Laboratory.

The EHF communication payload is to be launched by the Taurus Standard Small Launch Vehicle (SSLV) into a 6-8-, or 12-hr Molniya-type orbit. For this design, an 8-hr Molniya-type orbit was chosen with a 500-km (270 n.m.) perigee and a 27,000-km (14,578 n.m.) apogee. Worst-case eclipse for this orbit is 52 min. The EHF payload consists of a 0.81 m  $\times$  0.71 m  $\times$  0.15 m (32 in  $\times$  28 in  $\times$  6 in) structural box that supports the EHF antenna structure and houses the EHF receiver/transmitter and the telemetry, tracking, and command (TT&C) equipment. The EHF and TT&C antennas and the Earth sensor are located on the Earth face of this box, which is affixed to the Earth face of the MPS bus. Optical solar reflectors are mounted on the north face of the structural box and provide radiation of heat of the traveling wave tube amplifiers (TWTA). Figure 2 shows the EHF payload.

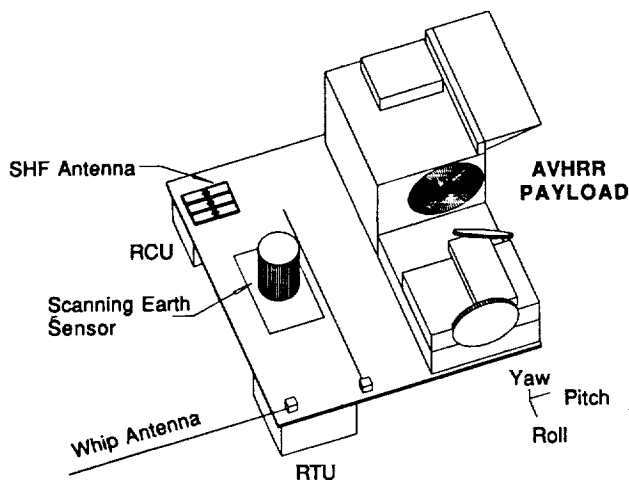


Fig. 1. Earth face with AVHRR payload.

**SPACECRAFT BUS CONFIGURATION**

The two payloads mentioned were suggested by the Defense Advanced Research Projects Agency (DARPA) as typical payloads for this spacecraft. DARPA also expressed in the Statement of Work (SOW) that the spacecraft be compatible with both the Pegasus Air Launched Vehicle (ALV) built by Orbital Sciences Corporation and Hercules Aerospace Company and the Taurus Standard Small Launch Vehicle (SSLV) also built by Orbital Sciences Corporation. The SOW requires that the spacecraft have a design life of three years.

A preliminary design of this MPS bus was performed employing as much modularity as possible. The MPS is a three-axis stabilized satellite with silicon solar-cell panels and nickel-hydrogen (NiH<sub>2</sub>) batteries for power, and hydrazine propulsion. Thermal

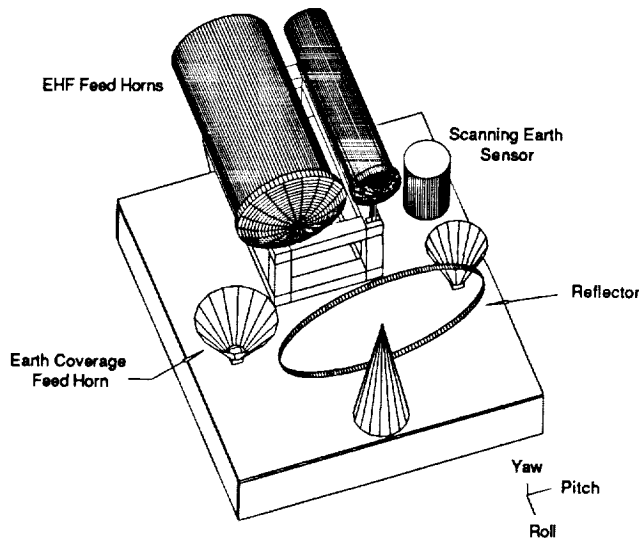


Fig. 2. EHF payload.

control is passive, using optical solar reflector (OSR) material, conductive paths, insulation, paints, and coatings. Detailed analysis was done in the areas of orbit analysis, electrical power, attitude control, thermal analysis, propulsion, telemetry, tracking and control, and structure design.

The MPS bus is designed to allow attachment of various payloads to the Earth face. Modular subsystem components allow the addition or enhancement of MPS performance. The attitude control subsystem, for example, has a precision sensor subsystem (PSS) to augment the basic sensor subsystem (BSS) allowing greater pointing accuracy from  $0.5^\circ$  to  $0.01^\circ$  depending on the mission requirements. The bus as shown in Fig. 3, is a 122.5-kg (270 lb) rectangular box with all the subsystems necessary to fly a variety of orbits and missions.

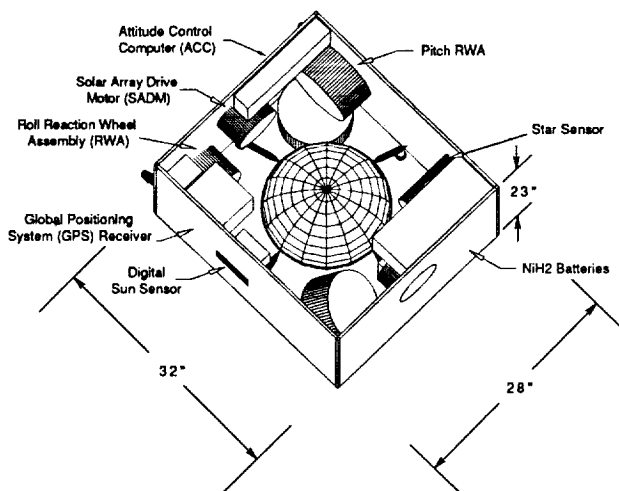


Fig. 3. Multipurpose satellite bus configuration.

**Pegasus Air Launched Vehicle (ALV)**

The Pegasus ALV is a three-stage, solid-propellant, winged rocket designed for the insertion of small payloads into orbit. The 15.2-m (50 ft) long, 1.278-m (50 in) diameter booster weighs 19,052 kg (42,000 lb) and is carried aloft by a conventional transport/bomber-class aircraft (B-52, B-747, L1011). The payload capability for the ALV is shown in Fig. 4.

**Taurus Standard Small Launch Vehicle (SSLV)**

Taurus is a four-stage, inertially-guided, three-axis stabilized, solid-propellant launch vehicle. The design incorporates a Pegasus first, second, and third stage on a Peacekeeper booster. Taurus is fully transportable with rapid launch site establishment. Initial performance estimates are described in Table 1.

The Taurus SSLV will be required to launch the EHF payload into its 8-hr Molniya orbit because of the additional lift not available from the ALV. The 1.27-m (50 in) diameter  $\times$  2.28-m (90 in) long dynamic envelope of the shroud allows for the addition of a third solar array panel per side if needed [the 1.17-m (46 in) diameter Pegasus shroud allowing only two panels per side]. Two solar arrays are sufficient for the two payloads under this study.

**ORBIT ANALYSIS**

Table 2 contains orbit parameters of the two payloads. Argument of perigee is undefined for the AVHRR orbit since it is circular. A highly inclined orbit results from the required global coverage and low altitude. Careful selection of the inclination produces a Sun-synchronous orbit. Finally, spacecraft currently performing missions similar to the AVHRR mission locate their ascending nodes within a couple of hours of the Earth's terminator (the line that separates the sunlit side from the dark side). This design also finds ascending node within two and a half hours of the terminator.

Parameters of the EHF payload orbit are also summarized in Table 2. The EHF communication mission requires a Molniya-type orbit. An 8-h Molniya-type orbit was selected. The EHF communication mission addresses the deficiency of geosynchronous communication satellites to provide high-latitude

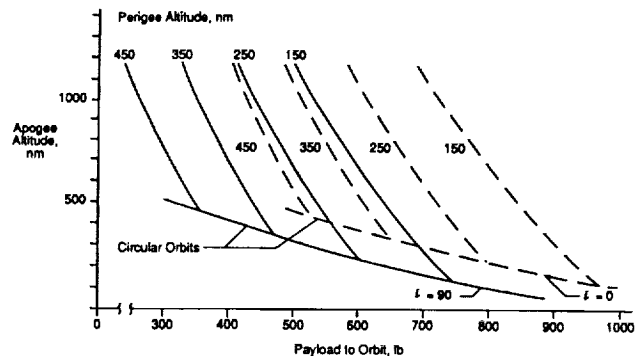


Fig. 4. Pegasus ALV launch capability<sup>(3)</sup>.

TABLE 1. Molniya-type orbits for SSLV ballasted vehicle.

| Perigee           | Apogee                 | Period | Payload         | Enhanced        |
|-------------------|------------------------|--------|-----------------|-----------------|
| 500 km (270 n.m.) | 39,632 km (21400 n.m.) | 12 hrs | 88 kg (194 lb)  | 208 kg (458 lb) |
| 500 km (270 n.m.) | 27,360 km (14773 n.m.) | 8 hrs  | 123 kg (277 lb) | 260 kg (573 lb) |
| 500 km (270 n.m.) | 20,270 km (10945 n.m.) | 6 hrs  | 164 kg (362 lb) | 315 kg (694 lb) |
| 500 km (270 n.m.) | 12,330 km (6658 n.m.)  | 4 hrs  | 246 kg (542 lb) | 432 kg (953 lb) |

TABLE 2. Summary of orbital parameters.

| Payload             | AVHRR               | EHF Communications      |
|---------------------|---------------------|-------------------------|
| Orbit Type          | Sun-synchronous     | Molniya                 |
| Period              | 101.5 min           | 8 hr                    |
| Semi-major Axis     | 7212 km (3894 n.m.) | 20,307 km (10,965 n.m.) |
| Eccentricity        | 0.0                 | 0.661                   |
| Inclination         | 98.75°              | 63.43°                  |
| Ascending Node      | 3:30 PM/8:30 PM     | N/A                     |
| Argument of Perigee | N/A                 | 270°                    |

coverage. A highly inclined, very eccentric orbit was studied with perigee located at the southernmost point in the orbit. The high eccentricity yields a longer loiter time over the northern hemisphere (nearly 90%). The choice of inclination was based on the critical inclination to remove rotation of the line of apsides. This minimizes the effects of perturbations on the orbital elements making the orbit easier to maintain. Although perigee is at 270°, it can be located at 90° if the extreme southern latitudes are of interest. Northern hemisphere coverage is assumed for this design.

Orbit selection for both missions was designed to eliminate orbit maintenance requirements. The Defense Meteorological Satellite Program (DMSP) uses the same orbit as the AVHRR mission. SMSP has several payloads, one of which is very similar to the AVHRR. DMSP performs no orbit maintenance during its lifetime.

The EHF payload orbit was analyzed for zonal harmonics  $J_2$  through  $J_7$ , resulting in a 500-yr period for rotation of the perigee. Perigee will move less than 2.5° for the satellite's mission life. The changes in inclination and eccentricity over the satellite's lifetime are also very small.

#### AVHRR Payload Mission

The AVHRR mission is Sun-synchronous, with the longitude of the ascending node move along the Earth's equator rather than remaining fixed in inertial space. The longitude of the ascending node travels once around the equator in one year. If the plane of the equator and the plane of the ecliptic were coplanar, then the Sun would remain in the same relative location with respect to the orbit. Since they are not coplanar, the location of the Sun depends on the season. The AVHRR orbit analysis was directed at determining Sun angles on the satellite, Sun angles on the solar arrays, and eclipse periods.

The primary motivation for this analysis is to ensure that the placement of the AVHRR payload on the spacecraft will prevent sunlight from shining in the sensor field of view and to prevent illumination of the thermal radiator. The basic approach is to define vectors normal to each of the satellite's faces. These vectors are the roll, pitch, and yaw axes and their negatives. Another vector is defined to point from the satellite directly at the Sun. The angle of incidence of sunlight striking a satellite face is the angle between the Sun vector and the vector normal to the satellite face. This angle shall be referred to as the Sun angle of a particular face. If the Sun angle is 0°, then the Sun is shining directly on the satellite face. If the Sun angle is greater than 90°, then the satellite face is oriented away from the Sun and has no incident sunlight.

The orbit is assumed fixed in inertial space for the period of one orbit. The angle between the Sun vector and the orbit normal vector is then a constant. The Sun angle on the satellite's pitch face and negative pitch face also remains constant for that orbit since the satellite's pitch axis is parallel to the orbit normal vector. The Sun angles on the remaining four faces vary as shown in Fig. 5 for the first day of winter. All four faces experience the same Sun angle profile, but shifted in time. The orbit's ascending node is at 8:30 p.m.

The plots for the other seasons are similar in general shape but contain a phase shift and a change in amplitude. Figure 6 examines the Sun angle profile on the +roll face for the first day of all four seasons.

A second study involves the solar array Sun angle over the orbit and the required rotation angle to minimize the solar array Sun angle. Rotation of the solar arrays only provides two locations in each orbit where the resulting solar array Sun angle is zero. Figure 7 shows the seasonal solar array rotation angles. Figure 8 illustrates the worst-case solar array Sun angles over a year. Rotation angle profiles will be required either by onboard

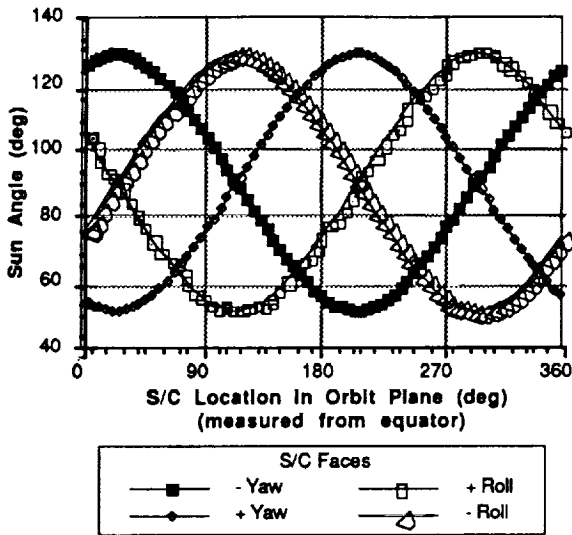


Fig. 5. First day of winter Sun angles on spacecraft faces vs. orbital position (8:30 p.m. ascending node).

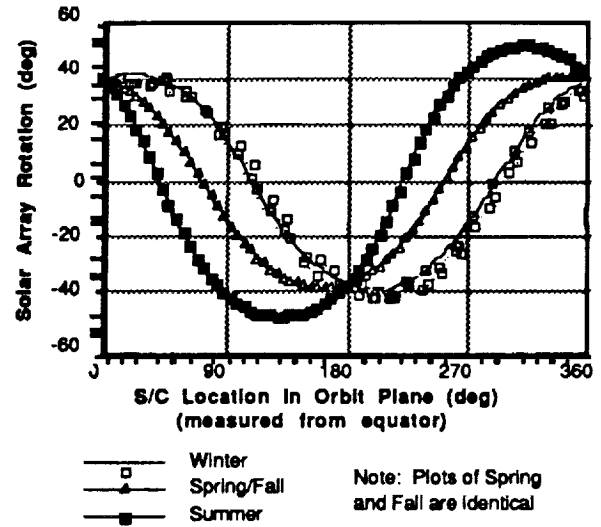


Fig. 7. Solar array rotation angle vs. orbital position and season.

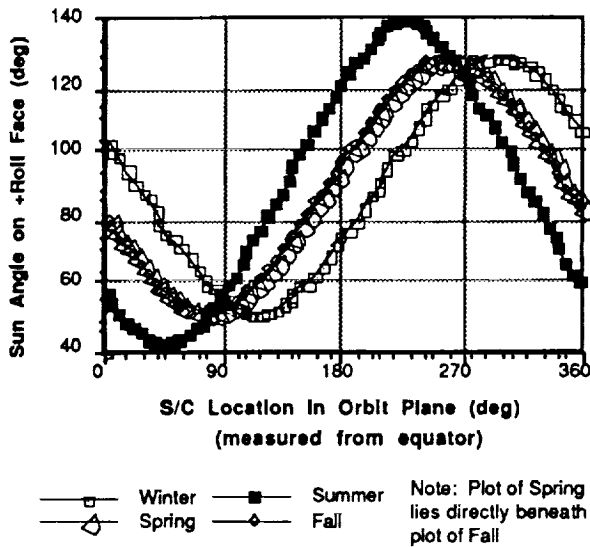


Fig. 6. Sun angle on +roll face vs. orbital position first day of winter (8:30 p.m. ascending node).

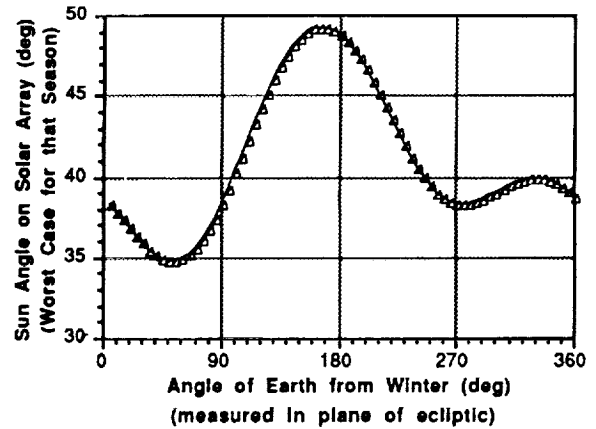


Fig. 8. Worst-case Sun angles vs. time of year.

processing with a Sun sensor or by updated control sequences from the ground.

Eclipse information for the AVHRR mission orbit is required for sizing of the batteries and solar arrays. Eclipse duration for the time of year is shown in Fig. 9.

**EHF Payload Mission**

The analysis of the EHF payload mission does not require the same level of analysis as the AVHRR orbit. The EHF spacecraft is free to rotate about its yaw axis. The satellite is then free

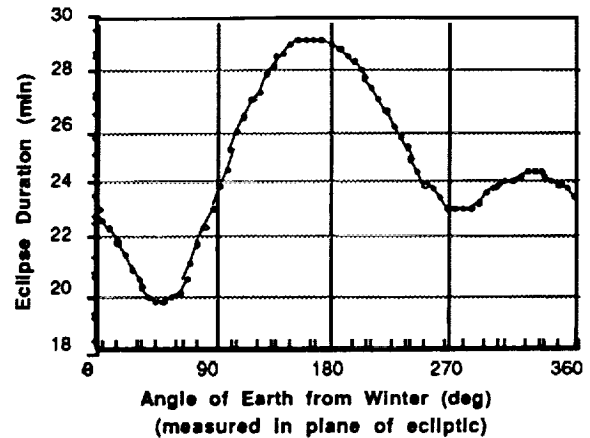


Fig. 9. Eclipse duration vs. time of year.

TABLE 3. Eclipse duration for EHF payload mission.

|                                     |         |
|-------------------------------------|---------|
| True Anomaly at Eclipse Entry (deg) | 70.587  |
| True Anomaly at Eclipse Exit (deg)  | 131.715 |
| Eclipse Duration (min)              | 52.079  |

to position its solar arrays with zero angle of incidence everywhere in the orbit. The required angle of rotation about the yaw axis, however, has not been examined.

The worst-case eclipse in terms of duration is when the portion of the orbit in eclipse passes directly through the center of the Earth's shadow cylinder. This condition is a function of the longitude of the ascending node. In addition, worst-case eclipse will occur when the portion of the orbit in eclipse is as close to apogee as the geometry will allow. An inclination of 63.43° and an argument of perigee of 270° prevent the apogee from ever entering eclipse. With perigee at the southernmost point in the orbit, the worst-case scenario is created on the first day of winter. The center of the eclipse occurs 113.5° past perigee. Table 3 presents the worst-case eclipse duration.

**ELECTRICAL POWER SUBSYSTEM**

The electrical power subsystem (EPS) consists of solar panels of silicon photovoltaic cells and NiH<sub>2</sub> batteries. Power control electronics will maintain bus voltage at 28 V. The bus will be fully regulated by employing a shunt regulator for periods of solar array operations and will use a boost regulator during periods of battery operations. Table 4 summarizes the power requirements for both the AVHRR and EHF payload missions.

**Solar Array Design**

The MPS bus is designed to have two symmetric solar arrays. The AVHRR and EHF configurations require two solar arrays of two panels each. An additional panel may be added to each side if some future payload requires it; however, only the Taurus SSLV can accommodate the increased volume. Silicon cells were chosen for cost and reliability. The cells selected were the same as those used in INTELSAT VI.

The solar arrays on the EHF payload will be Sun tracking to maintain panel orientation perpendicular to the Sun's rays. This is accomplished through freedom of movement about the longitudinal axis of the arrays and through satellite rotation about the yaw axis. The AVHRR solar panels will, as nearly as possible, be oriented perpendicular to the Sun's rays. The AVHRR operational requirements do not allow for the rotation of the

TABLE 4. System power summaries (normal operations).

| Element             | AVHRR (W) | EHF (W) |
|---------------------|-----------|---------|
| MPS Bus Subtotal    | 166.4     | 114.8   |
| Mission Instruments | 28.0      | 115.0   |
| MMS Harness Loss    | 4.0       | 4.0     |
| System Reserve      | 4.0       | 4.0     |
| Satellite Total     | 201.8     | 237.8   |
| With cosine effect  | 313.9     | N/A     |

TABLE 5. Solar cell characteristics.

| Characteristics            | K7 Silicon cell                                  |              |              |  |
|----------------------------|--|--------------|--------------|--|
| Power BOL (28°C) (mW)      | 307.8  |              |              |  |
| Power EOL (28°C) (mW)      | 230.8  |              |              |  |
| BOL                        |  |              |              |  |
| $I_{mp}$ (A)               | $V_{mp}$ (V)                                     | $I_{sc}$ (A) | $V_{oc}$ (V) |  |
| 0.644                      | 0.478  | 0.6887       | 0.590        |  |
| Size (cm)                  | 2.5 × 6.2  |              |              |  |
| Thickness (cm)             | 0.02   |              |              |  |
| Material                   | Si   |              |              |  |
| Base Resistivity W-cm/type | 10/N/P   |              |              |  |
| Front junction depth (mm)  | 0.2  |              |              |  |
| Back surface field         | Yes  |              |              |  |
| Back surface reflector     | Yes  |              |              |  |
| Contact metallization      | TiPdAg   |              |              |  |
| Front contact width (cm)   | 0.06   |              |              |  |
| Anti-reflective coating    | TiO <sub>2</sub> /Al <sub>2</sub> O <sub>3</sub> |              |              |  |
| Cover type                 | CMX microsheet with anti-reflective coating      |              |              |  |
| Cover thickness (cm)       | 0.021  |              |              |  |
| Cover adhesive             | DC 93-500  |              |              |  |
| Cover front surface        | Textured   |              |              |  |

TABLE 6. Solar array summary.

|                                  | AVHRR | EHF  |
|----------------------------------|-------|------|
| Number cells series              | 22    | 22   |
| Number cells parallel            | 68    | 80   |
| Total number cells               | 1496  | 1760 |
| Area needed (m <sup>2</sup> )    | 2.31  | 2.72 |
| Area available (m <sup>2</sup> ) | 2.81  | 2.81 |

spacecraft about the yaw axis. Therefore, some loss of potential power is introduced from the effect of the angle of incidence, which reaches a maximum of 50°. Using the data from Table 4 and the cell characteristics from Table 5, the actual array panel area was determined and the results summarized in Table 6.

**Battery Design**

The battery for eclipse power is a 12-amp-hr NiH<sub>2</sub> battery manufactured by Eagle Picher. The battery is made in a two-cell common pressure vessel (CPV). Dimensions of each CPV are approximately 8.89 cm (3.5 in) diameter by 15.2 cm (6 in) height. Using a 28-V bus with constant current charge, the number of CPV cells is limited to eight. A NiH<sub>2</sub> battery was chosen because of the high number of charge/discharge cycles the bus may experience. The AVHRR payload, because of its 833 km (450 n.m.) low Earth orbit (LEO), for example, will experience over 15,000 cycles in its three-year design life. The number of charge/discharge cycles the EHF payload will experience may only be 1000. Because the bus was designed to accommodate these and other payloads in various orbits, the battery recharge requirements will vary. For this reason, the recharge circuitry must have the capability to be selectable or be comprised of modular components.

The AVHRR payload configuration draws 100.6 W during eclipse. The recharge rate is determined from the duration of the sunlight period and the amount of power removed. Assuming that 90% of the sunlight period was used to recharge the battery,

the AVHRR charge rate was chosen to be  $C/4$ ; this is only slightly below the maximum recommended charge rate of  $C/3$ , where  $C$  is the battery capacity in amp-hr. This allows for a third of the orbit in eclipse for LEO and a 10% overcharge required for high charge/discharge cycles.

The EHF payload utilizes only 80.7 W during eclipse. Because of the longer sunlight periods and smaller power drawn, the charging rate of this configuration is only  $C/10$ . The battery would be trickle-charged in seasons where the Molniya-type orbit has no eclipse. Table 7 gives the battery summary.

**Radiation Effects**

Radiation effects and shielding requirements were examined for the AVHRR's circular orbit and the EHF's 8-hr Molniya orbit using the JPL Solar Cell Radiation Handbook. The degradation for the AVHRR configuration was based on an annual equivalent of 1 MeV electron fluence assuming solar maximum for the three-year mission. Apogee for the 8-hr Molniya orbit extended into the Van Allen belts, exposing the solar cells to large fluences. Equivalent 1 MeV fluences for 5-min increments of orbital time were calculated for this orbit. Total fluence per orbit, per year, and three-year, lifetime were derived, and the impact on the solar cells calculated. Radiation effects for one year are summarized in Table 8 for both orbits, where  $I_{sc}$  is the short-circuit current, and  $V_{oc}$  is the open-circuit voltage for a solar cell at maximum power ( $P_{max}$ ).

**ATTITUDE CONTROL SUBSYSTEM**

The attitude determination and control subsystem (ADCS) provides precise attitude pointing for the AVHRR or similar payloads in a low 833-km (450 n.m.) circular orbit, and a less accurate determination for the EHF or other communications payload in a Molniya-type orbit. This dual objective is met by using two subsystems for the different requirements, the precision sensor subsystem (PSS) and the basic sensor subsystem (BSS). The PSS and BSS are used for precise positioning, whereas the BSS alone can be used for less stringent requirements. Both subsystems consist of sensors to determine attitude, an onboard processor for control, and an inertial reference system consisting

of an assembly of three orthogonal gyro assemblies (GA). The BSS and PSS share the same components where possible. The attitude control subsystem (ACS) is driven by either the PSS or BSS and consists of three primary reaction wheel assemblies (RWA) with a fourth skewed to provide redundancy, and two magnetic torque rods (MTR) for momentum dumping. Six 0.89-N (0.2 lbf) thrusters can be used for momentum dumping in case of failure of the MTRs or if excessive momentum buildup occurs.

The PSS relies primarily on a celestial sensor assembly (CSA) for attitude determination previously used aboard the DSP Block 5D-3 satellite. The CSA is a strap-down star mapper with a  $10.4^\circ$  field of view. The star sensor measures star transits across a detector and provides an input to the attitude control computer (ACC). The user provides the satellite, approximately once per day, the 80 brightest stars that will be in view of the CSA. The ACC also receives input from the GA and an onboard global positioning system (GPS) receiver. The ACC uses the GPS receiver data and the uplinked catalog to predict star transits that are then compared with actual transits from the CSA to determine attitude error. Gyro drift is then calculated. The inertial attitudes rates from the gyros (corrected for drift in the ACC by the CSA) and the attitudes estimate from the CSA are combined in a Kalman optimal estimation algorithm to provide an attitude determination accuracy of  $0.01^\circ$  as required by the AVHRR payloads. The PSS uses the BSS for backup and initial attitude determination. The GPS receiver provides accurate ephemeris data required by the CSA. Figure 10 shows the PSS block diagram.

The BSS consists of a conical scanning Earth sensor (ES), a digital Sun sensor (DS), the GA, RWAs, ACC, GPS receiver, and MTRs. A scanning ES is required by the wide range of possible altitudes. The ES scans the 14- to 16- $\mu$ m infrared radiance profile of the Earth to determine pitch and roll error, while the DS determines the angle between the pitch axis and the Sun. This information, together with the ephemeris data from the AC and

TABLE 7. Battery summary.

|                  | AVHRR   | EHF     |
|------------------|---------|---------|
| Charge required  | 76.8 W  | 30.7 W  |
| Charging rate    | $C/4$   | $C/10$  |
| Charge time      | 59 min  | 6.5 hrs |
| Available sun    | 64 min  | 7.1 hrs |
| Battery capacity | 12 A-hr | 12 A-hr |

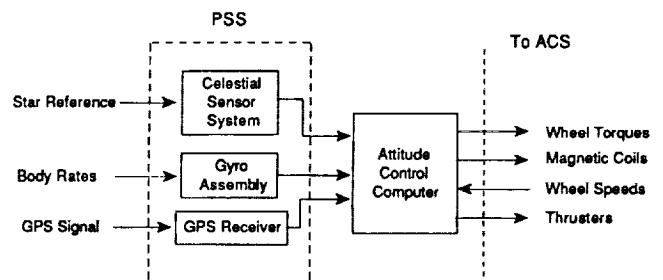


Fig. 10. Functional block diagram of precision sensor subsystem.

TABLE 8. Radiation annual fluence summary (MeV).

|                   | AVHRR        |                  | EHF          |                  |
|-------------------|--------------|------------------|--------------|------------------|
|                   | $I_{sc}$     | $V_{oc} P_{max}$ | $I_{sc}$     | $V_{oc} P_{max}$ |
| Trapped electrons | $4.59E + 11$ | $4.59E + 11$     | $3.18E + 13$ | $3.18E + 13$     |
| Trapped protons   | $8.64E + 12$ | $1.47E + 13$     | $3.82E + 15$ | $1.59E + 15$     |
| Totals            | $9.10E + 12$ | $1.52E + 13$     | $3.85E + 15$ | $1.62E + 15$     |

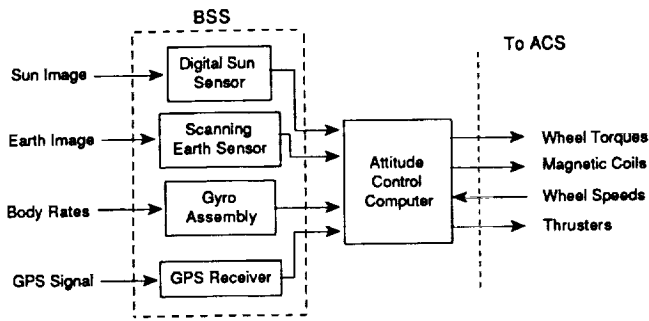


Fig. 11. Functional block diagram of basic sensor subsystem.

GPS receiver, provides yaw error. The BSS can provide better than  $0.5^\circ$  accuracy in each of the three axes. Figure 11 is a functional block diagram of the BSS.

The Attitude Control Subsystem (ACS) is driven by the output of the ACC, which controls the RWAs to correct attitude errors. The RWAs input to the ACC is the load current and wheel speed. The current is used to determine if an overload condition exists, in which case the ACC shuts down the wheel and starts the backup RWA. The wheel speed is used as feedback and to determine if momentum dumping is required. When the momentum reaches the maximum for the wheel, the torque coils are commanded to dump the excess momentum. In case of excessive rate buildup, as determined by differentiators in the circuitry, thrusters are fired to slow the rate to within acceptable limits. The block diagram for the ACS is shown in Fig. 12.

The yaw motion of the satellite in the Molniya-type orbit is modeled as in HILACS<sup>(1)</sup>. This report considers only the attitude control of the meteorological payload. Solar gravity gradient, magnetic, and aerodynamic disturbance torques were modeled in a first-order approximation for the design. The spacecraft was modeled as a rigid body with nonrotating, rigid solar arrays. The equations of motion for a three-axis stabilized

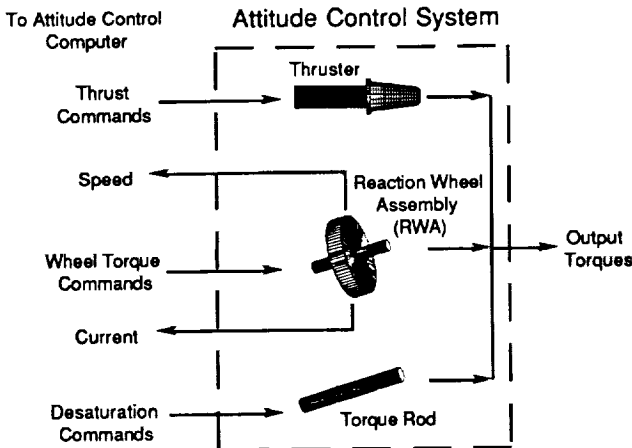


Fig. 12. Functional diagram of attitude control subsystem.

spacecraft were used<sup>(2)</sup> and analysis was done using MATLAB<sup>®</sup> on a PC. Figures 13 through 16 show the resulting error in pitch, roll, and yaw and the pitch wheel speed over one orbit.

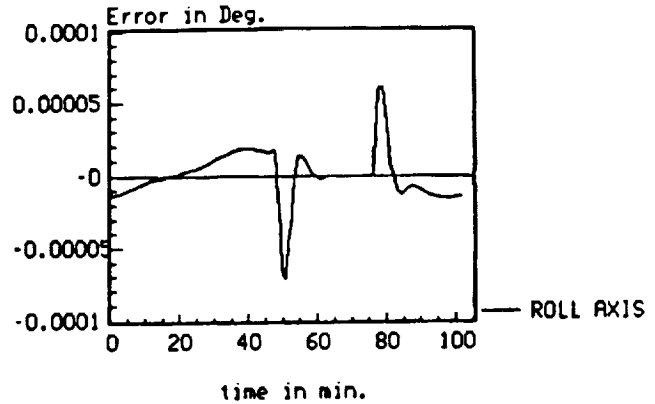


Fig. 13. Roll error for one orbit.

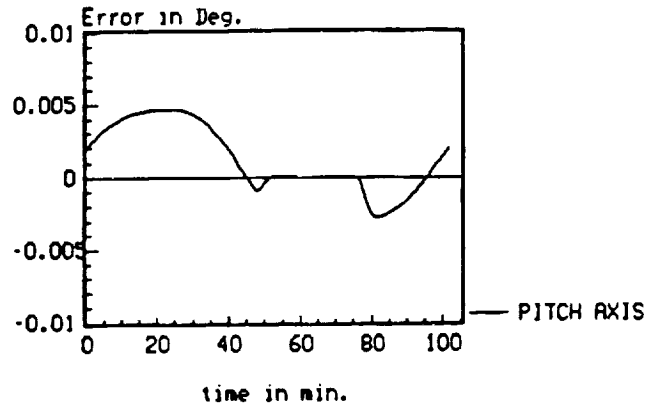


Fig. 14. Pitch error for one orbit.

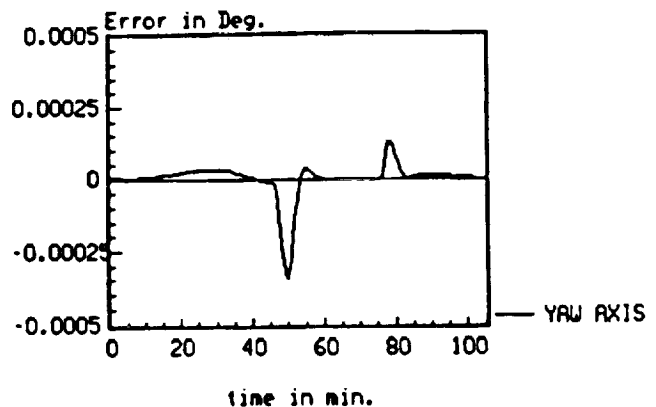


Fig. 15. Yaw error for one orbit.

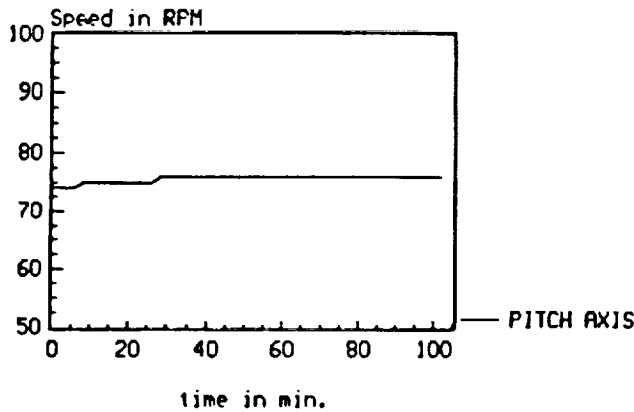


Fig. 16. Pitch wheel speed for one orbit.

The pitch wheel will require periodic desaturation due to the secular torques along the pitch axis (solar and aerodynamic). The pitch MTR will be energized at 250 rpm wheel speed and powered off at 75 rpm. The torque rods will provide a 10-amp-m<sup>2</sup> magnetic dipole that will result in 0.006 N-m of torque over the Earth's geomagnetic poles for the 833 km (450 n.m.) altitude of the circular orbit. The pitch torque rod will be energized within ± 30° of the north and south geomagnetic poles; and the roll-yaw rod (required) powered within ± 30° of the geomagnetic equator. The desaturation scheme for the Molniya-type orbit is dependent upon the longitude of the ascending node. Basically, the roll-yaw rod will be used near the equatorial crossing and the pitch rod near perigee. As can be seen from the plot of the wheel speeds, the pitch wheel gains about 6 rpm for every 5 orbits, resulting in about 17 orbits between MTR cycles. The roll and yaw wheels should not require desaturation due to the cyclic nature of the disturbance torques. The satellite will maintain a 0.01° pointing accuracy during desaturation.

**THERMAL CONTROL SUBSYSTEM**

An initial analysis was conducted to determine the approximate area required to radiate the thermal energy generated based on the power summaries of the spacecraft. The thermal energy dissipated by the EHF payload was estimated to be 148 W and for the AVHRR payload, 115 W. The area required for the EHF payload radiator is 0.48 m<sup>2</sup> (744 in<sup>2</sup>), and 0.37 m<sup>2</sup> (573.5 in<sup>2</sup>) for the AVHRR configuration. It should be noted that the AVHRR assembly has approximately 0.19 m<sup>2</sup> (300 in<sup>2</sup>) in OSR already installed.

Operating temperatures for the solar arrays were calculated for the 2.81 m<sup>2</sup> (30.2 ft<sup>2</sup>) arrays assuming values of 0.8 array absorptance, 0.95 packing efficiency, 0.8 array front emittance, and 0.7 array back emittance. The steady-state operating temperatures for summer solstice and winter solstice are given in Table 9.

Thermal analysis of the spacecraft was done using the PC-ITAS® software package by ANALYTIX Corporation. The model consisted of 145 surfaces for calculating the temperatures at

TABLE 9. Solar array operating temperatures.

| T <sub>op</sub> | EHF    | HVHRR  |
|-----------------|--------|--------|
| Summer Solstice | 45.3°C | 12°C   |
| Winter Solstice | 50.4°C | 34.6°C |

various points on the spacecraft. The number of nodes was limited to approximately 165 by the amount of memory on the computer. This was deemed sufficient for this preliminary design. The analysis considered only steady-state temperatures for the two different orbits.

This preliminary analysis indicates that, with proper selection of coatings and materials, the temperatures of the various equipment can be maintained within operating ranges. There are specific nodes that are too cold or too hot, but, since these are identified, corrective action can be implemented. Corrective action in these cases would be to insulate or link by conduction the equipment to the radiator.

**PROPULSION SUBSYSTEM**

The propulsion subsystem consists of six 0.89-N (0.2 lbf) thrusters made by Rocket Research Corporation (model number MR103C), a 0.41-m (16 in) diameter tank made of titanium alloy manufactured by TRW Pressure Systems, Inc., one pressure transducer, and one pressure regulator to monitor the pressure throughout the system. The MR103C minimizes space required for mounting. The MR103C is also the lightest of the 0.89-N thrusters considered. An 8-μm filter is incorporated to screen the impurities remaining in the fuel.

The system is installed primarily as a backup system for reaction wheel desaturation, orbit maintenance, and orbit stationkeeping, and has no redundancy. The propulsion system will be used to correct minor errors in the orbit after separation. On orbit, the system will provide ΔV for stationkeeping. Figure 17 shows a schematic of the propulsion subsystem. Figure 18 shows the placement of thrusters on the MPS bus.

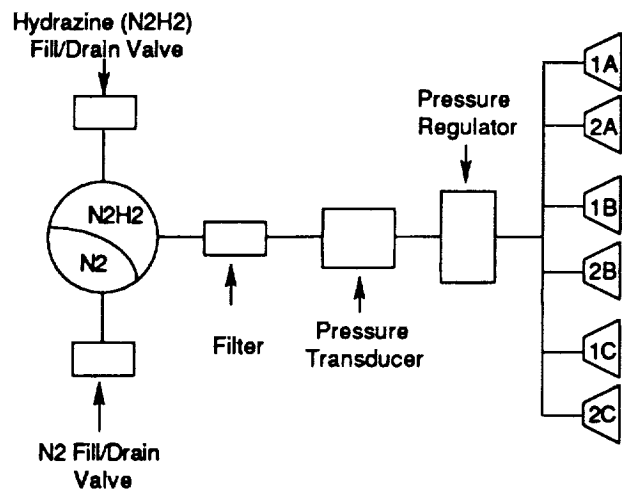


Fig. 17. Propulsion subsystem schematic.

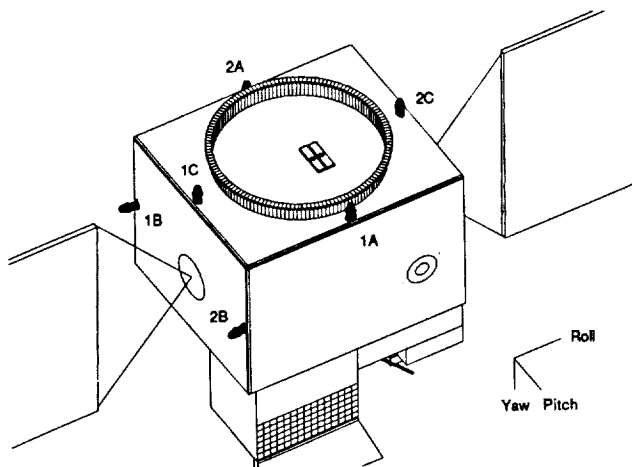


Fig. 18. Location of thrusters.

Thruster operations can be performed with or without the solar arrays deployed to desaturate the reaction wheels along any axis.  $\Delta V$  maneuvers can only be provided in the +yaw or the +roll directions. The positive roll thrusters are placed to provide  $\Delta V$  for orbit maintenance without the need for reorientation of the spacecraft. Major orbit changes will require reorientation of the spacecraft to align the flight path of the spacecraft along the +z axis. Deactivation of some equipment may be required for major orbit corrections. The two thrusters along the east face could possibly impinge on the solar panels, depending on the angular position of the arrays. An electronic cutout cam would have to be installed to prevent accidental firing and subsequent damage to the arrays. It is unlikely that this would affect AVHRR operations as the arrays operate  $\pm 50^\circ$  of the roll/yaw plane. The EHF payload may require the arrays to rotate  $\pm 90^\circ$  roll/yaw plane necessitating close management of solar array and thruster operations. The thrusters along the positive roll axis are canted out at an angle of  $8^\circ$  as an additional precaution.

**TELEMETRY, TRACKING, AND COMMAND**

The telemetry, tracking, and command (TT&C) package for the MPS bus is designed to be compatible with the Air Force Space-Ground Link Subsystem (SGLS) for satellite control. TT&C is designed in the bus to operate at super-high frequencies (SHF) that correspond to channel 1 of the SGLS ground terminal as given in Table 10.

The TT&C package sends and receives data from the payload and/or the anti-Earth-face antenna through command-controlled switches that allow the ground terminal to shift between payload

TABLE 10. TT&C operating frequencies.

|                     |              |
|---------------------|--------------|
| Command Uplink:     | 1.763721 GHz |
| Telemetry Downlink: | 2.2 GHz      |
| Carrier 1:          | 2.2025 GHz   |
| Carrier 2:          | 2.1975 GHz   |

antennas and the anti-Earth-face antenna. The anti-Earth-face antenna is a four-element microstrip antenna that uses the same elements as the AVHRR antenna and has a gain of 2.5 dB. The switches may be aligned such that during launch and activation, TT&C will be accomplished with the SGLS system channel 1 to the anti-Earth-face antenna. The payload TT&C is activated and the anti-Earth-face telemetry downlink is put on standby once the satellite is on station. The anti-Earth-face command receiver will remain active in case the satellite attitude control system fails.

The remote tracking unit (RTU) takes commands from the antennas and payloads in the SGLS format and demodulates and decodes them for the remote command unit (RCU) on up-link. The RTU also modulates and encodes telemetry signals from the RCU for down-link. The RTU block diagram is shown in Fig. 19.

The RCU receives a command from the RTU and passes it to the microprocessor for command recognition and execution. Data is gathered from all sensors and the payload and compiled into a telemetry down-link signal for the RTU. The signal uses frequency-shift-key (FSK) modulation to avoid phase ambiguities, and will be encoded to provide some error correction. Figure 20 shows the block diagram of the RCU.

A global positioning system (GPS) receiver is used for tracking below 20,000 km altitude. The satellite will most likely be receiving lower-powered side-lobes requiring significant antenna gain in order to achieve the 34 dB C/N ratio needed to receive analog data. A tracking beacon in the RCU can be turned on

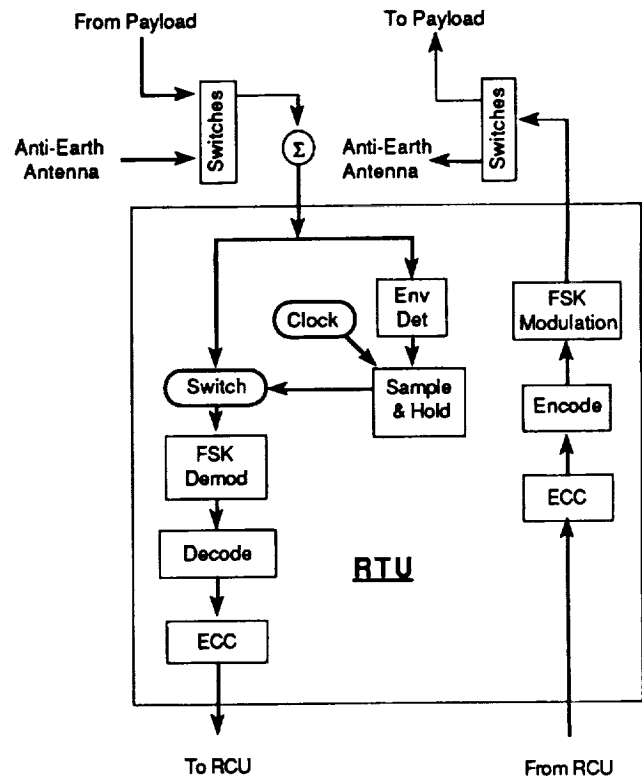


Fig. 19. Remote tracking unit.

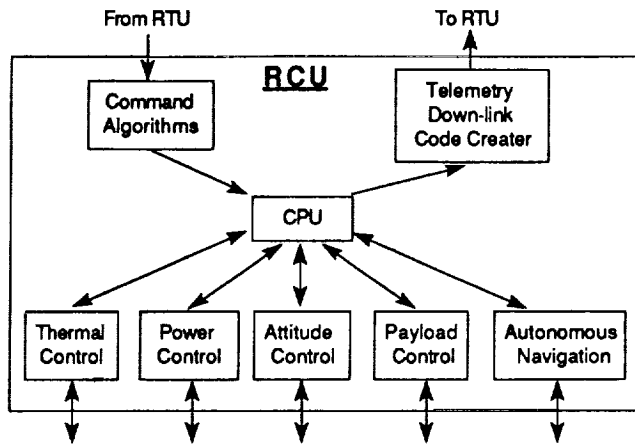


Fig. 20. Remote command unit.

with a command signal, and manual range and range rate tracking can be accomplished in the event the GS receiver is not accurately predicting the position of the satellite. The tracking beacon is intended for standby use allowing 15.2 m (50 ft) and 0.037 m/s (0.120 ft/s) resolution.

**STRUCTURE DESIGN**

The spacecraft bus structure is designed to fit within the 1.17-m (46 in) diameter Pegasus shroud with two folding solar panels and within the Taurus shroud with three, if required. A rectangular design was chosen for simplicity and ease of assembly. The bus is built on a rectangular frame that is composed of hollow rectangular cross-section tubing made from 6061-T6 aluminum. Five load-supporting honeycomb panels with aluminum faceskins are attached to the frame, one being the anti-Earth face. The sixth side of the spacecraft bus is the Earth/payload face. The entire spacecraft is mounted to Pegasus with a standard Marmon clamp assembly. Total weight of the dry standard bus structure is 20.4 kg (45 lb) for the AVHRR configuration and 26.8 kg (59 lb) for the EHF configuration. Launch design accelerations are given in Table 11. The structure margins of safety for the various components are given in Table 12.

TABLE 11. Accelerations at payload interface [m/s<sup>2</sup>].

| Flight Mode    | X (Roll) | Y (Pitch) | Z (Yaw) |
|----------------|----------|-----------|---------|
| Captive Carry  | +8.82    | +8.06     | +34.3   |
|                | -6.66    | -9.04     | -13.7   |
| Powered Flight | +0       | +4.9      | +27.4   |
|                | -83.3    | -4.9      | -9.8    |

TABLE 12. Margins of safety.

| Component Mix Load | Expected                                | Yield Load of Safety     | Margin |
|--------------------|---|--------------------------|--------|
| Aluminum Frame     | 6.2E06 Pa [900 psi] (compression)       | 255.1E06 Pa [37,000 psi] | 32     |
| Aluminum Frame     | 86.9E06 Pa [12,600 psi] (bending)       | 255.1E06 Pa [37,000 psi] | 1.9    |
| Aluminum Frame     | 6.89E06 Pa [1,000 psi] (shear)          | 206.8 Pa [30,000 psi]    | 29     |
| Honeycomb Panel    | 196 m/s <sup>2</sup> [20 g]             | 255.1E06 Pa [37,000 psi] | 1.1    |
| Honeycomb Panel    | 78.6E06 Pa [11,406 psi] (facing stress) | 165.5E06 Pa [24,000 psi] | 1.1    |

**ACKNOWLEDGMENTS**

The 1990 design project team would like to thank B. Agrawal for his guidance and assistance throughout the 11-week quarter. His continuous support was sincerely appreciated and ensured the success of the project. We are also indebted to G. Myers, T. Ha, D. Wadsworth, and R. Adler of the Naval Postgraduate School, who consistently made themselves available to answer our questions. M. Brown, C. Merk, S. Coffey, M. Zedd, R. Morris, P. Carey, and N. Davinic of the Naval Research Laboratory also contributed to the success of the project. W. Cummings of MIT Lincoln Laboratory and L. Flinn, R. Sudol, and P.-A. Stiffier of Space Applications also made significant contributions. Finally we appreciate the continued interest of J. Burke, our NASA representative from the Jet Propulsion Laboratory.

**REFERENCES**

1. National Oceanic and Atmospheric Administration Technical Report NESDIS, *Final Report on the Modulation and EMC Considerations for the HPRP Transmission System in the Post NOAA-M Polar Orbiting Satellite Era*, U. S. Dept. of Commerce, Washington D. C., June 1989.
2. Agrawal B. M., *Design of Geosynchronous Spacecraft*, Prentice-Hall, 1986.
3. Lindberg R. E., "Brief to the Space Test Program Tri-Service Experiment Review," 9 May 1989.

## PROJECT WISH: THE EMERALD CITY

THE OHIO STATE UNIVERSITY

532-18

160608

P-4

## INTRODUCTION

Project WISH (Wandering Interplanetary Space Harbor) is a three-year design effort currently being conducted at The Ohio State University. Its goal is the design of a space oasis to be used in the exploration of the solar system during the mid-twenty-first century. This spacecraft, named Emerald City, is to conduct and provide support for missions to other planetary bodies with the purpose of exploration, scientific study, and colonization. It is to sustain a crew of between 500 and 1000 people at a time, and be capable of traveling from a nominal orbit to the planets in reasonably short flight times. Such a ship obviously presents many technical and design challenges, some of which have been examined through the course of Project WISH.

This year, Phase II (1990-1991) of Project WISH was carried out. The basic design of the Emerald City resulting from Phase I (1989-1990) was taken and improved upon through more detailed analysis and revision. At the core of this year's study were orbital mechanics, propulsion, attitude control, and human factors. Throughout the year, these areas were examined and information was compiled on their technologies, performances, and relationships. Then, using the data obtained through these studies, two specific missions were designed: an envelope mission from a nominal orbit of 4 AU to Saturn and a single-point design for a specific mission from the Earth to Mars. The latter was designed in view of the special interest that Mars is attracting for near-future space exploration. The mission to Saturn has all the first six planets within its flight envelope in less than or equal to a 3-year flight time at any time upon demand, and it has Uranus in its flight envelope most of the time upon demand. These mission studies provided data on the approximate size, weight, number of engines, and other important design values that would be required for the Emerald City.

## ORBITAL MECHANICS

Consideration of orbital mechanics dealt primarily with finding the  $\Delta V$ s for transfers from a nominal orbit to a target planet in a given time. The original design requirement was for the Emerald City to be able to go from a nominal orbit to any planet in the solar system in three years or less. However, this requirement was modified in order to reduce the  $\Delta V$ s required so as to give the project a more workable design problem. First, the planets were categorized according to their envisioned role in manned space exploration during the mid-twenty-first century. The ability of the Emerald City to make transfers to a planet was then based on what category the planet fell into. The first category includes Earth, Mars, and Jupiter, planets that were felt to be very important. The design goal for the first category

was to be able to make a transfer to one of these planets 100% of the time on demand in three years or less. In the second category of planets were those deemed important, namely Venus, Saturn, and Uranus. The design goal for this category was to be able to make transfers to these planets most of the time in flight times of up to five years. The final category consists of planets deemed to be unimportant for Project WISH and is made up of Mercury, Neptune, and Pluto. It is envisioned that there would be little need for a ship such as the Emerald City to make transfers to these planets, and thus any capabilities to reach them would be an added bonus.

Once these new requirements were identified, the  $\Delta V$ s needed to make transfers to the planets were examined. This was done by using a high-impulse orbital mechanics computer code and the concept of the synodic period, which is the time it takes for a certain orientation to recur between two orbiting bodies. The synodic period is important because the  $\Delta V$ s will essentially repeat cyclically with a period given by the synodic period. The  $\Delta V$ s required for all the planets were found over one sample synodic period for a range of nominal orbit radii and flight times. These results were then analyzed by finding the percentage of the synodic period that a transfer could be made under a certain  $\Delta V$  level. These percentages were used to compare the ability of the Emerald City to reach the different planets from various nominal orbits. Based on the results from this analysis, a circular nominal orbit of 4 AU was selected, which met or exceeded all the design requirements mentioned earlier for a round trip  $\Delta V$  of 50 km/s. This value for  $\Delta V$  was then given to the propulsion group for their system analysis.

Another problem examined by orbital mechanics was  $\Delta V$  minimization. In this study, the effects of finite thrust levels were incorporated along with the equations for a free-flight orbit. From these equations, an optimization problem was formulated, with an objective function given by the total  $\Delta V$ . The constraints were based upon the limits of initial acceleration, total flight time, burn times, and a rendezvous condition that insures that the Emerald City and the target planet meet. Although the problem was set up and all the functional relationships were determined, the computer coding of the problem into an optimization routine is left for next year (1991-1992), Phase III of Project WISH.

## PROPULSION

The propulsion system of the Emerald City was the subject of much work during Phase II of Project WISH. The first step in the analysis of the propulsion system was the examination of the equations relating to the propulsion parameters such as the thrust, exit velocity, specific impulse, burn times, etc. By graphing these equations, relationships were noted and an

estimate of the order of magnitude of these parameters was obtained. It was observed that for a ship such as the Emerald City, with very large mass expected and high  $\Delta V$  requirements, a propulsion system capable of providing enormous amounts of impulse at high specific impulse and thrust levels would be needed. It was felt that, of the potential propulsion systems in the twenty-first century, the gas-core nuclear rocket offered the most promise as the propulsion system for the Emerald City.

The gas-core nuclear rocket consists of five different components: the pressure shell, the moderator, the turbo pump, the nozzle, and the radiator. It uses the thermal energy generated by the fissioning fuel,  $U^{233}$ , which is in a gaseous state at very high temperatures. The turbopump pumps liquid hydrogen around the circumference of the pressure shell to aid in the cooling process of the moderator. Next, the liquid hydrogen is pumped into the cavity where the gaseous  $U^{233}$  is located and the fission process is occurring. At this time, the hydrogen is heated to very high temperatures and expelled through the nozzle to produce thrust. The moderator is present to block and reflect neutrons, which allow the fission chain reaction to be maintained.

The gas-core nuclear rocket was selected because of the relatively high values for thrust,  $F$ , and specific impulse,  $I_{sp}$ . These parameters, along with values for the cavity diameter and the ratio of the  $U^{233}$  volume to the cavity volume were estimated in order to calculate the propulsion system component masses. A computer program was written to find these masses as well as the mass flow rates of the uranium and hydrogen. This program also calculated temperatures as well as other engine parameters in the cavity, at the throat, and at the exit.

Next, the number of engines that would be required for a mission was found. This figure is given by the formula

$$n = \frac{m_{dry} I_{sp} g}{F_i t_{pr}} (e^{\frac{\Delta V}{I_{sp} g}} - 1) \quad (1)$$

where  $m_{dry}$  is the dry mass of the Emerald City,  $F_i$  is the thrust of one engine,  $t_{pr}$  is the burn time, and  $\Delta V$  is the change in velocity that is required for the given mission. Once the number of engines is found, the total mass of the propulsion system and hence the payload mass can be found.

### HUMAN FACTORS

To provide life support for 500-1000 people on a ship with an expected lifetime of at least 50 years, a system was needed that required little or no resupply. Because of the magnitude of Project WISH, even a system that could be 99% efficient will waste thousands of kilograms of water a year. This fact virtually eliminates using mechanical systems for life support for the Emerald City. Attention therefore turned to organic-based methods for providing life support, such as biosphere technology, which could provide a life support system that would be 100% efficient. Biospherics is a rising science that studies the way the Earth naturally recycles all food, water, and waste. Using information from the Biosphere II project in Arizona,

volume and mass requirements for the crew section of the Emerald City were estimated. These results were then used as constraints for the design of the crew section.

Another problem in the area of human factors was the need for artificial gravity. Previous experience in space has shown that without gravity bones immediately begin to decalcify and muscles weaken and atrophy. Effects of long-term exposure to zero-g are not completely understood, but research appears to indicate further deterioration that would reduce the possibility of returning to life in a 1-g environment. The crew section was therefore designed to be a torus rotating about a central pole to provide some level of artificial gravity. The relationship between spin rate ( $\omega$ ), gravity level ( $n_g$ ), and distance from the rotating axis ( $r$ ) is found to be

$$r = \left(\frac{30}{\pi}\right)^2 \frac{n_g g}{\omega^2} \quad (2)$$

Possible sizes of the torus were found using this equation and the constraints on the three variables. One rpm is the upper limit for spin rate because of attitude control power requirements and the limits of human endurance. A maximum gravity level of 0.8 was used to size the torus because it was felt that this would limit the ill effects of extended weightlessness while reducing the structural mass that would be required for the larger torus radius at 1 g.

The final issue examined this year was radiation. Guidelines for exposure were determined from recommendations of the National Council on Radiation Protection and Measurements. The 5 rem/year limit was based on a 3% increased risk of getting cancer. The major radiation sources for the Emerald City are from the power and propulsion systems, solar flares, and cosmic radiation. Of these, cosmic radiation is of the most concern because the crew is constantly exposed to it, and the only way to protect against it is to shield the entire crew section. Of the most common materials in space applications, liquid hydrogen is the most effective shield because it does not contain neutrons that can be scattered by incident radiation. A 14-m layer of liquid hydrogen attenuates the dose from cosmic rays to just below the 5 rem/year limit. Dose rates from the exhaust of the engines and solar flares are high, but only last from 1 to 2 weeks. Specifically, the radiation from the engine plume was computed for the propulsion system parameters. When these sources of radiation are present, protection can be obtained by moving the crew to areas with extra shielding, thus keeping down the mass of the Emerald City.

### ATTITUDE CONTROL

The vehicle dynamics of the Emerald City were studied during Phase I (1989-1990) of Project WISH. The attitude-stable configurations of the spacecraft (assumed to be rigid body, although this assumption will be revised next year) were determined from this study. Phase II placed more emphasis on the attitude control aspect of the problem. A study was conducted to determine the state response due to specified initial disturbances and the attitude control design requirements needed to damp out these disturbances.

The first step in the study was to determine a thruster configuration that would be used for attitude control. This configuration consisted of four clusters yielding independent control couples about the centroidal principal moments of inertia axes parallel to the torus plane. Next, the control torques on the spacecraft were calculated using this cluster configuration. This thruster configuration matrix was then substituted into the gyroscopic state equations of a spinning body, which were obtained during Phase I of the project. The control software package MATLAB was then used to design linear quadratic regulator (LQR) controls. The root-mean-square power,  $P_{rms}$ , required to damp out the disturbances, was then calculated by using the equation

$$P_{rms} = \frac{V_{ex} I_x n^2}{2D_t} \left( \frac{S^*}{\tau_c} \right)^{1/2} \quad (3)$$

where  $V_{ex}$ ,  $I_x$ ,  $n$ , and  $D_t$  are the thruster jets' exhaust velocity, mass moment of inertia about the  $x$  axis, and the diameter of the living quarters (torus) of the spaceship. The parameters  $S^*$  and  $\tau_c$  are nondimensional control power and control time, respectively, obtained via the particular state feedback control design and the initial disturbances. The attitude power requirement was the influencing factor in keeping the spin rate below 1 rpm. The next step was the calculation of the propellant mass required for the attitude control systems and the calculation of the thrust requirements at each cluster location by studying the control input profiles. The results of this study are shown in Table 2 for the particular missions discussed earlier.

#### REPRESENTATIVE MISSION DESIGNS

Once the individual disciplines of Project WISH had been studied in detail, an attempt was made to produce a representative design for the Emerald City. Since the idea of Project WISH is for the Emerald City to handle a wide variety of missions, two contrasting cases were considered to find the range of the design parameters. The first one is the Saturn envelope mission with a three-year flight time and a round trip  $\Delta V$  of 50 km/s, which is near the upper bound of  $\Delta V$  set for the propulsion system. The second mission is a single-point design that depicts a transfer from about 1 AU outside the sphere of influence of the Earth to Mars with a  $\Delta V$  of 12.6 km/s and a flight time of 1.54 yr. This would be a more common mission that the Emerald City might be required to undertake, carrying new colonists and supplies that had been shuttled to the Emerald City just outside the Earth's sphere of influence, supplying the martian colonies with materials from Earth. It was felt that analyzing these two missions would yield good estimates of the bounds for the size, mass, and configuration of the Emerald City.

The missions described above were analyzed using a methodology based on considerations discussed in the previous sections. Human factors were used to set volume and mass requirements for the torus, which was based on the crew size selection. These were based on data from the Biosphere II project and estimates for the structural and shielding masses needed. Then, a dry mass of the spacecraft was estimated and the propulsion system parameters (number of engines, propellant

required, burn time, total engine mass) were found from orbital mechanics and propulsion considerations. The mass of the torus section, the propellant, and the engines were subtracted from the dry mass to obtain the payload mass. This payload mass represents cargo as well as other subsystems that have not been considered yet (power, heat rejection, attitude control thrusters, tankage, etc.). The center pole was sized to store fuel and propellant and the center of mass of the ship was found. Mass moments of inertia were then calculated and these values were used in the study of the attitude control system.

The results from the design studies can be found in Tables 1 and 2. Table 1 lists the mission requirements for the two missions and then the different masses and ship sizes. Table 2 uses the values found for these missions and finds the attitude control requirements for a given gyroscopic initial disturbance. Figure 1 shows how some of the variables listed in these tables are defined.

TABLE 1. Emerald City Design Parameters

|                                   | Saturn Envelope<br>Mission | Earth to Mars           |
|-----------------------------------|----------------------------|-------------------------|
| Crew                              | 1000                       | 500                     |
| $\Delta V_{total}$ (km/s)         | 50                         | 12.6                    |
| $\Delta V_1$ (km/s)               | -                          | 5.1                     |
| $\Delta V_2$ (km/s)               | -                          | 7.5                     |
| $t_{pr,total}$ (days)             | 20                         | 11.53                   |
| $t_{pr,1}$ (days)                 | -                          | 5                       |
| $t_{pr,2}$ (days)                 | -                          | 6.53                    |
| $F_t$ , thrust/engine (N)         | $4.44 \times 10^5$         | $4.44 \times 10^5$      |
| $I_{sp}$ , specific impulse (sec) | 5000                       | 5000                    |
| number of engines                 | 172                        | 33                      |
| $m_o$ (total, kg)                 | $4.16 \times 10^9$         | $1.295 \times 10^9$     |
| $m_p$ (propellant, kg)            | $2.658 \times 10^9$        | $2.947 \times 10^8$     |
| $m_{dry}$ (dry, kg)               | $1.5 \times 10^9$          | $1 \times 10^9$         |
| $m_1$ (payload, kg)               | $3.457 \times 10^8$        | $2.165 \times 10^8$     |
| $m_w$ (engine, kg)                | $4.4376 \times 10^7$       | $8.514 \times 10^6$     |
| $m_{torus}$ (torus, kg)           | $1.111 \times 10^9$        | $7.746 \times 10^8$     |
| $m_1 / m_o$                       | 0.083                      | 0.167                   |
| $m_p / m_o$                       | 0.639                      | 0.228                   |
| $V_{LH2}$ (m <sup>3</sup> )       | $3.742 \times 10^7$        | $4.151 \times 10^6$     |
| $r_{pole}$ (m)                    | 100                        | 50                      |
| $h_w$ (m)                         | 20                         | 20                      |
| $h_p$ (m)                         | 1200                       | 528                     |
| $h_c$ (m)                         | 50                         | 21                      |
| $R$ (m)                           | 700                        | 700                     |
| $r$ (m)                           | 37                         | 26                      |
| $z_{centroid}$ (m)                | 432                        | 69                      |
| $I_z$ (kg m <sup>2</sup> )        | $5.6144 \times 10^{14}$    | $3.8061 \times 10^{14}$ |
| $I_x, I_y$ (kg m <sup>2</sup> )   | $9.9568 \times 10^{14}$    | $2.1731 \times 10^{14}$ |
| max/min g-levels                  | 0.8/0.72                   | 0.8/0.74                |
| $\omega$ (spin rate, rpm)         | 0.99                       | 0.99                    |
| $r_x$ (m) / $r_z$ (m)             | 489/367                    | 410/542                 |

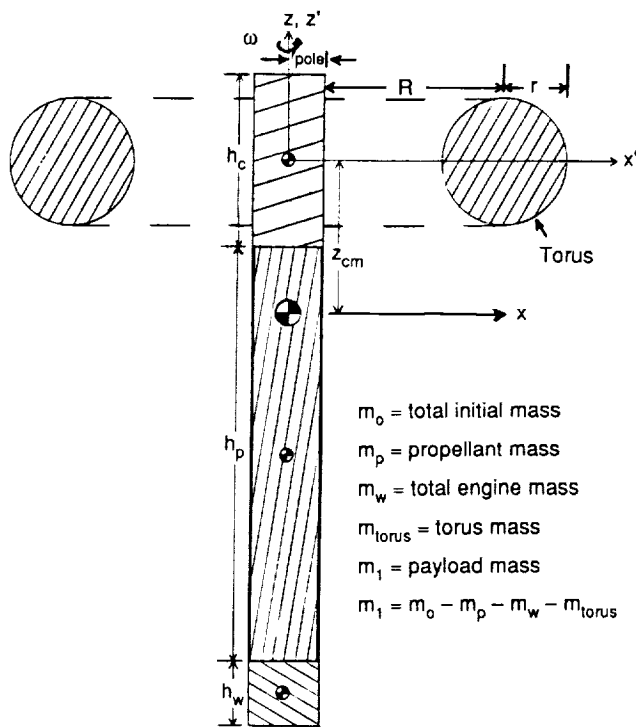


TABLE 2. A representative attitude control system design  
 ( $\theta$ s are rotations about the respective body axes).

| $I_z / I_x$           | 0.56   | 1.75                  |
|-----------------------|--|-----------------------|
| Initial Disturbance   | $[\theta_x, \theta_y, \dot{\theta}_x, \dot{\theta}_y] = [1.1 \ .1n \ .1n \ .1n]$ |                       |
| $P_{rms}$ (W)         | $6.176 \times 10^{12}$   | $7.86 \times 10^{11}$ |
| $m_{p,control}$ (kg)  | $2.105 \times 10^7$  | $3.458 \times 10^6$   |
| $F_{control,max}$ (N) | $2.988 \times 10^9$  | $1.911 \times 10^9$   |
| $t_{control}$ (sec)   | $\sim 100$   | $\sim 100$            |

Fig. 1. Definition of design parameters.

## FROM ORBITAL DEBRIS CAPTURE SYSTEMS THROUGH INTERNAL COMBUSTION ENGINES ON MARS

OLD DOMINION UNIVERSITY

593-12  
160609  
P. 8

The investigation and conceptualization of an orbital debris collector was the primary area of design. In addition, an alternate structural design for space station *Freedom* and systems supporting resource utilization at Mars and the moon were studied. Hardware for production of oxygen from simulate Mars atmosphere was modified to permit more reliable operation at low pressures (down to 10 mb). An internal combustion engine was altered to study how Mars atmosphere could be used as a diluent to control combustion temperatures and avoid excess Mars propellant production requirements that would result from either methane-rich or oxygen-rich, methane-oxygen combustion. An elastic loop traction system that could be used for lunar construction vehicles was refined to permit testing. A parabolic heat rejection radiator system was designed and built to determine whether it was capable of increasing heat rejection rates during lunar daytime operation. In addition, an alternate space station truss design, utilizing a pre-integrated concept, was studied and found to reduce estimate EVA time and increase the structural integrity when compared to the original Warren truss concept.

An orbital-debris-capturing spacecraft design which could be mated with the Orbital Maneuvering Vehicle was studied. The design identified Soviet C-1B boosters as the best targets of opportunity in Earth orbits between an altitude of 900 km and 1100 km and at an inclination of 82.9°. A dual robot pallet, which could be spun to match the tumbling rate of the C-1B booster, was developed as the conceptual design.

### INTRODUCTION

Students participated in six space systems design projects during the 1990-91 academic year. Design teams investigated alternate truss structure designs for Space Station *Freedom*; an orbital debris capturing unit; a locomotion system for lunar construction vehicles; a focusing radiator system for lunar heat rejection applications; production of oxygen from Mars atmosphere, and methane/oxygen-fueled engines for Mars applications. Mars oxygen production and lunar construction vehicle systems were continuations of previous design projects, while the other four projects were initiated during the present academic year. The participation of J. P. Raney, who was on loan from NASA Langley Research Center, is gratefully acknowledged.

The orbital debris capturing system and the space station truss designs were primarily paper studies, while the other four projects involved designing and building hardware that can be used to evaluate the specific design through further testing. The Mars oxygen processor assembly was rebuilt in order to eliminate leaks that have compromised earlier tests when conducted at subatmospheric pressures. The track system for a lunar construction vehicle has reached a design stage where its performance can be evaluated under simulated operating conditions. An internal combustion engine was modified to use methane fuel and pure oxygen, diluted subsequently with carbon dioxide, to study how stoichiometric methane-oxygen mixtures can be used for internal combustion engines on Mars. A focused parabolic collector system was designed and built to operate in a cryogenically cooled vacuum environment to investigate infrared heat rejection efficiency in the presence of a columnated sun-lamp heat source.

### ORBITAL DEBRIS COLLECTOR

The population of objects in low Earth orbit (LEO) is currently monitored by the North American Aerospace Defense Command (NORAD). It catalogs and determines trajectories and orbital decay rates for all objects that can be observed and tracked by its ground-based radar systems. Currently, NORAD is capable of tracking objects as small as 4-10 cm in diameter. Those data show that the LEO environment is crowded with space debris. At this time, it is accepted that the population density of orbital debris is not yet prohibitive for spacecraft. However, this could easily change, particularly if any major collisions occur. A large effort has gone into determining the future amount and type of orbital debris. Even if no more launches were made, the level of orbital debris is expected to continue to grow from continuing collisions that generate more fragments. A literature search was conducted to determine primary types of debris and their population distributions to conceptualize the design of the debris collector. D. Kessler<sup>(1)</sup> has documented the growth and size of orbital debris in LEO and has targeted specific regions that need immediate debris removal. These regions are ranked by likelihood of impending collisions. The present design study has focused on developing methods for collection and removal of debris in regions that contain large objects in collisionally unstable orbits. By collisionally unstable, it is meant that the population density of objects of a particular orbital interval is sufficiently high that there is a significant probability of a self-sustaining series of collisions occurring from a single initial collision. The main reasons for the decision to target large objects are that large pieces of debris are relatively easy to capture and there is a dangerous potential for larger objects to dis-

integrate into millions of postcollision fragments. The exact regions of interest lie between altitudes of 700 and 1000 km, and between angles of inclination of 70° and 85°.

The debris in this region is largely of Soviet origin<sup>(2,3)</sup>. The initial target selection process focused on possible types of debris that could be collected. In this region the Soviets deploy three types of satellites: navigation, oceanographic, and ferret. Many of these satellites are accompanied by their associated spent second-stage booster rockets. Finally, there is a very large number of fragments that have been generated by these satellite programs. Evaluation of the debris types show that the second stage of the Cosmos C-1B booster has many features that argue for priority in cleanup. It is present in large quantity, it presents a very large target cross-section to possible debris collisions, and rocket bodies have the tendency to spontaneously explode due to failure of fuel tanks.

An in-depth survey showed that the population of orbiting Cosmos C-1B second-stage boosters was sufficiently high to justify them as a specific target for removal. There are 59 Cosmos C-1B rocket bodies at an angle of inclination of 82.9°. Their distribution at this angle of inclination over various altitudes is shown in Fig. 1.

Restricting attention to C-1B boosters, the problem is determining exactly what type of motion the orbiting booster might possess. J. Turner of NASA Marshall Space Flight Center provided results from a Martin Marietta Corporation study<sup>(4)</sup> that determined that these bodies evolve rapidly to a rotational motion about their major axis (principle moment of inertia), as shown in Fig. 2. It was also determined that uncontrolled bodies in LEO will typically have rotation rates of up to 7 rpm, which dictated the design requirements for this study.

To intercept a rotating body in space, a conceptual orbital debris collector (ODC) kit was developed that was to be mounted aboard the orbital maneuvering vehicle (OMV). The OMV was assumed to provide all power, tracking, and orbital transport needs, placing further limits on the present design. The two main features of the current kit are its spin table and arm/cradle assemblies. The required spin table was a flat circular plate 14' in diameter and 1" thick. It provided the rotating

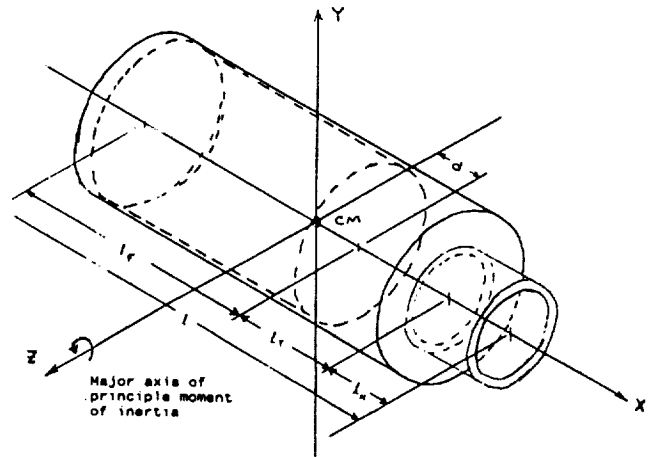


Fig. 2. Rotational motion of rocket bodies in low Earth orbit.

base for the robotic retrieval arms. The current design utilizes a DC motor to provide the torque required to adjust the spin table's angular velocity to that of the rotating rocket body. Also included in this design, for purposes of postcapture deceleration, is a compressed gas diaphragm brake mechanism. The brake mechanism has been designed to stop all rotational motion of a captured Cosmos C-1B within five minutes of brake initiation. The other main components of the ODC kit are the robotic arms and cradles. Figure 3 shows a three-dimensional CADAM graphic illustration of the proposed conceptual kit. The arms were analyzed through the use of NASTRAN. Aluminum tubing with an outer diameter of 8 cm and an inner diameter of 6 cm was chosen as the construction material for the structure. The chosen dimensions provided a large factor of safety in terms of the estimated applied load.

A complete mechanisms analysis was performed to determine a configuration that could exhibit rectilinear motion. The ability to perform rectilinear motion was deemed important because

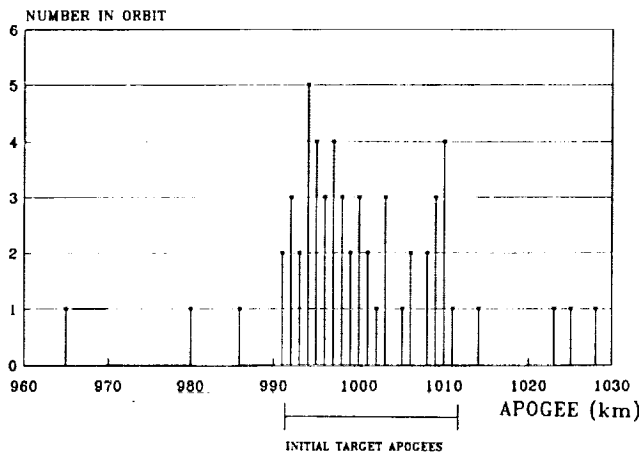


Fig. 1. Distribution of Cosmos C-1B rocket bodies.

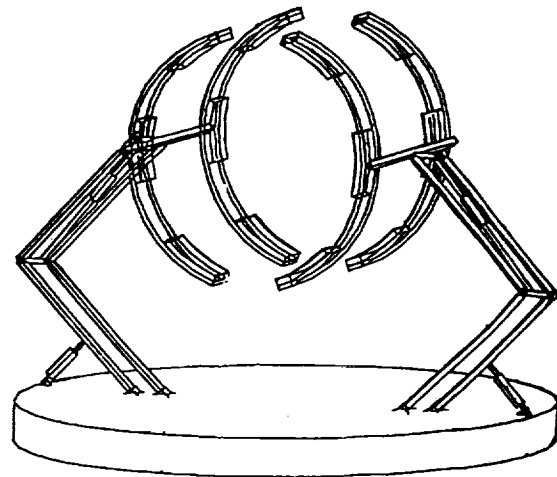


Fig. 3. Conceptualized orbital debris collector.

it would free any operator or operating system of anticipating the final landing point. Errors at this phase of operation could result in setting the body into chaotic motion, thus destroying the ODC/OMV assembly. For the rectilinear motion a double four-bar mechanism was selected. The motion of this mechanism is to be controlled by linear motor actuators, for which position and velocity requirements have been computed. It is important to note that the cradle dimensions were sized specifically for the C-1B, and that soft contact pads are to be placed, as shown in Fig. 3, on the cradles to minimize contact jarring.

Several calculations of velocity change necessary to deorbit the captured debris proved the feasibility of an OMV/ODC disposal mission in terms of requiring OMV performance levels well within the capabilities of the OMV thrusters. However, more work is needed to determine exact fuel requirements and mission utility limits. Sample missions were outlined to demonstrate the various stages and modes of operation required for particular missions. More important features of these sample missions included the use of the space shuttle for deployment of the assembled OMV/ODC and the use of a matched orbital velocity for initial approach to minimize plume impingement.

Future work on this project should include optimizing the configuration of the arms using more advanced materials, such as Kevlar or Spectra Fiber. More orbital mechanics must be done to obtain more precise data on fuel consumption and ranges of missions. It is also recommended that an experimental program be set up to determine structural loads and control system performance at rendezvous as well as to study the effects of misaligned interceptions.

### SPACE STATION TRUSS DESIGN

While NASA has been working on Space Station *Freedom* designs for over 10 years, they have been plagued by budgetary constraints. Recent budget problems have forced NASA engineers to look for alternative designs. Since the basic truss structure is a key element in any space station design, the purpose of this project is to define an alternative truss design for the space station and compare it with the original one. The alternative design had to meet the functional requirements established by NASA and by congressional mandates.

The functional requirements are mission oriented. The truss structure must serve as the backbone of the station and secure the habitat and laboratory modules. It must carry the photovoltaic (PV) arrays that provide power to the crew and scientists aboard the station. Also, the truss structure must have an effective life of at least 30 years and be capable of withstanding a catastrophic failure of a single member. Therefore, the truss structure must maintain the structural and geometric stability of the station as a whole. Congress has determined that the space station should be easily assembled in space and has dictated that the cost be much less than estimated originally. Therefore, this design group has studied an alternative truss structure design concept that satisfies the functional requirements mentioned above and addresses the congressional mandates. As seen in Fig. 4, the alternative design employs an eight-sided regular polygon with a nominal 4 m diameter (between opposite sides). Each octagonal element is separated by 1-m truss members and diagonal stiffeners opposite in direction along the surface.

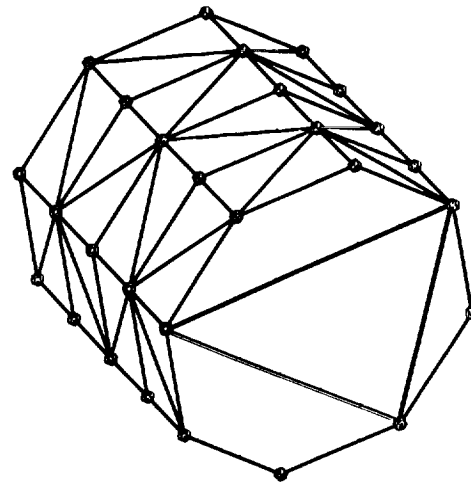


Fig. 4. Schematic of basic structural element for alternative design.

Internally, a triangular truss assembly provides additional stiffness. Each internal triangular stiffener is placed longitudinally, every 4 m. Overall, the alternate design is cylindrical and approximately 100 m long. The truss is assumed to carry three PV arrays and several habitat/laboratory modules as shown schematically in Fig. 5. Each shuttle flight will deliver a 12-m long, preassembled section of the station. This assembly approach reduces dramatically the amount of time required to construct the station in orbit. It was estimated that 17 shuttle flights will be required to deliver all sections of the space station truss to LEO.

Analysis of the alternative design was performed using NASTRAN/PATRAN. The design was compared to the original space station truss design for evaluation. A Warren-type truss was implemented in the original or baseline design. The

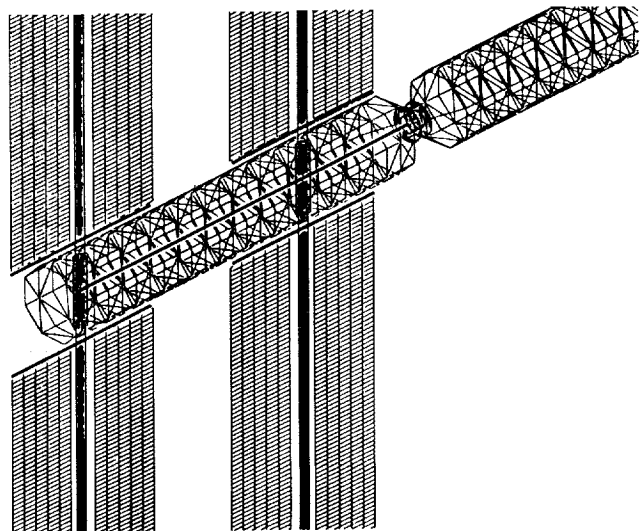


Fig. 5. Schematic of structural module attached to solar array.

deflection estimates, obtained from a static analysis, showed that the alternative truss was superior to the original design. Vibrational results of the design have not been finalized yet. Therefore, additional work should be performed on the vibrational characteristics of the alternative space station truss. The estimated number of shuttle flights required for the alternative design was approximately half that required by the original design and less time was required to construct the preassembled truss, thus reducing the total EVA time.

**ELASTIC LOOP TRACK DESIGN**

An Elastic Loop Mobility System (ELMS) design was selected as the traction system for Old Dominion University's 1990 Lunar Construction Utility Vehicle (LCUV) design<sup>(5)</sup>. The concept was studied previously by Lockheed Corporation<sup>(6)</sup> for use on a Mars explorer vehicle. The goal of the 1991 design group was to evolve the ELMS hardware sufficiently to enable testing and evaluation.

The ELMS combines the traction capabilities of tracks with the light weight and relatively low power consumption of wheels. The ELMS employs an elastic loop that grips the lunar soil in a manner similar to a traction chain on a bulldozer. Unlike a chain-link track, the elastic track was made of a single band of material shaped in a loop. In addition to transporting the body of the vehicle, the ELMS protected the instrumentation of the LCUV. The two loops also assisted in the suspension of the LCUV by suspending the drive drums above rocks and other obstacles that would otherwise jar the vehicle.

As can be seen in Fig. 6, the elastic loop rides on two drive drums. Tension on the loop is supplied by the spring assemblies that are mounted onto pivot plates. Two rollers on each loopwheel assembly provide guidance and aide in keeping proper tension on the loop. A 22-gauge, type-304 stainless steel sheet was selected for elastic loop construction. Unfortunately, the thickness chosen was too thin to suspend the vehicle as desired. However, the modified suspension system had attributes appropriate for further testing.

The suspension system must maintain proper tension on the loop and dampen vibrations. Proper operation of a suspension system prevents shock loads from reaching the hull of the LCUV.

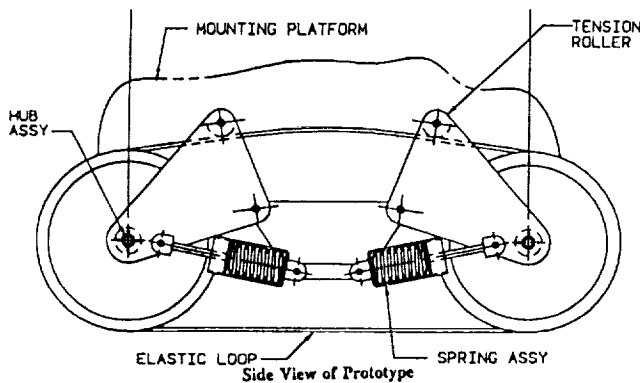


Fig. 6. Side view of elastic loop track system.

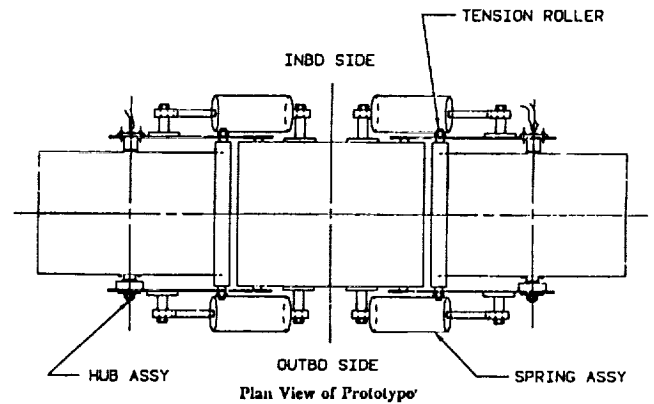


Fig. 7. Plan view of elastic loop track system.

This is accomplished by the utilization of four spring assemblies on each loopwheel as seen in Fig. 7. A close-up view of a spring assembly is shown in Fig. 8. If the spring constant,  $\kappa$ , is low the springs will allow pitching motion of the vehicle in starting and braking situations. Springs with higher  $\kappa$  values have a higher energy absorption ability than the softer springs, but little cushioning effect<sup>(7)</sup>.

Several assumptions were made in the design of the spring/suspension assemblies. These assumptions involved lunar temperature fluctuations and the lunar dust/soil problem. The nature of the lunar environment poses many problems for the design of an LCUV. The lunar day lasts 27.3 days with approximately two weeks of sunlight and two weeks of darkness. In addition, the surface temperature can range from 374 K during the lunar day to 120 K during the lunar night<sup>(8)</sup>. These temperature fluctuations will cause subsequent expansions and contractions of the spring assemblies, thus changing the tolerances. The first assumption, therefore, is that lunar temperature fluctuations will not affect tolerances. Ground laboratory studies of lunar soil samples from different regions of the lunar surface have shown that the mechanical properties of the upper layer of the lunar soil can vary over a wide range and depend on both the depth of the upper fine-grained layer and the degree of packing<sup>(9)</sup>. Final designs must protect the suspension system from lunar dust.

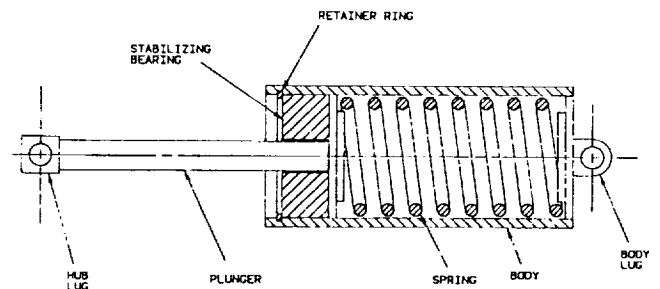


Fig. 8. Schematic of spring assembly.

The spring system incorporates coulomb damping as a method to reduce vibration. In coulomb damping, dry sliding friction forces dissipate energy from a vibrating system by opposing the motion between two members in contact. In the present case, relative motion between the plunger and body of the spring assembly is responsible for frictional damping. The energy dissipated in damping causes the magnitude of the vibration to decrease continuously until the system comes to rest.

Eight spring assemblies (four per loopwheel) were required for a complete traction system. They were attached on an adjustable track to allow them to be oriented in different directions. A loosely fitted loop would require the spring assemblies to be mounted further apart than when they were located on a tight loop. Other items used to maintain tension on the loop were the tension rollers (see Fig. 7). In order to guide the loop across the suspension system, two rollers were scheduled to be mounted onto each loopwheel. However, testing of different materials for the loop demonstrated that the rollers were not required for the stainless steel loop. When necessary, the rollers and the spring assemblies could be attached to the pivot plates to provide a balanced system.

Direct current motors were used on the ELMS for both propulsion and steering. Each loop utilized two 90-V motors that were synchronized in both rotational speed and direction. By varying the voltage between the two loops, thrust could be varied between the two loops. Thus, a moment would be created that, in effect, turned the vehicle when the loops were driven in opposite directions.

The drive motors were encased in individual drive hubs to prevent lunar particles from interfering with their performance. Though variances in loop thrust were desirable for turning the vehicle, variances in motor rpm were not. Unsynchronized motors tended to imbalance the vehicle by pivoting the body forward or backward. Such a condition strained the other motors, sometimes to the point of shearing keys along the motor mounts.

In summary, an overall system design has been produced that can be used to test propulsive performance and steering. Although the 22-gauge stainless steel loop is less rigid than desired, the loop system still exhibits sufficient elasticity and damping to warrant further testing.

### PARABOLIC REFLECTOR

Recently, Costello and Swanson<sup>(10)</sup> proposed a lunar radiator design that incorporated a flat, two-sided radiator with a specular, parabolic reflector. Their analysis showed that if the edge of the rectangular radiator were on the symmetry plane of the reflector and its upper edge terminated below the focal line (Fig. 9), improved lunar-daytime heat rejection could be accomplished when the reflector tracked the Sun. A system was built to test their predictions.

A cylindrical vacuum chamber (12" diameter by 12" high) was built that could accommodate a parabolic reflector with a 6" x 8" aperture. The focal length of the reflector was 2.5" and the infrared radiator unit was constructed as a sandwiched, electrically heated 2" x 6" plate. Solar heating was simulated using a sun lamp that was columnated through a Fresnel lens. Both units were located outside the vacuum chamber above a window located in the chamber's top surface. The inner

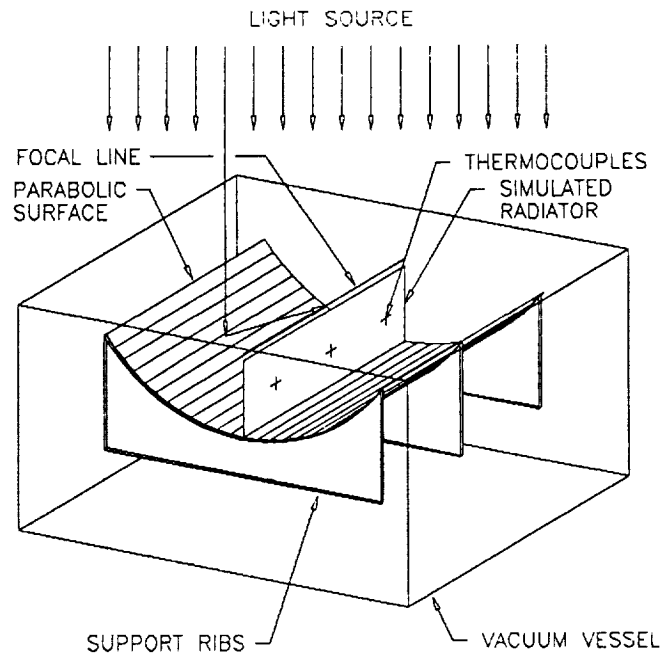


Fig. 9. Schematic view of radiator-reflector experiment.

surfaces of the vacuum chamber were coated with flat black paint and the cylindrical chamber wall was cooled using liquid nitrogen to simulate deep space.

The reflector contour was cut from wood using a numerically controlled milling machine and the reflector surface was produced using a thin layer of Kapton coated with vacuum-deposited aluminum. The infrared heater-plate was coated with flat black paint and a thermocouple was epoxied between the plates and the inner resistive heating element.

Preliminary tests were conducted that measured the transient rate at which the reflected and unreflected radiator was heated and cooled in the presence of the simulated solar heat source. Both sets of measurements showed that the reflected radiator was more efficient than the unreflected unit. However, the tests were not performed with adequate control to permit anything but qualitative interpretation. It is anticipated that an upgraded version of this system will be developed in time for the 1992 conference.

### METHANE ENGINE OPERATION ON MARS

If carbon dioxide and water are the feedstock ingredients for propellant production systems on Mars, methane and oxygen are the logical products. A fully operational chemical plant will produce a stoichiometric mix of methane and oxygen products and the energy required to produce those should be minimized. As a result, a dedicated propellant plant is most efficient when oxygen and methane are used in stoichiometric proportions. However, engine combustion temperatures are excessive for stoichiometric combustion, a noncombustible diluent is preferred to either fuel-rich or oxidizer-rich combustion to avoid wasting methane or oxygen. A logical diluent on Mars would

be unprocessed Mars atmosphere. Depending on the engine operating conditions, the atmospheric gas could be mixed using either a "supercharger" or by carrying precompressed gas. Regardless of the form of supply, questions concerning the range of acceptable levels of carbon dioxide for efficient engine operation should be addressed. Under what operating conditions are performance and operability requirements met without resulting in significant carbon buildup or without causing other processes to occur that limit engine reliability, maintainability, or performance?

A Megatech Mark III laboratory engine was modified to use gaseous methane, oxygen, and carbon dioxide as the fuel and oxidizer mixture. The original unit was a 4-stroke, 0.5-horsepower (370 W) engine, using methanol. The unit was modified so that gaseous fuel, oxidizer, and carbon dioxide were supplied through independently valved lines, and each flow was monitored via rotometers, as shown in Fig. 10. The compression ratio of the engine could be varied between 3 and 4. Preliminary tests were conducted operating the engine at 3:1. Typical engine performance curves for a mixture of 0.25 CH<sub>4</sub>, 0.5 O<sub>2</sub>, and 0.25 CO<sub>2</sub> are shown in Figs. 11 and 12.

Unlike a liquid-fueled, air-oxidizer engine, the pressurized fuel and oxidizer were capable of providing some work via the pressurization of the cylinder. Hence, the performance of the engine was corrected by deducting the amount of work that could be extracted via adiabatic expansion of the propellant products.

Initial tests showed that the engine did not operate in a "steady-state" mode in the sense that the crank shaft speed (rpm) varied cyclically during controlled fuel-oxidizer supply operation. The cyclic behavior was also observable via changes in the color of the combusting gases (which could be monitored through the glass cylinder wall). Further testing is required to establish operating envelopes for Mars applications.

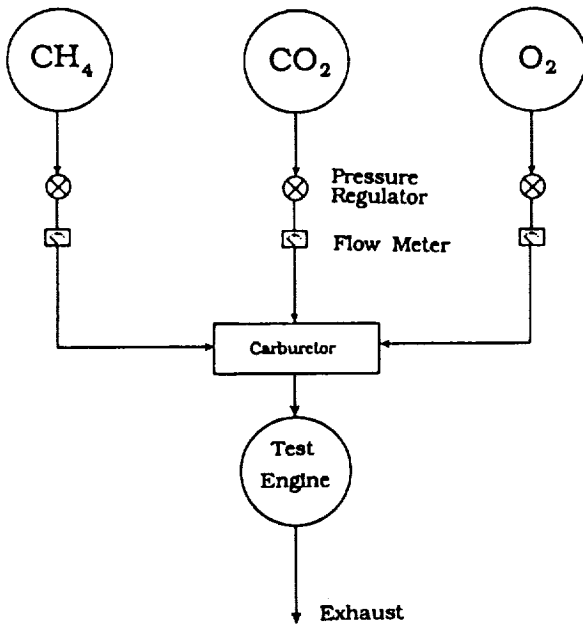


Fig. 10. Schematic of gas supply system for engine tests.

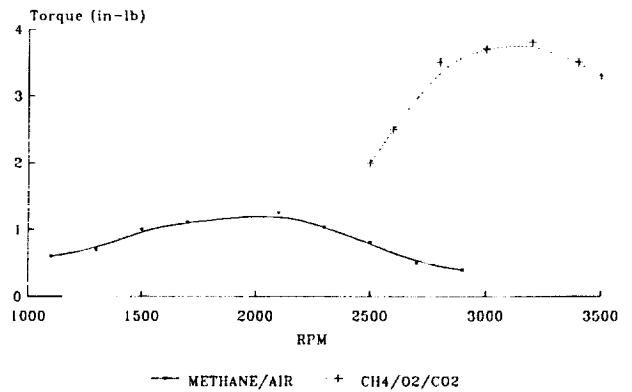


Fig. 11. Comparison of engine torque performance for methane/air combustion with CH<sub>4</sub>, CO<sub>2</sub>, 2O<sub>2</sub>.

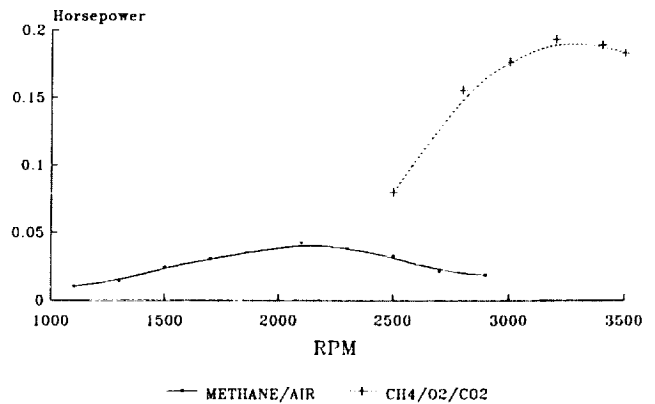


Fig. 12. Comparison of engine horsepower performance for methane/air with CH<sub>4</sub>, CO<sub>2</sub>, 2O<sub>2</sub>.

### MARS OXYGEN PROCESSOR

Production of oxygen from Mars' atmosphere was identified in 1979 as an early opportunity for extraterrestrial resource utilization at Mars<sup>(11)</sup>. Subsequently, a demonstration system was designed and built with support from the Planetary Society and USRA that produces oxygen from simulated martian atmosphere<sup>(12)</sup>. Operation and evaluation of that system has continued to evolve, but difficulties have been experienced in performing tests below 1 bar pressure. Air leaks have compromised the experiments performed at simulated martian operating conditions. A design group was charged with evaluating the instrumentation and system piping to determine how to eliminate leaks and modify the instrumentation to measure system performance more accurately.

The present Mars oxygen processor system is shown schematically in Fig. 13. Testing showed that the original piping layout had employed three types of stainless steel tubing with leaks produced from one tubing type. In addition, the procedure

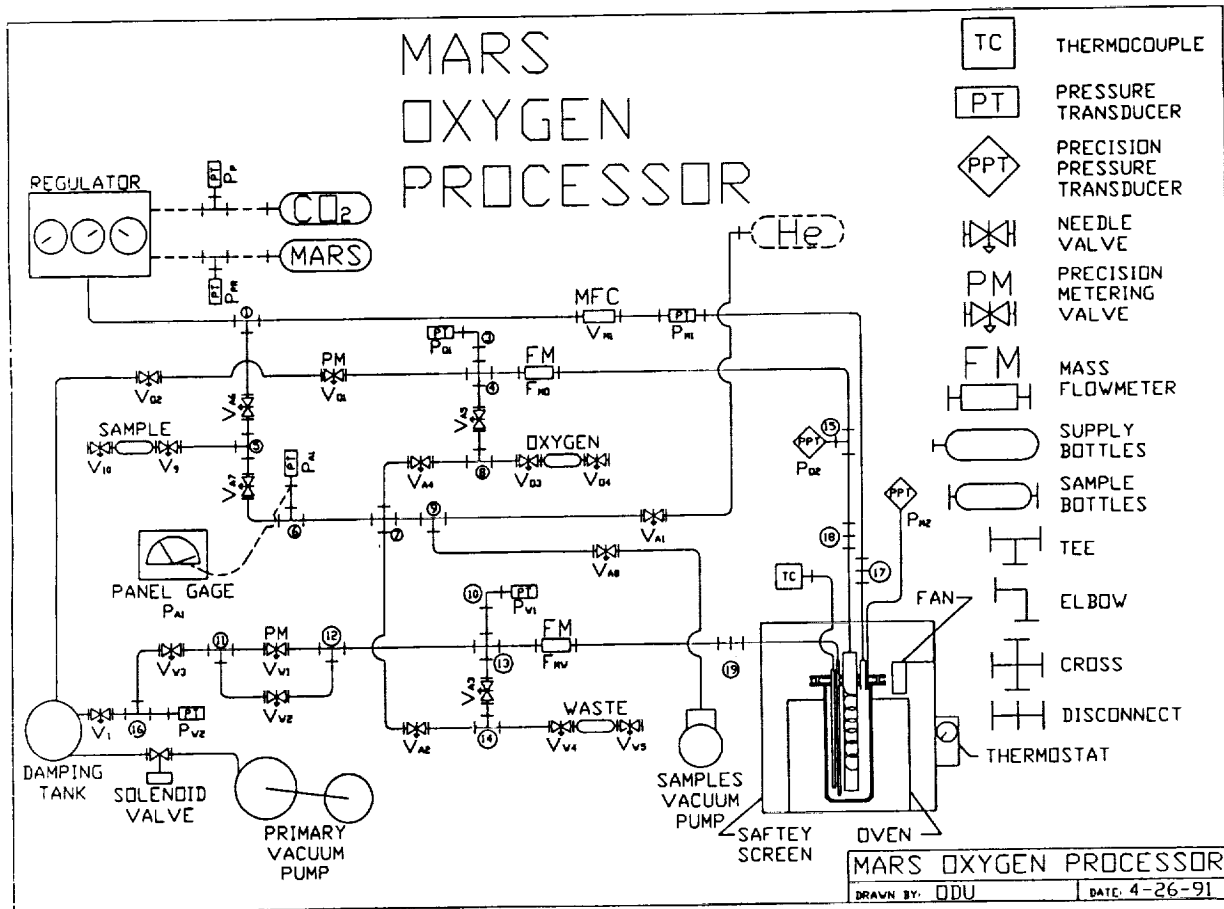


Fig. 13. Schematic of Mars oxygen processor layout.

used to disassemble and reassemble the tubing connections produced leaks. Tubing was standardized and procedures were developed to control the system assembly process. A procedure was also developed that enabled the pressure transducers, employed throughout the layout, to be checked periodically against a calibrated reference source. While these aspects of the system design were tedious (including discovery of a programming error in reading temperature via the data acquisition system), the oxygen processor unit is now capable of low-pressure operation. Tests will be run during the summer of 1992.

**CONCLUSIONS**

Students have engaged in space system design projects ranging from conceptual design of an orbital debris capture system through developing procedures to improve measurement quality for operational hardware. The space debris capturing strategy is both novel and worthy of further consideration by NASA. A specific orbital volume 82.9° inclination, 1000 km altitude contains 59 spent Soviet C1-B rocket bodies. The hardware-oriented projects have all evolved toward producing useful systems that can ultimately lead to publication-quality results.

**REFERENCES**

1. Kessler D. J. (1989) Current orbital debris environment. In *Orbital Debris from Upper Stage Breakup* (J. P. Loftus Jr., ed.). *Prog. Astronaut. Aeronaut.*, 121, 2-12.
2. King-Helle D. G. et al. (1987) *The RAE Table of Earth Satellites (1957-1986)*. Stockton Press, New York.
3. NASA Office of Public Affairs (1991) *Satellite Situation Report*, Vol. 27, No. 4, NASA Goddard Space Flight Center, Greenbelt, Maryland.
4. Cable D. A. et al. (1986) *Concept Definition Study for Recovery of Tumbling Satellites, Vol. 1*. Executive Summary, Martin Marietta, Denver Aerospace Division, Contractor Report MCR-86-1329, (NASA Contract NAS8-36609).
5. Old Dominion University. (1990) Design of an autonomous lunar construction vehicle. In *Proc. 6th Annual Summer Conference*, pp. 169-173. NASA/USRA University Advanced Design Program, NASA Lewis Research Center, NASA CR-187041.
6. Trautwein W. (1972) *Design, Fabrication and Delivery of an Improved Elastic Single Loop Mobility System (ELMS)*. Lockheed Missiles and Space Co., NASA Contractor Report NASA CR-123841.
7. Hohl G. H. Torsion-bar spring and damping systems of tracked vehicles. *J. Terramechanics*, 22, pp. 195-196.
8. *The Lunar Split Mission: A Robot Constructed Lunar Base Scenario*, Summer Design Report for the NASA/USRA Advanced Space Design Program, p. 62. NASA Johnson Space Center.
9. Lenonovich A. K. et al. (1972) Investigations of the mechanical properties of the lunar soil along the path of Lunakhod 1. *Space Research XII*, Akademie-Verlag, Berlin.

10. Costello F. A. and Swanson T. D., (1990) *Lunar Radiators with Specular Reflectors*. AIAA/ASME 5th Joint Thermophysics and Heat Transfer Conference, Seattle, Washington.
11. Stancati M. L., Niehoff J. C., Wells W. C. and Ash R. L., (1979) *Remote Automated Propellant Production: A New Potential for Round Trip Spacecraft*. AIAA Conference on Advanced Technology for Future Space Systems, NASA Langley Research Center, AIAA Paper No. 79-0906.
12. Ash R. L., Werne J. A., and Haywood M. B., (1989) pp. 479-487. Design of a Mars oxygen processor In *The Case for Mars III*, (C. Stoker, ed.), AAS Science and Technology Series, 75.

**MARS SAMPLE RETURN MISSION  
TWO ALTERNATE SCENARIOS  
PENNSYLVANIA STATE UNIVERSITY**

534-66  
160610  
P. 4

Two scenarios for accomplishing a Mars Sample Return mission are presented herein. Mission A is a low-cost, low-mass scenario, while Mission B is a high-technology, high-science alternative.

Mission A begins with the launch of one Titan IV rocket with a Centaur G' upper stage. The Centaur performs the trans-Mars injection burn and is then released. The payload consists of two lander packages and the orbital transfer vehicle, which is responsible for supporting the landers during launch and interplanetary cruise. Near Mars, the landers separate—one bound for a polar site and the other for an equatorial site. After descending to the surface, the landers deploy small, local rovers to collect samples. The rovers return these samples to the landers for loading on the direct return rockets, which return the samples directly to the Earth's surface.

Mission B starts with four Titan IV launches, used to place the components of the planetary transfer vehicle (PTV) into orbit. The fourth launch payload is able to move to assemble the entire vehicle by simple docking routines. Once complete, the PTV begins a low-thrust trajectory out from low Earth orbit, through interplanetary space, and into low Mars orbit. It deploys a communications satellite into a one-half sol orbit and then releases the lander package at 500 km altitude. The lander package contains the lander, the Mars ascent vehicle (MAV), two lighter-than-air rovers (called Aereons), and one conventional land rover. The entire package is contained within a biconic aeroshell. After release from the PTV, the lander package descends to the surface, where all three rovers are released to collect samples and map the terrain. The Aereons attempt to circumnavigate Mars and collect samples from a wide variety of sites, while the land rover examines a local area more thoroughly. The Aereons are equipped with small sample return rockets that can return their samples to the lander in the event that an Aereon is incapable of returning to the lander itself. Once all samples have been collected, they are loaded onto the MAV and launched into orbit. The PTV then collects the samples and returns them to Earth orbit for recovery.

### INTRODUCTION

Penn State's design project for the 1990-91 academic year was the Mars Sample Return mission, currently under study by the Human and Robotic Spacecraft Office (HRSO) at Johnson Space Center.

The Mars Rover Sample Return Mission Science Objectives Document<sup>(1)</sup> states, "The objectives of the MRSR mission are twofold: (1) To reconstruct the geological, climatological, and biological history of Mars and determine the nature of its near-surface materials, (2) To obtain key environmental information and test key technologies necessary to maximize the safety and effectiveness of eventual human exploration."

A Mars Sample Return mission will "address the above goals by doing in situ analyses and returning a suite of intelligently selected samples representative of the planet's diversity."

The students participating in this year's design class were given a list of desired sample types and amounts, with the task being to acquire some or all of the sample set and return it to Earth by the year 2010. For the Fall '90 semester, the class was challenged to examine several alternative methods of achieving their mission and to evaluate the alternatives based on their own established criteria. For the Spring semester, the class was divided into two mission design teams, and each was given a mission scenario compiled from interesting features of the previous semester's designs. The two teams were composed of several groups, with each being responsible for a specific mission element of its team's scenario. Figures 1 and 2 depict the two mission scenarios. The suggested sample set is presented in Table 1.

This class comprises the required senior-level design sequence at Penn State and consists of two credits of conceptual and preliminary design in the Fall, followed by two credits of detailed design in the Spring.

TABLE 1. Suggested sample set.

|                      |                     |
|----------------------|---------------------|
| Regolith             | 50 g                |
| Rock Fragments/Chips | 1000 g              |
| Pebbles              | 2085 g              |
| Boulder Specimens    | 70 g                |
| Core Sample          | 1256 g              |
| Atmosphere           | 160 cm <sup>3</sup> |

### MISSION A

Mission A is a low-cost, low-mass mission scenario satisfying the following mission requirements:

1. All mission elements had to fit on one launch vehicle without assembly or construction in Earth orbit;
2. The trans-Mars injection had to be performed by the upper stage on the launch vehicle;
3. No Mars orbit operations, such as a satellite or a rendezvous, were permitted;
4. The mission had to use two landers, each with a small, land-based rover and a direct launch-to-Earth return vehicle.

These requirements were developed after a review of the previous semester's preliminary design work.

The scenario designed to meet these requirements can be seen in Fig. 1. A single Titan IV/Centaur G' launch is used to boost the payload on a trajectory to Mars. The payload consists

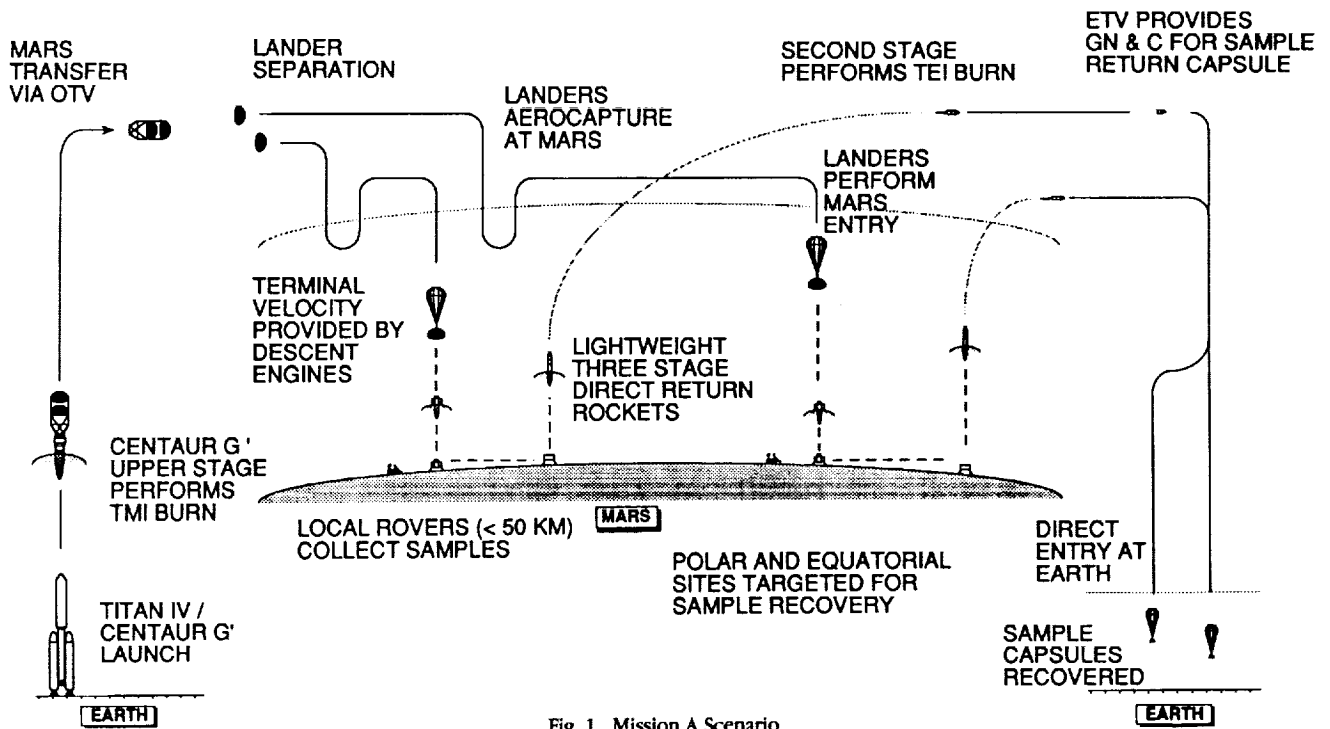


Fig. 1. Mission A Scenario

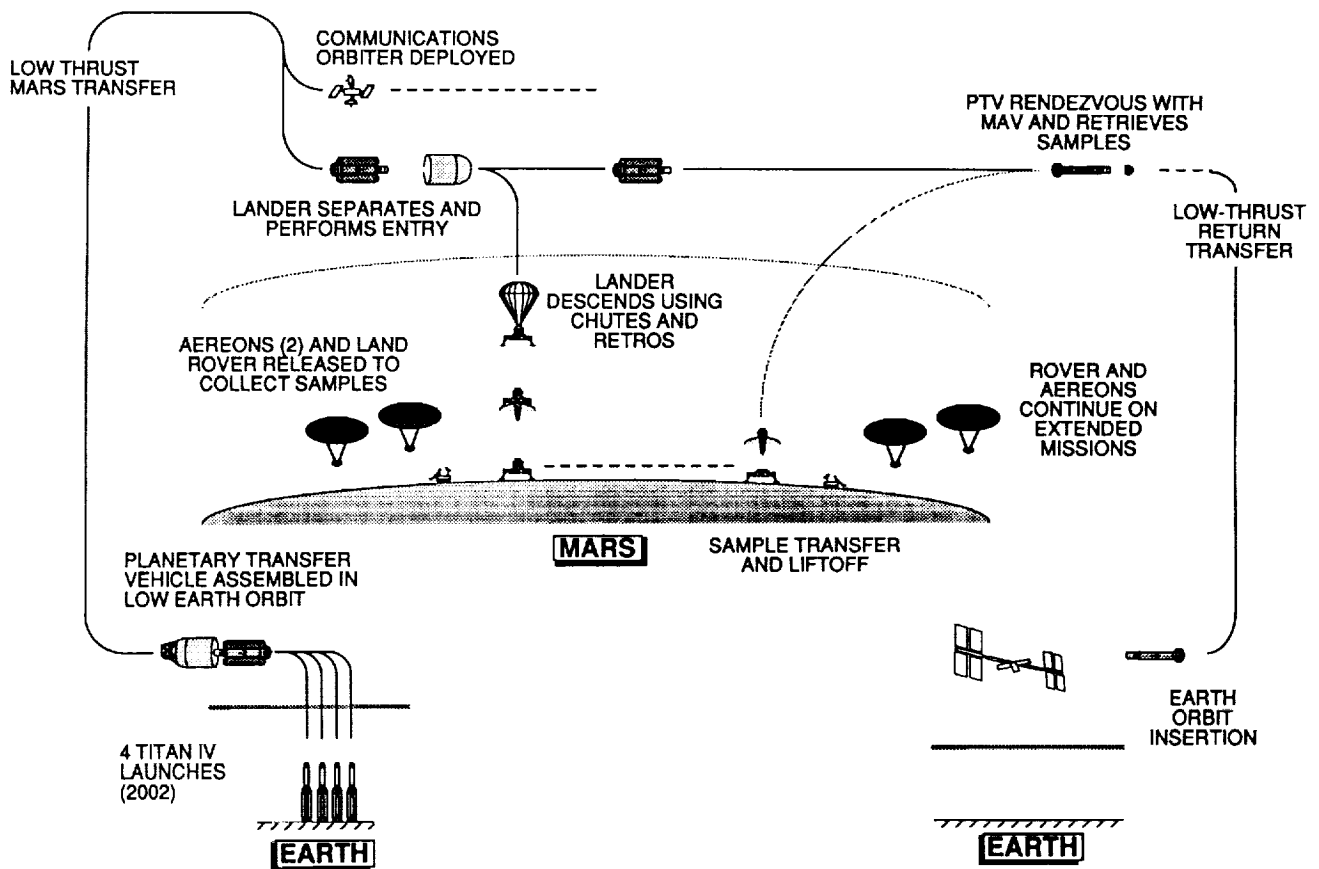


Fig. 2. Mission B Scenario

of two lander vehicles supported by an orbital transfer vehicle (OTV). The OTV supports the landers during launch and interplanetary cruise and uses shared systems to reduce mass and avoid unnecessary duplication. This means that the OTV has access to the landers' communications, power, and computer systems. It does, however, have its own attitude and control system to make course corrections as necessary. As the OTV approaches Mars, it is jettisoned, and the two landers continue on independently—one bound for a polar landing site and one for an equatorial site.

The landers aerocapture into separate orbits, and then proceed to land. They have blunt aeroshells similar in shape to those used on the Viking missions, but made to withstand both an aerocapture and an atmospheric entry. Once the entry process is complete, the aeroshells are jettisoned, and the parachutes deployed. The parachutes slow the landers to a velocity of approximately 60 m/s at an altitude of 1.5 km. At this time, the parachutes are discarded, and the retrorockets begin to fire. There are four retrorockets per lander, and they use a hydrazine/ NTO propellant combination to slow the lander for a soft landing.

Once on the surface, the landers collect a contingency sample of regolith and atmosphere to insure at least a partial mission success should a rover fail. The landers are also responsible for collecting the core sample, which they do after obtaining the contingency samples. The Mars sample acquisition vehicles (MSAVs) are then deployed.

The MSAVs are small, local rovers that range no more than 1 km from the lander. Each MSAV is an articulated, three-body, six-wheeled vehicle powered by a modular radioisotope thermoelectric generator (MOD-RTG). It is semiautonomous, and therefore dependent on instructions from Earth to execute complicated procedures. The MSAV has two arms: one for high-strength work and one for high-precision work. Both arms have access to a number of tools for acquiring samples and a variety of analysis equipment to determine the fitness of a candidate sample. Samples worth keeping are placed in small teflon bags that are then placed in a basket on the rover. When the MSAV has completed collecting samples, it returns to the lander. The lander uses its robotic arm to remove the basket from the rover and place it aboard the direct return rocket (DRR).

The DRR is a three-stage vehicle capable of returning a sample return capsule directly from the martian surface to an Earth splashdown. The first two stages are simple, solid-propellant rocket stages using an advanced, high specific impulse propellant. Together these stages move the payload into a low Mars orbit, and then perform the trans-Earth injection. The third stage of the DRR is the Earth transfer vehicle (ETV). It is based on the kinetic kill vehicle (KKV) developed for the Strategic Defense Initiative and provides guidance, navigation, and control for the sample return capsule as it returns to Earth. Once the capsule has been placed on its reentry trajectory, the ETV detaches and the capsule continues on an unpowered entry. The small size of the capsule keeps it from generating much heat, so an ablative heat shield and passive thermal control devices are sufficient to protect the samples from damage.

This mission was costed using the Advanced Space Systems Costing Model developed by Kelly Cyr at Johnson Space Center<sup>(2)</sup>. Each mission element was costed separately, and the results are shown in Table 2.

TABLE 2. Mission A costs (in millions of U.S. dollars).

|                                      |      |
|--------------------------------------|------|
| Launch Costs (Titan IV/Centaur G')   | 265  |
| Orbit Transfer Vehicle               | 552  |
| Landers (2)                          | 1746 |
| Mars Sample Acquisition Vehicles (2) | 708  |
| Direct Return Rockets (2)            | 230  |
| Total Mission Cost                   | 3236 |

### MISSION B

Mission B is a high-science-return, high-technology scenario, and was designed under the following requirements:

1. Multiple launches were permitted, but Earth-orbit assembly was limited to simple docking routines (i.e., no on-orbit construction);

2. An orbital transfer vehicle, using radioisotope engines for propulsion, was to be used to transfer all mission elements from low Earth orbit to low Mars orbit and then back again upon completion of the mission. The transfer vehicle was to remain in Mars orbit while surface operations were conducted;

3. A communications and tracking satellite was to be included and deployed in an appropriate Mars orbit;

4. A lander was required, and was to be responsible for delivering three rovers to the planet's surface. Additionally, the lander was to include an ascent vehicle that would deliver the collected samples to the waiting transfer vehicle;

5. Two of the rovers were to be small, lighter-than-air (LTA) vehicles based on the Aereon principle. These rovers were required to attempt to circumnavigate Mars, collecting small amounts of samples from a large variety of sites. In case an LTA rover failed to return sufficiently close to the lander, a minirocket could be included to attempt to launch the collected samples to the vicinity of the lander;

6. The third rover was to be a large, land-based rover responsible for investigating the area near the lander in detail. This rover was also to collect the majority of the samples, including those the LTA rovers were unable to collect due to weight limitations;

7. All rovers were to deliver their samples back to the lander for delivery to orbit via the ascent vehicle.

These requirements were developed after a review of the preliminary scenarios developed during the Fall '90 semester.

The mission designed to fulfill these requirements can be seen in Fig. 2. Four Titan IVs launch their payloads into low Earth orbit. The first two payloads consist of one tank of ammonia each. The third payload consists of the communications satellite and the lander package, which contains all the vehicles operating on the martian surface. The final launch contains the central module of the planetary transfer vehicle (PTV), which consists of the third and final ammonia tank, the sample retrieval bay, and the transfer vehicle's subsystems. The central module then maneuvers on-orbit to rendezvous with and connect to the other sections.

Once the PTV is fully assembled, it begins a low-thrust spiral out of Earth orbit. The PTV's radioisotope engines produce thrust by heating a working fluid and expanding it out from a diverging nozzle in a similar manner to a nuclear thermal engine. A

decaying radioactive isotope provides the heat. Ammonia was chosen to be the working fluid due to its relatively high density and high specific impulse. This configuration results in a total thrust of approximately 10 N, with a specific impulse between 800 and 1200 s.

Upon reaching the vicinity of Mars, the PTV spirals into a low orbit. Along the way, it releases the communications satellite into a roughly circular 9300-km orbit that has an orbital period of approximately one-half a martian day. This will allow the satellite to be in contact with each vehicle on the surface, including the Aereons, for a considerable amount of time each day.

After the PTV settles into a 500-km orbit, it releases the lander package, which subsequently begins an atmospheric entry. The lander package is contained in a biconic aeroshell that slows the lander to Mach 2 at an altitude of 6 km. At this time, the aeroshell is jettisoned, and the parachutes are deployed to slow the lander further. The conical ribbon chutes are made of Kevlar and are designed to bring the lander's speed to 60 m/s at an altitude of 1.5 km before being discarded as the retrorockets begin to fire. The retrorockets use a hydrazine/H<sub>2</sub>O<sub>2</sub> combination and slow the lander sufficiently to provide a soft landing.

Once on the ground, the lander collects the contingency samples and loads them onto the Mars ascent vehicle (MAV) prior to releasing the rovers. The rovers are then deployed to collect their samples. The landing site is at Candor Mensa, a proposed landing site for a manned mission, and has a number of geologically interesting features within range of the land rover.

The Aereons' primary mission is to collect information about the martian surface as they attempt to circumnavigate the planet. The principal means of doing this is by using the instruments on board to conduct *in situ* analysis. Additionally, the Aereons will collect a few regolith and atmospheric samples along the way. The Aereons function using the Aereon principle developed by Andrews in 1862; it holds that certain orientations of an ellipsoid balloon generate thrust as the vehicle ascends or descends. Using this thrust, the Aereon can pilot its way to a specific location with some accuracy. The Aereon is filled with hydrogen gas that is stored in tanks on the lander until the Aereons are deployed. Additionally, there are ballast balloons that can be filled with martian air as needed to cause the Aereon to ascend or descend. Once an Aereon has collected its samples (totalling no more than 7 kg per vehicle), it will attempt to return to the lander. Since the accuracy of the Aereons' navigation

may be insufficient to bring them within range of the land rover, each is equipped with a small sample return rocket with a range of approximately 200 km and capable of carrying all the Aereon's collected samples. These rockets are equipped with radio beacons so that they can be located by the land rover.

The land rover is a large, three-bodied, six-wheeled vehicle with a range of at least 200 km. It is equipped with the sample acquisition robotic system (SARS), a set of tools and scientific instruments that permit the rover to be very selective when examining a candidate sample. The SARS is also equipped with two robotic arms for acquiring the samples. A 6-degree-of-freedom (DOF) acquisition arm will perform jobs requiring high strength, while a 7-DOF manipulator arm will perform those jobs that require more precision. The rover will use the SARS to collect almost 60 kg of samples, including regolith, core samples, boulder chips, pebbles, and rock fragments. As the samples are collected, the rover will make periodic stops at the lander to have its samples loaded onto the MAV. This procedure will prevent all the samples from being lost in the case of a mission-ending accident for the rover. The rover also supports the Aereons by moving to retrieve samples from them or their sample return rockets, in the event that they are unable to return precisely to the lander.

This mission was also costed using the Advanced Space Systems Costing Model<sup>(2)</sup>. Each mission element was costed separately, and the resulting mission costs are shown in Table 3.

TABLE 3. Mission B costs (in millions of U.S. dollars).

|                               |      |
|-------------------------------|------|
| Launch Vehicles (4 Titan IVs) | 1000 |
| Planetary Transfer Vehicle    | 1200 |
| Communications Satellite      | 367  |
| Lander and MAV                | 2936 |
| Land Rover                    | 905  |
| Aereons (2)                   | 1266 |
| Total Mission Cost            | 7674 |

## REFERENCES

1. Carr M. et al. Mars Rover Sample Return: Science Objectives Document. JPL Document No. D-6247. February 1, 1989.
2. Cyr K. "Cost Estimating Methods for Advanced Space Systems." SAWE Paper No. 1856, Index Category No. 29. July 29, 1988.

**MARS HABITAT**  
**PRAIRIE VIEW A&M UNIVERSITY**

35-54  
160611  
p 11

### INTRODUCTION

The College of Engineering & Architecture at Prairie View A&M University has been participating in the NASA/USRA Advanced Design Program since 1986. The interdisciplinary nature of the program allowed the involvement of students and faculty throughout the College of Engineering & Architecture for the last five years. The research goal for the 1990-1991 year is to design a human habitat on Mars that can be used as a permanent base for 20 crew members. The research is being conducted by undergraduate students from the Department of Architecture.

### OBJECTIVE

The purpose of this study is to develop a conceptual design for a permanently manned, self-sustaining martian facility to accommodate a crew of 20 people. The goal is to incorporate the major functions required for long-term habitation in the isolation of a barren planet into a thriving ecosystem.

These functions include the living area, research laboratories, medical clinic, greenhouse, command control, materials processing, life support system, power source, and a launch pad. The harsh environment of Mars is not conducive to life as we know it. Cosmic radiation, thin atmosphere, extreme cold, dust storms, and the absence of surface water and food must be overcome for humans to survive on Mars.

### GENERAL CONCEPT

The general concept of the design is to create a comfortable, safe living environment for the 20 crew members for a stay of 6 to 12 months on Mars. This self-contained environment would accommodate five main facilities: living facilities, working facilities, service facilities, medical facilities, and a greenhouse. The main design task is to focus on the internal layout while investigating the appropriate structure, materials, and construction of these facilities.

Two different concepts, an inflatable structure and a space-frame structure have been investigated.

### MODULAR ASSEMBLY REUSABLE STRUCTURE MARS BASE (LAVAPOLIS)

#### Concept

Construct inflatable modules in a lava tube, using the modular assembly reusable structure (MARS) system (Fig. 1).

#### Site

The selection of an appropriate site is critical to the long-term success of the Mars base. An equatorial site is most economically accessed from low Mars orbit, and simplifies rendezvous maneuvers. The most striking geological features, Olympus Mons, the largest volcano in the Solar System, and Valles Marinaris, the colossal canyon, are located there.

The site chosen for Lavapolis is at the base of Ceraunius Tholus, a 115-km-wide, 22-km-high volcano in Northeast Tharsis at 24°N, 97°W, at the area where an impact crater has pulverized a 2-km-wide channel.

#### Assumption

A lava tube exists in the region described that satisfies the requirement for habitability. It must be accessible, have structural integrity, and dimensions of not less than 200 ft wide, 50 ft high, and 400 ft deep for this proposed scheme.

#### Rationale for Construction in a Lava Tube

The large covered volumes that are naturally created by the flow of molten lava underground that drains away, can provide radiation shielding for the entire base without having to move a lot of dirt. The thermal mass regulates the internal temperature to be relatively constant at any time. The environment is calm year round, minimizing the load on the HVAC system, and is protected against frequent dust storms. The time required to locate and prepare a lava tube for habitation is less than the time it would take to cover a base with 3 ft of soil. Also, the sheltered volume available in a lava tube is much larger than that which can be constructed, and requires less structural mass for the pressurized modules. The basaltic rock of a tube can be processed to form glass structural panels that can be used to seal and pressurize large segments of the lava tube for future expansion.

#### Structure

The modular assembly reusable structure (MARS) system consists of inflatable cylinders supported at the ends with lightweight aluminum rings. The rings are composed of 8 segments, 3 ft wide, which join together to form a 30-ft-diameter circle, and are spaced 30 ft on center. The cylinders are made of pneumatic material and connect the space between two rings, with the same 30-ft diameter. Attaching the circular walls made of pneumatic material to the rings on either side of the cylinder forms on MARS module (Figs. 2 and 3).

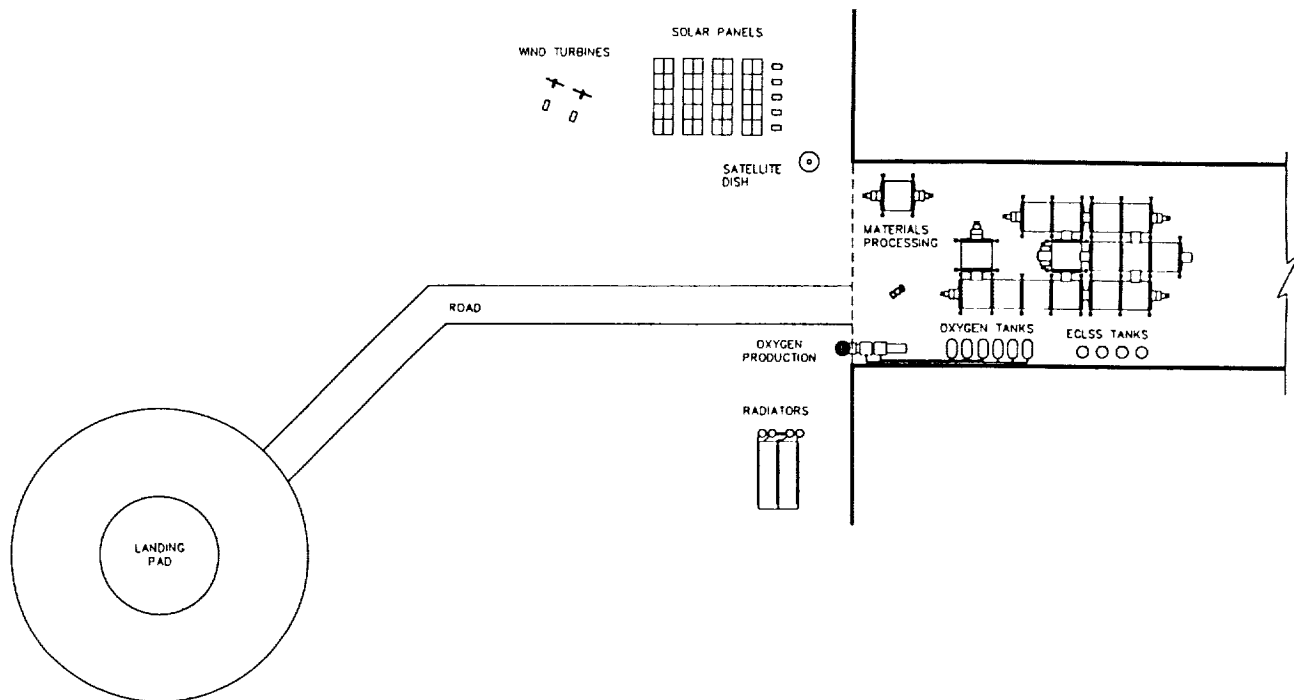


Fig. 1. Site Plan.

The floor joists span the length of the cylinder and connect to a beam spanning the ring. This beam carries the floor loads to the ring, through several short beams, to a column on either side of the ring, then down to the mat foundation. The floor and ceiling heights are variable depending upon functional requirements and can be easily modified as the needs change. Additional cylinders can be connected to the habitat without having to depressurize the existing structure. The MARS system deploys large expandable volumes using reusable, lightweight, modular components, and connections, which require minimum packing space.

#### Architecture (Exterior)

The organization of the base is a linear pattern, corresponding to the geometry of the MARS system, and contextually with the tubular nature of the site. The modules are arranged in a functional composition with resulting aesthetics derived from the orientation of the module's flat round, or convex square elevations, juxtaposed with the columns. The oblong form of adjoining cylinders with the repetitive column spacings resembles a Roman basilica, creating a sense of traditional architecture.

#### Architecture (Interior)

The interior spatial complexities are achieved through the variations in floor and ceiling heights, combined with the arrangement of inflatable furniture and partitions that allow for

long views through several open modules or define small intimate spaces (Figs. 4, 5, and 6).

Level changes of a couple of feet can be made with the use of stairs, while ladders and manual elevators are provided for separations in floors of several feet.

The sizes of internal volumes are similar to those on Earth, because any perception of home is beneficial to the psychological wellbeing of the inhabitants.

There are two means of egress from every module, one of which will lead to an air-lock toward the exterior. A group of modules can be sealed and isolated in case of contamination or fire.

#### Future Expansion

The future expansion of the base will entail the processing of basaltic rock into structural glass panels and connections. Large segments of the lava tube can be sealed and pressurized making it possible to landscape and construct buildings that incorporate architectural styles from around the world to create an international garden city.

### PREFABRICATED SPACE FRAME STRUCTURES HEXAMARS

#### Concept

The concept is to construct a space-frame structure that consists of a central core and secondary modules radiating from

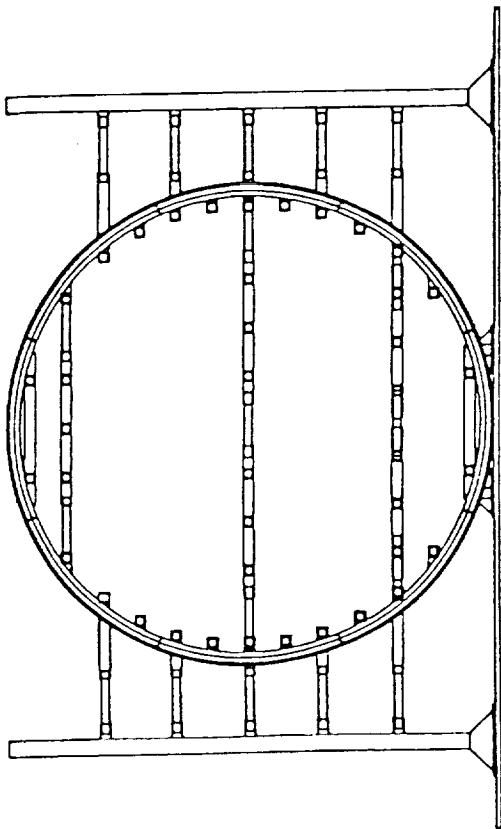


Fig. 2. Cross Section.

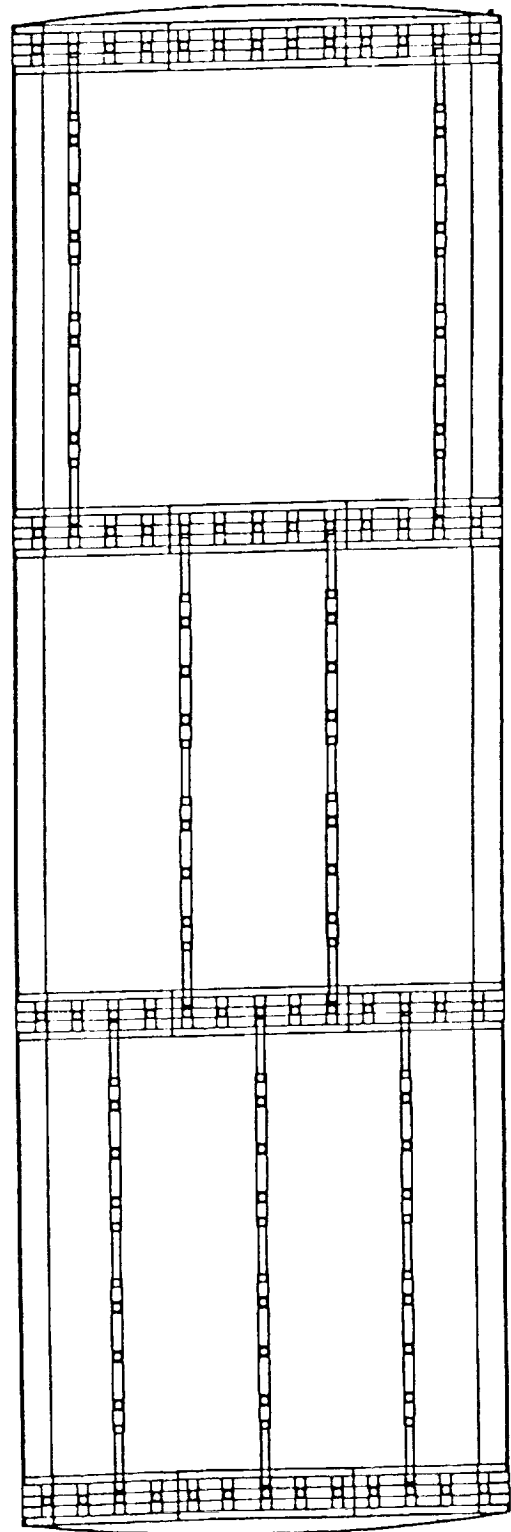


Fig. 3. Longitudinal Section.

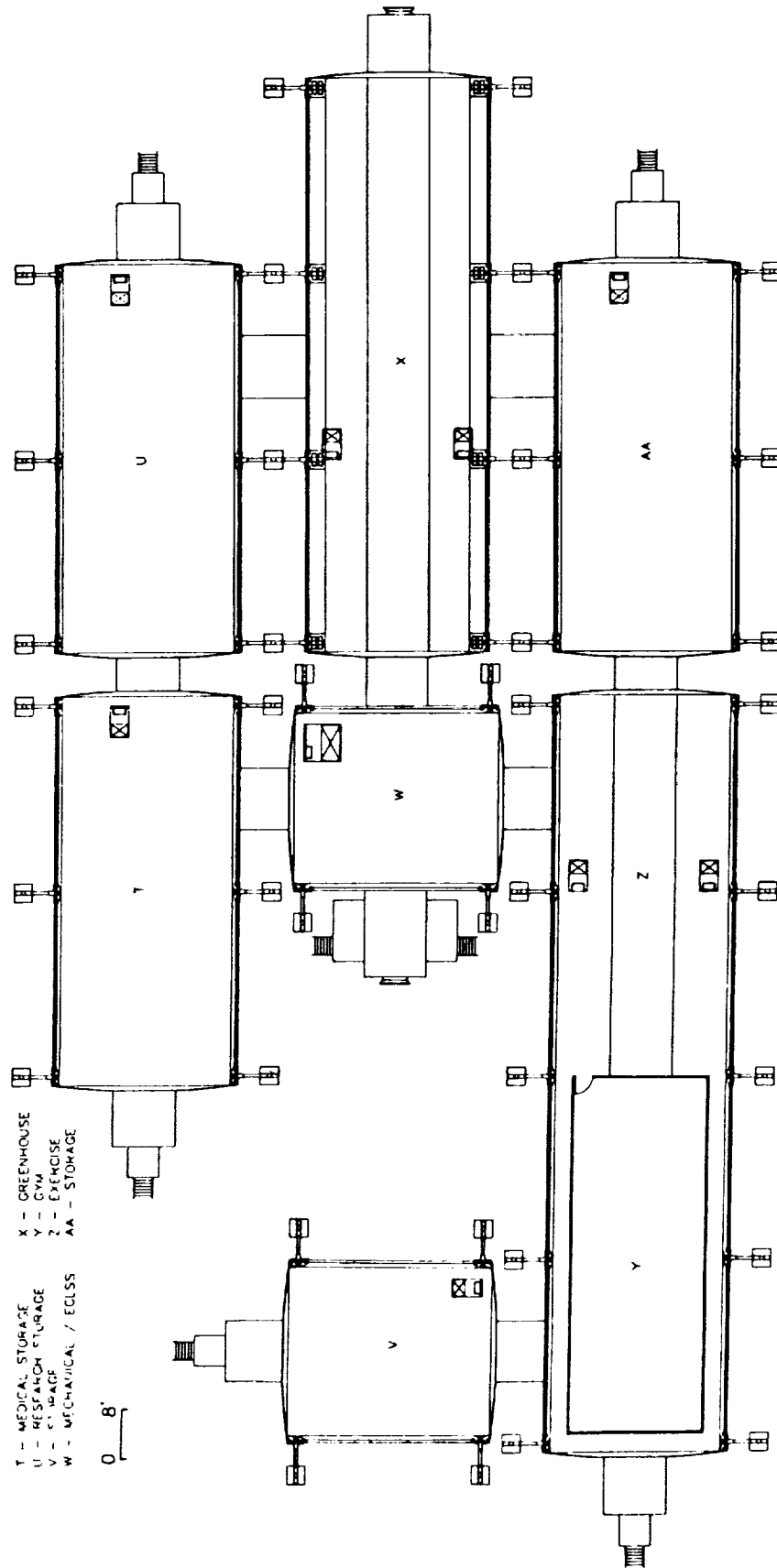


Fig. 4. First Floor Plan.

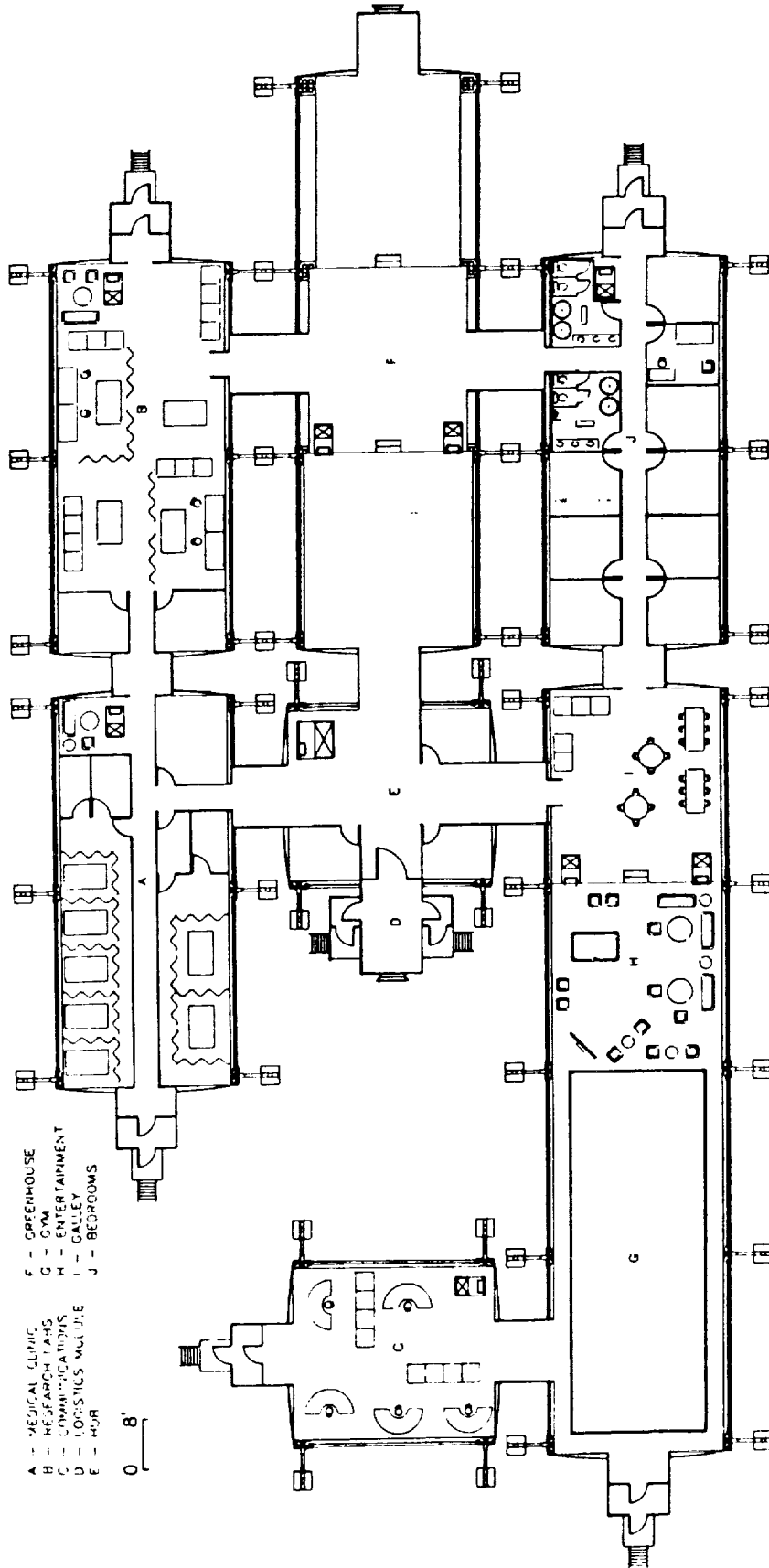


Fig. 5. Second Floor Plan.

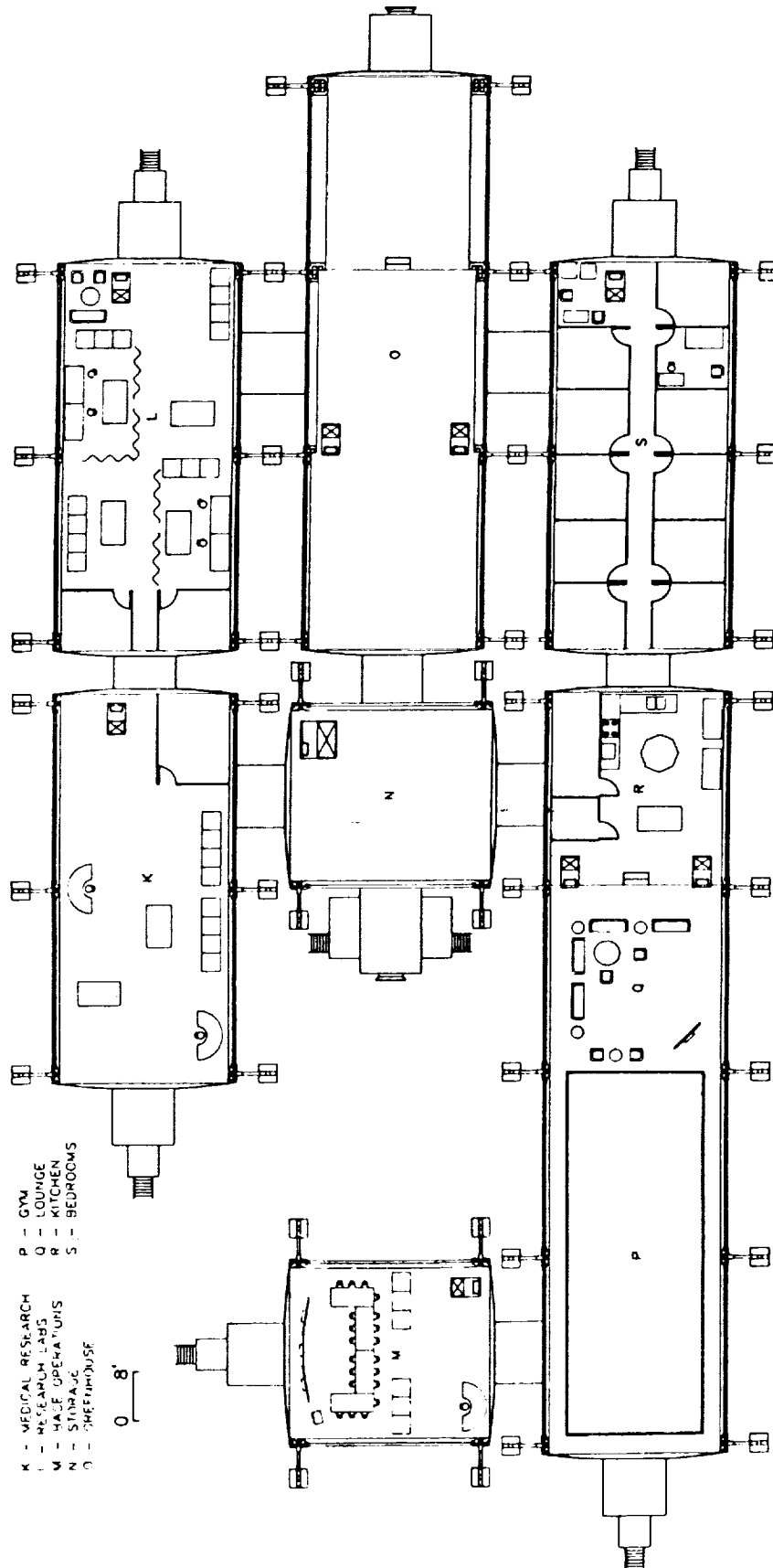


Fig. 6. Third Floor Plan.

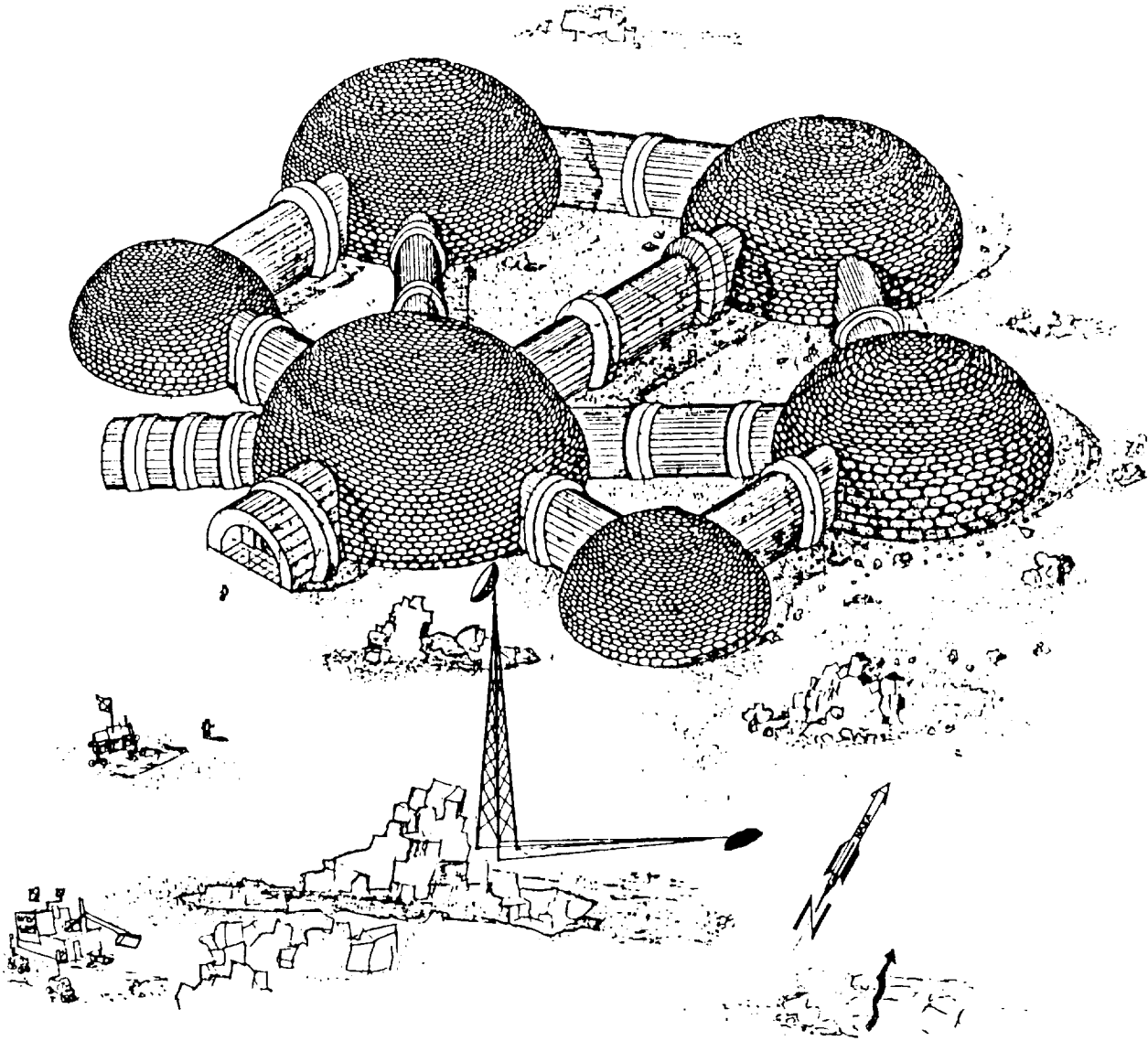


Fig. 7. Isometric of Hexamars.

the core. The sphere-shaped modules will be partially buried below the martian surface. Interchangeable structural members are used in the construction of this habitat (Figs. 7 and 8).

**Site Location**

The site location is 3°N latitude 99°E longitude between Pavonis Mons and Ascreaus Mons. The site is compatible to the angle of the spacecraft entering Mars orbit. It is also close to the equator and has relatively moderate temperature conditions.

**Assumptions**

1. There will be a temporary habitat located near or at the site of an earlier mission that satisfies the requirements for a short-term habitation.
2. The prefabricated space-frame structure, as well as other prefabricated material, will be shipped to the site before the long-term crewmembers arrive.
3. Partial construction and preparation for the long-term habitat will be done by crewmembers or robotics from a previous mission on Mars.

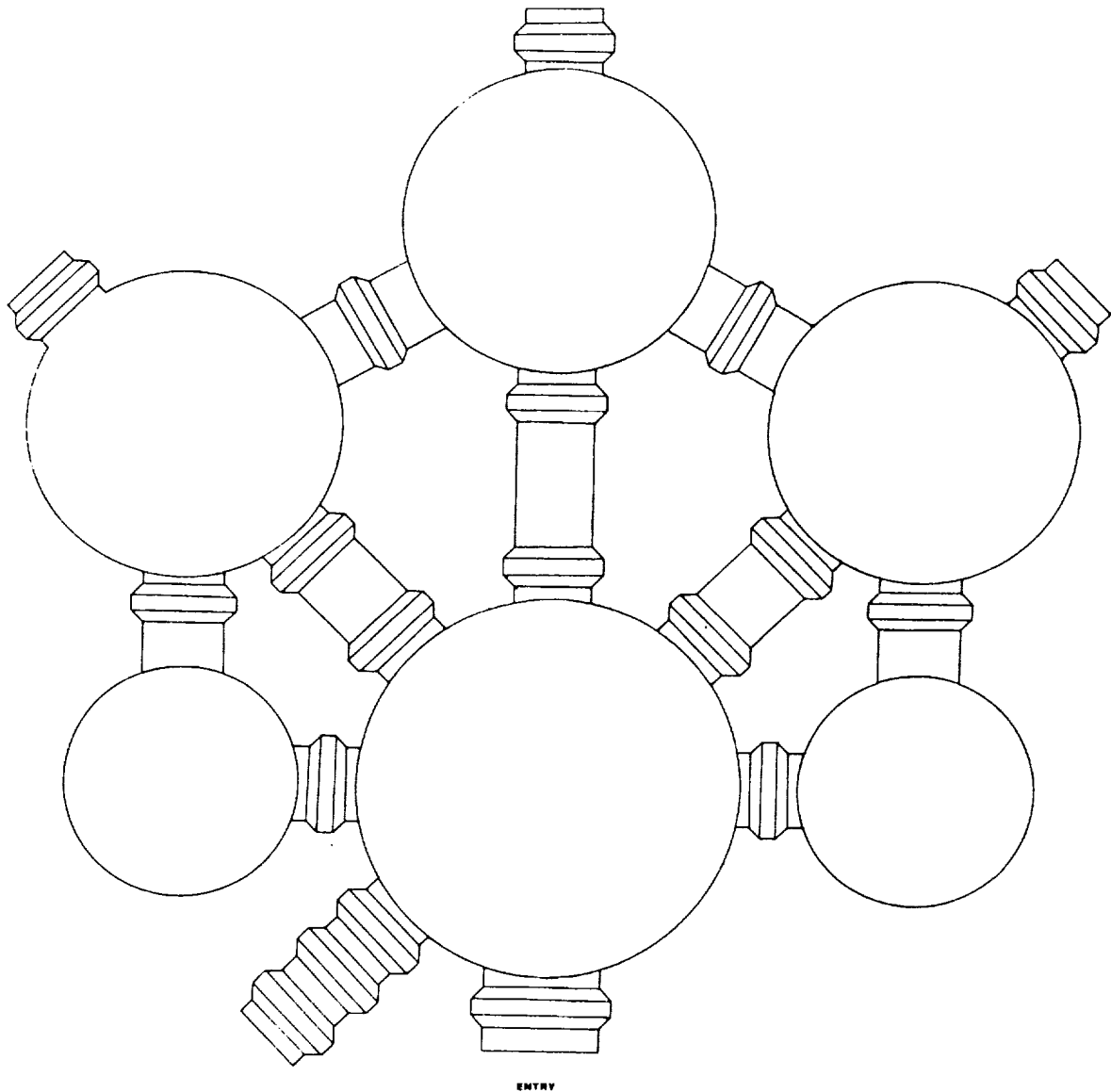


Fig. 8. Roofplan.

4. The construction of the long-term habitat will occur in phases.

#### Structure

The prefabricated frame structures are individual structural members generally fabricated in tubular shapes of metal. Each member is usually stressed axially, either in compression or tension. At the ends of each member, there is a specified connector installed to allow for both construction and expansion.

The internal structure consists of (1) six telescoping hexagonal core columns; (2) six peripheral ribs; (3) radial floorbeams; (4) circumferential joists; (5) intermittent floorjoint; and (6) secondary bracing.

A mat foundation transfers all loading of the interior to the exterior support structure from six hard points.

The module shell consists of prefabricated spare-frame and titanium panels on the exterior, with Kevlar 29 for the interior module shell wall, Nextel for floor panels, and foam-rigidized walls for partition walls.

#### Methods of Construction

##### *Steps of assembly.*

1. Create five holes and grade them for the mat foundation to be set in them.
2. After the self-deploying foundation is in place, the space frame structure is connected to the foundation.

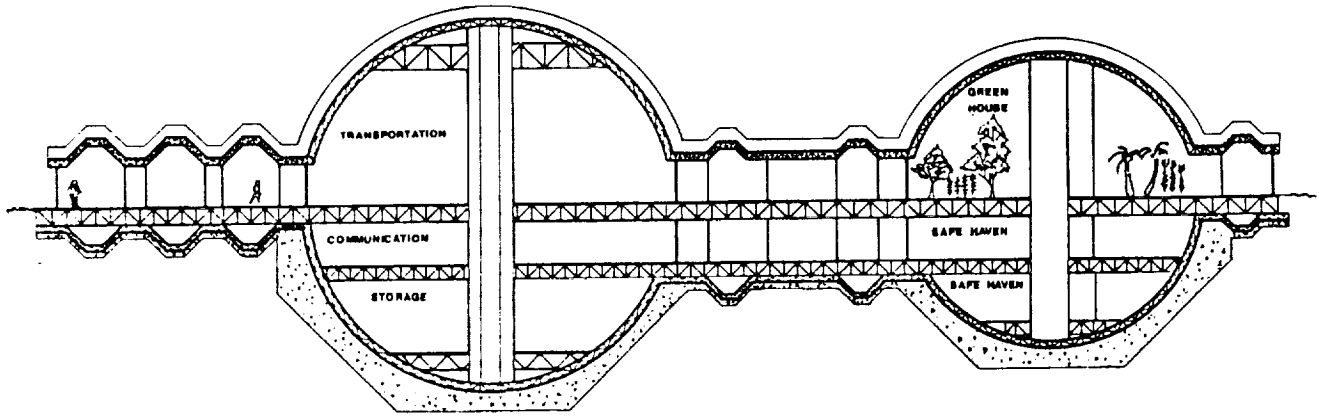


Fig. 9. Section B-B.

## LEGEND

- 1 COMMUNICATION
- 2 BASE COMMAND
- 3 RESTROOMS
- 4 CREW QUARTERS
- 5 MEDICAL CLINIC
- 6 DINING
- 7 KITCHEN
- 8 RESTROOMS & SHOWERS
- 9 SICK BAY
- 10 VEGETATION LAB
- 11 SOIL LAB
- 12 OXYGEN STORAGE
- 1A OFFICE
- 2A CONSTRUCTION EQUIPMENT STORAGE

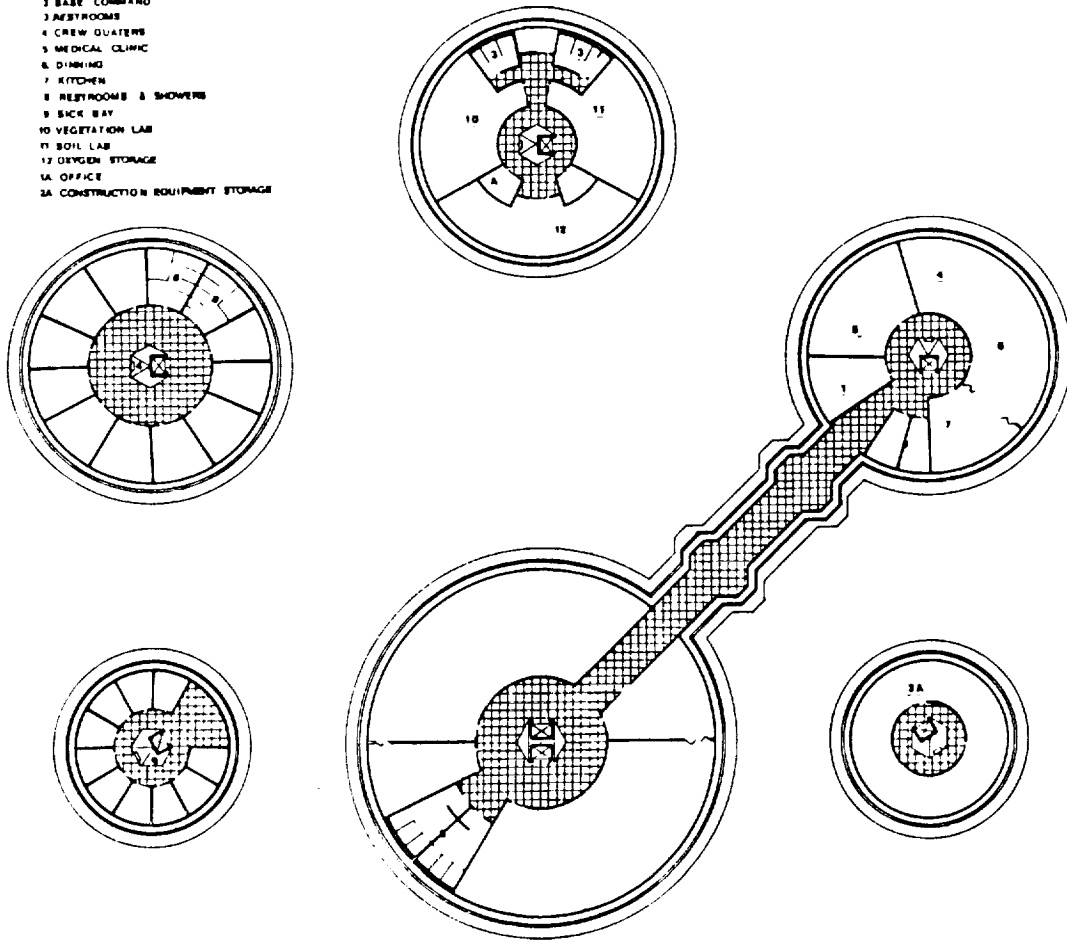


Fig. 10. Plan 3.

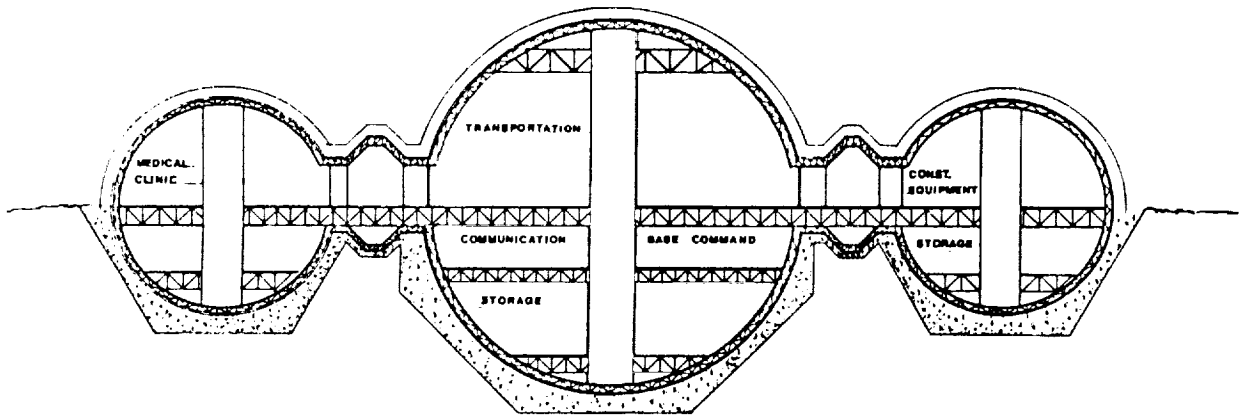


Fig. 11. Section A-A.

**LEGEND**

- A TRANSPORTATION
- B WORK AREA CONSTRUCTION
- C GREEN HOUSE
- D OFFICE
- E STORAGE
- F RESTROOMS
- G ATMOSPHERIC LAB
- H CHEMICAL
- I EXERCISE ROOM
- J KITCHEN DINING
- K ENTERTAINMENT
- L DENTAL CLINIC
- M CLINIC AREA
- N RESEARCH
- O OXYGEN STORAGE

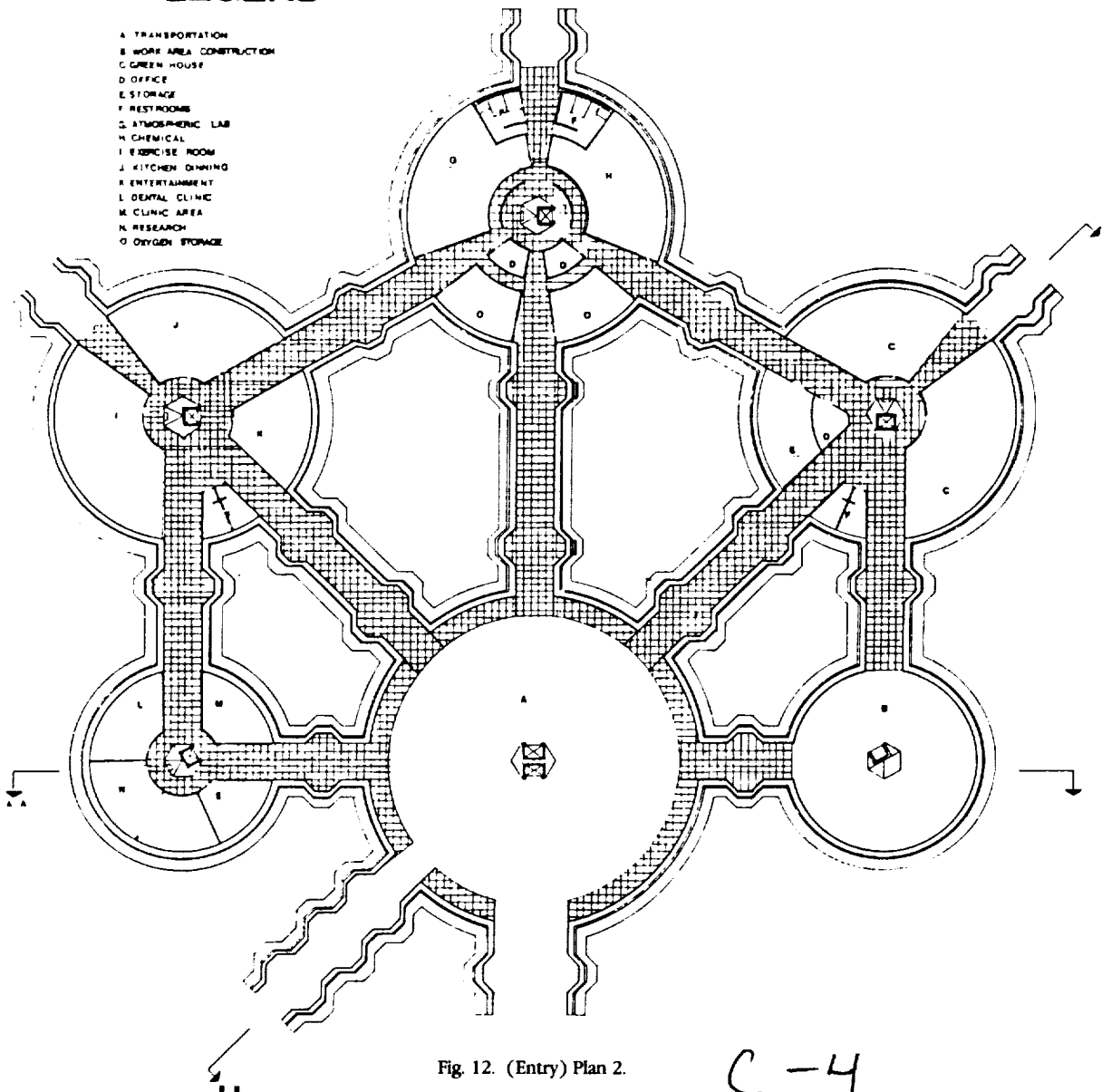
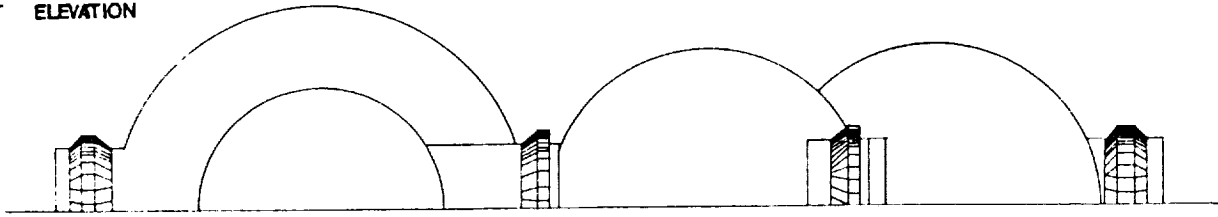


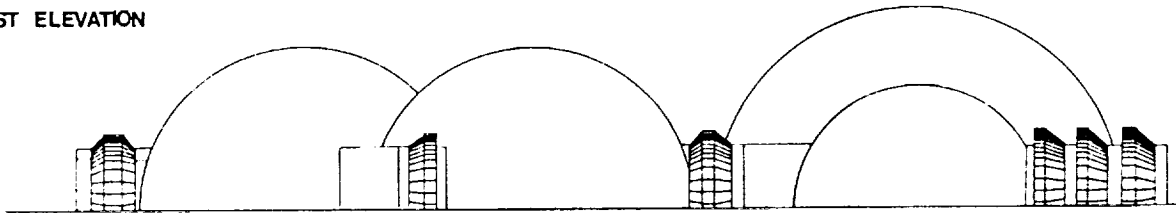
Fig. 12. (Entry) Plan 2.

C-4

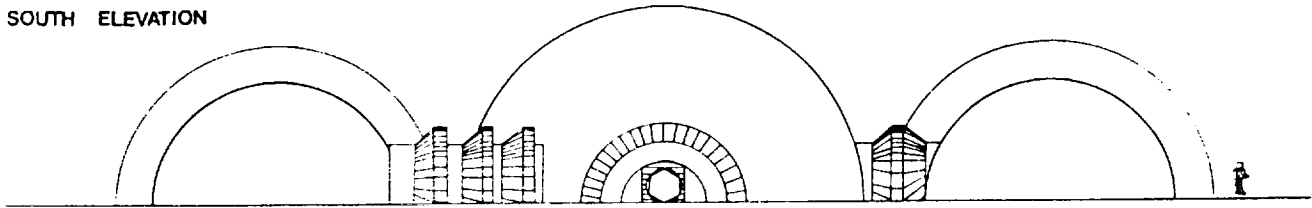
EAST ELEVATION



WEST ELEVATION



SOUTH ELEVATION



NORTH ELEVATION

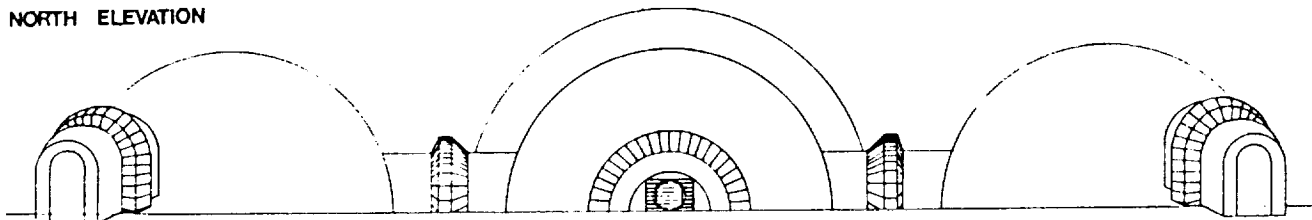


Fig. 13. Elevations.

3. Four columns in the membrane structure are connected to the foundation.

4. The space-frame structure is packaged with the internal telescopic columns, internal framing, and initial life support.

5. As the space-frame structure is pressurized, the Nextel flooring will be put into position.

The construction of the space-frame structure will occur in five phases.

1. Phase 1 is the safe haven, which includes the dining room and kitchen, exercise room, entertainment, crew rooms, and storage (Fig. 9).

2. Phase 2 will be the crew quarters, which includes the medical facilities, bathroom, wardroom, and storage (Figs. 10 and 11).

3. Phase 3 is the transportation bay, which consists of the base command and communication unit, and transportation port (Fig. 12).

4. Phase 4 will be the greenhouse and service facilities. These facilities include plants, animals, oxygen storage tanks, construction equipment, and storage (Figs. 10 and 12).

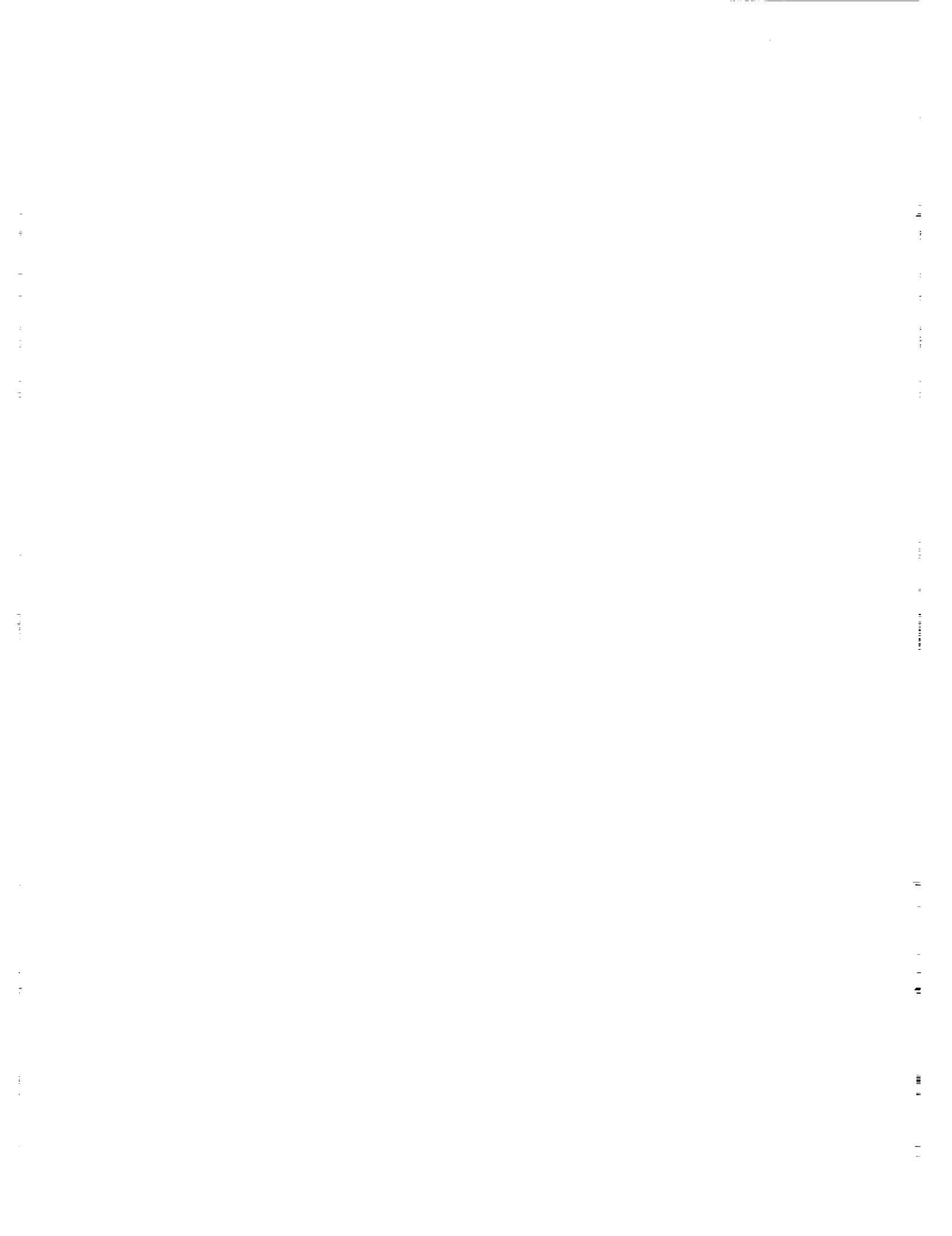
5. Phase 5 will be the laboratories, which consist of soil, chemical, vegetation, and atmospheric labs and storage (Fig. 10).

**Future Expansion**

The future expansion of the long-term base will entail constructing and adding more prefabricated space-frame modules to the existing long-term base, thereby creating a colony of prefabricated modules with multiple functions (Fig. 13).

**ACKNOWLEDGMENTS**

Project Director and Faculty Advisor is Ikhlas Sabouni, Ph.D. Faculty Advisor is Marshall V. Brown, P.E., Interim Dean. Student participants were Dale Ayers, Woody Bryant, Vernadette Gardner, Brock Harrell, Sherrill Hilton, Ronald Livingston, Damian Ohale, Jose Villanueva, Ricardo Watson, and David Ways.



## SELENIA: A HABITABILITY STUDY FOR THE DEVELOPMENT OF A THIRD GENERATION LUNAR BASE

UNIVERSITY OF PUERTO RICO

536-54  
166612  
P 9

### INTRODUCTION

When Apollo astronauts landed on the Moon the first generation of lunar bases was established. They consisted essentially of a lunar module and related hardware capable of housing two astronauts for not more than several days.

Second generation lunar bases are being developed, and further infrastructure, such as space station, orbital transfer, and reusable lander vehicles will be necessary, as prolonged stay on the Moon is required for exploration, research, and construction for the establishment of a permanent human settlement there. Human life in these habitats could be sustained for months, dependent on a continual flow of life-support supplies from Earth.

Third-generation lunar bases will come into being as self-sufficiency of human settlements becomes feasible. Regeneration of water, oxygen production, and development of indigenous construction materials from lunar resources will be necessary. Greenhouses will grow food supplies in engineered biospheres. Assured protection from solar flares and cosmic radiation must be provided, as well as provision for survival under meteor showers, or the threat of meteorite impact. All these seem to be possible within the second decade of the next century. Thus, the builders of Selenia, the first of the third-generation lunar bases are born today.

During the last two years students from the School of Architecture of the University of Puerto Rico have studied the problems that relate to habitability for prolonged stay in extraterrestrial space. An orbital personnel transport to Mars developed originally by the Aerospace Engineering Department of the University of Michigan was investigated and habitability criteria for evaluation of human space habitats were proposed. An important finding from that study was that the necessary rotational diameter of the vessel has to be on the order of two kilometers to ensure comfort for humans under the artificial gravity conditions necessary to maintain physiological well being of passengers, beyond the level of mere survival.

### A THIRD GENERATION LUNAR BASE

"Selenia" is derived from Selene, the name of the Greek goddess who personifies the Moon (Fig. 1). Our lunar settlement is named Selenia in recognition of the mythologic notion of the kind of experience to be encountered as humans actually populate Earth's closest neighbor, the Moon.



Fig. 1. Selenia, a Greek Goddess.

Selenia is a settlement of one hundred inhabitants working on lunar exploration, indigenous materials development for the sustenance of the settlement and for export, astronomical observation, and general research under reduced gravity conditions. Located at Lacus Veris on the Mare Orientale region,<sup>(1)</sup> its appearance is like a bullseye (Fig. 2) because of the presence of several large concentric crater rims at the very edge of the nearside of the Moon.

Selenia, a self-sufficient human settlement, will produce enough revenue to make it economically feasible by exporting products in addition to the production necessary for its own sustenance from lunar resources and recycling.

It consists of a 120-ft-diameter craterlet covered by a geodesic structure with tunnels to house underground personal quarters (Fig. 3). Three Social Nodes will be located at the juncture of the tunnels, each containing a lobby-lounge, a gym, a galley, a dining-conference-library area, an infirmary, a chapel, and a

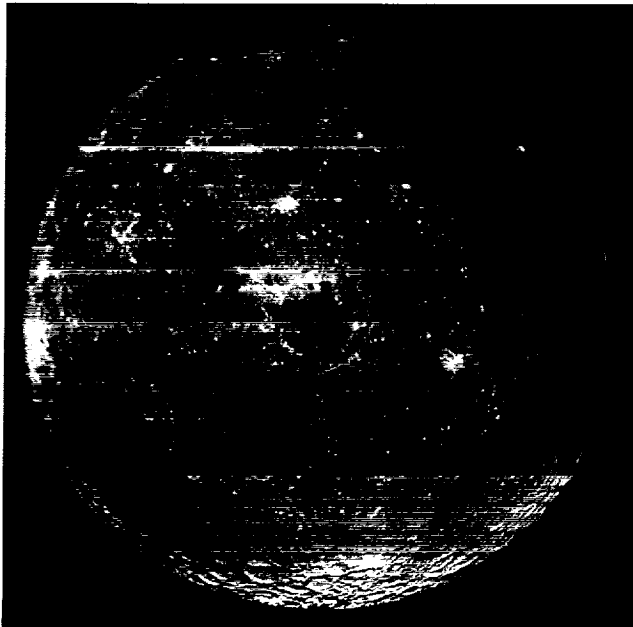


Fig. 2. NASA Photo 37327.

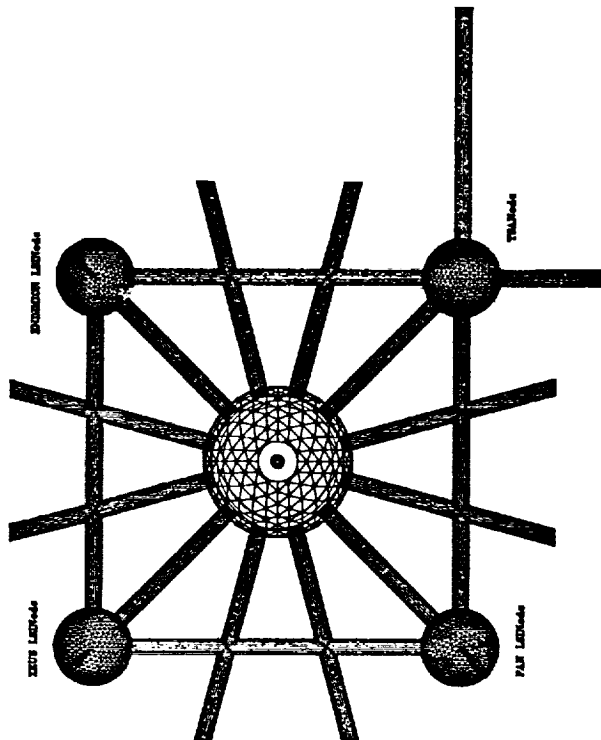


Fig. 3. Floor plan of Selenia.

surface-access igloo. A Transportation and Surface Access Node is located at the juncture of the surface-access tunnels, completing the square and housing equipment and parking spaces for pressurized surface transports. The northward surface

access tunnel points toward the takeoff and landing facility two and a half km away, and the tunnel going east leads toward the energy field.

The heart of Selenia is the four-level craterlet (Fig. 4). The lower level houses a "lung" system for storage, regeneration, and odor control of the air supply. The second level is for water recycling and by-product extraction. The third level will hold the food production facility that requires protection from solar flare radiation. Above will be the food production facility that requires less protection, and over it, a park-like common, that will house communal activities and will provide facilities for recreation, lunar sports, and artistic performances. There will be a centralized elevator for access to all levels and the Observation Tower to monitor nearby surface operations and to enjoy the sights.

Anthropometrics for low-gravity lunar habitation were studied, and color schemes, illumination patterns, and interior decoration considered, aiming to fulfill the habitability criteria developed earlier for the NASA/USRA project<sup>(2)</sup>.

**HABITABILITY CONCEPT DEFINITION**

Habitability, as defined earlier by University of Puerto Rico students could be summarized as "that state of equilibrium, which results from the interaction between components of the Individual-Architecture-Mission Complex; which allows a person to sustain psychological homeostasis, adequate performance, and acceptable social relationships."<sup>(2)</sup>

A diagram was developed to communicate the interdependence of the three parts of the complex (Fig. 5). Individual stress due to isolation, interpersonal stress due to confinement, and impersonal stress induced by a totally artificial or alien environment may cause a person to suffer psychological impairment, which may hinder the fulfillment of the mission or even the individual's motivation for survival in such an

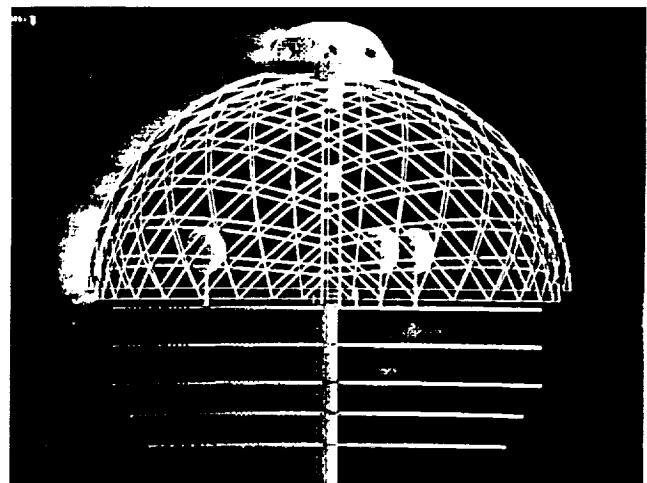


Fig. 4. Cross-Section of Main Craterlet Dome.

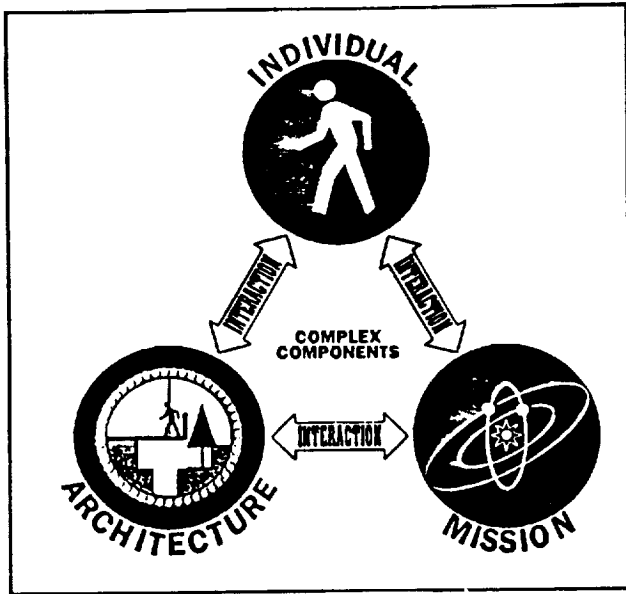


Fig. 5. Habitability Concept Diagram.

environment. The mission, together with the individual's values can provide the proper motivation and drive for striving to accomplish expected goals. But since psychology is shaped by physicality, it is the architecture that is the key to providing quality of life. Sights, motions, and sounds, as well as careful consideration of all sensory stimuli must be envisioned and provided for before we can design an appropriate environment for human inhabitants in extraterrestrial space.

**ARCHITECTURAL DESIGN CONCEPT DEVELOPMENT**

In the next century, we will be exploring farther in the Solar System. It will be more economical to base such operations on the Moon than on Earth, because of reduced gravity that will require less energy to assemble hardware and gather mineral resources. By that time the Moon could be providing fuel to power the Earth. Helium-3, which the solar wind has deposited in the lunar regolith over millennia, could be collected and transported to fusion plants on Earth. According to the NASA Lunar Helium-3 Fusion Power Workshop, of April 1988, one ton of helium-3 could meet the U.S. annual energy needs by the year 2015<sup>(3)</sup>. Thus the Moon could become the future substitute for the oil-producing countries of today as an energy supplier.

Infrastructure will include launch systems capable of transporting passengers to a space station, transferring to a lunar transportation node, or Orbital Transfer Vehicle, which will carry them on to lunar orbit; and a lunar landing craft capable of maneuvering from orbit into the landing and takeoff facility of the base. From such a port, several kilometers from the base, lunar rovers will provide transportation for people and cargo.

As the rover approaches Selenia, little will be seen apart from the lunar landscape, since most of its architectural features lie under the surface or will be covered under a 3'-6' layer of

bagged regolith for shielding (Fig. 6). Only the antennae, the surface access igloos, and the micrometeorite shields at the entrance would stand out. The rover will enter through tunnels carved out of the rock and built under the regolith to a Transportation and Surface Access Node.

Selenia will have to generate its own foodstuffs, recycle its own water and oxygen, and maintain its own ecological balance. Its main feature will be a domed craterlet that contains a Closed Environmental Life Support System (CELSS), which will house several biomes, biomachines, and agroindustrial features, protected to ensure survival of the colony. The rest of the social life of the lunar settlers will take place in their work, rest, and leisure places around the CELSS.

**LACUS VERIS LOCATION**

The site selected was one of a group recommended by the Solar System Exploration Division of the NASA Johnson Space Center in the northwest quadrant of Mare Orientale at 87.5°W, 13°S, a multiring crater structure. At the limb of the nearside of the Moon the Earth sinks below the horizon for eight Earth days for every lunar day, giving it some of the advantages of a farside site location. Many topographical and geological features can be observed within a relatively short distance on the lunar surface.

**INHABITANT DESCRIPTION**

The success of any mission depends to a great measure on the dynamic interaction among participants and Earth support. It is very important to analyze the characteristics of these people and ensure that the architectural design of the habitats take into account factors such as age, sex, physical conditioning, interests, and purpose to contribute positively to the development of good group dynamics.

There are three Leisure and Social Interaction Nodes called Endymion, Zeus, and Pan. Thirty-three inhabitants will be associated with each LSINode as a subcommunity, sharing leisure activities and meals, and will have coinciding work and rest schedules. The following classification or distribution is deemed optimal: 27% of the population will work in mining related endeavors (e. g., materials engineers, explorers, etc.); 21% will work on astronomical observations and research; 33% will work on exploitation or production of prime material for export to Earth and the Solar System; and 15% will work in administration of the base, physical, social, and health maintenance.

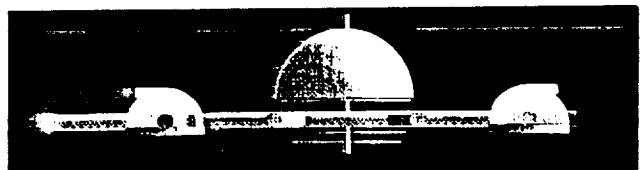


Fig. 6. A Cross-Section through Selenia.

## LIFESTYLE ANALYSIS

An important aspect of the social, scientific, and economic development of the base is the lifestyle of its inhabitants. Living conditions should not be limited to mere survival, but should include quality and style within a Selenite society. Life in Selenia will follow a terrestrial calendar and will accommodate the human circadian cycle. Selenia will have a 365.25-day year, 24-hour day, with the difference that weekdays will be displaced one third, that is, eight hours difference among the different LSINode subcommunities. This will make possible a three-shift work schedule so that all operations may be uninterrupted. This schedule seeks to conform to the needs of the base dwellers, except that it makes it impossible to have total community reunions. To eliminate this drawback weekends could alter the schedules to allow for total community sharing. In Pan, the weekend takes one third of Saturday, and one third of Monday. In Endymion, two thirds of Monday, and in Zeus, two thirds of Saturday. All LSINode subcommunities will coincide one and a third day on part of Saturday and Sunday. Schedules for the weekend will allow for general assemblies, festivities, and sports tournaments. In addition this would be an appropriate time for departure of personnel and arrival of new dwellers with reception from the Selenite community.

The lunar month is a little over twenty-eight days. For convenience they have been grouped into four weeks of seven days each. There will be eight days in which the Earth will be just below the horizon. Therefore one of the weeks of the month and its corresponding weekend will be significantly different than others in Selenia. For optimum conditions at arrival and departure times, as well as the communal celebrations, position of Earth and Sun in relation to the base must be considered.

Of all these conditions (sunrise, Earth-rise and sunset) Earth-rise seems to be the most appropriate for arrival and departure of dwellers because of good communications and visibility. The days in which Earth falls below the horizon will be the most appropriate for astronomers to make observations that are not possible from Earth, seeking more answers and questions about our universe.

## PERSONNEL CATEGORIES

Work will be generally classified in four categories.

**Mining-exploration:** These will be mostly engineers who will be studying the geology, topography and resources available on the Moon to pave the way for future extraction, resource utilization, and export. They will develop and test new construction techniques in a reduced gravity environment.

**Astronomy-astronautics:** Research and observations in the reduced gravity, airless, and slowly rotating environment of the Moon can accomplish feats impossible on Earth.

**Lunar resource exploitation:** This is the most important personnel category on the base from the commercial point of view. It will include engineers, physicists, chemists, biologists, and ecologists, who will be producing prime material for export to enhance quality of life on Earth, to sustain life on the Moon, and to further exploration of the Solar System. Many will be concentrated in the CELSS, and the biomes of Selenia's main

craterlet for production of food, recycling of air and water, and essentials such as clothing and medicines. Some will be gathering energy-rich materials such as helium-3, searching for life-sustaining substances, such as trapped water and oxygen, and producing hardware in reduced gravity for base operations and export.

**Maintenance-administration:** These will be people employed in the LSINodes, CELSS, and TSANode, taking charge of kitchen-galley, medical center-infirmary, and general physical, social, and health maintenance. People involved in government will generally be from this group, but participatory democracy should incorporate others to represent all sectors and categories of dwellers.

## GOVERNANCE

Life in Selenia will require a system of government to supply the needs of the people and to maintain an orderly way of conducting affairs. This special kind of community of gifted and educated individuals of different nationalities, would require that they agree to abide by an established system and to strive to work for its improvement in harmony with each other.

Participatory democracy is based on the people as the source of power delegated to elected authorities that make decisions on their behalf. In Selenia such decisions cannot be taken in complete isolation from Earth. A system should include an economy in which private enterprise, property, and work remuneration are agreed upon by the Selenite community. There should be a willingness to surrender individual freedoms and afford a greater degree of central control as long as this represents a guarantee for community and personal survival.

Individual dwellers would be classified in two groups: those who intend to go back to Earth and those who intend to remain permanently on the Moon. The first group might insist that their remuneration for work on the Moon be transferable back to Earth. The latter group could develop a different sense of remuneration and private property. Wealth will still be related directly to power and influence, but mutual help will be the norm to insure communal subsistence.

Property ownership on the Moon is a similar problem to that place in Antarctica, which lawyers refer to as *res nullius*<sup>(4)</sup>. Is the Moon like Antarctica, a place whose ownership is to be claimed by those who have been there, or have settled there? Or should it belong to no one, and therefore to all humanity? Nations that have established Antarctic bases have agreed to terms of mutual cooperation, without resigning to their claims to sectors of the land. Could we envision this as the proper model for dealing with lunar property claims, or should we assume that because one nation got there first and planted its flag, the Moon is already part of that nation's territory? What will happen when another power contests such a claim and arrives to start exploiting lunar resources for its own benefit? Could an international body such as the U.N. or some other alliance of space-faring nations intervene to see that the interests of all humankind are upheld as potential conflicts arise? Can the U.S. act as a benevolent leader in this endeavor, incorporating the efforts of other nations to widen the base of human and material resources available?

Governance of Selenia must take into account these factors, and provide a system of checks and balances to prevent greedy, ambitious, corrupt, or dictatorial leadership from taking over.

### SOCIAL WELFARE

It is unrealistic to assume that social ills such as crime will never reach our Selenite community. An effective judiciary system should be in place, capable of swift action in agreement with all national jurisdictions involved. Habcapsule confinement, movement monitoring using electronic devices, financial sanctions, and extradition to nation of origin, are some of the measures that could be used in Selenia to enforce the law.

Accidents and emergencies could happen, but preventive measures must be taken, since in some instances they could be devastating and could place survival in jeopardy. Epidemics, fire, air leaks, malfunction of life support systems, falls, injuries, or meteorite collisions could happen, and plans of action should be in place before the emergency occurs. The following are possible ways of dealing with these emergencies.

**Shielding:** A 3'-6' bagged regolith shield will cover all vital structures of Selenia and would protect it from small meteorites and thermal, cosmic, and solar flare radiation. Compartmentalization, as in submarines, and redundancy of life support systems will increase possibilities of survival in case of impact by more massive bodies. For micrometeorite collision protection a thin metallic membrane would suffice over the sensitive part, since they tend to vaporize on contact (Fig. 7).

**Evacuation and air lock systems:** In case of fire, malfunction of life support systems, or atmospheric depressurization, sensing devices will automatically activate air lock systems to insure survival. They could be locally overridden to allow for the evacuation of individuals.

**Medical emergencies:** Each LSINode contains an infirmary, which serves as a medical center, where physicians and paramedics provide health services to each subcommunity, monitoring the effects of reduced gravity on the dwellers, prescribing pharmaceuticals and exercise regimes to maintain muscle tone and bone strength. In case of epidemics, selected habcapsules or even one of the LSINode infirmaries could be quarantined. In case of death, provision to return a body to loved ones on Earth should be made, but dwellers should be encouraged to donate their bodies for scientific and medical purposes.

### NORMS AND VALUES

Cultural diversity among inhabitants of the base may bring also norm and value clashes. Behavior that may be perfectly acceptable in one society may be offensive in another. Religion, language, race, nationality, and other cultural traits of the individuals in the Selenite community will influence their norms and values.

**Religion:** Christians, Buddhists, Muslims, Jews, and non-believers could coexist in Selenia, as long as there be no fanatic proselytizing or coercion from one to the others. Spiritual welfare can add to the quality of life of the Selenite community and fulfillment of individuals. Thus, a chapel is provided in each LSINode for private meditation, as well as for group worship.

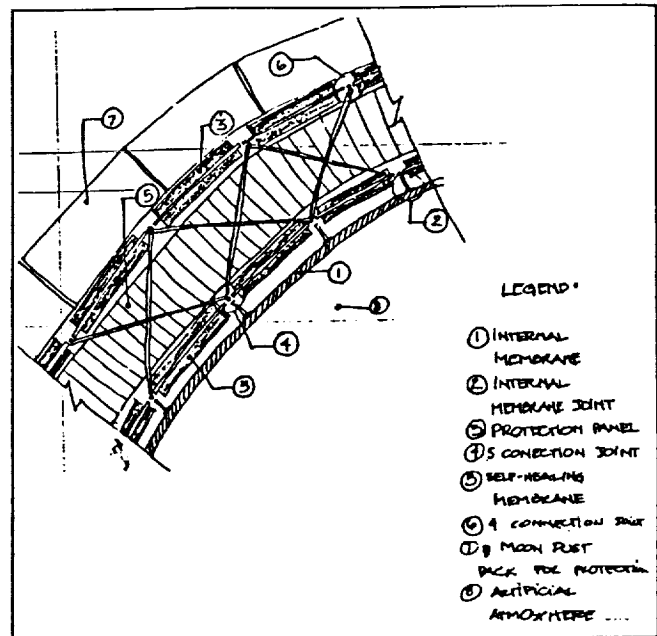


Fig. 7. Section of Shielding and Structure of Main Craterlet.

**Language:** Each human language has a culturally determined cosmic vision and set of values imbedded in it. Conceivably, languages used in Selenia would be selected on the basis of those spoken by the settlers and their nations of origin, like the United Nations.

**Culture, Race and Nationality:** Even if the U.S. is to be the leading nation because of its historical role of leadership in the conquest of extraterrestrial space, other nations, races, and cultures must be incorporated if it is to become truly an endeavor of all humankind.

**Sex and matrimony:** In a conservative western society sex is expected to be confined to heterosexual, monogamous matrimony. In recent times sex has been viewed as a way of enjoying intimate relationships with other persons, who may or may not be of the opposite sex. Traditionally humans have found ways to sublimate sexual drives and channel such a powerful source of energy into creative fulfillment, rather than seeking hedonistic personal satisfaction.

**Offspring:** In the initial stages at Selenia, there will be no appropriate environment for rearing children. It will not be until humans decide to stay permanently in the reduced gravity environment of the Moon that we will have a first generation of human extraterrestrials. When we can understand the impact of reduced gravity upon reproductive processes we will be able to decide whether or not offspring should be reared in Selenia.

**Etiquette:** In most societies there are norms for social interaction. In Selenia some of these will be imported from Earth and agreed upon by the dwellers. Others will eventually evolve there as particular Selenite customs and traditions.

**Liberals vs. conservatives:** In all human societies there is always the tension between those who want to keep the comfort of the known and resist change, and others who boldly want to go beyond experience, seeking innovation. A balance will

have to be established to limit personal expression without stifling the enrichment of community mores to maintain quality of life in the Selenite society.

### ASSEMBLY PROCESS

On the circumference of the craterlet that will contain CELSS, 12 tunnels will be carved from lunar rock under the regolith. Ten of these will house 18 Habicapsules containing living quarters in an area highly protected from radiation, meteorite impact and major temperature changes, with airlock systems to guarantee survival of major parts of the community in case of failure of life support systems or atmospheric decompression for a period of time. Two of the tunnels will be used for circulation to the core of the Main Craterlet. The advantage of locating these facilities under the surface is that inhabitants could live assured of protection from lethal radiation, meteorite impact, and extreme temperature variations. For the construction of these tunnels we envision that something like the Texas A & M University Subselenian Tunneler Melting Head Device could be used (Fig. 8): "It consists of a tunneler which would melt through the Lunar material, leaving behind glass-lined tunnels. The tunneler uses a nuclear generator, which supplies the energy to thermally melt the regolith about its cone shaped head. Melted regolith is excavated through intakes in the head and transferred to a truck that hauls it to the surface. The tunnel walls are solidified to provide support lining by using an active cooling system about the midsection of the tunneler."<sup>(5)</sup>

This machine is fast and capable of making 15'-maximum-diameter tunnels, but has the limitation that it cannot make small-diameter curved tunnels. The twelve tunnels made with this device will be transversely connected by four others that form a 230' square, and will be used for circulation and other community activities. On each of the corners of the square there will be 70'-diameter nodes, three of which will serve as the Leisure and Social Interaction centers of the three subcommunities, and a fourth will house the Transportation and Surface Access facilities. Each will provide a way to the surface. The TSANode will have two additional upward sloping tunnels, one leading eastward toward the energy field, and one leading northward, toward the takeoff and landing facility.

The Main Craterlet, as well as the Nodes are domed by a geodesic structure from which an airtight membrane will be hung to contain the atmosphere, and above which a self-healing

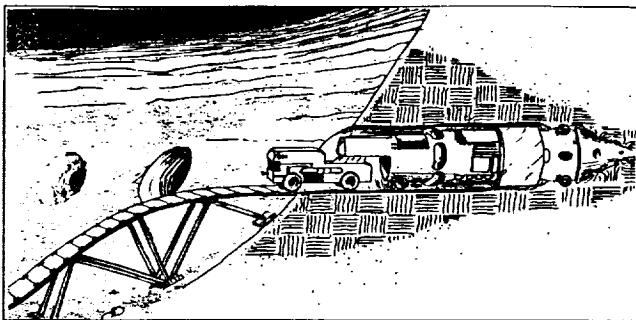


Fig. 8. Subselenian Tunneler by Texas A&M students.

protective layer will be placed. Above that, bagged regolith will be placed to create adequate protection from radiation and extreme temperatures. Structural redundancy is employed to insure the integrity of the form in case of local failures. For the regolith bagging system we envision something like the device developed by the Georgia Institute of Technology Textile Engineering Department called "Lunar Regolith Bagging System." (Fig. 9): "This design consists of a rotating brush, protective shroud, metering funnel, prefabricated bags on a roll with built-in drawstrings, a cutter to cut filled bags from the roll, a clutch mechanism to pull the drawstrings closed, and a magnetic control arm to hold the bags open while filling."<sup>(6)</sup>

This layer of regolith is capable of protecting the dwelling places from lethal radiation, extreme temperatures, and small meteorite impact.

### BASE DESCRIPTION

Selenia covers an area of 268,731.83 sq ft and encloses a volume of 1,149,377.70 cu ft. There are four nodes in the corners of the base quadrangle, located in each of the corners, forming something like a baseball diamond.

The Main Craterlet covers an area of 45,238.93 sq ft and a volume of 452,389.34 cu ft, which encloses the 120-ft diameter craterlet found in Lacus Veris (Fig. 10). Except for the upper commons, it will be divided horizontally in 12 almost identical

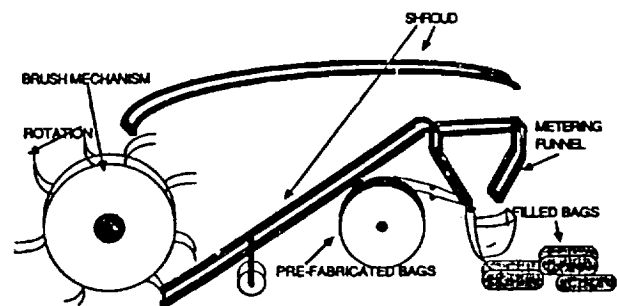


Fig. 9. Regolith Bagging System by Georgia Tech students.

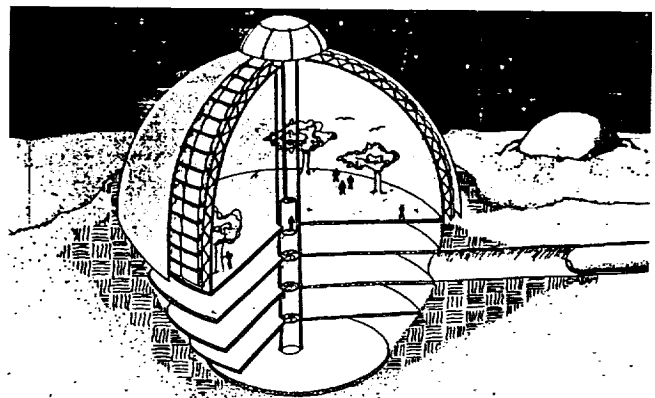


Fig. 10. View of Main Craterlet Levels.

compartmentalized sectors that will contain the following features at each of its levels. The lower level houses air recycling, processing, handling, and deodorizing equipment in 31,415.93 sq ft. We refer to it as a "lung," because of its physiological role in the life of the base. Thus, it is placed in the most protected location on the center of the base. The second level houses water processing and sewer plants in 38,013.27 sq ft. The third level, which is at the Habcapsule tunnels levels, holds a CELSS with animal and vegetable foodstuff producing biomachines in containers that can be transported into the Habcapsule tunnels for protection from extreme solar flare radiation in an area of 45,238.93 sq ft. The fourth level, also of 45,239.93 sq ft serves as a hydroponic and aeroponic greenhouse. The fifth level is covered by the cupola and is a commons for communal and recreational activities in 45,238.93 sq ft. An observatory is located in 615.44 sq ft at the top of this array for monitoring surface operations near the base or enjoyment of the sights. All levels are interconnected by an elevator 6 ft in diameter.

**Habcapsules:** From the Main Craterlet CELSS, 12 tunnels 141 ft long and 15 ft in diameter will radiate. These will be for circulation, and 10 of them will also hold 18 habitational capsule units, each holding living quarters for 6 inhabitants. Each capsule is 80 ft long, and covers an area of 1902.86 sq ft (Fig. 11). Ten Habcapsules are located inside the quadrangle of the base and eight just outside on the nodule connecting tunnels. Those external connections could be extended for future growth of the base.

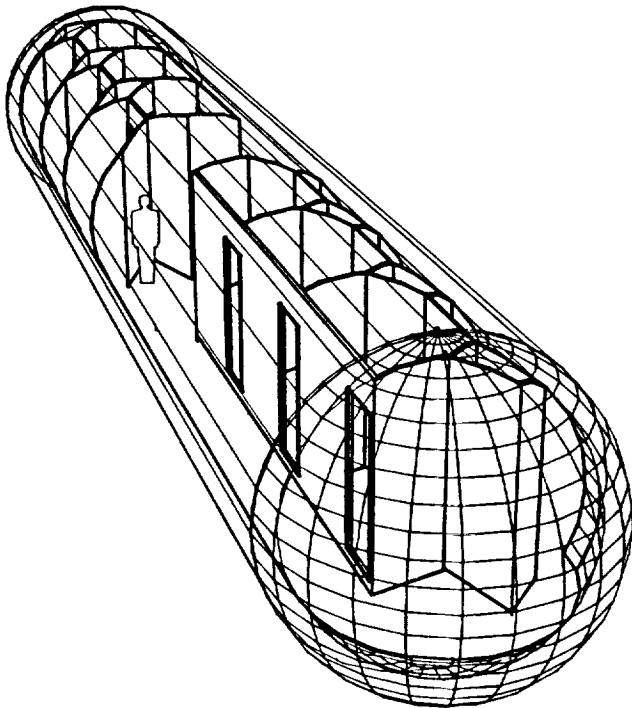


Fig. 11. View of Habcapsules.

**LSINodes:** Leisure and Social Interaction Nodes are 70-ft-diameter hemispherical spaces, covering 3,848.45 sq ft in three levels. The first one houses spaces for recreation and social interaction and includes lobby-lounge, 1,087.68 sq ft, a meeting room for each subcommunity; gym of 728.64 sq ft, a place where physical fitness acquires a new importance if one intends to ever go back to a terrestrial environment; dining-conference in 960.96 sq ft, where meetings, banquets, and other social functions will take place; kitchen-galley, 543.84 sq ft, where meal preparation will take place; and 251.33 sq ft public toilets. Even though the gym is a place for exercising, physical training activities can take place outside it. Monkey bar racing in the circulation tunnels, and Moon-gliding in the commons could be developed to maintain upper body tone. Above the kitchen, there will be a library, which inhabitants can use for research as well as recreational reading.

The highest level of the LSINodes is a surface access igloo of 281.01 sq ft, reached through a ladder or through a 6'-diameter elevator from the interior, and from a "T" shaped access tunnel on the surface. Around the elevator the public bathrooms are located in the first level. The second level houses an infirmary in 610 sq ft, and the third level houses a chapel. Under this array there is a "lung," which serves as part of the life support system of the base, in 3,848.45 sq ft.

**TSANode:** This is the Transportation and Surface Access Node (Fig. 12). Its 70 ft diameter is derived from the turning radius of the Subseleonian Tunnel, and it covers an area of 3,848.45 sq ft. It consists of an open space that serves mostly as a parking place for surface operations vehicles and materials storage. Ten rover vans and two cargo vehicles can be placed there. In addition to the three corner tunnels, which all Nodes have, the TSANode will also have an eastward tunnel leading toward the energy field and a northward tunnel leading toward the landing and launching array.

**Energy Field:** It is located at least 3 km from the base in the eastward direction (Fig. 13). It contains a solar collector array and fuel cells. Further away is a multimewatt nuclear power plant to provide energy to the base during the lunar night.

**Launching and Landing Facilities:** Consists of a main terminal 2.5 km from the base toward the equator, where there are four landing-launching pads. There is also a linear sling mass accelerator 0.5 km away that takes advantage of the lunar rotation and the near-equatorial location of the base.

#### APPLICATION OF THE HABITABILITY CRITERIA

**Personal Identification:** Astronauts and cosmonauts have expressed their need to feel that they are not aliens during their space missions, but to feel part of a family of humans who have been privileged to experience an alien environment with adequate protection for survival and with quality of life enhancements. To satisfy this need inhabitants should have the option of individual dwelling quarters, where personal objects could impart a homey character to the living environment. Other areas of the base will also contribute to personal identification by adopting familiar forms, characters, and styles, and where holographic projections will recreate specific reproductions of terrestrial places.

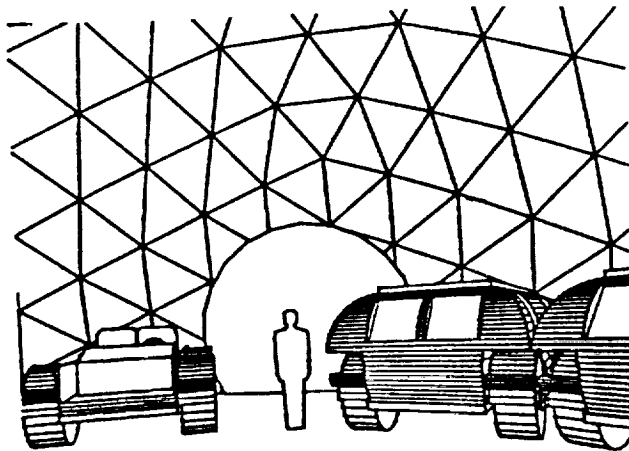
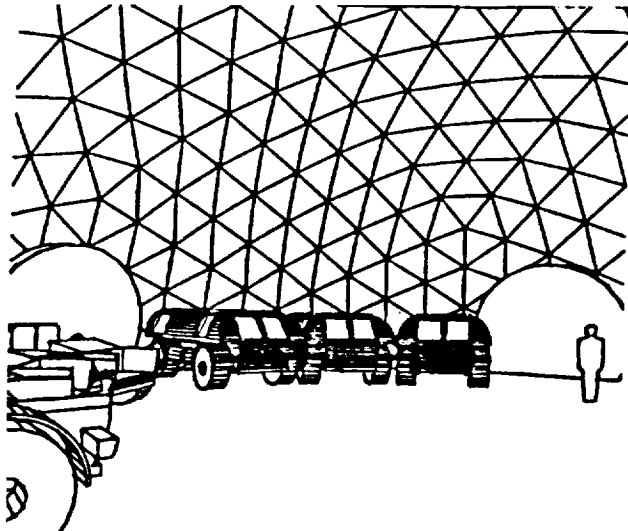


Fig. 12. Views of TSANode.



Fig. 13. View of Master Site with Accessory Facilities.

**Social Interaction:** In prolonged stays in space it seems important for humans to feel the presence of others. Besides company and security, it is necessary to promote positive interpersonal dynamics and good social interaction. Hallways between Habcapsules, and the commons at the Main Craterlet, and spaces at the LSINodes such as the lounges and the dining room will be places designed to promote social interaction.

**Mental Landscapes:** "Acute Places" are referenced in psychology as enclosed spaces. It is important that they contain symbolic elements that would evoke memories and sensations from previous experiences. These are called "mental gardens." They can help people transcend their immediate physical reality through images, photos, forms, spatial sensations, colors, textures, and materials. The mythology, legends, and decoration in the base should contribute to fulfilling this need.

**Privacy:** Among inhabitants of the base, social dynamics should be promoted, but privacy or occasions of solitude should also be provided. Their absence has been demonstrated to be an irritant to humans in restricted environments. It seems reasonable to assign each individual a place each can call his or her own.

**Contact with Nature:** There is great contrast between what we call architecture, and nature. Prolonged stay on the Moon will immerse individuals in the base to a totally alien, artificial environment. The unstabilizing effect that this causes could be offset by gardens and places of contact with animals in the base, such as the Biomes and the CELSS. Habcapsules will have small gardens at the rounded ends. Growing crops and feeding the animals of the CELSS, activities to be shared among all members of the community, will promote a healthy contact with nature, as well as visits to the commons in the upper level of the Main Craterlet.

**Equalitarian Conditions:** These will promote more relaxed interpersonal relationships among dwellers, making the work on the mission easier and more productive. Arbitrary rank or hierarchical distinctions are not conducive to the best relationships. In architectural terms such equalitarian conditions are reflected in the quality, location, and size of the rooms.

**Variety:** Psychological studies suggest that similar elements or very repetitive features in an acute place are boring and cause irritability and environmental stress. Habitable places in the base need variety. Decoration at the LSINodes, and rotation of housekeeping tasks should fulfill this criterion.

**Aleatoric Conditions:** Space travelers have expressed their appreciation for pleasant surprises that depart from daily routine and promote enjoyment of changes. Inhabitants of Selenia will celebrate special events to enhance the routine of ordinary days. The sights of the observatory, the flowering of crops in the CELSS, in the Habcapsule gardens, and in the commons will allow dwellers to enjoy happenings. The lighting of hallways could be programmed to vary aleatorically to simulate weather variation in terrestrial environment or to suit special activities.

**Functionality:** To be considered habitable, a place must satisfy physical and psychological needs. Also it must house all the hardware necessary to perform the work to fulfill the mission in the base. As an example, the "lungs," the recycling systems, the self-healing membranes, the airlocks, and their redundancy will ensure human life.

**Comfort:** This includes conditions such as illumination, color schemes, temperature, humidity, pressure, and atmospheric composition that can be accurately determined according to standards, and applied to the design of Selenia.

**Stability and Security:** Stability refers to inertia that resists forces causing motion or distortion. Human reflexes and muscle tone developed on Earth under a normal 1 g will find alien an environment of only 1/6 g. The lunar base will offer color coding systems to identify doors, walls, and floors, and different patterns to compensate for the sense of instability or insecurity resulting from such alien conditions.

**Sensory Stimulation:** It is fundamental that dwellers need as close to normal and as varied as possible a range of stimuli. Sensations are the primary human experience. Surfaces in the lunar base should be treated with color, which will stimulate the visual sense in a meaningful coding system, as well as texture, which will stimulate tactile sense and would help solve acoustic and friction problems in a 1/6-g environment. Simulated windows with video showing the exterior of the base will also serve this criterion.

**Music and Environmental Sound:** The problem of silence in the extraterrestrial environment will be offset by the sounds generated by the life support systems machinery, air handling units, etc.

**Sense of Orientation:** Characteristics of light can be used to transmit information. Color, as function of wavelength, aids in discerning shapes. Color effects in the interior design of the base are one way to meet the criterion of sense of orientation and also the criterion of comfort. Location of a color stimulus, be it on ceiling, floor, or walls, can make a great difference in the character of a dwelling, its perceived form and size, and its psychological perception.

## CONCLUSIONS

Additional questions require further study and research for the continuation of this study, which has tackled many problems but left many questions unanswered. These will constitute an agenda for future years.

**Self-healing membrane:** The chemistry of fluids, which make membranes self-healing, is known and has many applications on Earth. An example is the kind of substance used in emergency automobile tire repair cannisters. But how would such a substance could perform in the vacuum of extraterrestrial space?

**Refinement of the Habitability Criteria:** Research underway at Biosphere 2 will help answer important questions such as: What is the volume required for a CELSS per inhabitant? What is the biome composition that more efficiently supports an artificial ecology? What are the empirically tested parameters in reduced gravity anthropometry?

**Growth of the lunar base:** The question of further growth of the base must be addressed. Is it better to develop other lunar bases in modular stages, or should they be allowed to expand indefinitely, as in the case of terrestrial cities? What

is the ideal size for a Selenite community? What are the determinants and parameters that should be considered to reach a conclusion? Is there a critical size at which a self-sufficient community is no longer possible?

**Reduced gravity furniture design:** Further development of furniture design is necessary, considering the anthropometrics of the lunar environment. The idea of edible furniture materials to ensure survival under catastrophic circumstances is worth exploring.

**Illumination and lighting effects:** The use of environmental lighting to change the character of an acute place, holography to create environments that evoke mental landscapes, fractals to introduce aleatoric variations in decorative patterns of walls, and photo-sensitive membranes to vary transparency to create a new sense of indoor-outdoor relationships are some of the items that should be explored as resources for the specific design of the lunar base.

**New activities:** Lifestyle in the Selenite community will create the need for new kinds of sports and new festivities to enhance the routine of ordinary days and new forms of social interaction developed to suit the particular circumstance and inhabitants of the base.

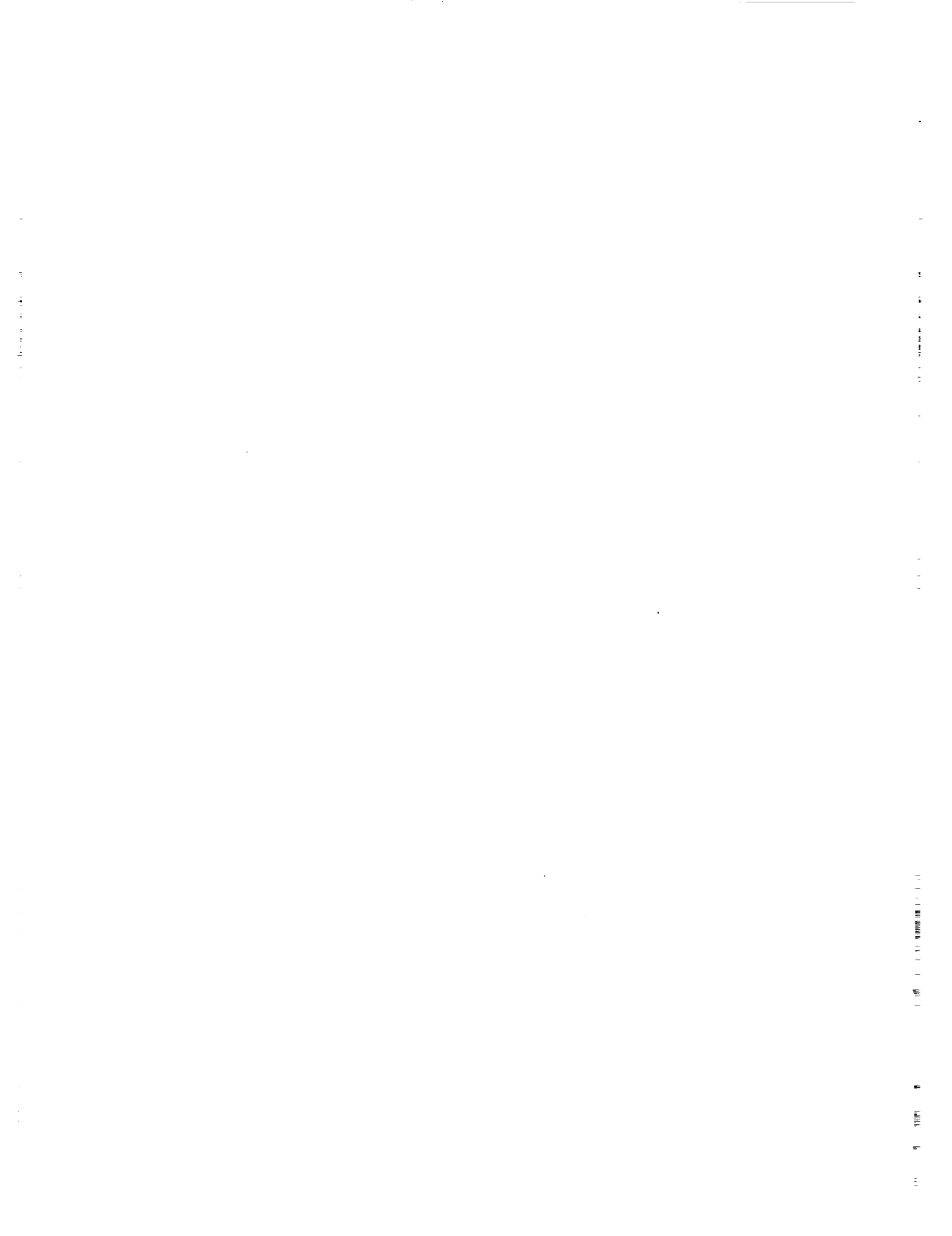
We could be heading toward the development of a design manual for architects of lunar bases. However, our immediate aspiration is to raise consciousness regarding the contribution that architectural designers can make to the conquest of space and to call upon people in that field to reflect upon this new frontier.

## ACKNOWLEDGMENTS

Students participating in the project were Iván Amy, Nilangely Arzón, Nelson Corchado, Yiramari Dávila, Alicia Díaz de León, Mareni Estrada, Norma Lozada, Héctor Maldonado, Samuel Marquez, Daniel Silva, Frances Villarini. Other project members were Aureo F. Andino, A.I.A., Professor, Erik Von Gundlach, Teaching Assistant, Hernán Torres, P.E., Technical Consultant, Osvaldo Budet, M. Arch. (Candidate), Rendering Consultant, and Nelson Ortiz, B.E.D. (Candidate), Model Consultant.

## REFERENCES

1. Alred J. (1989) *Lunar Outpost*, Johnson Space Center, Houston, Texas. pp. 23-24.
2. Andino A. et al. (1989) *Habitability: Camelot III*, University of Puerto Rico, Rio Piedras.
3. Auburn F. M. (1982) *Antarctic Law and Politics*, Indiana University Press, Bloomington.
4. Freeman M. (1990) "Mining Helium on the Moon to Power the Earth", in *21st Century Science and Technology*, Vol. 3, No. 3.
5. NASA/USRA University Advanced Design Program: (1989-1990) *Subselenian Tunneler Melting Head Design*, Texas A&M University.
6. NASA/USRA University Advanced Design Program: (1989-1990) *Lunar Regolith Bagging System*, Georgia Institute of Technology.



## THE LIGHTCRAFT PROJECT

## RENSSELAER POLYTECHNIC INSTITUTE

-37-16  
160 613

P. 6

Rensselaer Polytechnic Institute has been developing a transatmospheric "Lightcraft" technology which uses beamed laser energy to propel advanced shuttlecraft to orbit. In the past several years, Rensselaer students have analyzed the unique combined-cycle Lightcraft engine, designed a small unmanned Lightcraft Technology Demonstrator, and conceptualized larger manned Lightcraft — to name just a few of the interrelated design projects.

The 1990-91 class carried out preliminary and detailed design efforts for a one-person "Mercury" Lightcraft, using computer-aided design and finite-element structural modeling techniques. In addition, they began construction of a 2.6 m-diameter, full-scale engineering prototype mockup. The mockup will be equipped with three robotic legs that "kneel" for passenger entry and exit. More importantly, the articulated tripod gear is crucial for accurately pointing at, and tracking the laser relay mirrors, a maneuver that must be performed just prior to liftoff.

Also accomplished were further design improvements on a 6-inch-diameter Lightcraft model (for testing in RPI's hypersonic tunnel), and new laser propulsion experiments. The resultant experimental data will be used to calibrate Computational Fluid Dynamic (CFD) codes and analytical laser propulsion models that can simulate vehicle/engine flight conditions along a transatmospheric boost trajectory. These efforts will enable the prediction of distributed aerodynamic and thruster loads over the entire full-scale spacecraft.

## INTRODUCTION

Rensselaer's concept of an advanced "Lightcraft" (space shuttle) relies on beamed energy propulsion to greatly lower launch weight and to improve specific impulse. Beamed energy propulsion employs a remote energy source to deliver power to the vehicle through a direct, line-of-sight transmission link. The vehicle is equipped with a receiving antenna which reflects this power into a "propulsion energy converter." The latter device transforms the received beam energy into usable thrust.

Rensselaer's futuristic aerospace transportation system is based upon orbiting Satellite Power Stations (SPS) which transmit energy to the Lightcraft, in the form of a laser (or microwave) beam. The Rensselaer design team concentrates its attention on the *vehicle technology* only, and assumes the feasibility of an SPS power grid. A Lightcraft is slaved to the beamed power that energizes its multicycle airbreathing engine. This advanced airbreathing propulsor consumes a very small amount of propellant (e.g., 5 to 10% of TOGW) mostly in the final two engine modes: the *MHD-Fanjet*, and *rocket* for orbital insertion<sup>(1)</sup>.

Figure 1 is an artist's concept of a single-place Mercury Lightcraft under a laser boost to orbit. Note that the vehicle is axisymmetric, and is still in the first engine mode, which produces laser-generated thrust upon the aft centerbody surface shortly after takeoff. The laser beam is brought in from above, reflected by the large annular primary optics onto smaller secondary (cylindrical reflecting) optics located under the engine cowl. The beam is finally brought to a tight focus across the vehicle aftbody, causing air breakdown and the formation of spherical (or cylindrical) blast waves that momentarily contain high pressures. These high pressures act to produce engine thrust.

Several of the Lightcraft's major interior features are visible in Fig. 1. The passenger (or pilot) is seated in a reclined position in the center of the capsule. Trackball controls are integrated with the chair armrests, and advanced flat-screen color displays



Fig. 1. Artist's Conception of Mercury Lightcraft.

facilitate a friendly interface between the pilot and the mission computers. The pilot's luggage is stowed in twin compartments under the armrests, and steps are recessed into the interior surface of the door for easy entrance and egress. Robotic tripod landing gear and a small propellant tank are placed under the pilot within the aftbody. Altogether, these key features create an ergonomic environment for the passenger or pilot during the short ascent (approximately three minutes), and brief travel time (a maximum of 45 minutes to any point on the globe).

This academic year, our Advanced Design class completed the detailed design of the Mercury Lightcraft components and began construction of a full-scale engineering prototype mockup.

Other students designed and constructed experimental apparatus used in proof-of-concept tests on the Lightcraft's laser engine. The overall progress of each design team is summarized below.

**PROTOTYPING OF THE MERCURY LIGHTCRAFT**

At the beginning of the 1990/91 academic year, the design class was divided into seven teams, six of which worked on the prototype mockup design. The various prototype design teams are listed in Table 1.

TABLE 1. Mercury Lightcraft Mockup Design Teams

|         |                                       |
|---------|---------------------------------------|
| Team 1: | Exterior Aeroshell and Door           |
| Team 2: | Human Factors and Information Systems |
| Team 3: | Robotic Tripod Landing Gear           |
| Team 4: | Annular Shroud and Actuation System   |
| Team 5: | Primary Optics and Engine Mockup      |
| Team 6: | Major Structure                       |

Team 1, the Exterior Aeroshell and Door team, was responsible for designing and constructing an accurate exterior surface for the prototype, and for integrating a retractable door into the vehicle. The Human Factors team designed and began construction of an ergonomic interior for the Lightcraft and started work on the computer-based flight control/simulation system. The Landing Gear team designed and constructed a single full-scale robotic landing gear leg. The Shroud and Actuation System team designed and constructed the vehicle's annular shroud; they also developed the concept for a shroud translation system needed for the Lightcraft's variable geometry airbreathing engine inlet. The Primary Optics team designed a manufacturing process for the prototype's primary receptive optics and applied this process in fabricating a full set of 24 mirrors. Finally, the Major Structure team designed the load-bearing primary structure for the prototype mockup.

**Exterior Aeroshell and Door**

The Exterior Aeroshell and Door team was responsible for designing and constructing the external surface of the prototype mockup. Dimensioned engineering drawings of the external surface are shown in Fig. 2. The Aeroshell design team chose epoxy/fiberglass composites to keep the exterior surface lightweight, and, for ease of construction, to build the aeroshell in identical quarters. They began by first building an accurate male mold.

To assure an accurate cross-sectional mold contour, full-scale CAD drawings were traced onto two 3/4" plywood silhouettes and mounted at 90° to each other. Then a large number of bulkheads (spaced about 4-inches apart) were attached to this rigid frame, as shown in Fig. 3. Next, blue styrofoam was glued between the bulkheads and sanded down to form a smooth external contour; a rigid layer of epoxy/fiberglass was then applied to the external surface. CAD drawings were again used to create a stiff aluminum template that could be rotated about the vehicle axis of symmetry, to both generate and check the male mold surface contour. Automotive body filler was then

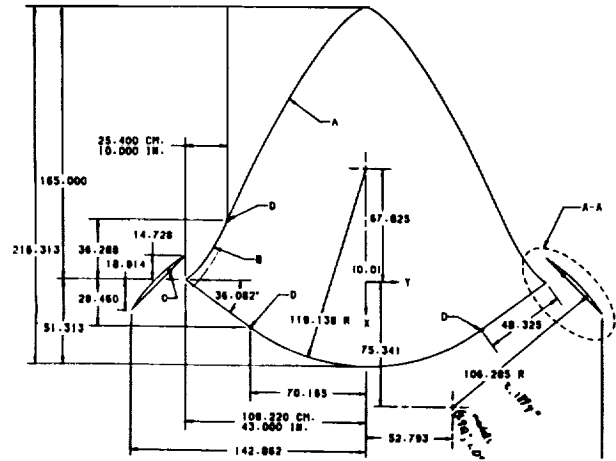


Fig. 2. Engineering Drawing of Mercury Lightcraft with Dimensions.

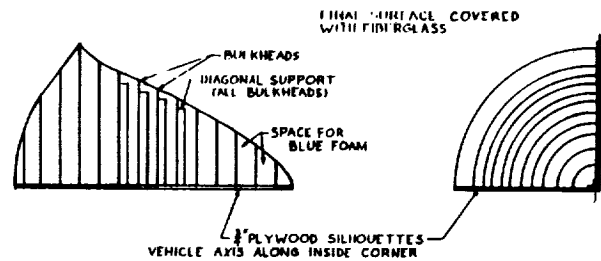


Fig. 3. Schematic of Male Mold Construction.



Fig. 4. Complete Male and Female Molds.

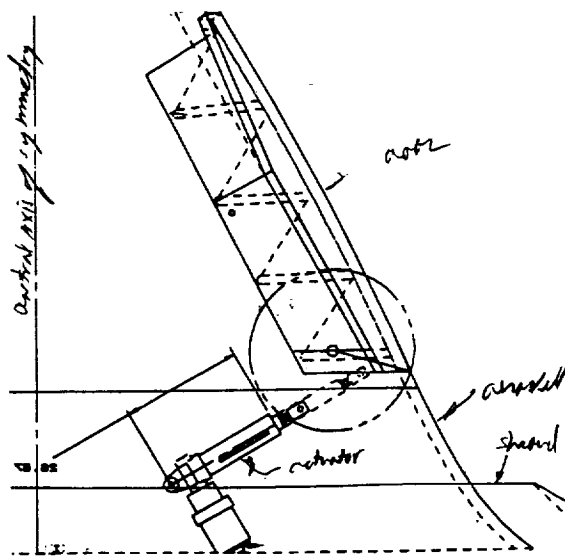


Fig. 5. Schematic of Door Actuation System.

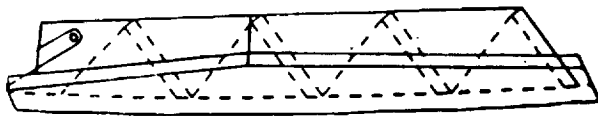


Fig. 6. Stairs are Integrated into the Lightcraft Door.

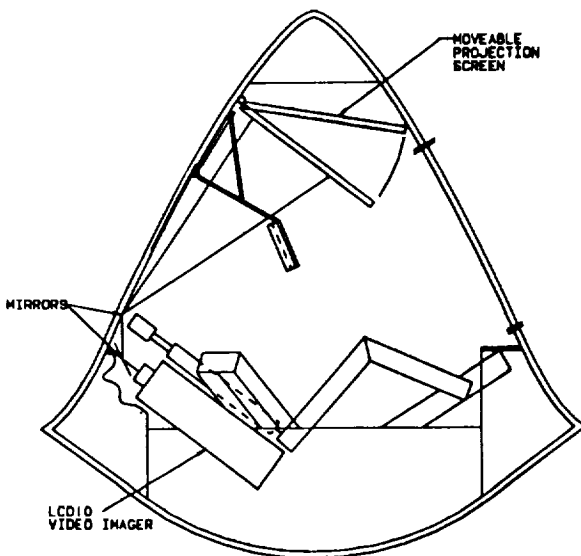


Fig. 7. Schematic of Prototype Mockup Interior Design.

swept across the surface to make it exactly conform to the template. Finally, a female mold was pulled off the male mold. The finished molds are pictured in Fig. 4.

The next step for the Aeroshell team is the construction of four composite sandwich skins which will be joined together to make the exterior surface of the prototype mockup. This composite sandwich will consist of two layers of 10 oz./yd<sup>2</sup> fiberglass cloth on both sides of a 1/4" thick foam core for increased stiffness. The aeroshell has several areas where openings are needed (e.g., for the door, tripod landing gear, etc.); these will be devoid of foam, to eliminate delamination problems.

In parallel with the spacecraft mold effort, the Aeroshell team designed and began construction of the mockup's retractable door (see Figs. 1 and 5). The fiberglass/foam/epoxy door is to be deployed with a four-bar linkage by a single Duff-Norton electromechanical actuator with a 6-inch throw (see Fig. 5). The staircase has five steps that are integrated with the interior surface of the door (see Fig. 6). The preliminary design for the door is essentially complete, but refinements are necessary.

### Human Factors and Information Systems

The Human Factors and Information Systems team was responsible for the interior design of the prototype mockup, including a comfortable chair for the passenger/pilot, a user-friendly interface with mission computers, and a ventilation and lighting system. A schematic outline of the prototype interior is portrayed in Fig. 7. Flat screen displays and (possibly) a projection video screen monitor will communicate information to the pilot, and twin trackball I/O devices will control these displays. The pilot chair, shown in Fig. 8, is positioned for maximum comfort while accommodating 99% of the adult population.

### Robotic Tripod Landing Gear

The mission of the Robotic Tripod Landing Gear team was to design, analyze, and construct a prototype tripod landing gear system capable of safely positioning the Lightcraft mockup in all required entrance, egress, and satellite-tracking orientations. The landing gear system had to be robotically actuated because the vehicle must tilt to approximately 26° from normal, in any direction, as it tracks the laser power relay satellite just prior to liftoff. Shown in Fig. 9 is a schematic diagram of the gear, each of which is actuated by two Duff-Norton electro-mechanical actuators with a 12-inch throw and 1500-lb load capacity. A single landing gear leg was actually constructed from 6061-T6 aluminum, and actuators are now being exercised for initial checkout. During the design effort, a finite-element stress analysis was performed on the gear. This analysis indicated that the gear was over-designed, having a minimum factor of safety of about five.

Work was also initiated on the computer control system for the landing gear. For a given vehicle orientation, the control system must predetermine the deployed length for each of the six actuators and then guide the actuators to this position along a safe path (see Fig. 10). A computer program was written to achieve this end, and to explore the envelope of possible

prototype orientations. This code proved to be not only an effective design tool, but also the first step towards developing a landing gear control system.

**Annular Shroud and Actuation System**

The Lightcraft's shroud and support struts were designed and constructed from aluminum by the Annular Shroud and Actuation System team. To fabricate an accurate male mold, 63 aluminum ribs were first cut from 1/8"-thick 6061 T6 aluminum on a numerically controlled milling machine. These ribs were then fastened together and the exterior surface was taped to form a smooth male mold, which represents a full-scale 1/24th segment of the annular shroud. Next this mold was taken to a local foundry to cast 24 replica shroud segments out of aluminum. Figure 11 shows the partially assembled shroud, placed about the wooden templates which bound the interior mockup of the Lightcraft prototype.

As mentioned above, the annular shroud must be translated to accurately simulate the variable geometry feature of the Lightcraft inlet. This will be accomplished by 24 Duff-Norton screw actuators, equally distributed around the perimeter, all connected with universal joints and driven by a single electric motor. A schematic diagram of the cross-section for one shroud actuation section is shown in Fig. 12. Construction and debugging of the complete actuation system is the principal remaining task for this design team.

**Primary Optics and Engine Mockup**

The Primary Optics and Engine Mockup team had several goals: to design an effective manufacturing process for the prototype's primary optic mirrors; to use this process in constructing 24 identical mirrors; and to design and fabricate four MHD generator mockups for the Lightcraft's MHD-Fanjet engine. The team decided to fabricate the primary optic mirrors from 1/8"-thick acrylic plastic mirror material, by thermomechanically deforming it in an accurate mold-press to produce precisely contoured, highly reflective mirrors. The manufacturing process involved several stages of heating in both boiling water and an electric oven before the acrylic material was finally inserted into the molds and pressed into shape.

Mockups of the laser-heated MHD generators incorporated the same acrylic plastic mirror material, and strategically placed light sources to simulate the luminosity produced in actual operation. The MHD generator design also incorporated a pressurized CO<sub>2</sub> fog system to simulate the high velocity MHD exhaust stream.

**Primary Structure**

The Primary Structure team was responsible for designing the load-bearing structure of the Lightcraft prototype mockup. This structure had several dominant requirements: it must protect the pilot from all possible failure modes, as well as provide hardpoints for the landing gear, door and shroud actuation systems, and the seat. An additional requirement was that the structure must provide lift points so that the prototype mockup can be maintained and transported to other locations.



Fig. 8. Detail of Prototype Pilot Chair.

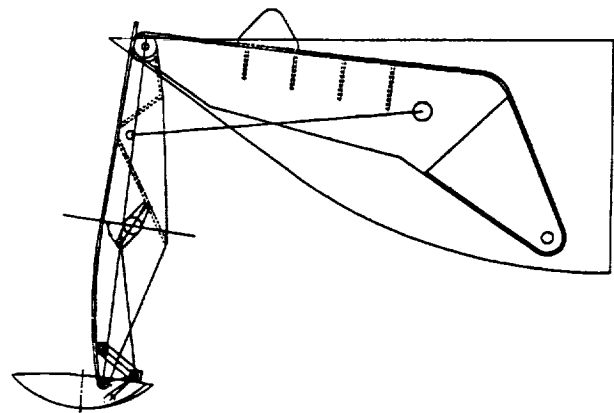


Fig. 9. Schematic of Robotic Tripod Landing Gear.

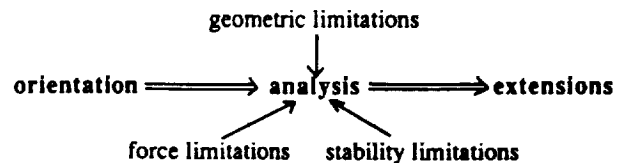


Fig. 10. Landing Gear Control System Moves Lightcraft Between Safe Orientations.

The primary structural design utilizes three U-channels (which house the robotic landing gear), and twin annular bulkheads to provide mounting points for the aeroshell, all actuation systems, and the pilot seat. A roll cage is positioned around the pilot to protect against possible catastrophic failure of the robotic landing gear system; also, both upper and lower structurally-reinforced lift points are provided (see Fig. 13).



Fig. 11. Shroud Assembled Around Lightcraft Contour.

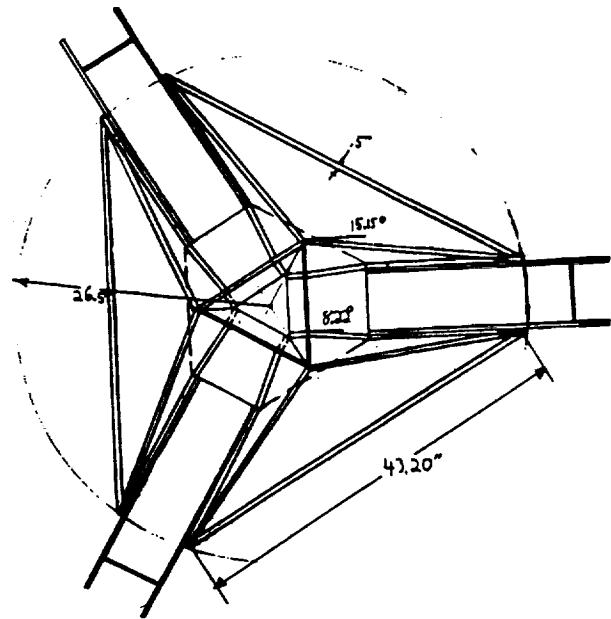


Fig. 13. Schematic of Lightcraft Major Structure.

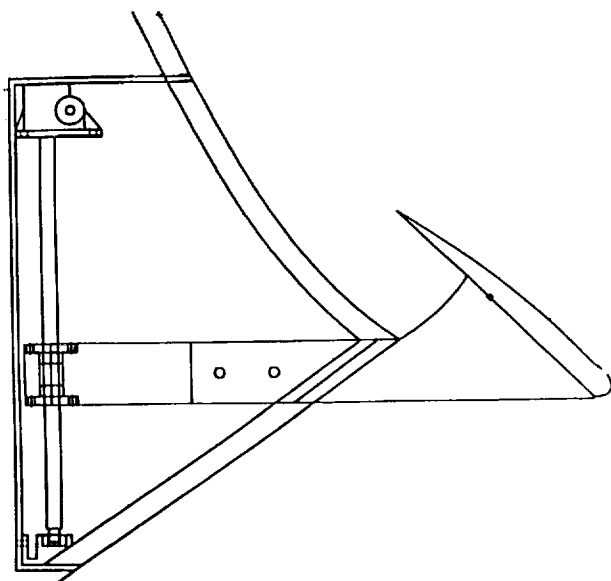


Fig. 12. Schematic of Shroud Actuation System.

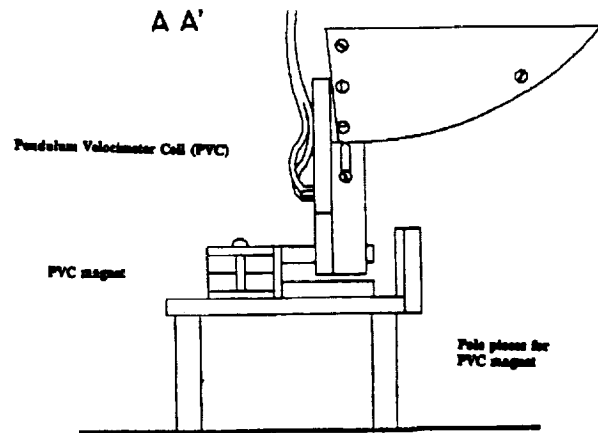


Fig. 14. Pendulum Motion is Measured By a Coil (PVC) Moving Through a Stationary Magnetic Field.

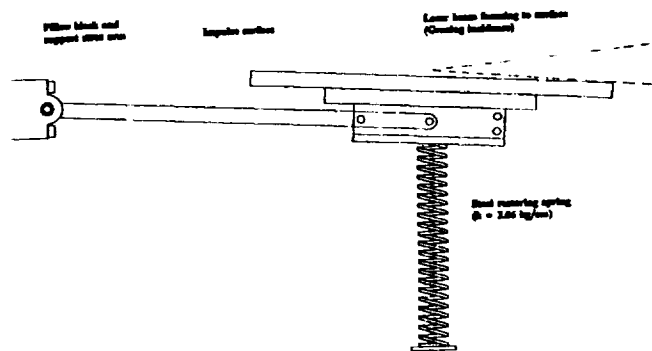


Fig. 15. Schematic of Horizontal Pendulum.

## EXPERIMENTAL APPARATUS

Another design team worked apart from those dedicated to the Lightcraft mockup. These students designed experimental equipment that was constructed with the aid of the Rensselaer SC machine shop, and then tested with a 1- $\mu$ m Nd-glass laser at the Naval Research Laboratory (NRL) in Washington, DC. A detailed description of the experimental equipment and the actual tests is contained in reference 2. Basically, the static engine performance measured in this first year of airbreathing laser propulsion tests at NRL was roughly equivalent to that demonstrated by the first afterburning turbojets. The potential for further improvement is promising.

These laser propulsion experiments used ballistic pendulums to measure the impulse delivered by the laser-induced breakdown of air (at standard sea-level atmospheric pressure). The pendulums were mounted either horizontally or vertically, and the impulse was measured by the voltage induced in a wire coil that moved through the poles of a small permanent magnet (see Fig. 14).

The horizontally mounted pendulum required that the target surface be supported by a coiled spring in order to produce the same characteristic motion as the vertical pendulum (see Fig. 15).

## SUMMARY AND FUTURE WORK

The prototype mockup of a single-person Mercury Lightcraft is now underway. Male and female molds of the spacecraft exterior aeroshell have been completed, and the Lightcraft door is nearly 50% complete. The prototype seat, flight computer I/O devices, electromechanical actuators for the landing gear (and door), and three flat plasma display screens have been acquired. One complete robotic landing gear leg has been assembled, finite-element structural analysis of the gear has been performed, and actuation software programming has been initiated. The annular shroud, support struts, and primary receptive optics have been fabricated, and the shroud actuation system has been designed.

In addition, several proof-of-concept experiments are also underway to validate the Lightcraft propulsion system. Hypersonic inlet testing and CFD verification of the results have been performed<sup>(3,4)</sup>. Laser propulsion tests are well underway, and results indicate promising performance<sup>(2)</sup>.

Next year's design class will complete the design and construction of the Mercury Lightcraft prototype mockup. The robotic landing gear will be activated and fully tested, and the possibility of creating a Transatmospheric Flight Simulator will be explored. Both hypersonic and laser propulsion testing may be continued, and the aerodynamic testing will be expanded

to include low supersonic and subsonic regimes. As with last year's class, the 1991/92 design class will be exposed not only to the spacecraft design process, but also to the engineering prototyping process as well. Much progress is expected toward the goal of an operational Lightcraft technology.

## ACKNOWLEDGMENTS

Paper compiled and written by Don G. Messitt (Teaching Assistant) and Professor Leik N. Myrabo (Faculty Advisor). This project was supported by a contract from NASA/USRA under the Advanced Design Program. The design work was accomplished during the 1990/91 academic year by two separate classes.

Members of the Fall 1990 design class were K. Amberge, G. Brown, D. Chang, K. Downes, S. Dunham, M. Harvey, J. Jeffrey, J.C. Krok, A. Kurgan, M. Mohd Tahir, E. Monsen, M. Mustafa, J. Nieto, M. Obrist, M. Petervary, K. Richard, J. St. Angelo, P. Stiles, N. Torres-Olivencia, and R. Vehlow.

Members of the Spring 1991 design class were D. Abd Manap, R. Augi, P. Blanchet, D. Cox, J. Davis, M. Fiori, E. Hintereder, T. Hyland, C. Jackson, S. Kaluczky, J. Kinton, J. Lewandowski, A. Lockhart, J. McGinley, K. Mogan, S. Mullady, D. Napoli, C. Nguyen, K. Richard, J. St. Angelo, R. Spriggs, J. Stewart, R. Wallner, M. Waters, M. Werner, and M. Wojcik.

John St. Angelo and Matt Werner were selected to present their class design projects at the summer conference.

This paper is an Executive Summary of a larger document which is available from the Faculty Advisor. A special thanks is given to Ms. Lisa Kohout, our mentor at NASA Lewis Research Center. We would also like to acknowledge Professor Henry T. Nagamatsu for his insight and guidance in the hypersonic testing, laser propulsion experiments and CFD simulations. Finally, we must thank the RPI IMS Science Center Machine Shop personnel for their expert help in constructing the prototype mockups designed by the students.

## REFERENCES

1. Myrabo, L.N. and students, "Apollo Lightcraft Project," NASA/USRA Advanced Design Program, Rensselaer Polytechnic, August 1991.
2. Lyons, P.W., Myrabo, L.N., Jones, R.A., Nagamatsu, H.T., and Manka, C., "Experimental Investigation of a Unique Airbreathing Pulsed Laser Propulsion Concept," AIAA Paper 91-1922, June 1991.
3. Jones, R.A., Myrabo, L.N., Nagamatsu, H.T., and Minucci, M.A.S., "Experimental Investigation of a 3-D Scramjet Inlet for Laser Propulsion at Mach Numbers of 10 to 25 and Stagnation Temperatures of 800 to 4100K," AIAA Paper 91-0012, January 1991.
4. Messitt, D.G., Myrabo, L.N., Jones, R.A., and Nagamatsu, H.T., "Computational vs. Experimental Performance of an Axisymmetric Hypersonic Inlet for Laser Propulsion," AIAA Paper 91-2547, June 1991.

ASPEC—SOLAR POWER SATELLITE

THE UNIVERSITY OF TEXAS, AUSTIN

S38-18  
160614  
p. 5

INTRODUCTION

The solar power satellite (SPS) will provide a clean, reliable source of energy for large-scale consumption. The system will use satellites in geostationary orbits around the Earth to capture the Sun's energy. The intercepted sunlight will be converted to laser beam energy that can be transmitted to the Earth's surface. Ground systems on the Earth will convert the transmissions from space into electric power. Figure 1 shows the overall system concept.

The preliminary design for the SPS consists of one satellite in orbit around the Earth transmitting energy to a single ground station. The SPS design uses multilayer solar cell technology arranged on a 20 km<sup>2</sup> planar array to intercept sunlight and convert it to an electric voltage. Power conditioning devices then send the electricity to a laser, which transmits the power to the surface of the Earth. A ground station will convert the beam into electricity. Typically, a single SPS will supply 5 GW of power to the ground station. Due to the large mass of the SPS, about 41 million kg, construction in space is needed in order to keep the structural mass low. The orbit configuration for this design is to operate a single satellite in geosynchronous orbit (GEO). The GEO allows the system to be positioned above a single receiving station and remain in sunlight 99% of the time.

Construction will take place in low Earth orbit (LEO); array sections, 20 in total, will be sailed on solar wind out to the GEO location in 150 days. These individual transportation sections are referred to as solar sailing array panels (SSAPs). The primary truss elements used to support the array are composed of composite tubular members in a pentahedral arrangement. Smart segments consisting of passive and active damping devices will increase the control of dynamic SPS modes.

PROJECT BACKGROUND

Modern society is based on technology that depends primarily upon burning fossil fuels as an energy source. Unfortunately, dependence on this form of energy has many associated problems. Regional, political, and religious conflicts can disrupt worldwide distribution of fossil fuels, which can threaten world stability and peace. The search for alternative sources of energy has led to the development of solar power. Compared to fossil fuels, the Sun promises to be an infinite source of energy. Technology has already created the means to harness the power of the Sun cheaply and efficiently without the drawbacks of fossil fuels. This study builds upon a concept formulated in 1968 by Peter Glaser and on research conducted in the late 1970s on Satellite Power Systems. ASPEC's objectives are to make an integrated satellite design and to update previous findings with the application of modern technologies.

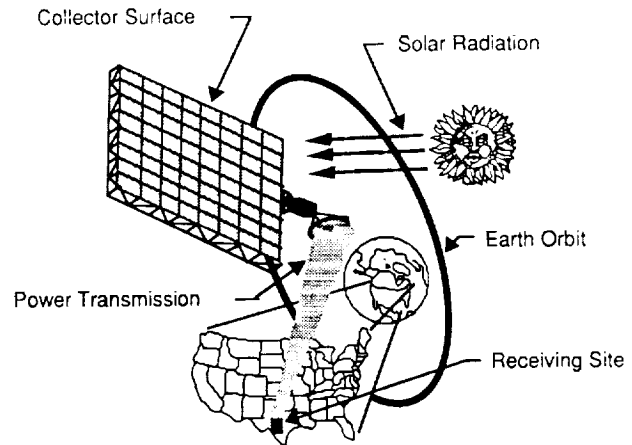


Fig. 1. Overall system concept.

SYSTEM GUIDELINES

Guidelines for the Satellite Power System design have been established by the Request for Proposal in the form of assumptions and requirements. The following are selected assumptions used to guide system development: (1) technology available by the year 2000; (2) cost is not a design parameter; (3) launch failure rate is 1%; and (4) weight growth factor of 15% should be reflected in final mass estimates. The following are the basic system requirements: (1) the SPS will supply 5 GW to a ground site; (2) damage to Earth and space environment is minimal; (3) space debris from construction/operation is minimal; and (4) system life is 30 years.

SOLAR TECHNOLOGY

The selection of a solar to electrical energy conversion method is a primary consideration in realizing the SPS concept. This study researched the two methods of energy conversion considered to be feasible for use by the year 2000, solar dynamic systems and solar photovoltaic cells. After completing research on these two types of energy conversion methods, solar photovoltaic cells were selected for use on the SPS. This selection was based upon a comparison of the relative advantages and disadvantages of the two conversion methods.

ASPEC proposes to reduce the costs of the solar array by using plastic lenses to concentrate sunlight onto small-area single crystals. The concentrator lens/solar cell approach has additional advantages over single crystal units. Since the cells are small and located behind lightweight optics, they are shielded for improved radiation resistance leading to higher end-of-mission performance. Also, the use of smaller size solar cells leads to

higher manufacturing yields. As Fig. 2 shows, assuming one defect per wafer, the material utilization is 90% in the small concentrator cell approach, as opposed to 64% for large flat plate solar cells. Lightweight, plastic Fresnel lenses have been chosen for the SPS design. In addition to their low weight, the lenses can be manufactured easily and inexpensively in mass quantities<sup>(1)</sup>.

In the last decade, solar cells have consisted of a single layer of material converting a specific range of the solar spectrum to electricity. Efficiencies as high as 24% in the space environment have been recorded using this approach. Recent breakthroughs in solar technology have led to the development of double- and triple-layer cells. Current work with two-layer tandem cells has produced cells achieving efficiencies as high as 31%<sup>(2)</sup>. Predictions have been made for three-layer tandem cells with conversion efficiencies of 48.6%. Such highly efficient cells are ideally suited for the SPS, resulting in a reduction of the number of cells and the size of array panels needed to produce 5 GW.

The Solar Technology subgroup conducted research to select the appropriate materials for each layer of the stacked cell. Current research indicated GaAs and AlGaAs as prime candidates for the top layer. Silicon, GaSb, or InP are possibilities for the second layer. The most work remains to be completed in the manufacturing of the third layer. By the year 2000, based upon trends in solar technology, the major candidate for the bottom layer is InGaAsP<sup>(3)</sup>. In developing efficient multilayer solar cells, each layer must be made transparent to certain frequencies of light used in the lower cells. To accomplish this, the solid metal backing normally used to collect and conduct the current on conventional cells is eliminated. In its place is a grid of fine metal lines on the top of the cell that perform the same function<sup>(2)</sup>.

The concept of a multiple stack concentrator cell is demonstrated in Fig. 3. The concentrating lens is fixed above the stack (typically at a height of 1"). Light passes through the lens and is focused onto the smaller cell assembly where it first strikes a prismatic Entech cover. This cover bends the light around the metal gridlines on the surface of the solar cell.

**ORBITS AND CONTROLS**

Control of the SPS is accomplished by integrating the components used on SSAPs into a complete system once at the GEO station. The SSAPs will be assembled at a space factory in LEO.

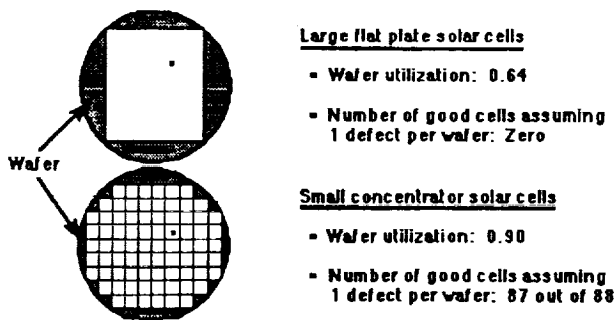


Fig. 2. Small concentrator cells lead to higher manufacturing yields.

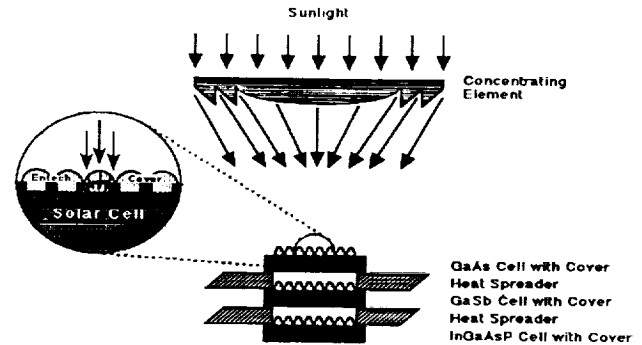


Fig. 3. Multistack solar cell.

All the materials required for this will be sent up to LEO with a heavy lift launch vehicle (HLLV). This could be accomplished with a smaller vehicle, but even with an HLLV that can carry  $2.5 \times 10^5$  kg to LEO, it will take at least 165 launches.

Each SSAP will consist of a 1-sq-km section of the solar array, four gimbaled ion thrusters, two cylindrical pressure vessels that each contain 77,200 kg of argon, and an attitude reference determination system (ARDS). The ARDS consists of a charged coupled device (CCD), Sun sensor, two CCD star sensors, a set of three rate gyros, and a processor that will interpret the sensor readings and control the thrusters. The total mass of each SSAP is  $2.055 \times 10^6$  kg. Figure 4 shows an SSAP.

After the SSAP is assembled, it will spiral out with a constant tangential, low thrust to GEO where the fully assembled SPS will be. The SSAP will power itself with its solar array that will remain perpendicular to the Sun's rays. The SSAP will also have batteries for power during shadow. The transfer will be powered by four ion engines; preliminary calculations show that the resulting thrust should be tangential to the transfer path. The total time of this transfer is approximately 150 days.

Once the SSAPs arrive at GEO, they will be integrated into the SPS. This will be done by telerobotics. The thrusters and ARDS will be removed from each of the SSAPs and the SSAPs will be joined together to form the SPS. The thrusters will be attached to the corners of the SPS (20 at each corner), one pair of ARDSs will be located at each corner of the SPS, one pair will be located at the center of mass of the SPS, and one pair will be located on each side of the transmission dish. The processors will be removed from the remaining six ARDSs and evenly spaced along the SPS array and converted to monitor damage. The leftover sensor and gyros will be stored with the robots in case they are needed later as replacement parts. The thruster system features an argon ion bombardment thruster reaction control system operating an average of 36 thrusters at a time. Each thruster is an argon ion bombardment thruster with a specific impulse of 13,000 sec and a thrust of 23 N. They require 1275 kW of power, and a 1-m aperture. The thruster system will be controlled by the attitude control computer. The attitude control computer will receive its information for the processors from each of the ARDSs.

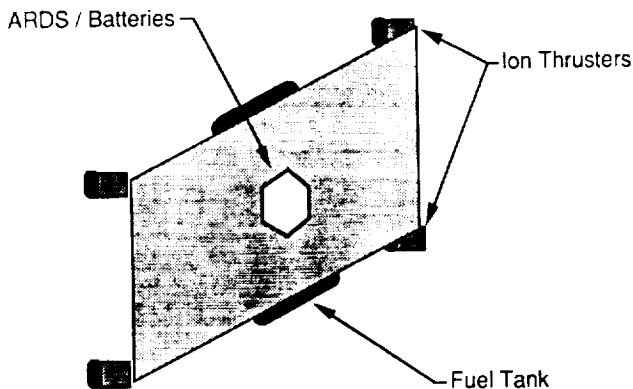


Fig. 4. Configuration of an SSAP

### POWER TRANSMISSION

The Power Transmission subsystem studies selected a CO<sub>2</sub> laser-based subsystem. Laser and microwave were compared based on five criteria: size of transmission optics, efficiency, flexibility of system, development of technology, and area of ground station required.

Size of transmission optics was considered the most important criterion. Depending on the type of laser chosen, the transmitting antenna will be 10 m to 60 m in diameter and weigh from 10,000 to 100,000 kg<sup>(4)</sup>. The next criterion is electric-to-beam conversion efficiency. Laser conversion is estimated to have significantly lower efficiency (30%-80%, depending on the type of laser) than microwave conversion (80%-90%)<sup>(4)</sup>. This is the only area where the laser concept falls below that of the microwave. Flexibility of the system is incorporated into future possible operating scenarios. Since the laser beam is small, it could be employed for aircraft propulsion or to provide power for spacecraft or space stations. The development of laser technology is behind that of microwave, but research is continuing to advance laser capabilities, especially in SDIO studies. Finally, the area of the ground station is a relatively minor criteria, because the cost of purchasing real estate may be considered negligible when compared to the other costs of this project. The amount of area required for a ground station to receive a laser beam (about 200 acres) is much smaller than the area required to receive a microwave beam (about 80,000 acres)<sup>(4)</sup>. After considering and weighing the previously described criteria, ASPEC chose laser as the best mode of power transmission for the SPS.

The Laser Power Transmission Subsystem (LPTS) will consist of four major elements: electrical power supply, the closed cycle laser, heat removal, and optics. These elements are detailed in the following section. A side view of the LPTS is shown in Fig. 5.

The LPTS will require some power conditioning of electricity that is produced by the solar arrays. This power conditioning is needed to convert lower-voltage solar cell power into high-voltage power for laser pumping. This can be done at an efficiency of 95% or higher<sup>(5)</sup>.

Four types of laser considered were the carbon dioxide laser, carbon monoxide laser, iodine solar pumped laser, and semi-

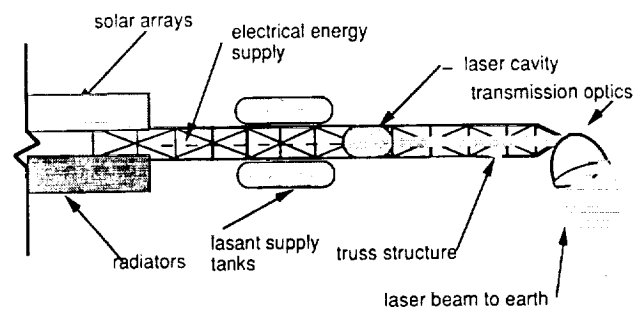


Fig. 5. Laser subsystem—side view (not to scale).

conductor diode lasers. The first electrically driven laser developed was the carbon dioxide (CO<sub>2</sub>) laser. It has a wavelength of 10.6  $\mu\text{m}$ . A geosynchronous satellite will require a 60-m-diameter aperture to beam a 10-m-diameter spot on the ground. As of 1989, the CO<sub>2</sub> laser is the most developed high-powered gas laser and promises an open cycle efficiency of greater than 60% operating at 409 K<sup>(5)</sup>.

The heat removal element of the LPTS consists primarily of radiators. If it is assumed that the selected CO<sub>2</sub> laser can operate at 80% efficiency, then 1.316 GW will be absorbed by the lasant and must be removed continuously to maintain the lasant at operating temperature. This task will be performed by radiators nearly 1.22 sq km in area. The radiators will be located near the transmission end of the SPS, underneath the solar arrays, in order to protect the radiators from heating and solar degradation<sup>(6)</sup>.

An adaptive optical system employing active controls to remove beam aberration aims and focuses the laser radiation. The transmitting aperture expands the narrow beam from the laser device and corrects for any beam distortion. A Cassegrain aperture configuration using a large concave primary mirror and a small convex secondary mirror is employed. The primary mirror surface is composed of small mirrors supported by 5 actuators on a truss structure. The combination of these actuators and mirror segments conforms the primary mirror to the desired shape<sup>(7)</sup>.

### SAFETY

There are many safety concerns associated with beaming lasers to Earth. The primary concern is the effect laser beams might have on humans in the vicinity of the reception site. This problem is avoided by locating the receiving site in an area of sparse population and building a fenced buffer zone around the target area. Another safety concern is whether airplanes will be able to fly through this beam. A radiation level as high as 1.5 W/cm<sup>2</sup> is permitted for aircraft, but the system will beam as much as 10 w/cm<sup>2</sup> to the ground. Thus, airplane flights will have to be restricted away from the vicinity of the beam<sup>(4)</sup>.

## STRUCTURES

With a required solar array area on the order of 20 sq km (about 7 sq m), the SPS will be by far the largest man-made structure ever placed in orbit. The supporting truss structure is required to support the cell arrays, support the subsystems, and give accuracy to the pointing of the arrays. Three types of trusses were considered: tetrahedral, A-frame, and pentahedral. The pentahedral truss combines ease of serviceability and load handling efficiency. This design contains no tension members while allowing access to the square sub-arrays, which easily lend themselves to modular design. As a result of these advantages, the pentahedral truss was chosen to be the primary supporting structure for the SPS.

## MATERIALS

The choice of materials is another important consideration in the design of the SPS structure. Availability, low manufacturing costs, and a large amount of existing performance data make conventional alloys primary candidates for use as materials for structural members. Aluminium alloys feature a high stiffness-to-density ratio and excellent workability and a low level of magnetism. Unfortunately, aluminum's low yield strength may be prohibitive<sup>(6)</sup>. Composites combine high strength, extremely light weight, low thermal conductivity, and tailorable elastic properties making them another worthy candidate for use as structural member materials. Effective oxidation coatings are essential, however, because even slight damage to the surface (which may be ignored with conventional alloys) can destroy the integrity of the composite fibers, resulting in a catastrophic failure. In addition to the special coating, electrical grounding must be achieved by using conductive strips located throughout the structure. As a result of these drawbacks, composites have been previously relegated to roles as secondary structures<sup>(6)</sup>. New developments in the field, however, are occurring at a rapid pace, and it is thus not unreasonable to expect that solutions to such problems may be found in the very near future<sup>(8)</sup>.

As a result of these projected developments, composites have been chosen as the primary material for the SPS truss structure. Specifically the material data for DuPont Kevlar 49 was used in all structural calculations.

## SMART STRUCTURES

The large, flexible supporting structure required by the SPS will require an advanced structural control system. Active structural elements that will be able to independently vary their damping coefficients will be dispersed throughout the structure where they will automatically respond to minimize any damaging effects. Active members using electrorheological (ER) fluids as a stiffening mechanism show particular promise<sup>(9)</sup>. Electrorheological fluids possess the unique property of a viscosity that varies with an applied electric field. As a result, a nearly immediate increase in damping in response to structural vibrations

is possible. Besides controlling the damping electronically, a structural increase in damping can be accomplished by using an elastomer between layers in the composite tubes. The inner and outer tubes can then shear independently and excess energy is absorbed in the elastic layer.

## MODULAR CONSTRUCTION

Due to the sheer size of the SPS, it is not feasible to attempt to assemble the entire satellite in LEO and then transport it to GEO. Thus, the structure must be designed with some degree of modularity. The SPS will be constructed from a number of individual SSAPs. The SSAPs are in turn composed of smaller individual solar panels. These panels will also be incorporated into individual modules containing their own lenses, solar cells, and rigid backing structures. Thus, the solar panels are designed to be easily removed and replaced. Construction of the SPS will take too long and be far too dangerous to make human assembly feasible. Thus, most of the assembly tasks will be performed robotically.

Launches from Earth will primarily carry preprocessed materials into LEO where an orbiting "space factory" will extrude the tubular members and assemble the truss structures. This eliminates the need for a collapsible structure designed to fit inside the payload bay of a launch vehicle. Prototype remote facilities for manufacturing structural members and constructing truss structures like the Grumman beam builder have already been built and tested.

The primary steps in assembly of the SPS are: (1) Establish a "space factory" in LEO with facilities to manufacture the structural elements and assemble the SSAPs; (2) Launch the pre-processed structural materials for manufacture of structural elements. The solar panels will be manufactured on Earth and launched for assembly in LEO; (3) Assemble the truss structure from its individual elements and mount the solar panels until an entire SSAP is produced; (4) Transport the SSAP to GEO using ion thrusters powered by electricity generated by the SSAP itself; and (5) Rejoin final assembly in GEO as robots assemble the arriving SSAPs to form the operational SPS.

## ROBOTIC MAINTENANCE

Robots will be used extensively to perform both routine maintenance and unscheduled repairs of the SPS. The robotic maintenance system will be primarily composed of two robots mounted on a railing fixed to the SPS. As shown in Fig. 6, the mounting rail will move the robots over the length of the SPS, while the robots themselves will move transversely along the rail. This system, which operates much like an ordinary computer plotter, allows any point on the SPS to be easily reached. These rail-mounted robots will be primarily used to perform routine repairs, especially replacement of damaged solar cells. The mounting rails will extend around the edge of the SPS to allow the robots to service the rear of the structure. Direct human involvement will only be required if a problem arises that is too complex to be handled entirely by the robots.

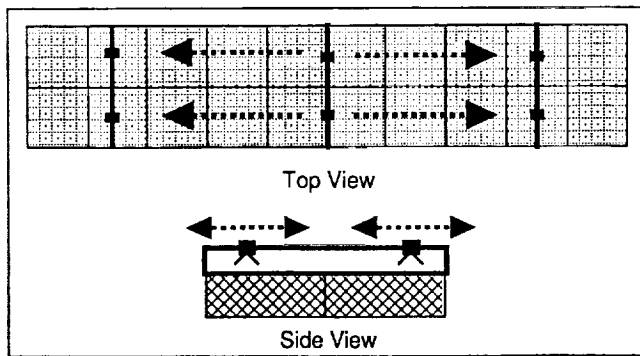


Fig. 6. Rail mounted robot concept.

#### REFERENCES

1. O'Neill, M. J., Piszczor, Domed Fresnel Lens Concentrator Technology. *Space Photovoltaic Research and Technology 1988*, pp. 286-289.
2. Fraas, Lewis and Avery, James E. (1990) *Over 30% Efficient Tandem Gallium Solar Cells for Use with Concentrated Sunlight*, p. 299. Boeing High Technology Center, Seattle.
3. Negley, G. H., Rhoads (1988) A Three Solar Cell System Based on Self-Supporting Transparent AlGaAs Top Solar Cell. *Space Photovoltaic Research and Technology 1988*, pp. 190-194.
4. Bain, Claud N. (1978) *Potential of Laser for SPS Power Transmission*, U.S. Department of Energy Contract No. E.G.-77-C-01-4024.
5. DeYoung, R. J., et. al., (1988) One-Megawatt Solar Pumped and Electrically Driven Lasers for Space Power Transmission. *Proceedings of the Intersociety Energy Conversion Engineering Conference*, Vol. 3, pp. 710-711. NASA Langley Research Center.
6. Baer, Tony (1984) Space Station Thermal Control, *Mechanical Engineering*, December, 1984.
7. Hertzberg, A. and Sun, K. C. (1989) New Energy Conversion Techniques in Space, Applicable to Propulsion. *Proceedings of the Second Beamed Space Power Workshop*, p. 78. NASA Langley Research Center.
8. Stevens, Tim (1990) Carbon Fiber, Poised to Dominate, *Mechanical Engineering*, 35-38.
9. Choi, S. B., Thompson, B. S., and Gandhi, M. V. (1989) Smart Structures Incorporating Electro-Rheological Fluids for Vibration-Control and Active-Damping Applications: An Experimental Investigation. *Proceedings of the 1989 ASME Design Technical Conferences—12th Biennial Conference on Mechanical Vibration and Noise*, pp. 17-21. American Society of Mechanical Engineers, New York.



**B&T—LUNAR LANDERS**

**THE UNIVERSITY OF TEXAS, AUSTIN**

**INTRODUCTION**

In the early twenty-first century, astronauts will return to the Moon and establish a permanent base. To achieve this goal safely and economically, B&T Engineering has designed an unmanned, reusable, self-unloading lunar lander. The lander is designed to deliver 15,000-kg payloads from an orbital transfer vehicle (OTV) in a low lunar polar orbit and at an altitude of 200 km to any location on the lunar surface.

**MISSION/TRAJECTORIES**

Initially the OTV transfers the lander from low earth orbit (LEO) to low lunar orbit (LLO). For maximum efficiency, the Earth-Moon transfer will be performed during the nodal alignment of LEO with the Moon's orbit. From a stable 200-km lunar polar parking orbit, the lander will wait for the orbit to align with the landing site longitude and then descend to the desired position on the Moon to deliver the payload. After the lander unloads the payload, it returns to the same polar orbit to await the arrival of another payload from an OTV. The total  $\Delta V$  required for one mission is 3.594 km/s.

**PAYLOAD SYSTEM**

The payload is carried on the top of the lander by a trolley system. The trolley system consists of a chain-driven pallet that rides on two rails. The drive system consists of a continuous chain connected to the pallet's rear wheels and to a high-torque drive motor. The drive system is sealed to protect it from lunar dust contamination. The pallet and payload are supported in flight by detachable hardpoints. In order to unload the payload, these hardpoints are detached and the pallet travels along the rails over the side of the lander and down to the lunar surface. Then the payload is detached from the trolley and the pallet is retracted. Although the payload is left on the surface, it is protected from the effects of the ascent engines by a distance of over 9 m and a minimum of blast shielding. The unloading sequence and the side of of the lander is shown in Fig. 1.

**DOCKING AND REFUELING**

Docking between the lander and the OTV is accomplished automatically (Fig. 2). First, the lander soft docks with extendable columns on the OTV and then the columns are retracted, pulling the lander into a hard dock with the payload. Refueling is accomplished through fuel lines running through the support

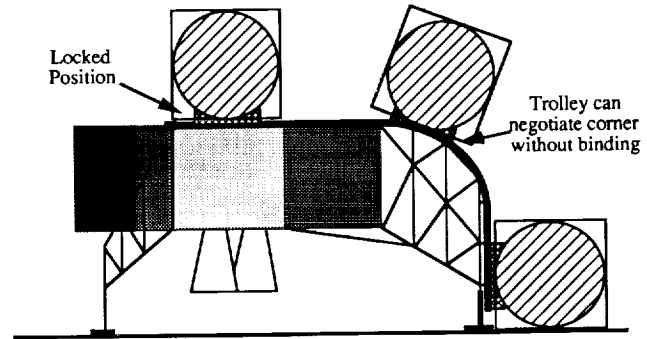


Fig. 1. The unloading sequence.

packaging of the payload. After refueling, the lander will detach with the payload from the OTV and begin the descent sequence of the mission.

**LANDER STRUCTURE**

The lander is made of four modular tank/subsystem boxes that surround the central engine/subsystem box containing the main engines and avionics. These boxes have a rigid frame constructed of thin-wall box beams and honeycomb sandwich panels. These panels provide torsional stiffness as well as thermal and dust protection. In addition to being supported by the structural boxes, the tanks have internal stiffeners/baffles. The lunar lander will touch down on a four-strut asymmetrical landing gear configuration (Figs. 3 and 4). These struts will be equipped with a terrain-adaptive system to help keep the lander level on uneven terrain.

**PROPULSION SUBSYSTEM**

The main propulsion system consists of three  $H_2/O_2$  engines capable of providing 30,000 lb of thrust each. Only two engines are needed to lift the lander, and each engine has a  $10^\circ$  gimbal capability for thrust correction in case of engine out and to adjust for center of mass location. In order to simplify the refueling process, the Reaction Control System (RCS) also uses hydrogen and oxygen. The RCS consists of vernier thrusters

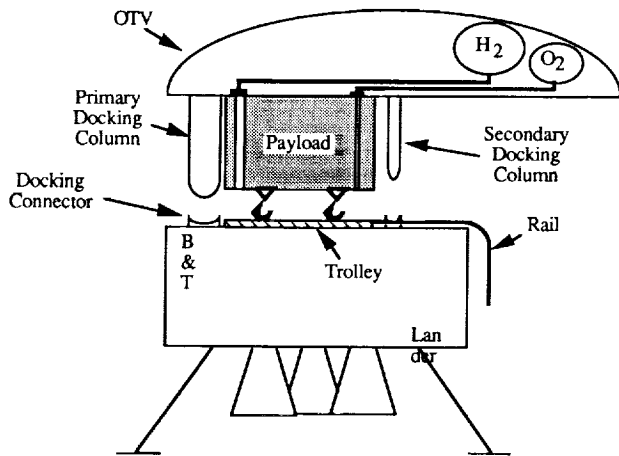


Fig. 2. Lander docking with OTV.

for low-thrust maneuvers and primary thrusters for more substantial attitude changes. The RCS motors are placed at symmetrical positions around the lander on a horizontal plane.

**POWER SUBSYSTEM**

The electrical power is supplied by a system of sodium-sulfide batteries for high-power and mission operations, and gallium-arsenic solar photovoltaic arrays for recharging and on-orbit power during the time spent between missions. The photovoltaic arrays will be stored except when the lander is in LLO. These systems provide a peak power of 11 kW and nominal power of 0.5 kW. Peak power will be used for short durations in operations such as engine gimbaling and unloading. Nominal power is consumed by the lander systems that are in continuous operation.

**GUIDANCE, NAVIGATION, AND CONTROL**

The Guidance, Navigation, and Control (GN&C) subsystem will provide the lander with the ability to follow a preprogrammed mission objective. Guidance will be provided using two inertial measurement units (IMU) and two dual-cone scanners with Sun fans to periodically update the IMUs. These systems provide all orbital parameters and attitude information to the navigation system. Navigation will consist of software in the central computer and a link with the communication subsystem to allow for input command signals to change or correct the mission. In addition, a global or lunar positioning system will provide position information as the lander approaches the lunar surface. Rendezvous radar with transponders will be used for docking and refueling with the OTV as well as for the future case of landing near a lunar base. High-precision imaging radar with obstacle avoidance software will provide the capability to land autonomously on the lunar surface. The guidance and navigation systems will send signals through the central digital computer to notify the control system when maneuvers are required. The control system will consist of RCS for relatively large attitude adjustments, a control moment system for fine tuning the attitude during proximity operations, and engine gimbaling for c.m. adjustments.

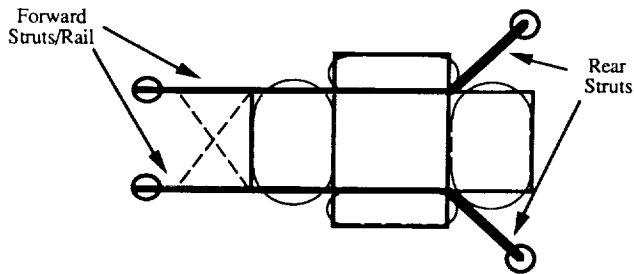


Fig. 3. The strut configuration.

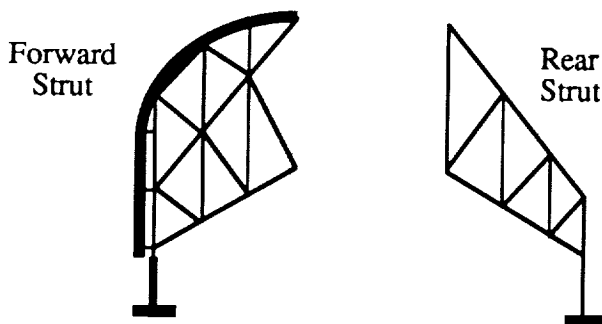


Fig. 4. The landing struts.

**COMMUNICATIONS**

The three main communication links considered in this report are lander-Earth, lander-OTV, and lander-lunar base. For lander-Earth communications, a steerable S-band antenna will be used with infrared sensors for pointing. For lander-OTV communications, X-band radar will be used for rendezvous and a low-power VHF antenna will be used for transmission of data to be relayed to Earth. The low-power VHF antenna will also be used for communication with a lunar base. The communication with Earth will be performed through the Tracking Data Acquisition System (TDAS), the replacement for the present (Tracking Data Relay Satellite System) TDRSS system.

### **THERMAL CONTROL**

The lander employs passive as well as active systems to maintain the temperature of the lander's subsystems. The lander's top side is designed to face away from the Sun to radiate heat more efficiently. Radiators from active cooling systems are placed on this side, and the bottom side is insulated and covered with reflective coatings to protect the lander from the Sun's heat.

While the cryogenic fuel of the lander is only protected by passive thermal systems, the boiloff of the fuel is still useable by the RCS thrusters.

### **LANDER MASS STATEMENT**

The total deorbit mass of the lander is 49,376 kg, which includes a 15,000-kg payload and 24,586 kg of propellant.



# SPACELY'S ROCKETS—PERSONNEL LAUNCH SYSTEM/FAMILY OF HEAVY LIFT LAUNCH VEHICLES

P. 3

THE UNIVERSITY OF TEXAS, AUSTIN

## INTRODUCTION

During 1990, numerous questions were raised regarding the ability of the current shuttle orbiter to provide reliable, on-demand support of the planned space station. Besides being plagued by reliability problems, the shuttle lacks the ability to launch some of the heavy payloads required for future space exploration, and is too expensive to operate as a mere passenger ferry to orbit. Therefore, additional launch systems are required to complement the shuttle in a more robust and capable Space Transportation System.

In December 1990, the Report of the Advisory Committee on the Future of the U.S. Space Program, headed by Norm Augustine, advised NASA of the risks of becoming too dependant on the space shuttle as an all-purpose vehicle. Furthermore, the committee felt that reducing the number of shuttle missions would prolong the life of the existing fleet. In their suggestions, the board members strongly advocated the establishment of a fleet of unmanned, heavy lift launch vehicles (HLLVs) to support the space station and other payload-intensive enterprises.

Another committee recommendation was that a space station crew rotation/rescue vehicle be developed as an alternative to the shuttle, or as a contingency if the shuttle is not available. The committee emphasized that this vehicle be designed for use as a personnel carrier, not a cargo carrier. This recommendation was made to avoid building another version of the existing shuttle, which is not ideally suited as a passenger vehicle only.

The objective of this project was to design both a Personnel Launch System (PLS) and a family of HLLVs that provide low-cost and efficient operation in missions not suited for the shuttle.

## PERSONNEL LAUNCH SYSTEM DESIGN

The PLS vehicle is designed primarily for space station crew rotation and emergency crew return. Therefore, a nominal complement of eight passengers is provided for. Studies have indicated that a small, reusable, lifting-body spacecraft can operate at greater cost effectiveness, reliability, and safety than the shuttle. The personnel vehicle is carried into low Earth orbit by a partially reusable, man-rated version of the heavy lift vehicles codesigned in this project.

The final design of the PLS vehicle is depicted in Fig. 1. It has an overall length of 36 ft and an overall width of 27 ft. The weight of this vehicle is 30,000 lb. The vehicle has provisions for eight passengers and a flight crew of two for a maximum mission duration of three days.

The interior of the craft is shown in Fig. 2. Although it is meant to be a payload-intensive vehicle, the PLS is designed to carry a minimum of space station resupply with specific cargo area designed into the craft. More cargo area can be gained by removing the passenger seats when the PLS vehicle does not have a full crew complement.

The PLS vehicle is designed to be boosted into orbit by launching it serially from a man-rated rocket. To ensure crew safety during ascent, the final design provides for an on-pad abort, as well as an abort during ascent if an emergency situation arises.

## HEAVY LIFT LAUNCH VEHICLE DESIGN

The mission of the family of HLLVs is to place large, massive payloads into Earth orbit with payload flexibility being considered foremost in the design. Because of this concern, the final design of three launch vehicles was found to yield a payload capacity range from 20 Mt to 200 Mt. These designs include the use of multistaged, high-thrust liquid engines mounted on the core stages of the rocket. Payload flexibility is provided by the use of multiple strap-on solid rocket boosters. The final design of the FHLLV project consists of three basic configurations: the SR-1, the SR-2, and the SR-3. These vehicles are shown in comparison in Fig. 3.

The SR-1 is the smallest vehicle in the launch vehicle family. It has a payload capacity of 20-95 Mt depending on the number of SRBs used, and whether or not a second stage is employed. Figure 4 illustrates the basic dimensions of the SR-1 in the 72-Mt configuration. This configuration employs two SRBs and the second stage. The SR-1 can mount two or four SRBs as required to increase the payload capacity.

The first stage of the all-liquid-propelled core utilizes three SSME-35s for propulsion, and is a cylindrical structure that houses the oxidizer and fuel for the first stage in separate tanks. The first stage is 31 ft in diameter and 149 ft tall. The second stage of the SR-1 relies on two unmodified SSMEs for thrust. It has a diameter of 24 ft and a length of 82 ft without the payload shroud. Overall, the SR-1 stands 357 ft tall, and has a width of nearly 70 ft. The gross lift-off weight and stage dimensions for the SR-1 are shown in Fig. 4.

The SR-2 is the medium capacity vehicle in the launch vehicle family. It has a payload capacity of 40-150 Mt depending on the number of SRBs used and whether or not the second stage is employed. Figure 5 illustrates the basic dimensions of the SR-2 in the 100-Mt configuration. This configuration employs

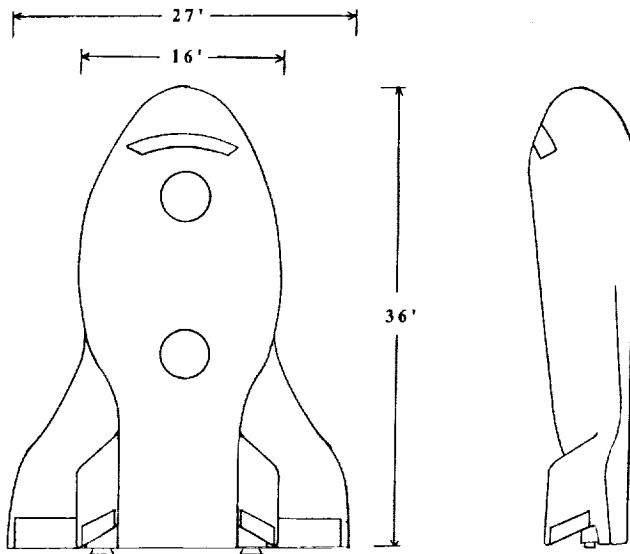


Fig. 1. PLS exterior concept.

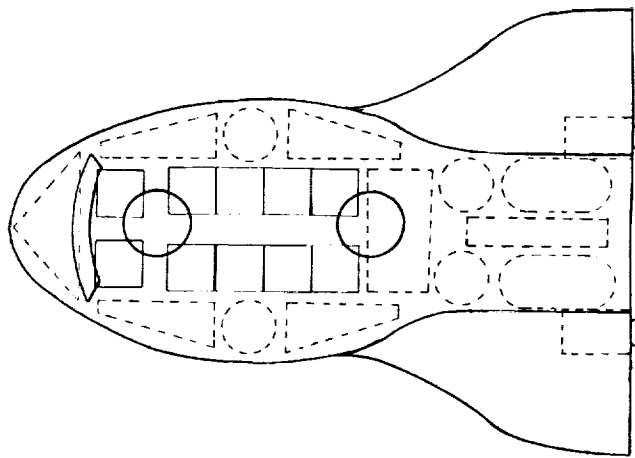


Fig. 2. The interior diagram of the PLS.

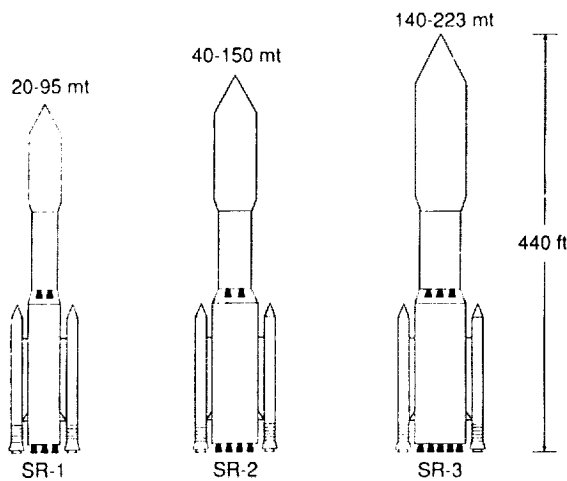


Fig. 3. Launch vehicle family.

|                        |                     |
|------------------------|---------------------|
| <b>GLOW</b>            | <b>5,328,660 lb</b> |
| <b>Payload Shroud</b>  | <b>3307</b>         |
| <b>2nd Stage</b>       |                     |
| <b>Structural Mass</b> | <b>47,058</b>       |
| <b>Propellant Mass</b> | <b>306,004</b>      |
| <b>2 SSME's</b>        |                     |
| <b>1st Stage</b>       |                     |
| <b>Structural Mass</b> | <b>122,355</b>      |
| <b>Propellant Mass</b> | <b>1,178,083</b>    |
| <b>3 SSME-35's</b>     |                     |
| <b>2 SRB's</b>         |                     |

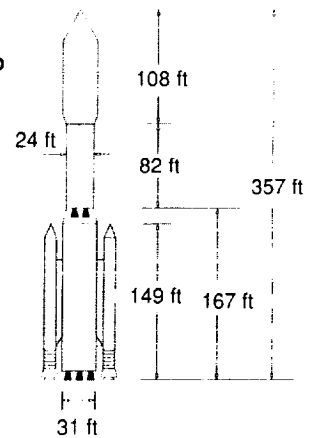


Fig. 4. The SR-1 launch vehicle.

two SRBs and the second stage. The SR-2 can employ two, four, or six SRBs as required to increase the payload capacity.

The first stage of the all-liquid-propelled core utilizes five SSME-35s for propulsion and is 40 ft in diameter and 149 ft tall. The second stage of the SR-2 relies on two or three unmodified SSMEs as needed for thrust. The second stage has a diameter of 31 ft and a length of 82 ft without the payload shroud. Overall, the SR-2 stands 384 ft tall, and has a width of nearly 76 ft. The gross lift-off weight and stage weights for the SR-2 are shown in Fig. 5.

The SR-3 is the largest vehicle in the launch vehicle family. It has a payload capacity of 140-200 Mt depending on the number of SRBs used. Figure 6 illustrates the basic dimensions of the SR-3 in the 200-Mt configuration. This configuration employs six SRBs. The SR-3 can mount two, four, six, or eight SRBs as required to increase the payload capacity.

The first stage of the all-liquid-propelled core utilizes eight SSME-35s for propulsion. It is 50 ft in diameter and 149 ft tall. The second stage relies on two or three unmodified SSMEs as needed for thrust; it has a diameter of 40 ft and a length of 82 ft without the payload shroud. Overall, the SR-3 stands 440 ft tall, and has a width of nearly 86 ft. The gross lift-off weight and stage weights for the SR-3 are shown in Fig. 6.

Both the PLS and family of HLLV systems designed by Spacefly's Rockets fit neatly into the planned evolution of the U.S. space program. The PLS, if actually constructed, would provide more efficient manned access to space on a routine schedule of flights. This in turn, alleviates fears that the Space Station *Freedom* will be built without a guaranteed crew return vehicle. The construction of the family of heavy lift launch vehicles would give the U.S. unprecedented launch capacity for any program being pursued, and potentially provide the inexpensive commercial access to space. Thus, the hopes of the Space Exploration Initiative and other projects can be realized by finally having a heavy lift system available.

|                        |                     |
|------------------------|---------------------|
| <b>GLOW</b>            | <b>5,496,064 lb</b> |
| <b>Payload Shroud</b>  | <b>6,614</b>        |
| <b>2nd Stage</b>       |                     |
| <b>Structural Mass</b> | <b>78,446</b>       |
| <b>Propellant Mass</b> | <b>509,915</b>      |
| <b>2 SSME's</b>        |                     |
| <b>1st Stage</b>       |                     |
| <b>Structural Mass</b> | <b>203,925</b>      |
| <b>Propellant Mass</b> | <b>1,963,472</b>    |
| <b>5 SSME-35's</b>     |                     |
| <b>2 SRB's</b>         |                     |

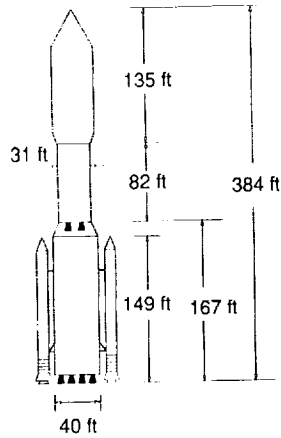


Fig. 5. SR-2 launch vehicle.

|                        |                      |
|------------------------|----------------------|
| <b>GLOW</b>            | <b>12,399,460 lb</b> |
| <b>Payload Shroud</b>  | <b>11,023</b>        |
| <b>2nd Stage</b>       |                      |
| <b>Structural Mass</b> | <b>125,662</b>       |
| <b>Propellant Mass</b> | <b>817,702</b>       |
| <b>3 SSME's</b>        |                      |
| <b>1st Stage</b>       |                      |
| <b>Structural Mass</b> | <b>326,281</b>       |
| <b>Propellant Mass</b> | <b>3,141,555</b>     |
| <b>8 SSME-35's</b>     |                      |
| <b>6 SRB's</b>         |                      |

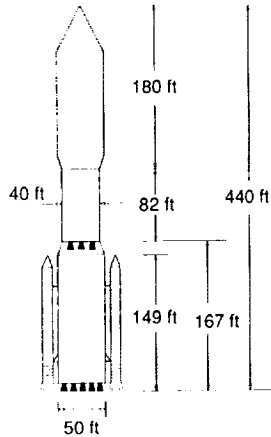


Fig. 6. The SR-3 launch vehicle.



**RS LANDERS—LUNAR LANDER****THE UNIVERSITY OF TEXAS, AUSTIN**

160 617

p. 3

**INTRODUCTION**

The future of the U.S. space program outlined by President Bush calls for a permanently manned lunar base. A payload delivery system will be required to support the buildup and operation of that lunar base. In response to this goal, RS Landers has developed a conceptual design of a self-unloading, unmanned, reusable lunar lander. The lander will deliver a 7000-kg payload, with the same dimensions as a space station logistics module, from low lunar orbit (LLO) to any location on the surface of the Moon.

**LUNAR LANDER DESIGN**

The proposed design has been named "La Rotisserie" and is shown in Fig. 1. It consists of a lander, unloader, and payload. The payload and the unloader are loaded in an inverted position on top of the lander. After postlanding stabilization on the lunar surface, the entire structure will rotate 180° with respect to the legs. This rotation will take at least 30 minutes in order to minimize dynamic loads exerted on the rotation mechanisms.

When the rotation is complete, the unloader will be lowered to the surface. The unloader will then drive out between the legs and deliver the payload to its desired location. In order to avoid excessive engine plume damage, the distance between the landing location and a possible lunar base should be about 2 km. Therefore the range of the unloader was set at 5 km. Once the payload is delivered, the unloader can return to LLO with the lander, or it can remain on the surface to await the lander's return.

**MAIN ENGINES**

Solid-core nuclear motors were chosen for use on the lunar lander. These motors have an optimistically projected specific impulse of 1200 s and thrust-to-weight ratio of 11.3. The fuel used is liquid hydrogen. The maximum required thrust occurs during the descent phase of the mission, and it is 22,584 lbf.

It is not currently known whether a three-motor configuration or a single-motor configuration would be superior for use on the lander. For conventional motors, the three-motor configuration is recommended for situations of engine out. There are studies being done to determine the effect of clustering nuclear motors. It may be necessary to use one nuclear motor with redundant turbopumps. However, all calculations and estimations took place assuming a three-motor configuration. The internal arrangement of fuel tanks and subsystems is shown on Fig. 2.

**UNLOADING MECHANISMS**

The detailed design of the mechanical components of the various payload unloading mechanisms is beyond the scope of this study; however, there are a few areas that have been considered during their study. The types of electric motors, bearings, and drive train or gear reduction system have been of interest.

The motors that are most promising for the La Rotisserie concept use direct current, deliver moderate torque, medium rotation rates (around 1000 rpm), and are of a brushless design. These are the most suitable for working in the lunar environment due to their efficiency and durability.

Coated bearings are recommended for use on the lunar lander. Lubricants will prove to be ineffective in the harsh lunar environment. They will either become filled with dust, freeze up, or boil off. Possible bearing coatings include Teflon®, Nomex®, and diamond. Diamond coatings can be applied using chemical vapor deposition.

Finally, a harmonic drive system is recommended for use on the lunar lander. Harmonic drives have fewer moving parts than the conventional gear box. Therefore they are less massive and have fewer losses. Harmonic drive systems use flexible splines that wear faster than conventional gear box components; however, with the advent of advanced materials, the harmonic drive can be designed to meet the lander's requirements in the near future.

**TRAJECTORIES**

The lander trajectories have been designed and optimized using a computer program called Lander developed by Eagle Engineering in Houston, Texas, to simulate the ascent and descent phases of a lunar landing mission.

The landing site location of the Apollo 15 mission was chosen for the lunar lander simulation. The resulting total  $\Delta V$ s were 1.839 km/s for ascent and 1.92 km/s for descent. The flight times were 50 min for ascent and 63.25 min for descent. The use of the solid core thermal nuclear propulsion system has provided more flexible parameters for trajectory optimization than conventional propulsion.

**STRUCTURES AND MATERIALS**

The lander structure provides connectivity and integrity to all the lander's systems. The central box of the lander structure carries all the loads generated by the subsystems. This box is a truss structure enclosed by honeycomb core panels. The truss structure is strong enough to support the loads generated by

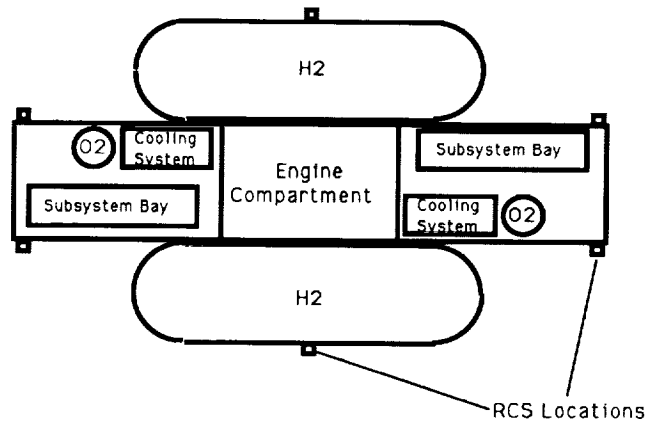
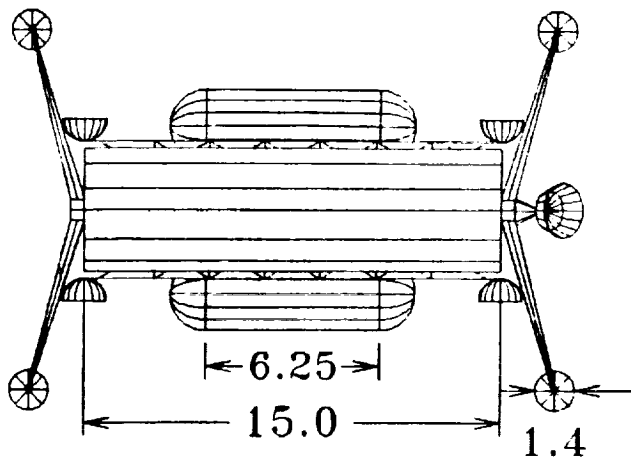


Fig. 2. The subsystem and tank arrangement in the lander.

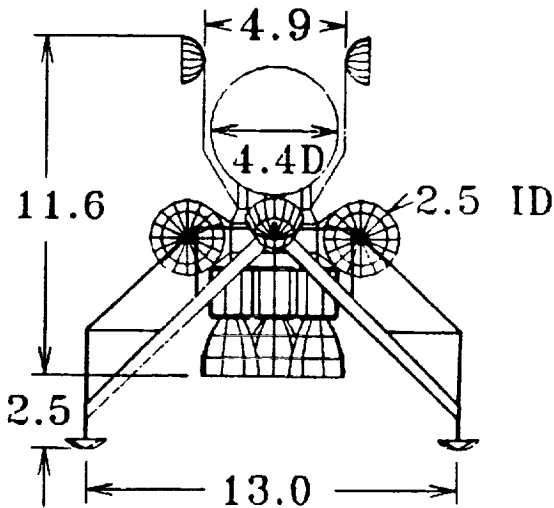
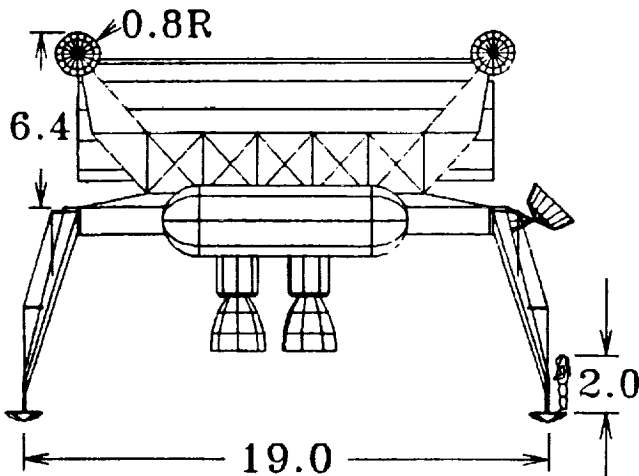


Fig. 1. The dimensions of La Rotisserie lander (meters).

the subsystems, and its lightweight panels protect the subsystems from solar radiation, dust, and micrometeorites.

The landing gear is composed of four struts that are lightweight planar trusses with landing pads similar to the Apollo lunar module. To enable the lander to remain level on an incline of up to 8°, a terrain adaptive system is incorporated into the landing gear.

Aluminum-lithium alloys were chosen as the main construction material for the lander. In addition to having the advantages of standard aluminum alloys, they can have a high tensile strength (over 100 ksi), along with increased weldability and a higher cryogenic strength.

#### GUIDANCE, NAVIGATION, AND CONTROL

The purpose of the guidance, navigation, and control (GNC) system is to determine the linear and angular position, velocity, and acceleration of the lander, to compare those data with the desired state, and to make corrections when necessary. The desired state of the lander will be provided by the predetermined trajectory analysis for each specific mission.

Three levels of sensors are used for redundancy. During optimum operating conditions, several components of each level of redundancy will be used. The primary, secondary, and emergency sensor arrays rely on a radar imaging/altimeter system, several sets of accelerometers and gyros, a transponder system, a close proximity altitude detection device, and the communications system. The communications system is only used as a sensor for emergency situations.

The onboard navigation computer will be a fault-tolerant high-performance computer. The rapid pace of computer and software development has shown that the advanced system required can be developed, and, additionally, have little mass and power consumption. The navigation computer will be responsible for monitoring the output and status of each sensor, monitoring the status of and providing input for each of the control devices, and providing an interface between the two.

The lander will use three control techniques: momentum exchange devices, small directional thrusters, and gimballed/throttled main engines. While some redundancy exists using all three systems, the optimum operating conditions will use each technique where best suited.

The control of the unloader will be primarily automated with a remote control system as a backup. The unloader will have optical sensors that will inform the unloader's onboard computer of obstacles. The computer will then instruct the wheel motors to make the required adjustments. The unloader will be in constant communication with the lander, in case it becomes necessary to employ the back up remote control system.

### COMMUNICATIONS

The communications systems provide three basic functions: telemetry, command, and tracking. The system must enable the following communication links: (1) lander to Earth; (2) lander to OTV; and (3) lander to unloader.

S-band (2.3 GHz) will be used for direct communications between the lander and Earth. The antenna on the lander will be a parabolic dish with pointing capabilities similar to that on the Apollo spacecraft. The Apollo pointing system is sufficient for the communication link with Earth.

It is recommended that a communications satellite be placed in a halo orbit on the L2 Lagrangian point. The satellite would allow transmissions to be made between the lander and Earth when the lander is on the farside of the Moon.

Communications between the OTV and the lander will be done with a VHF system. The antennas for this system will be dipoles and therefore there will not be a need for pointing. This system will be used during docking. Once the lander is docked with the OTV a data feed umbilical will be connected to the lander by means of a manipulator arm on the OTV.

The lander and unloader will communicate using a UHF system. The UHF receivers and transmitters are small, lightweight, and require little power. The UHF antennas are also small and there is no need for pointing.

### POWER/THERMAL CONTROL

The energy for the power system is provided by the heat generated during engine cool-down cycles. A power conversion loop transforms the heat into electrical energy, which is then stored in rechargeable NaS batteries on the lander and the unloader. The conversion loop also serves to cool down the nuclear motors and keep the batteries at a higher operating temperature.

Two sets of batteries provide 11 kWhr of power on both the lander and the unloader. The power for the unloader allows it to carry the payload 5 km at a speed of 2.5 km/hr. In the event that the unloader remains on the surface for an extended period, two solar arrays totalling 20 sq m, mounted on the unloader, will be used. The GaAs/Ge arrays are able to recharge the batteries fully in about one solar day.

Thermal control will be accomplished using several methods. The first method will employ the use of a cryogenic refrigeration system that will be powered by the power generation loop. The second method will employ the use of 2.5" of multilayer

insulation on the propellant tanks and other areas that require thermal control. Heat exchangers on the power generation loop will also be used to keep certain areas of the lander warm.

The final method that will be used is two radiation/thermal protection umbrellas. These umbrellas will be deployed from the landing struts after the complete rotation sequence has been performed. The umbrellas will help to reduce the workload on the refrigeration system.

### MASS ESTIMATES

When delivering a payload of 7000 kg, the total deorbit mass of the lander will be 21,584 kg. In addition to the payload mass, this deorbit mass includes 9780 kg of inert mass and 4804 kg of fuel. The mass of the lander is broken down in Table 1.

TABLE 1. Mass estimate for La Rotisserie.

| Item                        | Mass (kg) |
|-----------------------------|-----------|
| Payload                     | 7,000     |
| Inerts                      |           |
| Structure                   |           |
| (Lander)                    | 2,290     |
| (Unloader)                  | 1,200     |
| 3 Engines w/Shielding       | 3,000     |
| RCS                         | 600       |
| Fuel Tanks w/Insulation     | 820       |
| Power System                | 700       |
| Refrigeration System        | 500       |
| Rotation Motors and Winches | 300       |
| GN and C                    | 150       |
| Data Processing             | 40        |
| Communication               | 50        |
| Thermal Control             | 130       |
| Total Inert Mass            | 9,780     |
| Fuel                        |           |
| Descent                     | 2,876     |
| Ascent                      | 1,508     |
| RCS                         | 420       |
| Total Fuel Mass             | 4,804     |
| Deorbit Gross Mass          | 21,584    |



# SPECS—ORBITAL DEBRIS REMOVAL

THE UNIVERSITY OF TEXAS, AUSTIN

542-18  
160618  
p. 2

## OVERVIEW

The debris problem has reached a stage at which the risk to satellites and spacecraft has become substantial in low Earth orbit (LEO). This research discovered that small particles posed little threat to spacecraft because shielding can effectively prevent these particles from damaging the spacecraft. The research also showed that, even though collision with a large piece of debris could destroy the spacecraft, the large pieces of debris pose little danger because they can be tracked and the spacecraft can be maneuvered away from these pieces. Additionally, there are many current designs to capture and remove large debris particles from the space environment. From this analysis, it has been decided to concentrate on the removal of medium-sized orbital debris, that is, those pieces ranging from 1 cm to 50 cm in size.

The current design incorporates a transfer vehicle and a netting vehicle to capture the medium-sized debris. The system is based near an operational space station located at  $28.5^\circ$  inclination and 400 km altitude. The system uses ground-based tracking to determine the location of a satellite breakup or debris cloud. These data are uploaded to the transfer vehicle, which proceeds to rendezvous with the debris at a lower altitude parking orbit. Next, the netting vehicle is deployed, tracks the targeted debris, and captures it. After expending the available nets, the netting vehicle returns to the transfer vehicle for a new netting module and continues to capture more debris in the target area. Once all the netting modules are expended, the transfer vehicle returns to the space station's orbit where it is resupplied with new netting modules from a space shuttle load. The new modules are launched by the shuttle from the ground and the expended modules are taken back to Earth for removal of the captured debris, refueling, and repacking of the nets. Once the netting modules are refurbished, they are taken back into orbit for reuse. In a typical mission, the system has the ability to capture 50 pieces of orbital debris. One mission will take approximately six months and the system is designed to allow for a  $30^\circ$  inclination change on the outgoing and incoming trips of the transfer vehicle.

## TRANSFER VEHICLE

The transfer vehicle is the part of the debris removal system that moves the nets, netting vehicle, and netting modules close to the debris that is targeted for capture. A basic layout of the vehicle is shown in Fig. 1.

The transfer vehicle is capable of  $30^\circ$  of inclination change on both legs of the trajectory. To accomplish the large inclination change without massive amounts of fuel, the transfer vehicle uses ion engines for thrust. This allows the fuel to be reduced

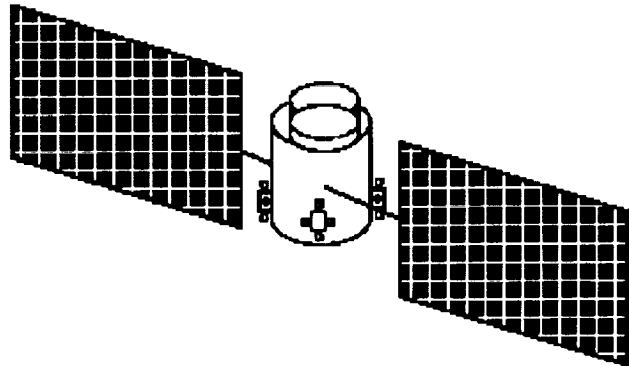


Fig. 1. The layout of the transfer vehicle.

to 10% of the amount that would be used if chemical engines were used. To provide the 35 kW of power that the 10 ion engines require, the transfer vehicle uses two high-efficiency solar arrays. The vehicle also has batteries that will provide power while the vehicle is in the shadow of the Earth.

The transfer vehicle weighs approximately 8000 kg. When it is fully loaded with the netting modules, propulsion module, and fuel, the transfer vehicle weighs 30,000 kg. Once the netting vehicle has captured the debris and returned to the transfer vehicle, the total mass of the transfer vehicle is about 21,000 kg. This reduction in weight is due to the fuel that is spent during the capture of the debris.

Control of the transfer vehicle is provided by control moment gyroscopes. The gyros will perform the fine attitude adjustments required as the vehicle makes its rendezvous with the debris. For large maneuvers and momentum dumping, the vehicle also includes RCS thrusts similar to those used by the space shuttle.

Navigation of the transfer vehicle is done by a combination of onboard calculations and data from the ground. Initially, the transfer vehicle receives data about the location of the debris and its location from external sources. From the data, the vehicle plots an intercept course. The vehicle proceeds along its trajectory and modifies it as new data are received about the location of the vehicle with respect to the debris.

The transfer vehicle receives this data from the command center located on Earth via a Ku-band communications link through the TDRSS satellite. The transfer vehicle relays any commands to the netting vehicle with a V-band communications system.

## NETTING VEHICLE

The netting vehicle is responsible for gathering the debris and returning it to the transfer vehicle. The layout of the netting vehicle and the modules is shown in Fig. 2.

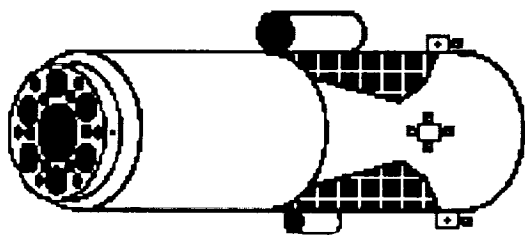


Fig. 2. The layout of the netting vehicle.

Once in the debris orbit, the netting vehicle uses its onboard infrared (IR) tracking system to locate and target a piece of debris. Once the debris is targeted, the netting vehicle does a Hohmann transfer into a slightly different orbit. This allows the netting vehicle to close in on the debris piece. As the vehicle closes in on the debris to a distance of about 25 km, the tracking switches to a LADAR (LAser Detection and Ranging) system.

The LADAR system provides more accurate ranging and location information to the netting vehicle as it approaches the debris. When the debris is within about 20 m of the debris, the vehicle will fire a net, capture the debris, and reel the net back into the netting module.

The netting vehicle will be controlled from the ground or elsewhere with teleoperated controls. This will prevent the netting vehicle from having to have extensive artificial intelligence. The communication is relayed to and from the netting vehicle using V-band link from the transfer vehicle through TDRSS. To provide the attitude adjustments, the vehicle will use control moment gyros in conjunction with RCS thrusters. The vehicle will also use hydrazine/nitrous oxide-fueled engines to provide the large orbital changes as the vehicle chases the debris.

Power is provided by solar arrays mounted on the surface of the spacecraft. This arrangement minimizes the surface area of the spacecraft in order to avoid possible collision with debris. The array is also oversized by 25% to compensate for degradation due to debris impacts.

The total mass of the netting vehicle after it leaves the transfer vehicle is 8076.5 kg. Upon gathering all the debris and returning to the transfer vehicle, the mass is reduced to 5183 kg, reflecting fuel expended.

## 1990-91 PROJECT SUMMARIES

## THE UNIVERSITY OF TEXAS AT AUSTIN

543-12

160619

P. 3

## INTRODUCTION

The Mechanical Engineering Department at The University of Texas at Austin participated in the NASA/USRA University Advanced Design Program on both an undergraduate and a graduate level during the 1990-91 academic year. The focus of study was on four design projects that fall into one of the following areas: (1) the establishment of a lunar base and (2) mission planet Earth. The design projects were incorporated into already existing design courses and students worked together in groups of three to five. A background of each area of study is provided, along with synopses, conclusions, and recommendations for further study for each design project.

## LUNAR BASE PROJECTS

## Background

NASA has a long-range goal of constructing a fully equipped, manned lunar outpost on the nearside of the Moon by the year 2015. The proposed outpost includes landing pads, an oxygen pilot plant, oxygen storage tanks, and an inflatable habitat. The lunar outpost mission consists of three phases: emplacement, consolidation, and utilization. The emplacement phase, to be completed by the year 2003, places a habitat with one-year life support capabilities on the Moon. Along with the initial habitat, the emplacement phase delivers laboratories, airlocks, and any required support systems. An expanded habitat, constructed during the consolidation phase, is scheduled to be completed by the year 2010. The expanded habitat contains crew quarters, science laboratories, medical facilities, and other facilities necessary for missions of long duration. The final phase, utilization, is the phase in which crew members conduct experiments on the Moon.

One of the primary design concerns during background research was the effect of the harsh lunar environment on humans and structures. NASA has been studying the Moon's environment for many years. During their studies, they found that radiation and extreme temperatures in the zero-atmosphere lunar environment pose a serious threat to human life and potential damage to structural materials. Tests on lunar soil, or regolith, showed that covering habitats with the soil can provide adequate protection from radiation and thermal effects. Prior to initiation of the emplacement phase, work crews and/or robots will excavate the lunar surface to provide a site for the initial habitat. This excavation process can provide some of the regolith necessary to cover the habitat.

Construction of the expanded habitat will begin at the conclusion of the emplacement phase. The expanded habitat houses larger crews for longer-duration missions than the habitat of the emplacement phase. NASA considered several alternate structures for the habitat during their initial studies. Structures considered include Space Station *Freedom*-derived modules, heavy lift launch vehicle diameter modules, prefabricated large-diameter cylinders, and inflatables. Inflatable structures consist of an outer shell, which acts as a pressure boundary, and internal structures, which provide support for floors and walls. Because of their low weight-to-volume-ratio, inflatable structures are especially useful in space applications. In addition to being lightweight, inflatable structures offer the advantage of being deflatable. Existing vehicles, such as the space shuttle, can transport the compact deflated structure into Earth orbit and a transport vehicle can transfer the structure to a lunar orbit and emplace the structure on the lunar surface. Due to weight, space, and fuel considerations, an inflatable structure can be transported at a lower cost than a prefabricated structure. For these reasons, NASA chose inflatable structures as the most feasible solution for conceptual design.

The construction of an outpost on the Moon presents many challenging and unique problems. The excavation and transportation of lunar regolith for this construction will require highly specialized equipment. This equipment must perform efficiently in the abrasive lunar environment at extreme temperatures, under intense radiation, and in a near-perfect vacuum. The highly abrasive lunar dust poses a constant threat to this equipment and other surfaces. Innovative solutions to these problems will be needed that minimize weight, space, power consumption, human exposure, and operating times. These solutions or designs should be adaptable to other tasks as well as performing their primary functions. The following three sections briefly summarize two undergraduate design projects completed during the fall semester of 1990 and a graduate design project completed in the spring of 1991.

## Inflatable Habitat Support Structures

This report presents a design for the internal support structures of an inflatable lunar habitat. The design solution includes material selection, substructure design, assembly plan development, and concept scale model construction. The internal support structures have been designed for an inflatable sphere that is 16 m in diameter with 5 interior levels.

After studying the proposed lunar habitat and background information, several project requirements were identified. The first project requirement was the development of substructure designs that satisfy the spatial and equipment layout concepts. Substructures include vertical supports, horizontal supports, and structural connections. During the design of the substructures, several construction materials were investigated. The next requirement was the development of an assembly plan for constructing the substructures. The assembly plan includes investigation of equipment to aid in habitat construction and investigation of assembly sequences. Site preparation, airlock design, inflatable shell design, and foundation design were not included in the project requirements.

The support structure design solution includes a cylindrical core, expandable trusses for horizontal support, a truss system for vertical support, and pins, nuts, bolts, and welds for connecting the members. The advantage of employing expandable trusses is that structures can be assembled on Earth, transported to the Moon in a compacted state, and be erected easily and efficiently on the lunar surface. Properties of 7075 T73 aluminum served as a basis for structural design. Assembly of the structures involves several stages including preassembling parts on Earth, shipping, preparation and arrival, and support structure assembly inside the inflated sphere.

Further research is recommended in several areas. Use of fiber-reinforced polymers for structural support may allow future designers to decrease the mass of the structure. Another area that deserves further consideration is the possibility of automated assembly. Also, possibilities of adapting the habitat to various geometries and environments should be considered in future designs. Finally, the building of a mock-up of the entire assembly to test assembly methods, loading conditions, and interior layout concepts is recommended.

### Design of Equipment to Excavate and Transport Regolith

The report entitled "Conceptual Design of Equipment to Excavate and Transport Regolith from the Lunar Maria" presents design concepts for excavation and transportation of lunar regolith as well as characterizing the regolith and determining the power requirements for excavation. The high cost of transporting payloads to the lunar outpost from Earth can be reduced by fabricating products from material available on the lunar surface. Excavation and transportation of lunar materials for processing will require highly specialized and efficient equipment.

After studying the design concepts of the proposed lunar outpost, three important project requirements were identified. The first requirement was to characterize the material properties and elements composing lunar regolith. The next requirement was to conceptually design the equipment needed for mining operations and transportation. This equipment needed to achieve three basic functions: loosening, collecting, and transporting. Several design criteria for this equipment were specified including safety, modularity, simplicity, minimum power consumption, minimum mass and volume, and reliability. The final requirement was to calculate the power requirements for excavation and transporting the lunar regolith to a processing site.

A modular Main Drive Unit (MDU) has been designed to provide mobility for loosening, collection, and transport function modules. The MDU is powered by fuel cells and travels on hemispherical wheels. It serves as the source of mobility and electrical power for its modular attachments. The MDU is designed to operate by telecontrol from the lunar base.

A scarifier has been designed to loosen, a bucket conveyor to collect, and a haul-dump unit to transport the lunar regolith. The scarifier and bucket conveyor are connected to one MDU and a regolith bin used for hauling and dumping is attached to another MDU. The scarifier has a variable depth of cut and organizes the regolith into a row to make collection easier. The bucket conveyor is powered by a motor that receives electrical energy from the MDU. During operation, a haul-dump unit closely follows the scarifier/conveyor assembly and is loaded continuously. Several haul-dump units can be employed to increase efficiency of the system. The power required to operate each MDU to operate is calculated to approximately 35 kW.

Further research is recommended in five areas. More information is needed about lunar soil mechanics, particularly those properties that vary with depth. The fine portion of regolith is most valuable, so adding a beneficiation process to the excavation process will prevent the collection of large pieces of regolith. Large rocks can interrupt the operation of equipment and a method for handling the rocks needs to be devised. More research needs to be done on the automation of equipment on the Moon. Finally, a regolith bagging system should be developed that can be attached to the excavation and transportation equipment.

### Design of Equipment for Lunar Dust Removal

The objective of this project was to design a system or a device that will effectively remove lunar dust from material surfaces in a zero-atmosphere, one-sixth gravity environment. The scope of the project was restricted to the design of a device capable of removing the dust from delicate optical surfaces such as camera lenses and mirrors. A design capable of successfully removing lunar dust from optical surfaces may be extended to cleaning other devices where surface finish is not of great importance.

After studying the characteristics of lunar dust and the problems associated with dust contamination, several project requirements were identified. The use of various energy domains for removing dust in a one-sixth gravity, zero-atmosphere environment had to be characterized. A device or system capable of removing lunar dust from optical surfaces without degrading the surface finish was to be designed. The last requirement was to propose methods of preventing lunar dust from accumulating on finished surfaces.

Several possible design concepts including electrostatics, fluids, and mechanical cleaning devices were explored. Electrostatics appear to be feasible yet are not practical due to the large amount of power required, large system mass, and possible safety problems. Mechanical cleaning alternatives are inadequate due to the probable damage to the optical surface, but are energy-efficient and could be effective on surfaces where surface finish is not of great importance. A design concept employing a compressed gas was chosen for detailed investi-

gation due to its apparent feasibility for portability and dust removal without damage to optical surfaces.

The dust removal concept developed consists of a small astronaut/robotic-compatible device that removes dust from contaminated surfaces with a small burst of gas. The design is composed of two major parts: a handle with gas exit nozzles and a removable pressurized gas storage tank. Either carbon dioxide or nitrogen can be used as the cleaning medium. Gas is released through three 6-mm-diameter focused nozzles by actuating a trigger on the handle. The three-nozzle design delivers 0.3 N of thrust with a mass flow rate of 48 g/min. A possible secondary application of this device is that it may be adapted for use as a fire extinguisher.

Upon completion of the design, several conclusions and recommendations for further study were made. This design employs circular nozzles, but the use of slit orifices should be researched in the rarified gas regime as a slit may produce a more useful thrust area. Also, these nozzles were designed with the constraint of not allowing the expelled gas to condense. This condensation could possibly be used beneficially to carry dust off surfaces without damaging them. And finally, the process of removing dust is time consuming and expensive, so methods of preventing dust contamination should be employed where possible.

## MISSION PLANET EARTH

### Background

"Mission Planet Earth" seeks to use space and aeronautics technology for the sole purpose of improving the Earth. These issues include ozone deterioration, ecological improvements, weather studies, ocean studies, and the prevention of harmful effects produced from previous and future space missions. The project discussed in this section concerns the latter of these issues, the deorbiting of space debris in Earth orbit.

It has been common practice to abandon used space vehicles and equipment and leave them in Earth orbit even though they can remain there for many years. Of the approximately 7000 objects currently tracked by NORAD only about 5% are operating vehicles. These objects consist of abandoned satellites, discarded

upper rocket stages, other debris, and debris resulting from collisions between these objects. These inevitable collisions result in self-propagation of the debris over time even if the addition of new debris is halted entirely.

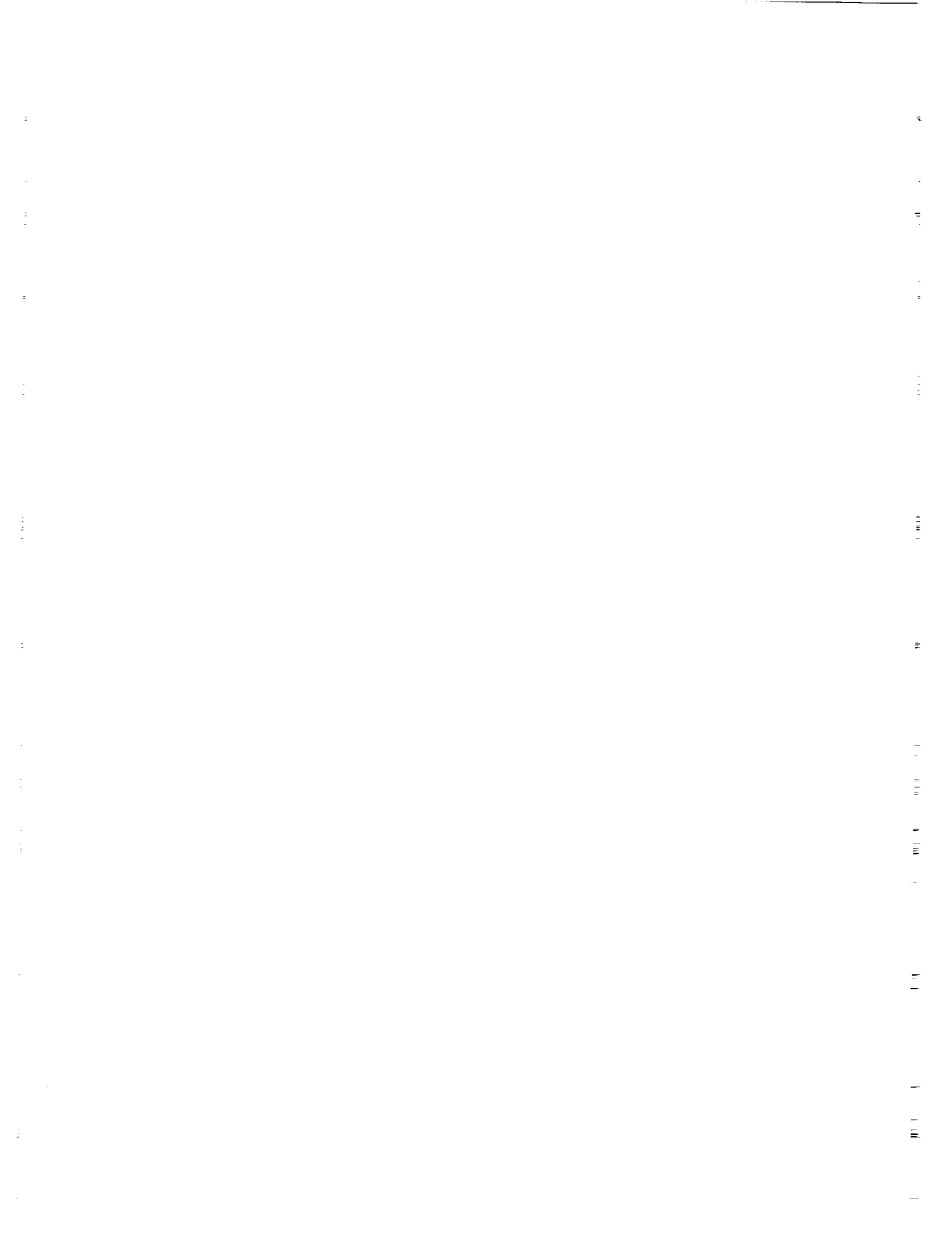
Two major problems result from space debris. A collision with debris can cause serious if not fatal damage to a functioning spacecraft. This results in considerable expense in designing for survivability. The second problem concerns mission planning. The launch of any vehicle becomes complicated as paths must be planned away from the known trajectories of all objects being tracked. The danger of collisions increases as new debris masses are added to an already self-propagating problem.

### Design of an Unmanned, Reusable Vehicle to Deorbit Debris

An unmanned, reusable Deorbiting Vehicle (DOV) has been designed that uses the NASA Orbital Maneuvering Vehicle (OMV) command/propulsion modules and a Chain-And-Bar-Shot (CABS) module to deorbit space debris. This design is based on maximum reusability and component modularity. As a matter of fact, debris deorbiting with the attachment of a specialized module was considered in the original specifications of the OMV.

The CABS module contains projectiles that are designed to impart enough kinetic energy to deorbit a debris mass on the order of 2000 kg. Each projectile consists of a set of perimeter rods that are connected to a central core by aramid cords. The projectile is fired at high velocities from a rail-gun barrel that imparts a spin on the projectile, centrifugally spreading the rods into a whirling circle with enough area to capture debris. The rods are connected with strips of mylar to ensure uniform spacing and to increase the chances of capture. The CABS module carries six projectile packages in a revolver-type magazine that may be replenished in orbit.

The active removal procedure of the DOV will not solve the debris problem entirely. Space activity at the present rate will cause the debris problem to worsen even as a removal process is underway. The self-propagating debris will continue a geometric growth as well. A debris prevention plan is necessary and conventions should be established to protect the orbital environment from future damage.



MARS AQUARIUS MISSION AND TITAN EXPLORER

U. S. NAVAL ACADEMY

544-66

160620

P. 4

MARS AQUARIUS MISSION

Philosophy

The Mars Aquarius Mission is designed to carry out several scientific studies of the surface and subsurface of Mars with an emphasis on locating subterranean water. This mission is a precursor to a manned mission to Mars. A manned mission will require an extended stay on the planet's surface, and an accessible source of water will greatly simplify life support requirements. Using data from previous Mars observations, four sites have been selected as possible locations of subsurface water. The Aquarius spacecraft carries one penetrator for each of these sites.

Penetrators

Two hundred and fifty-five days after launch, all four penetrators will be simultaneously released from the spacecraft and injected on hyperbolic trajectories toward their respective landing sites. Upon atmospheric entry, each has a heat shield and a parachute that will decelerate the penetrator into a ballistic approach. Landing accuracy is approximately 5 km. Impact will occur at velocities from 80-100 m/s. Depending on the composition of the landing site, at impact the lower housing of the penetrator will be blasted 4-6 m further into the soil.

The penetrators carry instruments to carry out several experiments. The neutron spectrometer and alpha-backscatter/XRF spectrometer will detect the presence of water throughout the surface, subsurface, permafrost layers, and atmosphere. The gamma ray spectrometer will determine the abundance of most major and minor elements, as well as a few trace elements, near the surface of Mars. Temperature probes will measure the planet's temperature-depth profile. Accelerometers and a seismometer will analyze the structure of the planet and seismic activity. Also, a 360° camera/imager will provide visual data on landing sites.

Each penetrator carries a 2-W microradioisotope thermoelectric generator, as well as lithium batteries for power. Data is relayed up to the orbiter via a half-wave dipole antenna and a 0.5-W transmitter at a maximum rate of 11.1 kbytes/s at 220 MHz. A diagram of the penetrator is shown in Fig. 1.

Communications

The Mars Aquarius communications system must be able to receive commands from Earth, transmit signals to the penetrators to initiate their transmission of data, receive and store this data, and telemeter both this data and status reports back to Earth. Basic components of the communications system include a 3-m Earth-pointing dish and a half-wave turnstile reflector Mars-

pointing antenna, each used for both transmitting and receiving. Both antennas are mounted on the despun section of the spacecraft. The groundbased component of the communications will involve the use of a 70-m dish, part of NASA's Deep Space Network (DSN).

A 500-km orbit was chosen for the spacecraft orbiter. This orbit provides for low path loss for the uplink, and also provides the necessary overhead time of three minutes needed for data reception from the penetrators. Upon reception of data from the penetrators, the orbiter will store it in memory until a predetermined time to downlink via DSN. The orbit is designed so that any given penetrator can uplink four times a day. This requires maximum storage of 31.9 kbits. Downlink will take 30 minutes at 19 kbps and 8.4 GHz.

Power and thermal control

The power system chosen for the Aquarius is a solar array of eight panels. This system met the requirements of vehicle weight, power required, and safety. Maximum power needed

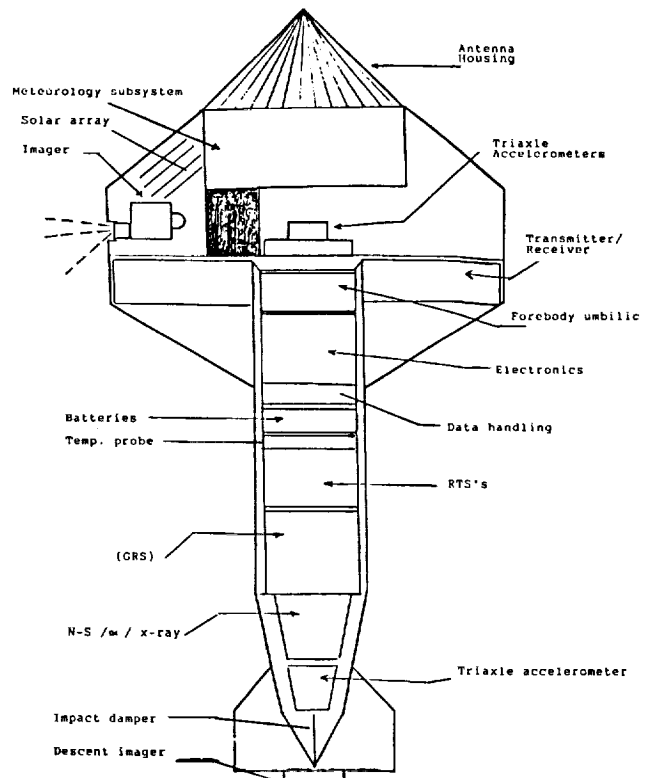


Fig. 1. Aquarius Penetrator.

304 INTENTIONAL BLANK

onboard the spacecraft is 340 W. Each panel is 5.747 m<sup>2</sup>, and each panel alone is capable of producing the 340-W requirement. Since the spacecraft is spin stabilized, however, the panels are wrapped around it so that enough solar cells are always in maximum incidence. Due to the polar orbit of the orbiter, there will be times of solar eclipse. Maximum eclipse time will be 41.03 min. Power during these times will be provided by 22 NiCd batteries in series, which will be reconditioned after each period of use in eclipse.

Thermal constraints onboard are nearly entirely determined by the batteries. The NiCd cells must be kept within -10° to 25°C. The spinning spacecraft otherwise allows the sun to evenly heat the orbiter against the cold of outer space. Both active and passive temperature regulation are employed on the spacecraft. Multithermal insulation blankets used on the despun section, black paint on the antennas, aluminum on the propellant tanks, and a stainless steel heat shield over the 490-N engine comprise the passive portion. Active systems include two heaters for eclipse periods when no sunlight can provide heat, and an active louver system for heat dissipation should temperatures rise too high. Figures 2 and 3 show top and side views of the Aquarius spacecraft and include elements of the communications, propulsion, power, and thermal systems.

**Aerodynamics and aerobraking**

To conserve spacecraft weight, a minimum energy transfer is utilized. The spacecraft will begin the Mars transfer from

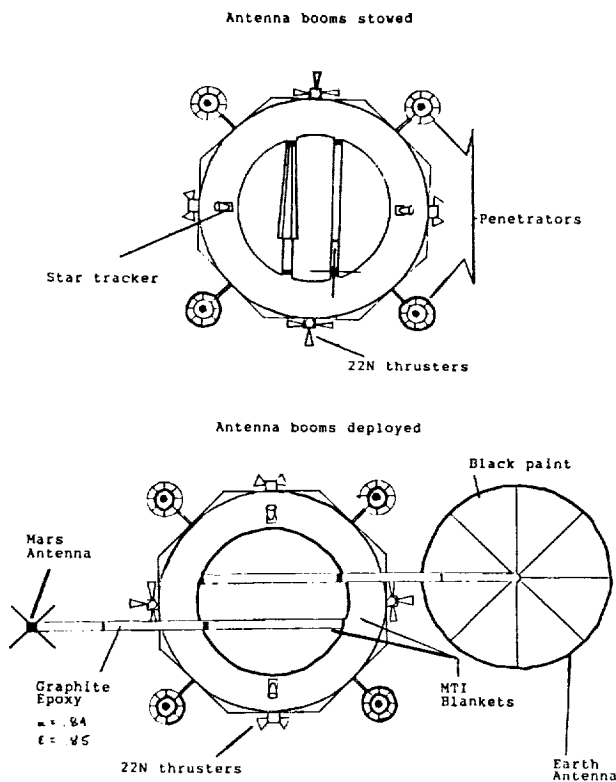


Fig. 2. Aquarius Spacecraft, Top View.

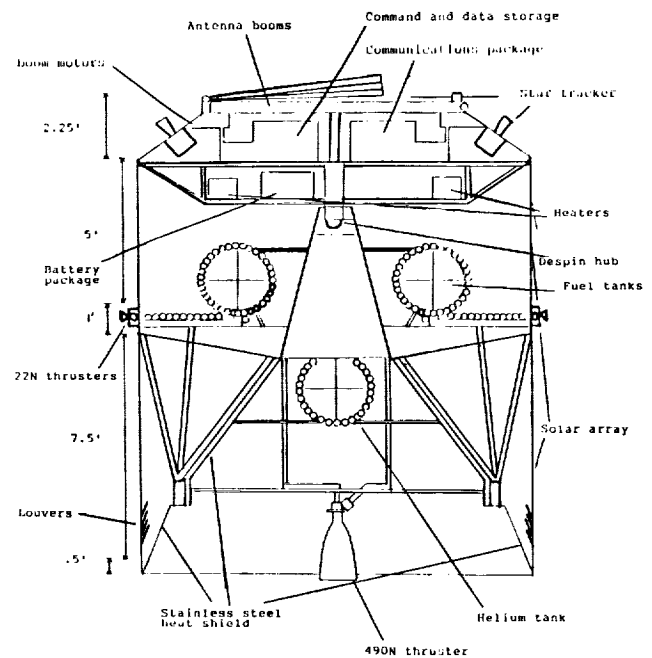


Fig. 3. Aquarius Spacecraft, Side View.

an Earth parking orbit of 300 km. A 3.696-km/s ΔV will place the spacecraft on a Hohmann transfer to Mars. The thrust vector will also place the spacecraft in Mars' ecliptic plane. This is a plane change of 6.5° from the parking orbit's 28.5° inclination. The entire transfer will take 258.96 days. Three quarters of the way to Mars, the 490-N engine will impart a ΔV of 0.459 m/s, placing the spacecraft on a path that will result in a polar martian orbit. Mars capture will be accomplished using aerobraking. This greatly reduces fuel requirements for the spacecraft. The spacecraft will enter the martian atmosphere at a flight path angle of -20° with a velocity of 4.159 km/s. The aerobraking maneuver will slow the spacecraft by 0.6323 km/s, resulting in an elliptical orbit with a periapsis of 100 km and an apoapsis of 500 km. At apoapsis a ΔV of 27.6 m/s will place the spacecraft in a circular orbit. The aerobrake is a blunt body with a lift-to-drag ratio of 1:2. It is composed of an isogeometric grid of ceramic tiles and unfolds after the spacecraft is removed from the shuttle bay. The optimum launch date has been calculated as April 26, 2001.

**Propulsion**

The propulsion system must provide for the transfer of the spacecraft from Earth orbit to Mars, and for stationkeeping once the martian orbit is attained. The space shuttle will deploy the Aquarius spacecraft with its transfer kick motor into a 300-km Earth orbit, positioning it in the proper attitude for transfer. At this time the aerobrake will be deployed and the 3-m Earth communications dish extended. The 3.696-km/s ΔV is provided by the Orbus 21 Transfer Orbit Stage (TOS), a solid rocket booster that will carry 5347 kg of propellant. The TOS uses three-axis stabilization. During transit the spacecraft's y axis will be perpendicular to the Sun, allowing the solar panels to achieve

maximum incidence. Three-axis stabilization will be used at this time. The spacecraft has four star trackers onboard for this purpose. Attitude control is provided by a bipropellant system of one 490-N engine and twelve 22-N thrusters. Upon achieving Mars orbit, the despin hub will be unlocked and the spacecraft will be spun up to 25 rpm. Star trackers on the despin section will provide stationkeeping data. The Aquarius spacecraft has sufficient fuel onboard for a minimum of two martian years of service, after which time the spacecraft will be placed in planetary quarantine for probable future restart. The spacecraft can then be used again as a communications relay for future missions.

### TITAN EXPLORER

The Titan Explorer is a scientific research probe consisting of an orbiter and a lander designed to travel to Saturn's largest moon, Titan, to conduct various experiments, make observations, and send data back to Earth. The probe will be placed in a circular orbit around Titan and will make preliminary estimates of Titan's atmospheric composition and structure, measurements of magnetic fields, observations of the dynamics of Titan's atmosphere, and radar observations of the topography of Titan.

The lander will be deployed by the probe after the orbit around Titan has been established. It will attempt to measure the composition and variations of the atmosphere as it descends, land on either a solid or liquid surface, and determine the conditions and composition of Titan's surface.

The Titan Explorer is 10 m long and octagonal in shape along its main axis. A high-gain dish antenna, folded and stored on the top of the spacecraft makes its height 2.4 m. The total mass of the spacecraft without fuel is 2743 kg. It will be launched by NASA's space shuttle in the year 2015 and will use a nuclear propulsion system to send it on a six-year journey to Titan. Upon reaching Titan, it will use at least 15 different scientific instruments to accomplish its objectives of studying Titan's emissions, magnetic field, atmosphere, weather systems, and surface composition and conditions.

Saturn's distance from Earth and the Sun makes just reaching Titan a significant problem. Titan Explorer will get to Saturn using a gravity assist flyby of Jupiter. It will first be launched into a 300-km-altitude Earth orbit by the shuttle. A velocity change of 3.8 km/s will be used to move it to the plane of the ecliptic. Another  $\Delta V$  burn of 6.3 km/s will put the spacecraft approximately on a Hohmann transfer orbit to Jupiter, which will take approximately 2.7 years. It will fly past Jupiter at a distance of 206,700 km, gaining about 10.0 km/s from this flyby. It will travel for another 2.8 years and then use a 5.87 km/s burn to reach a parking orbit with a radius of 1.3 million km around Saturn. It will then use a Hohmann transfer around Saturn to get to its circular orbit around Titan, 2000 km above its surface. The launch window for this trajectory is primarily constrained by the angular relationship between the Sun, Jupiter, and Saturn. The first practical launch window would open late in 2015.

In order to use this trajectory, a propulsion system significantly better than those available today will be needed to avoid having to carry extremely large amounts of fuel. It was assumed that by the proposed launch in 2015, such a system, specifically

a nuclear thermal rocket, could be developed to provide all of the velocity changes necessary for this trajectory. Recent studies have proposed such a system that would use a particle bed reactor made up of uranium and carbon alloy pellets. The reactor will be used to heat hydrogen gas to temperatures of 2400-3000 K and then eject it through an exhaust nozzle. With a specific impulse of roughly 1000 s, preliminary estimates have proposed a rocket 3.05 m  $\times$  1.22 m that would have a mass of 1134 kg and would deliver over 34,000 kg of thrust. This rocket would require 10,580 kg of fuel to complete the proposed trajectory. Six hydrazine thrusters are also located at various places on the spacecraft, but these will be used primarily for maintaining and altering its orientation.

Power for the main spacecraft will be provided by radioisotope thermoelectric generators (RTG) which use thermoelectric couples to produce electrical energy from the heat given off by the natural radioactive decay of radioisotope fuel. The RTGs will be used to power the scientific instruments, command and data handling system, communications systems, heaters, pumps, and electric motors. The total estimated power requirement for the orbiter is 390 W. The most recently developed RTG is the General Purpose Heat Source (GPHS)-RTG. Its high specific power (54.4 W<sub>e</sub>/kg) make it a good candidate to provide the large amount of power required by this mission. The Titan Explorer will use two such RTGs that will be deployed on extendable booms after launch. They have the capacity to provide 580 W at the beginning of the mission. After the six-year transit to Titan, their total output will have decayed to 475 W.

Attitude determination and control will be performed by Sun sensors and star trackers supplying data to a three-axis stabilization system with momentum wheels. The momentum wheels provide the spacecraft with some gyroscopic stiffness while three-axis corrections and adjustments will be made by six hydrazine thrusters. The Titan Explorer's orbiter carries six scientific instruments to gather preliminary information concerning Titan's atmospheric composition and dynamics, surface topography, and magnetic field. A solid-state imaging camera will be used to determine atmospheric structure, motions, and radiative properties and will study relative cloud motions. A photo-polarimeter-radiometer will measure the temperatures and energy balance of the atmosphere, as well as cloud characteristics and composition. An ultraviolet spectrometer will use spectra to study the atmosphere above the clouds. The orbiter also carries a gamma-ray spectrometer which will attempt to investigate the composition of surface elements by measuring gamma-ray emission characteristics. A radar altimeter will be used to provide some topographic mapping of the surface in an effort to determine the amount of liquid and solid surface and possibly adjust the entry trajectory of the lander. A magnetometer, extended from the spacecraft by a boom, will measure any magnetic field that exists around Titan. These six instruments require approximately 77 W of power.

Communications with the spacecraft will be conducted through DSN. It is assumed that DSN's current transmission/receiving rates of up to 12 GHz will be improved to allow a rate of 15 GHz by mission launch time. The primary communications system onboard the spacecraft uses a 5.8-m-diameter parabolic dish high-gain antenna that will require

118 W of power and will broadcast at a frequency of 15 GHz to meet the required data transfer of 135 kbps. A secondary system will consist of two parabolic dish low-gain antennas. They are each 1.35 m in diameter and will operate at frequencies of 14.9 GHz and 14.8 GHz. During the probe's journey to Titan, the high-gain antenna will be folded along the top of the spacecraft and covered by a protective shroud. Until it is deployed when the probe reaches Titan, the secondary antennas will be used. When the lander is deployed, the orbiter communications systems will act as a communications relay between the lander and Earth. Two dipole antennas will be used to communicate with the lander.

The lander is designed to survive entry into Titan's atmosphere, safely land on either a solid or a liquid surface, and float if the latter situation is encountered. It is made up of a 1-m-diameter spherical housing mounted on a flat, 1.3-m platform base. The bottom half of the lander is surrounded with a vacuum-filled shroud. While attached to the orbiter, the lander is encased in a conical atmospheric-entry aeroshell and is carried on the front of the spacecraft. It will be deployed once the orbit around Titan has been established and preliminary observations have been made by the orbiter's scientific instruments. Four hydrazine thrusters mounted in the atmospheric entry shell will be used to maneuver the lander out of the path of the orbiter, adjust the lander module's orientation, and start it on its entry trajectory. Once the lander unit has entered the atmosphere, a pilot chute will be deployed, which will pull off the aft cover which, in turn, releases the main parachute. Once the main chute has been deployed, the conical heat shield will be jettisoned and the lander will drift slowly to Titan's surface, studying atmospheric composition and conditions as it descends.

Power for the lander will be provided by a scaled-down version of the GPHS-RTG. This smaller version will be a little more than half the size of a normal GPHS-RTG. It will provide an estimated power output of 136 W after six years. Multilayer Kapton blankets will be used to insulate the RTG from other lander systems and a double closed loop system will transfer excess heat from the RTG to an atmospheric radiator. Mylar and Kapton multilayer blankets will also be used to insulate the lander from the extremely cold temperatures of Titan's surface (estimated to be about 94 K).

The lander will carry scientific instruments to be used during the descent phase and others to be used while on the surface. The atmospheric structure experiment will study the variation

with altitude of the temperature, pressure, and density of the atmosphere as well as conditions of cloud levels, internal cloud structure, and the depths and altitudes of cloud layers. A net flux radiometer will provide a better understanding of Titan's radiation budget. A neutral mass spectrometer will be used to determine the abundances of the major components of the atmosphere at different altitudes and will also analyze samples of the surface of Titan. A nephelometer will be carried to locate cloud layers, make direct measurements of cloud structure, and determine the character of the particles in the main clouds. The camera and navigation system determines characteristics of surface topography and morphology. The lander will carry a cryogenic xenon sample collector and an alpha-particle instrument and an *in-situ* chemical analysis instrument will be used to analyze collected samples. A micro gas chromatograph will determine the distribution and molecular forms of the biogenic elements (C,H,N,S,O,P).

Communications with the orbiter will be conducted via the lander's two omnidirectional, quarter wavelength, dipole antennas. The orbiter will use a beacon system to let the lander know when it is within sight and able to receive data. The lander's system will have a maximum data transfer rate of 50 kbps. The command and data handling system can store up to 3 Gbits of data, which equals 9.5 orbits of data.

The goals of the Titan Explorer mission are to reach and successfully establish an orbit around Titan, enter Titan's atmosphere, safely land on its surface, and survive to send back enough data to answer many of the basic questions about this planet-like moon. To complete such a mission, some assumptions had to be made concerning technological advances achievable by the year 2015. Provided such advances can be made, Titan Explorer should be able to successfully perform its mission.

#### ACKNOWLEDGMENTS

Mars Aquarius Mission summary prepared by Ensigns Brian Dulla, Christina Glaser, Jason Lopez, Jeffrey Lucas, Michelle Reyes, and James Rimrodt.

Titan Explorer summary prepared by Ensigns Stephen Philpott, Paul Diedrich, Terry Ladau, David Lagassa, and John Soma.

# THERMION: VERIFICATION OF A THERMIONIC HEAT PIPE IN MICROGRAVITY

UTAH STATE UNIVERSITY

545-34  
160261  
p. 4

## INTRODUCTION

The Idaho National Engineering Laboratory (INEL) is conducting intensive research in the design and development of a small excore heat-pipe-thermionic space nuclear reactor power system (SEHPTR). The SEHPTR spacecraft will be able to supply 40 kW of power in any given orbit. Figure 1 shows a conceptual diagram of the SEHPTR spacecraft. The key components in this reactor are the thermionic heatpipes. The heat pipes have two major functions: (1) to convert heat energy into electrical energy, and (2) to radiate the excess heat to space.

Thermionic power conversion is the process of converting heat energy into electrical energy with no moving parts. Heat is applied to the cathode surface, as shown in Fig. 2. This heat will boil off electrons that will jump across the gap to the cooler surface of the anode, which will cause a potential difference between the two plates and induce a current through the load.

Thermionic power conversion is incorporated as part of the heat pipe. The heat pipe, which is being developed by Thermacore Inc., is actually two heat pipes. It uses a radial heat pipe, called the emitter, and an axial heat pipe collector, as shown in Fig. 3. The emitter heat pipe will pass the heat from the nuclear core to the cathode surface. The collector heat pipe keeps the anode surface cooler by transferring the heat from the anode surface and radiating it to space.

## Design Project

This year's design project was in collaboration with the Idaho National Engineering Laboratory to design a space flight-demonstration of a scaled-down thermionic heat pipe. The mission of this satellite would be to demonstrate the performance of an integrated thermionic heat pipe device in micro-gravity. During the course of the design, we developed two design concepts: Thermion-I and Thermion-II.

**Thermion-I.** Thermion-I is a small satellite that will have a one-year mission. A solar collecting mirror will be used to focus the Sun's energy into a cavity that will transfer the heat into a 6-cm heat pipe. The 6-cm heat pipe is a scaled down version of the 40-cm heat pipe that will be used in SEHPTR. The satellite will be flown as a secondary payload on the Delta II.

**Thermion-II.** Thermion-II is a more brute-force approach to conducting the experiment. Instead of being deployed from the Delta II, it will be permanently mounted to the second stage. Thermion-II will use batteries rather than the Sun to heat the heat pipe. Because of the limited number of batteries we can launch on the Delta II due to their weight, the experiment will last only a little more than a day.

## Design Considerations

Confirmation that the thermionic heat pipe will operate in a microgravity environment is the primary performance driver for this Thermion mission. To confirm this, temperature measurements of the heat pipe are necessary. Measurement of the power generated will also be needed to prove that the device works properly.

## Design Evolution of Thermion-I

Thermion-I had five major design criteria: Test a 6-cm thermionic heat pipe module (THPM); Use solar energy to heat the THPM; Small satellite; 1-year mission; and Secondary payload in a Delta II as launch vehicle. A summary for each subsystem on Thermion-I follows.

**Heat pipe testing system.** The heat pipe temperature will be monitored through 12 thermocouples: 6 distributed over the emitter heat pipe surface and 6 distributed over the collector heat pipe surface.

The thermionic power conversion of the heat pipe will be approximately 11%. A 6-cm heat pipe requires 1050 W of heat energy. It will convert 11% of the 1050 W into electrical energy (116 W). The electrical power breaks down into a 0.7 voltage and a current of 165 amp. The power pick-off points on the heat pipe are at 1000 K. This makes measuring the voltage and current with conventional techniques very difficult. We have chosen to measure the power lost through heat ( $I^2 R$  losses) and calculate what the power is.

**Solar collection system.** A parabolic mirror that is  $58.6 \times 41.6$  in ( $148.8 \times 105.7$  cm) will be used to collect 2050 W of the Sun's energy. The mirror will focus the energy into a cavity that resembles Planck's black body box (see Fig. 4). Once the energy is trapped into the cavity, it will conduct into the heat pipe.

**Attitude control and determination system.** The mirror has a pointing requirement of  $\pm 0.75^\circ$ . To achieve this accuracy, the following sensors and actuators are used: wide-angle Sun sensor, high-accuracy Sun sensor, horizon-crossing sensor, photodiodes, torque rods (magnetometer), and momentum wheel.

**Satellite structure and configuration system.** The structure consists of a bus, mirror, mirror support, payload, payload arm, and internal components. Figure 4 shows the satellite in its deployed configuration.

**Data management system.** Data acquisition is the main task of data management. The data will be collected and transmitted in a store-and-forward manner. The data will be dumped to a ground station every eight hours.

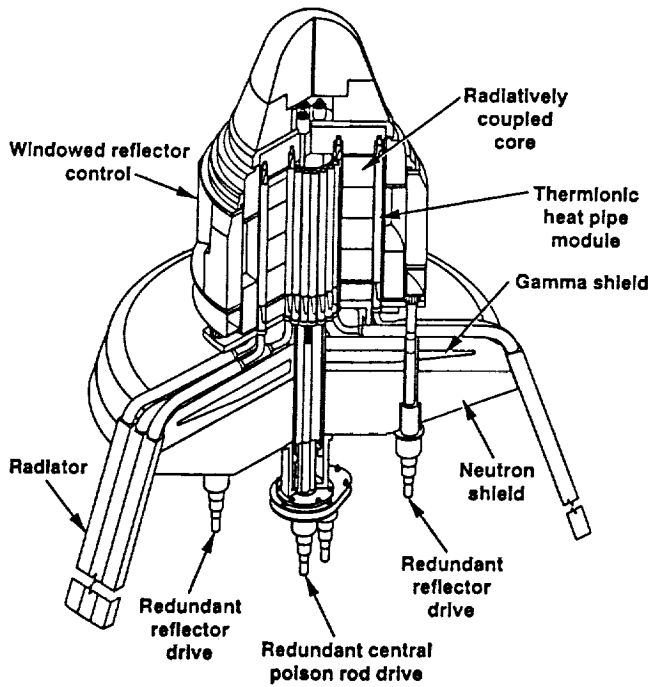


Fig. 1. Space nuclear reactor power system (SEHPTR).

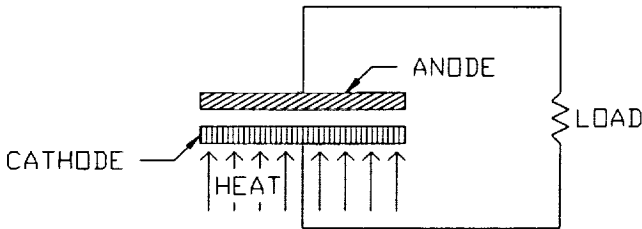


Fig. 2. Thermionic power conversion converts heat energy into electrical energy.

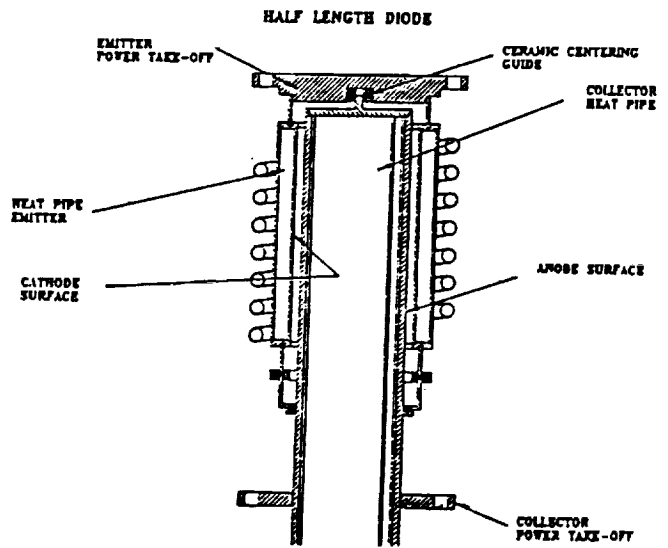


Fig. 3. Heat pipe design by Thermacore.

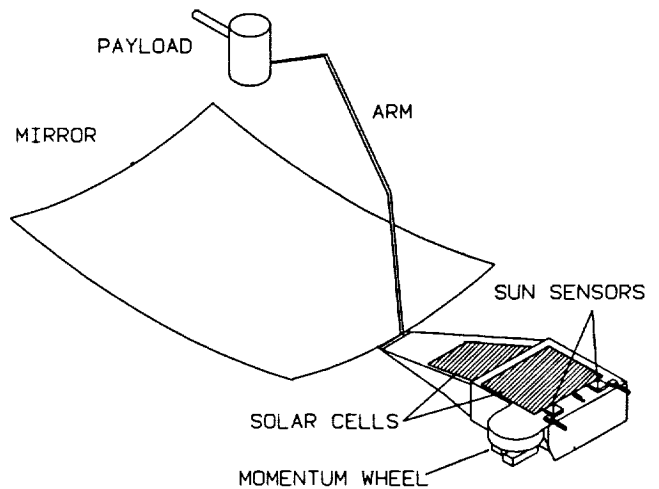


Fig. 4. Thermion-I satellite in its deployed configuration.

**Communications system.** Since the satellite's attitude control will be tracking the Sun, a near omnidirectional antenna is needed. Two transmitting antennas will use S-band to downlink data to a mobile ground station. Two receiving antennas will be used to uplink any information that might be needed.

**Power system.** The power generated by the thermionic heat pipe cannot be turned into useful power for operation of the satellite. Therefore, silicon solar cells were placed on top of the satellite to generate the required operating power. Nickel-cadmium batteries will be used when the satellite is in the shadow of the Earth. These batteries will then be charged on the Sun side of the orbit.

**Launch vehicle interface and deployment system.** There will be several global positioning satellite (GPS) missions in the next few years with available space on the Delta II secondary

stage to launch a small satellite. Thermion-I was designed to fit in the secondary payload volume of the Delta II. The satellite is mounted to the Delta II via a Marman clamp. Once the Delta II secondary stage has reached a circular orbit of 375 n.m. explosive bolts will fire and eject Thermion-I from the vehicle into its circular orbit.

**Thermal management system.** Temperature extremes of the Thermion-I satellite were determined by considering the hottest and coldest orbits. A 90-min orbit was assumed with 60 min of this orbit in the Sun. The hottest orbit is during the 60 min that the satellite is in the Sun and appropriate instruments are turned on. In this case, all the onboard components will stay within their operating temperature ranges. The coldest orbit is where the satellite stays in the shadow of the Earth for over 30 min. All the components except the

Sun sensors and the solar cells stayed within their temperature limits. This is of little concern because those components will not be operating in the shadow of the Earth. Three watts of power have been incorporated into the power system for heater use, and emissive coatings can be used to bring the instruments into their operating temperature ranges, if deemed necessary.

**Test and evaluation system.** The test and evaluation system has been investigating ways of ensuring mission success. Test procedures have been developed to validate instrument operation.

**Conclusions.** The Thermion-I satellite has a mass of 85.19 lb (38.64 kg) and will cost less than \$1.2 million for construction of the satellite. Integration for mounting to the Delta II will cost approximately \$1 million.

## THERMION II

### Introduction

Half way through the design of the satellite Thermion-I, it was realized that the thermionic heat pipe module (THPM) need only be tested in a space environment. A free-flying satellite is just one of several solutions. Flight on NASA's KC-135 parabolic test platform, or on a sounding rocket such as the STARFIRE or JOUST series were considered. They provide 30 seconds, 5 minutes, and 15 minutes of microgravity, respectively. We finally settled on flying, as Thermion-I does, on the Delta II launch vehicle. The Delta II can provide months of microgravity and is capable of carrying up to 340 kg as a secondary payload. Unlike Thermion-I, Thermion-II will merely be an appendage to the Delta II; it will not separate. Instead of using a solar collector, Thermion-II will use 253 kg of alkaline cells to power an electric tungsten grid heater on the THPM. Flying on the Delta II gives the best combination of low cost and performance. The experiment can run continuously for 21 hours using the alkaline cells or for 63 hours using lithium cells. Thermion-II will complete an identical test of the THPM as Thermion-I, but for a much shorter time. Thermion-II's THPM is 65% larger than the THPM presently proposed on Thermion-I and much closer to the full-scale THPM proposed for the Small Excure Heat-Pipe-Thermionic Space Nuclear Power System (SEHPTR).

The U.S. Air Force and Idaho National Engineering Laboratory (INEL) would like to conduct a test of THPM because it is a critical component of SEHPTR. SEHPTR is a space nuclear reactor nominally capable of generating 40 kW of power. Due to its extremely toxic nature and high cost, it is desirable to conduct realistic tests of critical new components. Thermion-II will simulate the reactor heat load on the THPM using an electric heater.

**Description.** Thermion-II is composed of five elements: four battery pallets of 480 alkaline cells each and one payload module. They are fixed to the secondary payload volume of the Delta II launch vehicle as shown in Fig. 5. Two pallets plus the payload module are on one side, while the remaining two battery pallets are 180° around on the other side of the Delta II second stage.

**Payload description.** The THPM is actually two heat pipes in one. The outer one is shorter. It is called the emitter. The inner and longer heat pipe is called the radiator. It radiates

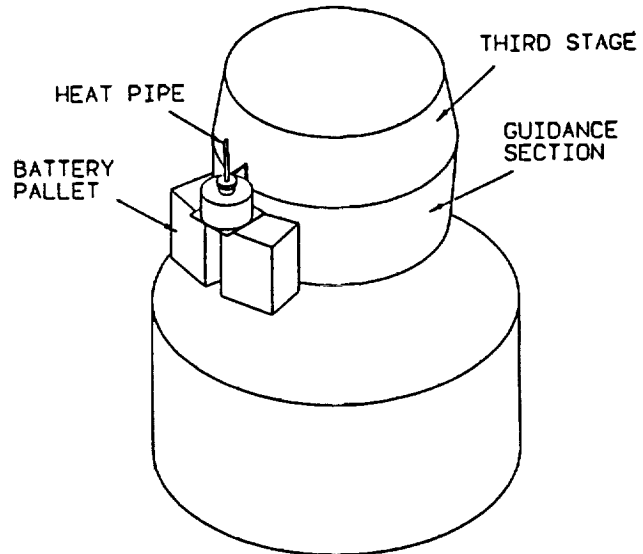


Fig. 5. Thermion-II in Delta II secondary volume.

the heat from the nuclear reactor core. The emitter converts 11% of the heat transferred through it into electric power. The other 89% of the heat energy is carried away by the radiator heat pipe. Nominally, the heat input surface of the emitter is at 1925 K. The radiator's surface is 1000 K. So the THPM has two functions: (1) to generate electricity and (2) to transport heat away from the reactor core. Figure 6 shows the SEHPTR reactor design.

**Nominal payload for Thermion-II.** Thermion-II can test any scale THPM, but as the heat pipe gets larger, the required input power gets larger. The duration of the experiment is reduced because of the finite amount of energy available from the batteries. As a baseline, Thermion-II will test a one-quarter length heat pipe. This is equivalent to a heat pipe with a 10-cm emitter length and an approximate radiator length of 70 cm. The final dimensions on the test THPM are not set because the scale of heat pipe has not been decided on, and so the final performance of THPM has not yet been determined. However, Utah State University has been working closely with Thermacore, Inc., the likely manufacturer of the THPM, and the finalization of parameters is imminent.

### System-Level Requirements of Thermion-II

The requirements of Thermion-II are to simulate the thermal environment of SEHPTR's nuclear reactor core on a scaled version of THPM on orbit, measure the performance, and telemeter data to the ground. Other requirements are to provide a structure to fly in the Delta II secondary payload volume that supports the required batteries and THPM, design a low cost alternative to Thermion-I, and provide a safe and reliable design.

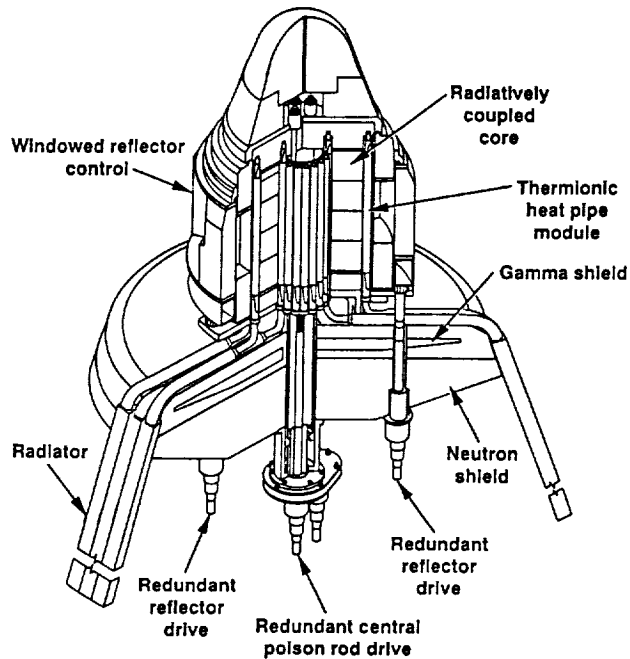


Fig. 6. The THPM inside the SEHPTR reactor.

### Design Philosophy

The design philosophy of Thermion-II (1) takes a simple, straightforward approach to the THPM space test, and avoids unproven systems and items of questionable safety; (2) offers a low-cost option (if it is simple to design and understand, it will be easy and inexpensive to implement).

### Mission Description

The THPM test requires a microgravity environment for some length of time. The THPM should be exposed to an environment that closely matches that of its intended use, inside a reactor core. To achieve this, the THPM payload will be mounted to the Delta II secondary payload volume along with batteries,

power control system computer, and interface to the Delta II telemetry system. Once the orbit has been achieved, the primary payload will separate from the Delta II and the Delta II will zero the rotation rates of the second stage and activate the experiment. From this time on, the Delta II will provide only telemetry capability. No active attitude control system will remain, and some power will be diverted from the batteries to power the Delta II telemetry system. Detailed integration with the Delta II has not been seriously addressed, and it is anticipated that use of its telemetry system will be involved.

Using a one-quarter length THPM, the experiment may be operated continuously for 21 hours or longer if variable heating rates are applied to THPM. For example, the high amount of control of an electric-based heater allows for very slow and very fast heating of the THPM.

### Conclusions

Thermion-II is not a satellite and, consequently, is free of the cost, complexity, and development time that a satellite requires. Thermion-II capitalizes on existing systems onboard the Delta II (attitude control and telemetry) and does not depend on external power sources. Because it has no moving parts, there is no question of mechanical reliability. Thermion-II can also be developed and flown in much less time than satellite.

Thermion-II is versatile since it has excellent control over heating rates of the electric heater. This is a closed loop system. Transients can be simulated and excess power input may also be simulated. While Thermion-I may run for a year, it has the drawback that it cycles the THPM every orbit due to the loss of the Sun when it is in Earth's shadow.

Thermion-II should be pursued if a 21-h test or a series of 21-h tests (several Thermion-IIs) will satisfy the reliability and functional concerns of the THPM in a space environment. Finally, Thermion-II can be optimized using lithium cells instead of alkaline cells. This will triple the experiment time. However, lithium cells have had an explosive history. If the cells are not internally fused they may overheat and explode when shorted, and although modern lithium cells are much safer, their legacy remains. The cost of qualifying them for flight may exceed their benefit.

**SOLAR ELECTRIC PROPULSION CARGO SPACECRAFT FOR MARS MISSIONS**

**VIRGINIA POLYTECHNIC INSTITUTE AND STATE UNIVERSITY**

546-20  
160622  
P. 4

One of the topics available to the 1990/91 Aerospace Engineering senior class was the development of a preliminary design of an unmanned cargo ferry that would support the Mars mission by bringing equipment and supplies from a low Earth orbit (LEO) to a low Mars orbit (LMO).

Several previous studies initiated by NASA have indicated that low-thrust transportation systems seem to offer the best performance for Mars missions. Such systems are characterized by long spiral times during escape and capture maneuvers, high payload mass fractions, and, typically, low propellant mass fractions. Of two main low-thrust candidates, nuclear electric propulsion (NEP) and solar electric propulsion (SEP), only the first one received extensive consideration because it seemed to represent the most promising concept for a manned mission to Mars. However, any sustained Mars initiative will have to include an unmanned cargo transportation system, for which an SEP concept deserves very careful consideration.

The key assumptions and requirements established in cooperation with the Space Exploration Initiative office at the NASA Langley Research Center were

1. Vehicle is assembled at the Space Station *Freedom* (SSF).
2. Earth-to-orbit delivery of the vehicle components, propellant, and payload is via shuttle-C.
3. Vehicle's cargo mass is 61,000 kg.
4. Vehicle delivers cargo to LMO at an altitude of 500 km and inclination of 70°.
5. Vehicle returns (without cargo) to SSF.
6. Vehicle should be reusable for at least three missions.
7. Vehicle is powered by ion argon thrusters.

Two configurations have been developed by two student teams, working mostly independently.

**FLAT SOLAR ARRAY CONFIGURATION**

The first configuration, SEMM1 (Solar Electric Mars Mission 1) uses 24 self-deployable flexible blanket solar arrays anchored to two square-bay truss beams (Fig. 1). Before the final SEMM1 design was chosen, various options were analyzed and compared with an overall goal of minimizing the total initial mass while accepting relatively long trip times (up to about three years for a round trip). Both trip time and specific impulse ( $I_{sp}$ ) directly affect the amount of power required, which in turn strongly influences the mass of the spacecraft. The key characteristics of the selected SEMM1 are  $I_{sp}$  of 8000 s, initial power of 3.15 MW<sub>e</sub>, initial thrust (near Earth) of 60 N, and LEO to LMO trip of 654 days.

The SEMM1 solar arrays provide a total cell area of 10,370 m<sup>2</sup> to produce 3.15 MW<sub>e</sub> power near Earth. The solar cells will be of a multibandgap type, using indium phosphide (InP) as a top layer and gallium antimonide (GaSb) as a bottom cell.

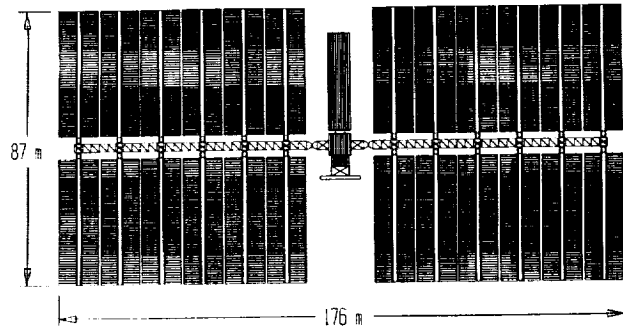


Fig. 1. Planar solar array configuration.

This combination has been studied and experimented with at Boeing and Entech. A small amount of cell output current will be drawn from the main feed to be rerun back through the cell in a forward-bias configuration to keep the cell materials above 100°C for self-annealing of the InP cell from the electron- and proton-induced radiation damage. High potential efficiency of the cell (22.5% InP + 8% GaSb) at air mass zero (AMO) conditions will be reduced by about 4% because GaSb cell's efficiency decreases somewhat at higher operating temperatures. Taking this into account as well as the physical and electrical losses (wiring/mismatch and forward-bias current) and the losses expected due to irreversible degradation after a long journey, the effective efficiency has been projected to be 22% throughout most of the trip to Mars, and about 2% less after the first round trip.

The InP/GaSb cells will be arranged into arrays by using extendable flat solar panels similar to a few prototype arrays flown on the space shuttle. These prototypes were demonstrated to have adequate stiffness and deployability in a space environment. Selection of the flat panel arrays instead of those using optical concentrators was strongly influenced by three factors: in-space assembly time, launch packaging, and pointing accuracy. Extendable arrays are light-weight, do not require high pointing accuracy, are self-deployable, and are compact when stowed. Twenty-four arrays of the SEMM1 extend out from two long truss beams. The beams are attached to the sides of the ship by means of rotational  $\alpha$ -joints, forming two "wings," with six arrays fore and aft, on each wing. Each array consists of two solar panel blankets that are held in tension by a mast extending between them (Fig. 2). The  $\alpha$ -joints allow the two wings to rotate about one axis and they transmit the electrical power to the central (main) body. The mass of the solar arrays, including wiring, truss beams, and  $\alpha$ -joints is 15,320 kg.

The SEMM1 propulsion system consists of 13 (including 3 redundant units) 2-m-diameter, gimbal-mounted ion thrusters, each capable of developing 6 N thrust at  $I_{sp}$  of 8000 s. Ten

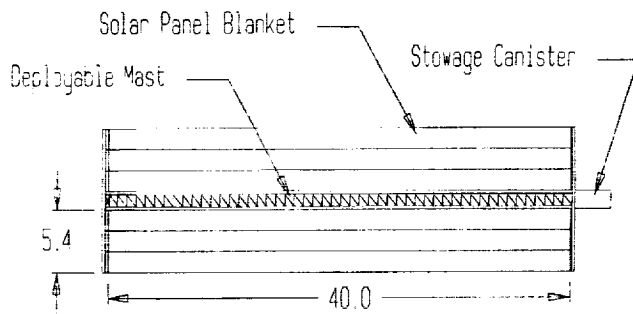


Fig. 2. Deployable solar panel blankets.

thrusters will operate during Earth-escape spiral, and four will operate near Mars. A lifetime of the thrusters is projected to be between 15,000 and 20,000 hr. High  $I_{sp}$  and large thruster diameter should result in a high thruster efficiency of 0.81.

The power generated by the solar arrays must be conditioned into a form suitable for the thrusters and the onboard systems. The power processing units (PPU) supply and control the power for discharge/cathode, neutralizer, screen, and accelerator. The overall PPU efficiency is assumed to be 95%, and the heat generated by the electrical components will be dissipated to space by radiators mounted on the sides of the propulsion module.

The argon propellant (23,840 kg) will be cryogenically stored at a temperature of 85 K in a 17.3 m<sup>3</sup> ellipsoidal tank. The tank is a two-shell type with a vapor-cooled shield surrounding it, and will be equipped with internal heaters to vaporize argon during thrusting operation, as well as with a refrigeration system to reliquefy boiled-off argon during coasting periods. An extensive meteoroid/debris protection and thermal insulation will be provided for the argon storage.

The SEMM1 main body structure is made of graphite-epoxy box trusses that hold the thruster module, power conditioning units, auxiliary power system (batteries), navigation, guidance and communications equipment, and array orientation and vehicle control systems. The cargo container is attached to the front of the main body. Three shuttle-C launches will be needed to deliver to LEO all the spacecraft components. The total initial mass of the spacecraft (at LEO) is approximately 118,000 kg offering a payload mass ratio of nearly 52%.

**FRESNEL LENS CONCENTRATOR ARRAY CONFIGURATION**

The second configuration (SEMM2) uses two hexagonal shaped arrays that collect solar power by a Fresnel lens concentrator/multistacked cell system (Fig. 3). Spacecraft sizing and low-thrust trajectory analyses were aimed mainly at low total initial mass of the spacecraft and low propellant and thrusting time requirements. These considerations, combined with an assumption of high solar cell efficiency, led to a  $I_{sp}$  of 10,300 s, power requirement of around 3.5 MW, and LEO to LMO trip duration of around 960 days.

The system chosen to provide the solar power is a three-solar-cell stack proposed by Barnett and Trumble<sup>(1)</sup> and a Fresnel lens concentrator (Figs. 4 and 5). The cell will use a six-terminal

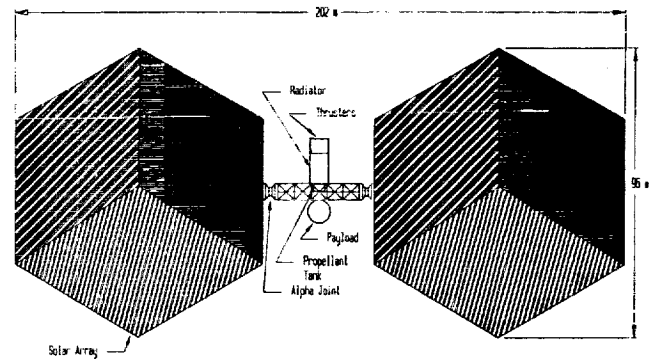


Fig. 3. Fresnel lens concentrator array configuration.

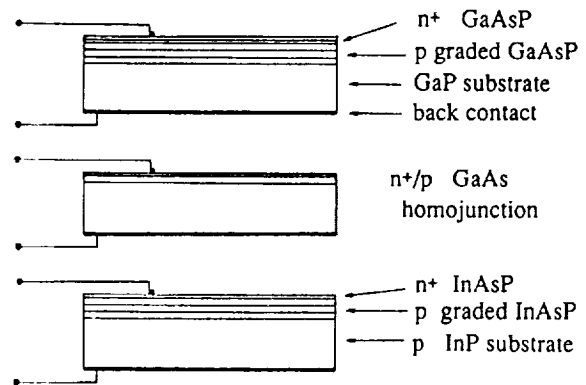


Fig. 4. Three-solar-cell stack.

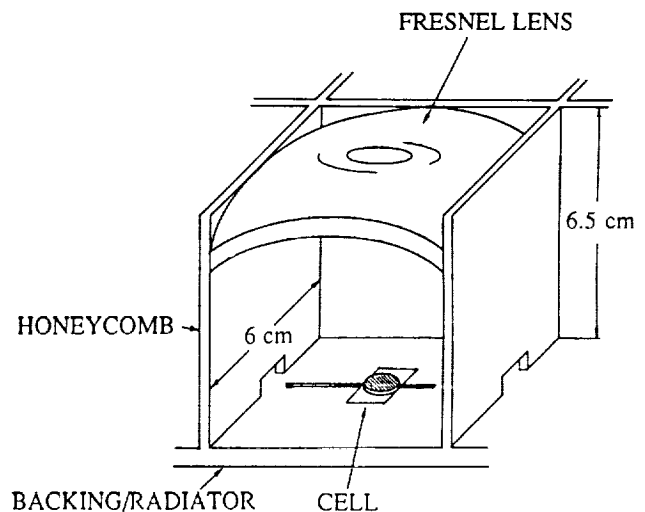


Fig. 5. Fresnel lens module.

wiring configuration to minimize current mismatch losses that may be caused by different degrees of radiation damage to the three solar cells. The GaAsP-on-GaP top cell, which determines the performance of the triple stack, is the most advanced wide-bandgap cell currently under development. The state-of-the-art GaAs cell will serve as the middle cell. The InAsP bottom cell is least developed and even when "immature" can only improve the total conversion efficiency by scavenging the low-energy photons from the top two cells. A theoretical efficiency limit of this triple solar cell stack is 42.8% at AMO and a practical system efficiency of 35.9% is predicted<sup>(1)</sup>. In application to our spacecraft, an efficiency of 27% was assumed to account for the high operating temperature of about 150°C and the radiation damage occurring during the three Mars missions.

The array is made up of small modules, 6 cm on each side and 6.48 cm high (Fig. 5). Each module consists of a Fresnel lens dome that concentrates the incident sunlight on the 6-mm-diameter cell, a honeycomb supporting structure, a multistacked cell, and a back radiator panel to dissipate excess heat. Each lightweight silicone Fresnel lens has a thin protective diamond film coating on the upper surface of the lens. The thin-wall honeycomb structure is made of graphite-epoxy with a protective coating. This structure provides a simple way to create a rigid array with less weight penalty than other array systems. The array is designed to allow a maximum deflection of 2°. A wall height of 6.48 cm was chosen as a compromise between strength, low mass, and shuttle-C space requirements. The array wiring is designed to minimize both the weight and the power loss.

Solar array support structure is designed to be resistant to out-of-plane deformations and vibrations. It is constructed of three concentric "rings" of tetrahedral pyramid-shaped elements. Each element is assembled from six half-conical strut members made of anodized-aluminum-coated graphite epoxy. The total mass of the solar arrays, without  $\alpha$ -joints and trusses connecting to the main body, is about 13,000 kg.

The electric propulsion system consists of 17 ion engines including 5 redundant units. Twelve engines will operate near Earth producing a maximum thrust of 60 N. Each engine has a beam diameter of 130 cm and its beam power, discharge power, and neutralizer power are 252.6, 20.8, and 1.7 kW, respectively. To provide a lifetime of 20,000 to 25,000 hr, a ring-cusp magnetic configuration and a moderate beam current density are selected; it is also possible to add a small amount of nitrogen to the discharge chamber. The engine efficiency is assumed to be 0.714 and the power processing efficiency is 0.95. The total mass of the propulsion system is 9140 kg.

The argon propellant mass of 24,200 kg is stored cryogenically in a cylindrical tank (2.6 m diameter, 4.1 m length) with hemispherical end caps. The tankage mass, including protective shield/insulation, electrical heaters, Stirling refrigeration unit, propellant lines, valves, and controls, is 820 kg.

The central supporting structure of the ship uses orthogonal tetrahedral truss cells. The mass of this structure including engine mounts, cargo bay, and rotational  $\alpha$ -joints is estimated at 3600 kg. The attitude/orientation control system of the ship and solar array is based on the control moment gyroscopes (CMG) and small electric thrusters. The communications and navigation systems employ 6 antennas (2 high gain and 4 omnidirectional;

Ka- and X-band), transponders, command data, and handling subsystems based on low-power 32-bit processors, and navigation subsystem based on 3 star trackers, 3 dry inertial measurement units, and 11 solar sensors.

Earth-to-LEO delivery of the ship components, propellant, and payload will require three shuttle-C launches. The total initial mass of the spacecraft is approximately 116,000 kg, resulting in a payload mass ratio of nearly 53%.

## CONCLUSIONS

An SEP cargo spacecraft using high  $I_{sp}$  and either planar or concentrator arrays offers a very high payload mass fraction (around 52%) and a low initial mass of the system. Implementation of the SEP system will require a significant advance in solar cell technology and a further development of large ion thrusters. If the pace of the progress in solar cell technology made over the past 10 years is sustained, we may expect that during the next 15-18 years efficiencies and resistance to radiation damage can be increased to and beyond the levels assumed in our studies, i.e., AMO efficiencies of 22% and 27% for the planar and concentrator arrays, respectively. In laboratory tests, planar InP cells have attained a value of 18.8% AMO, and GaAs concentrator cells exceeded 22%. Both types have shown potential to be highly resistant to the natural radiation environment. Incorporation of new developments in surface passivation, front surface shaping, and dot junction geometry may result in concentrator GaAs efficiencies approaching 28% at concentrations of around 100. Supperlattice solar cells (comprising layers of different semiconductor materials) and tandem cells currently under development in several laboratories and proposed for our vehicles, offer a further significant improvement in cell performance. Because the bulk recombination losses can be drastically reduced in such cells, very high collection efficiencies are possible. In addition, an increased lifetime of minority carrier should result in a very high resistance to radiation damage and, thus, in a significant extension of the lifetime of solar cells. As far as ion engine life is concerned, there are no inherent or strong reasons why the lifetimes of high-power, large-diameter ion engines should not be comparable to those of the current engines and subject to further improvement so as to reach 15,000-25,000 hr.

We anticipate that high-performance/long-lifetime solar cells will become available for space applications by 2005-2010, and at that time SEP propulsion system will be highly competitive if not superior to nuclear electric propulsion (NEP), because it is likely to offer a higher payload fraction, no environmental concerns, and lower launch and assembly costs. The increased NEP costs are associated with an initial safe Earth orbit higher than LEO.

## ACKNOWLEDGMENTS

SEMM1 design team members were C. E. Callaghan, M. D. Crowe, M. R. Mickney, C. K. Montgomery, M. J. Swis, S. Thoden, and R. Walters. SEMM2 team members were A. Chiles, J. Fraser,

A. Halsey, D. Honeycutt, B. Mc Gough, D. Paulsen, B. Spear, L. Tarkenton, and K. Westley. Project advisors were Dr. A. K. Jakubowski (VPISU) and D. A. Haynes (NASA Langley Research Center).

#### REFERENCES

1. A. M. Barnett, T. M. Trumble, G. H. Negley, S. L. Rhoads, J. B. McNeely, and N. E. Terranova, "A Three-Solar-Cell Mechanically Stacked, Multijunction System With Energy Conversion Efficiencies Greater Than 30% AMO," 22nd IECEC Conference, Vol. 1, Aug. 1987.

# ANTARES: A LOW COST MODULAR LAUNCH VEHICLE FOR THE FUTURE

UNIVERSITY OF WASHINGTON

547-15

160623

p. 12

The single-stage-to-orbit launch vehicle Antares is a revolutionary concept based on identical modular units, enabling the Antares to efficiently launch communications satellites, as well as heavy payloads, into Earth orbit and beyond. The basic unit of the modular system, a single Antares vehicle, is aimed at launching approximately 10,000 kg (22,000 lb) into low Earth orbit (LEO). When coupled with a standard Centaur upper stage it is capable of placing 4000 kg (8800 lb) into geosynchronous Earth orbit (GEO). The Antares incorporates a reusable engine, the Dual Mixture Ratio Engine (DMRE), as its propulsive device. This enables Antares to compete and excel in the satellite launch market by dramatically reducing launch costs. Antares' projected launch costs are \$1340/kg (\$610/lb) to LEO, which offers a tremendous savings over launch vehicles available today.

Inherent in the design is the capability to attach several of these vehicles together to provide heavy lift capability. Any number of these vehicles can be attached depending on the payload and mission requirements. With a seven-vehicle configuration, the Antares' modular concept provides a heavy lift capability of approximately 70,000 kg (154,000 lb) to LEO. This expandability allows for a wide range of payload options, such as large Earth satellites, Space Station *Freedom* matériel, and interplanetary spacecraft, and also offers a significant cost savings over a mixed fleet based on different launch vehicles.

## INTRODUCTION

The expanding applications of communications and military satellites over the last decade have increased the demand for reliable, low-cost launch vehicles. Recent projections made by the Office of Commercial Space Transportation (OCST) indicate that the average number of payloads launched per year will continue to increase<sup>(1)</sup>. NASA has estimated that 11-14 shuttle flights per year are needed to construct and supply the proposed Space Station *Freedom*<sup>(2)</sup>. Other analysis done by NASA, the Air Force's Space Systems Division, and the NASP program reveal that a vehicle able to lift 9000 kg (20,000 lb) into low earth orbit (LEO) could carry 80% of NASA's civil payloads, 60% of the Defense Department's payloads, and nearly all commercial payloads<sup>(3)</sup>. With a backlog of payloads waiting to be launched and a projected increase in the number of launches needed in the future, the current U.S. launch fleet, composed of reusable space shuttle orbiters and expendable launch vehicles (ELVs), will not be able to adequately meet these demands.

The space shuttle, initially hailed as America's dependable, low-cost, all-purpose launch vehicle, has encountered numerous technical problems, causing delays to scheduled launches. Originally, in the early 1970s, NASA projected that a reusable shuttle would deliver payloads to orbit for one-tenth the cost of any expendable launch vehicle available at that time<sup>(4)</sup>. However, in order to achieve these cost savings, the shuttle had to be flown frequently, allowing the operations costs to be spread out over many missions. As late as 1981, NASA's Office of Space Transportation System Operations was predicting that the shuttle could achieve a flight rate of 40 missions per year<sup>(4)</sup>, but unexpected delays to scheduled launches have severely reduced this number, resulting in the current high cost of launching payloads on the orbiters. Being a man-rated vehicle, the shuttle requires multiple redundant systems to ensure the safe launch and return of the crew. This causes increased system complexity and can reduce efficiency. This has required NASA to create

a "standing army" of engineers and technicians to keep the space shuttle orbiters in operation and on schedule. The man hours involved significantly increase the shuttle's launch costs, making it less attractive to potential launch customers. The reduction in the number of launches per year caused by delays, and the increased cost to consistently maintain the space shuttle reduces its effectiveness as a reliable vehicle for launching satellites and space probes.

With the delays of the shuttle reducing the number of launches available, commercial and military satellite launch customers have had to rely on expendable launch vehicles, such as the Atlas, Delta, and Titan<sup>(4)</sup>. However, the ELVs, originally developed in the 1960s as intermediate range ballistic missiles (IRBMs), and intercontinental ballistic missiles (ICBMs), impose mass and size restrictions that limit their payload capacities. These restrictions have created a gap in the payload range to geosynchronous Earth orbit (GEO) between 1500 kg (3300 lb) and 4000 kg (8800 lb). Arianespace, a consortium of European aerospace companies and banks, predicts that satellites heavier than 1200 kg, particularly in the 2000- to 3000-kg range, will dominate the future<sup>(5)</sup>. Without an American expendable launch vehicle that is able to compete in the 1500-kg to 4000-kg payload range, and with the uncertainty of space shuttle launches, U.S. companies have turned to Arianespace for their launch needs<sup>(2)</sup>. To date, Arianespace has effectively captured a 50% share of the satellite launch market<sup>(5)</sup>.

The high cost of launching a satellite on the shuttle or an ELV places another constraint on satellite manufacturers. It currently costs from \$50,000 to \$120,000/kg (\$22,700 to \$54,500/lb) to launch a payloads into GEO<sup>(6)</sup>. To reach LEO, the cost range is from \$6,600 to \$26,450/kg (\$3,000 to \$12,000/lb)<sup>(7)</sup>.

The mass and size restrictions and high launch costs of the current mixed fleet of space shuttle orbiters and ELVs have severely hindered America's ability to compete in the satellite launch market. It is apparent that a new, flexible and cost-effective launch vehicle must be developed to ensure America's

continued presence as a leader in the commercial launch market. Current vehicles under consideration, such as the Advanced Launch Development Program (ALDP), formerly the Advanced Launch System (ALS)<sup>(8)</sup>, and the fly back single-stage-to-orbit (SSTO) manned vehicle<sup>(9)</sup>, do not meet the above mentioned criteria. The ALDP is designed as a heavy lift launch vehicle, thus limiting its effectiveness for launching payloads into orbit to a small percentage of the market. The totally reusable manned SSTO requires many additional systems that not only increase the overall cost of the vehicle, but make it more complex. As evident from the problems experienced by the shuttle, very complex vehicles tend to encounter more technical problems, which in turn increase launch costs.

Antares, the new launch vehicle proposed in this report, is the flexible and cost-effective launch system that will be able to meet the nation's growing launch needs both in the near and long term. Antares is a single-stage-to-orbit launch vehicle that can deliver a wide range of payloads. The basic Antares vehicle for LEO and GEO missions uses a single advanced reusable liquid hydrogen and liquid oxygen engine, the Dual Mixture Ratio Engine (DMRE), as its main engine<sup>(10)</sup>. The DMRE is retrieved for reuse in future missions via the Engine Return Unit (ERU), resulting in a substantial reduction of the launch costs. For LEO missions, the Antares vehicle has the capability to be clustered together to provide heavy lift. The LEO mission vehicles (see Fig. 1), which are identical modular units, can

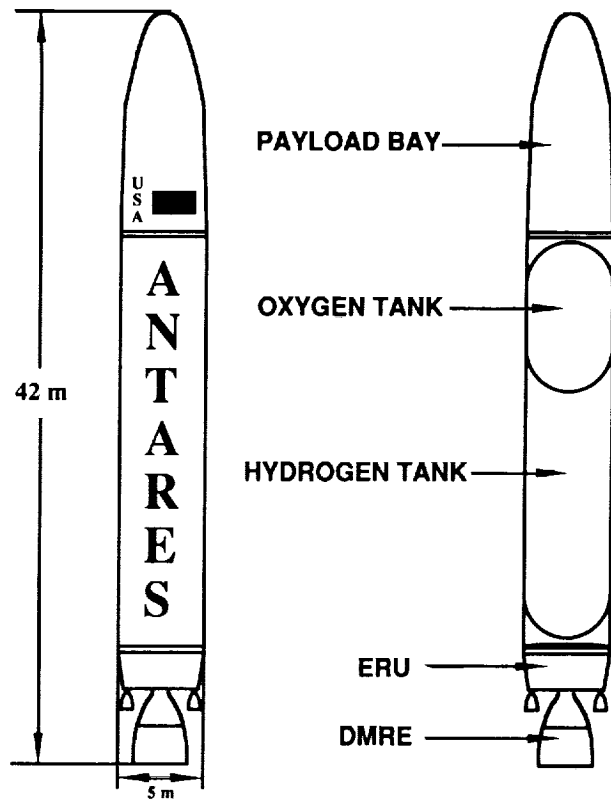


Fig. 1. Antares I configured for LEO missions.

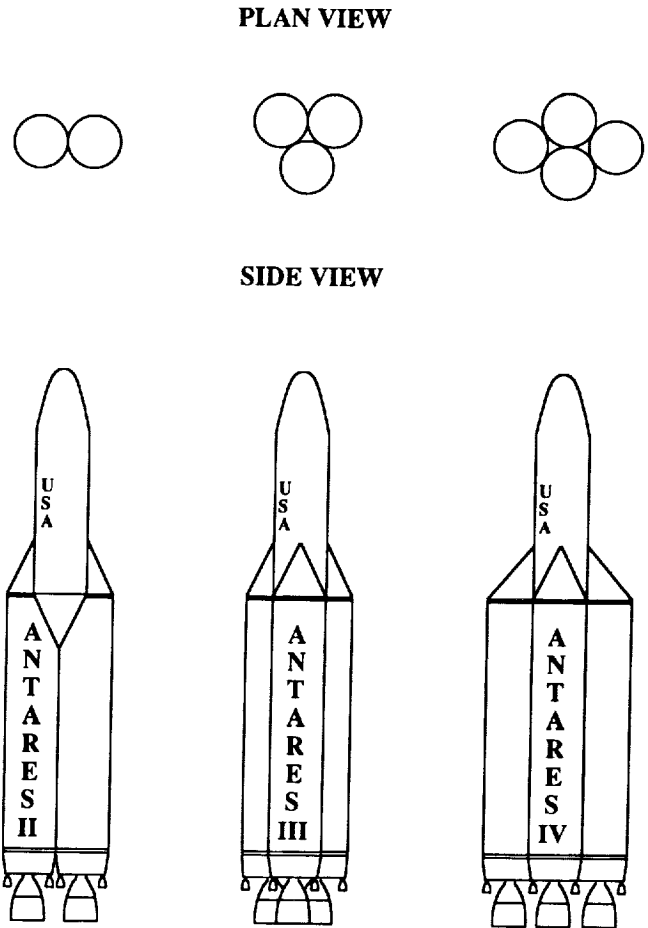


Fig. 2a. Antares modular configurations.

be combined to form various modular configurations, from a two-booster configuration (Antares II), up to a seven-booster configuration (Antares VII), as illustrated in Fig. 2. This modular concept reduces cost on the basis that a large, heavy lift vehicle is a cluster of simple, generic boosters, thus giving Antares an unprecedented advantage over any other existing or proposed launch vehicle. The Antares vehicle used for GEO missions is basically the same as the LEO mission vehicle (see Fig. 3). It executes a suborbital trajectory and uses a Centaur upper stage to deliver the payload into GEO. With a reusable engine and the concept of simple modular systems, Antares provides a low-cost, reliable alternative to the existing fleet of launch vehicles.

For Antares to be successful, it must recapture a large portion of the U.S. satellite market that has been lost to Arianespace. One Antares vehicle can place a payload of 4000 kg (8800 lb) into GEO, thus allowing it to effectively compete against Arianespace for launch customers. Antares' modular capability provides another distinct advantage over other launch vehicles and is instrumental in making the Antares a potentially dominant player in the commercial launch market. The ability to attach several vehicles together provides launch customers with a wide range of payloads to LEO, from 10,000 kg (22,000 lb) with Antares I to 70,000 kg (154,000 lb) with Antares VII. The low launch costs of the Antares vehicle, \$1340/kg (\$610/lb) to LEO and

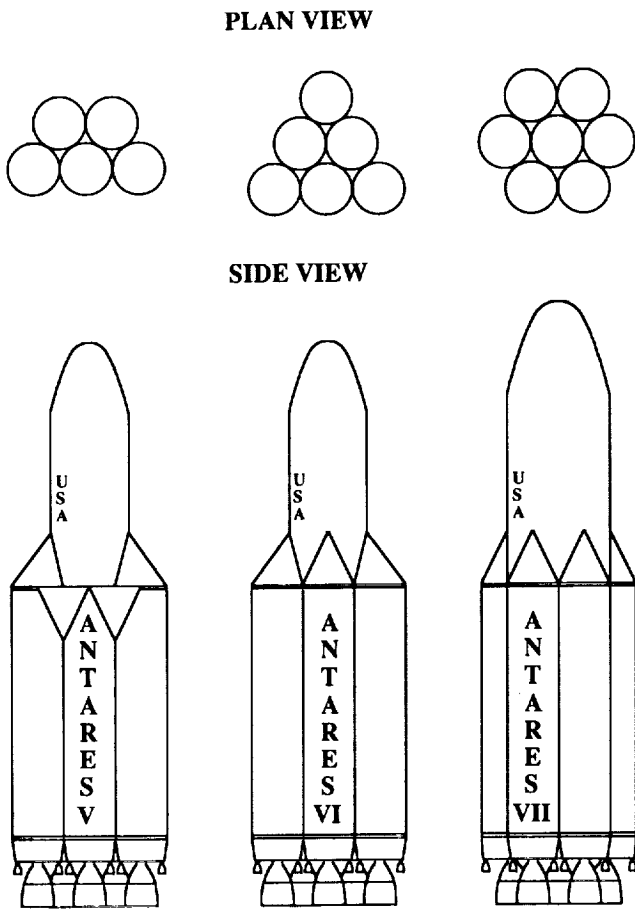


Fig. 2b. Antares modular configurations.

\$16,200/kg (\$7350/lb) to GEO, cannot be matched by any existing launch vehicles. Antares' unique ability to deliver a variety of payloads into LEO and GEO and its low launch costs, allow it to effectively compete not only against Arianespace, but other foreign competitors such as China and Japan. The concept of modularity and the cost savings attributed to reusable engines makes Antares a reliable, inexpensive, and flexible launch vehicle.

This report provides a summary of the design of the Antares vehicle. It includes LEO and GEO mission profiles, the Antares' main systems: ERU, propellant tanks, structural connectors, and fairings, and the benefits of modular configurations. An evaluation of the cost per unit mass to launch payloads into orbit concludes the report.

**MISSION PROFILES**

All mission scenarios, whether destined for LEO or GEO, begin in the flight integration building. In an effort to maintain a high launch rate it is essential to reduce the length of time that a launch vehicle spends on the launch pad. With the exception of the space shuttle, all current U.S. launch vehicles are integrated

in an upright position on the launch pad. This often requires an extended length of time during which the pad cannot be used for other missions. The approach offered with the Antares vehicle will reduce the time required on the launch pad by performing vehicle integration in a horizontal position at a site located away from the launch pad. The major components of the Antares and its payload can be joined and checked out in the protection and safety of a climate-controlled facility. When engineers and customers are satisfied with the integration, the vehicle will travel to the launch site horizontally on a railed vehicle specifically designed to hold the Antares during integration and transportation. The Antares will be translated to an upright position at the launch site by the transport vehicle. The transport vehicle will then retreat to a safe distance when the operation is complete. By performing only final checkout and fueling procedures on the launch pad, significant savings in pad occupancy time can be attained. This system is very similar to the Soviet approach to launch vehicle integration and it holds potential improvements in ground operation efficiency and hence launch costs.

To help compare the Antares with other U.S. launch vehicles, sample mission profiles are performed with launches originating at the Kennedy Space Center (KSC). This provides for a launch

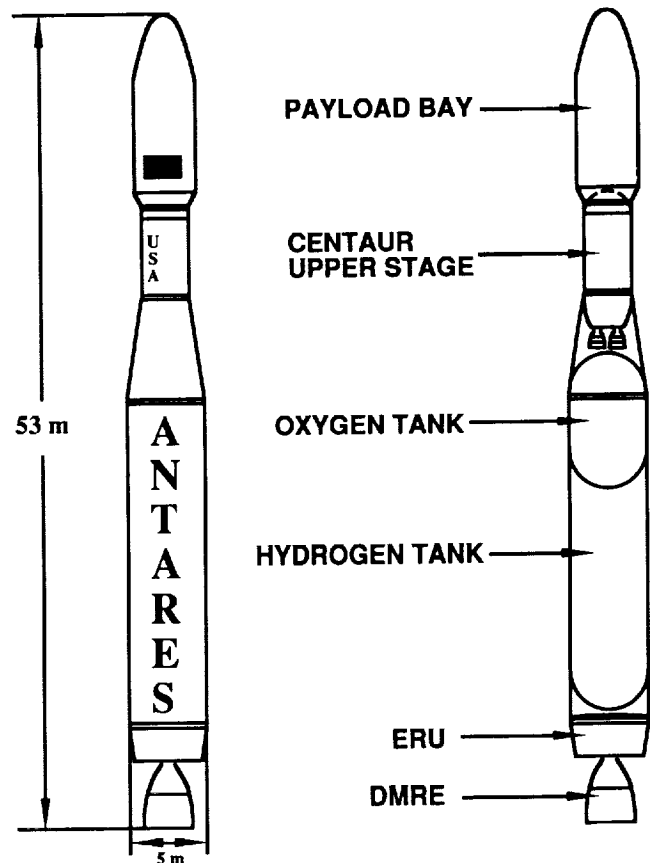


Fig. 3. Antares I configured for GEO missions.

latitude similar to many other vehicles. KSC is located at 28.5° N, and an east launch from here provides for insertion into an orbit of 28.5° inclination.

**LEO Mission**

At rollout, the dry mass of the LEO Antares is 23,000 kg (50,600 lb). Payload mass for LEO missions makes up 10,000 kg (22,000 lb) of this, while the other 13,000 kg (28,600 lb) is components of the vehicle. They consist of the Engine Return Unit (ERU), the propellant tank structure, and the payload fairing. An illustration of the LEO launch sequence is shown in Fig. 4.

The Antares is designed to use a DMRE. It is a staged combustion cycle engine concept studied by Pratt and Whitney Co.<sup>(10)</sup> specifically for SSTO applications, which require high thrust at liftoff and high  $I_{sp}$  at altitude. It burns liquid oxygen and hydrogen and operates at a high oxidizer-to-fuel ratio (12:1)

early in the flight, providing for high thrust levels during the boost phase of the mission. High thrust is critical at takeoff when the mass of the vehicle is greatest. Later in the flight the oxidizer-to-fuel ratio is reduced to 6:1. This sustainer phase lowers the engine's thrust but increases the specific impulse. The gross liftoff mass of the vehicle is 197,600 kg (435,500 lb). At takeoff the DMRE produces 2460 kN (553,000 lb) of thrust at an  $I_{sp}$  of 333 s. This gives the Antares an initial thrust-to-weight ratio of 1.27. The DMRE has a translatable nozzle that allows the expansion ratio to be changed during flight. At an altitude of 12 km (40,000 ft) the nozzle extension is lowered, increasing the area ratio from 40:1 to 150:1. This adds approximately 28,000 lb to the vacuum thrust and 18 s to the vacuum  $I_{sp}$ . At an altitude of 27 km (88,000 ft) the mass of the Antares has been reduced to approximately half of its original value. At this point in the flight the oxidizer-to-fuel mixture ratio is reduced to 6:1, the thrust drops to 417,000 lb, and the  $I_{sp}$  is increased to 467 s.

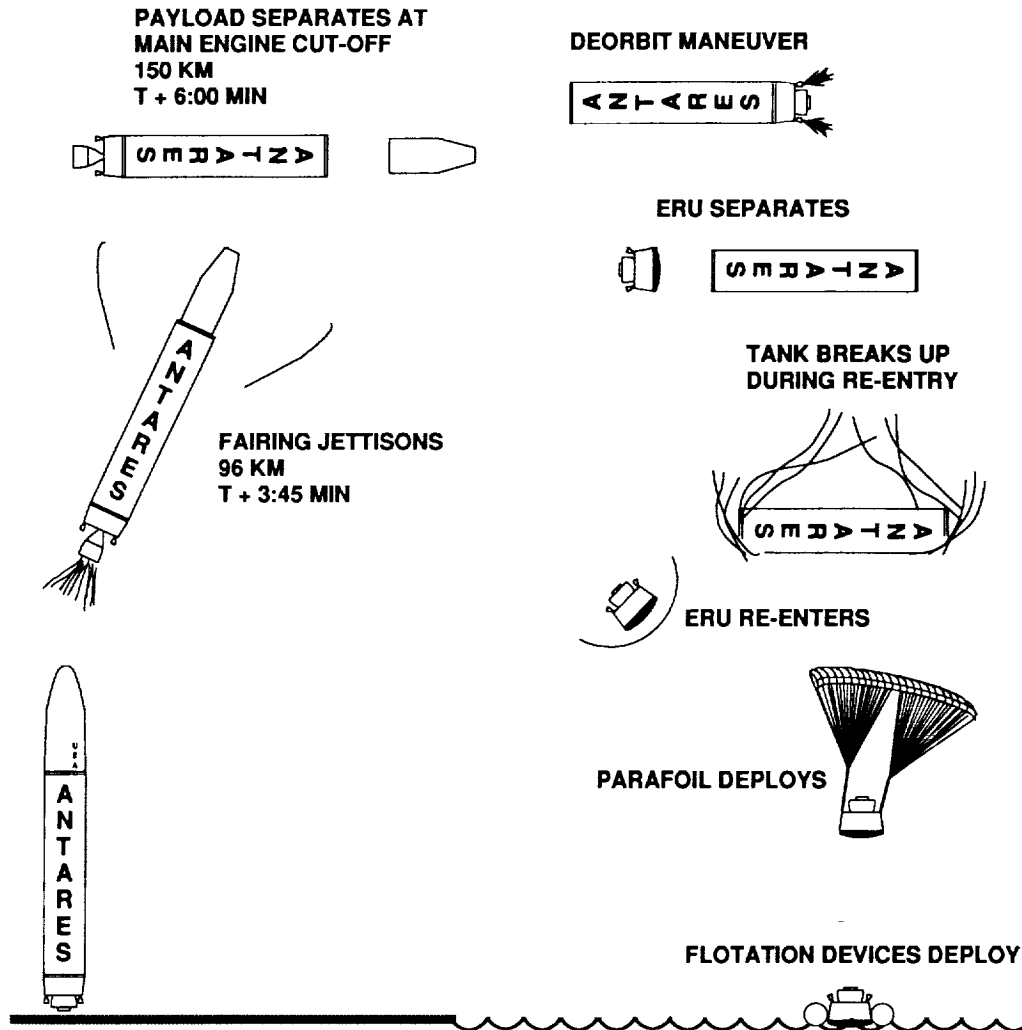


Fig. 4. LEO mission profile.

When the Antares reaches the upper atmosphere, the drag and frictional heating experienced at the payload fairing become negligible. This allows for the fairing to be jettisoned, as it is no longer required to protect the payload. The payload fairing is deployed at an altitude of 96 km (317,000 ft), and decreases the mass of the vehicle by 1400 kg (3090 lb).

Burnout is achieved six minutes after liftoff with the completion of orbital insertion into a 150-km  $\times$  300-km elliptical orbit of 28.5° inclination. This orbit was chosen for the sample profile analysis, as it provides the satellite with a wide range of final orbital altitudes which require minimal  $\Delta V$  from the satellite. The total  $\Delta V$  required for this LEO mission profile is 9.3 km/s.

After orbital insertion is achieved, the Antares separates itself from the payload and orients itself for a reentry maneuver. The Antares is capable of remaining in the 150  $\times$  300-km parking orbit for several days as it waits for the proper reentry window. At the appropriate time, the DMRE's nozzle retracts and the ERU performs a deorbit burn. The ERU and the tanks separate so that they reenter at different locations. This is desirable, as the ERU is to be retrieved, while the tanks are to be discarded so that they burn up in the atmosphere. Small solid rocket motors push the tanks into a long shallow trajectory that will cause them to be destroyed by atmospheric heating. Any pieces that survive the flight will land harmlessly, far out to sea. The ERU maneuvers into a steep descent that allows it to splash down relatively close to the Florida coast, where it can be retrieved by ship. Once the ERU is retrieved, maintenance is performed on its components and it is integrated into another Antares vehicle for further service.

### GEO Mission

The mission to GEO also begins at KSC, but the final destination of the payload is in a much higher orbit that is equatorial rather than inclined. Both the LEO and GEO missions involve initial insertion into a 150  $\times$  300-km parking orbit. The GEO mission, however, performs this mission as a two-stage vehicle. In place of a LEO payload, a Centaur upper stage and GEO payload ride atop the Antares booster. The Centaur upper stage performs insertion into the parking orbit, the transfer to a Geosynchronous Transfer Orbit (GTO), and final insertion of the payload into GEO.

At liftoff, an optimum thrust-to-weight ratio of 1.27 is desired. Since a fueled Centaur and payload have a greater weight than a LEO payload, this is achieved by only partially filling the Antares propellant tanks. This results in a fueled Antares booster of 175,300 kg (383,800 lb), topped with a Centaur of 18,400 kg (40,600 lb) and a payload of 4000 kg (8,800 lb). The launch characteristics for the GEO mission profile (Fig. 5) are very similar to those of the LEO mission. The area ratio and oxidizer/fuel ratio change at altitudes corresponding to the LEO mission and have the same effects described above. The payload fairing is also deployed at altitude, reducing the mass of the vehicle by 1200 kg (2650 lb). Burnout of the Antares booster is achieved five minutes after liftoff, when the Centaur separates and begins its burn. The Antares booster begins to fall back to earth in a suborbital, ballistic trajectory. The ERU separates from the

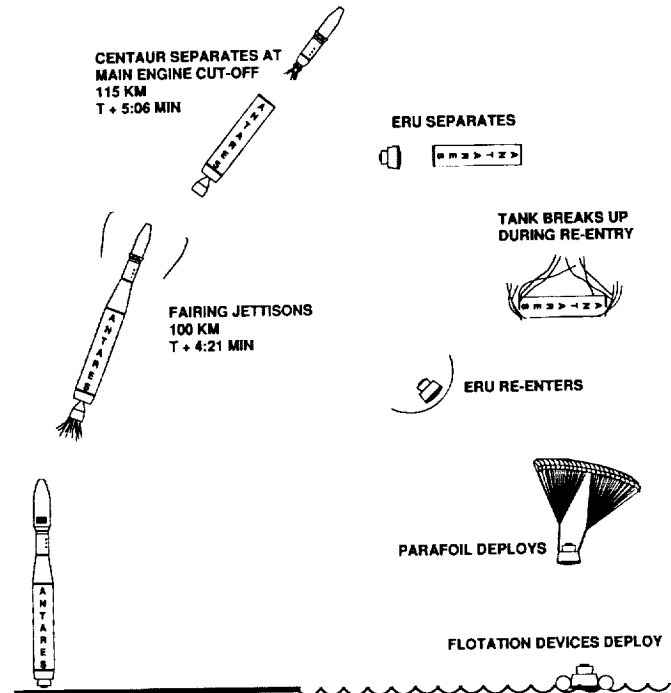


Fig. 5. GEO mission profile.

tanks for reentry and is recovered by ship approximately 2100 km east of KSC. The tanks are allowed to burn up on reentry, and are not reused.

The Centaur burns approximately half of its propellant in achieving insertion into the parking orbit. The remaining propellant is required for insertion of the payload into GEO. The Centaur waits in the parking orbit until the proper transition time. At the perigee of the parking orbit, the Centaur performs a burn to accelerate it into GTO. The optimum transfer involves a plane change at both the perigee and apogee of the GTO. The perigee plane change is from an inclination of 28.5° to 26.4°. The apogee of the GTO is at GEO, where the final plane change is performed and the satellite is released into a circular orbit of 0° inclination. Once separation of satellite and Centaur is complete, the Centaur places itself into a circular orbit 1000 km lower than the satellite. The  $\Delta V$ s for this mission are 9.17 km/s from launch to LEO and 4.24 km/s from LEO to GEO.

Analysis of the Antares' mission profile, in both LEO and GEO configurations, was performed with a trajectory optimization program called OPGUID, provided by NASA's Marshall Space Flight Center<sup>(11)</sup>. It performs a three-dimensional vector analysis of the rocket's trajectory, based on the initial and final conditions and the vehicle operating parameters. A separate program was used to determine the characteristics of both the deorbit and suborbital reentry of the ERU. Worst-case dynamic stability analysis was performed on the LEO Antares based on the flight characteristics predicted by OPGUID.

**ENGINE RETURN UNIT**

The Engine Return Unit (ERU), shown in Figs. 6-8, is the key element for the reusability concept of the Antares launch vehicle. It houses the DMRE, secondary propulsion, and avionics, which are the most expensive components of the vehicle. The ERU is designed to return these components to Earth, so that they may be reused on subsequent missions. The ERU makes up 5800 kg (12,800 lb) of the vehicle's 13,000 kg (26,600 lb) dry mass.

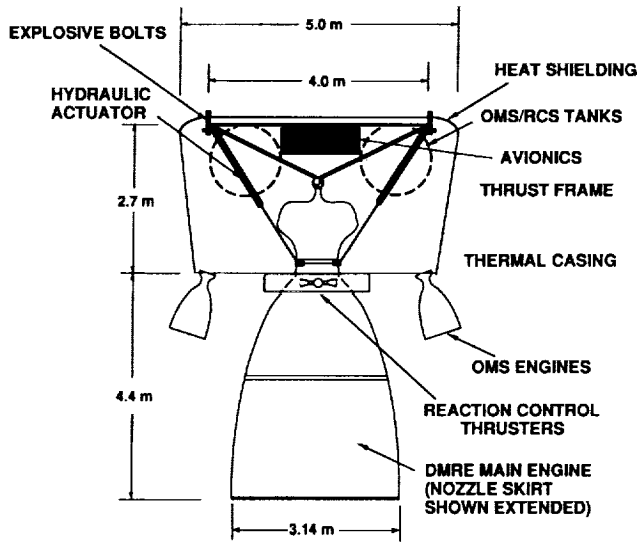


Fig. 6. Schematic cutaway view of Engine Return Unit (ERU): LEO configuration.

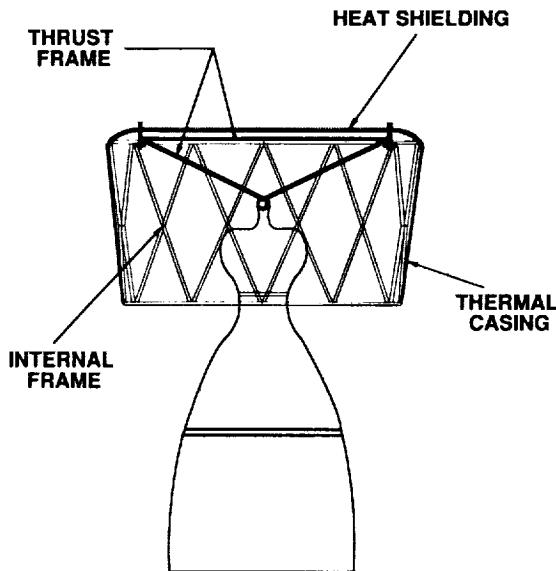
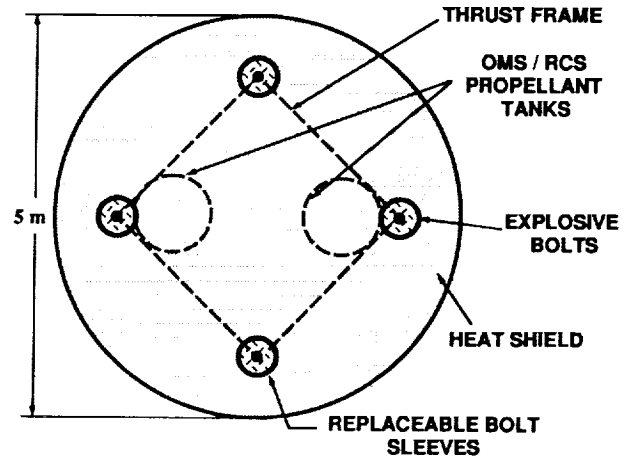
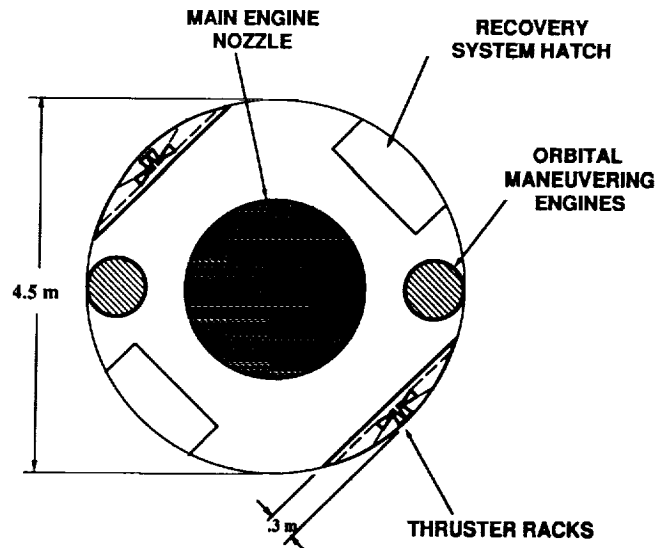


Fig. 7. ERU structural components. (For clarity OMS structure is not shown).



a) Top view



b) Bottom view

Fig. 8. End views of ERU.

The Antares uses the DMRE as its main engine because it is designed specifically for single-stage-to-orbit operations. The DMRE provides high thrust for the boost phase, which accelerates the vehicle quickly through the atmosphere. This is accomplished with a high mixture ratio of 12:1, and a low nozzle expansion ratio of 40:1. For the sustainer phase of the launch, the mixture ratio is reduced to 6:1 and the nozzle expansion ratio is increased to 150:1 to give a maximum specific impulse (see Table 1). The engine also has the ability to throttle to keep the vehicle's acceleration within the 4-g limit.

The ERU structure (see Fig. 7) is divided into three parts: the main thrust frame, the internal frame, and the outer heat shield. The thrust frame is designed to transfer the thrust of the DMRE through the fasteners that connect the ERU to the

propellant tank. The frame members consist of titanium tubes for maximum material strength per unit mass. The internal framing is a Kevlar composite structure that supports the ERU's outer casing and is strong enough to withstand the loads experienced during splashdown, which can be as high as 1400 kPa (~200 psi). Extra titanium frame structure is required to support the two orbital maneuvering engines used in conjunction with the LEO configurations. This structure is attached to the main thrust frame. A carbon-carbon ablating heat shield is mounted on the forward face of the ERU to absorb the heat of reentry.

TABLE 1. DMRE Performance Characteristics.

|                        | Boost Phase    | Sustainer Phase |
|------------------------|----------------|-----------------|
| Thrust (kN), (lbf)     | 2460 (553,000) | 2670 (417,000)  |
| $I_{sp}$ (sec)         | 334            | 467             |
| Mixture ratio (O/F)    | 12:1           | 6:1             |
| Expansion ratio        | 40:1           | 150:1           |
| Chamber Pressure (MPa) | 27.6           | 18.6            |

The avionics housed in the ERU are controlled by a distributed command and data handling system (C&DH). The guidance, navigation, and control system (GN&C) consists of an inertial navigation system (INS) and two horizon sensors. The communications subsystem uses a transponder that is compatible with the Space-Ground Link System (SGLS) on the S-band. The avionics themselves use approximately 100 W of power for both LEO and GEO missions. The ERU power supply consists of primary batteries as well as secondary rechargeable batteries for the longer term LEO missions. The total avionics mass is 500 kg.

For LEO missions, the Antares requires orbital maneuvering and deorbiting capability and an attitude control system. These are provided by an independent propulsion system integrated into the structure of the ERU (see Figs. 6 and 8). This secondary propulsion system becomes active after the payload has been deployed. The vehicle's attitude is maintained by a reaction control system (RCS) while it coasts in the parking orbit. The orbital maneuvering system (OMS) engines then decelerate the vehicle at the appropriate time, initiating the vehicle's deorbit trajectory. GEO missions do not require this additional hardware, as the Antares vehicle performs a suborbital flight.

Rocketdyne XLR-132 orbital maneuvering engines, which each produce 16.68 kN of thrust, are mounted on the ERU to carry out orbital maneuvers and perform the deorbit burn. Marquardt R-1E thrusters, which produce 110 N of thrust, provide reaction control for the Antares. They are housed in thruster racks, which are mounted onto the bottom of the ERU (see Figs. 6 and 8). This makes the thruster racks easily accessible and allows them to be reconfigured for modular Antares vehicles (see Fig. 9). Both the XLR-132 engines and the R-1E thrusters burn monomethyl hydrazine (MMH) and nitrogen tetroxide ( $N_2O_4$ ). These propellants are stored in spherical tanks that are mounted in the ERU as shown in Figs. 6 and 8. A high-pressure helium tank is located upstream of the propellant tanks, and pressure regulators are used to adjust the pressure to the required engine manifold inlet pressure.

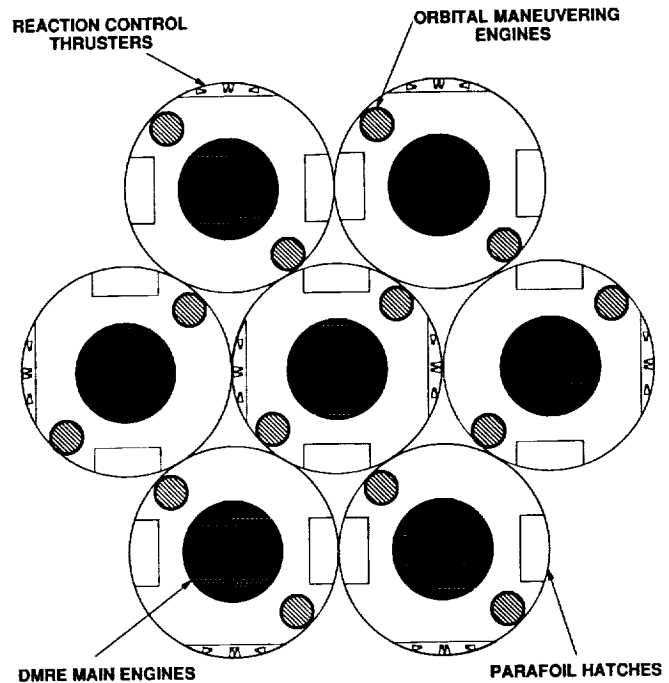


Fig. 9. Antares VII propulsion system configuration.

The separation system disconnects the ERU from the tank structure before reentry by means of explosive bolts extending from the thrust frame of the ERU. At the proper time, the bolts explode and expanding springs push the ERU and tank safely apart. No retractable doors are necessary to seal off the ERU to avoid sinking after a water landing because there is no pathway for water through the separation system components and into the ERU. This feature minimizes mass and reduces system complexity.

After separation from the tank, the ERU reenters the atmosphere, where it experiences a very high thermal load. The ERU is protected from this through the use of an ablating heat shield on the blunt forward surface. Blunt bodies dissipate a large fraction of the energy of reentry to the atmosphere, thus reducing the heat transferred to the vehicle. The ablator's function is to absorb the heat that is imparted to the vehicle. The material vaporizes, jettisoning the heat from the vehicle. A carbon-carbon composite is used as this material because of its high heat of vaporization.

A parafoil is deployed for the final phase of deorbit. This parafoil slows the vehicle so that it safely splashes down into the ocean, and allows some maneuvering capability just prior to splashdown. An inflatable flotation ring is deployed to give the ERU additional buoyancy and stability in the water. The ERU is recovered by ship and returned for refurbishment and reuse.

## PROPELLANT TANKS

The design of the Antares propellant tanks (Fig. 10) is based on the relationship between the forces and moments that are imposed on the oxidizer and fuel tanks and the ability of the

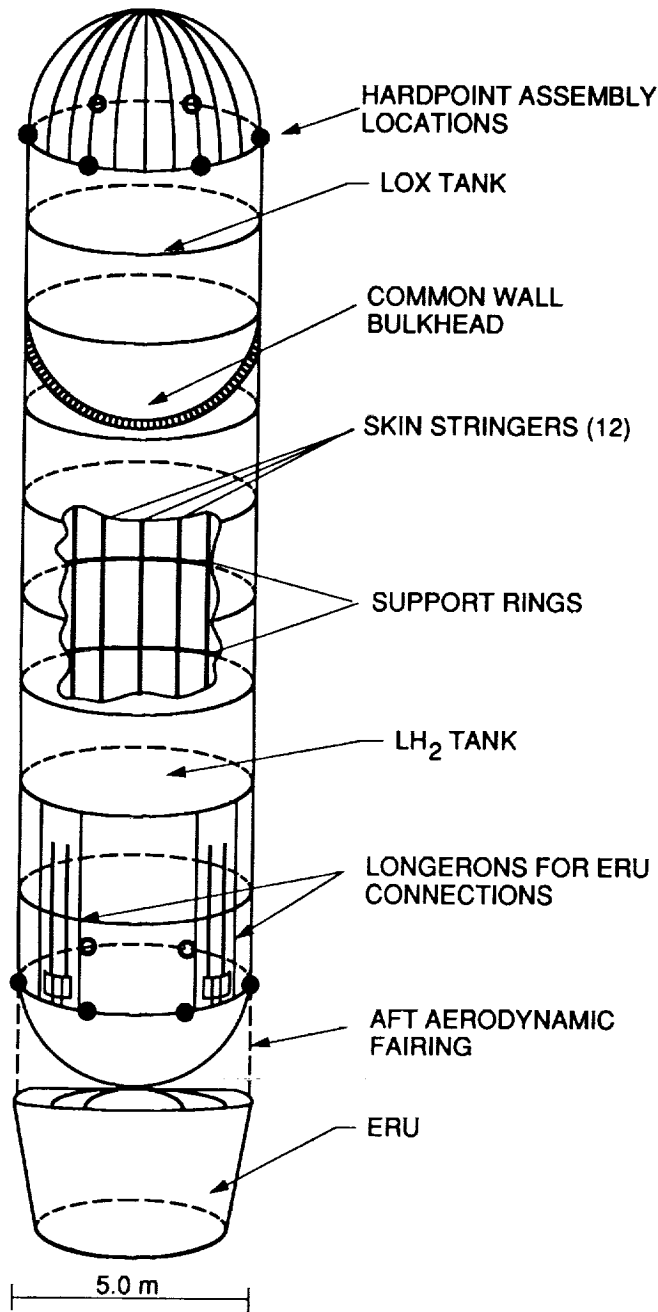


Fig. 10. Antares propellant tank.

tanks to withstand these loads. This relationship limits the minimum dimensions of the propellant tanks and corresponds to a minimum dry mass of the tank structure. The Antares encounters various combinations of axial, lateral, and shear forces prior to launch and during ascent, and is designed to withstand worst-case loading situations.

The lightweight propellant tanks are designed with the liquid hydrogen tank ( $292.4 \text{ m}^3$ ) below the liquid oxygen tank ( $140.3 \text{ m}^3$ ). A common wall bulkhead separates the two tanks.

The oxidizer and the fuel tanks are semimonocoque structures constructed of aluminum alloy 2219 and have a wall thickness of 2 and 2.2 mm respectively. The propellant tank structure is 23.5 m long, and has a constant diameter of 5 m. Through the use of supporting rings and stringers the tanks are self-supporting and do not require internal pressurization to maintain structural integrity. One of the key features of the Antares propellant tank structure is the common wall bulkhead that separates the fuel and oxidizer tanks. It is an aluminum 2219 honeycomb structure with an evacuated core to minimize the heat flux between the propellants. The tanks are externally insulated with polyurethane foam that is 10 mm thick for the liquid hydrogen tank and 5 mm for the liquid oxygen tank. The fuel and oxidizer are transferred to the ERU via 10-cm-I.D. external lines, constructed of Inconel 718. The mass of the complete tank system, including an estimation for slosh baffles, is 4200 kg. An inventory of the mass of each tank component is listed in Table 2.

TABLE 2. Tank Component Structural Masses.

| Component                         | Mass (kg)   |
|-----------------------------------|-------------|
| Liquid Oxygen Tank                |             |
| • Cylinder                        | 335         |
| • End Closure                     | 220         |
| • Support Rings                   | 100         |
| • Stringers                       | 70          |
| Liquid Hydrogen Tank              |             |
| • Cylinder                        | 1440        |
| • End Closure                     | 440         |
| • Support Rings                   | 440         |
| • Stringers                       | 280         |
| Common Wall Bulkhead              | 550         |
| Propellant Lines                  | 200         |
| Insulation                        | 125         |
| <b>Total Tank Structural Mass</b> | <b>4200</b> |

### CONNECTIONS

There is one connection device that is common to all Antares configurations. This is the ERU to tank connection (Fig. 11). The bottom of the liquid hydrogen tank is connected to the ERU via four struts. These connect to the four corners of the ERU's main thrust structure and attach to the sides of the liquid hydrogen tank via longerons, which extend up the tank walls. The total mass of the ERU-to-tank connection, including the aft aerodynamic skirt, is 1000 kg. Another major connection device is the inter-stage adapter (ISA) used on GEO missions. The ISA connects the liquid oxygen tank to the Centaur upper stage and transfers axial loads to the propellant tank walls. The ISA has a total mass of 1200 kg. A modified ISA is used as support for payloads on LEO missions. The ISA for the LEO Antares has a mass of 600 kg.

### PAYLOAD FAIRINGS

The design of the lightweight payload fairings is based on payload envelopes that are attractive to potential users of the Antares. The fairing shape minimizes aerodynamic loads while

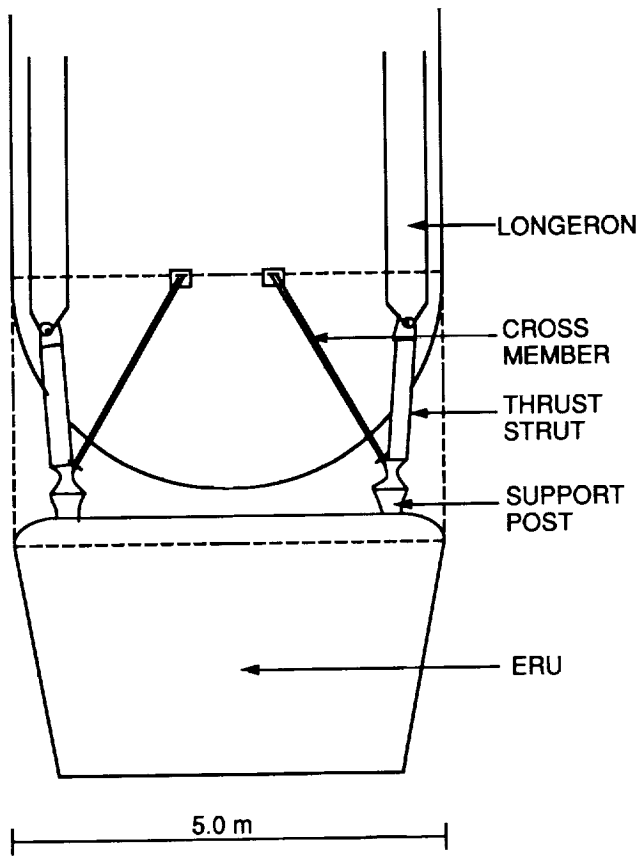


Fig. 11. ERU to tank connection.

maximizing the structural integrity. The sizes of Antares payload envelopes are in accordance with current and projected payload dimensions that can utilize the full payload capacity of Antares. Geostationary communications satellites have progressed toward increased circuit capacity and a longer life span. The more capable spacecraft are larger and heavier than their predecessors. Indications are that future communications satellites will be even larger still. The Antares GEO payload fairing accommodates today's communications satellites and the larger spacecraft of the future (see Fig. 12).

NASA's needs and industry projections dictated the initial LEO payload envelope dimensions. The *Civil Needs Data Base*<sup>(12)</sup>, maintained by NASA, contains several hundred entries describing NASA's current and projected payloads for delivery to LEO. A majority of these payloads have widths suited for delivery by the space shuttle (4.57 m) and are under 9000 kg. Such payload widths are accommodated by Antares' standard LEO fairing, shown in Fig. 12. The fairing base diameter is dictated by Antares I's single booster diameter (5.0 m). The standard LEO payload fairing will service more than 75% of NASA's LEO payloads. A larger payload envelope is provided for modular versions of the Antares (Fig. 2). The Antares III fairing has the same diameter as the Antares I, but has a length comparable to that of the shuttle's payload bay.

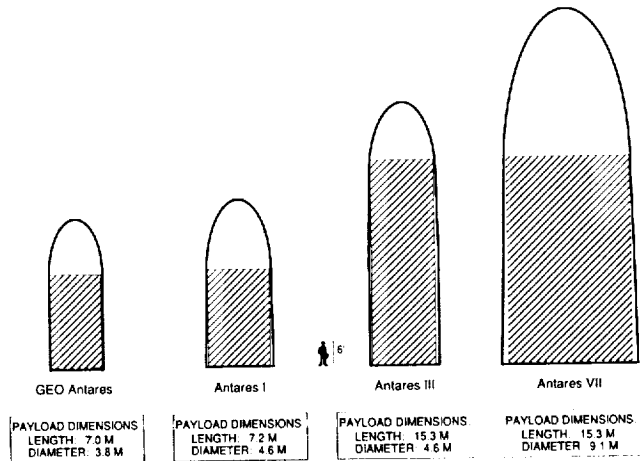


Fig. 12. Antares payload fairings.

The fairing of the Antares VII (Figs. 2b and 12) provides a payload envelope that is unique among current or planned U.S. launch vehicles. The envelope's diameter is approximately twice that of the Titan IV, while its length corresponds to the lengths of many larger payloads listed in the *Civil Needs Data Base*.

All fairings use a parabolic nose geometry with a length-to-diameter ratio of 1.2. This geometry allows a sizeable portion of the payload to be stowed inside the nose section, thus resulting in an overall reduction in length and mass of the cylindrical portion of the payload fairing. In addition, the continually curved shape resists collapse or buckling loads, thereby requiring less structural support in the nose cone shell.

The Antares' nose cone shell structural support is modeled in a manner similar to McDonnell Douglas' Titan IV nose cone (an isogrid arrangement). The benefit of using an isogrid is that the outer skin of the nose cone can be made less massive, due to the forces being transmitted through the isogrid truss. The nose cone tip's skin will be made from a carbon-carbon composite to withstand the high temperatures experienced during the maximum Q region of flight. The remaining skin will consist of Cycom NCG nickel-coated graphite fiber composite. This composite is specially designed to dissipate electrical charge, should a lightning strike to the nose occur. Acoustic blankets are inserted between the composite beams of the isogrid in the inner fairing wall to prevent excessive vibration transmission to the payload envelope.

The payload fairing is jettisoned from the vehicle at a prescribed altitude (~100 km). To perform this separation two rails that sandwich an explosive charge are used. When detonated, the explosive charge splits the fairing along its axis into two or more segments. Once split the segments rotate back on hinges until they reach an unhinging point and fall off.

### CONFIGURATIONS

One of the key features of the Antares is the ability to combine the boosters to provide expanded payload capabilities. The Antares is capable of attaching from two to seven boosters to

form its family of vehicles called the Antares II through the Antares VII. In the modular configurations the Antares units are attached using hard points that are a part of the propellant tanks. Two of the tanks' stiffening rings, one forward and one aft, contain six hard point attachment assemblies that allow up to six boosters to be attached to a central booster (see Fig. 10).

The modular configurations of Antares allow for expanded payload capabilities. Since each booster is identical to the Antares I, the payload capabilities are just multiples of the Antares I. The Antares family has a payload range of 10,000 kg (22,000 lb) for the Antares I to 70,000 kg (154,000 lb) for the Antares VII. This wide range of payloads gives the Antares an advantage over existing launch vehicles by providing the space launch market a fleet of vehicles with only one vehicle design.

An issue that must be addressed in the modular configurations is that of engine failure. If one of the engines were to fail in a modular configuration launch, the mission's success would be dependent upon when the failure occurred. If the failure occurs too early in the ascending phase of the mission, there is no alternative but to abort the mission. Beyond a certain point during ascent, the Antares can still complete its mission, in spite of an engine failure, by using an Emergency Propellant Communication System (EPCS).

The EPCS allows for the propellant from the booster with the failed engine to be shared with the engines that are still firing. This is done by interconnecting the propellant lines of the boosters that are joined together. This gives each ERU access to another unit's propellant. If there is an engine failure, the appropriate valves open, so that all the propellant is consumed and the mission is salvaged.

**COST ANALYSIS**

For the Antares vehicle to establish itself as the dominant launch vehicle in the 21st century it must be cost effective. To achieve this goal the Antares uses many cost saving techniques. One idea used to reduce cost was to design the Antares as a single-stage-to-orbit vehicle. Although this design is less efficient than multi-stage vehicles it lowers the cost by reducing the complexity of the vehicle and the costs of operation and support. Another technique is using the ERU to retrieve the DMRE and the avionics, which together can account for up to 70% of total vehicle cost. The savings achieved by reusing the expensive components of the Antares translate directly to a much lower cost per unit payload mass to the customer.

To determine the cost per unit payload mass for Antares, the Life Cycle Cost (LCC) had to be taken into consideration. The LCC consists of three basic costs: Research, Development, Test, and Evaluation (RDT&E) cost, the production cost which is a function of the Theoretical First Unit (TFU) cost, and the Operations and Support (O&S) cost. The RDT&E cost includes all of the design, analysis and testing of the Antares vehicle. The TFU cost indicates the production cost for one Antares vehicle and is the basis for computing the cost for multiple units in production. The O&S cost consists of the necessary operations for preparing the Antares for a launch and supplying personnel for these launches. Other factors that are added to the O&S cost are the recovery and the refurbishment costs for the ERU, and total propellant costs for the vehicle. All of

these costs are necessary to determine the expenditures required to put the Antares on line, and to calculate the cost per unit payload mass.

Before the LCC could be computed, the number of launches had to be estimated. The Antares mission model shows how many launches per year will be flown over the projected life span of 40 years. The mission model (see Fig. 13) proposes a maximum launch rate of 30 per year, and a total of approximately 900 launches over the program's anticipated life span.

For the cost analysis the Antares vehicle was separated into eight categories. These categories are the structure, thermal control, avionics, power, main propulsion, secondary propulsion, recovery system, and staging/ordnance (Table 3). Cost per kilogram values for the eight categories were used to determine the TFU and the RDT&E for the vehicle<sup>(12)</sup>. This was done simply by summing the masses of the components that fit into a specific category and multiplying the result by its respective cost per kilogram value. The results are shown in Fig. 14. RDT&E and TFU cost per kilogram values differ for ERU and tank components due to the differing complexity of these two systems. To compensate for this the category masses were separated into ERU and tank values. To determine the total production costs the TFU costs must be adjusted using a learning curve, which accounts for productivity improvements as more units are produced. The O&S cost is calculated using a linear slope approximation. It follows that the O&S cost increases as more flights are made but the average cost per flight decreases (see Fig. 15).

TABLE 3. Categories for Life Cycle Costs.

| Category             | Example of Components in Category            |
|----------------------|--|
| Structure            | Propellant tanks, fairings, ERU thrust frame |
| Thermal Control      | Insulation, heat shield, thermal casing      |
| Avionics             | On-board computers, accelerometers           |
| Power                | Batteries                                    |
| Main Propulsion      | DMRE engine, piping for the main vehicle     |
| Secondary Propulsion | OMS, RCS                                     |
| Recovery Systems     | Parafoils, flotation devices                 |
| Staging Ordnance     | Explosive bolts, range safety devices        |

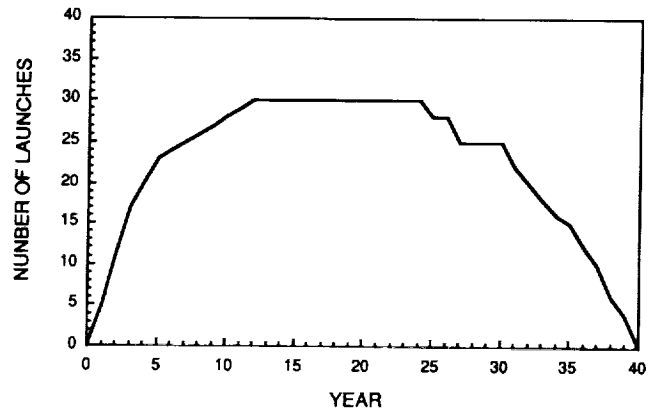


Fig. 13. Antares mission model.

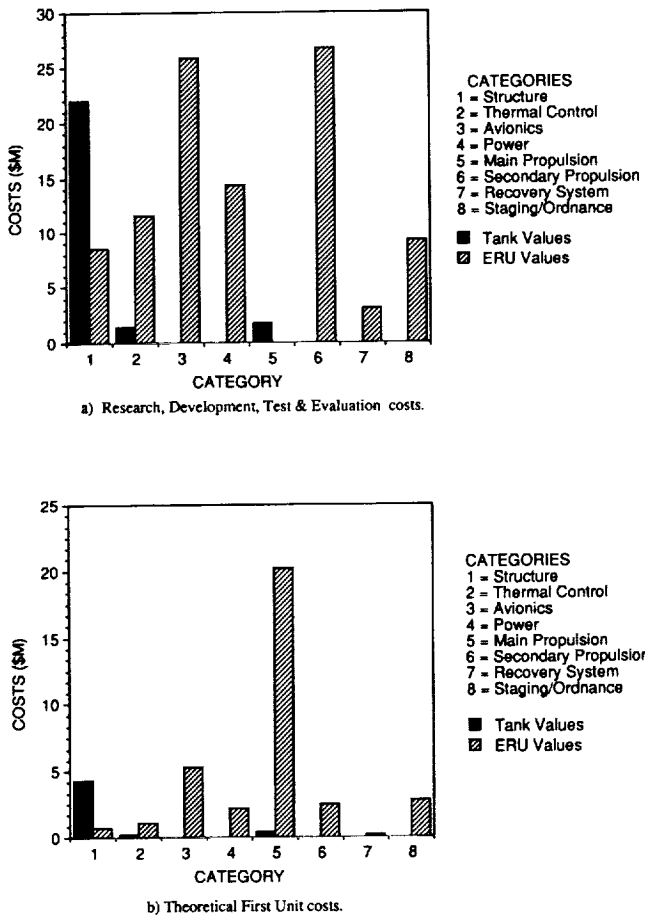


Fig. 14. Costs for tank and ERU components (in millions of 1991 dollars).

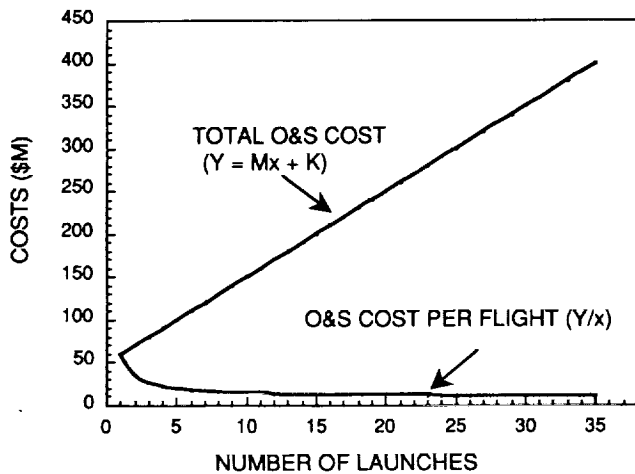


Fig. 15. Operations and Support cost per launch (in millions of 1991 dollars).

To determine the cost per unit payload mass for the Antares all of the previous data must be taken into account. The RDT&E costs are spread out over the 900 flights contained in the mission model. A model year is chosen to determine the average cost per unit payload mass. For our analysis the fifteenth year of service is chosen. In this year of service thirty launches are scheduled. The values obtained for production and O&S costs are averaged for the thirty launches to determine the launch cost for one vehicle. The cost per unit payload mass is obtained by simply dividing the average launch cost by the maximum payload delivered to LEO. The cost per unit payload mass to LEO for the Antares is \$1340/kg (\$610/lb).

The cost per unit payload mass to GEO is a direct function of the total LEO launch cost. To calculate the cost per unit payload mass to GEO, there are a few other factors that need to be addressed. These factors are the cost of the Centaur, which is the cost for the vehicle and all O&S necessary to launch it, and the additional components, mostly structure, necessary to attach the Centaur to the Antares. These costs are added directly to the total (RDT&E, TFU, and O&S) launch cost obtained in the LEO analysis. From this the GEO cost per unit payload mass is determined by simply dividing the total GEO launch cost by the Antares payload capabilities to GEO. The cost per unit payload mass to GEO is \$16,200/kg (\$7350/lb).

From the above data it is evident that the Antares vehicle is capable of providing launch services at a cost unmatched by any existing launch vehicle. The cost per unit payload mass to LEO for the Antares is approximately one-tenth that of the space shuttle and one-sixth of the current industry leader, the Ariane IV. For these reasons alone, it is evident that the Antares launch vehicle is prepared to make space affordable and to open this market to the world.

**CONCLUSION**

The Antares is a single-stage-to-orbit launch vehicle, designed for versatility and low cost. To achieve these goals a modular system based on single identical units is proposed. The basic unit of the modular system, a single Antares vehicle, is aimed at launching approximately 10,000 kg (22,000 lb) into LEO. When using the Centaur upper stage it is capable of placing 4000 kg (8,800 lb) into GEO. The Antares incorporates a reusable engine, DMRE, as its propulsive device. This enables Antares to compete and excel in the satellite launch market by dramatically reducing launch costs. Antares' projected launch costs are \$1340/kg (\$610/lb) to LEO, which offers a tremendous savings over launch vehicles available today.

The most cost-effective aspect of the Antares is its ability to return the main engine and reuse it in future launches. Since the engine accounts for the majority of the total vehicle cost, returning it results in a considerable savings, which can be returned to the customer in the form of a low cost per unit payload mass. Engine reusability is assuredly the wave of the future, if launching is ever to become economical. The Antares will pioneer the way to developing this new technology.

Antares' modular configurations accommodate a payload range of 10,000-70,000 kg to LEO, which is unmatched by any other launch vehicle. The ability to launch multiple booster configurations makes the Antares in itself a family of launch vehicles.

Thus the launch cost is greatly reduced because only one vehicle is developed to serve this large range of payload masses. Another cost reducing factor is that the Antares is conducive to inexpensive, large-scale production because the main booster is identical in all the modular configurations. This straightforward approach to production, similar to the commercial airplane industry, also assures a high level of reliability in that specific manufacturing methods, unique to the Antares vehicle, can be implemented because of its inherent long term usefulness as a competitive launch vehicle.

Another feature of the Antares that enables it to achieve its design goal is its ability to expand and meet the growing needs of the satellite market. The Antares' modular concept makes this expansion possible. Satellites are no longer bound to the small payload capacities of existing launch vehicles. In addition to an increased payload mass, the modular concept also accommodates an increased volumetric capacity. In effect, the Antares is an all-purpose vehicle ready to expand to future needs.

Antares' innovative design makes it an inexpensive and reliable launch vehicle, and because of Antares' unique features it is capable of encouraging expansion in the satellite industry. By making the one-time dream of low-cost vehicles a reality, Antares could help the U.S. regain its dominance in the commercial launch market.

#### REFERENCES

1. U.S. Department of Transportation, Office of Commercial Space Transportation, *The Future of the Commercial Space Launch Market: 1993-2005*, Decision Science Consortium, Inc. and Berner, Lanphier, and Associates, Inc., May 1991, pp. 8-30.
2. Frazer, L., "Lead, Follow or Get out of the Way," *Space World*, May 1988, pp. 12-15.
3. Payton, G. and Sponable, J.M., "Single Stage to Orbit: Counting Down," *Aerospace America*, April 1991, pp. 36-39.
4. Simon, M.C. and Hora, R.P., "Return of the ELVs," *Space World*, January 1988, pp. 15-19.
5. Jaeger, R.W. and Claudon, J., "Ariane - The First Commercial Space Transportation System," *The Fifteenth International Symposium on Space Technology and Science*, Volume II, Tokyo 1986, pp. 1431-1438.
6. Wertz, J.R. and Larson W.J., Editors, *Space Mission Analysis and Design*, Kluwer Academic Publishers, Dordrecht, The Netherlands, 1991, p. 671.
7. U.S. Congress, Office of Technology Assessment, *Access to Space: The Future of U.S. Space Transportation Systems*, OTA-ISC-415, U.S. Government Printing Office, Washington, DC, April 1990, p. 59.
8. DeMeis, R., "New Life for Heavy Lift," *Aerospace America*, March 1991, pp. 32-35.
9. Payton, G. and Sponable, J.M., "Designing the SSTO Rocket," *Aerospace America*, April 1991, pp. 40-45.
10. Limerick, C.D., "Dual Mixture Ratio H<sub>2</sub>/O<sub>2</sub> Engine for Single Stage to Orbit Application," *Journal of Propulsion and Power*, Vol. 7, No. 1, January - February 1991, pp. 31-36.
11. OPGUID Program, NASA - Marshall Space Flight Center, Courtesy of D. Mercier, August 1989.
12. NASA, *Civil Needs Data Base: FY90 Version*, NASA Technical Memorandum 103324, August 1990.
13. Jordan, J., Boeing Defense and Space Group, personal communications, April 1991.

## GENESIS II: ADVANCED LUNAR OUTPOST

UNIVERSITY OF WISCONSIN-MILWAUKEE

548-54  
160624  
P-6

This study investigated advanced, second-generation lunar habitats for astronauts and mission specialists working on the Moon. The work was based on design constraints set forth in previous publications. Design recommendations are based on environmental response to the lunar environment, habitability, safety, near-term technology, replacability and modularity, and suitability for NASA lunar research missions in the early 21st century. Scientists, engineers, and architects from NASA/JSC, Wisconsin aeronautical industry, and area universities gave technical input and offered critiques at design reviews throughout the process. The recommended design uses a lunar lava tube, with construction using a combination of Space Station *Freedom*-derived modules and lightweight Kevlar-laminate inflatables. The outpost includes research laboratories and biotron, crew quarters and support facility, mission control, health maintenance facility, and related areas for functional and psychological requirements. Furniture, specialized equipment, and lighting are included in the design analysis.

### PROJECT GENESIS

In the aftershock of the Space Shuttle *Challenger* disaster in 1986, scientists, professionals, and citizens around the world have been rethinking the role humans should play in space. Current discussion and planning has moved into the arena of long-duration missions and extraterrestrial habitation. On the 20th anniversary of "One giant leap for mankind," President Bush announced a goal to land people on the moon by 2005, and this time to stay. Plans for the near future in space include a permanently inhabited space station, a lunar outpost, and possibly a joint United States/Soviet Union mission to Mars.

*Project Genesis* is proposed to NASA<sup>(1)</sup> as a pair of lunar outposts and early-stage, permanently occupied habitats on the Moon. Called *Genesis I* and *II*, these evolutionary outposts will serve both as long-term testbeds for all materials, processes, and development strategies to be employed in a mature lunar colony and as testbeds for all processes to be employed in the exploration and eventual settlement of Mars.

Following guidelines provided by engineers and scientists at NASA's Johnson Space Center (NASA/JSC) and with the advice of aerospace engineers from the Astronautics Corporation of America and Orbital Technologies Corporation, the UW-Milwaukee Space Architecture Design Group has designed two complete habitats: *Genesis I*<sup>(2,3)</sup> and now *Genesis II*. *Genesis I* was planned for a crew of 8 to 12 persons on rotations of 6 to 9 months with a maximum duration of 20 months, and *Genesis II* for a second crew of 11 astronauts and mission specialists at a different site. For both outposts, crew gender, nationality, and ethnicity are expected to vary as the consortium of world aerospace partners become involved in scientific, architectural, and engineering communication. This paper summarizes the major design criteria and concepts which lead to the development of *Genesis II*<sup>(4,5)</sup>.

### GOALS AND PROCEDURE

The project was part of a continuing effort to research and design human settlements for the Moon and Mars. The pedagogic objective is to enhance architectural and architectural/engineering education through establishing an advanced space

architecture program that integrates architecture, engineering, planning, environment-behavior (EB) studies, and advanced construction technology. The project also aims to produce information and design solutions useful to the aerospace community, NASA, its prime contractors and subcontractors, and NASA/USRA schools in the area of long-duration habitation design.

The long duration of these planned events requires the involvement of architects, interior designers, industrial designers, planners, and other environmental design professionals in order to ensure environments suitable for human habitation and performance. To date, space design has been the province of the engineer and that profession's highly technical orientation. Long-range planning, systems integration, construction sequencing, and interiors environmentally suitable for humans are all areas in which the design professions have demonstrable expertise and in which they can exercise a positive and much needed influence. Thus has evolved *space architecture*, as the field is becoming known.

The design of *Genesis II* is based on the exploration of different scenarios<sup>(6)</sup>, a facility program<sup>(7)</sup>, the final design document from 1989-90<sup>(2,3)</sup>, and excellent critiques of *Genesis I* offered by NASA scientists and engineers. Additional resources included work on the design and full-scale mock-up of an inflatable lunar habitat<sup>(8)</sup> and independent study projects to collect and prepare research information<sup>(9,10,11)</sup>.

The process culminated in an integrative design studio in which architects and engineers, from first year undergraduates to first year graduate students worked together to investigate and develop *Genesis II*. Areas of detailed architectural and engineering design investigation included the implications of new lightweight, high-strength materials especially elastomers and thin films; character of the lunar environment; extraction of design relevant information from previous space experience, analogous situations, and simulations; and human factors analysis of the minimum space requirements for different lunar habitation and research functions in 1/6th gravity. The studio was conducted as a professional team project, with the faculty advisor directing the project and the three teaching assistants and other advanced students assuming the role of team leaders for various specialized functions. The class worked as one team, producing one final project, but was subdivided into various teams with

specific tasks and deadlines as the semester unfolded. Through all steps, the program stressed the systems approach to design.

### LUNAR BASE MISSION OVERVIEW

An advanced lunar must be:

1. Located at an Earth-facing equatorial location.
2. Constructed of lightweight durable materials requiring minimum EVA time.
3. Contained within the next generation of Earth-lunar transport systems: (a) space shuttle system, (b) heavy-lift launch vehicle such as the Shuttle-C with cargo capacity of 69,000 kg and cargo bay  $25 \times 4.5$  m, (c) low-Earth orbit Space Station *Freedom* (SSF) and associated platforms, and (d) the planned dual-use cislunar transport system composed of an orbital transfer vehicle (OTV) and a separate reusable lunar lander that transports construction components to the lunar surface along with crews and logistics.
4. Capable of housing 11 astronauts of different nationalities, genders, and specialties for periods of time up to 20 months with a normal change-out of 6-9 months.
5. Able to provide for all necessary life-support and quality of life systems including (a) anthropometrics and human factors, (b) health and safety, (c) EB issues of isolation and interaction, privacy, personal space, and territoriality, (d) habitability architectural issues in crew areas, crew support, operations of base, and design for productivity, and (e) space biosphere Controlled Ecological Life-Support System (CELSS) and Environmentally Controlled Life-Support System (ECLSS).
6. Built using integrated advanced space construction technology.
7. Responsive to the physics, geology, and natural environment of the Moon and appropriate "urban" design so as to retain the natural qualities of the Moon.
8. Capable of supporting five main mission operations: (a) lunar surface mining and production analysis for lunar oxygen (Lunox), helium 3 ( $\text{H}_3$ ), and other minerals; (b) lunar construction technology and materials testbed for testing high technology construction with inflatables, the use of lunar regolith for radiation shielding, lunar glass, lunar concrete, and sintering techniques using advanced telerobotic systems; (c) CELSS test facility; (d) lunar far side observatory; and (e) human factors and EB research facility to investigate habitability issues on the Moon including ongoing post-occupancy evaluations (POEs).

The first mission to establish the second-generation *Genesis II* outpost, expected to land on the moon between 2005 and 2009, could last as little as 14 days. The astronauts, architects, and engineers will live inside their lunar landing vehicle (LLV) and spend much of each day performing EVA building the outpost. Once all systems, subsystems, and backups have been verified, and the initial IOC has been achieved, expected by 2015, crew change-outs will occur every nine months to a year as the astronauts perform research and manufacturing operations on the lunar surface.

### LAYOUT OF THE GENESIS II LUNAR BASE

The proposed design is situated in a lunar lava tube near the Apollo 15 site, located at  $3^\circ\text{E } 25^\circ\text{N}$ , alongside Hadley Rille at Palus Putredinis (Marsh of Decay).

The site plan is zoned that the hazardous lava facility is approximately 3 km to the south and the mining facility is 1 km to the north, the habitat research area zone is 1.25 km to the west, and the solar array field and dissipation radiator field is near the habitat (see Fig. 1). The habitat itself is over a drilled and sintered opening to the safe confines of the lava tube.

Following extensive telerobotic research and exploration, the base will be developed in three stages spanning almost 10 years: (1) emplacement of an assembly facility and the erection of radiation protection truss-work with accompanying regolith covering; (2) integration of the balance of base components, construction of all surface facilities, drilling, exploding, and sintering of the shaft to the lava tube, and lowering and assembling the structural truss-work and initial crew quarters on the base of the lava tube; and (3) final IOC during which two large inflatables are lowered into the lava tube, inflated, and outfitted for expanded crew quarters and research space.

The proposed design is based on the use of Space Station *Freedom*-type hard modules, lightweight structural truss systems, and thin-film elastomer inflatables. The habitat and research areas are situated in the safety of the lava tube, away from radiation, sharp temperature fluctuations, and deadly solar flares. Storage and vertical circulation to and from the surface occurs through a Shuttle-C module installed in the sintered opening between the lava tube and the surface. Only logistics modules and the EVA chamber remain on the surface protected by truss-work covered with a minimum of 0.5 m of lunar regolith. The basic configuration—a giant H on its side—may be seen in Fig. 2. Details, shown in a series of plans and axonometric drawings, of the two-story habitation and laboratory inflatables, the crew support module with mission operations and health maintenance facilities on the bottom of the lava tube, and the logistics and EVA modules on the lunar surface may also be seen in Fig. 2.

As considerable emphasis was placed on the quality of life and the contribution that the designed environment can make to habitability in confined quarters<sup>(12)</sup>, more detailed designs are shown in Figs. 3 and 4 for individual spaces within the

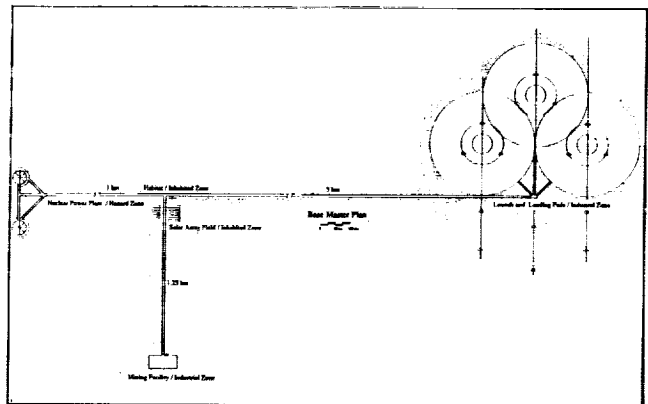


Fig. 1. Site plan for *Genesis II*, showing the launch and landing facility to the right, habitat/research facility near the center, power facility to the left, and mining below. Note: North is to the left.

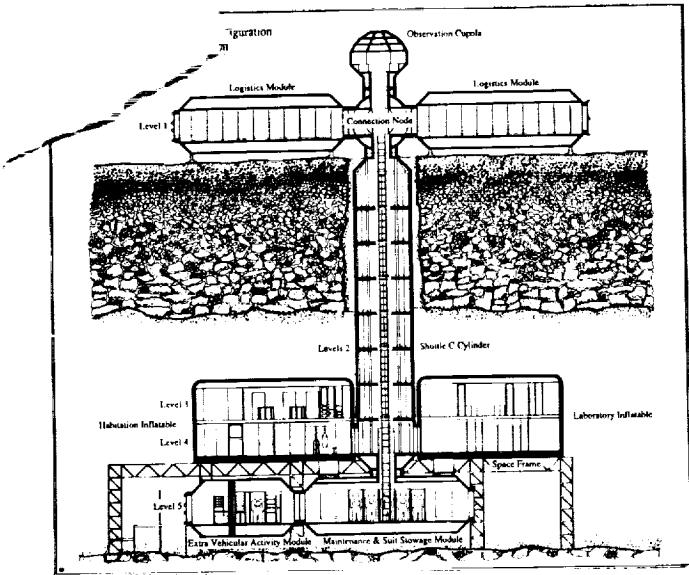


Fig. 2. Longitudinal section through *Genesis II*, showing the Shuttle-C vertical translation and storage module which connects the logistics and EVA modules and observation cupola on the moon's surface with the habitation and laboratory inflatables and mission control/crew support and maintenance/EVA modules on the surface of the lava tube.

crew habitat (e.g., the wardroom/dining room, a game room, the exercise facility, several arrangements of the crew quarters, the personal hygiene facility, a small library, several reading rooms, and a conservatory).

Detailed designs were also developed for mission operation workstations, health maintenance facility, and special furniture designs for the 1/6th gravity body position. Technical engineering details were developed for wall sections, hatch connectors, the lighting system, and the structural space-frame truss work<sup>(4)</sup>.

Finally, as the lunar outpost may need to expand into a more mature lunar colony, the system allows expansion to accommodate increments of 5-6 additional astronauts and mission specialists by adding inflatables along the length of the lava tube.

**DESIGN ADVANTAGES AND LIMITATIONS**

The second-generation *Genesis II* lunar habitat and research facility incorporates many design features, some well established, others yet untried. The principle design criteria influencing the design included safety, using advanced yet near-term technology, replacability and modularity, and minimizing volume and weight at lift-off; yet the driving force in the design was habitability—human factors and EB considerations to provide a reasonable quality of life during long stays in an alien environment.

Habitability criteria affected the design in many ways and places. Living and working spaces were separated, with the living spaces being in the inflatable habitation facility and the working spaces being in the inflatable laboratory facility and mission control on the lowest level of the lava tube. Movement through the Shuttle-C cylinder—the central circulation core—provides some transition between working and living spaces.

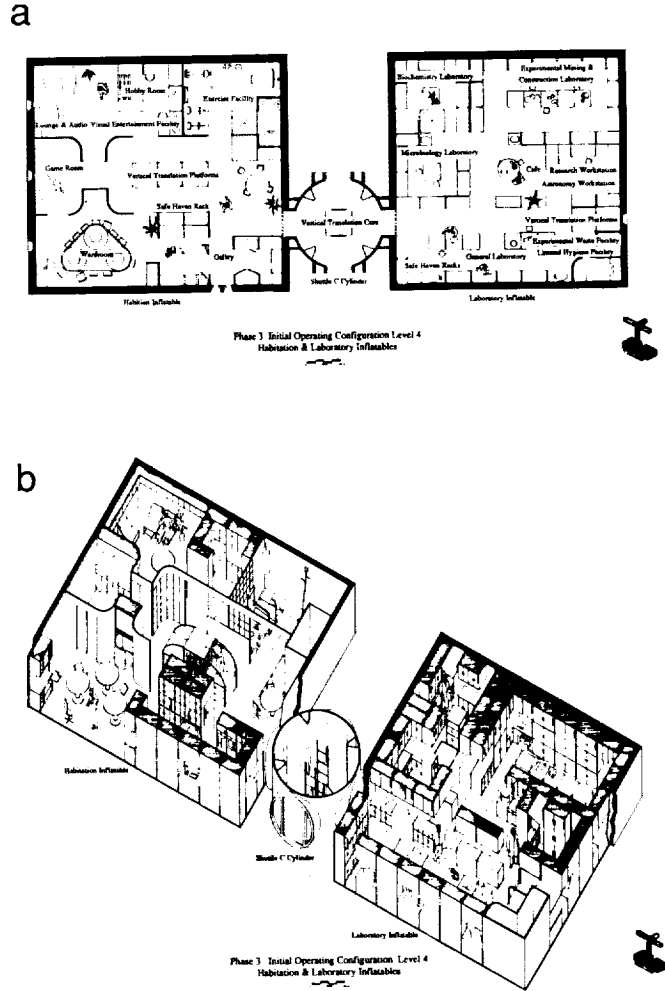


Fig. 3. a and b: IOC plan and axonometric of the lower level of the habitat and research facilities connected through the Shuttle-C circulation core. On the left is the galley, wardroom, a games room, lounge and AV entertainment facility, hobby room, and exercise facility, all arranged around a central atrium and vertical translation platforms up to the crew quarters. On the right are the research laboratories: a general lab, microbiology lab, experimental mining and construction telerobotic laboratory, an experimental waste facility connected with the biotron above and workstations for the lunar far-side observatory and for internal environment/behavior analyses and POEs of the base itself.

The character of the two types of spaces differs greatly (Figs. 3 and 4). The laboratory inflatable is organized in a series of bays with the extensive biotron upstairs accessible from peripheral translation platforms, while the habitation inflatable is organized around a central atrium and vertical translation platforms linking the two habitation floors. Within the research spaces an effort was made to separate different research functions from each other, while in the habitation area an effort was made to provide social and gathering space as well as visual connections between major spaces via the central atrium.

Balancing social interaction is the need for privacy. Upon advice of our consultants, and based on the research literature<sup>(13)</sup>, the individual crew quarters were made larger than

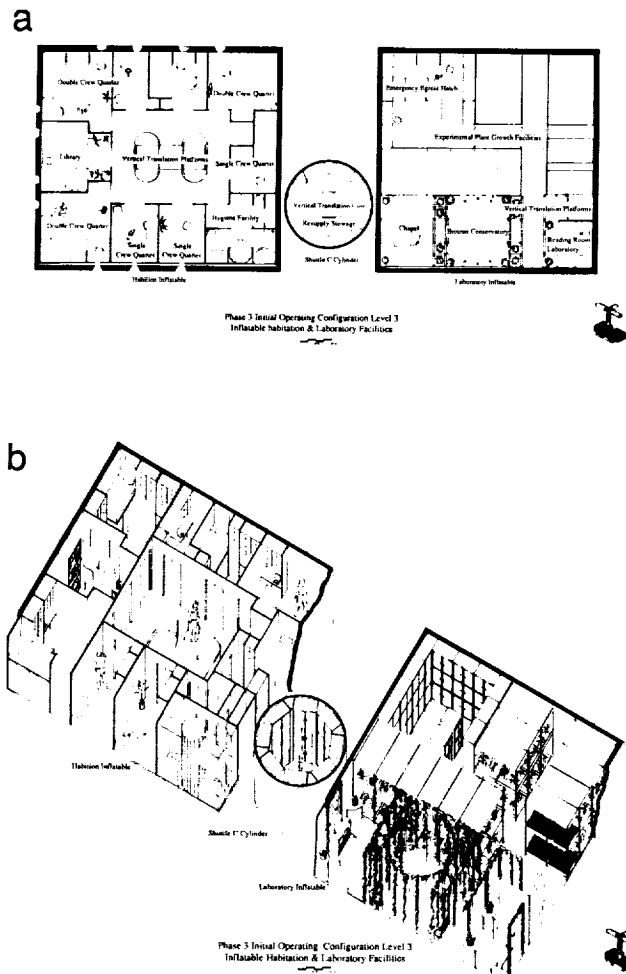


Fig. 4. a and b: IOC plan and axonometric of the upper level of the habitat and research facilities. On the left are a variety of individual and shared crew quarters. On the right is the experimental plant growth biotron. Note also the library, reading room, conservatory, and chapel for individual and small group retreat.

minimum and considerably larger than suggested from current NASA standards for Space Station *Freedom*<sup>(14)</sup>. A variety of single and double crew quarters were designed to allow choice, and to allow the possibility of an environment/behavior post-occupancy evaluation (POE) of their impacts over time.

To reinforce these private spaces, small spaces were created throughout the habitat for individual or small-group quiet activities, including a library and small games room in the habitation inflatable and a reading room, conservatory, and chapel borrowing from the natural character of the biotron in the research inflatable.

Safety influenced the design in many places, most notably in having dual means of egress from all points of the outpost, for example, the two EVA chambers allowing egress to the surface and to the open end of the lava tube.

The modular kit of parts allows ease of emplacement, interchangability, reconfiguration, and resupply. Pieces were sized to be transported through the hatches and moved from the

logistics modules to all parts of the base. To provide flexibility, a module of 1.2 m was chosen. The design also makes personalization of individual spaces—crew quarters and research laboratories—easy to accomplish.

Other important design constraints were the use of near-term technology and the minimization of volume and weight. The use of inflatable structures, using the latest in lightweight elastomer laminates, responded to both of these constraints. The technology needed to construct inflatables is not immediately available, but is near enough that it is practical and will be available prior to 2005. Inflatables work as a testbed for experimentation. They also collapse for transportation, resulting in low mass and volume. Once expanded in the lava tube, the inflatable provides a very large volume for its weight and thus greatly reduces the cost of the base.

A major asset of the design is its location inside a lava tube. This protects the base and its inhabitants from solar flares, meteorites, radiation, and temperature fluctuations. The extension of the habitat from the surface level to the base of the lava tube also allows two means of egress with exits on different levels. Use of the natural cavern of the lava tubes will prove cost effective relative to constructing space frames and moving great quantities of lunar regolith for protection. The constant temperature minimizes demands on the CELSS/HVAC system, also proving to be cost effective. EVA operations will be easier, with no worries about cosmic radiation. Finally, expansion is eased by adding additional inflatables without having to remove and provide additional regolith protection.

The natural zoning of the base can be seen as an advantage of this scenario, and a natural outgrowth of using a lava tube. The sensitive habitat and research zones are protected and isolated from the hazard zone of launch and landing, from the industrial manufacturing zones, and from the potentially hazardous nuclear energy zone.

Inside the base, the articulated zoning between work and leisure, and between public and private, mirrors—albeit in a microcosm—the equivalent urban zoning on Earth.

The furniture is potentially a breakthrough in lunar design (see Figs. 5 and 6). While there are no published data on anthropometrics in 1/6th gravity, our interpolations between 1 g and 0 g suggest what we have been calling a "1/6th body position." We have therefore designed a set of 1/6th gravity furniture for work and leisure.

Lastly, the design of *Genesis II* provides a variety of different situations and spaces, different in spatial size and configuration, and different in style and esthetics, with the flexibility to be personalized, allowing for the range of astronauts and mission specialists who will inhabit the base and for their different needs and personalities. The variety and flexibility are set up as an experimental system to enable POE and further refinement both on the lunar base and as input for martian travel and outposts.

#### AREAS FOR FUTURE RESEARCH AND DESIGN DEVELOPMENT

PDRs by NASA scientists and engineers and reviews offered of the work at national conferences, including the annual USRA conference, have suggested the following limitations and areas for further research and design development:

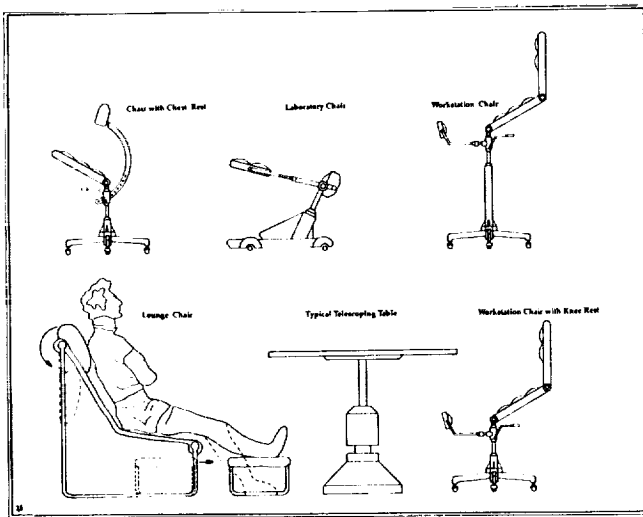


Fig. 5. Proposed experimental furniture designs for 1/6th gravity.

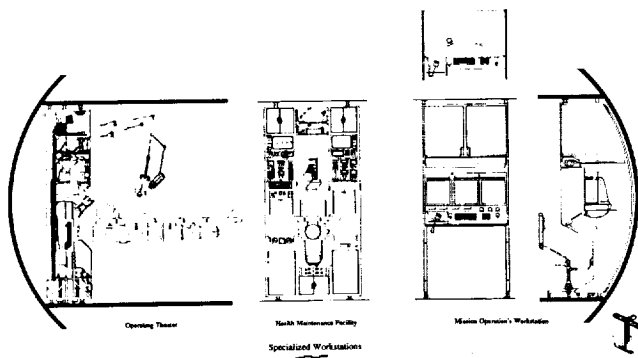


Fig. 6. Typical mission operations workstation designed to accommodate the 1/6th gravity body position. Note: Many other detailed design drawings—health maintenance facility, operating theater, suit maintenance facility, crew quarters, etc. have been developed and are included in the full report<sup>(4)</sup>.

1. The first question is the location of viable lava tubes. Survey missions must confirm locations, and subsequent exploration must determine their structural integrity.

2. Related is the question of how to stabilize the inner surfaces of lava tubes. Structural support systems may need to be devised that can be emplaced in an emergency.

3. Questions have been raised about inflatables, about likely bowing or what is known as the "oil canning effect," and about pressure and stress on their corners. Further study needs to be conducted—perhaps including computer simulations as well as laboratory tests—of the structural integrity of different inflatable shapes.

4. It is hoped that further work will be done on furniture design for 1/6th gravity, and, with NASA's assistance, on testing the furniture anthropometrically and functionally.

5. Some controversy surrounds the notion of providing safety through safe haven racks. Further exploration needs to be done on the relative advantages and disadvantages of safe havens as places versus as racks.

6. Questions could be raised about the modularity and relative openness of the plan. Some may question whether modularity leads to a sterile environment. We feel that modularity and the possibilities of interchangeability are absolutely critical in an extraterrestrial habitat and research facility. Once these facilities are in place, at considerable expense of launch and EVA construction time, it would be unreasonable to assume no subsequent changes in functional needs, or if there were, that it would require entirely new construction with new parts being transported from Earth. The modular system allows rapid change-outs as functional requirements change between crew change-outs (e.g., different crew compositions—men, women, couples; different mission research functions, etc.). Exploration does need to be done, however, on the relative merits of different modular systems, e.g., hexagonal versus the current rectilinear system.

7. Concern has also been expressed about sound transmission and safety from research accidents in a relatively open plan research facility. Of special concern would be the possible transmission of odors or germs from animal research. Each of the research areas can be isolated from all others in a matter of moments, and could be closed if noise is a problem. Nevertheless, the questions raised about modularity deserve considerable further research and design investigation.

8. The exercise facility will undoubtedly require more sound proofing from the rest of the crew quarters. Exercise machines cause noise and vibration, and require secure structural connections, neither of which has been adequately accounted for in the current design. New forms of NASA exercise counter-measure machines will be explored and incorporated in future work. A separate facility for group recreation may be needed. This will isolate excessive noise and vibrations from the ongoing base functions.

9. Other vibrations may occur from the movement of personnel and the operation of equipment. These vibrations may cause structural problems, and the resulting noise may also lead to an increase in crew member stress.

10. The medical facility on the ground level of the lava tube, very close, but not immediately adjacent to the research areas, may cause some concern. Better emergency circulation connection between the two may be required.

11. Only some attention has been given so far to the equipment needed for construction. Investigations need to be made of the relative merits of drilling, blowing, and laser cutting the hole between surface and tube. The reactions of the lava tube to vibrating machines during construction also needs careful exploration. Weight bearing features of the construction equipment relative to the strength of the lunar regolith over cavernous lava tubes needs careful exploration too. The details of the inflation of inflatables needs to be clarified. The exact equipment needed for construction, and the influence of this on the design itself, deserves further attention.

12. A number of mechanical engineering considerations were not investigated in this design, among them heat dissipation, capacity of thermal radiators, ventilation system, and detailed mechanical analysis.

13. The extensive length of the Shuttle-C translation core between the surface of the moon and the lava tube itself presents cause for concern. Considerable space is devoted to circulation. Movement between base locations must be efficient. In the event of an emergency, the crew must have easy access to safe haven locations. Further investigation needs to be conducted to determine if this is the most efficient circulation solution.

14. Questions could also be raised about the advisability of combining inflatables and hard modules in the lava tube itself. Why not use all inflatables, one might ask, given they have such a great volume to mass ratio? In the spirit of initial exploration, and conceiving the lunar base as a testbed for Mars, this scenario explored the use of both inflatables and modules, and the necessary connectors between the two.

15. Lastly, further attention needs to be given to the overall image of the habitat and research facility. Does the design tell us what we value as humans?

It is our firm belief that NASA should proceed with the lunar/Mars Space Exploration Initiative (SEI) toward the eventual exploration and habitation of both the Moon and Mars. First- and second-generation outposts will need to be developed, refined, and tested. We offer these conceptual designs as beginnings on the path to the eventual habitation of our near planets.

#### ACKNOWLEDGMENTS

Design and illustrations by Greg R. Busher, Adam L. Demler, Peter J. Dewitt, Joseph P. Fiber, Peter Frunceck, Gregory G. Gorski, Janis Huebner-Moths, Deborah Kishony, Scott Maner, Kerry L. Paruleski, Keith Prudlow, Patrick Rebholz, Daniel Rhone, Curtis W. Schroeder, and Christopher Trotier. Paper compiled and written by Gary T. Moore, Faculty Advisor. This project was supported by an Advanced Design Program grant from the Universities Space Research Association (USRA) under Grant NASW-4435 from the National Aeronautics and Space Administration. The full report is available in Fieber, Huebner-Moths & Paruleski (1991).

The Space Architecture Design Group would like to express appreciation for the continued support of the USRA ADP and for critical feedback and suggestions from Thomas Crabb, David Haberman, John Cain, Nancy Jaeger, Robert Weber, Wallace Fowler, Douglas Ryhn, Anthony Schnarsky, Mark Sothmann, Michael Roberts, John Connolly, Kriss Kennedy, James Burke, Stephen Paddock, and B. J. Bluth.

#### REFERENCES

1. Moore, G.T. (1991). Genesis lunar habitat. In American Institute of Aeronautics and Astronautics, *Final Report to the Office of Aeronautics, Exploration, and Technology, National Aeronautics and Space Administration on Assessment of Technologies for the Space Exploration Initiative (SEI)*. Washington, DC: American Institute of Aeronautics and Astronautics. Log No. 284.
2. Hansmann, T.L., & Moore, G.T. (Eds.) (1990). *Genesis Lunar Outpost: Criteria and Design*. Milwaukee: University of Wisconsin-Milwaukee, Center for Architecture and Urban Planning Research, Report R90-1.
3. Moore, G.T., Baschiera, D.J., Fieber, J.P., & Moths, J.H. (1990). Genesis lunar outpost: An evolutionary lunar habitat. In P. Thompson (Ed.), *NASA/USRA University Advanced Design Program: Proceedings of the 6th Annual Summer Conference*. Houston: Lunar and Planetary Institute. p. 241-254.
4. Fieber, J.P., Huebner-Moths, J., & Paruleski, K.L. (1991). *Genesis II: Advanced Lunar Outpost*. Milwaukee: University of Wisconsin-Milwaukee, Center for Architecture and Urban Planning Research, Report R91-2.
5. Moore, G.T., Fieber, J.P., Moths, J.H., & Paruleski, K.L. (1991). Genesis advanced lunar outpost II: A progress report. In J. Blackledge, C.L. Redfield & S.B. Seida (Eds.), *Space—A Call for Action: Proceedings of the Tenth Annual International Space Development Conference*. San Diego, CA: Univelt. p. 55-71.
6. Schnarsky, A.J., Cordes, E.G., Crabb, T., & Jacobs, M. (1988). *Space Architecture: Lunar Base Scenarios*. Milwaukee: University of Wisconsin-Milwaukee, Center for Architecture and Urban Planning Research, Report R88-1.
7. Baschiera, D., & 14 others (1989). *Program/Requirements Document for a Lunar Habitat*. Milwaukee: University of Wisconsin-Milwaukee, Center for Architecture and Urban Planning Research, Report R89-1.
8. Connell, R.B., Fieber, J.P., Paruleski, K.L., & Torres, H.D. (1990). *Design of an inflatable habitat for NASA's proposed lunar base*. Final report, Universities Space Research Association and NASA/Johnson Space Center.
9. Fieber, J.P. (1990). *An investigation of technological options in lunar construction*. Independent study report, Advanced Design Program in Space Architecture, Department of Architecture, University of Wisconsin-Milwaukee.
10. Huebner-Moths, J. (1991). *Environmental conditions of the Moon and Mars*. Independent study report, Advanced Design Program in Space Architecture, Department of Architecture, University of Wisconsin-Milwaukee.
11. Paruleski, K.L. (1990). *A comparative analysis of analogous situations, previous space exploration, simulated situations, and future conditions*. Independent study report, Advanced Design Program in Space Architecture, Department of Architecture, University of Wisconsin-Milwaukee.
12. Bluth, B.J. (1991). The Soviet space stations and extraterrestrial space experience. Wisconsin Young Astronauts Aviation and Space Conference, Brookfield, Wisconsin, March.
13. Moore, G.T. (1990). Environment-behavior issues in extraterrestrial space. In H. Pamir, V. Imamoglu & N. Teymur (Eds.), *Culture, Space, History*, Vol. 5. Ankara, Turkey: Middle East Technical University. p. 387-403.
14. NASA (1989). *Man-Systems Integration Standards: NASA Standard 3000*, Vol. 1, Rev. A. Houston: NASA/Johnson Space Center.

## ROTATIONAL FLUID FLOW EXPERIMENT

WORCESTER POLYTECHNIC INSTITUTE

549-34  
160625  
P-4

This project, begun in 1986 as part of the WPI Advanced Space Design Program, focuses on the design and implementation of an electromechanical system for studying vortex behavior in a microgravity environment. Most of the existing equipment was revised and redesigned by this project team, as necessary. Emphasis was placed on documentation and integration of the electrical and mechanical subsystems. Project results include reconfiguration and thorough testing of all hardware subsystems, implementation of an infrared gas entrainment detector, new signal processing circuitry for the ultrasonic fluid circulation device, improved prototype interface circuits, and software for overall control of experiment operation.

### INTRODUCTION

Many fluid mechanical phenomena involve dependence on more than one scaling parameter. A vortex is a good example of a practical concern when a design involves the flow of a liquid into an inlet. Understanding vortex formation is important, and involves three governing parameters. These parameters are the Reynolds number, the Froude number, and the Weber number, representing viscous, gravitational, and surface tension forces.

$$\text{Re} = \rho \frac{VD}{\mu}, \text{Fr} = \frac{V}{\sqrt{gD}}, \text{We} = \rho V^2 \frac{D}{\sigma}$$

A vortex can be described as a rotational flow that forms a low pressure region at its center. Vortices are typically found in pump systems and, most commonly, in a bathtub or kitchen sink drain. The effects of vortices extend into the areas of hydrodynamics, aerodynamics, and hydraulics, playing important roles in determining the efficiencies of systems.

### ADVANTAGE OF MICROGRAVITY

Pump performance can be altered significantly by designs that create an approach flow with large amounts of vorticity. For instance, a large vortex will cause a pump to pull air along with the fluid being pumped, which makes the pump less efficient and is characterized by surging of the pump system as vortices form and break. The result is unstable pump performance with undesirable accelerations and decelerations of the flow, and structural vibrations that lead to erosion of pump parts. Loss of pump efficiency due to vortices is estimated to be several percent.

Problems arise in scaling vortex flow from laboratory models to prototype dimensions, since experimenting with a full-size prototype is often not feasible. Results from models will be usable only if there are geometric, kinematic, and dynamic similitude. Geometric similarity requires the model and the prototype to be the same shape so all linear relationships between the model and the prototype are related by a constant scale factor. Kinematic similarity requires a constant scale factor

between the velocities of the model and the prototype. Dynamic similarity indicates that all force relationships between the model and the prototype are related by a constant scale factor. Therefore, if two flows are dynamically similar, they are also geometrically and kinematically similar.

On Earth it is rarely possible to achieve a this dynamic similitude. A simple observation reveals that if D is increased, the Reynolds number increases by that factor, while the Froude number decreases by the square root of that number. This non-linear relationship between the Reynolds and the Froude numbers preclude dynamic similitude between the model and the prototype. The way to maintain a linear relationship that will allow for a constant scale factor for different sizes of models (different D) is to vary gravity inversely with D. This cannot be achieved for gravities less than 1 g on Earth, but can be achieved in the GASCAN environment in the space shuttle.

The microgravity environment of space makes it possible to induce and vary gravity, which for this experiment, will be varied between micro-( $10^{-6}$ ) and 2-g. Both geometric and dynamic similitude between the model and the prototype may thus be achieved, and scale effects virtually eliminated.

### PROPOSED EXPERIMENT

The Rotational Fluid Flow Experiment is designed to study the effects of varying conditions on the strength of a rotational fluid flow in a non-terrestrial environment. To accomplish this, several devices have been designed and built to alter the gravitational level of a swirling fluid and to gather data on the effects of such variations.

The apparatus uses a small container, about the size of a beverage can, with a 1/4-in-diameter hole in the bottom. Liquid that flows out of the hole is returned to the container by a pump. The entire apparatus is rotated about an axis perpendicular to the container axis producing centripetal acceleration. The liquid collects in the bottom of the container and flows out the hole. For high enough flow, a vortex, similar to a bathtub drain vortex, will form in the container. The vortex can be measured by optically recording the liquid surface shape. Air entrainment can be detected by sensing air bubbles in the outlet tube.

## APPARATUS

A rotating platform supports all mechanical and electrical equipment needed to conduct the experiment. In addition to the major flow components, including the pump and the vortex chamber, there is a photographic data collection system composed of a camera, mirror, and flash. The mechanical hardware is divided into three major groups: the flow system, the rotating platform system, and the photographic system.

### Flow System

The major part of the experiment is the flow system. This system includes a positive displacement pump, the cylindrical chamber that will contain the vortex, aluminum tubing, and the bubble sensor (Fig. 1).

The vortex chamber is cylindrical and consists of an ultrasonic transducer mount, two cylindrical pieces of lucite (4-in ID  $\times$  1/4-in thick), a cap, and a base. The ultrasonic transducer mount is specifically designed to hold the transducers for the ultrasonic circulation meter. The mount does not have to be located at any particular height along the cylinder since the circulation of the vortex, once it has reached a steady state, is constant along the height of the cylinder. Presently, the transducer mount is located in the lower third of the cylinder so as not to obstruct the camera view of the vortex. Although the design of the base resembles that of the cap, the base has an 0.20-in diameter exit hole. To prevent fluid leakage from the cylinder, O-ring seals are used for all connections.

Another critical component of the flow system is the bubble sensor. On occasional experimental runs, it was observed that the vortex can gain such high vorticity that air bubbles begin to exit the cylinder and enter the pump. Since at low gravity levels it will be difficult to purge the flow system, a bubble sensor is used to detect the initial passage of bubbles. The bubble sensor is installed in the aluminum piping at the exit of the cylinder. If bubbles are detected, a feedback signal is generated.

The pump recycles the fluid exiting the vortex chamber back into the top of the chamber. Tangential injection creates a swirl-

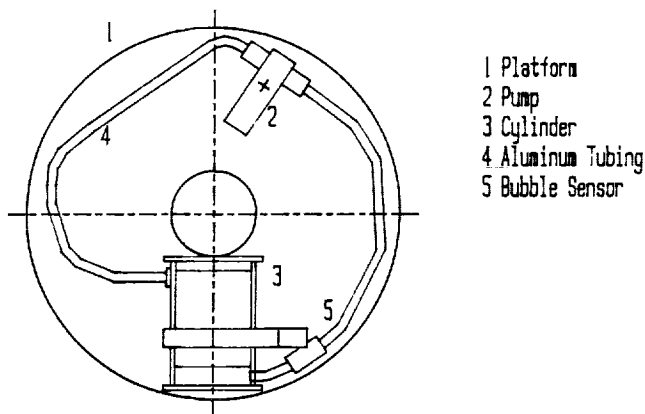


Fig. 1. Flow System

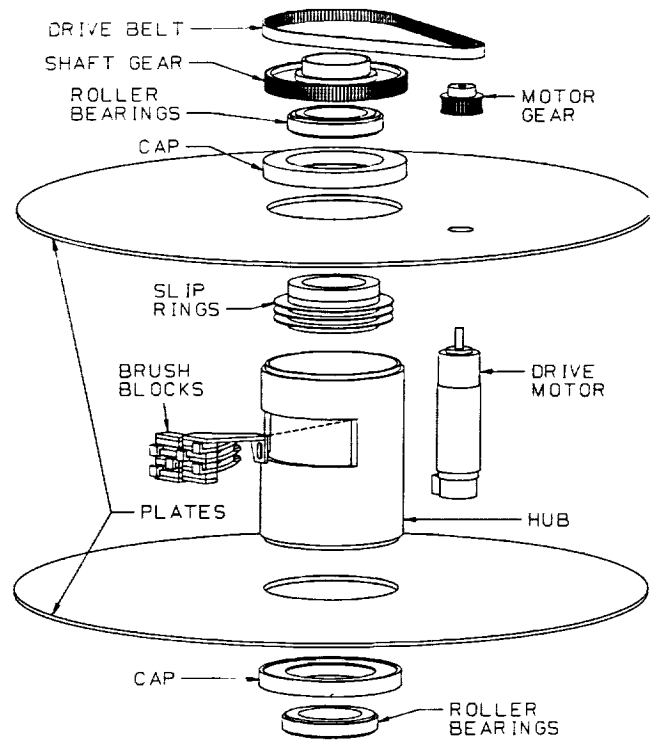


Fig. 2. Rotational Drive Equipment

ing mass of fluid that becomes a vortex. The drive motor for the pump is controlled using the onboard computer and a pulse-width modulated controller. The pump speed accurately determines flow rate so that independent measurement is not necessary. Based on results of extensive experiments conducted in the 1-g environment, the flow range for the pumping system was selected.

The cylinder is placed horizontally with the cap at the center of the platform and the base at the edge.

### Rotating Platform System

All equipment, both mechanical and electrical, is mounted on the platform (Fig. 2). This rotating platform is made from aluminum and consists of a hollow cylinder with two large, circular mounting plates, one at either end. The cylinder portion of the platform houses the mechanism by which the experiment is connected to the GASCAN mounting shaft, which forms the platform axle. The cylinder also houses the slip rings that carry electrical power to the experiment. The circular plates on the ends of the cylinder provide the surface to mount the experiment components and insure structural stability, including maintenance of a sufficiently high frequency for the first vibrational mode.

The central shaft of the structure is made of aluminum and is 2 in. It is hollow to allow the power cables to be run from the battery box to the other experiments, and for routing cables

to the NASA interface. Since the Rotational Fluid Flow Experiment is located at the bottom of the GASCAN, its installation is facilitated.

The slip rings are part of the power supply delivery system that are attached to the mounting shaft. The brushes are connected to the cylindrical portion of the platform. As the platform rotates, the brushes keep in constant contact with the slip rings, thus providing electrical power to the experiment. The input side of the slip rings is connected to the battery supply and the output side to the equipment in the experiment needing electrical power. Three different voltages are provided and all are switched on by a signal from crew.

An electric motor is used to rotate the experiment package. It is mounted to the top mounting plate of the rotating platform. The shaft of the motor protrudes far enough through the plate to allow for a small, toothed pulley to be attached to it. The pulley is essential to insure that the motor shaft and drive belt are positively connected. The pulley also has top and bottom edges to insure that the drive belt does not slide off the shaft.

The drive pulley is mounted onto the shaft just above the platform. The pulley serves a twofold purpose. First, it is fixed to the shaft, which enables the platform to rotate. The drive belt connects the pulley and the motor gear. Secondly, the collar used to attach the pulley to the shaft also serves as the top mounting bushing for the platform. The canister plate underneath and the pulley above prevent the platform from moving up and down on the shaft. The collar of the pulley is made of aluminum; the pulley itself is plastic. The pulley is fixed to the shaft with set screws.

The drive belt is a reinforced rubber belt. It is smooth on the outer side; the inner surface is notched to mate with the teeth of the pulleys. Since the notched surface of the belt exactly matches the teeth of the drive pulley, slipping of the belt is avoided.

The drive motor is controlled using a pulse-width modulated system to conserve electrical power. Signals to the controller come from the onboard computer system.

### Photographic System

The camera and flash provide a visual record of vortex formation. From the photographs, it will be possible to see vortex shape as a function of the  $g$ -levels being experienced (Fig. 3).

The camera experiment is a commercial unit that was modified for electronic activation. The camera selected was required to operate under expected environmental conditions, and to have features such as autowind, short focusing distance, flash capability, and the ability to be triggered by an electrical impulse. The greatest environmental concern is the low temperature that the camera and film will be exposed to when operating in orbit. The worst-case scenario, in which the space shuttle bay would be facing space for long periods of time, would result in a temperature as low as  $-30^{\circ}\text{C}$ . The camera must be able to operate at that temperature without experiencing mechanical and/or electrical failures in any of its components.

To evaluate the effects of temperature, tests were conducted on a 400 ASA black & white film. Pictures were taken immediately after the film was taken out of the freezer and then developed after refreezing the film. The film was virtually unaffected by

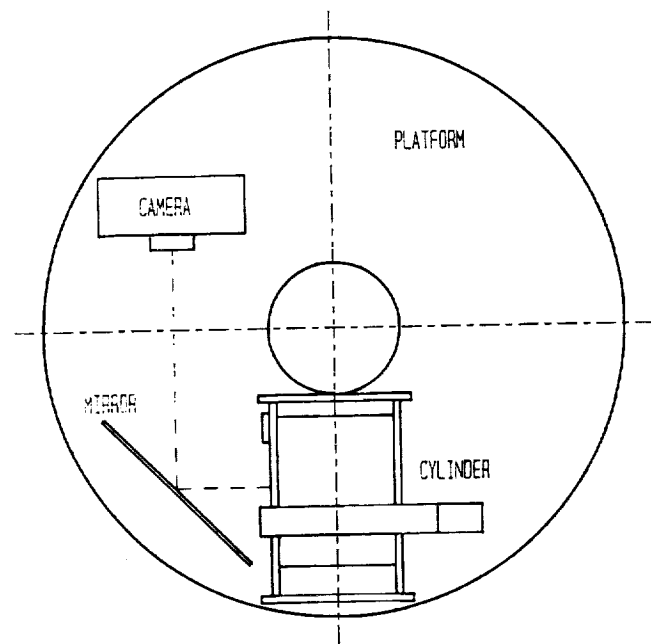


Fig. 3. Camera Arrangement

the low temperature environment and the pictures developed well. The only remaining concern is that when the film becomes brittle at these low temperatures, breakage might occur while the camera is winding to the next frame.

The camera that was chosen is a 35mm Pentax A4000 model, which can not only be electrically triggered, but has an autowind system built into the body. The camera must be capable of using alkaline batteries, since the use of lithium batteries is prohibited by NASA gas safety regulations.

The camera is controlled by the CPU, or Central Processing Unit, which also sends the signals to the pump and platform drive. The CPU first sends a signal to supply power to the camera and then a trigger signal to take a picture. After the picture is taken, the CPU sends another signal to disconnect the camera from the power source. This process is repeated every time the CPU sends a signal to the pump at the start of a new experimental run.

### HISTORY OF EXPERIMENT DEVELOPMENT

The Rotational Fluid Flow Experiment, begun in 1986 as part of the Worcester Polytechnic Institute's Advanced Space Design Program, required an investigation of design for experimental hardware, determination of significant parameters to be measured, and examination of a variety of measuring devices and controlling systems. In the five years that the experiment has been under development, many ideas for construction of different subsystems have been designed, constructed, tested, and, if not feasible, changed completely.

Developments during early years of the project included choosing the offset injection method over the rotating screen method to induce a vortex in the vortex chamber, as well as laying out the schematics of the fluid-flow subsystem (pump,

flowmeter, and piping, Fig. 4). The fluid-flow subsystem is the most important subsystem in the experiment since it produces the vortex. The pump recycles the water from the chamber back into the piping and across the flowmeter. The flowmeter's main function was to measure the volumetric flow rate of the fluid. As part of the electrical subsystems, work was begun on the different circuits that would monitor volumetric flow rate, flow circulation, core and dimple depth, effective gravity induced by the rotation of the platform, air entrainment within the piping layout, pressure and atmosphere conditions within the vortex chamber, as well as electrically activating and deactivating all the mechanical equipment to start and stop experimental runs. The measurements allow the calculation of the Reynolds, Froude, and Weber dimensionless parameters that describe the vortex flow at varying gravities. The scaling effects associated with vortex modeling can then be eliminated.

Other developments included determination of the working fluid and actual hardware procurement. The first piece of hardware developed was the rotating platform, that was designed as a modular component is independent of the rest of the experiment and can be used for other research in the future (Fig. 5). Once the hardware was manufactured, the drive motor and slip rings used to control the platform rotation were obtained. Another part of the experiment developed and built previously was the vortex formation cylinder. The cylinder is made of clear lucite and consists of three basic parts, the cylinder itself and the two end caps. The pump for the working fluid was also obtained with some aluminum tubing and steel fixtures to be used as piping for the flow system. Another major accomplishment of the previous groups was determination of the working fluid. The two major constraints of the working fluid are that the fluid maintain a constant viscosity in the extreme temperature differences experienced in the GASCAN and that the fluid be able to support vortices at a wide range of flow rates.

After studying the mechanics of the microgravity experiment, it was determined that an experiment based on Earth would be of significant value. The most persuasive reason for the on-Earth experiment was the feasibility of vortex formation even

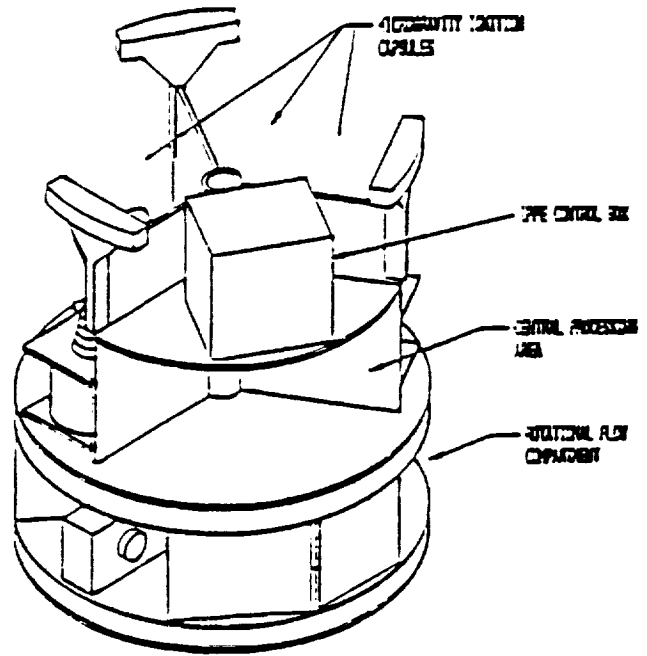


Fig. 5. GASCAN II Layout

with the unusual forces being placed on the fluid. It was unclear from static tests whether the data gathered by the microgravity test would be of use, or if a vortex would form at all. The on-Earth test is a slightly modified and simplified version of the space-based experiment. The most important modification is to suspend the cylinder from the edge of the rotating platform so that it can swing freely to the proper orientation for the speed of rotation. In this way, the resultant force vector is as close as possible to that which would be experienced in space.

Other testing determined the best placement for the camera and flash on the platform to avoid too much glare or too little light when the picture is taken.

During this project year several modifications were made to the existing electrical equipment, and some new components were added. Programs were written to test the functioning of the 8088 CPU, DS-64, MOR-800 boards, and 8155 and 8255 chips. The programs ran successfully and proved that those components operated properly. Also, each subcircuit in the gas entrainment detector was tested for proper operation once the design was completed and built. These tests also proved successful. Once all the electrical components were tested and their operation verified, they were interconnected and mounted. A complete software program was developed to control the function and timing requirements of the entire electro-mechanical system. After the program was written, a final, general test was run on the entire integrated system.

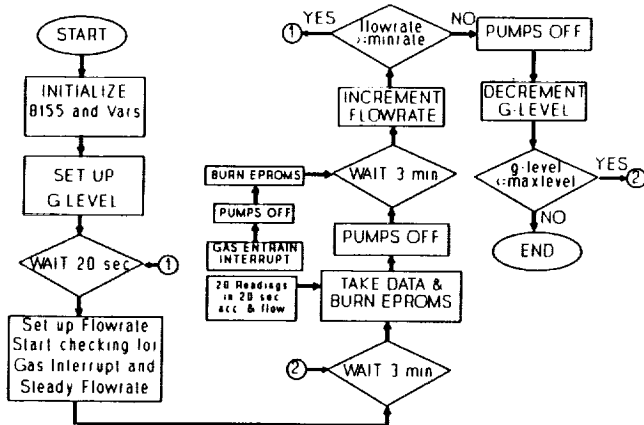


Fig. 4. Flow Chart Timing Diagram